ADVANCES IN THE PATHOGENESIS AND THERAPEUTIC STRATEGIES FOR NASOPHARYNGEAL CARCINOMA

EDITED BY: Jun Ma, Jan Baptist Vermorken, Yu-Pei Chen and Brian O'Sullivan
PUBLISHED IN: Frontiers in Oncology

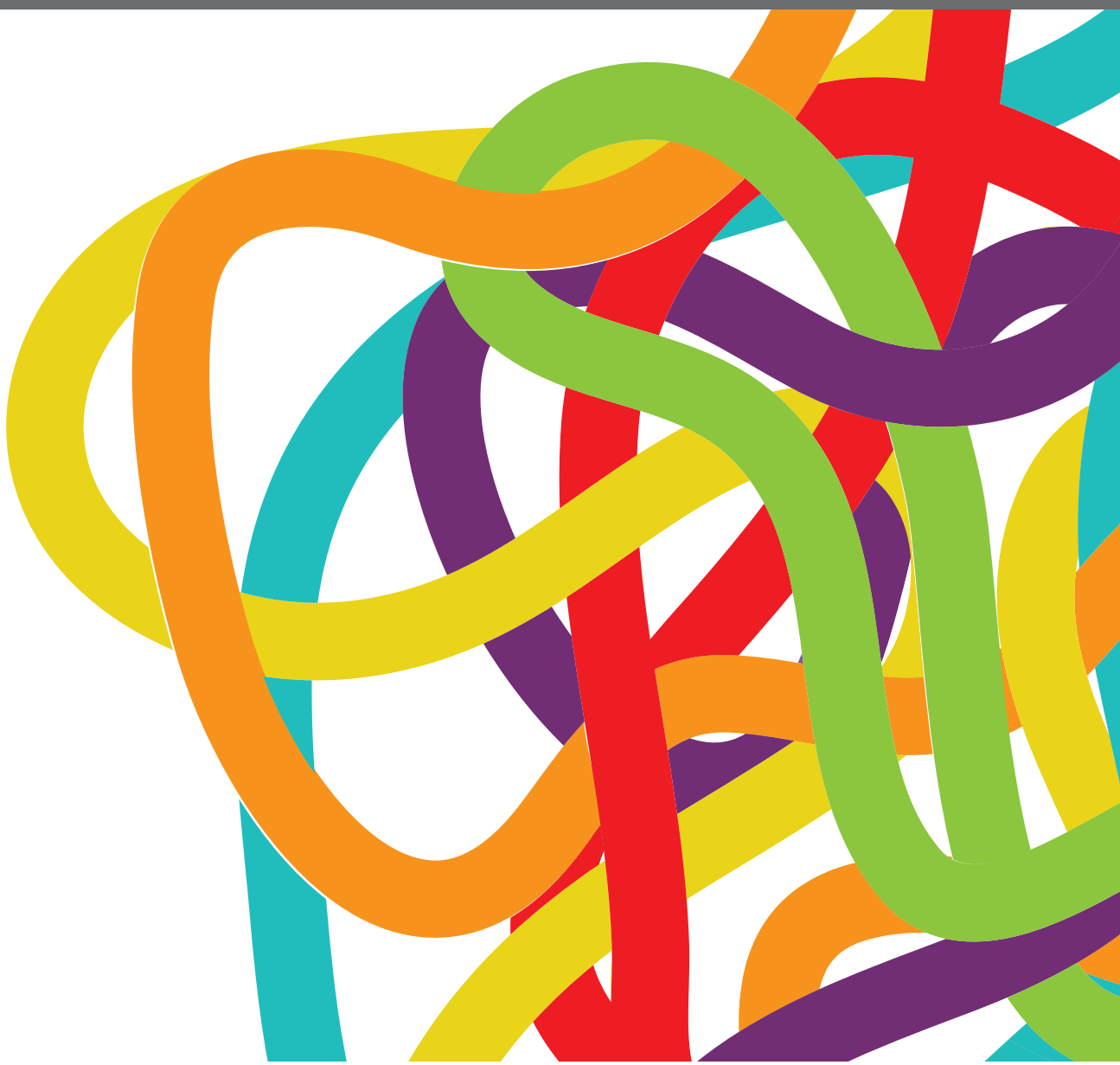

frontiers Research Topics

frontiers

ISSN 1664-8714
ISBN 978-2-88966-719-2
DOI 10.3389/978-2-88966-719-2

About Frontiers

Frontiers is more than just an open-access publisher of scholarly articles: it is a pioneering approach to the world of academia, radically improving the way scholarly research is managed. The grand vision of Frontiers is a world where all people have an equal opportunity to seek, share and generate knowledge. Frontiers provides immediate and permanent online open access to all its publications, but this alone is not enough to realize our grand goals.

Frontiers Journal Series

The Frontiers Journal Series is a multi-tier and interdisciplinary set of open-access, online journals, promising a paradigm shift from the current review, selection and dissemination processes in academic publishing. All Frontiers journals are driven by researchers for researchers; therefore, they constitute a service to the scholarly community. At the same time, the Frontiers Journal Series operates on a revolutionary invention, the tiered publishing system, initially addressing specific communities of scholars, and gradually climbing up to broader public understanding, thus serving the interests of the lay society, too.

Dedication to Quality

Each Frontiers article is a landmark of the highest quality, thanks to genuinely collaborative interactions between authors and review editors, who include some of the world's best academicians. Research must be certified by peers before entering a stream of knowledge that may eventually reach the public - and shape society; therefore, Frontiers only applies the most rigorous and unbiased reviews.
Frontiers revolutionizes research publishing by freely delivering the most outstanding research, evaluated with no bias from both the academic and social point of view. By applying the most advanced information technologies, Frontiers is catapulting scholarly publishing into a new generation.

What are Frontiers Research Topics?

Frontiers Research Topics are very popular trademarks of the Frontiers Journals Series: they are collections of at least ten articles, all centered on a particular subject. With their unique mix of varied contributions from Original Research to Review Articles, Frontiers Research Topics unify the most influential researchers, the latest key findings and historical advances in a hot research area! Find out more on how to host your own Frontiers Research Topic or contribute to one as an author by contacting the Frontiers Editorial Office: frontiersin.org/about/contact

ADVANCES IN THE PATHOGENESIS AND THERAPEUTIC STRATEGIES FOR NASOPHARYNGEAL CARCINOMA

Topic Editors:
Jun Ma, Sun Yat-sen University Cancer Center (SYSUCC), China
Jan Baptist Vermorken, University of Antwerp, Belgium
Yu-Pei Chen, Sun Yat-sen University Cancer Center (SYSUCC), China
Brian O'Sullivan, University Health Network, Canada

Citation: Ma, J., Vermorken, J. B., Chen, Y.-P., O'Sullivan, B., eds. (2021). Advances in the Pathogenesis and Therapeutic Strategies for Nasopharyngeal Carcinoma. Lausanne: Frontiers Media SA. doi: 10.3389/978-2-88966-719-2

Table of Contents

frontiers in Oncology

EDITORIAL
published: 09 March 2021
doi: 10.3389/fonc.2021.647809

Editorial: Advances in the Pathogenesis and Therapeutic Strategies for Nasopharyngeal Carcinoma

Kai-Bin Yang[1,2†], Cheng Xu[2†], Yu-Pei Chen[2], Jan Baptist Vermorken[3,4], Brian O'Sullivan[5] and Jun Ma[2]*

[1] Zhongshan School of Medicine, Sun Yat-sen University, Guangzhou, China, [2] State Key Laboratory of Oncology in South China, Department of Radiation Oncology, Collaborative Innovation Center for Cancer Medicine, Sun Yat-sen University Cancer Center, Guangzhou, China, [3] Department of Medical Oncology, Antwerp University Hospital, Edegem, Belgium, [4] Faculty of Medicine and Health Sciences, University of Antwerp, Antwerp, Belgium, [5] Department of Radiation Oncology, Princess Margaret Cancer Center, University of Toronto, Toronto, ON, Canada

Keywords: nasopharyngeal carcinoma, epstein barr virus, pathogenesis, therapeutic strategies, concurrent chemoradiotherapy, recurrence

Editorial on the Research Topic

Advances in the Pathogenesis and Therapeutic Strategies for Nasopharyngeal Carcinoma

BACKGROUND

Originating from the nasopharyngeal epithelium, nasopharyngeal carcinoma (NPC) is an Epstein-Barr virus (EBV)-related cancer that features an extremely uneven geographical and racial distribution. Its incidence varies widely from 30 in 100,000 individuals in endemic areas to <1 in 100,000 individuals within mainly white populations in non-endemic areas (1–3).

Given the anatomic constraints and the high radiosensitivity of NPC, radiotherapy (RT) is currently the mainstay of definitive treatment for non-metastatic disease (4). Over the past three decades, the management of NPC patients and, accordingly, their prognosis has shown great improvement (5). Firstly, the innovations in RT technology and the extensive application of intensity-modulated radiotherapy (IMRT) with advantageous dose distribution has improved locoregional control and reduced toxic effects on adjacent organs (6–8). In parallel, the prognosis was further improved with the addition of platinum-based chemotherapy to RT, especially for locoregionally advanced NPC (LANPC), probably owing to the improved distant control and enhanced sensitivity to RT. The survival benefits and safety of concurrent chemoradiotherapy (CCRT) and neoadjuvant chemotherapy (NACT) for LANPC have been confirmed by several clinical trials (9–15), and NACT+CCRT is currently the recommended therapy for LANPC in international guidelines (16, 17). However, certain controversies still exist in the management and prognosis of NPC, and a considerable number of studies have focused on tackling them. The present article sheds light on these challenges and the solutions proposed by various research groups.

LIMITATIONS IN RT

Although the improved locoregional control and reduced toxicities has been achieved in the era of IMRT, successful RT still relies on precise delineation and exact dose delivery to the target volume, which is time-consuming and susceptible to inter-observer variability despite the establishment of international contouring guidelines (18). In a retrospective study by Iacovelli et al., the predictive effect of the dose and volume parameters of RT for non-metastatic NPC was evaluated. Since there is a scarcity of medical evidence in non-endemic areas, this study can provide physicians

OPEN ACCESS

Edited and reviewed by:
Andreas Dietz,
Leipzig University, Germany

***Correspondence:**
Jun Ma
majun2@mail.sysu.edu.cn
orcid.org/0000-0002-1137-9349

† These authors have contributed equally to this work

Specialty section:
This article was submitted to Head and Neck Cancer, a section of the journal Frontiers in Oncology

Received: *30 December 2020*
Accepted: *16 February 2021*
Published: *09 March 2021*

Citation:
Yang K-B, Xu C, Chen Y-P, Vermorken JB, O'Sullivan B and Ma J (2021) Editorial: Advances in the Pathogenesis and Therapeutic Strategies for Nasopharyngeal Carcinoma. Front. Oncol. 11:647809. doi: 10.3389/fonc.2021.647809

and investigators with valuable information on the radiotherapy of patients with NPC. Automated delineation through deep-learning algorithms is an appealing option to overcome the shortcomings of artificial contouring. A fully-automated delineation method based on dual-sequence MRI of NPC was proposed by Ye et al. Integrating the different image features of NPC in T1W and T2W images using a dense connectivity embedding U-net, their method demonstrated efficient, accurate, and robust performance within an external validation dataset. In particular, its fully automated design makes it convenient to use.

THE CHALLENGE OF RECURRENCE

Another challenge in NPC treatment is recurrence, especially in patients with advanced disease, even after intensive treatment. After definitive IMRT, 5–10% of NPC patients develop locoregional recurrence, and most of them develop in the first 5 years of follow-up, especially in the first 2 years (19). Using 2 years as a cut-off, the recurrences were classified into early type and late type, and the clinical characteristics and prognostic factors of early vs. late relapses were investigated in a retrospective study by Li F. et al. Surveillance following anti-cancer treatment is another important strategy for tackling the high failure rate of locoregional control. The NPC surveillance guidelines provided by the National Comprehensive Cancer Network and European Society for Medical Oncology were evaluated by Zhou et al. in a retrospective study, and their results showed that most recurrences would be missed if either of the two guidelines was strictly followed, indicating an urgent need for improved surveillance algorithms. Additionally, the suspicion of a clinically recurrent event can be confused with complications associated with radiotherapy. For example, cervical spine osteoradionecrosis may be mistaken as metastasis due to the increased radiotracer uptake on a bone scan. In their retrospective study, Zhong et al. demonstrated the additional value of MRI in differentiating between cervical spine osteoradionecrosis and metastasis detected by bone scan, further enabling the early detection and treatment of recurrent diseases and the elimination of unnecessary intensive therapy for benign lesions. Besides surveillance, treatment of recurrences also remains a problem. Endoscopic nasopharyngectomy is one of the treatment options for local recurrence after radiotherapy. Site-specific and sinonasal-related quality of life (QoL) was shown to be impaired immediately after salvage nasopharyngectomy and to gradually recover to preoperative levels during long-term follow-up in a prospective study by Li W. et al.. Their results confirmed that endoscopic nasopharyngectomy is a valuable management option for local recurrence and indicated that gross-total resection was superior to subtotal resection considering the postoperative QoL.

IMPAIRED QoL AND TOXICITY

Another current challenge in NPC is the substantial burden of long-term toxicity and impaired QoL in survivors after successful anti-cancer treatment. McDowell et al. have provided a detailed review of the toxicity and long-term QoL data in prospective studies of chemotherapy and RT from both endemic and non-endemic areas. Factors affecting long-term QoL, the unmet needs of NPC survivors in the contemporary era, and potential and promising strategies to reduce the toxicity burden were all highlighted. Their review provided a profile of unmet needs in NPC survivors and, additionally, pointed out two major shortcomings in the presently available data to provide valuable guidance for future research. One of the shortcomings was that the vast majority of QoL and toxicity data was reported from the clinician's perspective, which may result in unintentional underestimation of symptoms and their severity. The second shortcoming was that statistically determined, rather than clinically meaningful, differences were more commonly reported.

Since more intensive therapies generally facilitate disease control at the expense of more severe toxicity, striking a balance between disease control and toxicity is key to the optimal treatment of all cancers, including NPC. To assist in the comprehensive evaluation of both the efficacy and toxicities of different cancer treatment options, the ASCO-VF and ESMO-MCBS frameworks were proposed (20, 21). In a field test of these two frameworks in the context of NPC, Zhang et al. reported significant variations in the toxicity data reported by different trials and inconsistent scores generated by ASCO-VF for treatments that were defined as "substantial clinical benefit" in ESMO-MCBS. Thus, there seems to be some inconsistency between the two frameworks, which requires more attention in the future. Given the additional toxicity and economic burden of CCRT and NACT, identification of the potential beneficiaries for these treatments to help avoid unnecessary chemotherapy is another feasible measure to achieve better balance between treatment efficacy and toxicity. In their Phase 2 Multicenter Clinical Trial, Huang et al. evaluated the efficacy of CCRT in stage II NPC in the IMRT era. In contrast to the results in another phase 3 trial adopting conventional 2-dimensional radiotherapy published previously (22), their results showed that CCRT failed to further improve the prognosis of stage II NPC compared with IMRT alone. Thus, additional concurrent chemotherapy may be unnecessary for stage II NPC in the IMRT era. Prediction of the potential beneficiaries for NACT in LANPC has also been extensively studied via two relevant retrospective studies from endemic areas. One of the studies targeted the entire LANPC population and established a prognostic index model that uses gender, T status, N status, LDH level, and EBV-DNA level to identify high-risk patients for additional NACT (Sun et al.), while the other one focused on the usually excluded T3N0-1 and T4N0 subgroups. Combining real-world and clinical trial data together, a risk stratification model including gender and EBV-DNA level was generated and validated using recursive partitioning analysis (Xu et al.). Notably, gender and EBV-DNA level were identified as risk factors in both studies, indicating their close association with the patient's prognosis.

PATHOGENESIS OF NPC

Besides the clinical studies on therapeutic strategies, research effort has also been devoted to deepening our understanding of the pathogenesis of NPC, with the intention of promoting the development of novel screening strategies and targeted

therapies with high efficacy and low toxicity, especially to better treat NPC recurrences and distant metastasis. Since NPC is consistently related to the EBV infection in endemic areas, extensive research has focused on the role of multiple viral latent gene products, such as EBNA1, LMP1, and LMP2, in the malignant transformation of the nasopharyngeal epithelium and EBV-targeting therapy for NPC. These studies and their findings have been reviewed in detail by Hau et al., who report that EBV-targeting therapeutic strategies for NPC include targeting EBV latent proteins and switching the latent cycle of EBV to the lytic cycle. Although no specific EBV-targeting therapeutic strategy has been approved for NPC at present, this strategy remains promising and appealing for this EBV-related malignancy.

Abnormal function of proto-oncogenes and tumor suppressor genes form a common pathogenic mechanism in all cancers, including NPC. Accordingly, Qin et al. reported a heterozygous mutation of p53, a well-known tumor suppressor gene, and its oncogenic effect through activation of the PI3K-Akt signaling pathway in NPC cells. Additionally, Wang et al. found that the internal ribosome entry sites of Bmi1, a proto-oncogene in polycomb-repressive complex 1, mediated its cap-independent translation in NPC cells.

Extensive application of high-throughput sequencing techniques has greatly promoted research on the pathogenesis of cancer. With the help of these techniques, the altered intestinal flora in NPC patients and circRNA expression profiles in NPC were revealed by Jiang et al. and Yang et al., respectively. While the alteration of flora might be useful in early screening and individualized prevention and treatment of NPC, the differentially expressed circRNAs and their target pathways might provide novel targets for NPC therapy.

OTHER LIMITATIONS

A notable shortcoming in research on NPC is that it is poorly studied in children and adolescents, probably due to its rarity in younger age groups. In a large cohort study of childhood and adolescent NPC treated with IMRT, the clinical significance of plasma EBV-DNA was confirmed (Qiu et al.). However, more research effort is required to facilitate optimization of treatment for patients from this group, as the findings for adulthood NPC may not be translatable to children and adolescents with NPC.

CONCLUSION

Despite the advances in research on the management and treatment of NPC over the past three decades, toxicity, recurrence, and standardization of RT remain major challenges, along with a lack of research about NPC in children and adolescents. Nonetheless, advances are being witnessed in research on the pathogenesis and therapeutic strategies of NPC. With concerted global research efforts, the current obstacles in NPC treatment will be overcome, and we are bound to win the battle against NPC eventually.

AUTHOR CONTRIBUTIONS

K-BY and CX drafted the manuscript. JM, JV, and BO'S revised the manuscript. All authors approved the submission.

FUNDING

This work was supported by grants from the National Natural Science Foundation of China (81930072); the Key-Area Research and Development Program of Guangdong Province (2019B020230002); the Natural Science Foundation of Guangdong Province (2017A030312003); the Health & Medical Collaborative Innovation Project of Guangzhou City, China (201803040003); the Innovation Team Development Plan of the Ministry of Education (No. IRT_17R110); and the Overseas Expertise Introduction Project for Discipline Innovation (B14035).

REFERENCES

1. Wei KR, Zheng RS, Zhang SW, Liang ZH, Li ZM, Chen WQ. Nasopharyngeal carcinoma incidence and mortality in China, 2013. *Chin J Cancer.* (2017) 36:90. doi: 10.1186/s40880-017-0257-9
2. Bray F, Ferlay J, Soerjomataram I, Siegel RL, Torre LA, Jemal A. Global cancer statistics 2018: GLOBOCAN estimates of incidence and mortality worldwide for 36 cancers in 185 countries. *CA Cancer J Clin.* (2018) 68:394–424. doi: 10.3322/caac.21492
3. Ferlay J, Colombet M, Soerjomataram I, Mathers C, Parkin DM, Piñeros M, et al. Estimating the global cancer incidence and mortality in 2018: GLOBOCAN sources and methods. *Int J Cancer.* (2019) 144:1941–53. doi: 10.1002/ijc.31937
4. Peng H, Chen L, Chen YP, Li WF, Tang LL, Lin AH, et al. The current status of clinical trials focusing on nasopharyngeal carcinoma: a comprehensive analysis of ClinicalTrials.gov database. *PLoS ONE.* (2018) 13:e0196730. doi: 10.1371/journal.pone.0196730
5. Chen YP, Chan ATC, Le QT, Blanchard P, Sun Y, Ma J. Nasopharyngeal carcinoma. *Lancet.* (2019) 394:64–80. doi: 10.1016/S0140-6736(19)30956-0
6. Peng G, Wang T, Yang KY, Zhang S, Zhang T, Li Q, et al. A prospective, randomized study comparing outcomes and toxicities of intensity-modulated radiotherapy vs. conventional two-dimensional radiotherapy for the treatment of nasopharyngeal carcinoma. *Radiotherap Oncol.* (2012) 104:286–93. doi: 10.1016/j.radonc.2012.08.013
7. Zhang B, Mo Z, Du W, Wang Y, Liu L, Wei Y. Intensity-modulated radiation therapy versus 2D-RT or 3D-CRT for the treatment of nasopharyngeal carcinoma: a systematic review and meta-analysis. *Oral Oncol.* (2015) 51:1041–6. doi: 10.1016/j.oraloncology.2015.08.005
8. Co J, Mejia MB, Dizon JM. Evidence on effectiveness of intensity-modulated radiotherapy versus 2-dimensional radiotherapy in the treatment of nasopharyngeal carcinoma: meta-analysis and a systematic review of the literature. *Head Neck.* (2016) 38(Suppl. 1):E2130–42. doi: 10.1002/hed.23977
9. Al-Sarraf M, LeBlanc M, Giri PG, Fu KK, Cooper J, Vuong T, et al. Chemoradiotherapy versus radiotherapy in patients with advanced nasopharyngeal cancer: phase III randomized Intergroup study 0099. *J Clin Oncol.* (1998) 16:1310–7. doi: 10.1200/JCO.1998.16.4.1310
10. Lin JC, Jan JS, Hsu CY, Liang WM, Jiang RS, Wang WY. Phase III study of concurrent chemoradiotherapy versus radiotherapy alone for advanced nasopharyngeal carcinoma: positive effect on overall and progression-free survival. *J Clin Oncol.* (2003) 21:631–7. doi: 10.1200/JCO.2003.06.158
11. Sun Y, Li WF, Chen NY, Zhang N, Hu GQ, Xie FY, et al. Induction chemotherapy plus concurrent chemoradiotherapy versus concurrent

chemoradiotherapy alone in locoregionally advanced nasopharyngeal carcinoma: a phase 3, multicentre, randomised controlled trial. *Lancet Oncol.* (2016) 17:1509–20. doi: 10.1016/S1470-2045(16)30410-7

12. Li WF, Chen NY, Zhang N, Hu GQ, Xie FY, Sun Y, et al. Concurrent chemoradiotherapy with/without induction chemotherapy in locoregionally advanced nasopharyngeal carcinoma: long-term results of phase 3 randomized controlled trial. *Int J Cancer.* (2019) 145:295–305. doi: 10.1002/ijc.32099
13. Cao SM, Yang Q, Guo L, Mai HQ, Mo HY, Cao KJ, et al. Neoadjuvant chemotherapy followed by concurrent chemoradiotherapy versus concurrent chemoradiotherapy alone in locoregionally advanced nasopharyngeal carcinoma: a phase III multicentre randomised controlled trial. *Europ J Cancer.* (2017) 75:14–23. doi: 10.1016/j.ejca.2016.12.039
14. Frikha M, Auperin A, Tao Y, Elloumi F, Toumi N, Blanchard P, et al. A randomized trial of induction docetaxel-cisplatin-5FU followed by concomitant cisplatin-RT versus concomitant cisplatin-RT in nasopharyngeal carcinoma (GORTEC 2006-02). *Ann Oncol.* (2018) 29:731–6. doi: 10.1093/annonc/mdx770
15. Zhang Y, Chen L, Hu GQ, Zhang N, Zhu XD, Yang KY, et al. Gemcitabine and cisplatin induction chemotherapy in nasopharyngeal carcinoma. *N Engl J Med.* (2019) 381:1124–35. doi: 10.1056/NEJMoa1905287
16. Colevas AD, Yom SS, Pfister DG, Spencer S, Adelstein D, Adkins D, et al. NCCN guidelines insights: head and neck cancers, Version 1.2018. *J Natl Compr Canc Netw.* (2018) 16:479–90. doi: 10.6004/jnccn.2018.0026
17. National Comprehensive Cancer Network. *NCCN Guidelines for Head and Neck Cancers (Version 1.2021)* Available online at: https://www.nccn.org/professionals/physician_gls/pdf/head-and-neck.pdf (accessed January 20, 2021).
18. Lee AW, Ng WT, Pan JJ, Poh SS, Ahn YC, AlHussain H, et al. International guideline for the delineation of the clinical target volumes (CTV) for nasopharyngeal carcinoma. *Radiotherap Oncol.* (2018) 126:25–36. doi: 10.1016/j.radonc.2017.10.032
19. Lee AW, Ma BB, Ng WT, Chan AT. Management of nasopharyngeal carcinoma: current practice and future perspective. *J Clin Oncol.* (2015) 33:3356–64. doi: 10.1200/JCO.2015.60.9347
20. Cherny NI, Dafni U, Bogaerts J, Latino NJ, Pentheroudakis G, Douillard JY, et al. ESMO-magnitude of clinical benefit scale version 1.1. *Ann Oncol.* (2017) 28:2340–66. doi: 10.1093/annonc/mdx310
21. Schnipper LE, Davidson NE, Wollins DS, Blayney DW, Dicker AP, Ganz PA, et al. Updating the american society of clinical oncology value framework: revisions and reflections in response to comments received. *J Clin Oncol.* (2016) 34:2925–34. doi: 10.1200/JCO.2016.68.2518
22. Chen QY, Wen YF, Guo L, Liu H, Huang PY, Mo HY, et al. Concurrent chemoradiotherapy vs radiotherapy alone in stage II nasopharyngeal carcinoma: phase III randomized trial. *J Natl Cancer Inst.* (2011) 103:1761–70. doi: 10.1093/jnci/djr432

Conflict of Interest: The authors declare that the research was conducted in the absence of any commercial or financial relationships that could be construed as a potential conflict of interest.

frontiers in Oncology

ORIGINAL RESEARCH
published: 29 November 2019
doi: 10.3389/fonc.2019.01343

Selection and Validation of Induction Chemotherapy Beneficiaries Among Patients With T3N0, T3N1, T4N0 Nasopharyngeal Carcinoma Using Epstein-Barr Virus DNA: A Joint Analysis of Real-World and Clinical Trial Data

Cheng Xu[1†], *Shu Zhang*[1†], *Wen-Fei Li*[1†], *Lei Chen*[1], *Yan-Ping Mao*[1], *Ying Guo*[2], *Qing Liu*[3], *Jun Ma*[1] *and Ling-Long Tang*[1*]

[1] *Department of Radiation Oncology, Sun Yat-sen University Cancer Center, State Key Laboratory of Oncology in South China, Collaborative Innovation Center for Cancer Medicine, Guangdong Key Laboratory of Nasopharyngeal Carcinoma Diagnosis and Therapy, Guangzhou, China,* [2] *Clinical Trials Centre, Sun Yat-sen University Cancer Center, State Key Laboratory of Oncology in South China, Collaborative Innovation Center for Cancer Medicine, Guangdong Key Laboratory of Nasopharyngeal Carcinoma Diagnosis and Therapy, Guangzhou, China,* [3] *Department of Medical Statistics and Epidemiology, School of Public Health, Sun Yat-sen University, Guangzhou, China*

Background and Purpose: Evidence for induction chemotherapy plus concurrent chemoradiotherapy (IC+CCRT) in nasopharyngeal carcinoma (NPC) was derived from landmark clinical trials excluding the T3N0, T3N1, T4N0 subgroups. This study used Epstein-Barr virus (EBV) DNA to select IC beneficiaries from the three subgroups.

Materials and Methods: Significant predictors of overall survival (OS) were identified using multivariate Cox analyses. Risk stratification was generated using recursive partitioning analysis (RPA). IC+CCRT was compared with CCRT in each risk stratification and in different subgroups. Individual-level data from a clinical trial (NCT01245959) was used for validation.

Results: Gender and EBV DNA were included in RPA-generated risk stratification, categorizing patients into low-risk (EBV DNA <2,000 copies/mL; female and EBV DNA ≥2,000 copies/mL) and high-risk groups (male and EBV DNA ≥2,000 copies/mL). The OS superiority of IC+CCRT over CCRT was only observed in the high-risk group (HR = 0.64, 95% CI = 0.43–0.97; $P = 0.032$). Subgroup analysis indicated the OS benefit was exclusively from the docetaxel–cisplatin–5-fluorouracil regimen (HR = 0.41, 95% CI = 0.22–0.78; $P = 0.005$). The status of the T3N1 subgroup as an IC beneficiary is more explicit than the T3N0 and T4N0 subgroups. IC+CCRT showed improved OS in the validation cohort combining high-risk cases of real-world data with clinical trial data (HR = 0.62, 95% CI = 0.42–0.94; $P = 0.023$).

OPEN ACCESS

Edited by:
David I. Rosenthal, University of Texas MD Anderson Cancer Center, United States

Reviewed by:
Sarbani Ghosh Laskar, Tata Memorial Hospital, India
Sjoukje F. Oosting, University Medical Center Groningen, Netherlands

****Correspondence:***
Ling-Long Tang
tangll@sysucc.org.cn

† These authors have contributed equally to this work and share first authorship

Specialty section:
This article was submitted to Clinical Diabetes, a section of the journal Frontiers in Oncology

Received: *14 September 2019*
Accepted: *15 November 2019*
Published: *29 November 2019*

Citation:
Xu C, Zhang S, Li W-F, Chen L, Mao Y-P, Guo Y, Liu Q, Ma J and Tang L-L (2019) Selection and Validation of Induction Chemotherapy Beneficiaries Among Patients With T3N0, T3N1, T4N0 Nasopharyngeal Carcinoma Using Epstein-Barr Virus DNA: A Joint Analysis of Real-World and Clinical Trial Data. Front. Oncol. 9:1343. doi: 10.3389/fonc.2019.01343

Conclusion: Patients with high-risk T3N1 NPC is the definite target population for receiving IC+CCRT in real-world practice. T3N0 and T4N0 subgroups need further investigations in future IC-related studies.

Keywords: nasopharyngeal carcinoma, Epstein-Barr virus, induction chemotherapy, concurrent chemoradiotherapy, recursive partitioning analysis

INTRODUCTION

As nasopharyngeal carcinoma (NPC) has the highest incidence in endemic areas such as Southern China, randomized controlled trials (RCTs) conducted in this region are incredibly important in optimizing clinical decision-making (1, 2). In excess of 70% of new cases are defined as locoregionally advanced NPC (LANPC; stage III–IVA), which is prone to distant metastasis and therefore requires intensive treatments over and above radiotherapy alone (3).

Since the INT 0099 trial successfully introduced chemotherapy for improved management of LANPC in 1998, various chemoradiotherapy schedules have been investigated using clinical trials (4–8). In the past two decades, concurrent chemoradiotherapy (CCRT) followed by adjuvant chemotherapy (AC) has been recommended by the National Comprehensive Cancer Network (NCCN) clinical guidelines as the standard treatment for LANPC due to its strong therapeutic intensity (9). However, a clinical trial from endemic area by Chen et al. reported that the additional AC induced severe gastrointestinal toxicities and low patient compliance (63%), which greatly restricted its broad practical application (5). Induction chemotherapy (IC) is used before radiotherapy and thought to be less toxic, improve tumor shrinkage, and lead to early eradication of micrometastases (10). The 2018 NCCN guidelines increased the recommendation of IC+CCRT from category III to IIA as one of the most appropriate treatments for LANPC, rendering it superior to CCRT (IIB) and equivalent to CCRT+AC (IIA) (11).

Three phase III RCTs from endemic areas provided supporting evidences for IC+CCRT (7, 8, 12). Cao et al. (7) investigated the cisplatin−5-fluorouracil (PF) IC regimen in LANPC excluding T3N0–1 subgroup and found IC+CCRT achieved higher 3-year disease-free survival than CCRT alone (82.0 vs. 74.1%; $P = 0.028$). Sun et al. (8) and Zhang et al. (12) individually explored docetaxel–cisplatin−5-fluorouracil (TPF) and gemcitabine–cisplatin (GP) IC regimens in LANPC excluding T3–4N0 subgroups. Both trials suggested that the additional IC can significantly improve 3-year overall survival (OS) compared with CCRT alone. Notably, target population of the three RCTs covered all LANPC but not T3N0–1 (7) or T3–4N0 (8, 12) subgroups, since these patients were crudely considered to have low risk of distant metastasis and not warranting additional IC. Although this inclusion criterion enhanced the power to detect survival benefits of IC+CCRT, it raised clinical questions that whether patients with T3N0, T3N1, and T4N0 NPC could benefit from IC, in that data on a relatively favorable subgroup is scarce and these patients are not always included in clinical trials. A phase III trial including all subgroups of LANPC patients in a non-endemic area reported non-significantly different OS between IC+CCRT and CCRT ($P = 0.059$) (13). Thus, the three subgroups (i.e., T3N0, T3N1, and T4N0) has become a potentially confounding factor that may exert effects on trial results, yet it has not been thoroughly investigated.

As the Tumor-Node-Metastasis (TNM) staging system only utilizes anatomical information, it solely may fail to identify IC beneficiaries from the three excluded subgroups. Epstein-Barr virus (EBV) DNA has been demonstrated to better refine risk stratification and guide individualized treatment in NPC (14). In this retrospective, joint analysis based on real-world and clinical trial data, we used pre-treatment EBV DNA and other critical predictors to select and validate the IC beneficiaries from these excluded T3N0, T3N1, and T4N0 NPC cases, with the purpose of providing real-world evidences to inform choices between treatment strategies in patients with T3N0, T3N1, and T4N0 NPC.

MATERIALS AND METHODS

Study Design, Data Source, and Population

A flow diagram depicting the study design and inclusion/exclusion criteria is presented as **Supplementary Figure 1**. Given the reliance on a big-data intelligence platform (YiduCloud Technology Ltd., Beijing, China), we generated a NPC-specific real-world dataset that was adopted to identify all untreated, non-metastatic cases that were initially diagnosed at Sun Yat-sen University Cancer Center (SYSUCC) between April 2009 to December 2015. All patients received radical treatments based on intensity-modulated radiotherapy (IMRT) and complete basic data were obtained for each patient. A detailed description of the intelligence platform is presented in **Supplementary Materials** and has been published in a previous study (15).

This study was approved by the Institutional Review Board and the Ethics Committee with the approval ID YB2018-71; the need for informed consent was waived. To ensure study integrity, original raw data have been uploaded to a public platform named Research Data Deposit (http://www.researchdata.org.cn) with the identifier RDDA2018000782.

Pre-treatment Workup

Clinical staging was guided by the 8th edition of the American Joint Committee on Cancer/Union for International Cancer Control (AJCC/UICC) manual. Pre-treatment examinations included complete medical history, physical examination, blood profile, nasopharyngoscopy, head-to-neck magnetic resonance imaging (MRI), chest radiography/computed tomography

TABLE 1 | Baseline characteristics of patients with T3N0, T3N1, and T4N0 NPC.

Characteristics	No. (%)	Univariate analysis of OS		Multivariate analysis of OS	
		HR (95% CI)	*P*	aHR (95% CI)	*P*
Age at diagnosis, years					
18–37	528 (19.6)	Reference		Reference	
38–44	769 (28.6)	1.48 (0.92–2.38)	0.108	1.42 (0.88–2.29)	0.148
45–52	655 (24.3)	1.10 (0.66–1.85)	0.715	1.12 (0.66–1.88)	0.678
≥53	740 (27.5)	2.38 (1.52–3.74)	<0.001	2.10 (1.32–3.31)	0.001
Gender					
Male	1,944 (72.2)	Reference		Reference	
Female	748 (27.8)	0.58 (0.40–0.84)	0.004	0.60 (0.41–0.87)	0.007
Histological type					
WHO type I–II	65 (2.4)	Reference		Reference	
WHO type III	2,626 (97.5)	0.34 (0.20–0.59)	<0.001	0.35 (0.20–0.60)	<0.001
Family history of cancer					
No	1,944 (72.2)	Reference		–	–
Yes	748 (27.8)	0.83 (0.60–1.16)	0.276	–	–
Comorbidity					
No	1,510 (56.1)	Reference		–	–
Yes	1,182 (43.9)	1.33 (0.98–1.79)	0.067	–	–
Cigarette smoking					
No	1,757 (65.3)	Reference		–	–
Yes	935 (34.7)	1.22 (0.91–1.63)	0.186	–	–
Alcohol consumption					
No	2,325 (86.4)	Reference		–	–
Yes	367 (13.6)	1.28 (0.87–1.89)	0.215	–	–
EBV DNA titer, copy/mL[a]					
<2,000	1,547 (57.5)	Reference		Reference	
≥2,000	1,145 (42.5)	2.09 (1.56–2.81)	<0.001	1.96 (1.45–2.64)	<0.001
Hb, g/L[a,b]					
<120.0 (110.0)	75 (2.8)	Reference		–	–
≥120.0 (110.0)	2,617 (97.2)	1.75 (0.82–3.73)	0.147	–	–
Albumin, g/L[a]					
<40.0	196 (7.3)	Reference		Reference	
≥40.0	2,496 (92.7)	0.42 (0.28–0.64)	<0.001	0.54 (0.35–0.82)	0.011
LDH, U/L[a]					
≤250	2,507 (93.1)	Reference		Reference	
>250	185 (6.9)	2.25 (1.51–3.37)	<0.001	2.00 (1.33–3.01)	0.001
CRP, mg/L[a]					
≤3.00	1,835 (68.2)	Reference		Reference	
>3.00	857 (31.8)	1.55 (1.16–2.06)	0.003	1.19 (0.88–1.60)	0.260
UICC/AJCC clinical stage					
T3N0	401 (14.9)	–	–	–	–
T3N1	2,098 (77.9)	–	–	–	–
T4N0	193 (7.2)	–	–	–	–
T category					
T3	2,499 (92.8)	Reference		Reference	
T4	193 (7.2)	2.30 (1.53–3.46)	<0.001	2.22 (1.47–3.34)	<0.001
N category					
N0	594 (22.1)	Reference		–	–
N1	2.098 (77.9)	0.84 (0.60–1.18)	0.313	–	–
Treatment					
CCRT	1,418 (52.7)	–	–	–	–
IC+CCRT	1,274 (47.3)	–	–	–	–

NPC, nasopharyngeal carcinoma; OS, overall survival; no., number; HR, hazard ratio; aHR, adjusted hazard ratio; CI, confidence interval; WHO, World Health Organization; EBV, Epstein-Barr virus; Hb, hemoglobin; LDH, serum lactate dehydrogenase; CRP, C-reactive protein; UICC, Union for International Cancer Control; AJCC, American joint Committee on Cancer; CCRT, concurrent chemoradiotherapy; IC, induction chemotherapy.

[a] *All of these variables were measured before treatment.*

[b] *Cut-off values of hemoglobin are 120 and 110 g/L for male and female, respectively.*

(CT), abdominal ultrasound, and skeletal scintigraphy; ^{18}F-fluorodeoxyglucose positron emission tomography-CT was used to replace the latter three items for detection of possible metastases in the lung, liver, and bones. Moreover, circulating cell-free EBV DNA was quantified using a real-time quantitative polymerase chain-reaction (PCR) assay; the detailed method for this has been described in a previous study (14).

Treatment

All patients underwent IMRT using the simultaneous integrated boost technique on 5 consecutive days every week. IC regimens consisted of PF regimen (80 mg/m^2 and 4,000 mg/m^2, respectively), docetaxel–cisplatin (TP; 75 and 75 mg/m^2, respectively), and TPF (60, 60, and 3,000 mg/m^2, respectively), every 3 weeks for 2–3 cycles. Concurrent chemotherapy was weekly (30–40 mg/m^2) or 3-weekly cisplatin (80–100 mg/m^2) treatment. Detailed information is shown in the **Supplementary Materials**.

TABLE 2 | Detailed treatment and prognosis of 2,692 patients with T3N0, T3N1, and T4N0 NPC.

Items	T3N0, no. (%)	T3N1, no. (%)	T4N0, no. (%)
No. of patients	401	2,098	193
Treatment			
CCRT	274 (68.3)	1,078 (51.4)	66 (34.2)
IC + CCRT	127 (31.7)	1,020 (48.6)	127 (65.8)
CCRT schedule			
3-weekly	280 (69.8)	1,548 (73.8)	155 (80.3)
Weekly	121 (30.2)	550 (26.2)	38 (19.7)
Accumulated DDP, mg	187	194	188
IC regimen			
TPF	40 (31.5)	454 (44.5)	68 (53.5)
PF	31 (24.4)	232 (22.7)	26 (20.5)
TP	56 (44.1)	334 (32.7)	33 (26.0)
Death (5th yr.)	16 (4.0)	128 (6.1)	23 (11.9)
Locoregional relapse (5th yr.)	15 (3.7)	123 (5.9)	20 (10.4)
Distant metastasis (5th yr.)	11 (2.7)	152 (7.2)	16 (8.3)
Bone	3	18	3
Lung	6	40	3
Liver	0	35	6
Multiple sites	2	45	3
Others	0	14	1
3-year OS (%)	97.3	95.7	91.2
5-year OS (%)	94.3	91.9	85.2
	Ref.	$P = 0.116$	$P = 0.001$
	–	Ref.	$P = 0.002$
3-year FFS (%)	93.5	88.5	83.3
5-year FFS (%)	90.6	84.9	76.6
	Ref.	$P = 0.003$	$P < 0.001$
	–	Ref.	$P = 0.014$
3-year LRRFS (%)	96.2	94.8	91.5
5-year LRRFS (%)	95.6	93.0	85.7
	Ref.	$P = 0.097$	$P = 0.002$
	–	Ref.	$P = 0.013$
3-year DMFS (%)	97.5	93.5	92.0
5-year DMFS (%)	96.8	91.6	90.6
	Ref.	$P = 0.002$	$P = 0.003$
	–	Ref.	$P = 0.511$

CCRT, concurrent radiochemotherapy; DDP, cisplatin; DMFS, distant metastasis-free survival; FFS, failure-free survival; IC, induction chemotherapy; LRRFS, locoregional relapse-free survival; NPC, nasopharyngeal carcinoma; No., number; OS, overall survival; PF, cisplatin−5-fluorouracil; Ref., reference; TPF, docetaxel–cisplatin−5-fluorouracil; TP, docetaxel–cisplatin; yr., year.

Follow-Up and Endpoints

Follow-up duration was measured from the day of diagnosis to the last visit or death. During the visits, head-to-neck MRI, chest radiography/CT, abdominal ultrasound, and skeletal scintigraphy were routinely performed, every 3 months during the first 2 years, then every 6 months for 3 years thereafter. Clinical suspicion of recurrence and distant metastasis were confirmed using cytological biopsies and imaging. The main endpoint was OS, measured from day of diagnosis until death due to any cause or the latest known date alive. Secondary endpoints were failure-free survival (FFS; from the date of diagnosis to failure, death, or last follow-up), locoregional relapse-free survival (LRRFS; to local/regional relapse), and distant metastasis-free survival (DMFS; to distant metastasis).

Statistical Analysis

Continuous variables were converted into categorical variables based on the interquartile range (IQR; age at diagnosis) and clinical cut-off values [hemoglobin (Hb), albumin, lactate dehydrogenase (LDH), and C-reactive protein (CRP)]. Robust evidence has indicated that pre-treatment EBV DNA can refine the TNM staging for NPC at the cut-off of 2,000 copies/mL (16), which was also supported by this study using the receiver-operating characteristic (ROC) curve analysis (**Supplementary Figure 2**). Actuarial survival rates were calculated using the Kaplan-Meier curve and compared using the log-rank test (17). Univariate and multivariate Cox regression models were performed to quantify the effect of variables on OS. Univariate Cox analysis was performed *a priori* via a hypothesis-driven method. Predictors with $P < 0.05$ in the univariate analysis were entered into the multivariate analysis to validate their significance by backward stepwise algorithm (18). Hazard ratios (HRs) and 95% confidence intervals (CIs) were used as the summary statistics.

In accordance with the optimized binary partition algorithm, we included all validated predictors for 5-year OS to perform recursive partitioning analysis (RPA) using the *rpart* package in R, with the purpose of distinctly categorizing heterogeneous patients into purified risk stratifications (19). The *prune* package in R was used to remove the excessive branches of RPA-generated risk stratification for realistic application (19).

Individual-level, 5-year follow-up data of the TPF trial (NCT01245959), which discarded the T3–4N0 NPC cases was used to establish validation cohorts (20). Essentially, we aim to use the real-world dataset of T3–4N0 NPC patients to establish pseudo-trial cohorts (basic characteristics of patients should be consistent with their counterparts in a clinical trial), combine these data with the trial data, and determine whether the

original trial results have changed significantly. Consequently, we validate the importance of additional IC to patients with T3–4N0 NPC. A three-step method was used to achieve this. Firstly, patients with T3–4N0 NPC at different risks were individually selected from the real-world dataset to produce two pseudo-trial cohorts. The sample size of T3–4N0 NPC was estimated according to its proportion, relative to the whole NPC population. Secondly, pseudo-trial cohorts of T3–4N0 NPC were processed to have similar baseline characteristics to the TPF trial, by using propensity score matching (PSM) to balance potential differences, since PSM can excellently mimic features of clinical trials and reduce selection bias caused by observed confounders (21). PSM was used in accordance with the nearest-neighbor algorithm without replacement. Thirdly, two validation cohorts were generated by combining pseudo-trial cohorts with the TPF trial data and verified by Kaplan-Meier survival analysis. C-index was used to measure the discriminatory performance of treatment via the *Hemins* package in R. All statistical analyses and figures were generated using SPSS, version 23.0 (SPSS Inc., Chicago, IL, USA) and R software, version 3.3.2 (http://www.r-project.org/). All tests were two-sided; $P < 0.05$ was significant.

RESULTS

Baseline Characteristics and Survival of Patients With T3N0, T3N1, T4N0 NPC

The baseline characteristics of 2,692 patients with T3N0, T3N1, and T4N0 NPC are shown in **Table 1**. The median age was 45 (IQR = 37–52) years, with a male-to-female ratio of 2.6:1.0. Non-keratinizing undifferentiated NPC (World Health Organization type III) accounted for the majority (97.5%) of all endemic cases. The proportion of patients with pre-treatment EBV DNA ≥2,000 copies/mL was 57.5%.

In the whole real-world dataset (N = 9,354), all survival curves were significantly disparate except for the comparison of stage II and the overall subgroups of T3N0, T3N1, and T4N0 NPC, which had equivalent OS, FFS, LRRFS, and DMFS (all $P \geq 0.063$; **Supplementary Figure 3**), indicating a good prognosis for T3N0, T3N1, and T4N0 NPC as a whole. As shown in **Table 2**, T3N1 had equivalent OS ($P = 0.116$) and LRRFS ($P = 0.097$) compared with T3N0, and equivalent DMFS ($P = 0.511$) compared with T4N0, suggesting homogeneity among patients with T3N0, T3N1, and T4N0 NPC.

RPA-Generated Risk Stratification

After adjustment in multivariate analysis, age ($P = 0.001$), gender ($P = 0.007$), histological type ($P \leq 0.001$), EBV DNA ($P \leq 0.001$), albumin ($P = 0.011$), LDH ($P = 0.001$), and T category ($P \leq 0.001$) were validated to have significant effects on OS (**Table 1** and **Supplementary Figure 4**). All validated predictors were included in RPA to generate risk stratification. After modification of branches based on automatic *rpart* algorithms, gender and EBV DNA were retained in the final model while inessential factors were discarded.

Figure 1A shows that 2,692 patients with T3N0, T3N1, and T4N0 NPC were categorized into two groups: low-risk group (n = 1,857; EBV DNA titer <2,000 copies/mL, female & EBV DNA titer ≥2,000 copies/mL) and high-risk group (n = 835; male & EBV DNA titer ≥2,000 copies/mL). The low-risk group had significantly higher OS compared with the high-risk group (HR = 2.45, 95% CI = 1.81–3.32; $P < 0.001$; **Figure 1B**). Patients with different EBV DNA status in the low-risk group had comparable OS ($P = 0.739$; **Supplementary Figure 5**).

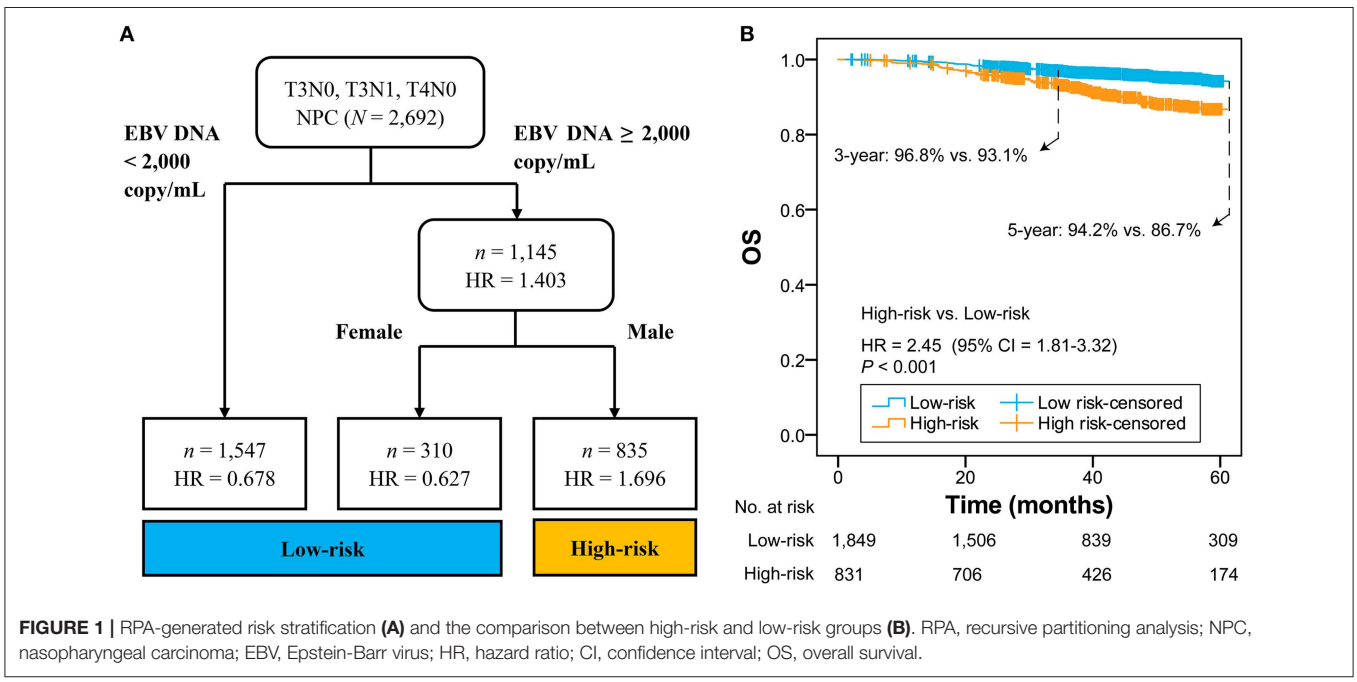

FIGURE 1 | RPA-generated risk stratification **(A)** and the comparison between high-risk and low-risk groups **(B)**. RPA, recursive partitioning analysis; NPC, nasopharyngeal carcinoma; EBV, Epstein-Barr virus; HR, hazard ratio; CI, confidence interval; OS, overall survival.

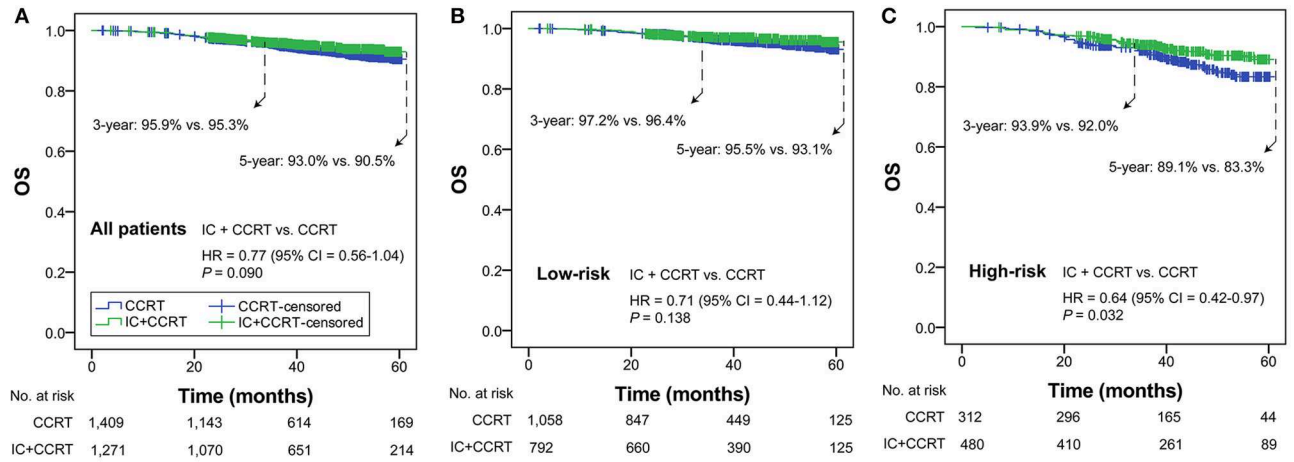

FIGURE 2 | Kaplan-Meier OS curves of IC+CCRT vs. CCRT in the overall T3N0, T3N1, and T4N0 NPC **(A)**, low- **(B)** and high-risk groups **(C)**. HR, hazard ratio; CI, confidence interval; OS, overall survival; IC, induction chemotherapy; CCRT, concurrent chemoradiotherapy.

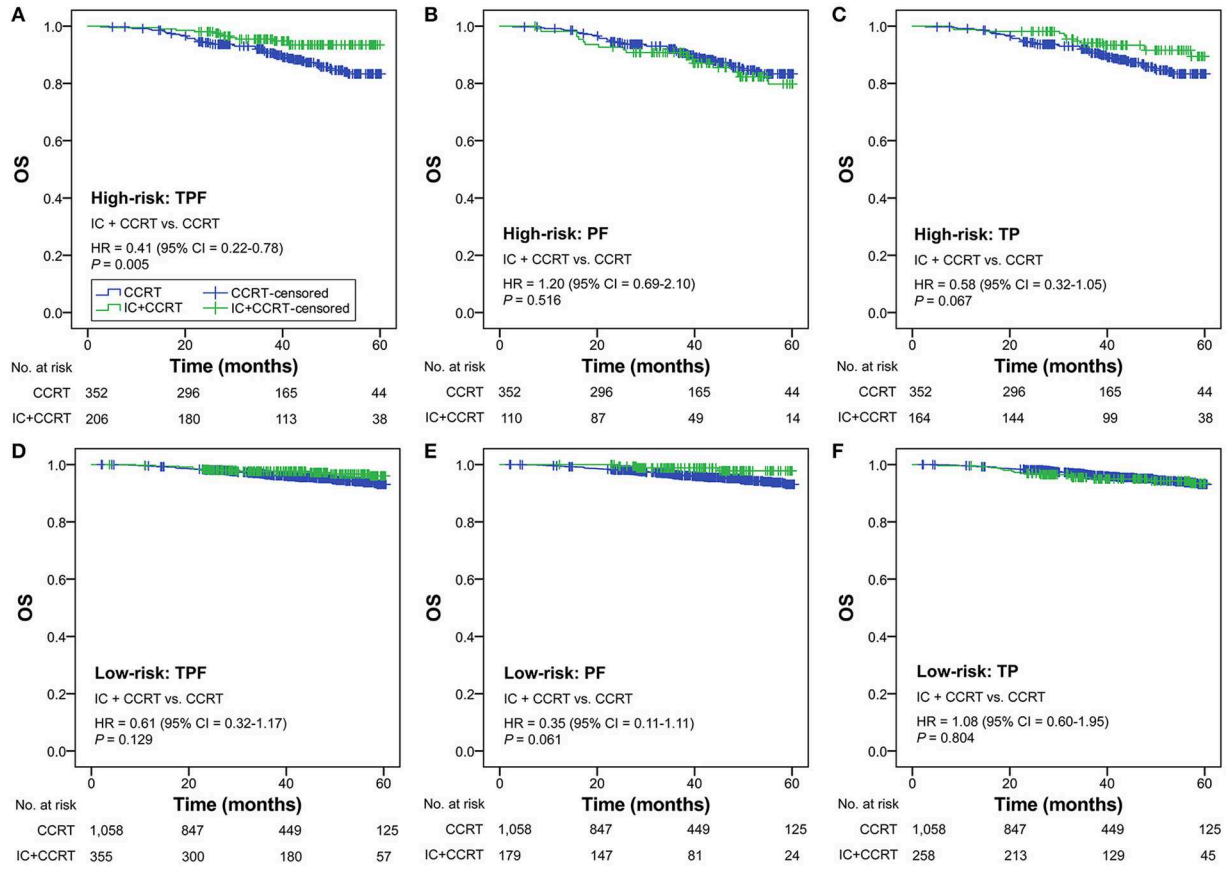

FIGURE 3 | IC+CCRT vs. CCRT in the subgroup analysis based on IC regimen [high-risk: TPF **(A)**, PF **(B)**, TP **(C)**; low-risk: TPF **(D)**, PF **(E)**, TP **(F)**] without adjustment. IC, induction chemotherapy; CCRT, concurrent chemoradiotherapy; TPF, docetaxel–cisplatin–5-fluorouracil; PF, cisplatin–5-fluorouracil; TP, cisplatin–5-fluorouracil.

Selection of IC Eneficiaries

In all patients with T3N0, T3N1, T4N0 NPC, OS was not significantly different in the comparison of IC+CCRT and CCRT (HR = 0.77, 95% CI = 0.56–1.04; $P = 0.090$). In the low-risk group, a non-significant difference in OS was observed between IC+CCRT and CCRT (HR = 0.71, 95% CI = 0.44–1.12; P

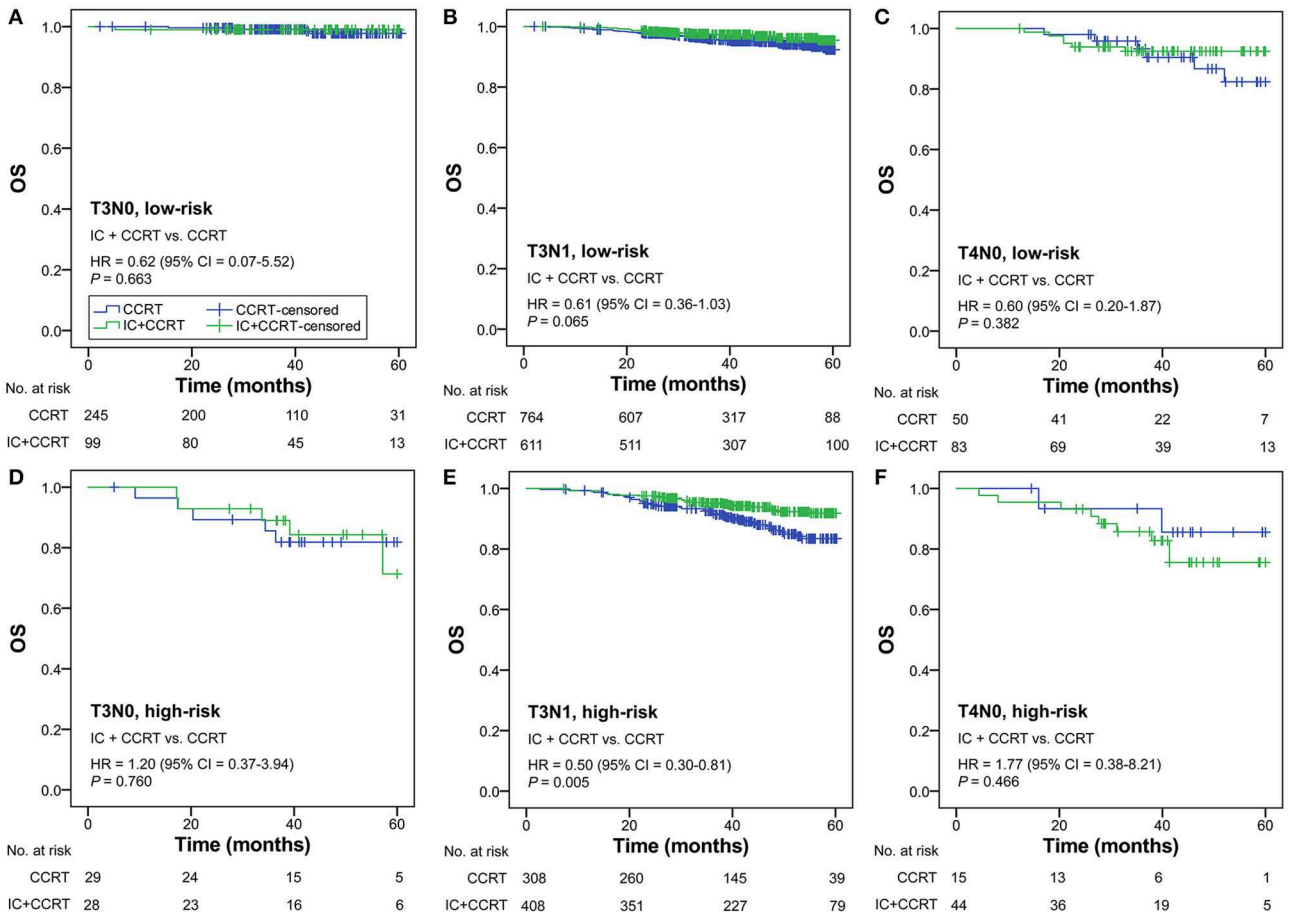

FIGURE 4 | IC+CCRT vs. CCRT in the subgroup analysis based on specific clinical stages [low-risk: T3N0 **(A)**, T3N1 **(B)**, T4N0 **(C)**; high-risk: T3N0 **(D)**, T3N1 **(E)**, T4N0 **(F)**]. IC, induction chemotherapy; CCRT, concurrent chemoradiotherapy.

= 0.138). In the high-risk group, patients receiving IC+CCRT had significantly improved OS compared with their counterparts receiving CCRT alone (HR = 0.64, 95% CI = 0.42–0.97; P = 0.032; **Figures 2A–C**).

Subgroup Analysis

Subgroup analysis was performed primarily based on IC regimens and specific LANPC subgroups. The improved, non-adjusted OS of IC+CCRT compared with CCRT was only observed in high-risk patients undergoing TPF (HR = 0.41, 95% CI = 0.22–0.78; P = 0.005) but not PF, TP, or any of the IC regimens in the low-risk group (all $P \geq 0.061$; **Figure 3**). Subgroup analysis was individually performed based on T3N0, T3N1, and T4N0 subgroups. Regardless of the specific clinical stages, low-risk patients treated by IC+CCRT generally had equivalent OS compared with those treated by CCRT alone (all $P \geq 0.065$). In high-risk patients, IC+CCRT was found to have significant survival benefit in OS compared with CCRT in the T3N1 subgroup (P = 0.005), but not in the T3N0 or T4N0 subgroups (**Figure 4**). The sample size of each treatment arm in T3N0 and T4N0 subgroups was very small, ranging from 15 to 44.

The RPA-generated risk stratification showed superb discriminatory ability in all subgroups, except for T4 category (P = 0.065; **Table 3**). After adjustment of covariates, the superiority of IC+CCRT over CCRT in OS was observed in the high-risk subgroup of age ≥53 years (P = 0.006), LDH ≤250 (P = 0.001), T3 category (P = 0.005), N1 category (P = 0.003), and TPF IC regimen (P = 0.003).

Validation of the Cohorts Based on Real-World and Clinical Trial Data

A total of 54 patients with T3–4N0 NPC was required to be incorporated into the TPF trial (n = 480) in accordance with the sample size ratio of 1 to 9. Eligible patients were individually selected from all of the T3–4N0 NPC group (n = 594) and high-risk T3–4N0 NPC group (n = 117) to match the trial baselines (e.g., TPF IC regimen, 3-weekly concurrent cisplatin, accumulated concurrent cisplatin ≥200 mg, age, and gender) and produce the validation cohort 1 and cohort 2, respectively. Both cohorts contained 534 patients comparing IC+CCRT with CCRT in LAPNC (267 vs. 267; **Figure 5A**).

As shown in **Figure 5B**, a significantly improved OS of IC+CCRT compared with CCRT was only observed in the

TABLE 3 | Subgroup analysis of RPA-generated risk stratification and IC+CCRT vs. CCRT with adjustment.

Variables	High risk vs. low risk		IC+CCRT vs. CCRT			
			High risk		Low risk	
	HR (90% CI)	*P*	aHR[a] (90% CI)	*P*	aHR[a] (90% CI)	*P*
Age, year						
18–37	3.30 (1.43–7.64)	0.005	0.94 (0.30–3.01)	0.922	0.81 (0.22–3.01)	0.749
38–44	2.81 (1.53–5.18)	0.001	0.47 (0.21–1.04)	0.061	0.83 (0.31–2.18)	0.700
45–52	3.29 (1.61–6.71)	0.001	0.89 (0.34–2.34)	0.810	1.11 (0.36–3.39)	0.862
≥53	1.71 (1.07–2.73)	0.024	0.34 (0.16–0.73)	0.006	0.50 (0.23–1.07)	0.076
Albumin, g/L						
<40.0	2.30 (1.02–5.18)	0.044	0.42 (0.14–1.25)	0.117	0.56 (0.13–2.39)	0.433
≥40.0	2.40 (1.73–3.33)	<0.001	0.67 (0.43–1.06)	0.085	0.78 (0.47–1.28)	0.320
LDH, U/L						
≤250	2.33 (1.68–3.25)	<0.001	0.44 (0.27–0.71)	0.001	0.79 (0.48–1.29)	0.343
>250	2.43 (1.09–5.46)	0.026	2.61 (0.75–9.08)	0.132	0.13 (0.02–1.02)	0.057
T category						
T3	2.51 (1.80–3.49)	<0.001	0.53 (0.34–0.83)	0.005	0.72 (0.43–1.21)	0.212
T4	2.16 (0.95–4.91)	0.065	1.80 (0.38–8.46)	0.456	0.60 (0.18–2.07)	0.422
N category						
N0	5.37 (2.85–10.11)	<0.001	1.42 (0.58–3.48)	0.444	0.74 (0.27–2.06)	0.567
N1	2.02 (1.43–2.85)	<0.001	0.48 (0.30–0.79)	0.003	0.65 (0.38–1.12)	0.119
IC regimen						
TPF	2.34 (1.63–3.35)	<0.001	0.38 (0.20–0.72)	0.003	0.62 (0.32–1.21)	0.159
PF	3.15 (2.19–4.54)	<0.001	1.16 (0.66–2.02)	0.613	0.37 (0.11–1.18)	0.092
TP	2.28 (1.60–3.24)	<0.001	0.58 (0.32–1.06)	0.078	1.10 (0.60–2.02)	0.757

RPA, recursive partitioning analysis; CCRT, concurrent radiochemotherapy; IC, induction chemotherapy; HR, hazard ratio; aHR, adjusted hazard ratio; LDH, lactate dehydrogenase; TPF, docetaxel–cisplatin−5-fluorouracil; PF, cisplatin−5-fluorouracil; TP, docetaxel–cisplatin.

[a]*aHR was adjusted for age, albumin, LDH, T category, N category, and IC regimen, except for the variable that is being analyzed.*

validation cohort 2 (HR = 0.62, 95% CI = 0.42–0.94; $P = 0.023$) but not cohort 1(HR = 0.66, 95% CI = 0.43–1.01; $P = 0.056$). Cohort 2 showed more obvious superiority of IC+CCRT over CCRT (HR: 0.62 vs. 0.65) and better discrimination performance (c-index: 0.560 vs. 0.557) than the long-term results of the TPF trial (**Figure 5C**).

DISCUSSION

With an increasing emphasis on IC in the NCCN guidelines, more robust studies are required to consider evidence on the comparison of IC+CCRT and CCRT in T3N0, T3N1, and T4N0 NPC, given that these patients had been excluded from a majority of IC-related trials and the evidence regarding optimal treatment strategy is limited. In December 2016, the U.S. Congress enacted $$*The 21st Century Cures Act*, which modified the Food and Drug Administration policies and inspired investigators to provide real-world evidence as supplements to clinical trials, in order to expedite the approval process for innovative research (22). This retrospective, joint analysis based on real-world and clinical trial data is the first attempt to identify IC beneficiaries among patients with T3N0, T3N1, and T4N0 NPC based on EBV DNA status (**Supplementary Figure 6**). We provide robust real-world evidence that can further complement the contemporary trial results.

The 8th edition AJCC/UICC staging system has successfully incorporated human papillomavirus infection status into the TNM classification of oropharyngeal carcinoma (23), which highlights the possibility of including non-anatomic factors to better differentiate the prognosis of EBV-related NPC. EBV is exclusively detected in tumor cells but not in normal nasopharyngeal epithelium; its cell-free DNA has the same polymorphism as the primary lesion tumor and is considered to be released into the peripheral circulation along with the tumor cells death of Lin et al. (24). Previous studies reported that circulating EBV DNA correlate with the tumor burden, stage classification, and survival of patients with NPC (25–27). The practical application of EBV DNA has expanded from initial diagnosis, detection of metastasis, to population screening and pre-treatment risk stratification (28–30). Only two recent studies have included incorporation of pre-treatment plasma EBV DNA into the 8th edition of TNM staging system (16, 31). These studies indicated that the risk of T3N0, T3N1, and T4N0 NPC could be refined by EBV DNA, since both plans covered the three subgroups. A previous retrospective study reported that patients with T3–4N0–1 NPC receiving CCRT could not benefit from additional IC, which may be influenced by the fact that EBV DNA was not used for the screening of IC beneficiaries (32). Similarly, in this study, we reported a non-significant difference in OS between IC+CCRT and CCRT in the whole patients with

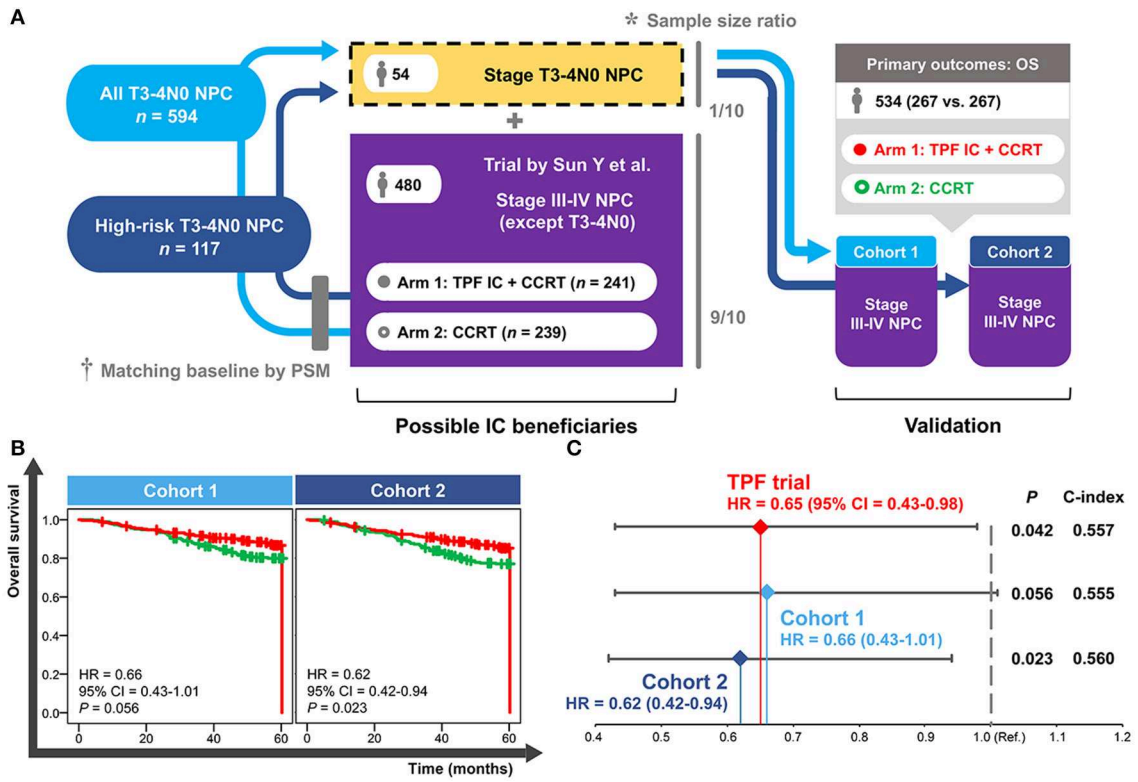

FIGURE 5 | Establishment **(A)** and validation **(B,C)** of the cohorts based on real-world and clinical trial data. *Sample size ratio was calculated based on the NPC-specific real-world dataset including 10,126 patients. †Baseline of the selected T3–4N0 NPC patients was matched with the trial data using the PSM method. NPC, nasopharyngeal carcinoma; PSM, propensity score matching; TPF, docetaxel–cisplatin–5-fluorouracil; IC, induction chemotherapy; CCRT, concurrent chemoradiotherapy; OS, overall survival; HR, hazard ratio; CI, confidence interval; Ref., reference.

T3N0, T3N1, and T4N0 NPC when they had not been stratified (**Figure 2A**). Therefore, high level EBV DNA may be an indicator for physicians to employ IC in LANPC.

Another validated predictor used for risk stratification in this study is gender. Although both genders had the same improved level of plasma EBV DNA, female patients obtained better OS benefits than males (**Supplementary Figure 5**). This result was in line with a previous finding, which reported that female is associated with better prognosis in NPC compared with male gender (33). One proposed hypothesis is that female hormones can promote immunological responses and confer higher resistance to oxidative damage (34).

This study demonstrated that the OS benefit for high-risk patients was mainly associated with the TPF regimen but not PF or TP IC regimens. The potent triple agent-based TPF regimen has been shown to be a promising prospect in LANPC, allowing patients to receive stronger intensity treatment, longer hospitalization, improved nursing care, and more supportive therapy than the PF regimen, while intensive management itself can lead to better prognosis (8, 13). In addition, the subgroup analysis based on specific clinical stages only supported the high-risk T3N1 subgroup, but not the T3N0 or T4N0 subgroups, as an IC beneficiary. This result should be regarded with caution, since statistical non-significance may be related to the insufficient sample size of two treatment arms in the high-risk T3N0 (28 vs. 29) and T4N0 (44 vs. 15) subgroups. The PF trial that included all LANPC subgroups except T3N0–1 NPC has recently been updated. It revealed a significant 5-year OS benefit of IC+CCRT compared with CCRT (80.8 vs. 76.8%; $P = 0.04$) (35), indicating that the T4N0 subgroup should receive IC+CCRT in clinical practice. Hence, the T3N1 subgroup may not be the only IC beneficiary, and all the three subgroups (T3N0, T3N1, T4N0) should be fully investigated. Since individual patient data of the PF trial is not accessible, we only performed the validation analysis using the 5-year data of the TPF trial (20), which successfully verified the effectiveness of RPA-generated risk stratification.

Several limitations to this study should be stated. First, it is important to recognize that different centers adopt different EBV DNA cut-off values, such as 4,000 copies/mL (36), 500 copies/mL (31), and 1,500 copies/mL (24). Moreover, the heterogeneity in PCR-based EBV DNA testing itself is an important problem, with sensitivity ranging from 53 to 96% (37). Assay harmonization of EBV DNA detection is a major hurdle that has to be overcome prior to incorporation of plasma EBV DNA as a clinical decision-making tool. In 2015, a workshop on harmonization of EBV testing for NPC was hosted by the National Cancer Institute. It offered valuable strategies for establishment of harmonized EBV DNA assays and key recommendations guiding future clinical use (37). Second, in this study, results were driven by the T3N1

subgroup (78%), and the OS superiority of IC+CCRT over CCRT in high-risk patients was only observed in the subgroup of T3 and N1 category. Although validation analysis confirmed that patients with high-risk T3–4N0 NPC could effectively benefit from IC, the sample size of T3N0 and T4N0 subgroups was too small to generate a reliable conclusion. Two robust phase 3 RCTs including all LANPC subgroups except T3–4N0 NPC had reported significant OS improvement of 6.0 and 4.3% from the additional TPF (8) and GP (12) IC regimens, respectively. Therefore, the status of the T3N1 subgroup as an IC beneficiary is more explicit than the T3N0 and T4N0 subgroups, while the latter two require more supporting evidences beyond this study. Third, the retrospective nature limits this study to some extent. This study was performed based on the 8th edition of the AJCC/UICC staging system for a better generalizability in real-world clinical practice. Although the clinical trial in validation analysis used the 7th edition of the AJCC/UICC staging system, the difference in staging systems was too subtle to exert obvious influence on results. Re-staging was not performed in this study because the transform of the staging system from the 7th edition into the 8th edition would compromise data integrity. Nonetheless, this real-world study offers essential information to clinical physicians and trialists, helping them make precise clinical decisions and refine future trial design.

CONCLUSION

RPA-generated risk stratification based on pre-treatment plasma EBV DNA provides good and robust efficacy of OS prediction in T3N0, T3N1, and T4N0 NPC. In comparison with CCRT, IC+CCRT leads to significantly improved OS for patients with high-risk T3N1 NPC, which is mainly due to the TPF IC regimen. Patients with high-risk T3N1 NPC is the definite target population for receiving IC+CCRT in real-world practice. T3N0 and T4N0 subgroups need further investigations in future IC-related studies.

DATA AVAILABILITY STATEMENT

The datasets for this study can be found in the public platform named Research Data Deposit (http://www.researchdata.org.cn) with the identifier RDDA2018000782.

ETHICS STATEMENT

The studies involving human participants were reviewed and approved by Institutional Review Board and the Ethics Committee of Sun Yat-sen University Cancer Center. Written informed consent for participation was not required for this study in accordance with the national legislation and the institutional requirements.

AUTHOR CONTRIBUTIONS

L-LT and CX: conceptualization. CX, QL, and YG: methodology. CX, LC, and Y-PM: software. CX and W-FL: validation. CX, SZ, and LC: formal analysis. SZ, YG, and Y-PM: investigation. W-FL and JM: resources. SZ and W-FL: data curation. CX and SZ: writing—original draft preparation. W-FL, JM, and L-LT: writing—review and editing. CX: visualization. L-LT: supervision, project administration, and funding acquisition.

FUNDING

This study was supported by grants from the National Natural Science Foundation of China (81930072), Key-Area Research and Development Program of Guangdong Province (2019B020230002), Natural Science Foundation of Guangdong Province (2017A030312003), Health & Medical Collaborative Innovation Project of Guangzhou City, China (201803040003), Innovation Team Development Plan of the Ministry of Education (No. IRT_17R110), Overseas Expertise Introduction Project for Discipline Innovation (111 Project, B14035).

ACKNOWLEDGMENTS

We thank YiduCloud (Beijing, China) Technology Ltd. for supporting the data extraction and processing.

SUPPLEMENTARY MATERIAL

The Supplementary Material for this article can be found online at: https://www.frontiersin.org/articles/10.3389/fonc.2019.01343/full#supplementary-material

REFERENCES

1. Siegel RL, Miller KD, Jemal A. Cancer statistics, 2018. *CA Cancer J Clin.* (2018) 68:7–30. doi: 10.3322/caac.21442
2. Wei KR, Zheng RS, Zhang SW, Liang ZH, Li ZM, Chen WQ. Nasopharyngeal carcinoma incidence and mortality in China, 2013. *Chin J Cancer.* (2017) 36:90. doi: 10.1186/s40880-017-0257-9
3. Mao YP, Xie FY, Liu LZ, Sun Y, Li L, Tang LL, et al. Re-evaluation of 6th edition of AJCC staging system for nasopharyngeal carcinoma and proposed improvement based on magnetic resonance imaging. *Int J Radiat Oncol Biol Phys.* (2009) 73:1326–34. doi: 10.1016/j.ijrobp.2008.07.062
4. Al-Sarraf M, LeBlanc M, Giri PG, Fu KK, Cooper J, Vuong T, et al. Chemoradiotherapy versus radiotherapy in patients with advanced nasopharyngeal cancer: phase III randomized Intergroup study 0099. *J Clin Oncol.* (1998) 16:1310–7. doi: 10.1200/JCO.1998.16.4.1310
5. Chen L, Hu CS, Chen XZ, Hu GQ, Cheng ZB, Sun Y, et al. Concurrent chemoradiotherapy plus adjuvant chemotherapy versus concurrent chemoradiotherapy alone in patients with locoregionally advanced nasopharyngeal carcinoma: a phase 3 multicentre randomised controlled trial. *Lancet Oncol.* (2012) 13:163–71. doi: 10.1016/S1470-2045(11)70320-5
6. Lee AW, Tung SY, Chua DT, Ngan RK, Chappell R, Tung R, et al. Randomized trial of radiotherapy plus concurrent-adjuvant chemotherapy vs radiotherapy alone for regionally advanced nasopharyngeal carcinoma. *J Natl Cancer Inst.* (2010) 102:1188–98. doi: 10.1093/jnci/djq258
7. Cao SM, Yang Q, Guo L, Mai HQ, Mo HY, Cao KJ, et al. Neoadjuvant chemotherapy followed by concurrent chemoradiotherapy versus concurrent chemoradiotherapy alone in locoregionally advanced nasopharyngeal

carcinoma: A phase III multicentre randomised controlled trial. *Eur J Cancer.* (2017) 75:14–23. doi: 10.1016/j.ejca.2016.12.039
8. Sun Y, Li WF, Chen NY, Zhang N, Hu GQ, Xie FY, et al. Induction chemotherapy plus concurrent chemoradiotherapy versus concurrent chemoradiotherapy alone in locoregionally advanced nasopharyngeal carcinoma: a phase 3, multicentre, randomised controlled trial. *Lancet Oncol.* (2016) 17:1509–20. doi: 10.1016/S1470-2045(16)30410-7
9. Pfister DG, Spencer S, Brizel DM, Burtness B, Busse PM, Caudell JJ, et al. Head and neck cancers, Version 2.2014. Clinical practice guidelines in oncology. *J Natl Compr Canc Netw.* (2014) 12:1454–87. doi: 10.6004/jnccn.2014.0142
10. Chua DT, Ma J, Sham JS, Mai HQ, Choy DT, Hong MH, et al. Long-term survival after cisplatin-based induction chemotherapy and radiotherapy for nasopharyngeal carcinoma: a pooled data analysis of two phase III trials. *J Clin Oncol.* (2005) 23:1118–24. doi: 10.1200/JCO.2005.12.081.
11. Pfister DG, Spencer S, Adelstein D, Adkins D, Brizel DM, Burtness B, et al. *National Comprehensive Cancer Network Clinical Practice Guidelines in Oncology (NCCN Guidelines®): Head and Neck Cancers. Version 1.2018.* Available online at: https://www.nccn.org/professionals/physician_gls/pdf/head-and-neck.pdf (accessed September 4, 2019).
12. Zhang Y, Chen L, Hu GQ, Zhang N, Zhu XD, Yang KY, et al. Gemcitabine and cisplatin induction chemotherapy in nasopharyngeal carcinoma. *New Engl J Med.* (2019) 381:1124–35. doi: 10.1056/NEJMoa1905287
13. Frikha M, Auperin A, Tao Y, Elloumi F, Toumi N, Blanchard P, et al. A randomized trial of induction docetaxel-cisplatin-5FU followed by concomitant cisplatin-RT versus concomitant cisplatin-RT in nasopharyngeal carcinoma (GORTEC 2006-02). *Ann Oncol.* (2018) 29:731–6. doi: 10.1093/annonc/mdx770
14. Xu C, Chen YP, Liu X, Li WF, Chen L, Mao YP, et al. Establishing and applying nomograms based on the 8th edition of the UICC/AJCC staging system to select patients with nasopharyngeal carcinoma who benefit from induction chemotherapy plus concurrent chemoradiotherapy. *Oral Oncol.* (2017) 69:99–107. doi: 10.1016/j.oraloncology.2017.04.015
15. Lv JW, Chen YP, Huang XD, Zhou GQ, Chen L, Li WF, et al. Hepatitis B virus screening and reactivation and management of patients with nasopharyngeal carcinoma: A large-scale, big-data intelligence platform-based analysis from an endemic area. *Cancer.* (2017) 123:3540–9. doi: 10.1002/cncr.30775
16. Guo R, Tang LL, Mao YP, Du XJ, Chen L, Zhang ZC, et al. Proposed modifications and incorporation of plasma Epstein-Barr virus DNA improve the TNM staging system for Epstein-Barr virus related nasopharyngeal carcinoma. *Cancer.* (2019) 125:79–89. doi: 10.1002/cncr.31741
17. Kaplan EL, Meier P. Nonparametric estimation from incomplete observations. *J Am Stat Assoc.* (1958) 53:457–81. doi: 10.1080/01621459.1958.10501452
18. Cox DR. Regression models and life-tables. *J R Stat Soc Series B Stat Methodol.* (1972) 34:187–220. doi: 10.1007/978-1-4612-4380-9_37
19. Atkinson EJ, Therneau TM. *An Introduction to Recursive Partitioning Using the RPART Routines*. Rochester, NY: Rochester Mayo Foundation (2000).
20. Li WF, Chen NY, Zhang N, Hu GQ, Xie FY, Sun Y, et al. Concurrent chemoradiotherapy with/without induction chemotherapy in locoregionally advanced nasopharyngeal carcinoma: Long-term results of phase 3 randomized controlled trial. *Int J Cancer.* (2019) 145:295–305. doi: 10.1002/ijc.32099
21. Stürmer T, Joshi M, Glynn RJ, Avorn J, Rothman KJ, Schneeweiss S. A review of the application of propensity score methods yielded increasing use, advantages in specific settings, but not substantially different estimates compared with conventional multivariable methods. *J Clin Epidemiol.* (2006) 59:437–47. doi: 10.1016/j.jclinepi.2005.07.004
22. Sherman RE, Anderson SA, Dal Pan GJ, Gray GW, Gross T, Hunter NL, et al. Real-world evidence - what is it and what can it tell us? *N Engl J Med.* (2016) 375:2293–7. doi: 10.1056/NEJMsb1609216
23. Amin MB, Edge SB, Greene FL, Schilsky RL, Gaspar LE, Washington MK, et al. *American Joint Committee on Cancer. AJCC Cancer Staging Manual*. 8th ed. New York, NY: Springer (2018).
24. Lin JC, Wang WY, Chen KY, Wei YH, Liang WM, Jan JS, et al. Quantification of plasma Epstein-Barr virus DNA in patients with advanced nasopharyngeal carcinoma. *N Engl J Med.* (2004) 350:2461–70. doi: 10.1056/NEJMoa032260
25. Leung SF, Zee B, Ma BB, Hui EP, Mo F, Lai M, et al. Plasma Epstein-Barr viral deoxyribonucleic acid quantitation complements tumor-node-metastasis staging prognostication in nasopharyngeal carcinoma. *J Clin Oncol.* (2006) 24: 5414–8. doi: 10.1200/JCO.2006.07.7982
26. Lo YM, Chan LY, Chan AT, Leung SF, Lo KW, Zhang J, et al. Quantitative and temporal correlation between circulating cell-free Epstein-Barr virus DNA and tumor recurrence in nasopharyngeal carcinoma. *Cancer Res.* (1999) 59:5452–5.
27. Ma BB, King A, Lo YM, Yau YY, Zee B, Hui EP, et al. Relationship between pretreatment level of plasma Epstein-Barr virus DNA, tumor burden, and metabolic activity in advanced nasopharyngeal carcinoma. *Int J Radiat Oncol Biol Phys.* (2006) 66:714–20. doi: 10.1016/j.ijrobp.2006.05.064
28. Chan KCA, Woo JKS, King A, Zee BCY, Lam WKJ, Chan SL, et al. Analysis of Plasma Epstein-Barr Virus DNA to Screen for Nasopharyngeal Cancer. *N Engl J Med.* (2017) 377:513–22. doi: 10.1056/NEJMoa1701717
29. Takes RP, Rinaldo A, Silver CE, Piccirillo JF, Haigentz M Jr, Suarez C, et al. Future of the TNM classification and staging system in head and neck cancer. *Head Neck.* (2010) 32:1693–711. doi: 10.1002/hed.21361
30. Wang WY, Twu CW, Chen HH, Jan JS, Jiang RS, Chao JY, et al. Plasma EBV DNA clearance rate as a novel prognostic marker for metastatic/recurrent nasopharyngeal carcinoma. *Clin Cancer Res.* (2010) 16:1016–24. doi: 10.1158/1078-0432.CCR-09-2796
31. Lee VH, Kwong DL, Leung TW, Choi CW, O'Sullivan B, Lam KO, et al. The addition of pretreatment plasma Epstein-Barr virus DNA into the eighth edition of nasopharyngeal cancer TNM stage classification. *Int J Cancer.* (2019) 144:1713–22. doi: 10.1002/ijc.31856
32. Wu LR, Yu HL, Jiang N, Jiang XS, Zong D, Wen J, et al. Prognostic value of chemotherapy in addition to concurrent chemoradiotherapy in T3-4N0-1 nasopharyngeal carcinoma: a propensity score matching study. *Oncotarget.* (2017) 8:76807–15. doi: 10.18632/oncotarget.20014
33. Xu C, Liu X, Chen YP, Mao YP, Guo R, Zhou GQ, et al. Impact of marital status at diagnosis on survival and its change over time between 1973 and 2012 in patients with nasopharyngeal carcinoma: a propensity score-matched analysis. *Cancer Med.* (2017) 6:3040–51. doi: 10.1002/cam4.1232
34. Yang Q, Cao SM, Guo L, Hua YJ, Huang PY, Zhang XL, et al. Induction chemotherapy followed by concurrent chemoradiotherapy versus concurrent chemoradiotherapy alone in locoregionally advanced nasopharyngeal carcinoma: long-term results of a phase III multicentre randomised controlled trial. *Eur J Cancer.* (2019) 119:87–96. doi: 10.1016/j.ejca.2019.07.007.
35. Austad SN, Fischer KE. Sex Differences in Lifespan. *Cell Metab.* (2016) 23:1022–33. doi: 10.1016/j.cmet.2016.05.019
36. Chan AT, Lo YM, Zee B, Chan LY, Ma BB, Leung SF, et al. Plasma Epstein-Barr virus DNA and residual disease after radiotherapy for undifferentiated nasopharyngeal carcinoma. *J Natl Cancer Inst.* (2002) 94:1614–9. doi: 10.1093/jnci/94.21.1614
37. Kim KY, Le QT, Yom SS, Pinsky BA, Bratman SV, Ng RH, et al. Current state of PCR-based Epstein-Barr virus DNA testing for nasopharyngeal cancer. *J Natl Cancer Inst.* (2017) 109:djx007. doi: 10.1093/jnci/djx007

Conflict of Interest: The authors declare that the research was conducted in the absence of any commercial or financial relationships that could be construed as a potential conflict of interest.

frontiers in Oncology

ORIGINAL RESEARCH
published: 06 December 2019
doi: 10.3389/fonc.2019.01346

Intestinal Flora Disruption and Novel Biomarkers Associated With Nasopharyngeal Carcinoma

*Haiye Jiang[1], Jian Li[2], Bin Zhang[3], Rong Huang[2], Junhua Zhang[2], Ziwei Chen[1], Xueling Shang[1], Xisheng Li[1] and Xinmin Nie[1]**

[1] Clinical Laboratory, Third Xiangya Hospital, Central South University, Changsha, China, [2] Department of Blood Transfusion, Third Xiangya Hospital, Central South University, Changsha, China, [3] Department of Anatomy and Neurobiology, Biology Postdoctoral Workstation, School of Basic Medical Sciences, Central South University, Changsha, China

Background: Nasopharyngeal carcinoma (NPC) is a malignant nasopharyngeal disease with a complicated etiology that occurs mostly in southern China. Intestinal flora imbalance is believed to be associated with a variety of organ malignancies. Current studies revealed that the destruction of intestinal flora is associated with NPC, and many studies have shown that intestinal flora can be used as a biomarker for many cancers and to predict cancer.

Methods: To compare the differences in intestinal flora compositions and biological functions among 8 patients with familial NPC (NPC_F), 24 patients with sporadic NPC (NPC_S), and 27 healthy controls (NOR), we compared the intestinal flora DNA sequencing and hematological testing results between every two groups using bioinformatic methods.

Results: Compared to the NOR group, the intestinal flora structures of the patients in the NPC_F and NPC_S groups showed significant changes. In NPC_F, *Clostridium ramosum*, *Citrobacter* spp., *Veillonella* spp., and *Prevotella* spp. were significantly increased, and *Akkermansia muciniphila* and *Roseburia* spp. were significantly reduced. In NPC_S, *C. ramosum*, *Veillonella parvula*, *Veillonella dispar,* and *Klebsiella* spp. were significantly increased, and *Bifidobacterium adolescentis* was significantly reduced. A beta diversity analysis showed significant difference compared NPC_F with NOR based on Bray Curtis ($P = 0.012$) and Unweighted UniFrac ($P = 0.0045$) index, respectively. The areas under the ROC curves plotted were all 1. Additionally, the concentrations of 5-hydroxytryptamine (5-HT) in NPC_F and NPC_S were significantly higher than those of NOR. *C. ramosum* was positively correlated with 5-HT (rcm: 0.85, $P < 0.001$). A functional analysis of the intestinal flora showed that NPC_F was associated with Neurodegenerative Diseases ($P = 0.023$) and that NPC_S was associated with Neurodegenerative Diseases ($P = 0.045$) as well.

Conclusion: We found that NPC was associated with structural imbalances in the intestinal flora, with *C. ramosum* that promoted the elevation of 5-HT and opportunistic pathogens being significantly increased, while probiotics significantly decreased.

OPEN ACCESS

Edited by:
Jun Ma,
Sun Yat-sen University Cancer Center (SYSUCC), China

Reviewed by:
Hai Hu,
Sun Yat-sen University, China
Qin Lin,
First Affiliated Hospital of Xiamen University, China
Lei Zhang,
Beihang University, China

****Correspondence:***
Xinmin Nie
niexinmin7440@sina.com

Specialty section:
This article was submitted to Head and Neck Cancer, a section of the journal Frontiers in Oncology

Received: *09 September 2019*
Accepted: *15 November 2019*
Published: *06 December 2019*

Citation:
Jiang H, Li J, Zhang B, Huang R, Zhang J, Chen Z, Shang X, Li X and Nie X (2019) Intestinal Flora Disruption and Novel Biomarkers Associated With Nasopharyngeal Carcinoma. Front. Oncol. 9:1346. doi: 10.3389/fonc.2019.01346

C. ramosum can be used as a novel biomarker and disease prediction models should be established for NPC. The new biomarkers and disease prediction models may be used for disease risk prediction and the screening of high-risk populations, as well as for the early noninvasive diagnosis of NPC.

Keywords: biomarker, nasopharyngeal carcinoma, familial, sporadic, intestinal flora, 5-HT

INTRODUCTION

Nasopharyngeal carcinoma (NPC) is a head and neck cancer (HNCC) caused by a malignant transformation of the nasopharyngeal epithelium. Based on the International Agency for Research on Cancer, nearly 129,000 new patients of NPC were diagnosed in 2018, and more than 70% of the new patients are from East and Southeast Asia. The NPC incidence rate in China has reached 3/100,000 (1, 2). The early symptoms of NPC are rare and not prominent, so NPC is not easily identified in the early stage; in addition, 70% of patients are at a locally advanced stage at the time of diagnosis (3), one of the major clinical symptoms is cervical lymph node enlargement. Early diagnosis, intervention and treatment are important prognostic factors for NPC patients and can significantly reduce their mortality. The causes of NPC are complicated and diverse and the currently recognized causes include genetic susceptibility, eating habits and Epstein-Barr virus (EBV) infection (4, 5). Multiple studies have reported that NPC shows a characteristic of family aggregation in low-risk populations and southern China (6–8). Epidemiological studies have also shown that people with a first-grade NPC family history are 4–20 times more likely to develop NPC than those who do not have a family history (9–11). The intestinal flora is a symbiotic microflora that inhabits the human intestinal mucosa (12), and its structural balance plays indispensable roles in various aspects including the immune response, metabolism of carcinogens and nutrient digestion (13, 14). Although there are many possible explanations for the formation of the intestinal flora, it is agreed that the intestinal flora is familial (15, 16), and this feature is probably related to the occurrence of familial tumors. It is worth noting that patients with familial colorectal cancer have similar imbalanced intestinal flora structures (17), which may cause a metabolic disruption of the intestinal metabolites and the disorders of the immune system, leading to cancer. Numerous studies have shown that changes in the intestinal microbiota are significantly associated with colorectal cancer (CRC) (18) and many extraintestinal malignancies (19), such as liver cancer (20), pancreatic cancer (21), melanoma (22), and breast cancer (23), there is a consensus that the dysbiosis of intestinal flora can promote cancer through provoking the magnification of immune response (19); meanwhile, it is found that intestinal microbiota can drive immune T cells proliferation and activation, which leads to the enlargement of cervical lymph nodes (24). Nevertheless, the hidden mechanisms of the interaction among intestinal flora, cancer and immune system remain exploiting completely (19, 25, 26). It is discovered that the dysbiosis of oral microbial structure is associated with HNCC (27), there are many similarities and connections between intestinal flora and oral microbiota (28), thus these discoveries above hinted us that the intestinal microbiota may modulate the development NPC by regulating the immune system. Moreover, a previous study found that radiochemotherapy significantly destroyed the balance of intestinal flora in NPC patients and that probiotic combination could significantly alleviate oral mucositis in NPC patients by improving the intestinal flora (29), which also prompted us that the intestinal flora may play an important role in the progression of NPC. In the meantime, one study reported that native spore-forming bacterium from the human intestinal flora played a major role in elevating the level of 5-HT in plasma from modulating enterochromaffin cells (ECs) (30).

5-HT is an important neurotransmitter and vasoactivator that is mainly synthesized and secreted by the central nervous system (CNS) and ECs, which has functions to regulate neurotransmitters and neuroendocrine (31). A variety of researches have found that 5-HT can stimulate the development and progression of multifarious cancers, such as prostate carcinoma (PC) (32), hepatocellular carcinoma (HCC) (33–35), CRC (36), small-cell lung cancer (SCLC) (37), pancreatic ductal adenocarcinoma (PDAC) (38, 39), cholanfiocarcinoma (40), breast cancer (41), ovary carcinoma (42), and glioma (43) and carcinoids (31) through the 5-HT receptor (5-HTR) subtypes like 5-HT1A, 5-HT1B, 5-HT2A, 5-HT2B etc. What interested us most is that a study has found that 5-HT1B was overexpressed in human NPC samples (44), which reminds us that 5-HT may play a crucial role in NPC development. This has aroused our great interest in research. *C. ramosum* is an anaerobic, Gram-positive spore-forming bacteria that produces immunoglobulin (Ig) A protease, which can be mainly found in intestinal tract (45). A previous study has shown that the metabolites of *C. ramosum* could stimulate the secretion of 5-HT from ECs, which can promote the level of 5-HT in plasma (46). These series of discoveries mentioned above have induced us to get a scenario that intestinal microbiota can promote the secretion of 5-HT to facilitate the progression of NPC.

Current screening methods for NPC include gene sequencing, EBV immunology and EBV DNA (47). However, these invasive methods are costly and time-consuming, so there is an urgent need to develop a new economical and non-invasive detection method for early NPC screening. This objective may be accomplished by using the specificity of the composition of the intestinal flora. Studies have shown that the intestinal flora can be used as a special biomarker for the screening of CRC with a sensitivity of 77.7% and a specificity of 79.5% (48, 49). The family-specific intestinal flora is also expected to be used for NPC screening.

In this study, we recruited familial NPC patients (NPC_F), sporadic NPC patients (NPC_S), and healthy controls (NOR) and performed the 16S rRNA sequencing of their intestinal floras and examined multiple clinical indicators of their blood. We compared the composition and biological functions of the intestinal floras among NPC_F, NPC_S, and NOR through bioinformatic methods, and explored the association between changes in the intestinal flora and NPC_F and NPC_S, elaborated the association that the intestinal flora had an impact on NPC by modulating the secreting of 5-HT, contemporary. We predicted the functions of each flora of NPC patients, aiming to establish the connection between every two groups through analyzing the intestinal flora of NPC patients. This study will lay a foundation for the application of the intestinal flora to the early diagnosis of NPC.

MATERIALS AND METHODS

Recruitment of Volunteers

We recruited 481 NPC patients and staged their tumor status with the American Joint Committee on Cancer (AJCC) 7th edition staging criteria (50). Excluded 243 patients with other diseases, excluded 50 patients who had received anti-tumor treatments, excluded 60 patients who had any drug treatments within 1 month, and excluded 44 patients with family history of any other tumors. Finally, 84 patients who met our requirements remained. And then, eight NPC patients [(46.4 ± 5) years old] with a NPC family history were selected, because the factors such as age, gender and BMI have influence on intestinal microbial structure, 24 sporadic NPC patients [(47.3 ± 3.3) years old] matched with familial NPC patients in age, gender and BMI were selected. At the same time, 87 healthy volunteers were recruited, and 27 healthy volunteers [(47.2 ± 3.4) years old] whose age, gender and BMI were matched with NPC patients were selected as controls.

We randomly recruited the NPC patients and healthy volunteers in the same area in China, who had a parallel dietary background. The recruited NPC group and healthy group were in line with the principle of randomized control, which could avoid various biases and balance the confounding factors including the nutrition and dietary intake (51, 52). The healthy volunteers were defined as those between 18 and 70 years old, with no history of NPC, no family history of NPC, no history of rhinitis, no history of any other diseases (such as hypertension, diabetes, gastrointestinal diseases, and immune diseases), and no smoking or drinking history, who did not receive any antibiotics or treatment 3 months prior to sample collection. None of the NPC patients had rhinitis or had used any antibiotics during the 3 months prior to sample collection, none of the patients had received any kind of treatment since being diagnosed NPC, including radiotherapy and chemotherapy. The study was reviewed by the Ethics Committee of the Third Xiangya Hospital of Central South University. Informed consent was signed by all subjects prior to participation.

Sample Collection

Fecal samples and blood samples were collected separately from each subject; venous blood collection was performed by professional nurses strictly in accordance with sterile and standardized procedures. Fecal samples were collected by the subjects themselves, before collecting the feces, we would teach the volunteers how to collect the feces, the procedures were as follows: Feces will be excreted on a piece of dry and clean paper, and the middle part of feces will be picked up with the pick stick of sterile feces collector and then placed it into the dry sterile feces collector immediately. After collection, the sterile feces collectors with feces were immediately placed on ice, to ensure the temperature was below 4°C and transported them to the biobank within 1 h, where they were stored at −80°C until DNA extraction (53). Sample collection, packaging, and storage procedures were strictly following the protocols and regulations of the Biobank of the School of Basic Medical Sciences, Central South University.

Testing of Blood Specimens

Detection of Routine Clinical Indicators for Blood

Blood routine test was performed using BC-6800 blood cell analyzer (Mindray, Shenzhen, China) within 8 h after collection of anticoagulated whole blood. Serum samples were tested using the 7600-020 automatic biochemical analyzer (Hitachi, Tokyo, Japan) for the detection of high-sensitivity C-reactive protein (hCRP), total cholesterol (TC), triglyceride (TG), total protein (TP), albumin (ALB), globulin (GLO), albumin to globulin ratio (A/G), total bilirubin (TBIL), blood urea nitrogen (BUN), uric acid (UA), alanine aminotransferase (ALT), fasting blood glucose (FBS), and bile acid (TBA).

Detection of 5-HT Concentration for Blood

Human sera were tested for 5-HT using a human 5-HT ELISA KIT (Mlbio, Shanghai, China) according to the manufacturer's instructions. In general, the steps were as follows: The standard and diluted samples were added to the standard well and sample well, respectively, at 50 μL per well. Then, the enzyme-linked reagent was added to each well and incubated at 37°C in the dark for 60 min. After repeated washing, chromogenic reagent was added for color development. In the end, the stop solution was added, and the OD value of each well was measured at the wavelength of 450 nm using a microplate reader (Biotek, USA). The concentration of 5-HT in the sample was calculated according to the standard curve.

DNA Detection in the Intestinal Microbes

DNA Extraction

The total DNA was extracted using the E.Z.N.A.® soil kit (Omega Biotek, Norcross, GA, USA) according to the manufacturer's instructions. The E.Z.N.A.® soil DNA kit permits efficient and dependable extraction of high-quality genomic DNA from various samples, including clinical samples (54, 55). The DNA concentration and purity were determined using a NanoDrop 2000 (Thermo Fisher Scientific, USA). The quality of the DNA extraction was assessed by electrophoresis using a 1% agarose gel. Finally, the 16S V3-V4

variable region was subjected to PCR amplification using the 338F (5′-ACTCCTACGGGAGGCAGCAG-3′) and 806R (5′-GGACTACHVGGGTWTCTAAT-3′) primers.

DNA Sequencing

The PCR products were isolated using a 2% agarose gel, purified and quantified. A PE 2*300 library was constructed using the purified amplification fragments according to the standard procedure of the TruSeqTM DNA Sample Prep Kit (Illumina, San Diego, USA). Finally, the DNAs were sequenced using the Miseq PE300 sequencer (Illumina, San Diego, USA).

Processing and Analysis of Sequencing Data

Sequence Processing

The amplicon sequence variant (ASV) was obtained after quality control, denoising and the removal of chimeras using the DADA2 method recommended by QIIME2 according to the raw sequence information (FASTQ format) (56). The ASV was compared with the GREENGENES database (57) (the database was aligned to the V3-V4 region according to the 338F/806R primers) and annotated. The ASV with 99% similarity was classified as one Operational Taxonomic Unit (OTU) to obtain the OTU classification information table. The OTUs were classified using the RDP classifier to obtain their numbers at different taxonomic levels.

Differential Flora Analysis

We determined the bacteria with differences in abundance among groups and samples using the Kruskal-Wallis, LEfSe and DEseq2 methods (58, 59) and adjusted the P value using the Benjamini-Hochberg method (60). In our study, an underestimated false discovery rate (FDR) (P-adjust in standard R packages) was used to rectify multiple measurements (61), the rectified FDR known as $P < 0.1$ was considered significant. The threshold value 0.1 for P-value was used mostly to be a significant threshold in human microbial genomics, to embrace the crucial taxa with small effect sizes (62–64). Kruskal-Wallis is a nonparametric test with no requirements for distribution and is appropriate for the bacterial flora analysis. To identify differential microbial species among the different groups, we used the linear discriminant analysis effect size (LEfSe) analysis based on the linear discriminant analysis (LDA) and assessed the significant differences with an LDA score >2.0 as the critical value. DESeq2 is a method for the differential analysis of counting data that allows multiple comparisons among groups to find microorganisms that differ significantly between two groups.

Alpha Diversity

To determine the abundance and homogeneity of the sample species composition, we calculated the alpha diversity indices including the observed OTUs, Shannon index and Faith's phylogenetic diversity index and compared the differences in the alpha diversity among groups. The observed OTUs was used to determine the abundance of OTUs in the samples, and the Shannon index was used to calculate the homogeneity of the samples. Faith's phylogenetic diversity index was used to calculate the distance from the OTU of each sample to the phylogenetic tree. The rarefaction curve showed the number and/or the diversity of the species and was used to determine the reliability of the sequencing data of the samples that indirectly indicated the species richness in the samples.

Beta Diversity

To determine the differences in the microbial community compositions among the different samples, we used the beta diversity index that was based on the Bray-Curtis and Unweighted UniFrac indices for analysis. Bray-Curtis is the most commonly used indicator in ecology that reflects differences among communities and it shows the information of species abundance. The Unweighted UniFrac distance is the distance between samples calculated based on the evolutionary relationship of the species systems that mainly considers the presence or absence of species. These two indices were used for the principal coordinate analysis (PCoA), and the principal coordinate combination with the largest contribution rate was used for graphing (65). To perform a statistical analysis of the PCoA analysis results, the results were subjected to a significant analysis using the nonparametric test analysis of similarities (Anosim).

Establishment of an Intestinal Flora Prediction Model

We also used the partial least squares discriminant analysis (PLS-DA) to predict the sample types corresponding to microbial communities (66). PLS-DA is a supervised analytical method that distinguishes groups using mathematical models, ignores random differences within groups and highlights systematic differences among groups. The classification performance among groups by PLS-DA based on intestinal flora markers can be evaluated using the receiver operator characteristic (ROC) curve. The area under the curve (AUC) is closer to 1, indicating that the prediction model obtained by the PLS-DA analysis is reliable, and multiple microorganisms differ in their abundances among groups.

Association Analysis Between Intestinal Flora and Clinical Variables

The redundancy analysis method (RDA) (67) was used to analyze the potential association between the intestinal flora and clinical variables based on relative abundances of microbial species at different taxa levels using the R package "vegan" (68), so that the important driving factors that affected the distribution of the flora could be obtained. In the RDA species sorting map, clinical variables were indicated by arrows, where the length of an arrow represented the degree of correlation between the clinical variable and the flora distribution (that indicated the size of the variance). An acute angle between arrows indicated a positive correlation between two clinical variables, and an obtuse angle indicated a negative correlation. Each point represented a species, and the larger the point, the more abundant the species. To determine if a clinical variable was significantly correlated with a microbial community or species, we calculated the Spearman correlation coefficient between the microbial species and clinical variables, which is shown in the correlation heat map.

Intestinal Flora Function Prediction

We used PICRUSt software (69) to predict the function of intestinal flora based on the 16S species information and KEGG function information. The principle of PICRUSt is to deduce the microbial genomic function region from the 16S rRNA sequence information, the sequenced 16S rRNA information is corresponded to the genomic functional prediction spectrum in the GREENGENES database to predict the metabolic function of the microbiota (69, 70). According to the depth of annotation, KEGG function can be annotated at three levels. In addition, we performed the principal component analysis (PCA), Dunn test and Duncan analysis for the predicted functions, and corrected the *P*-values using the Bonferroni method (71). Through PCA we calculated the principal components with the largest contribution to represent most of the variation of the samples (72). Dunn test and Duncan analysis are two kinds of significant analysis methods, the Dunn test is mainly used for pairwise comparison, while the Duncan analysis is used for multiple comparison. The results were displayed in a PCA map of the prediction function, a bar chart of the KEGG pathway at the second level and a bar chart of significant KEGG pathway comparing the three groups.

According to the PLS-DA analysis, the three distinct clusters indicated that the intestinal floras of the NPC_F, NPC_S, and NOR groups were clearly differentiated into three independent clusters, indicating that the composition of intestinal flora was significantly different among the three groups. All the AUCs were 1, suggesting that the prediction model established based on the detected differential genus was perfect by using the PLS-DA analysis and that the intestinal flora related to the two groups of NPC were strong prediction factors and could be used as risk factors for NPC. For example, *C. ramosum* could be used as a strong prediction factor for NPC and is likely to be developed as a biomarker for high-risk populations and NPC.

To determine whether the structural differences among the three groups of intestinal flora corresponded to functional changes, we used PICRUSt to perform a functional prediction analysis of the 16S sequences and performed a PCA analysis of the predicted functions and a comparative analysis of the different KEGG-pathway levels.

RESULTS

Volunteer Characteristics

The demographic and clinical characteristics of 8 familial NPC patients, 24 sporadic NPC patients and 27 healthy volunteers are shown in **Supplementary Table 1**. The tumor stage of recruited 84 NPC, and 8 familial NPC and 24 sporadic NPC patients included in the study is shown in **Supplementary Table 6**. There were no significant differences between three groups of the basic characteristics in age, gender, race etc. The genetic map of familial NPC patients is presented in **Figure 1**.

Hematology Detecting Results

There are many differences between a variety of clinical indicators by statistical analysis among groups of multiple hematology test results (**Supplementary Table 2**). It's worth noting that the concentration of hCRP was significantly different between NPC: NOR ($P = 0.0047$), indicating that hCRP concentration was significantly higher in NPC patients than NOR. The concentration of 5-HT in serum was determined by ELISA (**Figure 2**). The concentration of 5-HT in serum of NOR group was (2.421 ± 0.300) ng/mL, for NPC_S group was (2.986 ± 0.207) ng/mL, and for NPC_F group was (3.813 ± 0.850) ng/mL. The concentration of 5-HT in NPC_F group was significantly higher than NOR ($t = 3.499$, $P = 0.0014$) and NPC_S ($t = 3.841$,

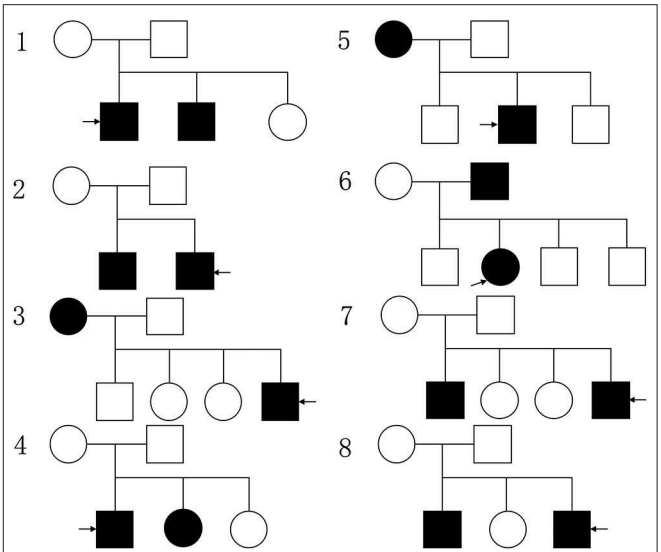

FIGURE 1 | The genetic map of familial NPC patients, the circle represents female, the square represents male, the black pattern represents the person with NPC, while the blank one means the healthy person; the pattern indicated by the arrow represents the patient participating in the study.

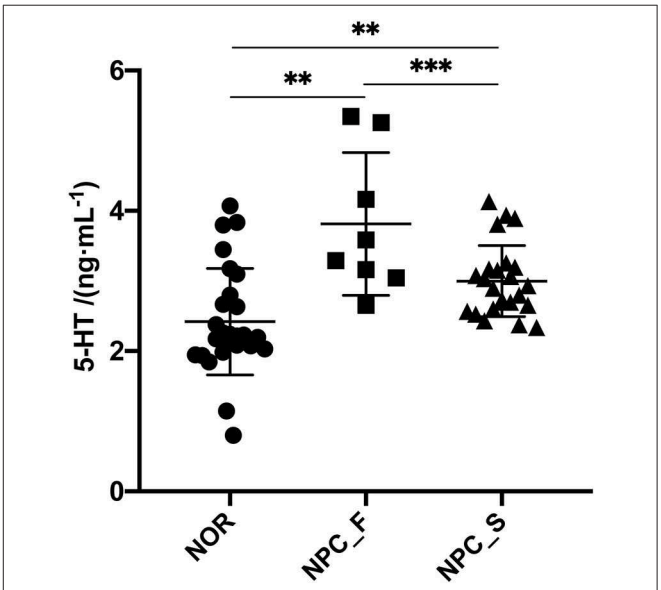

FIGURE 2 | The concentration of 5-HT in sera of the healthy controls (NOR), familial NPC patients (NPC_F), and sporadic NPC patients (NPC_S) groups, $^{**}P < 0.01$, $^{***}P < 0.001$.

$P = 0.0003$), and the concentration of 5-HT in NPC_S group was significantly higher than the NOR group ($t = 2.997$, $P = 0.0046$).

DNA Sequencing Results of Intestinal Flora and Statistical Analysis

Species Abundance and Diversity

A total of 3,200,797 available raw readings were obtained from all 59 samples, with an average reading of 54,251 ± 4,044 per sample. After CD-HIT clustering and NAST alignment, 1,828,692 unique representative sequences were generated and total of OTUs was 2,894. Petal diagram (**Figure 3A**) and phylogenetic tree (**Figure 3B**) were drawn with three groups' OTUs. The dilution curve (**Figures 4A,B**) constructed from the sequenced data has been basically stable, indicating that the sequenced data has been basically stable at this sequencing depth, and we have obtained the diversity of most of the microbiome contained in the samples.

At the phylum level for all species corresponding to the categorizable sequence, the main phylum is Firmicute, followed by Bacteroidete, Proteobacteria, Actinobacteria, and Verrucomicrobia (**Figure 5A**). Compared with the NOR group, the proportions of Proteobacteria in NPC_F ($P = 0.0045$) and NPC_S ($P = 7.57E\text{-}05$) were significantly increased. The distribution of the three groups at the genus and species levels is shown in (**Figures 5B,C**). It is found that the composition of the microorganisms in the three groups is distinctly different at different taxonomic levels.

Differences in Intestinal Flora Structure Between Groups

Based on the analysis of the DESeq2 method (**Supplementary Table 3**), the relative abundances between NPC_F and NOR were significantly different in 23 genus and 28 species; the relative abundances between NPC_S and NOR were significantly different in 9 genus and 17 species. And the relative abundance between NPC_F and NPC_S were significantly different in 13 genus and 22 species. Compared with the NOR group, the relative abundances of 8 genus such as *Clostridium*, *Veillonella,* and *Burkholderia* were significantly increased in NPC_F, while the relative abundances of 15 genus including *Akkermansia*, *Megamonas*, and *Roseburia* were significantly reduced in NPC_F. Compared with NOR, 8 species were significantly increased in NPC_F, such as *C. ramosum*, *Bacteroides fragilis*, *Citrobacter* spp. etc. While 20 species such as *A. muciniphila*, *Roseburia* spp., and *Gemmiger formicilis* were significantly reduced. In the NPC_S group, *Klebsiella*, *Veillonella*, *Clostridiaceae* spp., *Clostridium*, *Holdemania* etc., were increased significantly; at the species level, 14 species including *C. ramosum*, *Veillonella parvula*, *Veillonella dispar*, *Klebsiella* spp. were increased significantly in NPC_S, while *Mogibacteriaceae* spp., *Clostridiales* spp., *RF39* spp. etc., were reduced significantly. These differential genus and species can be used to construct a predictive model for the identification between familial NPC patients and sporadic NPC patients with healthy controls. Compared with NPC_S, *C. ramosum*, *Clostridium symbiosum*, *Blautia producta*, *Ruminococcus gnavus* etc., were significantly increased in NPC_F, while *Klebsiella* spp., *Prevotella stercorea* etc., were significantly increased in NPC_S.

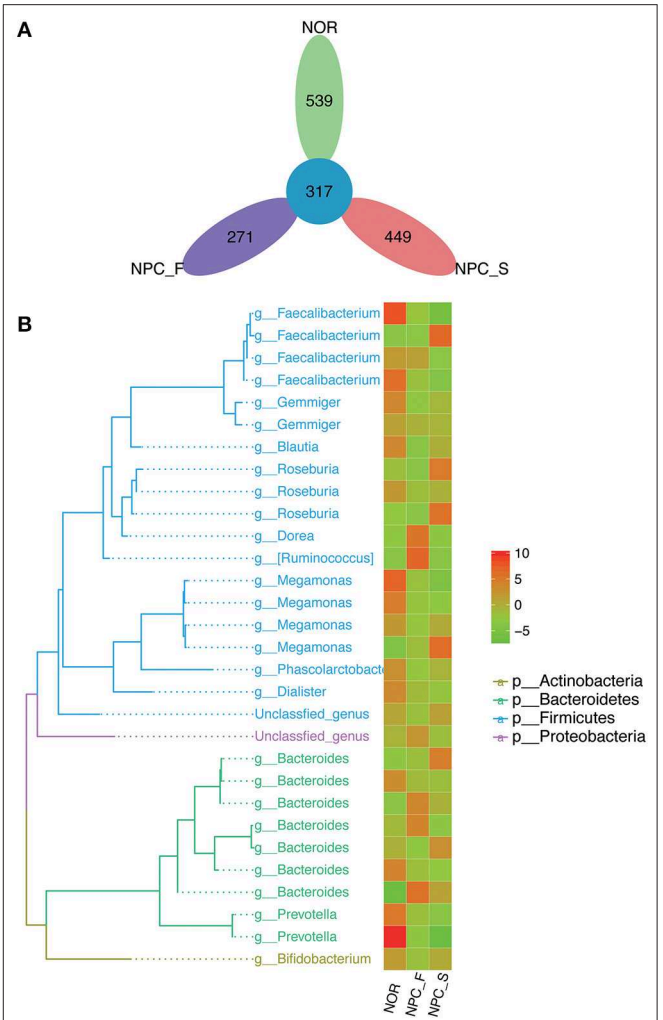

FIGURE 3 | Comparison of OTUs and phylogenetic tree map, **(A)** petal diagram based on OTUs of the healthy controls (NOR), familial NPC patients (NPC_F) and sporadic NPC patients (NPC_S) group. **(B)** Phylogenetic tree map, the phylogenetic tree on the left consists of nodes and branches, the different color of the branches represents the classification at different phylum levels, each terminal node represents an OTU, the corresponding classification of the OTU at the genus level is showed at the end of the branch. The heat map on the right clusters the standardized abundance of the genus corresponding to the left, through value-color gradient, the redder the color, the larger the value, the richer the abundance (phylum to genus: p, phylum; g, genus). Abundance standardization: the absolute abundance of each sample minus the mean absolute abundance of the genus and divided by the standard deviation; the normalized mean abundance is 0 and the standard deviation is 1.

From our current study, we evaluated the main intestinal flora commonly affected by diet, and found that some bacterium such as *Lactobacillus* spp. and *Faecalibacterium prausnitzii* can generate major metabolic byproducts including short chain fatty acid (73, 74); while *Enterococcus* spp., *Streptococcus* spp., and *Helicobacter pylori* were opportunistic pathogens in some cases (75–77), showing no significant difference between NPC patients

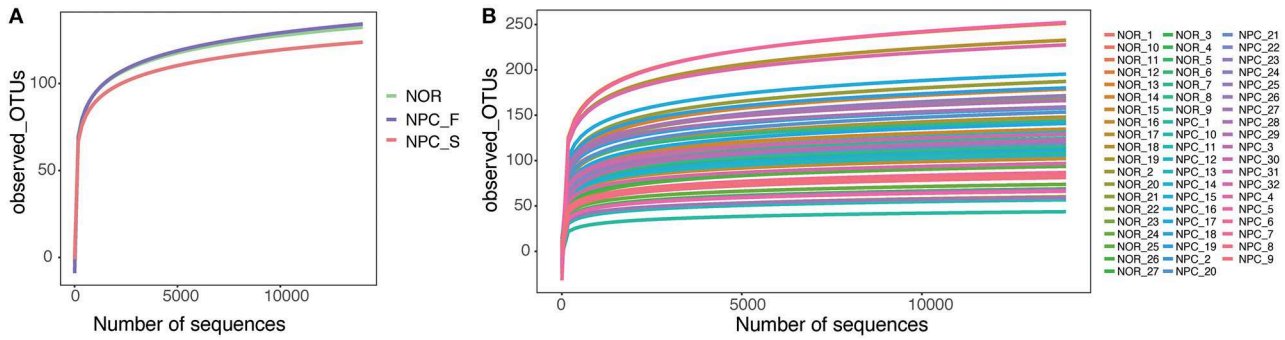

FIGURE 4 | Dilution curve in observed_OTUs, **(A)** Dilution curves of the healthy controls (NOR), familial NPC patients (NPC_F), and sporadic NPC patients (NPC_S) groups. **(B)** Dilution curves of all of the samples.

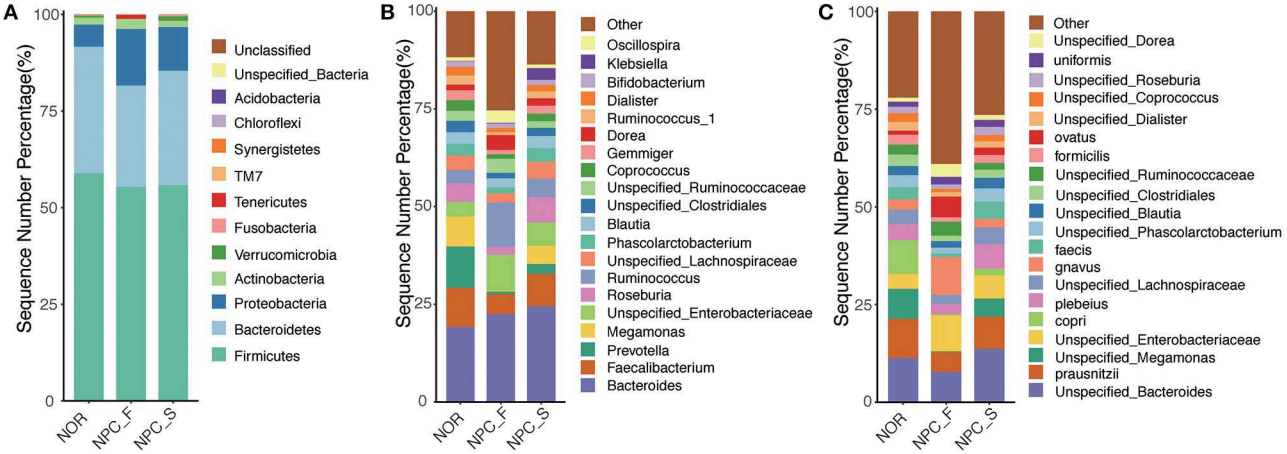

FIGURE 5 | Comparison of relative taxa abundance among the healthy controls (NOR), familial NPC patients (NPC_F), and sporadic NPC patients (NPC_S) groups at phylum, genus and species levels. **(A)** The bar chart of relative taxa abundance among the three groups at phylum levels. **(B)** The bar chart of relative taxa abundance among the three groups at genus levels. **(C)** The bar chart of relative taxa abundance among the three groups at species levels.

and healthy volunteers. Nevertheless, some other bacterium may be affected by diet, like *Clostridium* spp., *Bacteroides* spp., *Roseburia* spp., *Eubacterium* spp., and *Escherichia coli* which were mainly rich in NPC, while *Bifidobacterium* spp., *Alistipes* spp., *Bilophila* spp., and *A. muciniphila* were mainly found in healthy volunteers. The above measures and findings inferred us that the influence of nutrition and diet on gut microbiota between the comparison of NPC and healthy people can be neglected.

The results of LEfSe were shown in **Figures 6**, **7**. Comparision among the three groups, *Clostridium*, *Eubacterium* etc., were increased significantly in NPC_F, and *Bilophila* increased significantly in NPC_S. At the species level, compared with NOR, it was found that *C. ramosum*, *C. symbiosum* were increased significantly in NPC_F, while *A. muciniphila* was significantly reduced in NPC_F; *C. ramosum* and *V. dispar* increased significantly while *B. adolescentis* decreased significantly in NPC_S.

The first two main coordinates PC1 and PC2 with the largest contribution rate were obtained by using PCoA analysis (the explanatory variations were Bray-Curtis: 12.2 and 6.5% (**Figure 8A**), and Unweighted UniFrac: 12.4 and 7.1% (**Figure 8B**), respectively. Intestinal flora of NPC_F, NPC_S, and NOR groups was not completely clustered in the PCoA diagram.

According to the PLS-DA analysis (**Figure 8C**), the three distinct clusters indicated that the intestinal floras of the NPC_F, NPC_S, and NOR groups were clearly differentiated into three independent clusters, indicating that the composition of intestinal flora was significantly different among the three groups. All the AUCs were 1 (**Figure 8D**), suggesting that the prediction model established based on the detected differential genus was very good by using the PLS-DA analysis and that the intestinal flora related to the two groups of NPC were strong prediction factors and could be used as risk factors for NPC. For example, *C. ramosum* could be used as a strong prediction factor for NPC and is likely to be developed as a biomarker for high-risk populations of NPC and NPCs.

The observed OTUs, shannon and faith's phylogenetic diversity indices of the intestinal flora between the three

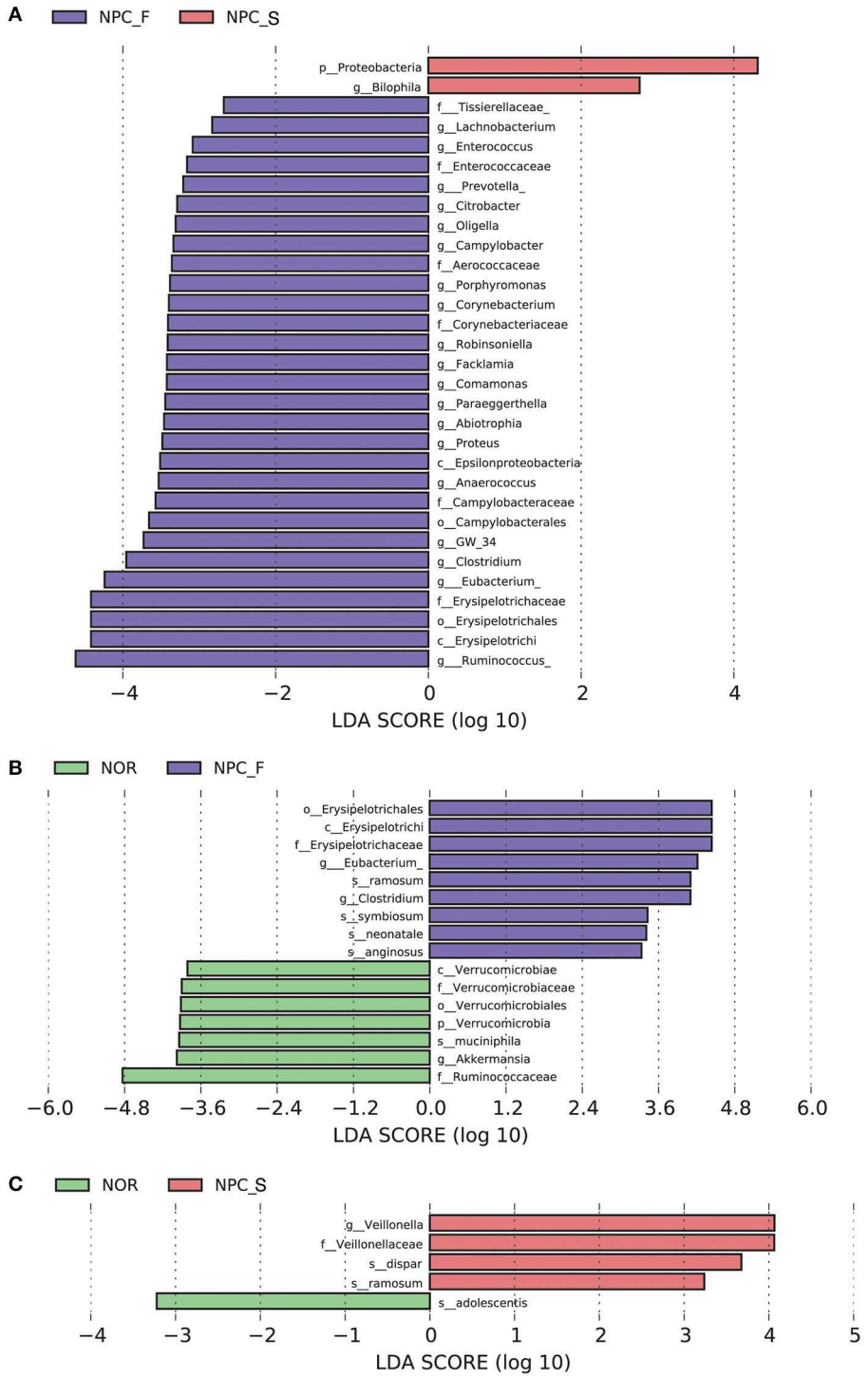

FIGURE 6 | Characteristics of intestinal flora composition in the healthy controls (NOR), familial NPC patients (NPC_F), and sporadic NPC patients (NPC_S) groups. **(A)** Diagram of the LDA scores calculated at genus levels among NOR, NPC_F and NPC_S groups, enriched taxa of NPC_S are directed with a positive value (red), while enriched taxa of NPC_F are directed with a negative value (purple). Only the LDA score > 2 are shown in the figure. **(B)** Diagram of the LDA scores calculated at species level between NOR and NPC_F groups, enriched taxa of NPC_F are directed with a positive value (purple), enriched taxa of NOR are directed with a negative value (green). **(C)** Diagram of the LDA scores calculated at species level between NOR and NPC_S groups, enriched taxa of NPC_S are directed with a positive value (red), enriched taxa of NOR are directed with a negative value (green). (phylum to species: p, phylum; c, class; o, order; f, family; g, genus; s, species).

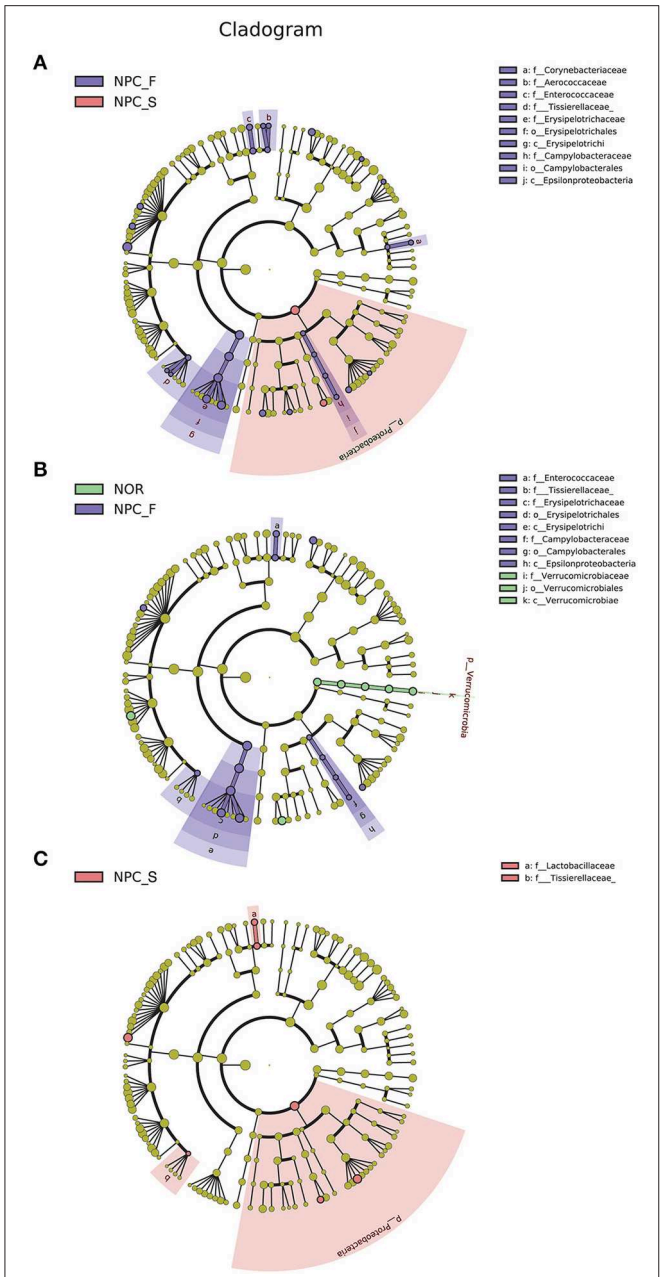

FIGURE 7 | Enriched flora in the healthy controls (NOR), familial NPC patients (NPC_F), and sporadic NPC patients (NPC_S) groups are represented in a cladogram. The origin of the tree (bacteria) showed in the central point, the larger circles centered on the center represent decreasing species levels from phylum to genus (phylum to genus: p, phylum; c, class; o, order; f, family; g, genus). The relative abundance of the flora is showed by each circle's diameter. **(A)** LEfSe analysis cladogram of intestinal flora among NOR, NPC_F and NPC_S groups at genus level. **(B)** LEfSe analysis cladogram of intestinal flora between NOR and NPC_F at genus level. **(C)** LEfSe analysis cladogram of intestinal flora between NOR and NPC_S at genus level.

groups of NPC_F, NPC_S, and NOR were calculated, and the statistical analysis of alpha diversity between every two groups showed there was no significant difference (**Figure 9**, **Supplementary Table 4**). Statistical analysis of beta diversity between each two groups was conducted, based on Bray-Curtis distance index (**Figure 10A**, **Supplementary Table 5**), it was found that the differences in beta diversity between NPC_F and NPC_S ($P = 0.018$), NPC_F and NOR ($P = 0.012$), were significant from each other, while that of the NPC_S and NOR ($P = 0.337$) was not significant; based on Unweighted UniFrac distance index (**Figure 10B**, **Supplementary Table 5**), the beta diversity between NPC_F and NPC_S ($P = 0.0045$), NPC_F and NOR ($P = 0.0045$) were significantly different, while that of between NPC_S and NOR ($P = 0.151$) was not significantly different. The NPC_F, NPC_S, and NOR groups had no significant difference in the gut microbial abundance and diversity. However, the NPC_F group was significantly different from the NPC_S group and the NOR group in the gut microbial structure, indicating the microbial structure of familial NPC patients was significantly altered relative to both sporadic NPC patients and healthy controls.

Statistical Analysis of Correlation Between Intestinal Flora and Clinical Variables

An RDA ranking map (**Figure 11A**) and a correlation heat map (**Figure 11B**) of NPC_F, NPC_S, and NOR group between intestinal flora at the genus level and clinical variables. Similarly, an RDA ranking map (**Figure 12A**) and a correlation heat map (**Figure 12B**) of NPC_F, NPC_S, and NOR group between intestinal flora at the species level and clinical variables. Based on the RDA ranking map, the correlation between total of the clinical variables and the intestinal flora was significant (at genus level: $P = 0.04$, **Figure 11A**; at species level: $P = 0.026$, **Figure 12A**), with the most relevant variables such as WBC, UA, FBS, 5-HT, BUN, TC, CREA.

Based on the genus-level RDA ranking map (**Figure 11A**) and the correlation heat map (**Figure 11B**), *Oscillospira* has a strong correlation with several clinical variables: positively correlated with hCRP (r: 0.32, $P = 0.012$); negatively correlated with BMI (r: −0.30, $P = 0.022$), TC (r: −0.37, $P = 0.0042$), UA (r: −0.36, $P = 0.0047$), and weakly positively correlated with TBA (r: 0.17, $P = 0.20$). Based on the species-level RDA ranking map (**Figure 12A**) and the correlation heat map (**Figure 12B**), *C. ramosum* was positively correlated with 5-HT (r: 0.85, $P = 2.81E-17$), and *V. dispar* was positively correlated with ALT (r: 0.30, $P = 0.020$).

Species Interaction Network Analysis

Figure 13A shows that *C. ramosum* is significantly associated with a variety of species, *C. ramosum* was positively correlated with opportunistic pathogens such as *R. gnavus* (r: 0.76, $P = 2.72E-12$), *Eubacterium dolichum* (r: 0.68, $P = 9.06E-07$), *C symbiosum* (r: 0.42, $P = 0.016$), and negatively correlated with the beneficial bacteria such as *Roseburia faecis* (r: −0.61, $P = 3.08E-07$) and *F. prausnitzii* (r: −0.49, $P = 9.20E-05$); which suggests that *C. ramosum* is probably a bacterium that affects the pathogenesis of NPC and provides us a direction for our future research on opportunistic pathogens and beneficial bacteria associated with *C. ramosum*. Meanwhile, *V. dispar* is positively correlated with *V. parvula* (r: 0.73, $P = 5.52E-11$) and *Haemophilus parainfluenzae* (r: 0.55, $P = 5.13E-06$).

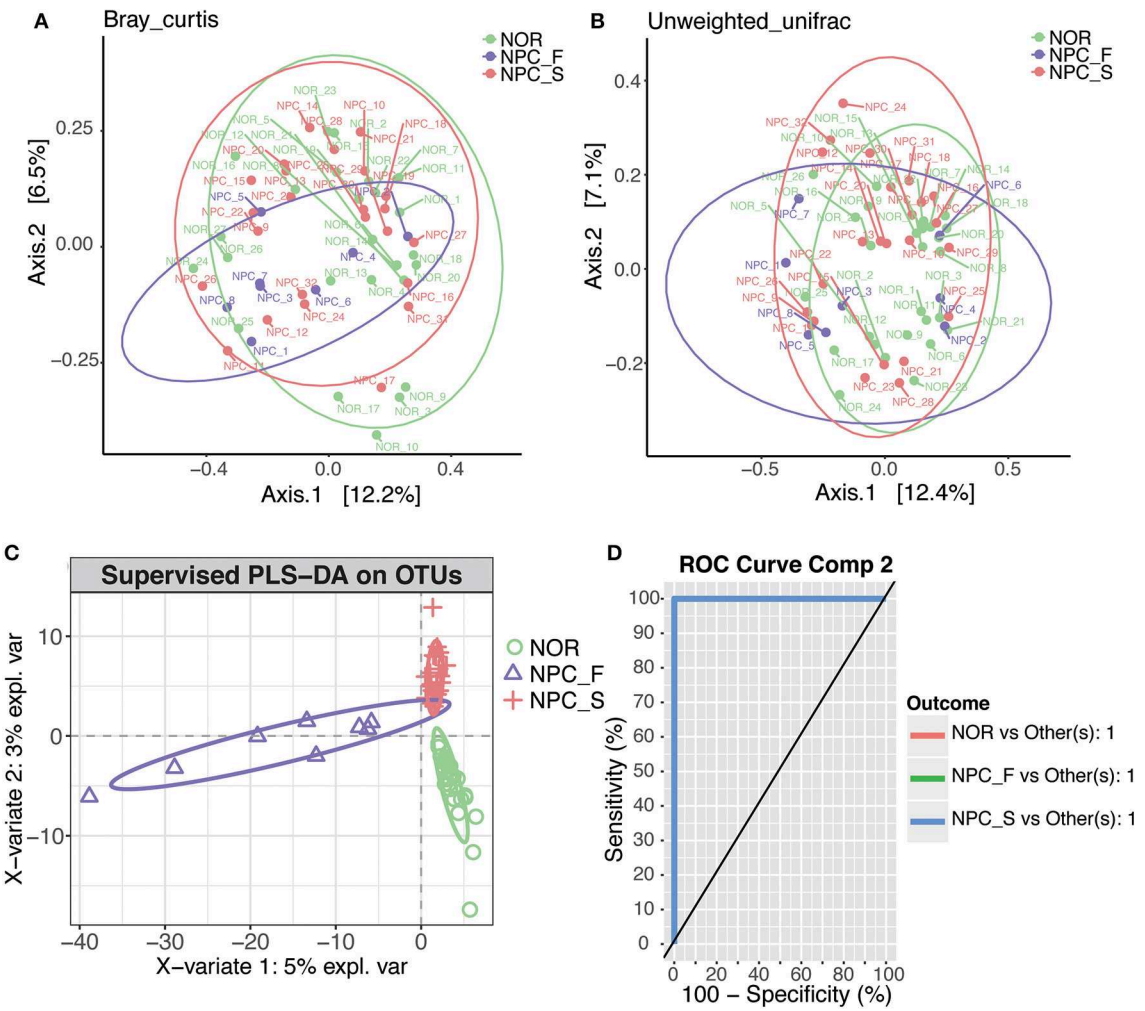

FIGURE 8 | PCoA and PLS-DA analysis of the microbiome among the healthy controls (NOR), familial NPC patients (NPC_F), and sporadic NPC patients (NPC_S) groups, different points or patterns are on behalf of different samples, different groups are showed in different colors, each large circle represents a group. The degree of discrepancy of the microbial structure of the samples is showed by the distance between the points or patterns. **(A)** Bray-Curtis PCoA based on the relative abundance of OTU (99% similarity level), NOR: green points, NPC_F: purple points, NPC_S: red points. **(B)** Unweighted UniFrac PCoA based on the relative abundance of OTU (99% similarity level), NOR: green points, NPC_F: purple points, NPC_S: red points. **(C)** The PLS-DA analysis on OTUs among the NOR, NPC_F and NPC_S groups, NOR: green circles, NPC_F: purple triangles, NPC_S: red crosses. **(D)** ROC analysis for the predictive value of the predictive model constructed based on PLS-DA analysis. The AUCs of the NOR, NPC_F and NPC_S groups all are 1.

Prediction of Intestinal Microbial Function

To determine whether the structural differences among the three groups of intestinal flora corresponded to functional changes, we used PICRUSt to perform a functional prediction analysis of the 16S sequences and performed a PCA analysis for the predicted functions (**Figure 13B**) and a comparative analysis of the predicted functions at the second KEGG-pathway level (**Figure 13C**). The comparison of enriched KEGG-pathway among NPC_F, NPC_S, and NOR groups by Dunn test is shown in the **Supplementary Table 7**. On the first KEGG-pathway level, the intestinal microbial function of NPC_F was found to be significantly correlated with HmnD (Human Diseases) ($P = 0.080$), the intestinal microbial function of the NOR group was significantly correlated with OrgS (Organismal Systems) ($P = 0.014$). On the second KEGG-pathway level, the gut microbial function of NPC_F was associated with neurodegenerative diseases ($P = 0.023$), lipid metabolism ($P = 0.073$); NPC_S was also associated with neurodegenerative diseases ($P = 0.045$); while the gut microbial function of NOR was mainly associated with immunity, digestion, endocrine system, energy, and nutrient digestion. At the same time, through Duncan test, it was found that the function of stilbenoid, diarylheptanoid, and gingerol biosynthesis in NPC_F was significantly increased (**Figure 13D**). The statement above shows that the predicted function of the intestinal flora can reflect the health status of the subjects. NPC patients are more susceptible to neurodegenerative diseases, and their intestinal function is more likely to be related to

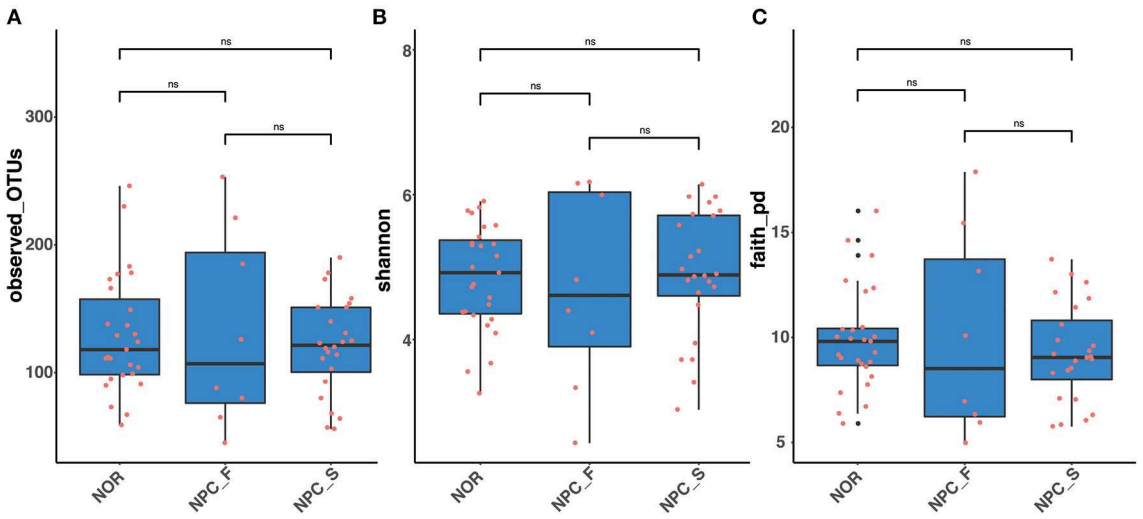

FIGURE 9 | The comparision of Alpha diversity among the healthy controls (NOR), familial NPC patients (NPC_F), and sporadic NPC patients (NPC_S) groups based on different indices. **(A)** Observed_OTUs. **(B)** Shannon index. **(C)** Faith's phylogenetics diversity index. ns, no significance, Wilcox_Test.

the synthesis of secondary metabolites and lipid metabolism; while the intestinal microbial function of the NOR group was mainly related to immunity, digestion, endocrine, energy, and nutrient digestion.

DISCUSSION

This study investigated the correlation between the changes in the intestinal flora and NPC by an examination of the intestinal flora and multiple clinical indicators of the blood of 8 carefully screened patients of familial NPC, 24 patients of sporadic NPC and 27 healthy controls and a comparison of the differences in their intestinal flora structures and biological functions. By analyzing the function of the intestinal floras of NPC patients, we aimed to provide a better biological marker for patients with familial and sporadic NPC and constructed a disease prediction model for high-risk populations.

In this study, we found that the intestinal microbiota structures of familial NPC patients and sporadic NPC patients were different from that of the healthy volunteers. At the phylum level, Proteobacteria were significantly increased in NPC_F and NPC_S. A previous study showed that the increased abundance of Proteobacteria was positively correlated with inflammatory diseases (78) such as nonalcoholic fatty liver disease (NAFLD) (79, 80), colitis (81, 82), inflammatory bowel diseases (IBD) (83–85), Crohn's disease (CD) and ulcerative colitis (UC) (86), and asthma and chronic obstructive pulmonary disease (COPD) (87, 88). The Proteobacteria in the mouth are significantly associated with the severity of mucositis in patients with NPC (89). Some bacterial components (such as Lipopolysaccharide, LPS) in the opportunistic pathogenic bacteria of the Proteobacteria phylum may produce pro-inflammatory factors that can cause cancer through activating the host's pattern-recognition receptors (such as Toll-like receptors, TLRs) (90).

C. ramosum and opportunistic pathogens such as *Citrobacter* spp., *Veillonella* spp., *Prevotella* spp., *Campylobacter* spp. in the intestinal flora of familial NPC patients were significantly increased, while the abundances of the anti-inflammatory bacteria *A. muciniphila*, and butyrate-producing bacteria *Roseburia* spp. were significantly decreased. *C. ramosum*, *V. parvula*, *V. dispar,* and *Klebsiella* spp. were significantly increased in sporadic NPC patients, and the abundance of the probiotic *B. adolescentis* was significantly decreased.

Compared to the NOR group, the *C. ramosum* in both of the NPC_F and NPC_S groups was significantly increased. Using ELISA, we found that the levels of 5-HT in the sera of patients in the NPC_F and NPC_S groups were significantly higher than those in the NOR group, and *C. ramosum* was significantly associated with 5-HT. *C. ramosum* is a spore-forming, indigenous intestinal bacteria, whose metabolites can irritate ECs to secret 5-HT (46). It was found that *C. ramosum* is an important opportunistic pathogen in clinical (91–93). At the same time, several studies have discovered that some of the metabolites of the spore-forming microbiota from human gastrointestinal flora can modulate the elevation of 5-HT from ECs (30, 94, 95). More than 90% of 5-HT in the human body is biosynthesized by ECs, which plays a crucial role in human physiological function through activation of the different 5-HT receptors on different kinds of cells, such as intestinal epithelial cells (96), platelets (97) and immune cells (98). In addition, it was discovered that there are many kinds of 5-HTR subtypes on a variety of cancers, including PC (32), HCC (33–35), CRC (36) etc. 5-HT could promote the development and progression of these cancers by activating the 5-HTR subtypes, such as 5-HT1A, 5-HT1B, 5-HT2A, 5-HT2B (44, 99). 5-HT1B was overexpressed in human NPC samples (44), which reminded us that the elevated 5-HT in plasma in NPC could promote the progression of NPC through 5-HTR. These findings suggest that the significantly elevated *C. ramosum* in the intestinal flora of NPC patients

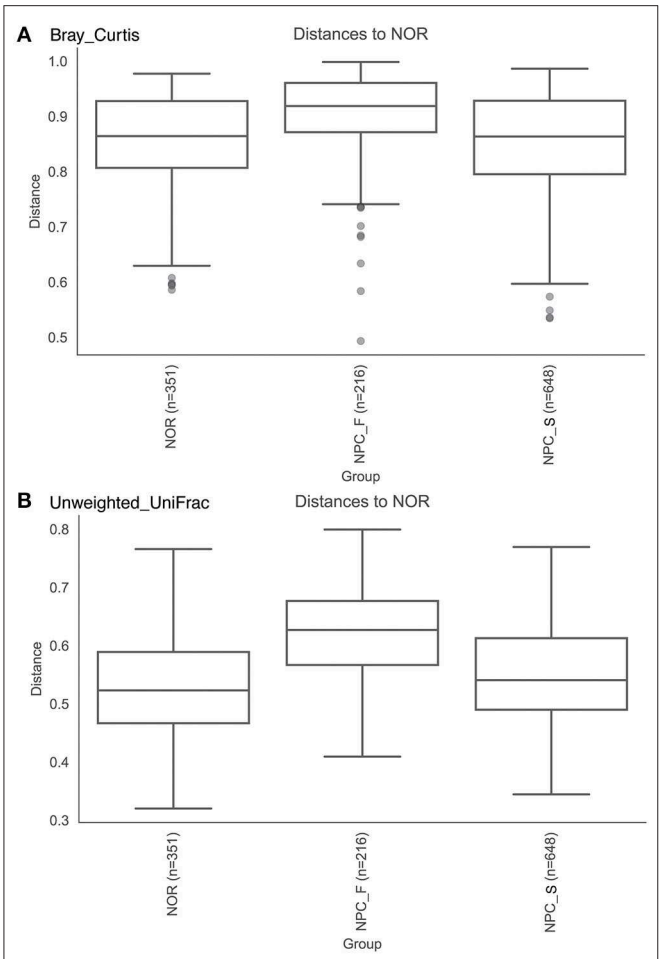

FIGURE 10 | The comparision of Beta diversity among the healthy controls (NOR), familial NPC patients (NPC_F), and sporadic NPC patients (NPC_S) groups based on different indices. **(A)** Bray-Curtis distance index, Anosim. **(B)** Unweighted UniFrac distance index, Anosim.

may affect the development and progression of NPC through increasing the 5-HT levels in the blood. We also found that both the *C. ramosum* and 5-HT were significantly higher in the NPC_F group than those in the NPC_S group, and this outcome may have occurred because NPC_F patients had family histories of NPC.

In the human body, *A. muciniphila* is an anti-inflammatory probiotic (100) that exerts beneficial effects on the host through regulating the mucin metabolism and immune responses, and *A. muciniphila* also shapes the composition of the host intestinal flora (101). Previous studies have found that reduced *A. muciniphila* levels are associated with the development and progression of many malignant tumors such as CRC and breast cancer and that *A. muciniphila* has a positive effect on the response of tumors to chemotherapeutic drugs and immune checkpoint inhibitors and improves the intestinal microbial composition (102, 103). Our study found that *A. muciniphila* was significantly reduced in patients with familial NPC. Therefore, we hypothesized that the reduction of *A. muciniphila* in patients with familial NPC lead to decreased levels of mucin metabolites beneficial to the host, which disrupts the homeostasis of the barrier function and immune function of the host intestine and eventually triggers NPC.

Roseburia spp. was significantly reduced in patients with familial NPC. *Roseburia* spp. is one of the main bacteria that generate the butyrate required by the human body that suppresses the growth and proliferation of tumor cells through multiple pathways (104–106). One study showed that the siblings of CD patients had similar disruptions of intestinal flora as CD patients, manifested by a low abundance of *Roseburia* spp. (107), suggesting that *Roseburia* spp. is familial. We believe that the familial nature of *Roseburia* spp. is probably related to the familial nature of NPC, which may explain the significant reduction in the butyrate supply in patients with familial NPC due to the significant reduction of butyrate-producing *Roseburia* spp. in their intestinal flora. The reduced butyrate may lead to an abnormal expression of genes related to NPC in the body and an enhanced Warburg effect of cancer cells, which then promotes tumor development and progression.

V. parvula and *V. dispar* were significantly increased in patients with sporadic NPC. NPC patients often have clinical symptoms such as cervical lymph node enlargement, nasal congestion and blood stasis. A previous study found that *Veillonella* spp. was significantly increased in CD patients (108). *V. parvula* is associated with many inflammatory diseases such as endocarditis (109), meningitis (110), and bacteremia (111). *V. dispar* is significantly increased in autoimmune hepatitis, and it was found that this bacterium was positively correlated with the serum AST level and the extent of disease activity (112). ALT and AST both reflect liver damage, with ALT being more sensitive. Our study found that *V. dispar* was positively correlated with ALT. *Klebsiella* spp. is significantly increased in sporadic NPC, and a previous study showed that *Klebsiella* spp. is one of the most common bacteria that causes infections in tumor patients (113). *Klebsiella* spp. is the main bacterium in the oral flora during the immunosuppression of cancer patients, which may lead to severe local or systemic disease in these patients (114). We believe that the changes in the intestinal flora of patients with sporadic NPC can lead to the disruption of the immune function by promoting inflammation that triggers cancer and may also affect the liver function. Therefore, special attention should be paid to the liver function during diagnosis and treatment. We found that *B. adolescentis* was significantly reduced in patients with sporadic NPC. *Bifidobacterium* is a probiotic that is mainly found in the intestine of breastfed infants (115), and this bacterium can metabolize dietary fiber to produce acetate and lactate, which can be further metabolized to produce propionate and butyrate (116, 117). Propionate and butyrate are beneficial to the physiological function of various tissues and organs *in vivo* (118). Previous studies have found that *Bifidobacterium* has an anti-inflammatory effect *in vivo* (119–122), and several studies have shown that the substances produced by *B. adolescentis* have anti-inflammatory activity (123–125). In summary, the increases in the pro-inflammatory

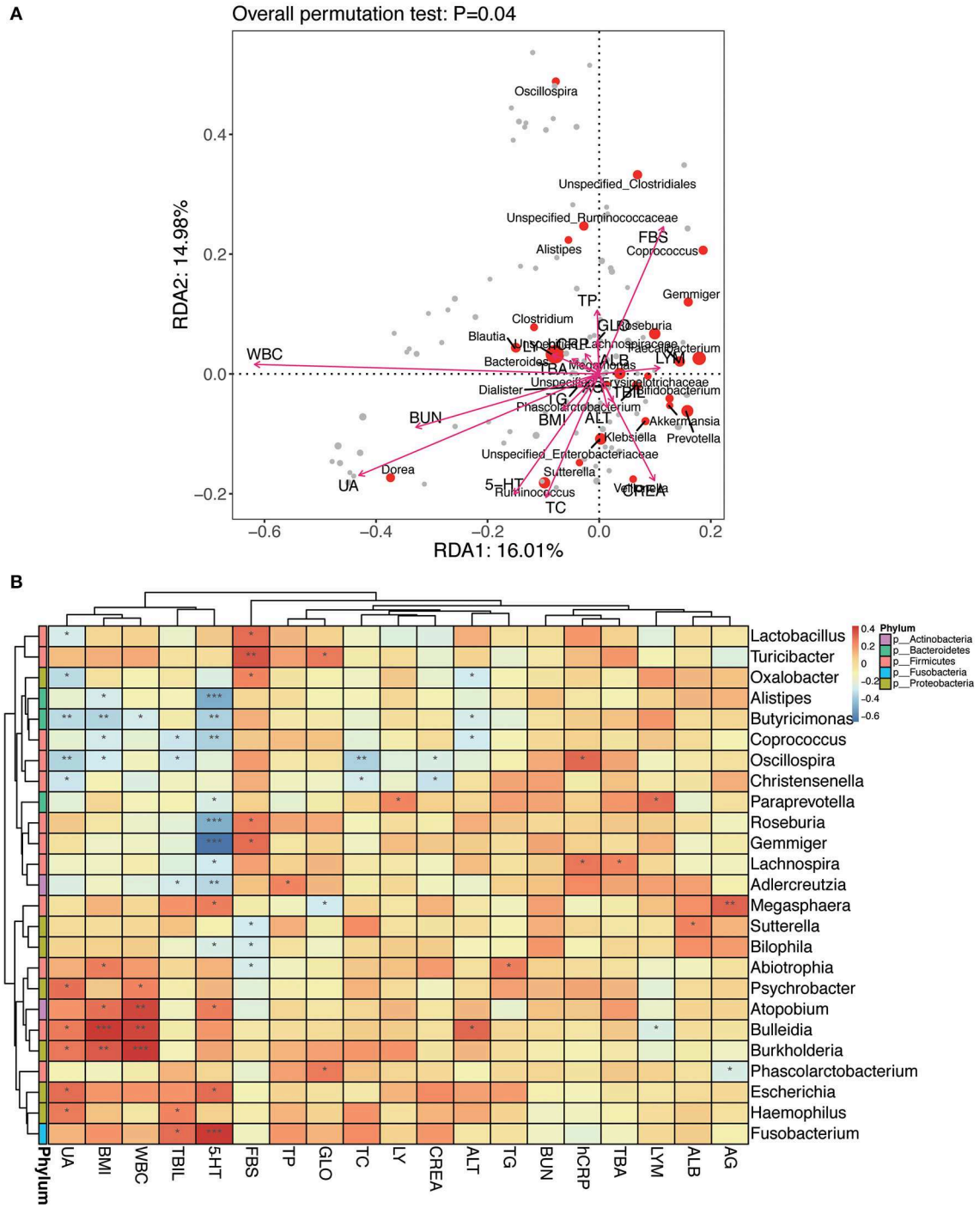

FIGURE 11 | The relationship between intestinal flora and clinical variables at the genus level. **(A)** RDA ranking map. RDA1:16.01% and RDA2:14.98% represent the magnitude of the percentage of variance interpreted in the direction of the two axes, respectively; clinical variables were indicated by arrows, the length of an arrow represented the size of the variance between the clinical variable and the flora distribution. An acute angle between two arrows indicated a positive correlation between two clinical variables, and an obtuse angle indicated a negative correlation. Each point represented a species, and the larger the point, the more abundance of the species. **(B)** Heat map for Spearman correlation analysis between intestinal flora and clinical variables at the genus level. X-axis: clinical variables, Y-axis: genus. The branches of the figure on the left indicates the classification of phylum. *R*-values (rank correlations) are shown in different colors in the heat map, the figure on the right shows the color gradient corresponding to different *R*-value; $P < 0.05$ is showed in the figure. $^{*}P < 0.05$, $^{**}P < 0.01$, $^{***}P < 0.001$.

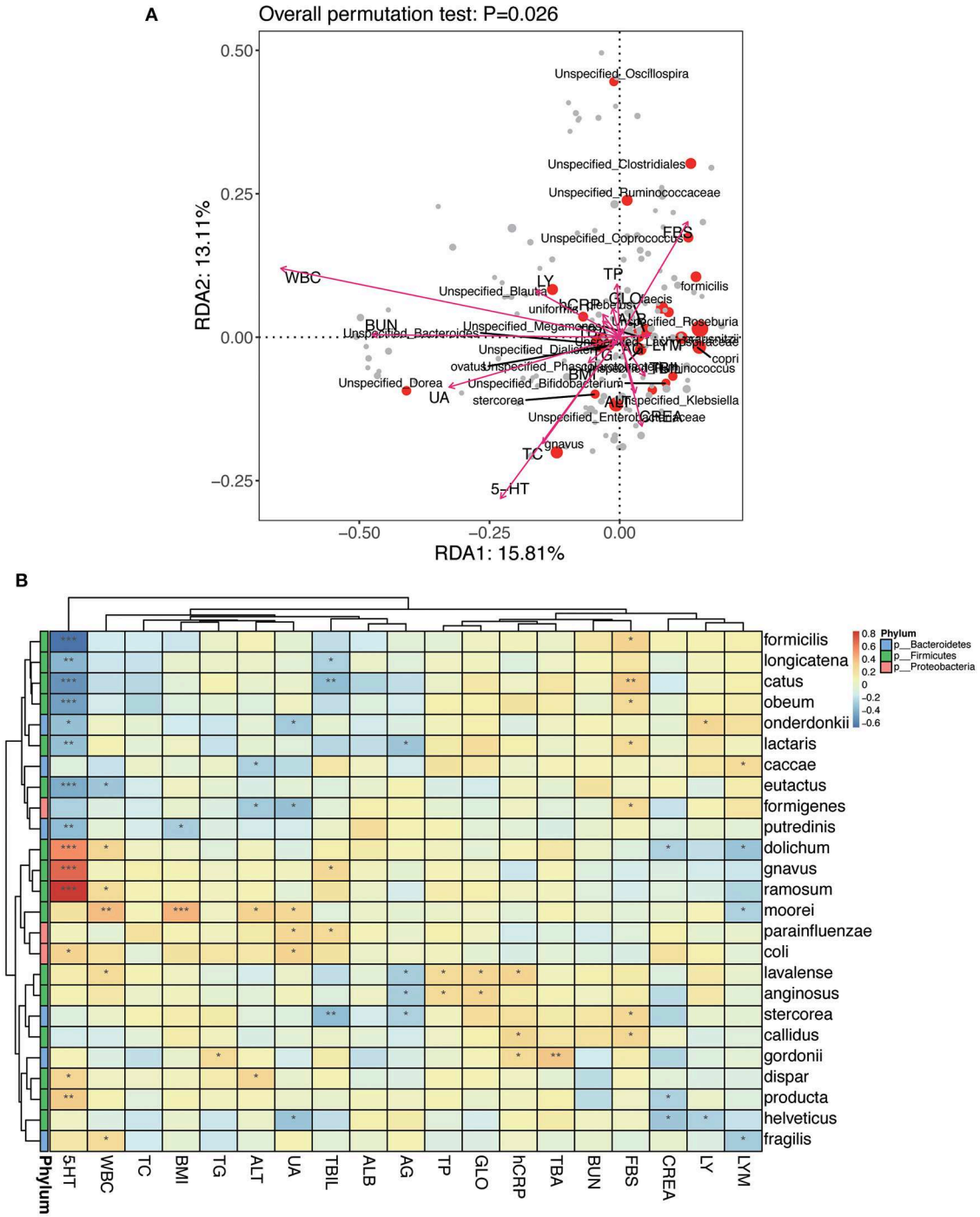

FIGURE 12 | The relationship between intestinal flora and clinical variables at the species level. **(A)** RDA ranking map; RDA1:15.81% and RDA2:13.11% represent the magnitude of the percentage of variance interpreted in the direction of the two axes, respectively. **(B)** Heat map for Spearman correlation analysis between intestinal flora and clinical variables at the species level. $^{*}P < 0.05$, $^{**}P < 0.01$, $^{***}P < 0.001$.

bacteria *C. ramosum*, *V. parvula,* and *V. dispar* and the reduction of the anti-inflammatory bacterium *B. adolescentis* in patients with sporadic NPC may lead to the physiological dysfunction of the body by inducing an inflammatory status that promotes tumor formation.

The relative abundances of *Oscillospira* in the NPC_F and NPC-S groups were increased, and *Oscillospira* was positively correlated with hCRP, negatively correlated with the body-mass index (BMI) and weakly and positively correlated with TBA. *Oscillospira* is an anaerobic bacterium whose abundance

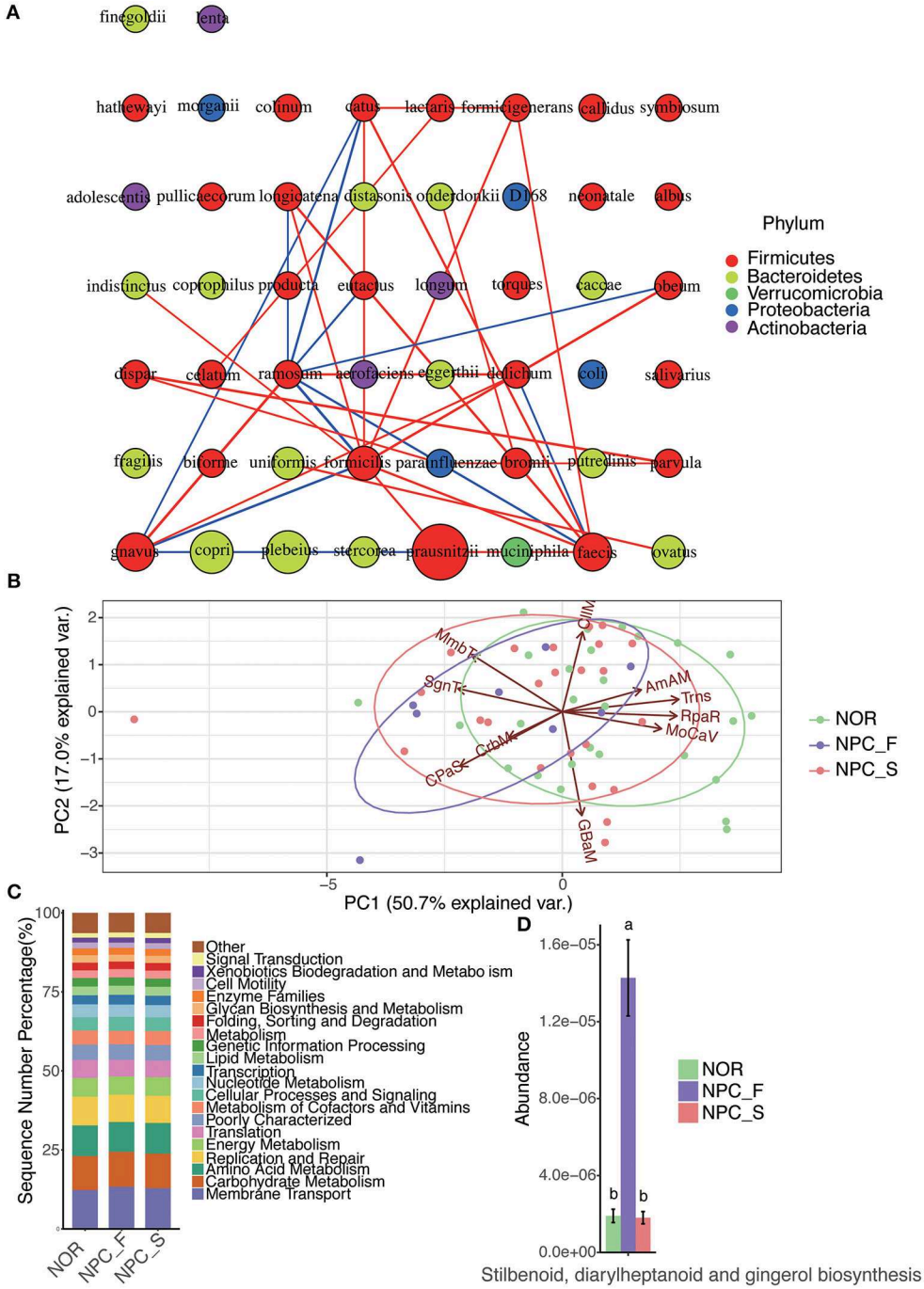

FIGURE 13 | The intestinal flora interaction network analysis and functional PICRUSt analysis among the healthy controls (NOR), familial NPC patients (NPC_F) and sporadic NPC patients (NPC_S) groups. **(A)** The map of the species interaction network analysis; a circle represents a bacteria, the size of the circle represents its relative abundance, different color represents different classification at phylum level, the line between the circles represents the correlation between the two bacteria is significant ($P < 0.05$), the red color of the line represents a positive correlation, while the blue one represents the negative correlation, the line is more rough, corresponding correlation coefficient value is greater. **(B)** The diagram of PCA analysis for the predicted functions on the second KEGG-pathway level; The PC1-axis (50.7%) and PC2-axis (17.0%) represent the contribution of the two principal components to the sample difference are 50.7% and 17.0%, respectively, each point represents a sample, each circle represents a group (NOR in green, NPC_F in purple and NPC_S in red), and the arrow direction and length represent the direction and dominant ability of the prediction function in the group, respectively. (AmAM, Amino Acid Metabolism; CIIM, Cell Motility; CPaS, Cellular Processes and Signaling; CrbM, Carbohydrate Metabolism; GBaM, Glycan Biosynthesis and Metabolism; MmbT, Membrane Transport; MoCaV, Metabolism of Cofactors and Vitamins; RpaR, Replication and Repair; SgnT, Signal Transduction; Trns, Translation). **(C)** The bar chart of the predicted functions at the second KEGG-pathway level. **(D)** The bar chart of the abundance of the function of stilbenoid, diarylheptanoid and gingerol biosynthesis of the NOR, NPC_F and NPC_S groups, the value of a and b represent that there is significant difference in abundance of this function compared NPC_F with NOR, and NPC_F with NPC_S groups.

is negatively correlated with BMI (126, 127) and is significantly reduced in CD (128) and NAFLD (129). These findings all suggest that *Oscillospira* not only reduces the BMI of the host, but the reduction in its abundance is positively correlated with inflammation. *Oscillospira* is the only genus that increased in the cecum during fasting in mammals (130). Compared to vegetarian diets, the TBA and the abundances of *Oscillospira* and anti-biliary bacterium were increased in the intestine of dietary intervened carnivorous volunteers (131). It has also been found that the abundance of *Oscillospira* was significantly increased by more than 4 times ($P = 0.041$) in the intestine of patients with cholelithiasis, (132) and it is highly likely that *Oscillospira* plays an anti-TBA role. This study showed that the abundance of *Oscillospira* was increased in NPC patients, which might be related to a progressive decline in appetite during the disease. Red meat consumption is associated with an increased risk of NPC (133) that further promotes the increase of *Oscillospira* by increasing bile acid levels. Opportunistic pathogens can elevate inflammatory factors through microbe-related molecular patterns (MAMPs), affecting the homeostasis of the body's immune system, which, in turn, induces cancer (134). *Oscillospira* may promote the elevation of hCRP levels through MAMPs.

CONCLUSION

The increase in the *C. ramosum* bacteria that promote the secretion of 5-HT is likely a key feature of the intestinal flora of human NPC patients. It is an urging issue to proceed additional studies with animal models, even with human models, to elaborate the mechanisms underlying the association among 5-HT, intestinal flora and NPC, with which we can manipulate the intestinal flora to screen, guard against and remedy NPC. The increases in *C. ramosum* and the opportunistic pathogens *Citrobacter* spp. and *Veillonella* spp. as well as the reduction of the anti-inflammatory bacteria *A. muciniphila* and butyrate-producing bacteria *Roseburia* spp. are key features of the intestinal flora of patients with familial NPC. The increases in *C. ramosum* and the pro-inflammatory bacteria *V. parvula* and *V. dispar* and the reduction in the anti-inflammatory bacteria *B. adolescentis* are probably characteristics of the intestinal flora of patients with sporadic NPC. Based on these characteristics, we can establish a predictive model for the intestinal flora of familial and sporadic NPCs, in which *C. ramosum*, a strong risk factor for NPC, may be used as a new biomarker for NPC patients. Based on this predictive model, we are likely to predict the disease risk in the population with a high risk of NPC and perform a non-invasive early screening for NPC using the biomarkers. However, this study is restricted by the limited number of enrolled patients. Based on the International Agency for Research on Cancer, the new cases of NPC only holding 0.7% of all diagnosed cancers in 2018 (1, 2). The incidence rate of NPC is 3.0/100 000 in China to 0.4/100 000 in white population (1, 2). The morbidity of NPC has been descending increasingly in recent years, the main decrement is from east and southeast Asia (135). The Third Xiangya Hospital is large and international hospital, from which we have got most of the cases based on the laboratory department. Considering the limited sample size, we also colaborated with other large hospitals, such as Hunan cancer hospital, to embrace more cases. Each of these cases has been carefully filtrated before being recruiting, and they are representative and precious. The discovery of this study also provided us a direction for our future research. Nevertheless, more studies with a larger number of NPC participants are needed to confirm this predictive model before being used in clinical. Through our findings, we may be able to monitor confirmed NPC patients and their intestinal flora and clinical indicators in the late disease stages and determine the relationship among the disease status, intestinal flora and clinical monitoring indicators, which may provide individualized methods to prevent and treat NPC.

DATA AVAILABILITY STATEMENT

The DNA sequencing data in this article is deposited in the NCBI BioProject database (https://www.ncbi.nlm.nih.gov/bioproject), with the accession number: PRJNA565548.

ETHICS STATEMENT

This study was conducted as per the recommendations of the Human Specimen Study guidelines of the Institutional Review Board (IRB) of the Third Xiangya Hospital, Central South University, with written informed consent taken from all subjects. All subjects gave written informed consent in accordance with the Declaration of Helsinki. The protocol was approved by the IRB of the Third Xiangya Hospital, Central South University. The IRB number is 2019-S478.

AUTHOR CONTRIBUTIONS

HJ, JL, BZ, RH, JZ, ZC, XS, and XL: sample collection. HJ: detected samples, organized data, and wrote the article. XN: designed experiment. All authors have read and critically revised the manuscript.

FUNDING

The New Xiangya Talent Project of the Third Xiangya Hospital, Central South University, China (No. 20160304).

ACKNOWLEDGMENTS

We thank all participants of this study. Thanks to the Biobank of the School of Basic Medical Sciences, Central South University, Changsha, China, for storing the collected samples for future study.

SUPPLEMENTARY MATERIAL

The Supplementary Material for this article can be found online at: https://www.frontiersin.org/articles/10.3389/fonc.2019.01346/full#supplementary-material

REFERENCES

1. Bray F, Ferlay J, Soerjomataram I, Siegel RL, Torre LA, Jemal A. Global cancer statistics 2018: GLOBOCAN estimates of incidence and mortality worldwide for 36 cancers in 185 countries. *CA Cancer J Clin.* (2018) 68:394–424. doi: 10.3322/caac.21492
2. Ferlay J, Colombet M, Soerjomataram I, Mathers C, Parkin DM, Piñeros M, et al. Estimating the global cancer incidence and mortality in 2018: GLOBOCAN sources and methods. *Int J Cancer.* (2019) 144:1941–53. doi: 10.1002/ijc.31937
3. Tang M, Lautenberger JA, Gao X, Sezgin E, Hendrickson SL, Troyer JL, et al. The principal genetic determinants for nasopharyngeal carcinoma in china involve the HLA class I antigen recognition groove. *PLoS Genet.* (2012) 8:e1003103. doi: 10.1371/journal.pgen.1003103
4. Lo KW, To KF, Huang DP. Focus on nasopharyngeal carcinoma. *Cancer Cell.* (2004) 5:423–8. doi: 10.1016/S1535-6108(04)00119-9
5. Tsao SW, Yip YL, Tsang CM, Pang PS, Lau VM, Zhang G, et al. Etiological factors of nasopharyngeal carcinoma. *Oral Oncol.* (2014) 50:330–8. doi: 10.1016/j.oraloncology.2014.02.006
6. Hsu WL, Yu KJ, Chien YC, Chiang CJ, Cheng YJ, Chen JY, et al. Familial tendency and risk of nasopharyngeal carcinoma in taiwan: effects of covariates on risk. *Am J Epidemiol.* (2011) 173:292–9. doi: 10.1093/aje/kwq358
7. Yuan JM, Wang XL, Xiang YB, Gao YT, Ross RK, Yu MC. Non-dietary risk factors for nasopharyngeal carcinoma in Shanghai, China. *Int J Cancer.* (2000) 85:364–9. doi: 10.1002/(SICI)1097-0215(20000201)85:3<364::AID-IJC12>3.0.CO;2-C
8. Zeng YX, Jia WH. Familial nasopharyngeal carcinoma. *Semin Cancer Biol.* (2002) 12:443–50. doi: 10.1016/S1044579X02000871
9. Friborg J, Wohlfahrt J, Koch A, Storm H, Olsen OR, Melbye M. Cancer susceptibility in nasopharyngeal carcinoma families - a population-based cohort study. *Cancer Res.* (2005) 65:8567–72. doi: 10.1158/0008-5472.CAN-04-4208
10. Liu Z, Chang ET, Liu Q, Cai Y, Zhang Z, Chen G, et al. Quantification of familial risk of nasopharyngeal carcinoma in a high-incidence area. *Cancer.* (2017) 123:2716–25. doi: 10.1002/cncr.30643
11. Ung A, Chen CJ, Levine PH, Cheng YJ, Brinton LA, Chen IH, et al. Familial and sporadic cases of nasopharyngeal carcinoma in Taiwan. *Anticancer Res.* (1999) 19:661–5. doi: 10.1016/S0041-1345(97)01181-0
12. Costello EK, Stagaman K, Dethlefsen L, Bohannan BJ, Relman DA. The application of ecological theory toward an understanding of the human microbiome. *Science.* (2012) 336:1255–62. doi: 10.1126/science.1224203
13. Chung H, Pamp SJ, Hill JA, Surana NK, Edelman SM, Troy EB, et al. Gut immune maturation depends on colonization with a host-specific microbiota. *Cell.* (2012) 149:1578–93. doi: 10.1016/j.cell.2012.04.037
14. Kamada N, Chen GY, Inohara N, Núñez G. Control of pathogens and pathobionts by the gut microbiota. *Nat Immunol.* (2013) 14:685–90. doi: 10.1038/ni.2608
15. Knoop KA, Holtz LR, Newberry RD. Inherited nongenetic influences on the gut microbiome and immune system. *Birth Defects Res.* (2018) 110:1494–503. doi: 10.1002/bdr2.1436
16. Ubeda C, Lipuma L, Gobourne A, Viale A, Leiner I, Equinda M, et al. Familial transmission rather than defective innate immunity shapes the distinct intestinal microbiota of TLR-deficient mice. *J Exp Med.* (2012) 209:1445–56. doi: 10.1084/jem.20120504
17. Dejea CM, Fathi P, Craig JM, Boleij A, Taddese R, Geis AL, et al. Patients with familial adenomatous polyposis harbor colonic biofilms containing tumorigenic bacteria. *Science.* (2018) 359:592–7. doi: 10.1126/science.aah3648
18. Gagnière J, Raisch J, Veziant J, Barnich N, Bonnet R, Buc E, et al. Gut microbiota imbalance and colorectal cancer. *World J Gastroenterol.* (2016) 22:501–18. doi: 10.3748/wjg.v22.i2.501
19. Rajagopala SV, Vashee S, Oldfield LM, Suzuki Y, Venter JC, Telenti A, et al. The human microbiome and cancer. *Cancer Prev Res.* (2017) 10:226–34. doi: 10.1158/1940-6207.CAPR-16-0249
20. Federico A, Marcello D, Giuseppe GC, Vittorio MO, Carmela L. Gut microbiota and the liver. *Miner Gastroenterol E Dietol.* (2017) 63:385–98. doi: 10.23736/S1121-421X.17.02375-3
21. Mima K, Nakagawa S, Sawayama H, Ishimoto T, Imai K, Iwatsuki M, et al. The microbiome and hepatobiliary-pancreatic cancers. *Cancer Lett.* (2017) 402:9–15. doi: 10.1016/j.canlet.2017.05.001
22. Gopalakrishnan V, Spencer CN, Nezi L, Reuben A, Andrews MC, Karpinets TV, et al. Gut microbiome modulates response to anti-PD-1 immunotherapy in melanoma patients. *Science.* (2018) 359:97–103. doi: 10.1126/science.aan4236
23. Mani S. Microbiota and breast cancer. *Approaches Underst Breast Cancer.* (2017) 151:217–29. doi: 10.1016/bs.pmbts.2017.07.004
24. Fleming C, Cai Y, Sun X, Jala VR, Xue F, Morrissey S, et al. Microbiota-activated CD103(+) DCs stemming from microbiota adaptation specifically drive gamma delta T17 proliferation and activation. *Microbiome.* (2017) 5:46. doi: 10.1186/s40168-017-0263-9
25. Hooper LV, Littman DR, Macpherson AJ. Interactions between the microbiota and the immune system. *Science.* (2012) 336:1268–73. doi: 10.1126/science.1223490
26. Lazar V, Ditu LM, Pircalabioru GG, Gheorghe I, Curutiu C, Holban AM, et al. Aspects of gut microbiota and immune system interactions in infectious diseases, immunopathology, and cancer. *Front Immunol.* (2018) 9:1830. doi: 10.3389/fimmu.2018.01830
27. Guerrero-Preston R, Godoy-Vitorino F, Jedlicka A, Rodríguez-Hilario A, González H, Bondy J, et al. 16S rRNA amplicon sequencing identifies microbiota associated with oral cancer, human papilloma virus infection and surgical treatment. *Oncotarget.* (2016) 7:51320–34. doi: 10.18632/oncotarget.9710
28. Aagaard K, Ma J, Antony KM, Ganu R, Petrosino J, Versalovic J. The placenta harbors a unique microbiome. *Sci Transl Med.* (2014) 6:237ra65. doi: 10.1126/scitranslmed.3008599
29. Jiang C, Wang H, Xia C, Dong Q, Chen E, Qiu Y, et al. A randomized, double-blind, placebo-controlled trial of probiotics to reduce the severity of oral mucositis induced by chemoradiotherapy for patients with nasopharyngeal carcinoma. *Cancer.* (2019) 125:1081–90. doi: 10.1002/cncr.31907
30. Yano JM, Yu K, Donaldson GP, Shastri GG, Ann P, Ma L, et al. Indigenous bacteria from the gut microbiota regulate host serotonin biosynthesis. *Cell.* (2015) 161:264–76. doi: 10.1016/j.cell.2015.02.047
31. Sarrouilhe D, Clarhaut J, Defamie N, Mesnil M. Serotonin and cancer: what is the link? *Curr Mol Med.* (2015) 15:62–77. doi: 10.2174/1566524015666150114113411
32. Dizeyi N, Bjartell A, Nilsson E, Hansson J, Gadaleanu V, Cross N, et al. Expression of serotonin receptors and role of serotonin in human prostate cancer tissue and cell lines. *Prostate.* (2004) 59:328–36. doi: 10.1002/pros.10374
33. Fatima S, Shi X, Lin Z, Chen GQ, Pan XH, Wu JC, et al. 5-Hydroxytryptamine promotes hepatocellular carcinoma proliferation by influencing β-catenin. *Mol Oncol.* (2016) 10:195–212. doi: 10.1016/j.molonc.2015.09.008
34. Liu S, Miao R, Zhai M, Pang Q, Deng Y, Liu S, et al. Effects and related mechanisms of serotonin on malignant biological behavior of hepatocellular carcinoma via regulation of Yap. *Oncotarget.* (2017) 8:47412–24. doi: 10.18632/oncotarget.17658
35. Soll C, Riener MO, Oberkofler CE, Hellerbrand C, Wild PJ, DeOliveira ML, et al. Expression of serotonin receptors in human hepatocellular cancer. *Clin Cancer Res.* (2012) 18:5902–10. doi: 10.1158/1078-0432.CCR-11-1813
36. Sui H, Xu H, Ji Q, Liu X, Zhou L, Song H, et al. 5-hydroxytryptamine receptor (5-HT1DR) promotes colorectal cancer metastasis by regulating Axin1/beta-catenin/MMP-7 signaling pathway. *Oncotarget.* (2015) 6:25975–87. doi: 10.18632/oncotarget.4543
37. Drozdov I, Kidd M, Gustafsson BI, Svejda B, Joseph R, Pfragner R, et al. Auto-regulatory effects of serotonin on proliferation and signaling pathways in lung and small intestine neuroendocrine tumor cell lines. *Cancer.* (2009) 115:4934–45. doi: 10.1002/cncr.24533
38. Jiang SH, Li J, Dong FY, Yang JY, Liu DJ, Yang XM, et al. (2017). Increased serotonin signaling contributes to the Warburg effect in pancreatic tumor cells under metabolic stress and promotes growth of pancreatic tumors in mice. *Gastroenterology.* 153:277–91.e19. doi: 10.1053/j.gastro.2017.03.008
39. Gurbuz N, Ashour AA, Alpay SN, Ozpolat B. Down-regulation of 5-HT1B and 5-HT1D receptors inhibits proliferation, clonogenicity and

invasion of human pancreatic cancer cells. *PLoS ONE.* (2014) 9:e105245. doi: 10.1371/journal.pone.0105245
40. Alpini G, Invernizzi P, Gaudio E, Venter J, Kopriva S, Bernuzzi F, et al. Serotonin metabolism is dysregulated in cholangiocarcinoma, which has implications for tumor growth. *Cancer Res.* (2008) 68:9184–93. doi: 10.1158/0008-5472.CAN-08-2133
41. Kopparapu PK, Tinzl M, Anagnostaki L, Persson JL, Dizeyi N. Expression and localization of serotonin receptors in human breast cancer. *Anticancer Res.* (2013) 33:363–70. doi: 10.1007/s10269-013-2254-1
42. Henriksen R, Dizeyi N, Abrahamsson PA. Expression of serotonin receptors 5-HT1A, 5-HT1B, 5-HT2B and 5-HT4 in ovary and in ovarian tumours. *Anticancer Res.* (2012) 32:1361−6. doi: 10.5455/medarh.2015.69.54-57
43. Merzak A, Koochekpour S, Fillion MP, Fillion G, Pilkington GJ. Expression of serotonin receptors in human fetal astrocytes and glioma cell lines: a possible role in glioma cell proliferation and migration. *Brain Res Mol Brain Res.* (1996) 41:1–7. doi: 10.1016/0169-328X(96)00058-7
44. Peters MAM, Meijer C, Fehrmann RSN, Walenkamp AME, Kema IP, de Vries EGE, et al. Serotonin and dopamine receptor expression in solid tumours including rare cancers. *Pathol Oncol Res.* (2019) p. 1–9. doi: 10.1007/s12253-019-00734-w
45. Senda S, Fujiyama Y, Ushijima T, Hodohara K, Bamba T, Hosoda S, et al. *Clostridium ramosum*, an IgA protease-producing species and its ecology in the human intestinal tract. *Microbiol Immunol.* (1985) 29:1019–28. doi: 10.1111/j.1348-0421.1985.tb00892.x
46. Mandić AD, Woting A, Jaenicke T, Sander A, Sabrowski W, Rolle-Kampcyk U, et al. *Clostridium ramosum* regulates enterochromaffin cell development and serotonin release. *Sci Rep.* (2019) 9:1177. doi: 10.1038/s41598-018-38018-z
47. Yu KJ, Hsu WL, Pfeiffer RM, Chiang CJ, Wang CP, Lou PJ, et al. Prognostic utility of anti-EBV antibody testing for defining NPC risk among individuals from high-risk NPC families. *Clin Cancer Res.* (2011) 17:1906–14. doi: 10.1158/1078-0432.CCR-10-1681
48. Liang Q, Chiu J, Chen Y, Huang Y, Higashimori A, Fang J, et al. Fecal bacteria act as novel biomarkers for noninvasive diagnosis of colorectal cancer. *Clin Cancer Res.* (2017) 23:2061–70. doi: 10.1158/1078-0432.CCR-16-1599
49. Yu J, Feng Q, Wong SH, Zhang D, Liang QY, Qin Y, et al. Metagenomic analysis of faecal microbiome as a tool towards targeted non-invasive biomarkers for colorectal cancer. *Gut.* (2017) 66:70–8. doi: 10.1136/gutjnl-2015-309800
50. Edge SB, Compton CC. The American Joint Committee on Cancer: the 7th Edition of the AJCC cancer staging manual and the future of TNM. *Ann Surg Oncol.* (2010) 17:1471–4. doi: 10.1245/s10434-010-0985-4
51. Spodick DH. The randomized controlled clinical trial. Scientific and ethical bases. *Am J Med.* (1982) 73:420–5. doi: 10.1016/0002-9343(82)90746-X
52. Gluud LL. Bias in clinical intervention research. *Am Journal Epidemiol.* (2006) 163:493–501. doi: 10.1093/aje/kwj069
53. Aagaard K, Petrosino J, Keitel W, Watson M, Katancik J, Garcia N, et al. The Human Microbiome Project strategy for comprehensive sampling of the human microbiome and why it matters. *FASEB J.* (2013) 27:1012–22. doi: 10.1096/fj.12-220806
54. Bürgmann H, Pesaro M, Widmer F, Zeyer J. A strategy for optimizing quality and quantity of DNA extracted from soil. *J Microbiol Methods.* (2001) 45:7–20. doi: 10.1016/S0167-7012(01)00213-5
55. Dauphin LA, Moser BD, Bowen MD. Evaluation of five commercial nucleic acid extraction kits for their ability to inactivate *Bacillus anthracis* spores and comparison of DNA yields from spores and spiked environmental samples. *J Microbiol Methods.* (2009) 76:30–7. doi: 10.1016/j.mimet.2008.09.004
56. Callahan BJ, McMurdie PJ, Rosen MJ, Han AW, Johnson AJ, Holmes SP. DADA2: high-resolution sample inference from Illumina amplicon data. *Nat Methods.* (2016) 13:581–3. doi: 10.1038/nmeth.3869
57. Bokulich NA, Kaehler BD, Rideout JR, Dillon M, Bolyen E, Knight R, et al. Optimizing taxonomic classification of marker-gene amplicon sequences with QIIME 2 ' s q2-feature-classifier plugin. *Microbiome.* (2018) 6:90. doi: 10.1186/s40168-018-0470-z
58. Love MI, Huber W, Anders S. Moderated estimation of fold change and dispersion for RNA-seq data with DESeq2. *Genome Biol.* (2014) 15:550. doi: 10.1186/s13059-014-0550-8
59. Mandal S, Van Treuren W, White RA, Eggesbø M, Knight R, Peddada SD. Analysis of composition of microbiomes: a novel method for studying microbial composition. *Microb Ecol Health Dis.* (2015) 26:27663. doi: 10.3402/mehd.v26.27663
60. Benjamini Y, Hochberg Y. Controlling the false discovery rate: a practical and powerful approach to multiple testing. *J R Stat Soc Ser B.* (1995) 57:289–300. doi: 10.1111/j.2517-6161.1995.tb02031.x
61. Lai Y. A statistical method for the conservative adjustment of false discovery rate (q-value). *BMC Bioinformatics.* (2017) 18:69. doi: 10.1186/s12859-017-1474-6
62. Ye Z, Zhang N, Wu C, Zhang X, Wang Q, Huang X, et al. A metagenomic study of the gut microbiome in Behcet's disease. *Microbiome.* (2018) 6:135. doi: 10.1186/s40168-018-0520-6
63. Klaassen MAY, Imhann F, Collij V, Fu J, Wijmenga C, Zhernakova A, et al. Anti-inflammatory gut microbial pathways are decreased during Crohn's Disease exacerbations. *J Crohn's Colitis.* (2019) 13:1439–49. doi: 10.1093/ecco-jcc/jjz077
64. Fang S, Xiong X, Su Y, Huang L, Chen C. 16S rRNA gene-based association study identified microbial taxa associated with pork intramuscular fat content in feces and cecum lumen. *BMC Microbiol.* (2017) 17:162. doi: 10.1186/s12866-017-1055-x
65. Vázquez-Baeza Y, Pirrung M, Gonzalez A, Knight R. EMPeror: a tool for visualizing high-throughput microbial community data. *Gigascience.* (2013) 2:16. doi: 10.1186/2047-217X-2-16
66. Rohart F, Gautier B, Singh A, Lê Cao KA. mixOmics: An R package for 'omics feature selection and multiple data integration. *PLoS Comp Biol.* (2017) 13:e1005752. doi: 10.1371/journal.pcbi.1005752
67. McCune, B., and Grace, J. B. *Analysis of Ecological Communities*. Gleneden Beach, OR: MjM software design (2002).
68. Dixon P. VEGAN, a package of R functions for community ecology. *J Veg Sci.* (2003) 14:927–30. doi: 10.1111/j.1654-1103.2003.tb02228.x
69. Langille MG, Zaneveld J, Caporaso JG, McDonald D, Knights D, Reyes JA, et al. Predictive functional profiling of microbial communities using 16S rRNA marker gene sequences. *Nat Biotechnol.* (2013) 31:814–21. doi: 10.1038/nbt.2676
70. Parks DH, Tyson GW, Hugenholtz P, Beiko RG. STAMP: statistical analysis of taxonomic and functional profiles. *Bioinformatics.* (2014) 30:3123–4. doi: 10.1093/bioinformatics/btu494
71. Jean Dunn O. Multiple comparisons among means. *J Am Stat Assoc.* (1961) 56:52–64. doi: 10.1080/01621459.1961.10482090
72. Ringnér M. What is principal component analysis? *Nat Biotechnol.* (2008) 26:303–4. doi: 10.1038/nbt0308-303
73. Chen X, Fruehauf J, Goldsmith JD, Xu H, Katchar KK, Koon HW, et al. *Saccharomyces boulardii* inhibits EGF receptor signaling and intestinal tumor growth in Apc(min) mice. *Gastroenterology.* (2009) 137:914–23. doi: 10.1053/j.gastro.2009.05.050
74. Miquel S, Martín R, Rossi O, Bermúdez-Humarán LG, Chatel JM, Sokol H, et al. Faecalibacterium prausnitzii and human intestinal health. *Curr Opin Microbiol.* (2013) 16:255–61. doi: 10.1016/j.mib.2013.06.003
75. Fisher K, Phillips C. The ecology, epidemiology and virulence of Enterococcus. *Microbiology.* (2009) 155:1749–57. doi: 10.1099/mic.0.026385-0
76. Waskito LA, Salama NR, Yamaoka Y. Pathogenesis of *Helicobacter pylori* infection. *Helicobacter.* (2018) 23(Suppl.1):e12516. doi: 10.1111/hel.12516
77. Chang AH, Parsonnet J. Role of bacteria in oncogenesis. *Clin Microbiol Rev.* (2010) 23:837–57. doi: 10.1128/CMR.00012-10
78. Shin NR, Whon TW, Bae JW. Proteobacteria: microbial signature of dysbiosis in gut microbiota. *Trends Biotechnol.* (2015) 33:496–503. doi: 10.1016/j.tibtech.2015.06.011
79. Kapil S, Duseja A, Sharma BK, Singla B, Chakraborti A, Das A, et al. Small intestinal bacterial overgrowth and toll-like receptor signaling in patients with non-alcoholic fatty liver disease. *J Gastroenterol Hepatol.* (2016) 31:213–21. doi: 10.1111/jgh.13058
80. Michail S, Lin M, Frey MR, Fanter R, Paliy O, Hilbush B, et al. Altered gut microbial energy and metabolism in children with non-alcoholic fatty liver disease. *FEMS Microbiol Ecol.* (2015) 91:1–9. doi: 10.1093/femsec/fiu002

81. Maharshak N, Packey CD, Ellermann M, Manick S, Siddle JP, Huh EY, et al. Altered enteric microbiota ecology in interleukin 10-deficient mice during development and progression of intestinal inflammation. *Gut Microbes.* (2013) 4:316–24. doi: 10.4161/gmic.25486
82. Selvanantham T, Lin Q, Guo CX, Surendra A, Fieve S, Escalante NK, et al. NKT Cell-deficient mice harbor an altered microbiota that fuels intestinal inflammation during chemically induced colitis. *J Immunol.* (2016) 197:4464–72. doi: 10.4049/jimmunol.1601410
83. Peterson DA, McNulty NP, Guruge JL, Gordon JI. IgA response to symbiotic bacteria as a mediator of gut homeostasis. *Cell Host Microbe.* (2007) 2:328–39. doi: 10.1016/j.chom.2007.09.013
84. Rehman A, Lepage P, Nolte A, Hellmig S, Schreiber S, Ott SJ. Transcriptional activity of the dominant gut mucosal microbiota in chronic inflammatory bowel disease patients. *J Med Microbiol.* (2010) 59:1114–22. doi: 10.1099/jmm.0.021170-0
85. Sartor RB. Microbial influences in inflammatory bowel diseases. *Gastroenterology.* (2008) 134:577–94. doi: 10.1053/j.gastro.2007.11.059
86. Gophna U, Sommerfeld K, Gophna S, Doolittle WF, Veldhuyzen van Zanten SJ. Inerences between tissue-associated intestinal microfloras of patients with Crohn's disease and ulcerative colitis. *J Clin Microbiol.* (2006) 44:4136–41. doi: 10.1128/JCM.01004-06
87. Marri PR, Stern DA, Wright AL, Billheimer D, Martinez FD. Asthma-associated differences in microbial composition of induced sputum. *J Aller Clin Immunol.* (2013) 131:346–52.e1-3. doi: 10.1016/j.jaci.2012.11.013
88. Pragman AA, Kim HB, Reilly CS, Wendt C, Isaacson RE. The lung microbiome in moderate and severe chronic obstructive pulmonary disease. *PLoS ONE.* (2012) 7:e47305. doi: 10.1371/journal.pone.0047305
89. Zhu XX, Yang XJ, Chao YL, Zheng HM, Sheng HF, Liu HY, et al. The potential effect of oral microbiota in the prediction of mucositis during radiotherapy for nasopharyngeal carcinoma. *Ebiomedicine.* (2017) 18:23–31. doi: 10.1016/j.ebiom.2017.02.002
90. Nakamoto N, Kanai T. Role of Toll-like receptors in immune activation and tolerance in the liver. *Front Immunol.* (2014) 5:221. doi: 10.3389/fimmu.2014.00221
91. García-Jiménez A, Prim N, Crusi X, Benito N. Septic arthritis due to *Clostridium ramosum*. *Semin Arthritis Rheum.* (2016) 45:617–20. doi: 10.1016/j.semarthrit.2015.09.009
92. Brook I. Clostridial infections in children: spectrum and management. *Curr Infect Dis Rep.* (2015) 17:8. doi: 10.1007/s11908-015-0503-8
93. Forrester JD, Spain DA. *Clostridium ramosum* bacteremia: case report and literature review. *Surg Infect.* (2014) 15:343–6. doi: 10.1089/sur.2012.240
94. O'Mahony SM, Clarke G, Borre YE, Dinan TG, Cryan JF. Serotonin, tryptophan metabolism and the brain-gut-microbiome axis. *Behav Brain Res.* (2015) 277:32–48. doi: 10.1016/j.bbr.2014.07.027
95. Ge X, Pan J, Liu Y, Wang H, Zhou W, Wang X. intestinal crosstalk between microbiota and serotonin and its impact on gut motility. *Curr Pharm Biotechnol.* (2018) 19:190–5. doi: 10.2174/1389201019666180528094202
96. Hoffman JM, Tyler K, MacEachern SJ, Balemba OB, Johnson AC, Brooks EM, et al. Activation of colonic mucosal 5-HT4 receptors accelerates propulsive motility and inhibits visceral hypersensitivity. *Gastroenterology.* (2012) 142:844–54.e4. doi: 10.1053/j.gastro.2011.12.041
97. Mercado CP, Quintero MV, Li Y, Singh P, Byrd AK, Talabnin K, et al. A serotonin-induced N-glycan switch regulates platelet aggregation. *Sci Rep.* (2013) 3:2795. doi: 10.1038/srep02795
98. Baganz NL, Blakely RD. A Dialogue between the immune system and brain, spoken in the language of serotonin. *ACS Chem Neurosci.* (2013) 4:48–63. doi: 10.1021/cn300186b
99. Sarrouilhe D, Mesnil M. Serotonin and human cancer: A critical view. *Biochimie.* (2019) 161:46–50. doi: 10.1016/j.biochi.2018.06.016
100. Zhang T, Li Q, Cheng L, Buch H, Zhang F. Akkermansia muciniphila is a promising probiotic. *Microb Biotechnol.* (2019) 12:1109–25. doi: 10.1111/1751-7915.13410
101. Derrien M, Belzer C, de Vos WM. Akkermansia muciniphila and its role in regulating host functions. *Microb Pathog.* (2017) 106:171–81. doi: 10.1016/j.micpath.2016.02.005
102. Niederreiter L, Adolph TE, Tilg H. Food, microbiome and colorectal cancer. *Dig Liver Dis.* (2018) 50:647–52. doi: 10.1016/j.dld.2018.03.030
103. Frugé AD, Van der Pol W, Rogers LQ, Morrow CD, Tsuruta Y, Demark-Wahnefried W. Fecal Akkermansia muciniphila is associated with body composition and microbiota diversity in overweight and obese women with breast cancer participating in a presurgical weight loss trial. *J Acad Nutr Diet.* (2018). doi: 10.1016/j.jand.2018.08.164. [Epub ahead of print].
104. Corfe BM. Hypothesis: butyrate is not an HDAC inhibitor, but a product inhibitor of deacetylation. *Mol BioSyst.* (2012) 8:1609–12. doi: 10.1039/c2mb25028d
105. Donohoe DR, Collins LB, Wali A, Bigler R, Sun W, Bultman SJ. The Warburg effect dictates the mechanism of butyrate-mediated histone acetylation and cell proliferation. *Mol Cell.* (2012) 48:612–26. doi: 10.1016/j.molcel.2012.08.033
106. Vander Heiden MG, Cantley LC, Thompson CB. Understanding the Warburg effect: the metabolic requirements of cell proliferation. *Science.* (2009) 324:1029–33. doi: 10.1126/science.1160809
107. Hedin CR, McCarthy NE, Louis P, Farquharson FM, McCartney S, Taylor K, et al. Altered intestinal microbiota and blood T cell phenotype are shared by patients with Crohn's disease and their unaffected siblings. *Gut.* (2014) 63:1578–86. doi: 10.1136/gutjnl-2013-306226
108. De Cruz P, Kang S, Wagner J, Buckley M, Sim WH, Prideaux L, et al. Association between specific mucosa-associated microbiota in Crohn's disease at the time of resection and subsequent disease recurrence: a pilot study. *J Gastroenterol Hepatol.* (2015) 30:268–78. doi: 10.1111/jgh.12694
109. Pérez-Jacoiste Asín MA, Fernández-Ruiz M, Serrano-Navarro I, Prieto-Rodriguez S, Aguado JM. Polymicrobial endocarditis involving Veillonella parvula in an intravenous drug user: case report and literature review of Veillonella endocarditis. *Infection.* (2013) 41:591–4. doi: 10.1007/s15010-012-0398-3
110. Bhatti MA, Frank MO. Veillonella parvula meningitis: case report and review of Veillonella infections. *Clin Infect Dis.* (2000) 31:839–40. doi: 10.1086/314046
111. Fisher RG, Denison MR. Veillonella parvula bacteremia without an underlying source. *J Clin Microbiol.* (1996) 34:3235–6. doi: 10.1002/(SICI)1097-4660(199612)67:4<397::AID-JCTB588>3.0.CO;2-D
112. Wei Y, Li Y, Yan L, Sun C, Miao Q, Wang Q, et al. Alterations of gut microbiome in autoimmune hepatitis. *Gut.* (2019). doi: 10.1136/gutjnl-2018-317836. [Epub ahead of print].
113. Wang SS, Lee NY, Hsueh PR, Huang WH, Tsui KC, Lee HC, et al. Clinical manifestations and prognostic factors in cancer patients with bacteremia due to extended-spectrum β-lactamase-producing *Escherichia coli* or Klebsiella pneumoniae. *J Microbiol Immunol Infect.* (2011) 44:282–8. doi: 10.1016/j.jmii.2010.08.004
114. Villafuerte KRV, Martinez CJH, Dantas FT, Carrara HHA, Dos Reis FJC, Palioto DB. The impact of chemotherapeutic treatment on the oral microbiota of patients with cancer: a systematic review. *Oral Surg Oral Med Oral Pathol Oral Radiol.* (2018) 125:552–66. doi: 10.1016/j.oooo.2018.02.008
115. Taft DH, Liu J, Maldonado-Gomez MX, Akre S, Huda MN, Ahmad SM, et al. Bifidobacterial dominance of the gut in early life and acquisition of antimicrobial resistance. *Msphere.* (2018) 3:e00441-18. doi: 10.1128/mSphere.00441-18
116. Belenguer A, Duncan SH, Calder AG, Holtrop G, Louis P, Lobley GE, et al. Two routes of metabolic cross-feeding between Bifidobacterium adolescentis and butyrate-producing anaerobes from the human gut. *Appl Environ Microbiol.* (2006) 72:3593–9. doi: 10.1128/AEM.72.5.3593-3599.2006
117. Reichardt N, Duncan SH, Young P, Belenguer A, McWilliam Leitch C, Scott KP, et al. Phylogenetic distribution of three pathways for propionate production within the human gut microbiota. *ISME J.* (2014) 8:1323–35. doi: 10.1038/ismej.2014.14
118. Koh A, De Vadder F, Kovatcheva-Datchary P, Bäckhed F. From dietary fiber to host physiology: short-chain fatty acids as key bacterial metabolites. *Cell.* (2016) 165:1332–45. doi: 10.1016/j.cell.2016.05.041
119. Imaoka A, Shima T, Kato K, Mizuno S, Uehara T, Matsumoto S, et al. Anti-inflammatory activity of probiotic Bifidobacterium: enhancement of IL-10 production in peripheral blood mononuclear cells from ulcerative colitis patients and inhibition of IL-8 secretion in HT-29 cells. *World J Gastroenterol.* (2008) 14:2511–6. doi: 10.3748/wjg.14.2511

120. Khokhlova EV, Smeianov VV, Efimov BA, Kafarskaia LI, Pavlova SI, Shkoporov AN. Anti-inflammatory properties of intestinal Bifidobacterium strains isolated from healthy infants. *Microbiol. Immunol.* (2012) 56:27–39. doi: 10.1111/j.1348-0421.2011.00398.x
121. Okada Y, Tsuzuki Y, Hokari R, Komoto S, Kurihara C, Kawaguchi A, et al. Anti-inflammatory effects of the genus Bifidobacterium on macrophages by modification of phospho-I kappaB and SOCS gene expression. *Int J Exp Pathol.* (2009) 90:131–40. doi: 10.1111/j.1365-2613.2008.00632.x
122. Wang, Z., Wang, J., Cheng,. Y., Liu, X., and Huang, Y. (2011). Secreted factors from *Bifidobacterium animalis* subsp. lactis inhibit NF-κB-mediated interleukin-8 gene expression in Caco-2 cells. *Appl Environ Microbiol.* 77:8171–4. doi: 10.1128/AEM.06145-11
123. Kawabata K, Baba N, Sakano T, Hamano Y, Taira S, Tamura A, et al. Functional properties of anti-inflammatory substances from quercetin-treated *Bifidobacterium adolescentis*. *Biosci Biotechnol Biochem.* (2018) 82:689–97. doi: 10.1080/09168451.2017.1401916
124. Kawabata K, Kato Y, Sakano T, Baba N, Hagiwara K, Tamura A, et al. Effects of phytochemicals on *in vitro* anti-inflammatory activity of *Bifidobacterium adolescentis*. *Biosci Biotechnol Biochem.* (2015) 79:799–807. doi: 10.1080/09168451.2015.1006566
125. Kawabata K, Sugiyama Y, Sakano T, Ohigashi H. Flavonols enhanced production of anti-inflammatory substance(s) by *Bifidobacterium adolescentis*: prebiotic actions of galangin, quercetin, and fisetin. *Biofactors.* (2013) 39:422–9. doi: 10.1002/biof.1081
126. Escobar JS, Klotz B, Valdes BE, Agudelo GM. The gut microbiota of Colombians differs from that of Americans, Europeans and Asians. *BMC Microbiol.* (2014) 14:311. doi: 10.1186/s12866-014-0311-6
127. Goodrich JK, Waters JL, Poole AC, Sutter JL, Koren O, Blekhman R, et al. Human genetics shape the gut microbiome. *Cell.* (2014) 159:789–99. doi: 10.1016/j.cell.2014.09.053
128. Walters WA, Xu Z, Knight R. Meta-analyses of human gut microbes associated with obesity and IBD. *FEBS Lett.* (2014) 588:4223–33. doi: 10.1016/j.febslet.2014.09.039
129. Zhu L, Baker SS, Gill C, Liu W, Alkhouri R, Baker RD, et al. Characterization of gut microbiomes in nonalcoholic steatohepatitis (NASH) patients: a connection between endogenous alcohol and NASH. *Hepatology.* (2013) 57:601–9. doi: 10.1002/hep.26093
130. Kohl KD, Amaya J, Passement CA, Dearing MD, McCue MD. Unique and shared responses of the gut microbiota to prolonged fasting: a comparative study across five classes of vertebrate hosts. *FEMS Microbiol Ecol.* (2014) 90:883–94. doi: 10.1111/1574-6941.12442
131. David LA, Maurice CF, Carmody RN, Gootenberg DB, Button JE, Wolfe BE, et al. Diet rapidly and reproducibly alters the human gut microbiome. *Nature.* (2014) 505:559–63. doi: 10.1038/nature12820
132. Keren N, Konikoff FM, Paitan Y, Gabay G, Reshef L, Naftali T, et al. Interactions between the intestinal microbiota and bile acids in gallstones patients. *Environ Microbiol Rep.* (2015) 7:874–80. doi: 10.1111/1758-2229.12319
133. Li F, Duan F, Zhao X, Song C, Cui S, Dai L. Red meat and processed meat consumption and nasopharyngeal carcinoma risk: a dose-response meta-analysis of observational studies. *Nutr Cancer Int J.* (2016) 68:1034–43. doi: 10.1080/01635581.2016.1192200
134. Weng M-T, Chiu Y-T, Wei P-Y, Chiang C-W, Fang H-L, Wei S-C. Microbiota and gastrointestinal cancer. *J Formos Med Assoc.* (2019) 118:S32–41. doi: 10.1016/j.jfma.2019.01.002
135. Tang LL, Chen WQ, Xue WQ, He YQ, Zheng RS, Zeng YX, et al. Global trends in incidence and mortality of nasopharyngeal carcinoma. *Cancer Lett.* (2016) 374:22–30. doi: 10.1016/j.canlet.2016.01.040

Conflict of Interest: The authors declare that the research was conducted in the absence of any commercial or financial relationships that could be construed as a potential conflict of interest.

frontiers in Oncology

ORIGINAL RESEARCH
published: 24 January 2020
doi: 10.3389/fonc.2020.00015

Differentiation of Cervical Spine Osteoradionecrosis and Bone Metastasis After Radiotherapy Detected by Bone Scan in Patients With Nasopharyngeal Carcinoma: Role of Magnetic Resonance Imaging

Xi Zhong[1†], Li Li[2†], Bingui Lu[1], Hainan Zhang[1], Lu Huang[1], Xinjia Lin[1], Jiansheng Li[1] and Jian Zhang[3*]*

[1] Department of Radiology, Affiliated Cancer Hospital & Institute of Guangzhou Medical University, Guangzhou, China,
[2] Department of Otolaryngology, The Third Affiliated Hospital of Guangzhou Medical University, Guangzhou, China,
[3] Department of Radiation Oncology, Affiliated Cancer Hospital & Institute of Guangzhou Medical University, Guangzhou, China

OPEN ACCESS

Edited by:
Jan Baptist Vermorken,
University of Antwerp, Belgium

Reviewed by:
Maria Cossu Rocca,
European Institute of Oncology (IEO), Italy
Cesare Piazza,
Fondazione IRCCS Istituto Nazionale dei Tumori, Italy

***Correspondence:**
Jiansheng Li
lijiansheng@gzhmu.edu.cn
Jian Zhang
zhangjian@gzhmu.edu.cn

[†]These authors have contributed equally to this work

Specialty section:
This article was submitted to Head and Neck Cancer, a section of the journal Frontiers in Oncology

Received: 07 November 2019
Accepted: 07 January 2020
Published: 24 January 2020

Citation:
Zhong X, Li L, Lu B, Zhang H, Huang L, Lin X, Li J and Zhang J (2020) Differentiation of Cervical Spine Osteoradionecrosis and Bone Metastasis After Radiotherapy Detected by Bone Scan in Patients With Nasopharyngeal Carcinoma: Role of Magnetic Resonance Imaging. Front. Oncol. 10:15. doi: 10.3389/fonc.2020.00015

Background: Osteoradionecrosis (ORN) of the cervical spine is a serious complication after radiotherapy (RT), which may show increased radiotracer uptake on a bone scan (BS) and be mistaken as metastasis. We aimed to assess the value of magnetic resonance imaging (MRI) in the differentiation of cervical spine ORN from bone metastasis after RT detected by BS in nasopharyngeal carcinoma (NPC).

Methods: In this retrospective study, 35 NPC patients who had undergone RT were enrolled, of whom 21 patients showed cervical spine ORN and 14 showed bone metastasis. New areas of increased radiotracer uptake in the cervical spine on a BS were noted in all patients, following which the patients underwent neck MRI for further assessment. Two radiologists independently reviewed two sets of images including a BS set and an MRI set (MRI with BS) and reached a consensus. The diagnostic sensitivity, specificity, and accuracy for ORN detection were calculated, and interobserver agreement was evaluated using the kappa test.

Results: A total of 75 cervical spine lesions were identified (44, ORN; 31 metastases). The BS set analysis showed that the diagnostic sensitivity, specificity, and accuracy were only 38.6, 48.3, and 42.7%, respectively, for differentiation of cervical spine ORN from bone metastasis. On the other hand, the MRI set analysis showed that the diagnostic sensitivity, specificity, and accuracy increased to 86.4, 90.3, and 88.0%, respectively. The interobserver agreement for the MRI set was determined to be very good ($\kappa = 0.92$).

Conclusion: MRI is a reliable technique for the further discrimination of emerging cervical spine lesions after RT detected by BS. Furthermore, it could be a better differential diagnosis technique for distinguishing ORN from metastasis and may help avoid a wrong assignment of the patient to a metastatic stage with indication for treatment with supplemental toxicity and a subsequent palliative strategy.

Keywords: nasopharyngeal carcinoma, osteoradionecrosis, cervical spine, magnetic resonance imaging, bone scan

INTRODUCTION

Nasopharyngeal carcinoma (NPC) is a malignant tumor with a very unique geographic distribution; it is mainly prevalent in southern China and Southeast Asia (1, 2). In the regions with NPC prevalence, NPC has been reported in approximately 50 per 100,000 persons annually and this incidence is almost 50 times higher than that in western countries (2). Radiotherapy (RT) has been identified as the primary therapeutic method for NPC, and post-RT adverse events have drawn a great deal of attention.

Post-RT adverse events in patients with NPC involving the central nervous system, including radiation encephalopathy, diffuse white matter injury, and optic neuritis, have been well-described (3). Osteoradionecrosis (ORN), with an incidence of 10.1%, is also a common complication after RT; it frequently develops in the mandible, maxilla, and skull base (4–6). Nevertheless, ORN in the cervical spine has been regarded as a rare complication, although the cervical vertebrae are often included in the irradiation field (6–9). Sometimes, cervical spine ORN may be misdiagnosed as bone metastasis, which may lead to patients accepting an unnecessary biopsy or harmful chemoradiotherapy (10–12).

Modern medical imaging has played a great role in the detection and characterization of bone disorders. Bone scan (BS) is considered as a sensitive enough technique for the detection of bone marrow diseases and has been widely applied for monitoring bone metastasis in patients with a malignancy (13). However, BS has a limitation in terms of specificity, because RT-induced bone complications, acute osteoporotic fractures, and the metastases may all result in increased uptake (14–16). MRI is quite sensitive for the detection of reactive marrow edema and fatty changes, and very helpful for the detection of soft-tissue masses. MRI has been proven to be valuable for distinguishing benign and malignant compression spinal fractures (17, 18), and differentiating RT-induced insufficiency fractures from metastases (14). However, few studies have assessed the MRI findings of ORN (10–12), and the role of MRI in the distinction of cervical spine ORN and metastasis remains unknown. Thus, the purpose of this study was to assess the additional value of MRI in the identification of cervical spine ORN and metastasis after radiotherapy in patients with NPC detected by BS.

MATERIALS AND METHODS

Patient Samples

The ethics committee of Affiliated Cancer Hospital & Institute of Guangzhou Medical University approved this retrospective study, and the requirement of patients' informed consent was waived. Between January 2013 and December 2016, data were reviewed for 2046 consecutive patients with pathology-proven NPC after RT. We found 73 patients showed new cervical spine lesions at follow-up BS. The following patients were included in this study: (1) patients with emerging areas of abnormal uptake in the cervical spine; (2) patients who underwent neck MRI for further assessment; and (3) patients for whom sufficient clinical and MRI follow-up data were available to resolve the diagnosis of lesions. The following patients were excluded from the study: (1) patients with an abnormal signal in the cervical spine on pretreatment MRI, (2) patients for whom MRI data were unavailable after lesion detection by BS; and (3) patients in whom the diagnosis of lesions could not be confirmed. Finally, 35 NPC patients who had undergone RT were enrolled, of whom 21 patients showed cervical spine ORN and 14 showed bone metastasis. The patient selection flowchart is shown in **Figure 1**.

MRI Acquisition

MRI was performed using a 1.5-T system unit (Achieva, Philips) with a 16-channel head-neck combined coil. The sequences included axial turbo spin-echo (TSE) T1-weighted imaging (T1WI); the parameters were as follows: TR/TE, 545/14 ms; field of view (FOV), 23 cm; slice thickness, 4 mm; gap, 4 mm; and matrix size, 328 × 220. Axial TSE T2-weighted imaging (T2WI) was also performed, the parameters for which were as follows: TR/TE, 3193/80 ms; FOV, 23 cm; slice thickness, 5 mm; gap, 5 mm; and matrix size, 228 × 185. Furthermore, coronal fat-suppression (FS) T2-weighted imaging (FS-T2WI) was performed, the parameters for which were as follows: TR/TE, 3224/165 ms; FOV, 26 cm; slice thickness, 5 mm; gap, 5 mm; and matrix size, 312 × 163. Axial and sagittal FS contrast-enhanced T1WI was also employed; parameters of contrast-enhanced T1WI were the same as those for the pre-enhanced T1WI in addition to the FS technique. Enhanced T1WI was performed after the patients had received intravenous gadopentetate dimeglumine (Magnevist, Bayer Schering) at a dose of 0.1 mmol/kg.

BS Acquisition

Whole-body BS was performed using a Philips SPECT scanner (Netherlands). Both anterior and posterior whole-body bone images were obtained 3 h after intravenous injection of 15–25 mCi 99 mTc-MDP; the scan parameters were as follows: matrix,

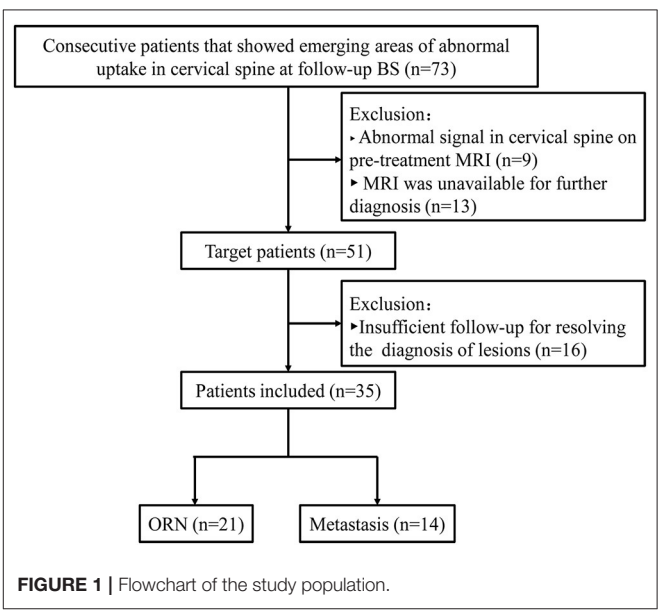

FIGURE 1 | Flowchart of the study population.

256 × 1,024; scanning speed, 15 cm/min; and acquisition energy window, 140 keV (±7.5%).

Image Analysis

All images were independently reviewed by two radiologists (observer 1, J.S.L, with 12 years of experience; observer 2, B.G.L, with 15 years of experience) and an agreement was reached. Two sets of images were designed to differentiate cervical spine ORN and metastasis, including a BS (BS images alone) set and an MRI set (MR images and BS images). Observers were only aware of the RT history but were blinded to patients' other clinical records, other imaging examination (CT, PET/CT) data, and the final diagnosis. Regarding the qualitative diagnosis, all cervical spine lesions were classified on a three-point scale as benign, malignant, or equivocal.

In the BS analysis, the observers were requested to record the abnormal uptake location and number of the cervical spine, as well as whether abnormal uptake was noted in other anatomical locations except for the cervical spine. If focal radiotracer uptake was greater than that in the anterior iliac spine, the lesion was classified as malignant (13, 17). A lesion was classified as benign if radiotracer uptake was equal to or lower than that in the anterior iliac spine and no abnormal uptake was noted in other anatomical locations except for the cervical spine. If a lesion was not classified as malignant or benign, it was classified as equivocal.

In the MRI set analysis, the number, location, MR signal characteristics (bone marrow edema change, degree, and pattern of enhancement), vertebral destruction, and body collapse of cervical spine lesions were recorded; any associated paravertebral soft-tissue masses were also recorded. In addition, other ancillary features were also documented, including abnormal enhancement or necrosis of the paravertebral muscle, abnormal neck lymphadenopathy (short axis larger than 1 cm), and radiation encephalopathy (REP). Regarding the qualitative diagnosis, the criteria for lesion classification as malignant were as follows: (1) presence of a distinct soft-tissue mass with abnormal enhancement on MRI (10, 17); and (2) absence of a distinct soft-tissue mass but presence of marked vertebral and heterogeneous enhancement on MRI and involvement of abnormal neck lymphadenopathy or meeting of the BS criteria for malignancy. The criteria for lesion classification as benign were as follows: (1) presence of only reactive marrow edema change with or without paravertebral muscle edema (19, 20); and (2) presence of an abnormal signal change on unenhanced images and homogeneous enhancement on contrast-enhanced images, and meeting of the BS criteria for benign lesions. If a lesion was not classified as malignant or benign, it was classified as equivocal.

Reference Standard

The final diagnosis of a cervical spine lesion was based on all available imaging investigations, clinical data, and follow-up MRI data for at least 6 months. The reference standard was as follows (10, 19): (1) lesions that shrank or remained stationary at MRI for more than 6 months without radiotherapy and/or chemotherapy were interpreted as ORN; and (2) lesions with progressive enlargement that presented as soft-tissue masses or distinctly regressed after radiotherapy and/or chemotherapy were identified as metastases. If a lesion's nature could not be confirmed by a follow-up procedure, it was excluded.

Statistical Analysis

Categorical data were expressed as numbers and frequencies (%), and continuous data were expressed as median and range. Interobserver agreement between observers was assessed using the kappa test and defined as follows (21): $1 \geq k > 0.8$, very good; $0.8 \geq k > 0.6$, good; $0.6 \geq k > 0.4$, moderate; $0.4 \geq k > 0.2$, fair; and $0.2 \geq k > 0$, poor. The diagnostic sensitivity, specificity, and accuracy were calculated based on the diagnostic scale. Pearson chi-square test (or Fisher test) was used for comparing differences in the incidence of imaging features between ORN and bone metastasis. Statistical tests were performed using SPSS 16.0 (SPSS Inc., Chicago, IL, USA); $P < 0.05$ indicated statistical significance.

RESULT

Patient Characteristics

A total of 35 patients were included, 60% (21/35) of whom were diagnosed with cervical spine ORN and 40% (14/35) were identified as metastasis. Among the patients with ORN, 23.8% (5/21) had undergone repeat RT to the neck, 66.7% (14/21) had developed ORN at multiple locations, and 76.2% (16/21) were symptomatic. In the patients with metastasis, 7.1% (1/14) had undergone repeat RT to the neck, 57.1% (8/14) had multiple lesions, and 57.1% (8/14) were symptomatic. Detailed patient characteristics are shown in **Table 1**.

TABLE 1 | Characteristics of NPC patients after RT enrolled in the study.

Characteristics	ORN ($n = 21$)	Metastasis ($n = 14$)
Median age (range)	51 (30–80) years	43 (23–65) years
Male/Female	17/4	9/5
RT dose (rang)	81 (68–154) Gy	74 (58–128) Gy
Median interval between RT and lesion detection (rang)	10 (2–96) months	10 (4–24) months
Overall stage#		
I	6 (28.6%)	1 (7.2%)
II	8 (38.1%)	3 (21.4%)
III	5 (23.8%)	7 (50.0%)
IV	2 (9.5%)	3 (21.4%)
Received repeat rt to the neck		
Yes	5 (23.8%)	1 (7.2%)
No	16 (76.2%)	13 (92.8%)
Clinical symptoms*		
Neck pain	16 (76.2%)	9 (64.3%)
Infection	6 (28.6%)	1 (7.2%)
Asymptomatic	5 (23.8%)	6 (42.8%)
Involvement of multiple lesions		
Yes	14 (66.7%)	8 (57.1%)
No	7 (33.3%)	6 (42.9%)

#According to the 7th UICC/AJCC staging system.
**A patient may show neck pain with infection.*
ORN, osteoradionecrosis.

Numbers and Locations of ORN and Metastasis of the Cervical Spine

Based on the reference standard, a total of 75 cervical spine lesions were identified, including 44 cases of ORN and 31 of metastases. As shown in **Table 2**, ORN most frequently developed in C1/C2 (**Figures 2–4**), accounting for 47.7% (21/44) of all lesions; the detailed locations of the ORN were as follows: C1, 10 sites; C2, 11 sites; C3, 5 sites; C4, 6 sites; C5, 6 sites; C6, 5 sites; and C7, 1 site. Cervical spine metastases were located at C1 (7 sites), C2 (5 sites), C3 (5 sites), C4 (3 sites), C5 (5 sites), C6 (4 sites), and C7 (2 sites).

BS Findings and Diagnostic Performance

As shown in **Table 3**, in the patient-wise analysis, the incidence of involvement with abnormal uptake in other anatomical locations except for the cervical spine in the metastasis group (**Figures 5**, **6**) was significantly higher than that in the ORN group (**Figure 2**) [64.3% (9/14) vs. 23.8% (5/21)], $P = 0.016$). In the lesion-wise analysis, only 61.4% (27/44) of the ORNs and 80.6% (25/31) of the metastases were detected on BS. The incidence of focal radiotracer uptake greater than the anterior iliac spine in metastases (**Figures 5**, **6**) was significantly higher than that in ORNs (**Figure 3**) [48.4% (15/31) vs. 11.4% (5/44), $P < 0.001$].

The qualitative assessment showed that 17 lesions of the 27 ORNs detected on BS were interpreted as benign, 5 lesions were classified as malignant, and the remaining 5 lesions showed equivocal findings; 15 lesions of the 25 metastases detected on BS were interpreted as malignant, 2 lesions were classified as benign, and the remaining 8 lesions showed equivocal findings. The diagnostic sensitivity, specificity and accuracy in the discrimination of ORN from metastasis were 38.6% (17/44), 48.3% (15/31), and 42.7% (32/75), respectively. The interobserver agreement between the two observers in the BS set was determined to be good ($k = 0.77$).

TABLE 2 | Number and locations of the ORN and metastasis of the cervical spine.

Location	ORN	Metastasis	Total
C1	10	7	17
C2	11	5	16
C3	5	5	10
C4	6	3	9
C5	6	5	11
C6	5	4	9
C7	1	2	3
Total	44	31	75

ORN, Osteoradionecrosis.

MRI Findings and Additional Diagnostic Performance

As shown in **Table 3**, in the patient-wise analysis, the incidence of involvement with cervical lymphadenopathy in the metastasis group (**Figure 6B**) was significantly higher than that in the ORN group [78.5% (11/14) vs. 9.5% (2/21), $P = 0.002$]. In the lesion-wise analysis, all lesions were detected by MRI, and the incidences of vertebral marrow edema (**Figures 2B**, **4B**) and paravertebral muscle edema (**Figure 3D**) in ORNs were significantly higher than those in metastases (95.5% (42/44) vs. 74.2% (23/31), $P = 0.007$; 45.5% (20/44) vs. 19.4% (6/31), $P = 0.017$, respectively]. In contrast, the incidence of vertebral soft-tissue mass in metastases (**Figures 5B,C**) was significantly higher than that in ORNs [38.7% (12/31) vs. 9.1% (4/44), $P = 0.002$].

For qualitative assessment, in the 44 cases showing ORNs, 38 lesions were interpreted as benign, 3 lesions were classified as malignant, and the remaining 5 lesions were considered to show equivocal findings. Of the 31 metastases, 28 lesions were interpreted as malignant, 3 lesions were classified as equivocal, and no lesion was classified as benign. For the discrimination of ORN from metastasis, with the addition of MRI, the diagnostic sensitivity, specificity, and accuracy increased to 86.4%

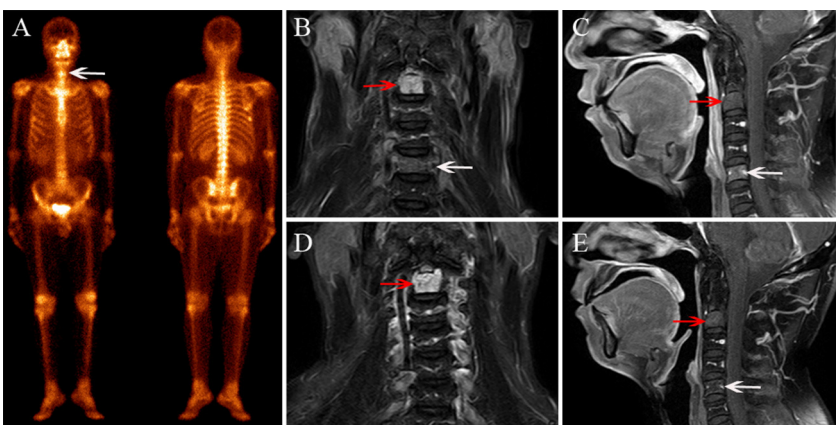

FIGURE 2 | A 42-year–old male diagnosed with cervical spine ORN after RT for NPC. **(A)** BS shows increased radiotracer uptake in C5 (white arrow) and the seventh right rib. **(B)** Coronal FS T2–weighted image shows hyperintensity in the C2 (white arrow) and C5 vertebra (red arrow). **(C)** Sagittal contrast-enhanced T1-weighted image shows mild enhancement in C2 and moderate enhancement in C5. **(D,E)** MRI follow-up examination after 8 months, coronal FS T2-weighted image **(D)**, and sagittal contrast-enhanced T1-weighted image **(E)** show that the signal change in C2 has remained stationary and the abnormal signal in C5 has disappeared.

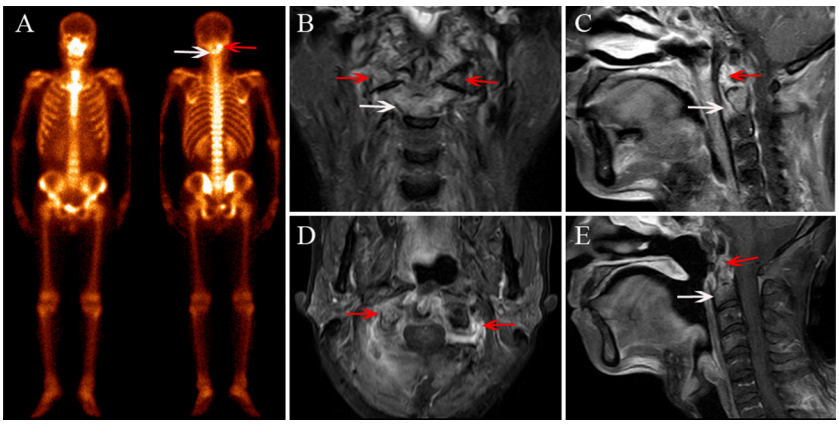

FIGURE 3 | A 56-year-old female diagnosed with cervical spine ORN after RT for NPC. **(A)** BS shows increased radiotracer uptake in C1 (red arrow) and C2 (white arrow). **(B)** Coronal FS T2-weighted image shows hyperintensity in C2 (white arrow) and the bilateral aspect of C1 (red arrow). **(C)** Sagittal contrast-enhanced T1-weighted image shows marked enhancement in lesions. **(D)** Sagittal contrast-enhanced T1-weighted image shows paravertebral muscle edema and marked enhancement change. **(E)** MRI follow-up after 6 months and a sagittal contrast-enhanced T1-weighted image shows that the lesion area has shrunken and the enhancement has declined.

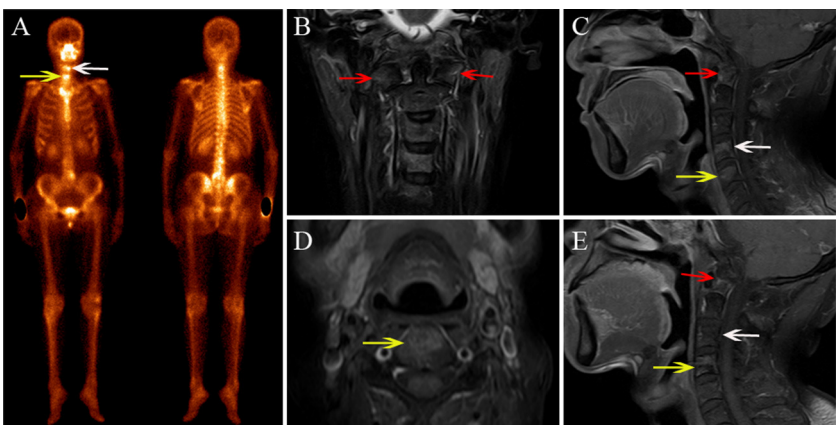

FIGURE 4 | A 48-year-old male diagnosed with cervical spine ORN after RT for NPC. **(A)** BS shows increased radiotracer uptake in C4 (white arrow) and C5 (yellow arrow). **(B)** Coronal FS T2-weighted image shows hyperintensity in the bilateral aspect of C1 (red arrow), C4, and C5. **(C,D)** Sagittal enhanced T1-weighted image **(C)** and axial enhanced T1-weighted image **(D)** show mild enhancement in the lesions. **(E)** MRI follow-up after 7 months; the sagittal contrast-enhanced T1-weighted image shows that the area of the lesions has shrunken and the enhancement has declined in C4 and C5, while the signal change of C1 has remained stationary.

(38/44), 90.3% (28/31), and 88.0% (66/75), respectively. The interobserver agreement in the MRI set was determined to be very good ($k = 0.92$).

DISCUSSION

Accurately distinguishing cervical spine ORN from metastasis is crucial in clinical practice. This study demonstrated that both ORN and metastasis could show increased radiotracer uptake on a BS, and BS showed comparatively low detection sensitivity and classification efficiency in the discrimination of ORN and metastasis. MRI showed additional value when used along with BS; the combined approach showed a better lesion detection rate and improved diagnostic sensitivity and specificity.

BS has been considered as one of the most common and accessible modern imaging procedures for monitoring bone metastasis in patients with malignancy. BS shows enough sensitivity for detecting metastasis, but it shows several limitations in specificity because many benign bone tumors, infections, and degenerative disease may also show abnormal radiotracer uptake (13, 15, 16, 22). Recently, BS has been applied for detecting RT-induced bone complications and has shown variable sensitivity in the detection of insufficiency fractures after RT for pelvic malignancy, with a detection rate ranging from 40 to 87.5% (14, 15, 23). In this study, BS showed a detection sensitivity of 61.4% for detecting ORN. Thus, novel imaging techniques need to be applied to improve the detection sensitivity of ORN.

MRI is an important alternative imaging modality for further assessment of vertebral benign and malignant diseases. However, the value of MRI in the characterization of cervical spine ORN has not been well-described. To date, only few studies have

discussed the MRI features of ORN that occurred in the upper (C1/C2) cervical spine (10–12), and ORN in other anatomical locations of the cervical spine was also only reported in some case reports (24–26). In this study, we found that ORN more frequently developed in C1/C2, which may be attributable to the fact that C1/C2 is adjacent to the nasopharynx and may be more susceptible to RT. Our study also demonstrated that 66.7% of patients with ORN showed devolution with multiple vertebras, which was consistent with the findings of previous studies (10, 11).

TABLE 3 | Findings of cervical spine lesions on BS and MRI.

Imaging findings	ORN	Metastasis	*P*
BS findings Patient-wise analysis (*n*)	21	14	
Abnormal uptake at other bone sites			
Yes	5 (23.8%)	9 (64.3%)	0.016
No	16 (72.2%)	5 (35.7%)	
Lesion-wise analysis (*n*)	44	31	
Detection rate	27 (61.4%)	25 (80.6%)	0.07
Radiotracer uptake greater than that in the anterior iliac spine	5 (11.4%)	15 (48.4%)	< 0.001
MRI findings			
Patient-wise analysis (*n*)	21	14	
Cervical lymphadenopathy			
Yes	2 (9.5%)	11 (78.5%)	< 0.001
No	19 (90.5%)	6 (42.9%)	
Radiation encephalopathy			
Yes	2 (9.5%)	0 (0%)	0.145
No	19 (90.5%)	14 (100%)	
Lesion-wise analysis (*n*)	44	31	
Vertebral marrow edema	42 (95.5%)	23 (74.2%)	0.007
Vertebral enhancement	42 (95.5%)	31 (100%)	0.141
Vertebral destruction	6 (13.6%)	10 (32.3%)	0.054
Vertebral soft-tissue mass	4 (9.1%)	12 (38.7%)	0.002
Vertebral body collapse	1(2.3%)	3 (9.7%)	0.163
Paravertebral muscle edema	20 (45.5%)	6 (19.4%)	0.017

ORN, Osteoradionecrosis.
Numbers in parentheses were used to calculate percentages; we calculated P-values by using the Pearson chi-square test (or Fisher test); P < 0.05 indicates a significant difference.

We found some MRI findings that could facilitate the differential diagnosis of cervical spine ORN from metastasis. First, patients with metastasis tended to show the involvement of cervical lymphadenopathy, with almost 80% of the patients showing cervical spine metastasis combined with cervical lymphadenectasis, which was also consistent with the results obtained by Wu et al. (10). Second, reactive vertebral marrow edema was the most common feature for ORN, with up to 95.5% of ORNs showing vertebral marrow edema change, and the bone marrow edema in ORN was frequently asystematic and homogeneous, but the marrow edema in metastasis was more likely to be circumscribed and asymmetrical. Third, reactive paravertebral muscle edema was also a distinctive ancillary feature that may be associated with ORN. In addition, a vertebral soft-tissue mass was a reliable symptom for detecting metastasis. Although, King et al. (11) indicated that some cervical ORN patients may also have soft-tissue masses adjacent to the cervical spine, we found that these lesions were usually less bulky, and the signal intensity of edema tended to be extensive and rarely showed an occupied effect. These findings exhibited by ORN likely reflect localized infectious and inflammatory processes (19, 20, 27). Meanwhile, the soft-tissue involvement in ORN may be more symmetric than that in metastasis. In summary, accounting for these meaningful findings, MRI may be a reliable technique for distinguishing ORN from bone metastasis, and the possibility of aggressive radiotherapy for patients due to misdiagnosis may be effectively avoided with the involvement of MRI.

With respect to the diagnostic efficiency in the identification of cervical spine ORN and metastasis, BS showed limited value

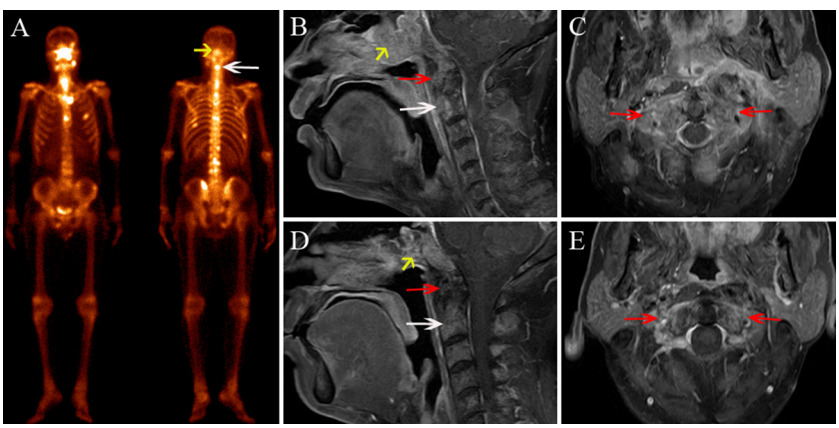

FIGURE 5 | A 53-year-old male diagnosed with skull base recurrence combined with cervical spine metastasis after RT for NPC. **(A)** BS shows increased radiotracer uptake in the skull base (yellow arrow) and C2 (white arrow), multiple ribs, thoracic vertebrae, and lumbar vertebrae, also show increased radiotracer uptake. **(B)** Sagittal contrast-enhanced T1-weighted imaging shows an enhanced soft-tissue mass in the skull base (yellow arrow), C1 (red arrow), and C2 (white arrow). **(C)** Axial contrast-enhanced T1-weighted image shows enhanced soft-tissue mass and bone destruction in the bilateral aspect of C1 (red arrow). **(D,E)** In an MRI follow-up 3 months after RT, the sagittal enhanced T1-weighted image **(D)** and axial enhanced T1-weighted image **(E)** show that the lesion area has shrunken and the enhancement has declined.

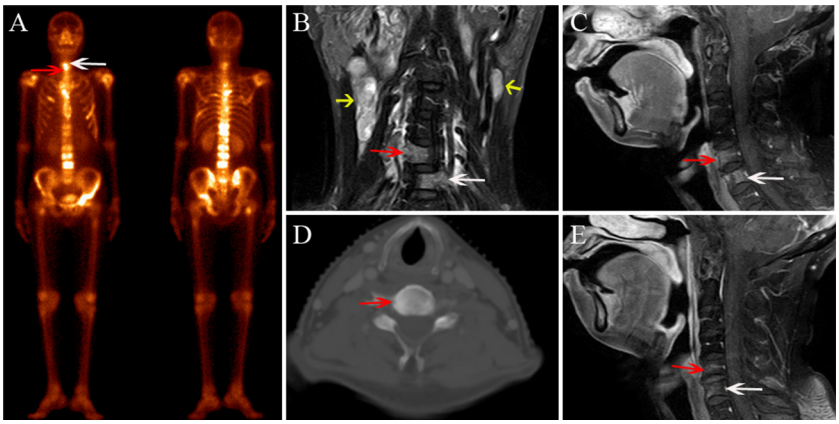

FIGURE 6 | A 68-year-old female diagnosed with bone metastasis after radiotherapy for NPC. **(A)** BS shows increased radiotracer uptake in C5 (white arrow) and C6 (red arrow); multiple ribs, thoracic vertebrae, lumbar vertebrae, and the right femoral neck also show increased radiotracer uptake. **(B)** Coronal FS T2-weighted image shows hyperintensity in C5 (white arrow) and C6 (red arrow), and multiple enlarged lymph nodes in both sides of the neck (yellow arrow). **(C)** Sagittal contrast-enhanced T1-weighted image shows marked and heterogeneous enhancement in C5 and C6. **(D)** CT localization image shows an osteogenic change in C5. **(E)** In the MRI follow-up 2 months after RT, the sagittal contrast-enhanced T1-weighted image shows that the area of the lesions has shrunken and the enhancement has declined.

for differential diagnosis. In our study, the diagnostic sensitivity, specificity, and accuracy using BS alone were only 38.6, 48.3, and 42.7%, respectively. This may be attributed to the relatively low lesion detection sensitivity on BS and the fact that a large number of lesions detected were classified as equivocal. We found that the diagnostic sensitivity increased to 86.4% and specificity increased to 90.3% with the addition of MRI. Meanwhile, 38.6% of ORNs and 19.4% of metastases that were not detected on BS were found on MRI, and the frequency of equivocal lesions was also reduced. These results were similar to those of several previous studies that assessed the added value of MRI or SPECT/CT to BS alone in the discrimination of RT-induced pelvic insufficiency fracture and pelvic metastasis in cervical cancer patients (13–15, 22). Therefore, the results of our study indicated that MRI could be a noninvasive technique for further discrimination of new cervical spine lesions detected by BS.

This study had several limitations. First, puncture pathologic evaluation was not available due to the high probability of fracture or hemorrhage; thus we used standardized clinical and MRI follow-up to confirm ORN or metastasis. Second, this was a retrospective study with a limited sample performed in a single center. Further prospective studies with larger sample sizes are needed to validate the results. Third, only routine MRIs were used to assess the diagnostic efficacy, and the potential performance of some functional MR imaging techniques, such as diffusion-weighted imaging (DWI), and perfusion-weighted imaging (PWI), need to be Friday, January 10, 2020 1:47 pm explored further.

In conclusion, both cervical spine ORN and metastasis can show increased radiotracer uptake on a BS in patients with NPC after RT, and MRI showed additional value in identifying these cervical spine lesions. MRI could be a better differential diagnosis technique for distinguishing ORN from metastasis and may avoid wrong assignment of patients to a metastatic stage with indications for treatment modalities with supplemental toxicity and a subsequent palliative strategy.

DATA AVAILABILITY STATEMENT

The datasets generated for this study are available on request to the corresponding author.

ETHICS STATEMENT

The studies involving human participants were reviewed and approved by Affiliated Cancer Hospital & Institute of Guangzhou Medical University. Written informed consent for participation was not required for this study in accordance with the national legislation and the institutional requirements. Written informed consent was not obtained from the individual(s) for the publication of any potentially identifiable images or data included in this article.

AUTHOR CONTRIBUTIONS

XZ and JZ: conceptualization, writing—original draft preparation, and supervision. LL, BL, and HZ: methodology. BL and JL: formal analysis. HZ, LH, and JL: investigation. XZ and LL: resources. LH and XL: data curation. JL and JZ: writing—review and editing. All authors read and approved the final manuscript.

FUNDING

This work was supported by the Guangzhou Health and Family Planning Science and Technology Project (20192A010020), the Guangzhou Key Medical Discipline Construction Project Fund (B195002004042), and the Youth Research Project of the Third Affiliated Hospital of Guangzhou Medical University (2018Q23).

REFERENCES

1. Torre LA, Bray F, Siegel RL, Ferlay J, Lortet-Tieulent J, Jemal A. Global cancer statistics, 2012. *CA Cancer J Clin*. (2015) 65:87–108. doi: 10.3322/caac.21262
2. Wee JT, Ha TC, Loong SL, Qian, CN. Is nasopharyngeal cancer really a "Cantonese cancer"? *Chin J Cancer*. (2010) 29:517–26. doi: 10.5732/cjc.009.10329
3. Rabin BM, Meyer JR, Berlin JW, Marymount MH, Palka PS, Russell EJ. Radiation-induced changes in the central nervous system and head and neck. *Radiographics*. (1996) 16:1055–72. doi: 10.1148/radiographics.16.5.8888390
4. Liu J, Ning X, Sun X, Lu H, Gu Y, Wang D. Endoscopic sequestrectomy for skull base osteoradionecrosis in nasopharyngeal carcinoma patients: a 10year experience. *Int J Clin Oncol*. (2019) 24:248–55. doi: 10.1007/s10147-018-1354-8
5. Teng MS, Futran ND. Osteoradionecrosis of the mandible. *Curr Opin Otolaryngol Head Neck Surg*. (2005) 13:217–21. doi: 10.1097/01.moo.0000170527.59017.ff
6. Kosaka Y, Okuno Y, Tagawa Y, Ueki N, Itoh K, Shinohara S, et al. Osteoradionecrosis of the cervical vertebrae in patients irradiated for head and neck cancers. *Jpn J Radiol*. (2010) 28:388–94. doi: 10.1007/s11604-010-0440-2
7. Cheung JP, Wei WI, Luk KD. Cervical spine complications after treatment of nasopharyngeal carcinoma. *Eur Spine J*. (2013) 22:584–92. doi: 10.1007/s00586-012-2600-9
8. Donovan DJ, Huynh TV, Purdom EB, Johnson RE, Sniezek JC. Osteoradionecrosis of the cervical spine resulting from radiotherapy for primary head and neck malignancies: operative and nonoperative management. case report. *J Neurosurg Spine*. (2005) 3:159–64. doi: 10.3171/spi.2005.3.2.0159
9. Prasad KC, Prasad SC, Mouli N, Agarwal S. Osteomyelitis in the head and neck. *Acta Otolaryngol*. (2007) 127:194–205. doi: 10.1080/00016480600818054
10. Wu LA, Liu HM, Wang CW, Chen YF, Hong RL, Ko JY. Osteoradionecrosis of the upper cervical spine after radiation therapy for head and neck cancer: differentiation from recurrent or metastatic disease with MR imaging. *Radiology*. (2012) 264:136–45. doi: 10.1148/radiol.12111714
11. King AD, Griffith JF, Abrigo JM, Leung SF, Yau FK, Tse GM, et al. Osteoradionecrosis of the upper cervical spine: MR imaging following radiotherapy for nasopharyngeal carcinoma. *Eur J Radiol*. (2010) 73:629–35. doi: 10.1016/j.ejrad.2008.12.016
12. Khorsandi AS, Su HK, Mourad WF, Urken ML, Persky MS, Lazarus CL, et al. Osteoradionecrosis of the subaxial cervical spine following treatment for head and neck carcinomas. *Br J Radiol*. (2015) 88:20140436. doi: 10.1259/bjr.20140436
13. Strobel K, Burger C, Seifert B, Husarik DB, Soyka JD, Hany TF. Characterization of focal bone lesions in the axial skeleton: performance of planar bone scintigraphy compared with SPECT and SPECT fused with CT. *Am J Roentgenol*. (2007) 188:W467–74. doi: 10.2214/AJR.06.1215
14. Zhong X, Li J, Zhang L, Lu B, Yin J, Chen Z, et al. Characterization of insufficiency fracture and bone metastasis after radiotherapy in patients with cervical cancer detected by bone scan: role of magnetic resonance imaging. *Front Oncol*. (2019) 9:183. doi: 10.3389/fonc.2019.00183
15. Zhang L, He Q, Jiang M, Zhang B, Zhong X, Zhang R. Diagnosis of insufficiency fracture after radiotherapy in patients with cervical cancer: contribution of technetium Tc 99m-labeled methylene diphosphonate single-photon emission computed tomography/computed tomography. *Int J Gynecol Cancer*. (2018) 28:1369–76. doi: 10.1097/IGC.0000000000001337
16. McLoughlin LC, O'Kelly F, O'Brien C, Sheikh M, Feeney J, Torreggiani W, et al. The improved accuracy of planar bone scintigraphy by adding single photon emission computed tomography (SPECT-CT) to detect skeletal metastases from prostate cancer. *Ir J Med Sci*. (2016) 185:101–5. doi: 10.1007/s11845-014-1228-7
17. Sung JK, Jee WH, Jung JY, Choi M, Lee SY, Kim YH, et al. Differentiation of acute osteoporotic and malignant compression fractures of the spine: use of additive qualitative and quantitative axial diffusion-weighted MR imaging to conventional MR imaging at 3.0 T. *Radiology*. (2014) 271:488–98. doi: 10.1148/radiol.13130399
18. Torres C, Hammond I. Computed tomography and magnetic resonance imaging in the differentiation of osteoporotic fractures from neoplastic metastatic fractures. *J Clin Densitom*. (2016) 19:63–9. doi: 10.1016/j.jocd.2015.08.008
19. Yung CS, Leung DKC, Cheung JPY. The prevalence and impact of cervical spine pathologies in patients with nasopharyngeal carcinoma. *Oral Oncol*. (2019) 90:48–53. doi: 10.1016/j.oraloncology.2019.01.013
20. Han P, Wang X, Liang F, Liu Y, Qiu X, Xu Y, et al. Osteoradionecrosis of the skull base in nasopharyngeal carcinoma: incidence and risk factors. *Int J Radiat Oncol Biol Phys*. (2018) 102:552–5. doi: 10.1016/j.ijrobp.2018.06.027
21. Landis JR, Koch GG. The measurement of observer agreement for categorical data. *Biometric*. (1977) 33:159–74. doi: 10.2307/2529310
22. Ndlovu X, George R, Ellmann A, Warwick J. Should SPECT-CT replace SPECT for the evaluation of equivocal bone scan lesions in patients with underlying malignancies? *Nucl Med Commun*. (2010) 31:659–65. doi: 10.1097/MNM.0b013e3283399107
23. Fujii M, Abe K, Hayashi K, Kosuda S, Yano F, Watanabe S, et al. Honda sign and variants in patients suspected of having a sacral insufficiency fracture. *Clin Nucl Med*. (2005) 30:165–9. doi: 10.1097/00003072-200503000-00004
24. Lim AA, Karakla DW, Watkins DV. Osteoradionecrosis of the cervical vertebrae and occipital bone: a case report and brief review of the literature. *Am J Otolaryngol*. (1999) 20:408–11. doi: 10.1016/S0196-0709(99)90083-2
25. Rashid MZ, Ariffin MH, Rhani SA, Baharudin A. Ibrahim, K. Osteoradionecrosis in subaxial cervical spine - a rare and devastating complication: a case report. *Malays Orthop J*. (2017) 11:53–5. doi: 10.5704/MOJ.1711.005
26. Kaltoft B, Kruse A, Jensen LT, Elberg JJ. Reconstruction of the cervical spine with two osteocutaneous fibular flap after radiotherapy and resection of osteoclastoma: a case report. *J Plast Reconstr Aesthet Surg*. (2012) 65:1262–64. doi: 10.1016/j.bjps.2012.02.014
27. Huang XM, Zheng YQ, Zhang XM, Mai HQ, Zeng L, Liu X, et al. Diagnosis and management of skull base osteoradionecrosis after radiotherapy for nasopharyngeal carcinoma. *Laryngoscope*. (2006) 116:1626–31. doi: 10.1097/01.mlg.0000230435.71328.b9

Conflict of Interest: The authors declare that the research was conducted in the absence of any commercial or financial relationships that could be construed as a potential conflict of interest.

frontiers in Oncology

ORIGINAL RESEARCH
published: 05 February 2020
doi: 10.3389/fonc.2020.00104

Heterozygous p53-R280T Mutation Enhances the Oncogenicity of NPC Cells Through Activating PI3K-Akt Signaling Pathway

Zhen-Qi Qin[1,2,3], *Qi-Guang Li*[2,3], *Hong Yi*[2,3], *Shan-Shan Lu*[2,3], *Wei Huang*[2,3], *Zhuo-Xian Rong*[2,3], *Yao-Yun Tang*[1] *and Zhi-Qiang Xiao*[1,2,3]*

[1] *Department of Otolaryngology Head and Neck Surgery, Xiangya Hospital, Central South University, Changsha, China,*
[2] *Research Center of Carcinogenesis and Targeted Therapy, Xiangya Hospital, Central South University, Changsha, China,*
[3] *The Higher Educational Key Laboratory for Cancer Proteomics and Translational Medicine of Hunan Province, Xiangya Hospital, Central South University, Changsha, China*

A heterozygous point mutation of p53 gene at codon 280 from AGA to ACA (R280T) frequently occurs in nasopharyngeal carcinoma (NPC) cell lines, and about 10% NPC tissues. However, the role of this mutation in the pathogenesis of NPC remains unclear. In this study, we generated p53 knockout (KO) NPC cell lines from CNE2 cells carrying heterozygous p53 R280T (p53-R280T) mutation and C666-1 cells carrying wild-type p53 by CRISPR-Cas9 gene editing system, and found that KO of heterozygous p53-R280T significantly decreased NPC cell proliferation and increased NPC cell apoptosis, whereas KO of wild-type p53 had opposite effects on NPC cell proliferation and apoptosis. Moreover, KO of heterozygous p53-R280T inhibited the anchorage-independent growth and *in vivo* tumorigenicity of NPC cells. mRNA sequencing of heterozygous p53-R280T KO and control CNE2 cells revealed that heterozygous p53-R280T mutation activated PI3K-Akt signaling pathway. Moreover, blocking of PI3K-Akt signaling pathway abolished heterozygous p53-R280T mutation-promoting NPC cell proliferation and survival. Our data indicate that p53 with heterozygous R280T mutation functions as an oncogene, and promotes the oncogenicity of NPC cells by activating PI3K-Akt signaling pathway.

Keywords: nasopharyngeal carcinoma, p53, R280T mutation, oncogenicity, Akt

OPEN ACCESS

Edited by:
Jan Baptist Vermorken, University of Antwerp, Belgium

Reviewed by:
Guiyuan Li, Central South University, China
Yingqin Li, Sun Yat-sen University Cancer Center (SYSUCC), China

***Correspondence:**
Zhi-Qiang Xiao
zqxiao2001@hotmail.com

Specialty section:
This article was submitted to Head and Neck Cancer, a section of the journal Frontiers in Oncology

Received: *30 July 2019*
Accepted: *20 January 2020*
Published: *05 February 2020*

Citation:
Qin Z-Q, Li Q-G, Yi H, Lu S-S, Huang W, Rong Z-X, Tang Y-Y and Xiao Z-Q (2020) Heterozygous p53-R280T Mutation Enhances the Oncogenicity of NPC Cells Through Activating PI3K-Akt Signaling Pathway. Front. Oncol. 10:104. doi: 10.3389/fonc.2020.00104

INTRODUCTION

Nasopharyngeal carcinoma (NPC) arises from the epithelial lining of the nasopharynx (1). It has a high prevalence in southern China, Southeast Asia, northern Africa and Alaska, with remarkable ethnic and geographic distribution (2). The annual incidence rate reaches 25 cases per 100,000 people in the endemic regions, which is about 25-fold higher than that in the rest of the world, posing one of the most serious public health problems in these areas (2). NPC is closely associated with the Epstein-Barr virus (EBV) infection and genetic susceptibility (3). Familial clustering of NPC has been observed not only in the southern Chinese population but also in the non-chinese, low-risk populations (4). It suggests that genetic alterations of tumor suppressor genes and proto-oncogenes may be important in NPC carcinogenesis.

P53 is a sequence-specific DNA binding protein, which consists of two N-terminal transactivation domains, a central DNA binding domain (DBD), a C-terminus including nuclear localization signals and an oligomerization domain needed for transcriptional activity (5). As the "guardian of the genome," p53 is important to suppress cancer development and progression. P53 mutations are observed in approximately half of the human cancers, most of which occur in the region encoding p53's DBD and lead to disordered p53 signaling pathway (6–8). P53 mutations often result in accumulation of the mutant p53 protein, which either loses tumor suppressor function or gains oncogenic activity. R280 residue located in the DBD of p53 gene plays an important role in DNA recognition and p53-DNA complex stability (9). In the p53 mutation database established by IARC, p53 mutation at codon 280 (R280T) was found in tumors originating from 30 types of human tissues such as bladder, breast, nasopharynx, accessory sinus and mouth larynx, and in a few tumor cell lines such as NPC, bladder carcinoma, breast carcinoma, gastric, and esophageal cancer cell lines (10). For NPC, the prevalence of p53 mutations is about 30% (11–16). Among them, a heterozygous point mutation of p53 gene at codon 280 from AGA to ACA (Arg changed to Thr) (R280T) was identified in the five NPC cell lines (CNE1, CNE2, TW06, TW01, and HONE1), with a mutation rate of about 10% in NPC tissues (15, 17–19). However, the functions of this heterozygous p53-R280T mutation in NPC remain unclear.

In this study, we generated p53 knockout NPC cell lines from CNE2 carrying heterozygous p53-R280T mutation (17) and C666-1 carrying wild-type (wt) p53 (15) using the CRISPR-Cas9 gene editing system. We found that knockout of heterozygous p53-R280T inhibited while knockout of wt p53 increased the oncogenicity of NPC cells. To explore the mechanism of heterozygous p53-R280T-promoting NPC cell oncogenicity, we compared the mRNA expression profiles in the heterozygous p53-R280T knockout and control CNE2 cells by mRNA sequencing, and found PI3K-Akt signaling pathway involved in the tumor-promotion effect of heterozygous p53-R280T mutation.

MATERIALS AND METHODS

Knockout of p53 in NPC Cell Lines Using the CRISPR-Cas9 Gene Editing System

Human NPC cell lines (CNE2, C666-1) were cultured and maintained in RPMI-1640 medium containing 10% (v/v) fetal bovine serum (FBS) (Thermo, USA) at 37°C. For p53 knockout, the guide RNA (gRNA) sequence was GCAGTCACAGCACATGACGG, which was designed using the website software from Massachusetts Institute of Technology (USA) (https://zlab.bio/guide-design-resources/). CNE2 and C666-1 cells were transfected with the plasmid pGK1.1 containing p53 gRNA and control vector pGK1.1, respectively. Forty eight hours after transfection, cells were treated with puromycin at a concentration of 3 μg/ml for 2 days. Then, a single cell was seeded into 96-well plates and cultured for 1 month, and knockout of p53 protein was evaluated by western blot, and DNA sequencing was used for confirmation. For DNA sequencing, genomic DNA was extracted from cells, and a 383-bp polymerase chain reaction (PCR) amplicon flanking the CRSPR-Cas9-targeted sites (GCAGTCACAGCACATGACGG) was generated using the primers 5′-TCACTTACCTCTCAGAGAC-3′ (forward) and 5′-ACAGGGCAGGTCTTGGCCGTT-3′ (reverse). The PCR product was purified and ligated into the pMD18-T vector. The recombinant plasmids were introduced into competent DH5α cells. Plasmid DNA was extracted and sequenced across the insert using one of the PCR primers in the Life Technologies Corporation (Shanghai, China). The sequence of p53 KO CNE2 (KO-41) cells after knockout by CRISPR-Cas9 gene editing system was 5′-GGAGGCTACACGACACTGACGAACATC-3′. The sequence of p53 KO CNE2 (KO-49) cells after knockout by CRISPR-Cas9 gene editing system was 5′-GGAGGCAGGGGTCCGGAGACTAAGTACA-3′ and 5′-GGAGGCACTGACGAAC-3′. The sequence of p53 KO C666-1 (KO-9) cells after knockout by CRISPR-Cas9 gene editing system was 5′-GGAGTACACGACACTGACGAACATCTACCG-3′. The sequence of p53 KO C666-1 (KO-29) cells after knockout by CRISPR-Cas9 gene editing system was 5′-GGAGTACACGACACTGACGAACATCTACCG-3′.

Western Blot

Proteins were exacted from cells using RIPA buffer, and subjected to SDS-PAGE separation, followed by blotting onto a PVDF membrane (Millipore, USA). Blots were incubated with antibodies against p53 (DO-1) (#sc-126, Santa Cruz, USA), phospho-AKT (Thr308; #4056, CST, USA), or AKT (#4691, CST, USA) overnight at 4°C, followed by incubation with HRP-conjugated secondary antibody for 1 h at room temperature. The signal was visualized with an enhanced chemiluminescence detection reagent (Millipore, USA).

Detection of Heterozygous p53-R280T Mutation in NPC Cell Lines

Sanger sequencing was performed to detect the heterozygous R280T mutation of p53 gene using genomic DNA extracted from NPC CNE2, 5-8F, 6-10B, and C666-1 cell lines. Mutation was confirmed by at least two independent PCR amplifications and a DNA sequencing reaction on both strands. Oligonucleotide primers were designed to amplify exon 8 of p53 gene. The primers used were: 5′-GCTGGGGAGAGGAGCTGGTG-3′ (forward) and 5′-GGTTCATGCCGCCCATGCAG-3′ (reverse). The products were examined by sequencing in the Sangon Biotech, Shanghai, China.

5-Ethynyl-2′-Deoxyuridine (EdU) Incorporation Assay

EdU incorporation assay was performed to detect cell proliferation as described previously by us (20). The assay was performed three times in triplicate.

Cell Counting Kit-8 (CCK-8) Assay

Cell proliferation was measured using a CCK-8 kit as described previously by us (20). The assay was performed three times in triplicate.

Flow Cytometry Analysis of Cell Cycle and Apoptosis

Flow cytometry analysis of cell cycle and apoptosis was performed as described previously by us (21). All assays were performed three times in triplicate.

Anchorage Dependent and Independent Colony Formation Assay

Plate colony formation assay and soft agar colony formation assay were performed to detect the anchorage dependent or independent growth of cells as described previously by us (22). All assays were performed three times in triplicate.

Tumor Formation Assay in Nude Mice

Nude male mice that were 4 weeks old were obtained from the Laboratory Animal Center of Central South University (Changsha, China) and were maintained under specific pathogen-free conditions. 5×10^6 cells resuspended in 200 μl of serum-free medium were subcutaneously injected into the flanks of mice ($n = 3$ mice each). The mice were monitored daily for palpable tumor formation, and tumor volume (in mm^3) was measured by a vernier caliper every 3 days and calculated by using the modified ellipse formula (volume = length × $width^2/2$). At the end of the experiments, the mice were killed by cervical dislocation, and tumors were excised, and weighted.

mRNA Sequencing

Total RNA was extracted from NPC cells with Trizol reagent (Invitrogen, USA). Two microgram RNA per sample was used as input material for the RNA sample preparations. Sequencing libraries were generated using NEBNext® Ultra™ RNA Library Prep Kit for Illumina® (#E7530L, NEB, USA), and index codes were added to attribute sequences to each sample. Briefly, mRNA was purified from total RNA using poly-T oligo-attached magnetic beads. First strand cDNA was synthesized using random hexamer primer and RNase H. Second strand cDNA synthesis was subsequently performed using buffer, dNTPs, DNA polymerase I and RNase H. The library fragments were purified

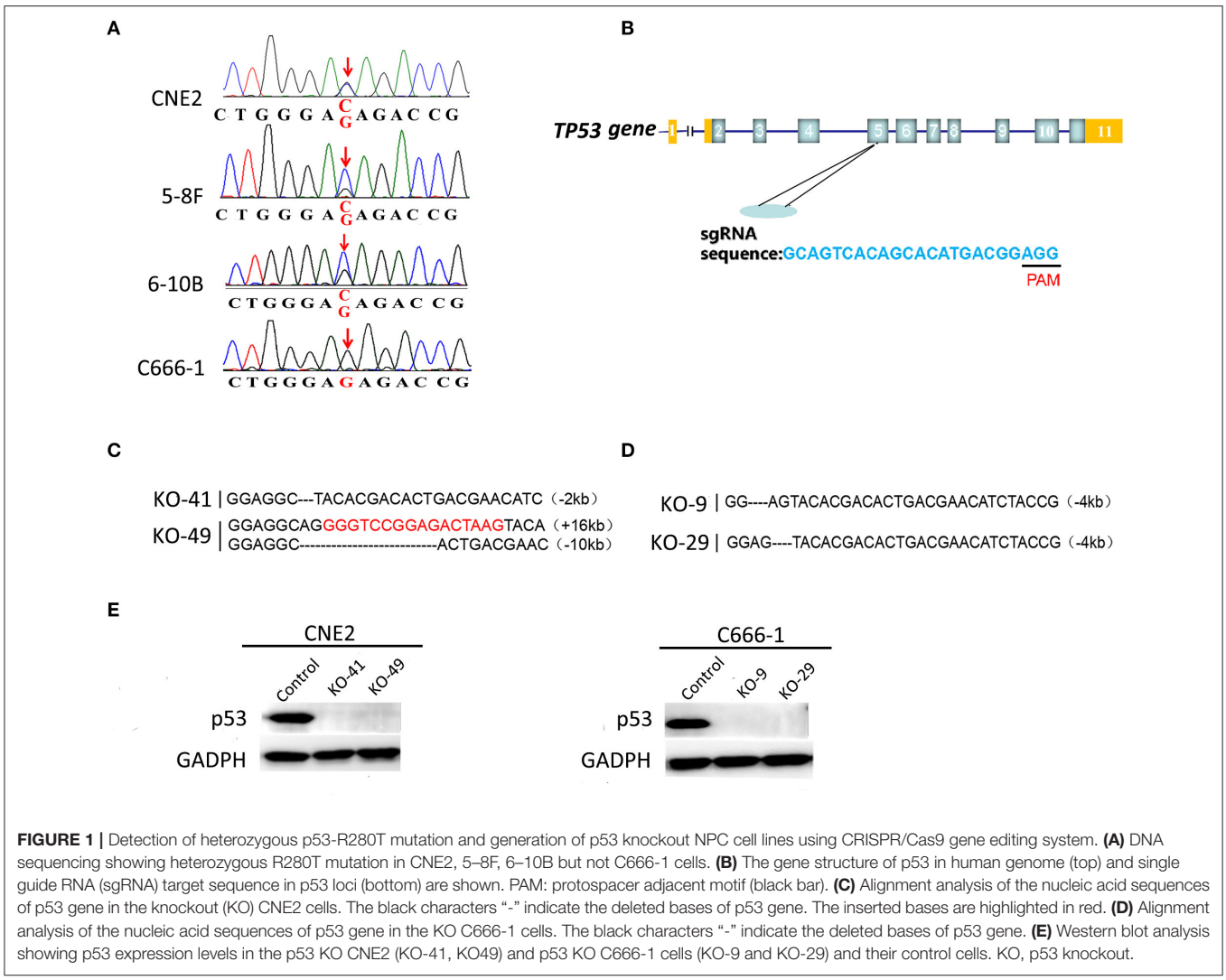

FIGURE 1 | Detection of heterozygous p53-R280T mutation and generation of p53 knockout NPC cell lines using CRISPR/Cas9 gene editing system. **(A)** DNA sequencing showing heterozygous R280T mutation in CNE2, 5–8F, 6–10B but not C666-1 cells. **(B)** The gene structure of p53 in human genome (top) and single guide RNA (sgRNA) target sequence in p53 loci (bottom) are shown. PAM: protospacer adjacent motif (black bar). **(C)** Alignment analysis of the nucleic acid sequences of p53 gene in the knockout (KO) CNE2 cells. The black characters "-" indicate the deleted bases of p53 gene. The inserted bases are highlighted in red. **(D)** Alignment analysis of the nucleic acid sequences of p53 gene in the KO C666-1 cells. The black characters "-" indicate the deleted bases of p53 gene. **(E)** Western blot analysis showing p53 expression levels in the p53 KO CNE2 (KO-41, KO49) and p53 KO C666-1 cells (KO-9 and KO-29) and their control cells. KO, p53 knockout.

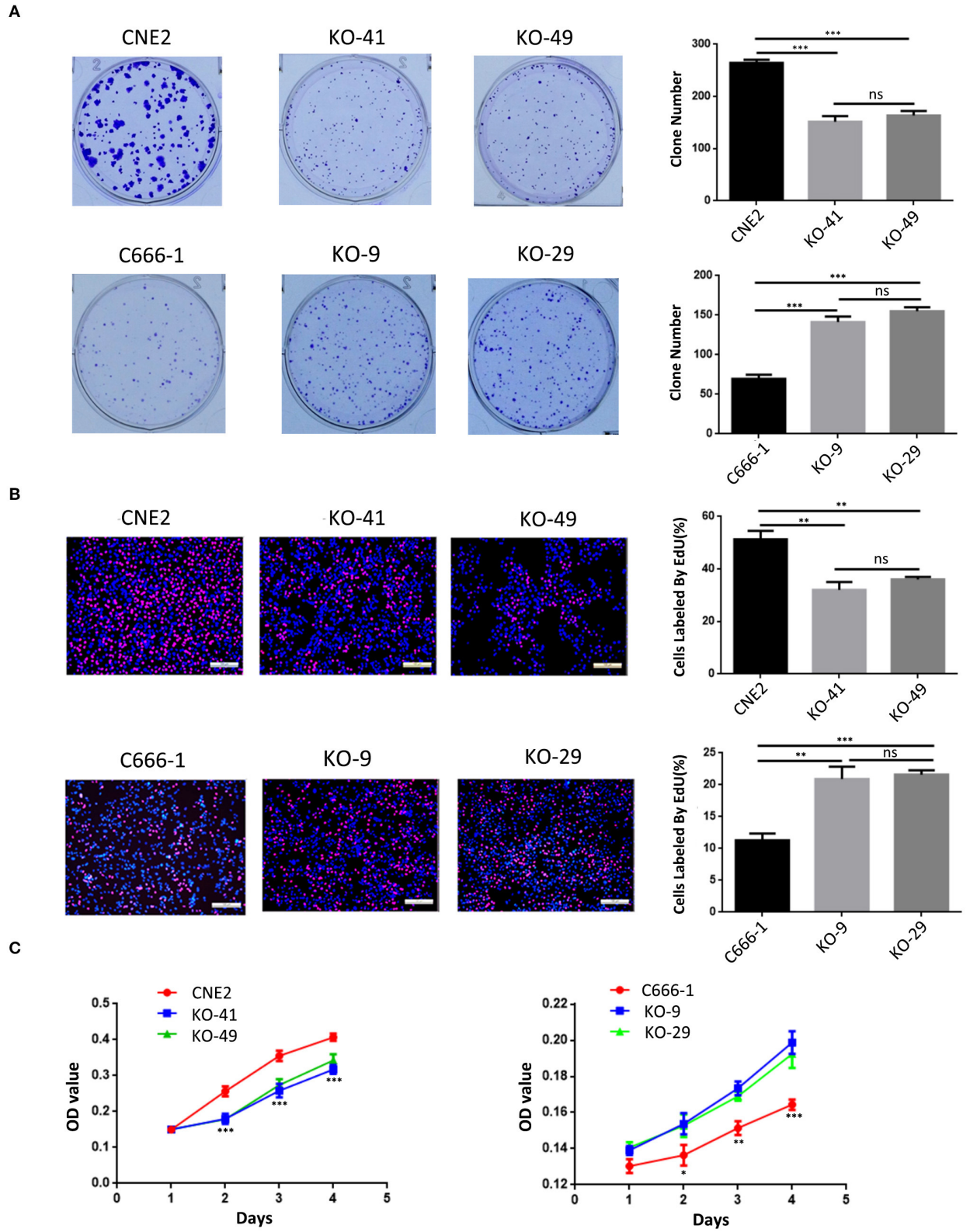

FIGURE 2 | The effect of heterozygous p53-R280T and wt p53 knockout on NPC cell proliferation. **(A,B)** Representative results (left) and statistical analyses (right) of cell proliferation detected by plate clone formation assay and EdU incorporation assay in the p53 KO CNE2 and C666-1 cells and their control cells. **(C)** CCK-8 assay showing cell proliferation in the p53 KO CNE2 and C666-1 cells and their control cells. *$P < 0.05$; **$P < 0.01$; ***$P < 0.001$; ns, no significance. KO, p53 knockout.

with QiaQuick PCR kits and elution with EB buffer, then terminal repair, A-tailing and adapter added were implemented. The aimed products were retrieved and PCR was performed, then the library was completed. The libraries were sequenced on an Illumina platform and 150 bp paired-end reads were generated. Reads count for each gene in each sample was counted by HTSeq v0.6.0, and FPKM (Fragments Per Kilobase Million Mapped Reads) was then calculated to estimate the expression level of genes in each sample. DESeq (v1.16) was used for differential gene expression analysis between two samples with biological

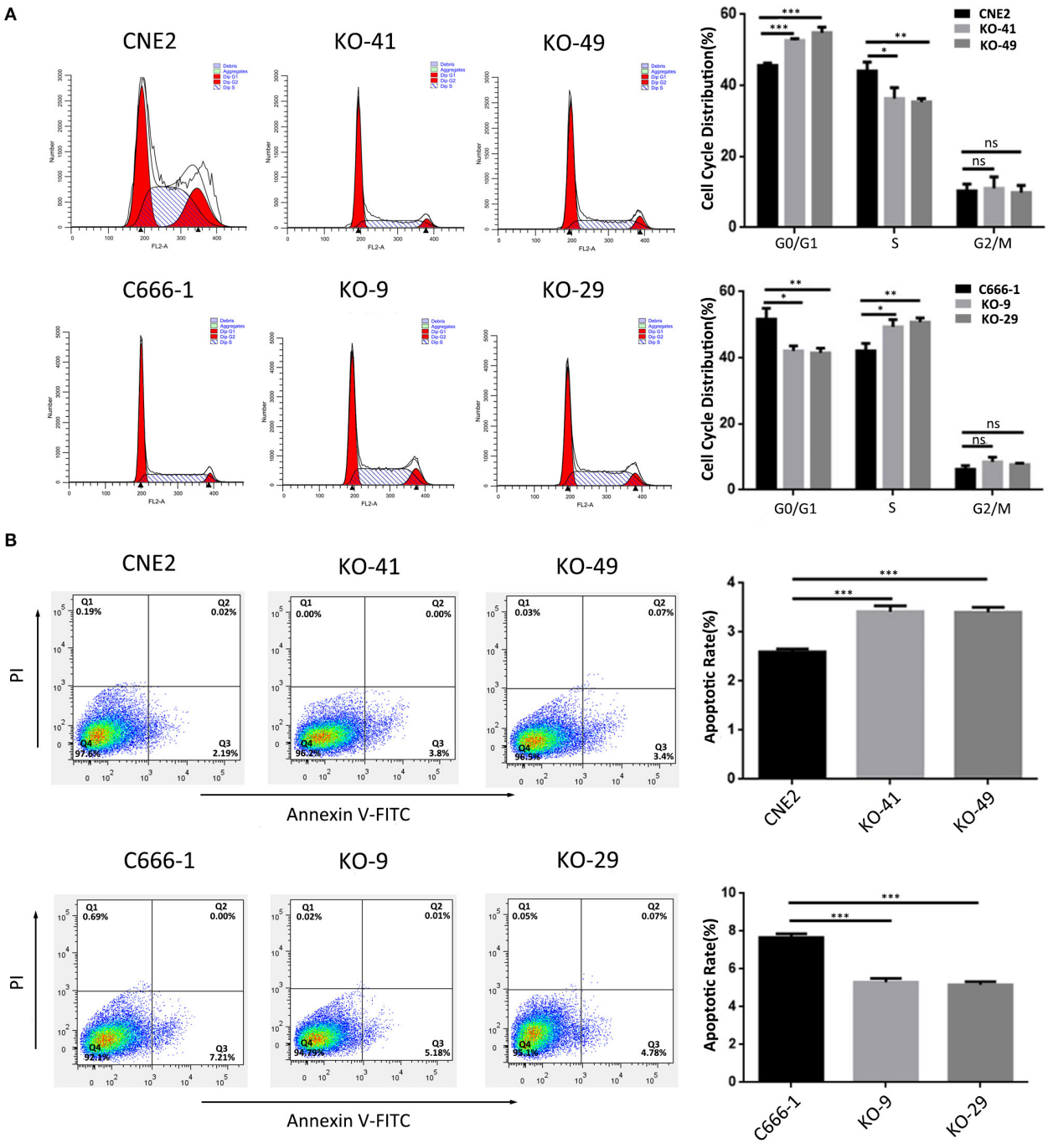

FIGURE 3 | The effect of heterozygous p53-R280T and wt p53 knockout on cell cycle and apoptosis of NPC cells. **(A)** Representative results (left) and statistical analyses (right) of cell cycle distribution analyzed by flow cytometry in the p53 KO CNE2 and C666-1 cells and their control cells. **(B)** Representative results (left) and statistical analyses (right) of cell apoptosis analyzed by flow cytometry in the p53 KO CNE2 and C666-1 cells and their control cells. $^{*}P < 0.05$; $^{**}P < 0.01$; $^{***}P < 0.001$; ns, no significance. KO, p53 knockout.

replicates using a model based on the negative binomial distribution. The DEGs standard is ($|\log_2$ Fold change$| \geq 2$, and $q < 0.05$). The GO enrichment of differentially expressed genes (DEGs) was implemented by the hypergeometric test, in which p-value is calculated and adjusted as q-value, and data background is genes in the whole genome. GO terms with $q < 0.05$ were considered to be significantly enriched. The KEGG enrichment of DEGs was implemented by the hypergeometric test. KEGG terms with $p < 0.05$ were considered to be significantly enriched.

qRT-PCR

Total RNA was extracted from NPC cells with Trizol reagent (Invitrogen, USA). One microgram of total RNA was reversely transcribed for cDNA using a RT kit according to the manufacturer's protocol and Oligo dT primer (Vazyme Biotech, China) according to the manufacturer's instruction. The RT products were amplified by real-time PCR using SYBR qPCR Master Mix kit (Vazyme Biotech, China) according to the manufacturer's instruction. The products were quantitated using 2^{-DDCt} method against GAPDH for normalization. The primer sequences were synthesized by the Sangon Biotech (Shanghai, China) and listed in **Supplementary Table S1**.

Statistical Analysis

All the quantified data represented an average of three times. Data are represented as mean ± SD. One-way analysis of variance or two-tailed Student's t-test was used for comparisons between

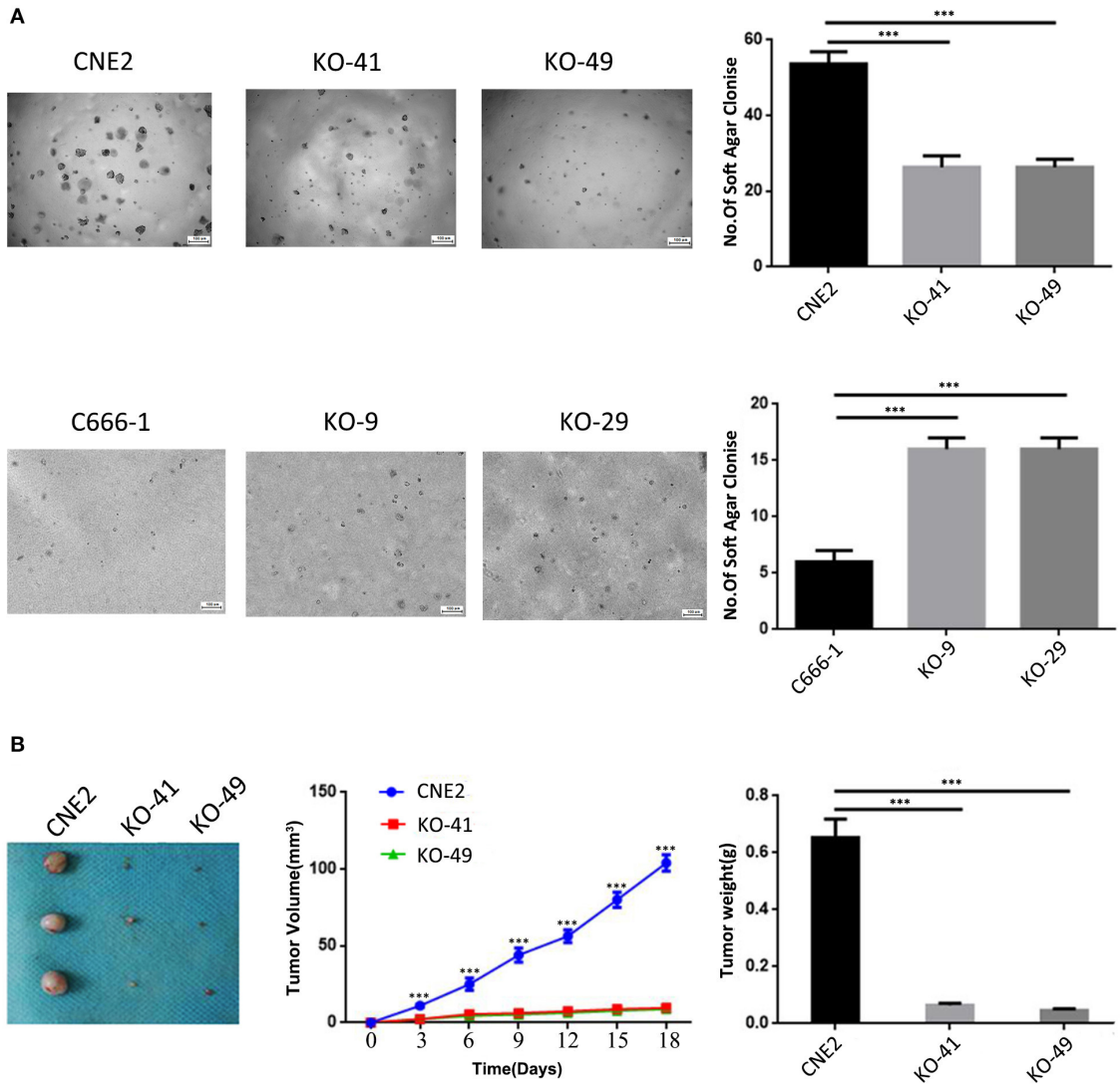

FIGURE 4 | The effects of heterozygous p53-R280T and wt-p53 knockout on anchorage-independent and xenograft growth of NPC cells. **(A)** Representative results (left) and statistical analyses (right) of soft agar colony formation ability in p53 KO CNE2 and C666-1 cells and their control cells. **(B)** The photography of xenograft tumors 18 days after subcutaneous implantation of p53 KO CNE2 cells and control cells (left), and growth curve and weight of xenograft tumors generated by p53 KO CNE2 cells and control cells (middle and right). $n = 3$ mice per group. ***$P < 0.001$. KO, p53 knockout.

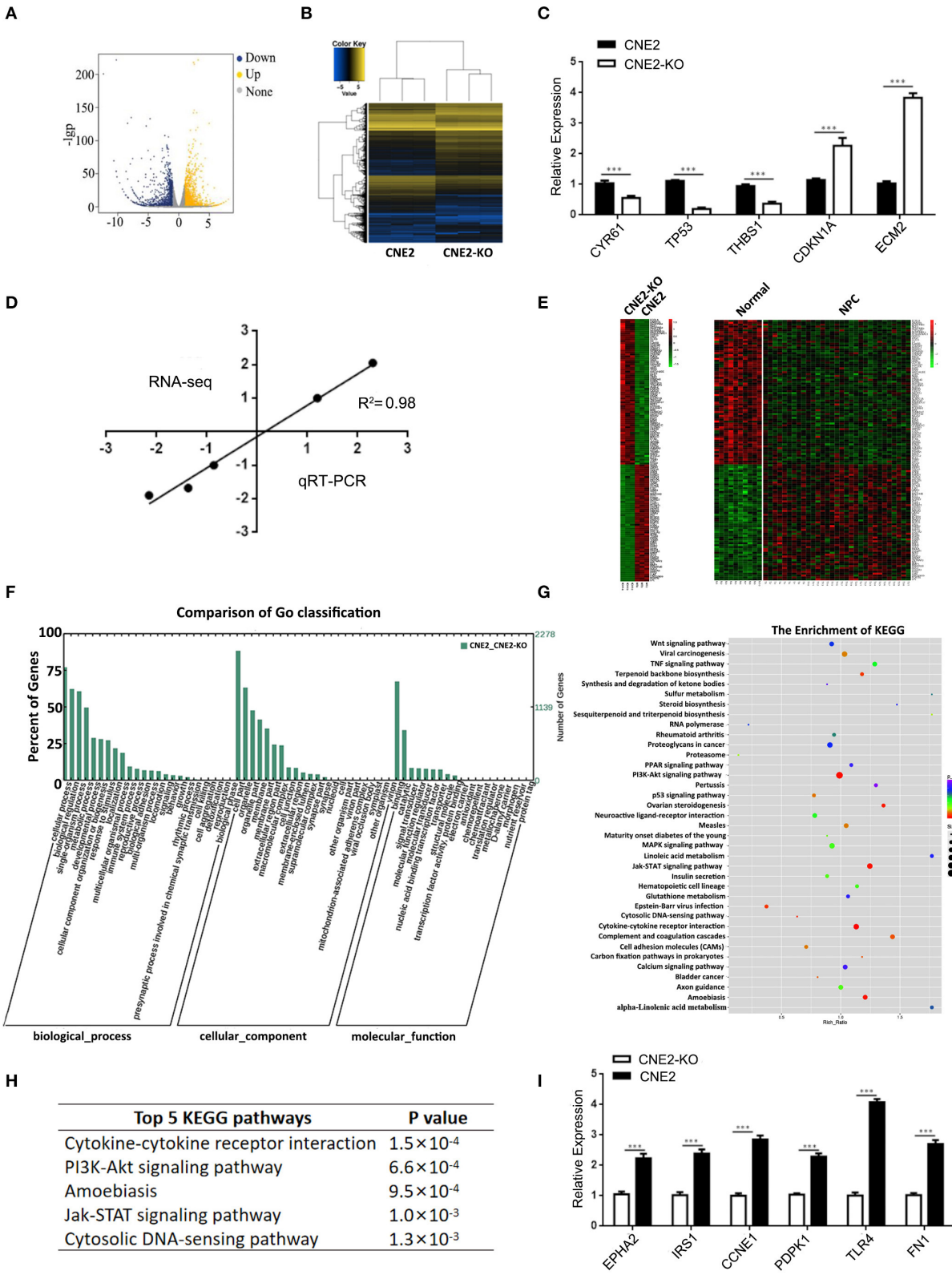

Top 5 KEGG pathways	P value
Cytokine-cytokine receptor interaction	1.5×10^{-4}
PI3K-Akt signaling pathway	6.6×10^{-4}
Amoebiasis	9.5×10^{-4}
Jak-STAT signaling pathway	1.0×10^{-3}
Cytosolic DNA-sensing pathway	1.3×10^{-3}

FIGURE 5 | Differentially expressed genes in the heterozygous p53-R280T KO CNE2 and control CNE2 cells. **(A)** mRNA-sequencing showing differentially expressed genes that change more than 2-fold in the p53 KO CNE2 and control CNE2 cells. Blue dots represent down-regulated genes and yellow dots represent up-regulated

(Continued)

FIGURE 5 | genes. **(B)** Hierarchical clustering of differentially expressed genes in the p53 KO CNE2 and control CNE2 cells. **(C)** qRT-PCR detection of the five differentially expressed genes identified by mRNA sequencing in the p53 KO CNE2 and control CNE2 cells. **(D)** Correlation of Log_2 fold change derived from mRNA sequencing with the Log_2 fold change obtained from qRT-PCR. **(E)** Integrated analysis of differentially expressed genes in p53 KO CNE2 vs. control CNE2 cells and primary NPCs vs. normal nasopharyngeal mucosal tissues. **(F)** GO enrichment analysis of differentially expressed genes in the p53 KO CNE2 and control CNE2 cells according to biological process, cellular component and molecular function. **(G)** KEGG enrichment analysis of the differential expression genes in p53 KO CNE2 and control CNE2 cells. **(H)** Top 5 KEGG pathways of enriched differentially expressed genes in the p53 KO CNE2 and control CNE2 cells. **(I)** qRT-PCR detection of 6 differentially expressed genes mRNA levels (EPHA2, IRS1, CCNE1, PDPK1, TLR4, and FN1) that enriched in PI3K-Akt signaling pathway and downregulated in the p53 KO CNE2 cells. ***$P < 0.001$. KO, p53 knockout; Normal, normal nasopharyngeal mucosal tissue.

groups. Differences were considered statistically significant when $P < 0.05$.

RESULTS

Heterozygous p53-R280T Mutation Occurs in NPC Cell Lines

Genomic DNA obtained from CNE2, 5-8F, 6-10B, and C666-1 cells was amplified and detected for mutations at codon 280 of p53 gene by Sanger sequencing. Alignment analysis of DNA sequences was performed using the NCBI BLAST. A heterozygous G changed to C point mutation at codon 280, position 2 (AGA coding for arginine changed to ACA coding for threonine) was detected in the CNE2, 5-8F, 6–10B cell lines (**Figure 1A**), which indicated that one allele was mutated, the other allele was retained as normal at codon 280. However, the amplified DNA sequences of p53 at codon 280 from C666-1 cells were exactly the same as the human wild-type (wt) p53 sequences, compared with the database (**Figure 1A**). The results confirmed that heterozygous p53-R280T mutation is present in CNE2, 5-8F and 6-10B cells, but not in C666-1 cells.

Generation of p53 Knockout NPC Cell Lines by CRISPR/Cas9 Gene Editing System

To study the roles of heterozygous p53-R280T mutation in NPC cells, we established p53 knockout (KO) CNE2 and C666-1 cell lines, in which p53 was knocked out at the chromosomal level by using CRISPR/Cas9 gene editing system. Single-guide RNA (sgRNA) was designed to delete exon 5 of the p53 gene (**Figure 1B**). Guide RNA (gRNA) vector and control vector were transfected into CNE2 and C666-1 cells, respectively. Sanger sequencing was used to identify the cell lines in which both alleles of p53 were deleted. The results showed that p53 was knocked out in the CNE2 cells (KO-41 and KO-49) (**Figure 1C**), and C666-1 cells (KO-9 and KO-29) (**Figure 1D**). Western blot analysis showed that there was no detectable p53 protein in the p53 KO CNE2 and C666-1 cells (**Figure 1E**). The results demonstrated that CNE2 and C666-1 cell lines with p53 KO are established.

Heterozygous p53-R280T Mutation Promotes NPC Cell Proliferation and Survival

We evaluated the effect of p53 KO on NPC cell proliferation by plate colony formation assay, EdU incorporation assay and CCK-8 assay. The results showed that p53 KO significantly suppressed cell proliferation in the CNE2 cells with heterozygous p53-R280T mutation, whereas significantly promoted cell proliferation in C666-1 cells with wt p53 (**Figures 2A–C**). Flow cytometric analysis of cell cycle distribution showed that p53 KO blocked G1/S phase progression in the CNE2 cells, whereas accelerated G1/S phase progression in the C666-1 cells (**Figure 3A**). Next, we analyzed the effect of p53 KO on the apoptosis of CNE2 and C666-1 cells by using flow cytometry. The results showed that p53 KO significantly increased cell apoptosis in the CNE2 cells, whereas significantly decreased cell apoptosis in the C666-1 cells (**Figure 3B**). Together, the results demonstrated that heterozygous p53-R280T mutation promotes NPC cell proliferation and survival.

Heterozygous p53-R280T Mutation Promotes Anchorage-Independent Growth and *in vivo* Tumorigenicity of NPC Cells

Soft agar colony formation assay and subcutaneous tumor formation experiment in nude mice were performed to determine the effects of heterozygous p53-R280T mutation on the anchorage-independent growth and *in vivo* tumorigenicity of NPC cells respectively. The results showed that p53 KO significantly decreased the formation ability of soft agar colony in the CNE2 cells, whereas significantly increased the formation ability of soft agar colony in the C666-1 cells (**Figure 4A**). Subcutaneous tumor formation experiment showed that p53 KO significantly decreased the *in vivo* growth of CNE2 cells in nude mice (**Figure 4B**). The results demonstrated that heterozygous p53-R280T mutation promotes the anchorage-independent growth and *in vivo* tumorigenicity of NPC cells.

Differentially Expressed Genes in the Heterozygous p53-R280T KO and Control CNE2 Cells

To explore the mechanism by which heterozygous p53-R280T mutation promotes the oncogenicity of NPC cells, we carried out mRNA sequencing in the p53 KO CNE2 (KO-41) and control CNE2 cells. As a result, a total of 2,612 differentially expressed genes (DEGs) (fold change≥2) were identified in the KO-41 and control CNE2 cells (**Figures 5A,B**). Of them, 1401 DEGs were upregulated and 1211 DEGs were downregulated in the KO-41 cells (**Supplementary Table S2**). To verify the mRNA sequencing results, qRT-PCR was conducted to detect the mRNA levels of 5 genes (CYR61, TP53, THBS1, CDKN1A, and ECM2) in the KO-41 and control CNE2 cells. The results showed that the relative expression patterns of the five genes

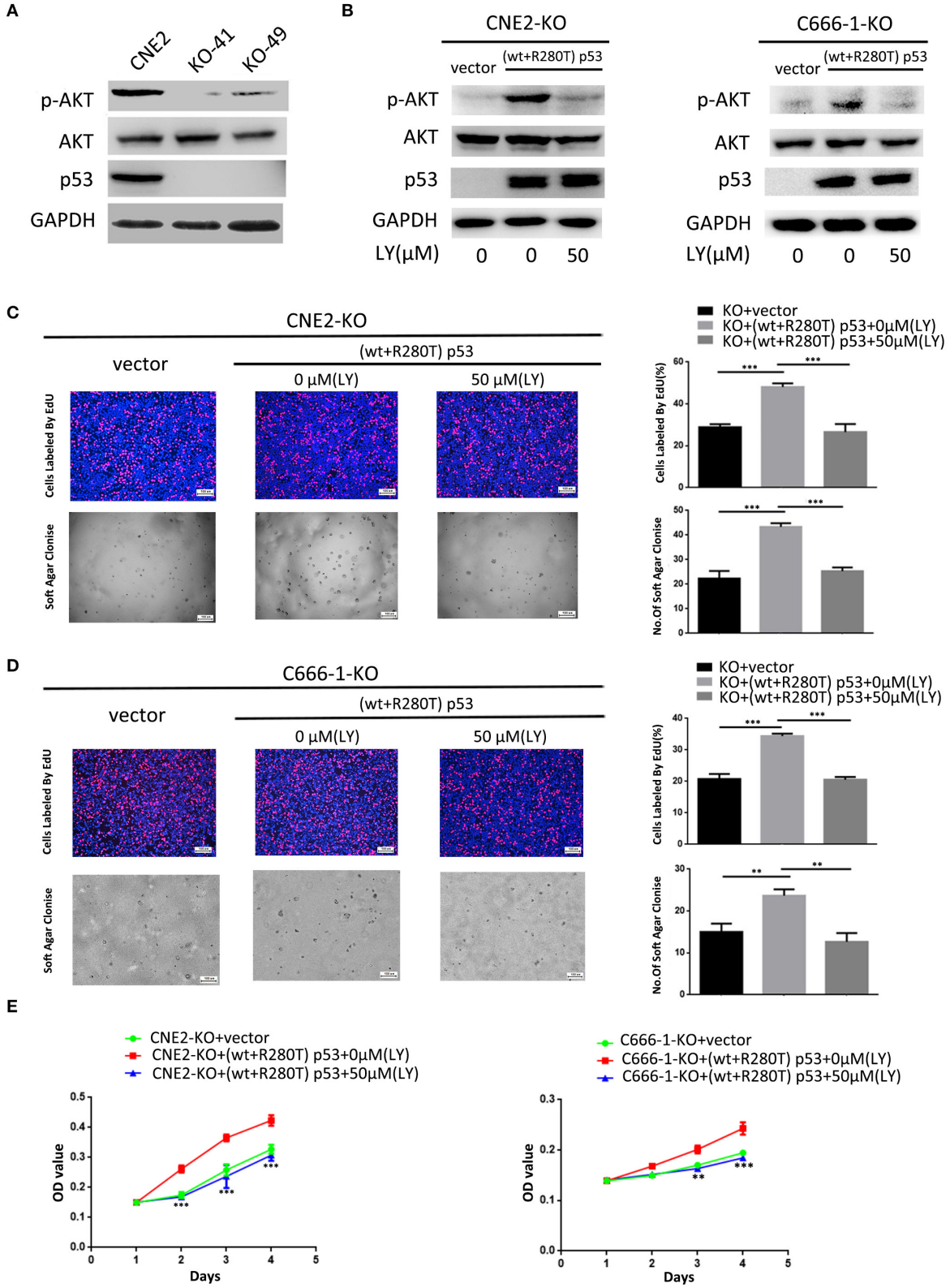

FIGURE 6 | PI3K-Akt signaling pathway mediates heterozygous p53-R280T mutation-promoting NPC cell proliferation. **(A)** Western blot analysis showing the levels of p-AKT(S308) in the p53 KO CNE2 and control CNE2 cells. **(B)** Western blot analysis showing the levels of p-AKT(S308) in the p53 KO CNE2 and C666-1 cells

(Continued)

FIGURE 6 | transiently transfected with p53-R280T mutation and wt p53 plasmid at a 1:1 ratio, followed by treatment with 50 μM LY294002 for 12 h. **(C,D)** Representative results (left) and statistical analyses (right) of cell proliferation detected by EdU incorporation assay and soft agar colony formation assay in the p53 KO CNE2 and C666-1 cells transiently transfected with p53-R280T mutation and wt p53 plasmid at a 1:1 ratio, followed by treatment with 50 μM LY294002 for 12 h. **(E)** CCK-8 assay showing cell proliferation in the p53 KO CNE2 and C666-1 cells transiently transfected with p53-R280T mutation and wt p53 plasmid, followed by treatment with 50 μM LY294002 for 12 h. $^{**}P < 0.01$, $^{***}P < 0.001$. Vector, transfected with an empty vector; KO, p53 knockout; LY, LY294002.

were consistent with mRNA sequencing data, with a correlation coefficient of 0.98 between qRT-PCR and mRNA sequencing results (**Figures 5C,D**). The results demonstrated that the mRNA sequencing results are reliable.

To investigate whether the DEGs in the p53 KO and control CNE2 cells are abnormally expressed in NPC biopsies, we downloaded the gene expression profile of NPC tissues from the GEO database (GSE12452) (23), and compared the DEGs with the differential gene expression profile of NPC tissues. The result showed that sixty-one mRNAs, such as PCNA, TIGAR, MMP1, FN1, SPARC and POSTN, upregulated in the CNE2 cells were also upregulated in NPC tissues; seventy-six mRNAs, such as CDKN2B, BCL6, KLF4 and TP53INP2, downregulated in the CNE2 cells were also downregulated in NPC tissues (**Figure 5E**, **Supplementary Table S3**), which suggests that these DEGs regulated by heterozygous p53-R280T mutation maybe participate in the carcinogenesis of NPC.

Gene Ontology and KEGG Pathways Enrichment Analysis of Differentially Expressed Genes

The 2612 DEGs identified in the present study were formulated into an XML-based input data set to query the GO database. The results showed that all DEGs were divided into three major groups: cellular component, molecular function and biological process, as well as 55 functional groups (**Supplementary Table S4**). In the cellular component, molecular function and biological process, 17, 14, and 24 functional groups were annotated respectively, many of which are involved in tumorigenesis, such as the regulation of cell growth, cell adhesion, antioxidant, and metabolic process (**Figure 5F**).

The 2612 DEGs were uploaded into the KEGG database for pathway enrichment analysis. The results showed that 37 pathways were found to be statistically enriched (**Supplementary Table S5**), including many pathways involved in tumor development and progression, such as cytokine-cytokine receptor interaction, PI3K-Akt signaling pathway, Jak-STAT signaling pathway and cytosolic DNA-sensing pathway (**Figures 5G,H**). Moreover, the expression of 66 genes in the PI3K signaling pathway was downregulated in the p53 KO CNE2 cells (**Supplementary Table S6**). qRT-PCR was performed to detect the mRNA levels of 6 differentially expressed genes (EPHA2, IRS1, CCNE1, PDPK1, TLR4, and FN1) that enriched in PI3K-Akt signaling pathway and downregulated in the p53 KO CNE2 cells. The results showed that the expression levels of these genes were reduced in the p53 KO CNE2 cells (**Figure 5I**). These results suggest that PI3K-Akt pathway signaling may be involved in heterozygous p53-R280T mutation-mediated NPC promotion.

Activation of PI3K-Akt Signaling Pathway Is Involved in Heterozygous p53-R280T Mutation-Mediated NPC Promotion

To investigate whether PI3K-Akt signaling pathway is involved in heterozygous p53-R280T mutation-mediated NPC promotion, we detected the levels of p-AKT in the KO-41, KO-49, and control CNE2 cells by western blot, and observed that p-AKT was significantly decreased in the KO-41 and KO-49 cells relative to control CNE2 cells (**Figure 6A**). Moreover, we transiently transfected p53 KO CNE2 and p53 KO C666-1 cells with wt p53 and p53-R280T mutation plasmid at 1:1 ratio (equal to transfection of heterozygous p53-R280T mutation), and then treated the cells with PI3K inhibitor LY294002. We observed that transfection of wt p53 and p53-R280T mutation plasmid at 1:1 ratio dramatically increased p-AKT levels in the p53 KO CNE2 and p53 KO C666-1 cells, which was abolished by LY294002 (**Figure 6B**). The results demonstrated that heterozygous p53-R280T mutation activated PI3K-Akt signaling pathway in NPC cells. Functionally, transfection of wt p53 and p53-R280T mutation plasmid at 1:1 ratio promoted *in vitro* cell proliferation of p53 KO CNE2 and p53 KO C666-1 cells, which was abolished by LY294002 (**Figures 6C–E**). Moreover, flow cytometric analysis showed that transfection of wt p53 and p53-R280T mutation plasmid at 1:1 accelerated G1/S phase progression and inhibited cell apoptosis in the p53 KO CNE2 and p53 KO C666-1 cells, which was abolished by LY294002 (**Figures 7A,B**). These results indicate that PI3K-Akt signaling pathway activation is involved in the tumor-promoting effects of heterozygous p53-R280T mutation in NPC cells.

DISCUSSION

In 1992, a heterozygous p53-R280T mutation was first detected in the NPC CNE2 and CNE1 cell lines (17). Consistent with this report, we also observed the same heterozygous mutation of p53 gene in the NPC CNE2, 5-8F, and 6-10B cell lines by Sanger sequencing. Previous study has shown that p53 gene is wild-type in the NPC C666-1 cell lines (15). We also did not find p53-R280T mutation in the C666-1 cells. The heterozygous p53-R280T mutation also exists in NPC tissues, with a mutation rate of about 10% (17). It is suggested that p53-R280T mutation may occur in primary tumors or may be acquired during the establishment or culture of cancer cell lines *in vitro* (17, 24). Nonetheless, the biological functions of heterozygous p53-R280T mutation in cancers remain unclear. To determine the roles of heterozygous p53-R280T mutation in NPC, we chose CNE2 with heterozygous R280T mutation and C666-1 with wt p53 gene to establish p53 knockout cell

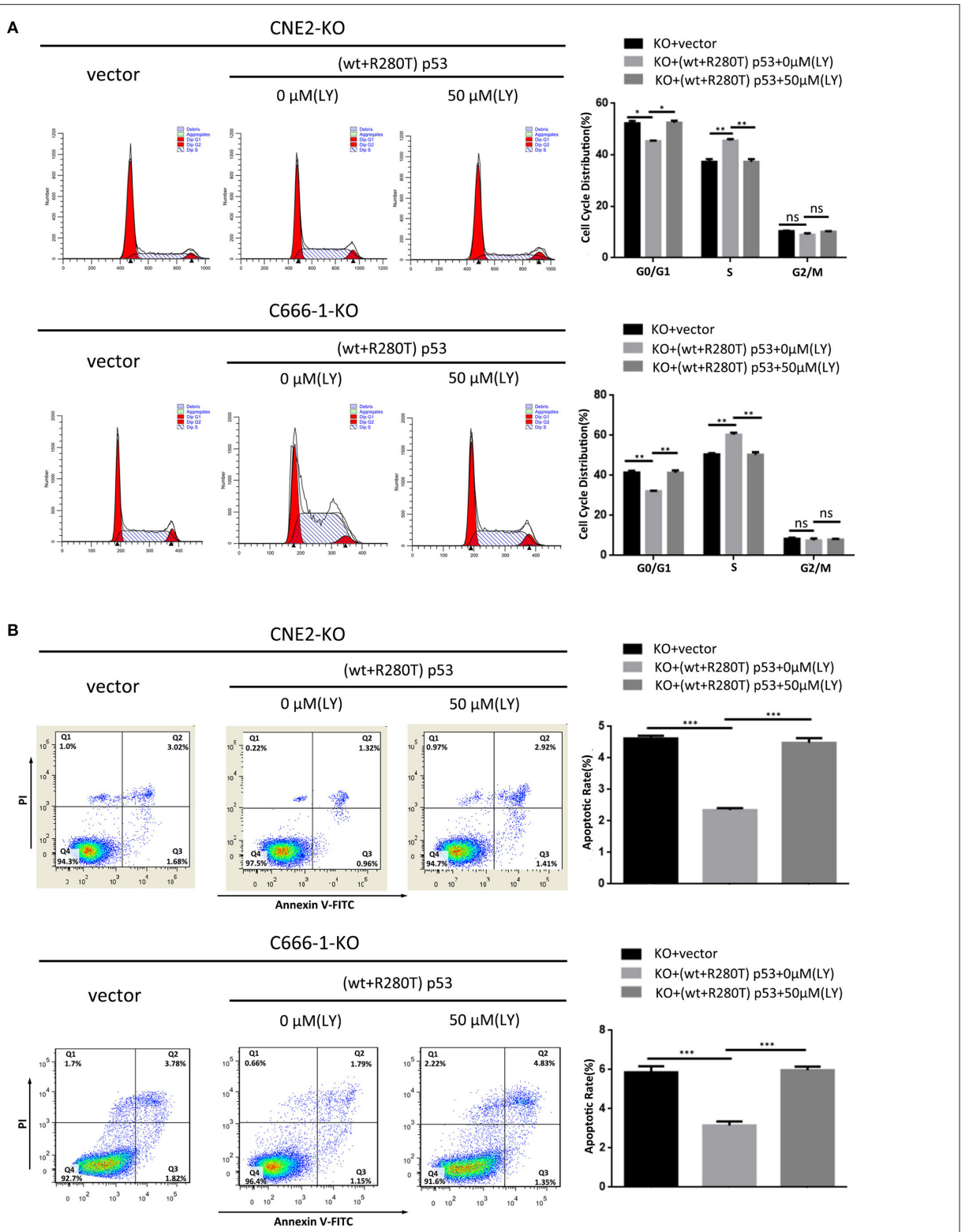

FIGURE 7 | PI3K-Akt signaling pathway mediates the effect of heterozygous p53-R280T on cell cycle and apoptosis of NPC cells. **(A)** Representative results (left) and statistical analyses (right) of cell cycle distribution analyzed by flow cytometry in the p53 KO CNE2 and C666-1 cells transiently transfected with p53-R280T mutation and wt p53 plasmid at a 1:1 ratio, followed by treatment with 50μM LY294002 for 12h. **(B)** Representative results (left) and statistical analyses (right) of cell apoptosis analyzed by flow cytometry in the p53 KO CNE2 and C666-1 cells transiently transfected with p53-R280T mutation and wt p53 plasmid at a 1:1 ratio, followed by treatment with 50 μM LY294002 for 12h. *$P < 0.05$; **$P < 0.01$; ***$P < 0.001$; ns, no significance. Vector, transfected with an empty vector; KO, p53 knockout; LY, LY294002.

lines. We found that knockout of endogenous p53 gene with heterozygous p53-R280T mutation suppressed NPC proliferation and increased NPC cell apoptosis, and inhibited the anchorage-independent growth and *in vivo* tumorigenicity of NPC cells. In contrast, knockout of wt p53 had the opposite effects on NPC cells. Moreover, transfection of wt p53 and p53-R280T mutation plasmid at 1:1 ratio, which is equal to heterozygous p53-R280T mutation, promoted NPC cell proliferation and survival in the NPC cells with endogenous p53 knockout. Our results indicate that heterozygous p53-R280T mutation gains oncogenic activities and functions as an oncogene in NPC cells.

To explore the mechanism by which heterozygous p53-R280T mutation is involved in the tumor promotion of NPC cells, we carried out mRNA sequencing in the p53 KO and control CNE2 cells, and observed that 1401 DEGs were upregulated, and 1211 DEGs were downregulated in the p53 KO CNE2 with heterozygous p53-R280T mutation. To investigated whether these DEGs were abnormally expressed in NPC biopsies, we compared these DEGs with the differential gene expression profile from NPC biopsies (GSE12452) (23), and observed that 61 mRNAs upregulated in the CNE2 cells were also upregulated in the NPC biopsies, and 66 mRNAs downregulated in the CNE2 cells were also downregulated in the NPC biopsies, suggesting that these DEGs regulated by heterozygous p53-R280T mutation maybe participate in the carcinogenesis of NPC. Besides, KEGG pathway enrichment analysis showed that the DEGs were statistically enriched in pathways related to cancer such as PI3K-Akt signaling pathway, Jak-STAT signaling pathway, MAPK signaling pathway, TNF signaling pathway and Wnt signaling pathway, which may be associated with the NPC promotion of heterozygous p53-R280T mutation. We also observed that the mRNA level of p53 target gene CDKN1A (p21) increased in the p53 KO CNE2 cells with heterozygous p53-R280T mutation. Previous report also shows that p53 silencing resulted in upregulation of p21 in CNE2 cells (25), supporting that heterozygous p53-R280T mutation gains oncogenic property in NPC cells.

PI3K plays an important role in cancer development and progression (26–32). Once activated, PI3K converts membrane-bound phosphatidylinositol 4, 5-biphosphate (PIP2) into phosphatidylinositol 3,4,5-triphosphate (PIP3) (33). PIP3 then recruits phosphoinositide-dependent kinase 1 (PDK1) to phosphorylate Akt at threonine 308. Subsequently, mTOR complex 2 (mTORC2) phosphorylates Akt at serine 473(Ser473) for AKT activation (34, 35). Thereafter, activated Akt interacts with downstream target proteins to regulate multiple biological processes. In the present study, mRNA sequencing of heterozygous p53-R280T KO CNE2 and control cells showed that heterozygous p53-R280T mutation activated PI3K-Akt signaling pathway, and transfection of wt p53 and p53-R280T mutation plasmid at 1:1 ratio dramatically increased p-AKT levels in the NPC cells with endogenous p53 KO, which was abolished by LY294002. The results demonstrated that heterozygous p53-R280T mutation activates PI3K-Akt signaling pathway in NPC cells. Importantly, blocking of PI3K-Akt signaling pathway abolished heterozygous p53-R280T mutation-promoting NPC cell proliferation and survival, indicating that heterozygous p53-R280T mutation promotes the oncogenicity of NPC cells by activating PI3K-Akt signaling pathway. Moreover, the genes enriched in PI3K-Akt signaling pathway, such as EPHA2, IRS1, FN1, PDGFRB, THBS1, CCND1, CCNE1, TLR4, FGFR1 and FLT1, promote the development and progression of NPC (36–46). Therefore, heterozygous p53-R280T mutation-activated PI3K-Akt signaling pathway may be involved in NPC carcinogenesis through theses target genes.

In summary, our data suggest that heterozygous p53-R280T mutation functions as an oncogene in NPC, and promotes the oncogenicity of NPC cells by activating PI3K-Akt signaling pathway. P53 knockout NPC cell lines and heterozygous p53-R280T mutation-associated DEGs provide a valuable tool to investigate the role and molecular mechanism of heterozygous p53-R280T mutation in NPC.

DATA AVAILABILITY STATEMENT

The datasets of mRNA-sequencing for this study can be found in the GEO: http://www.ncbi.nlm.nih.gov/geo/query/acc.cgi?acc=GSE130398.

ETHICS STATEMENT

All animal experimental procedures were performed in accordance with the Guide for the Care and Use of Laboratory Animals of Xiangya Hospital, Central South University, with the approval of the Institutional Animal Ethics Committee.

AUTHOR CONTRIBUTIONS

Z-QQ and Z-QX designed experiments. Z-QQ, Q-GL, and HY implemented experiments. Z-QQ, Z-QX, Q-GL, WH, S-SL, Y-YT, and Z-XR analyzed experimental results. ZQ-Q and Z-QX wrote the manuscript.

FUNDING

This work was supported by the National Natural Science Foundation of China (81874132, 81672687), the Natural Science Foundation of Hunan Province (2019JJ40486), and Shenzhen Municipal Government of China (KQTD20170810160226082).

SUPPLEMENTARY MATERIAL

The Supplementary Material for this article can be found online at: https://www.frontiersin.org/articles/10.3389/fonc.2020.00104/full#supplementary-material

REFERENCES

1. Wei WI, Sham JS. Nasopharyngeal carcinoma. *Lancet*. (2005) 365:2041–54. doi: 10.1016/S0140-6736(05)66698-6
2. McDermott AL, Dutt SN, Watkinson JC. The aetiology of nasopharyngeal carcinoma. *Clin Otolaryngol Allied Sci*. (2001) 26:82–92. doi: 10.1046/j.1365-2273.2001.00449.x
3. Bei JX, Li Y, Jia WH, Feng BJ, Zhou G, Chen LZ, et al. A genome-wide association study of nasopharyngeal carcinoma identifies three new susceptibility loci. *Nat Genet*. (2010) 42:599–603. doi: 10.1038/ng.601
4. Zeng YX, Jia WH. Familial nasopharyngeal carcinoma. *Semin Cancer Biol*. (2002) 12:443–450. doi: 10.1016/S1044579X02000871
5. Kastenhuber ER, Lowe SW. Putting p53 in context. *Cell*. (2017) 170:1062–78. doi: 10.1016/j.cell.2017.08.028
6. Kastan MB. Wild-type p53: tumors can't stand it. *Cell*. (2007) 128:837–40. doi: 10.1016/j.cell.2007.02.022
7. Gong Z, Huang H, Xu K, Liang F, Li X, Xiong W, et al. Advances in microRNAs and TP53 gene regulatory network. *Prog Biochem Biophy*. (2012) 39:1133–44. doi: 10.3724/SP.J.1206.2012.00015
8. Levine AJ, Finlay CA. Hinds PW. P53 is a tumor suppressor gene. *Cell*. (2004) 116:S67–S69. doi: 10.1016/S0092-8674(04)00036-4
9. Gomes AS, Trovão F, Andrade Pinheiro B, Freire F, Gomes S, Oliveira C, et al. The crystal structure of the R280K mutant of human p53 explains the loss of DNA binding. *Int J Mol Sci*. (2018) 19:E1184. doi: 10.3390/ijms19041184
10. IARC_TP53_Database. (2019) Available online at: http://www-p53.iarc.fr/ (accessed July, 2019).
11. Lo KW, To KF, Huang DP. Focus on nasopharyngeal carcinoma. *Cancer Cell*. (2004) 5:423–8. doi: 10.1016/S1535-6108(04)00119-9
12. Burgos JS. Absence of p53 alterations in NPC Spanish patients with Epstein-Barr infection. *Virus Genes*. (2003) 27:263–8. doi: 10.1023/A:1026347900050
13. Chang YS, Lin YJ, Tsai CN, Shu CH, Tsai MS, Choo KB, et al. Detection of mutations in the p53 gene in human head and neck carcinomas by single strand conformation polymorphism analysis. *Cancer Lett*. (1992) 67:167–74. doi: 10.1016/0304-3835(92)90140-Q
14. Van Tornout JM, Spruck CH III, Shibata A, Gonzalez-Zulueta M, Nichols PW, Chandrasoma PT, et al. Presence of p53 mutations in primary nasopharyngeal carcinoma (NPC) in non-Asians of Los Angeles, California, a low-risk population for NPC. *Cancer Epidemiol Biomarkers Prev*. (1997) 6:493–7.
15. Lin DC, Meng X, Hazawa M, Nagata Y, Varela AM, Xu L, et al. The genomic landscape of nasopharyngeal carcinoma. *Nat Genet*. (2014) 46:866–71. doi: 10.1038/ng.3006
16. Lung ML, Hu Y, Cheng Y, Li MF, Tang CM, O SK, et al. P53 inactivating mutations in Chinese nasopharyngeal carcinomas. *Cancer Lett*. (1998) 133:89–94. doi: 10.1016/S0304-3835(98)00209-2
17. Sun Y, Hegamyer G, Cheng YJ, Hildesheim A, Chen JY, Chen IH, et al. An infrequent point mutation of the p53 gene in human nasopharyngeal carcinoma. *Proc Natl Acad Sci USA*. (1992) 89:6516–20. doi: 10.1073/pnas.89.14.6516
18. Hwang JK, Lin CT. Co-localization of endogenous and exogenous p53 proteins in nasopharyngeal carcinoma cells. *J Histochem Cytochem*. (1997) 45:991–1003. doi: 10.1177/002215549704500709
19. Hoe SL, Sam CK. Mutational analysis of p53 and RB2/p130 genes in Malaysian nasopharyngeal carcinoma samples: a preliminary report. *Malays J Pathol*. (2006) 28:35–39. doi: 10.1002/joc.4252
20. Zheng Z, Qu JQ, Yi HM, Ye X, Huang W, Xiao T, et al. MiR-125b regulates proliferation and apoptosis of nasopharyngeal carcinoma by targeting A20/NF-κB signaling pathway. *Cell Death Dis*. (2017) 8:e2855. doi: 10.1038/cddis.2017.211
21. Zhu JF, Huang W, Yi HM, Xiao T, Li JY, Feng J, et al. Annexin A1-suppressed autophagy promotes nasopharyngeal carcinoma cell invasion and metastasis by PI3K/AKT signaling activation. *Cell Death Dis*. (2018) 9:1154. doi: 10.1038/s41419-018-1204-7
22. Xiao T, Zhu W, Huang W, Lu SS, Li XH, Xiao ZQ, et al. RACK1 promotes tumorigenicity of colon cancer by inducing cell autophagy. *Cell Death Dis*. (2018) 9:1148. doi: 10.1038/s41419-018-1113-9
23. Sengupta S, den Boon JA, Chen IH, Newton MA, Dahl DB, Chen M, et al. Genome-wide expression profiling reveals EBV-associated inhibition of MHC class I expression in nasopharyngeal carcinoma. *Cancer Res*. (2006) 66:7999–8006. doi: 10.1158/0008-5472.CAN-05-4399
24. Lo KW, Mok CH, Huang DP, Liu YX, Choi PH, Lee JC, et al. P53 mutation in human nasopharyngeal carcinoma. *Anticancer Res*. (1992) 12:1957–63
25. Vikhanskaya F, Lee MK, Mazzoletti M, Broggini M, Sabapathy K. Cancer-derived p53 mutants suppress p53-target gene expression–potential mechanism for gain of function of mutant p53. *Nucleic Acids Res*. (2007) 35:2093-104. doi: 10.1093/nar/gkm099
26. Zhao L, Vogt PK. Class I PI3K in oncogenic cellular transformation. *Oncogene*. (2008) 27:5486–96. doi: 10.1038/onc.2008.244
27. Courtney KD, Corcoran RB, Engelman JA. The PI3K pathway as drug target in human cancer. *J Clin Oncol*. (2010) 28:1075–83. doi: 10.1200/JCO.2009.25.3641
28. Engelman JA. Targeting PI3K signaling in cancer: opportunities, challenges and limitations. *Nat Rev Cancer*. (2009) 9:550–62. doi: 10.1038/nrc2664
29. Fulda S. The PI3K/Akt/mTOR pathway as therapeutic target in neuroblastoma. *Curr Cancer Drug Targets*. (2009) 9:729–37. doi: 10.2174/156800909789271521
30. Vogt PK, Hart JR, Gymnopoulos M, Jiang H, Kang S, Bader AG, et al. Phosphatidylinositol 3-kinase: the oncoprotein. *Curr Top Microbiol Immunol*. (2010) 347:79–104. doi: 10.1007/82_2010_80
31. Chen JZ. Targeted therapy of obesity-associated colon cancer. *Transl Gastrointest Cancer*. (2012) 1:44–57. doi: 10.3978/j.issn.2224-4778.2011.11.01
32. Chen JZ, Wang MB. The roles of miRNA-143 in colon cancer and therapeutic implications. *Transl Gastrointest Cancer*. (2012) 1:169–74. doi: 10.3978/j.issn.2224-4778.2012.07.01
33. Rubashkin MG, Cassereau L, Bainer R, DuFort CC, Yui Y, Ou G, et al. Force engages vinculin and promotes tumor progression by enhancing PI3K activation of phosphatidylinositol (3,4,5)-triphosphate. *Cancer Res*. (2014) 74:4597–611. doi: 10.1158/0008-5472.CAN-13-3698
34. Majchrzak A, Witkowska M, Smolewski P. Inhibition of the PI3K/Akt/mTOR signaling pathway in diffuse large B-cell lymphoma: current knowledge and clinical significance. *Molecules*. (2014) 19:14304–15. doi: 10.3390/molecules190914304
35. Sarbassov DD, Guertin DA, Ali SM, Sabatini DM. Phosphorylation and regulation of Akt/PKB by the rictor-mTOR complex. *Science*. (2005) 307:1098–101. doi: 10.1126/science.1106148
36. Li JY, Xiao T, Yi HM, Yi H, Feng J, Zhu JF, et al. S897 phosphorylation of EphA2 is indispensable for EphA2-dependent nasopharyngeal carcinoma cell invasion, metastasis and stem properties. *Cancer Lett*. (2019) 444:162–74. doi: 10.1016/j.canlet.2018.12.011
37. Tan P, Liu Y, Yu C, Su Z, Li G, Zhou X, et al. EphA2 silencing in nasopharyngeal carcinoma leads to decreased proliferation, invasion and increased sensitization to paclitaxel. *Oncol Lett*. (2012) 4:429–34. doi: 10.3892/ol.2012.746
38. Luo J, Wen Q, Li J, Xu L, Chu S, Wang W, et al. Increased expression of IRS-1 is associated with lymph node metastasis in nasopharyngeal carcinoma. *Int J Clin Exp Pathol*. (2014) 7:6117–24.
39. Wang J, Deng L, Huang J, Cai R, Zhu X, Liu F, et al. High expression of Fibronectin 1 suppresses apoptosis through the NF-κB pathway and is associated with migration in nasopharyngeal carcinoma. *Am J Transl Res*. (2017) 9:4502–11.
40. Zhen Y, Fang W, Zhao M, Luo R, Liu Y, Fu Q, et al. MiR-374a-CCND1-pPI3K/AKT-c-JUN feedback loop modulated by PDCD4 suppresses cell growth, metastasis, and sensitizes nasopharyngeal carcinoma to cisplatin. *Oncogene*. (2017) 36:275–85. doi: 10.1038/onc.2016.201
41. He S, Yang S, Niu M, Zhong Y, Dan Gao, Zhang Y, et al. HMG-box transcription factor 1: a positive regulator of the G1/S transition through the Cyclin-CDK-CDKI molecular network in nasopharyngeal carcinoma. *Cell Death Dis*. (2018) 9:100. doi: 10.1038/s41419-017-0175-4
42. Chen L, Zhou H, Guan Z. CircRNA_000543 knockdown sensitizes nasopharyngeal carcinoma to irradiation by targeting miR-9/platelet-derived growth factor receptor B axis. *Biochem Biophys Res Commun*. (2019) 512:786–92. doi: 10.1016/j.bbrc.2019.03.126

43. Cheng Y, Ho RL, Chan KC, Kan R, Tung E, Lung HL, et al. Anti-angiogenic pathway associations of the 3p21.3 mapped BLU gene in nasopharyngeal carcinoma. *Oncogene*. (2015) 34:4219–28. doi: 10.1038/onc.2014.353
44. Li Y, Xie G, Li L, Jiang Z, Yue Z, Pan Z. The effect of TLR4/MyD88/NF-κB signaling pathway on proliferation and apoptosis in human nasopharyngeal carcinoma 5-8F cells induced by LPS. *Lin Chung Er Bi Yan Hou Tou Jing Wai Ke Za Zhi*. (2015) 29:1012–5. doi: 10.13201/j.issn.1001-1781.2015.11.015
45. Lo AK, Dawson CW, Young LS, Ko CW, Hau PM, Lo KW. Activation of the FGFR1 signalling pathway by the Epstein-Barr virus-encoded LMP1 promotes aerobic glycolysis and transformation of human nasopharyngeal epithelial cells. *J Pathol*. (2015) 237:238–48. doi: 10.1002/path.4575
46. Sha D, He YJ. Expression and clinical significance of VEGF and its receptors Flt-1 and KDR in nasopharyngeal carcinoma. *Ai Zheng*. (2006) 25:229–34. doi: 10.1007/s11769-006-0026-1

Conflict of Interest: The authors declare that the research was conducted in the absence of any commercial or financial relationships that could be construed as a potential conflict of interest.

The reviewer GL declared a shared affiliation, though no other collaboration, with the authors to the handling Editor.

frontiers in Oncology

ORIGINAL RESEARCH
published: 14 February 2020
doi: 10.3389/fonc.2020.00119

Evaluation of the National Comprehensive Cancer Network and European Society for Medical Oncology Nasopharyngeal Carcinoma Surveillance Guidelines

*Guan-Qun Zhou†, Jia-Wei Lv†, Ling-long Tang, Yan-Ping Mao, Rui Guo, Jun Ma and Ying Sun**

State Key Laboratory of Oncology in Southern China, Department of Radiation Oncology, Collaborative Innovation Center of Cancer Medicine, Cancer Center, Sun Yat-sen University, Guangzhou, China

OPEN ACCESS

Edited by:
Paolo Bossi,
University of Brescia, Italy

Reviewed by:
Cessal Thommachan Kainickal,
Regional Cancer Center Thiruvananthapuram, India
Danilo Galizia,
Fondazione del Piemonte per l'Oncologia, Istituto di Candiolo (IRCCS), Italy

***Correspondence:**
Ying Sun
sunying@sysucc.org.cn

†*These authors have contributed equally to this work*

Specialty section:
This article was submitted to Head and Neck Cancer, a section of the journal Frontiers in Oncology

Received: *22 June 2019*
Accepted: *22 January 2020*
Published: *14 February 2020*

Citation:
Zhou G-Q, Lv J-W, Tang L, Mao Y-P, Guo R, Ma J and Sun Y (2020) Evaluation of the National Comprehensive Cancer Network and European Society for Medical Oncology Nasopharyngeal Carcinoma Surveillance Guidelines. Front. Oncol. 10:119. doi: 10.3389/fonc.2020.00119

Purpose: The National Comprehensive Cancer Network (NCCN) and European Society for Medical Oncology (ESMO) provide surveillance guidelines for nasopharyngeal carcinoma (NPC). We evaluated the ability of these guidelines to capture disease recurrence.

Materials and methods: All 749 NPC patients were stratified for analysis by T and N stage. We evaluated the guidelines by calculating the percentage of relapses detected when following the 2018 NCCN, 2015 NCCN, and 2012 ESMO surveillance guidelines, and related surveillance costs were compared.

Results: At a median follow-up of 100.8 months, 168 patients (22.4%) had experienced recurrence. Nineteen recurrences (11.3%) were detected using the 2018 NCCN, 53 (31.5%) using the 2015 NCCN and 46 (27.4%) using the ESMO guidelines. To capture 95% recurrences, surveillance would be required for 85.57 months for T1/2, 67.45 months for T3/4, 83.57 months for N0/1, and 55.80 months for N2/3 disease. In T1/2 disease, Medicare surveillance costs per patient were US$1642.66 using 2018 NCCN or ESMO and US$2179.81 using 2015 NCCN. Costs per recurrence detected were US$42,578.64, 62,088.70, and 73,329.76 using 2018 NCCN, 2015 NCCN, and ESMO, respectively.

Conclusions: If strictly followed, the NCCN and ESMO guidelines will miss more than two-thirds recurrences. Improved surveillance algorithms to balance patient benefit against costs are needed.

Keywords: national comprehensive cancer network, European Society for Medical Oncology, guidelines, surveillance, nasopharyngeal carcinoma

INTRODUCTION

Nasopharyngeal carcinoma (NPC) is radiosensitive and radiation was the mainstay definitive treatment. Though excellent control especially in local and regional disease can be achieved, recurrence after primary treatment is a major threat for NPC patients, particularly in patients who present with advanced stage NPC. Close follow-up can accurately assess treatment response as well as early detect the recurrent disease, and it can salvage a percentage of patients amenable to radical surgery or re-irradiation (1). However, intensive review can also incur considerable costs.

Despite an evident necessity, the optimal follow-up schedule and regimen for NPC patients after radical radiotherapy has not been thoroughly addressed. The National Comprehensive Cancer Network (NCCN) and European Society for Medical Oncology (ESMO) provide well-recognized follow-up guidelines for (2–4). However, these recommended surveillance protocols for NPC were somewhat contradicted. In the past many years, the NCCN recommended annual magnetic resonance imaging (MRI) for T3/4 or N2/3 disease due to the inaccessibility of the nasopharynx. In 2018, the NCCN updated their recommendations and suggested neither routine imaging of the nasopharynx nor the neck in patients without signs or symptoms, in view of the fact that in most cases recurrence is reported by patients themselves. Despite this change, the NCCN and the ESMO protocols are not uniform. Due to lack of prospective randomized data, there is no definitive evidence to clarify which regimen is most effective. As a result, there is significant heterogeneity in the follow-up strategies developed by different clinicians, leading to over- and underutilization of surveillance in certain patient populations (5). This variability of health care may translate into a unreasonable allocation of medical resources.

In the present study, we sought to evaluate the performance of the 2018 NCCN, 2015 NCCN, and 2012 ESMO guidelines by calculating how many NPC relapses could be detected when patients follow the surveillance recommendations of these guidelines. After that we calculated the duration of continuous monitoring at different sites in patients with different stages of NPC in order to detect 90, 95, and 100% of recurrent events. Finally, the average cost per recurrent event was compared for follow-up according to the guidelines and assumptions to detect 95% of recurrent events.

PATIENTS AND METHODS

Patient Population

After obtaining approval from the institutional review board of Sun Yat-sen University Cancer Center, we prospectively reviewed our NPC registry system, and identified 778 patients treated with radical intensity modulated radiation therapy (IMRT) or combined chemoradiotherapy for newly diagnosed, non-metastatic NPC between January 2003 and December 2010 at our Cancer Center. Written informed consent was obtained from each patient for their information to be used in research without affecting their treatment options or violating their privacy informed consent was obtained from the participants of this study. If the participants were under the age of 16, written informed consent was obtained from the parents or guardians of participants.

Treatment

All patients received radical IMRT for the entire course of treatment. Details regarding the IMRT techniques have been reported in a previous study (6). During the study period, the therapeutic principles in our institution recommended radiotherapy alone for NPC patients with stage I disease, concurrent chemoradiotherapy for patients with stage II, and concurrent chemoradiotherapy with or without neoadjuvant/adjuvant chemotherapy for stage III–IVb. If necessary, salvage treatments including brachytherapy, surgery, and chemotherapy, were provided in the cases of relapse or persistent disease.

Follow-Up

Because of the retrospective nature, the actual follow up interval and items of this study were not standardized. However, most patients underwent history and physical examination every 3 months for the first 2 years, every 6 months for up to 5 years and then annually. Post-treatment baseline MRI of the nasopharynx and neck within 3 months after treatment was compulsory. Nasopharyngoscopy, MRI of the nasopharynx and neck, chest radiography, or computed tomography (CT), abdominal ultrasonography or CT and whole-body skeletal scintigraphy were recommended to be performed annually or if clinically indicated by tumor recurrence.

Classification of Disease Recurrence

Recurrence disease was defined as relapse tumor at the primary site, regional lymph nodes, or distant sites that was radiographically or pathologically confirmed at least 30 days after treatment. Recurrences were classified by site as nasopharynx, neck, bone, chest, abdomen, or other sites. Using the location categories described above, it is possible to directly translate into the type of imaging or clinical examinations required for follow-up in each site. The first recurrence in each patient was counted as an event and all other recurrences were censored to avoid double counting. Recurrence that occurs simultaneously at multiple sites was individually counted.

Evaluation of Current Guidelines

Table 1 lists the recommended surveillance regimen according to the 2018 NCCN, 2015 NCCN, and 2012 ESMO guidelines. The ability of the guidelines was evaluated by calculating the total recurrences events that would be detected if patients were followed up strictly according to the strategies recommended by the guidelines. Because recurrences in the neck can be detected clinically or via imaging of the neck, the detection of recurrences in the neck was based on the time point recommended for physical examination; detection of recurrences in the nasopharynx, bone, chest and abdomen were via imaging of the nasopharynx, bone, chest or abdomen, respectively. To evaluate the guidelines, patients were stratified according to T and N classification (T1/2 vs. T3/4; N0/1 vs. N2/3). All patients

TABLE 1 | NCCN, ESMO, and AHNS oncologic surveillance schedules for NPC.

	Year 1	Year 2	Year 3	Year 4	Year 5	>5 years
2018 NCCN						
H&P exam	1–3 months	2–6 months	4–8 months	4–8 months	4–8 months	12 months
EBV serology	Consider EBV DNA monitoring					
Baseline imaging	Not routinely recommended					
Chest imaging	Chest CT with or without contrast as clinically indicated for patients with smoking history					
Abdominal imaging	Not mentioned					
Bone scan	Not mentioned					
2015 NCCN						
H&P exam	1–3 months	2–6 months	4–8 months	4–8 months	4–8 months	12 months
EBV serology	Consider EBV DNA monitoring					
Baseline imaging	Annual for T3–4 or N2–3 disease only					
Chest imaging	Annual low-dose chest CT for patients with high risk of lung cancer[#]					
Abdominal imaging	Not mentioned					
Bone scan	Not mentioned					
2012 ESMO						
H&P exam	Periodic examination of the nasopharynx and neck, cranial nerve function					
EBV serology	Post-treatment plasma/serum load of EBV DNA					
Baseline imaging	Used on a 6- to 12-month basis for the first few years for T3 and T4 tumors					
Chest imaging	Not mentioned					
Abdominal imaging	Not mentioned					
Bone scan	Not mentioned					

NCCN, National Comprehensive Cancer Network; ESMO, European Society for Medical Oncology; EBV, Epstein -Barr viral.
[#]Refer to patients aged 55–74 years and >30 pack-year history of smoking and smoking cessation <15 y or patients aged >50 years and >20 pack-year history of smoking and one additional risk factor (other than second-hand smoke) according to NCCN Guidelines Version 1. 2016 Lung Cancer Screening.

were restaged according to the 7th edition of the International Union Against Cancer/American Joint Committee on Cancer system (7).

Both the 2018 and 2015 NCCN guidelines use a time range (e.g., 1–3 months) for the frequency of the history and physical examination, which are too vague for evaluation and comparison; we used the median of the recommended time range (e.g., 2 months for 1–3 months). The 2012 ESMO guidelines suggest periodic history and physical examination; we used the frequency suggested by the 2015 NCCN. The ESMO guidelines suggest nasopharyngeal MRI on a 6–12 months basis for the first few years for T3 and T4 tumors; we specified this as nasopharyngeal MRI every 9 months for the first 5 years.

Medicare Cost Analysis

Using charges issued in 2017 by the Medical Insurance Administration Bureau of Guangzhou, China, the surveillance costs were estimated on a per-patient basis when the recommended follow-up schedules were strictly adhered to and completed, as shown in **Table 1**. The Chinese currency was converted to US dollars based on exchange rate and date [US$1.00 = ¥6.75 [¥ being the Chinese currency in 2017]]. The cost of capturing 95% recurrences was based on the following estimates: the frequency of the history and physical examination was similar to that recommended in the 2018 and 2015 guidelines; and including annual head and neck MRI, annual skeletal scintigraphy, annual chest CT, and annual abdominal CT. Finally, the cost of detecting one recurrent case in each stage group was calculated.

Statistical Analysis

The duration of follow-up required to find 90, 95, and 100% of recurrences at each location by stage stratification was determined by the cumulative frequency of time to relapse. For subgroups that the follow-up time required to detect 95% of recurrent could not be calculated for too few events, it was estimated to be half-way between the time for capturing 90 and 100%. Recurrence rates after treatment were estimated using the Kaplan–Meier and differences were calculated using log–rank tests. The required surveillance durations for the different stages of disease were compared using the Mann–Whitney *U*-test. All tests were two-sided, with $P < 0.05$ considered significant. Statistical analysis was performed using SPSS version 19.0 (IBM, Armonk, NY, USA).

RESULTS

Patient Demographics

A total of 778 consecutive patients with NPC were enrolled between January 2003 and December 2010. Twenty-nine patients were excluded for the following reasons: fewer than 3 months of follow-up ($n = 19$); insufficient staging

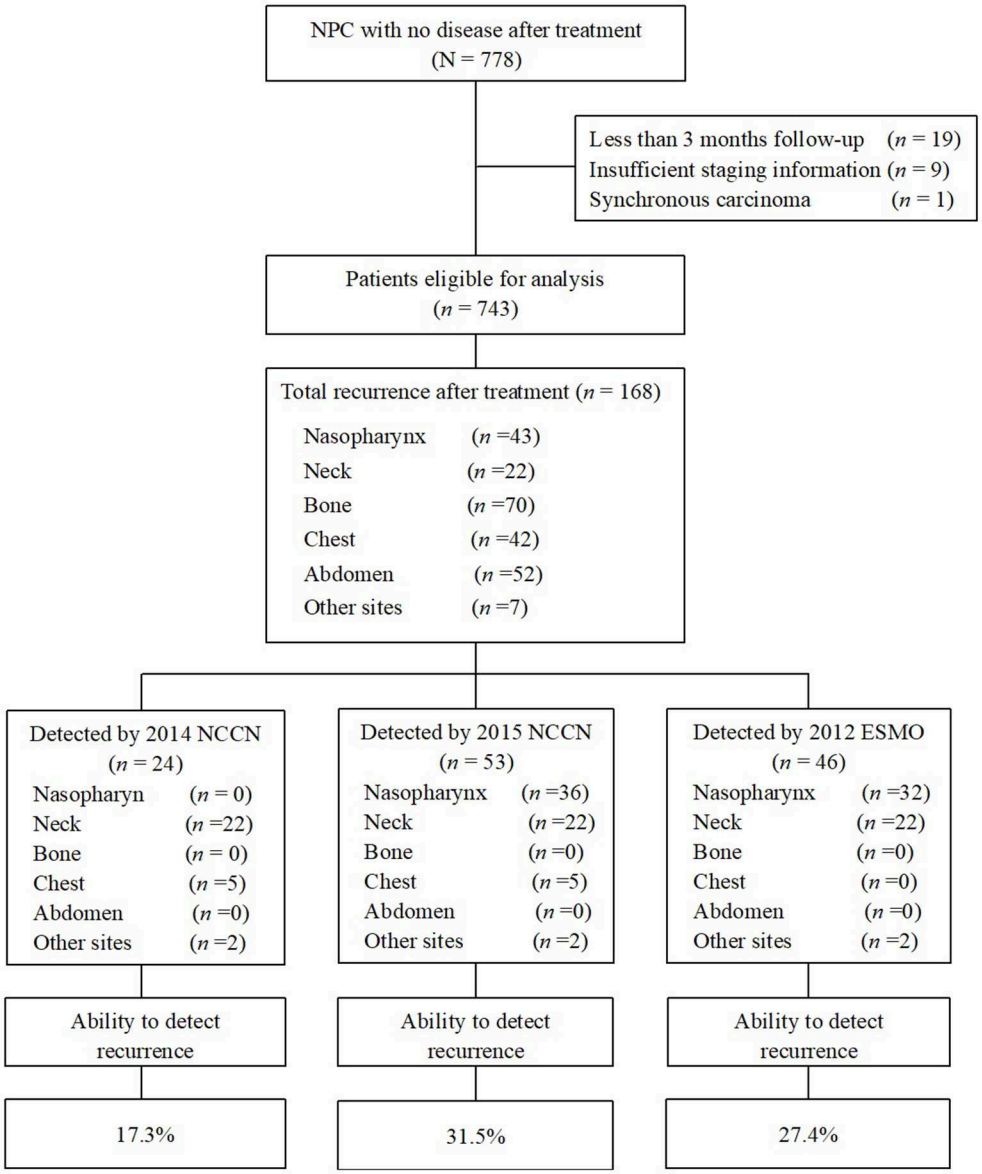

FIGURE 1 | Flowchart of patients enrolled in this study. Ability to detect recurrence (%) = recurrences detected if strictly follow the guidelines/the total number of recurrence after treatment ×100%. NPC, nasopharyngeal carcinoma; NCCN, National Comprehensive Cancer Network; ESMO, European Society for Medical Oncology.

information available (n = 9); or synchronous carcinoma (n = 1), and a total of 749 patients were eligible for analysis (**Figure 1**). Patient baseline demographic and disease features are summarized in **Table 2**. There were 580 men and 169 women, with a median age of 43.0 years [interquartile range (IQR) 36–51 years].

Survival Outcomes

Median post-treatment follow-up for the whole cohort was 100.8 months (IQR 81.4–120.1 months). Of the 749 patients, 168 (22.4%) developed disease recurrence, at a median of 20.6 months (IQR 11.6–38.3 months) after radiotherapy (range 0.8–93.8 months). Among the 168 patients who experienced recurrence, there were 70 bone recurrences (41.7%), 52 abdomen recurrences (31.0%), 43 nasopharynx recurrences (25.6%), 42 chest recurrences (25.0%), 22 neck recurrences (13.1%), and 7 recurrences in other sites (4.2%). A total of 31 patients (18.5%) had recurrence at two or more sites simultaneously. In patients with T3/4 disease, the most common site of recurrence was bone (40.2% bone, 29.1% abdomen, 28.3% nasopharynx, 26.8% chest, 10.2% neck, and 4.7% other). In patients with N2/3 disease, the majority of recurrences were in bone or abdomen (54.2% bone, 33.9% abdomen, 25.4% chest, 23.7% nasopharynx, 8.5% neck, and 5.1% other).

TABLE 2 | Patient baseline demographic and disease features.

Characteristics	All Patients (*N* = 749)	
	No. of patients	%
Age (years)		
≤50	553	73.8
>50	196	26.2
Sex		
Male	580	77.4
Female	169	22.6
Pathology type		
Non-keratinizing carcinoma	744	99.3
Keratinizing squamous cell carcinoma	5	0.7
Chemotherapy		
Yes	535	71.4
No	214	28.6
T category[†]		
T1–2	317	42.3
T3–4	432	57.7
N category[†]		
N0–1	593	79.2
N2–3	156	20.8
Stage[†]		
I–II	257	34.3
III–IV	492	65.7

T, tumor; N, node.
[†]*According to the 7th Union for International Cancer Control/American Joint Committee on Cancer staging system.*

Performance of Guidelines

When we evaluated the performance of the NCCN and ESMO guidelines to detect recurrences after therapy, we found that the 2015 NCCN surveillance protocol could only find 11.3% of all events. The updated 2018 NCCN T and N stage-adapted protocol improved the overall detection rate to 31.5% (**Figure 1**). Using a similar T stage-based approach, the 2012 ESMO guidelines enabled detection of 27.4% of all recurrences. Evaluating the ability of 2015 NCCN strategies according to different stage, we found it to be most limited for T1/2 and N2/3 patients, in whom <30% of recurrences would be detected (26.8 and 25.4%, respectively, **Table 3**). None of the guidelines were able to capture bone or abdominal relapses, because no imaging procedures are recommended for these sites. The 2018 and 2015 NCCN guidelines were able to capture 11.9% of the chest recurrences, with chest imaging recommended for patients with a history of smoking.

Location-Specific Recurrence Patterns

To capture 95% of recurrences, the required surveillance durations were 85.57 and 67.45 months for T1/2 and T3/4 disease ($P = 0.27$), 83.57 and 55.80 months for N0/1 and N2/3 disease, respectively ($P < 0.001$). When location-specific recurrence patterns were incorporated in the analysis for these stages, total surveillance duration of 60 months or longer was

TABLE 3 | Recurrences captured by the NCCN- and ESMO-prescribed surveillance guideline.

	Recurrences captured																			
	Total (*N* = 168)		By clinical stage[†]								By recurrence location									
			T classification				N classification				Nasopharynx (*n* = 43)		Neck (*n* = 22)		Bone (*n* = 70)		Chest (*n* = 42)		Abdomen (*n* = 52)		Other (*n* = 7)	
			T1–2 (*n* = 41)		T3–4 (*n* = 127)		N0–1 (*n* = 109)		N2–3 (*n* = 59)											
Guideline	**No.**	**%**	**No.**	**%**	**No.**	**%**	**No.**	**%**	**No.**	**%**	**No.**	**%**	**No.**	**%**	**No.**	**%**	**No.**	**%**	**No.**	**%**	**No.**	**%**
2018 NCCN	19	11.3	7	17.1	12	9.4	16	14.7	3	5.1	0	0	22	100	0	0	20	47.6	0	0	2	28.6
2015 NCCN	53	31.5	11	26.8	42	33.1	38	34.9	15	25.4	36	83.7	22	100	0	0	20	47.6	0	0	2	28.6
2012 ESMO	46	27.4	7	17.1	39	30.7	34	31.2	12	20.3	32	74.4	22	100	0	0	0	0	0	0	2	28.6

NCCN, National Comprehensive Cancer Network; ESMO, European Society for Medical Oncology.
[†]*According to the 7th Union for International Cancer Control/American Joint Committee on Cancer staging system.*

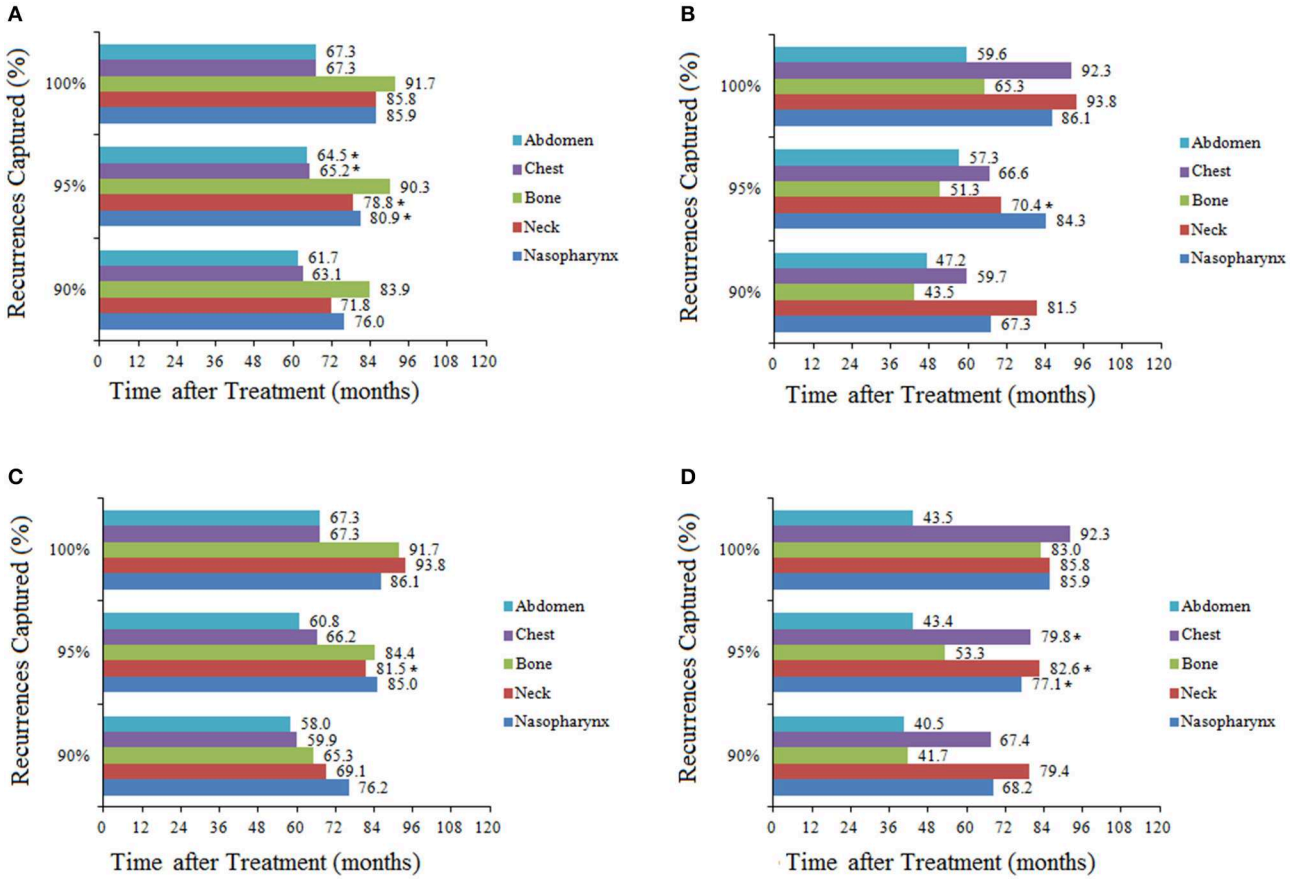

FIGURE 2 | Total duration of surveillance required to capture 90, 95, and 100% of recurrences in patients stratified by stage and recurrence location: **(A)** T1/2; **(B)** T3/4; **(C)** N0/1; **(D)** N2/3. *Estimated duration of surveillance due to there being few recurrences in these groups.

required to capture 95% of recurrences, with the exception of bone or abdomen recurrence in T3/4 and N2/3 patients. For example, to capture 95% of recurrences in T1/2 patients, surveillance of the nasopharynx would be required for 80.91 months, neck for 78.82 months, bone for 90.27 months, chest for 65.16 months, and abdomen for 64.50 months (**Figure 2**). In general, T1/2 and N0/1 patients required longer surveillance than T3/4 or N2/3 for the detection of recurrences in bone or abdomen. For example, to capture 95% of recurrences in N0/1 patients, surveillance of bone would be required for 84.4 months; in N2/3 patients, surveillance of bone would be required for only 53.3 months. The longest surveillance required at any site was bone in T1/2 patients (90.3 months); the shortest surveillance was abdomen in N2/3 patients (43.4 months; **Figure 2**).

To explore variations in recurrence with time according to stage, we analyzed the 5- and 10-year cumulative recurrence rates at each location (**Table 4**). Overall, the vast majority of recurrences occurred within the first 5 years, so the 5- and 10-year recurrence rates were similar. There was a consistent trend that the recurrence rate was the lowest in T1/2 group and the highest in N2/3 group for all sites except the neck. The recurrence rate in the neck was low for all stages, with no significant differences ($P = 0.76$ between T1/2 and T3/4, $P = 0.666$ between N0/1 and N2/3, $P = 0.162$ between stage I/II and stage III/IV). The lowest recurrence rate at any site was for the nasopharynx in T1/2 patients, with 5- and 10-year rates of 1.6 and 2.4%, respectively. The highest recurrence rate was observed in bone in patients with N2/3 disease, with 5- and 10-year rates of 22.2 and 22.9%, respectively.

Medicare Costs Compared Among Guidelines

Then we compared the total Medicare costs of follow-up according to different guidelines, and found that patients followed up under the 2018 NCCN regimen will incur the lowest cost ($1642.66 in 5 years per patients, **Table 5**). According the 2015 NCCN and 2012 ESMO guidelines, the highest cost (US$4484.69) would be incurred by patients with T3/4 or N2/3 disease because of the requirement for annual baseline imaging. Similarly, due to the baseline imaging recommended by the 2012 ESMO guidelines, a T3/4 patient would incur a greater cost for surveillance than a

TABLE 4 | Recurrence rates at 5 and 10 years by location among different stages.

	By T classification†			By N classification†		
Recurrence location	**T1–2**	**T3–4**	***P*#**	**N0–1**	**N2–3**	***P*#**
Any			<0.01			<0.01
No. of recurrence	41	127		109	59	
5-year recurrence rate, %	11.7	27.8		16.8	36.8	
10-year recurrence rate, %	13.1	30.2		18.8	38.2	
Nasopharynx			<0.01			0.023
No. of recurrence	7	36		29	14	
5-year recurrence rate, %	1.6	7.9		4.2	9.2	
10-year recurrence rate, %	2.4	9.2		5.3	10.1	
Neck			0.76			0.666
No. of recurrence	9	13		17	5	
5-year recurrence rate, %	2.7	2.8		2.7	3	
10-year recurrence rate, %	3	4.5		3.1	4	
Bone			0.03			<0.01
No. of recurrence	23	51		39	35	
5-year recurrence rate, %	6	12.1		6.1	22.2	
10-year recurrence rate, %	7.5	12.4		6.9	22.9	
Chest			<0.01			0.007
No. of recurrence	8	38		30	16	
5-year recurrence rate, %	2.3	8.9		5	10.4	
10-year recurrence rate, %	2.7	9.6		5.3	11.4	
Abdomen			0.01			0.002
No. of recurrence	15	41		36	20	
5-year recurrence rate, %	4.5	10		6.1	13.6	
10-year recurrence rate, %	4.9	10		6.3	13.6	
Other			0.07			0.166
No. of recurrence	1	7		5	3	
5-year recurrence rate, %	0.3	1		0.7	0.8	
10-year recurrence rate, %	0.3	2		0.9	2.6	

†*According to the 7th Union for International Cancer Control/American Joint Committee on Cancer staging system.*
#*P-values calculated using the Kaplan–Meier method.*

T1/2 patient. However, to capture 95% of recurrence cases, patients in all groups would incur surveillance costs of ∼US$6000, which would be greater than that incurred using the current guidelines.

Regarding the cost to detect per recurrence, we found that US$42,578.64 would be required to detect a recurrence following the 2018 NCCN guidelines. Following the stage-adapted surveillance protocol, detecting a recurrence in a patient with relatively earlier stage disease would cost much more than in a patient with advanced disease because of the lower recurrence rate in the former. For example, the cost per recurrence would be as high as US$62,088.70 in T1/2 patients but only US$44,863.95 in T3/4 patients following the 2015 NCCN recommendations. To capture 95% of all recurrences, the cost per case detected was much less than that incurred using the current guidelines, with US$50,338.69 required to detect a recurrence in patients with T1/2 disease, US$19,912.48 for T3/4, US$31,597.83 for N0/1, and US$17,187.99 for N2/3.

DISCUSSION

This large-scale study was the first to evaluate NCCN and ESMO follow-up guidelines for NPC. Our results suggested that if these follow-up recommendations from guidelines were strictly followed, it would lead to a large number of missed recurrences. Overall, the 2015 NCCN and 2012 ESMO strategies had an obvious advantage in detecting tumor recurrence because of the individualized recommendations for patients with different stages, yet we found that 69.5 and 72.6% of all recurrences would have been missed, respectively.

Because relapse site and time reflect patterns of recurrence, stratified follow-up according to the characteristics of recurrences can improve the efficiency of follow-up and increase the number of recurrences detected. In our analysis, most recurrences occurred in the first 5 years after treatment and later failures represented <10% of the total. This finding is consistent with previous data. Lee

TABLE 5 | Comparison of 2017 medicare costs associated with adhering to the NCCN and ESMO oncologic surveillance schedules and the costs that would be incurred if 95% of all recurrences were captured.

Surveillance strategy and risk group	2017 Total medicare Costs[†]	Cost per recurrence case detected
2018 NCCN[#§] (with ability to capture 11.3% of the recurrences)		
All patients	1,642.66	42,578.64
2015 NCCN[#§] (with ability to capture 31.5% of the recurrences)		
T1–2*	2,179.81	62,088.70
T3–4*	4,484.69	44,863.95
N0–1*	3,254.07	49,595.65
N2–3*	4,484.69	46,220.58
2012 ESMO[#] (with ability to capture 27.4% of the recurrences)		
T1–2*	1,642.66	73,329.76
T3–4*	3,747.87	40,423.99
To capture 95% of all recurrences[‡]		
T1–2*	6,264.65	50,338.69
T3–4*	5,712.88	19,912.48
N0–1*	6,253.04	31,597.83
N2–3*	6,237.52	17,187.99

NCCN, National Comprehensive Cancer Network; ESMO, European Society for Medical Oncology.

[#]The total cost in the first 10 years after treatment were estimated when strictly adhering to surveillance guideline.

[§]The 2018 and 2015 NCCN recommended annual low-dose chest CT for patients with high risk of lung cancer which represents only 4.82% of the whole patients, so the cost of chest imaging associated adhering to the 2018 and 2015 NCCN was ignored.

[*]According to the 7th edition of the International Union against Cancer/American Joint Committee on Cancer (UICC/AJCC) system.

*[†]Estimates based on total costs in dollars incurred by a single patient who has strictly followed and completed the recommended surveillance schedules as outlined in **Table 1**. H&P exam included both costs of a complete head and neck exam and fiberotic examination.*

[‡]Cost was calculated based on followed estimation: Frequency of H&P exam was similar to that the 2018 and 2015 recommended; baseline imaging included annually head and neck MRI, bone imaging included annually skeletal scintigraphy, chest imaging included annually chest CT, abdomen imaging included annually abdomen CT.

et al. reported that <10% of all local recurrences occurred after 5 years of treatment (8). Therefore, more intensive follow-up during the first 5 years may be justified to detect early locoregional recurrence. In addition, follow-up should continue indefinitely because late recurrences may occur and late recurrences usually have a better prognosis than early recurrences.

The prevailing use of IMRT and concurrent chemoradiotherapy for locoregionally advanced NPC has improved the locoregional control of this disease. As a consequence, distant recurrence has become a predominant pattern of treatment failure (9). However, the current NCCN and ESMO guidelines advocate no regular imaging to detect distant metastatic. The vast majority of early distant recurrences are missed following these guidelines. The most common metastatic sites for NPC include bone, lung and liver (10, 11), which were largely detected through imaging studies (12). Although NPC with distant metastasis was usually considered incurable (13), early detection and treatment of isolated asymptomatic disease could improve survival (14–17). Therefore, early diagnosis of metastatic NPC via routine body imaging instead of symptoms may be of great clinical value.

In our analysis, extending surveillance beyond the current recommendations and integrating routine body imaging in all patients to detect 95% of recurrences would require increased expenditure. The cost per recurrence detected in patients with T1/2 disease was almost three times that in patients with T3/4 disease, due to the better disease control and fewer recurrences in T1/2 patients. This study highlights the importance of developing more reasonable and accurate follow up strategies based on subtypes and risk of relapse, such that patient benefit can be balanced against Medical expense.

We recognize that a limitation of our study was the unstandardized follow-up due to its retrospective design. However, the instituted surveillance protocol was relatively uniform and <3% of patients in this study were lost to follow-up. Our analysis mainly focused on the follow-up period after treatment, while the optimail frequency of radiological examinations remained largely unknown due to the non-standardized follow-up protocol. In this study, the cost of radiological examinations was estimated on annual basis, but we recommend the exploration of more rational and individualized follow-up approaches.

In conclusion, the surveillance guidelines from NCCN and ESMO do not fully capture the recurrence of NCP after radical treatment. Extending surveillance to capture 95% of the recurrence events would lead to higher costs, while the cost per recurrence detected was much less than that incurred following the established guidelines. Detecting recurrence in patients with earlier disease was much more costly than in those with advanced disease. Therefore, the direction of further research was to identify personalized review strategies to balance the benefits of patients with medical costs.

DATA AVAILABILITY STATEMENT

All datasets generated for this study are included in the article/supplementary material.

ETHICS STATEMENT

The study was approved by the institutional review board of Sun Yat-sen University Cancer Center.

AUTHOR CONTRIBUTIONS

We declare that all authors are qualified. G-QZ, J-WL, JM, and YS had substantial contributions to the conception and design of the work, drafting the work, and revising it critically for important intellectual content or the acquisition. LT, Y-PM, and RG analyzed the data for the work. All authors provided approval for publication of the content. YS agreed to be accountable for all aspects of the work in ensuring that questions related to the accuracy or integrity of any part of the work are appropriately investigated and resolved.

FUNDING

This work was supported by grants from the National Natural Science Foundation of China (81872463), the Special Support Program of Sun Yat-sen University (16zxtzlc06), the Planned Science and Technology Project of Guangdong Province (2019B020230002), Natural Science Foundation of Guangdong Province (2017A030312003 and 2019A1515011863), Health & Medical Collaborative Innovation Project of Guangzhou City, China (201803040003), Innovation Team Development Plan of the Ministry of Education (No. IRT_17R110), Overseas Expertise Introduction Project for Discipline Innovation (111 Project, B14035).

REFERENCES

1. Tian YM, Tian YH, Zeng L, Liu S, Guan Y, Lu TX, et al. Prognostic model for survival of local recurrent nasopharyngeal carcinoma with intensity-modulated radiotherapy. *Br J Cancer*. (2014) 110:297–303. doi: 10.1038/bjc.2013.715
2. Chan A, Felip E. Nasopharyngeal cancer: ESMO clinical recommendations for diagnosis, treatment and follow-up. *Ann Oncol*. (2009) 20:123–5. doi: 10.1093/annonc/mdp150
3. Pfister D, Ang K, Brockstein B, Colevas A, Ellenhorn J, Goepfert H, et al. NCCN practice guidelines for head and neck cancers. *Oncology*. (2000) 14:163.
4. Chan AT, Gregoire V, Lefebvre JL, Licitra L, Hui EP, Leung SF, et al. Nasopharyngeal cancer: EHNS-ESMO-ESTRO Clinical Practice Guidelines for diagnosis, treatment and follow-up. *Ann Oncol*. (2012) 23(Suppl. 7):83–5. doi: 10.1093/annonc/mds266
5. Miller MC, Goldenberg D, Education Committee of American Head and Neck Society (AHNS). Do you know your guidelines? An initiative of the American Head and Neck Society's Education Committee. *Head Neck*. (2016) 38:165–7. doi: 10.1002/hed.24104
6. Li WF, Sun Y, Chen M, Tang LL, Liu LZ, Mao YP, et al. Locoregional extension patterns of nasopharyngeal carcinoma and suggestions for clinical target volume delineation. *Chin J Cancer*. (2012) 31:579–87. doi: 10.5732/cjc.012.10095
7. Edge SB, Compton CC. The American Joint Committee on Cancer: the 7th edition of the AJCC cancer staging manual and the future of TNM. *Ann Surg Oncol*. (2010) 17:1471–4. doi: 10.1245/s10434-010-0985-4
8. Lee AW, Foo W, Law SC, Poon YF, Sze WM, O SK, et al. Recurrent nasopharyngeal carcinoma: the puzzles of long latency. *Int J Radiat Oncol Biol Phys*. (1999) 44:149–56.
9. Lee N, Xia P, Quivey JM, Sultanem K, Poon I, Akazawa C, et al. Intensity-modulated radiotherapy in the treatment of nasopharyngeal carcinoma: an update of the UCSF experience. *Int J Radiat Oncol Biol Phys*. (2002) 53:12–22. doi: 10.1016/S0360-3016(02)02724-4
10. Al-Sarraf M, LeBlanc M, Giri PG, Fu KK, Cooper J, Vuong T, et al. Chemoradiotherapy versus radiotherapy in patients with advanced nasopharyngeal cancer: phase III randomized Intergroup study 0099. *J Clin Oncol*. (1998) 16:1310–7.
11. Chen L, Hu CS, Chen XZ, Hu GQ, Cheng ZB, Sun Y, et al. Concurrent chemoradiotherapy plus adjuvant chemotherapy versus concurrent chemoradiotherapy alone in patients with locoregionally advanced nasopharyngeal carcinoma: a phase 3 multicentre randomised controlled trial. *Lancet Oncol*. (2012) 13:163–71. doi: 10.1016/S1470-2045(11)70320-5
12. Tham IWK, Lu JJ. *Post-treatment Follow-Up of Patients with Nasopharyngeal Cancer*. Berlin: Springer Berlin Heidelberg (2010).
13. Jin Y, Cai XY, Cai YC, Cao Y, Xia Q, Tan YT, et al. To build a prognostic score model containing indispensible tumour markers for metastatic nasopharyngeal carcinoma in an epidemic area. *Eur J Cancer*. (2012) 48:882–8. doi: 10.1016/j.ejca.2011.09.004
14. Fandi A, Bachouchi M, Azli N, Taamma A, Boussen H, Wibault P, et al. Long-term disease-free survivors in metastatic undifferentiated carcinoma of nasopharyngeal type. *J Clin Oncol*. (2000) 18:1324–30. doi: 10.1200/JCO.2000.18.6.1324
15. Shen L, Li W, Wang S, Xie G, Zeng Q, Chen C, et al. Image-based multilevel subdivision of M1 category in TNM staging system for metastatic nasopharyngeal carcinoma. *Radiology*. (2016) 280:805–14. doi: 10.1148/radiol.2016151344
16. Shen LJ, Wang SY, Xie GF, Zeng Q, Chen C, Dong AN, et al. Subdivision of M category for nasopharyngeal carcinoma with synchronous metastasis: time to expand the M categorization system. *Chin J Cancer*. (2015) 34:450–8. doi: 10.1186/s40880-015-0031-9
17. Pan CC, Lu J, Yu JR, Chen P, Li W, Huang ZL, et al. Challenges in the modification of the M1 stage of the TNM staging system for nasopharyngeal carcinoma: a study of 1027 cases and review of the literature. *Exp Therap Med*. (2012) 4:334–8. doi: 10.3892/etm.2012.584

Conflict of Interest: The authors declare that the research was conducted in the absence of any commercial or financial relationships that could be construed as a potential conflict of interest.

frontiers in Oncology

ORIGINAL RESEARCH
published: 19 February 2020
doi: 10.3389/fonc.2020.00166

Fully-Automated Segmentation of Nasopharyngeal Carcinoma on Dual-Sequence MRI Using Convolutional Neural Networks

Yufeng Ye[1,2†], Zongyou Cai[3,4†], Bin Huang[3,4], Yan He[5,6], Ping Zeng[7], Guorong Zou[5,6], Wei Deng[1,2], Hanwei Chen[1,2] and Bingsheng Huang[2,3*]*

[1] Department of Radiology, Panyu Central Hospital, Guangzhou, China, [2] Medical Imaging Institute of Panyu, Guangzhou, China, [3] Medical AI Lab, School of Biomedical Engineering, Health Science Center, Shenzhen University, Shenzhen, China, [4] Shenzhen University General Hospital Clinical Research Center for Neurological Diseases, Shenzhen, China, [5] Department of Oncology, Panyu Central Hospital, Guangzhou, China, [6] Cancer Institute of Panyu, Guangzhou, China, [7] Department of Radiology, Shenzhen University General Hospital, Shenzhen, China

OPEN ACCESS

Edited by:
Yu-Pei Chen,
Sun Yat-sen University Cancer Center (SYSUCC), China

Reviewed by:
Jun-Lin Yi,
Chinese Academy of Medical Sciences & Peking Union Medical College, China
Wei Jiang,
Guilin Medical University, China

***Correspondence:**
Hanwei Chen
docterwei@sina.com
Bingsheng Huang
huangb@szu.edu.cn

† These authors have contributed equally to this work and share first authorship

Specialty section:
This article was submitted to Head and Neck Cancer, a section of the journal Frontiers in Oncology

Received: *22 September 2019*
Accepted: *30 January 2020*
Published: *19 February 2020*

Citation:
Ye Y, Cai Z, Huang B, He Y, Zeng P, Zou G, Deng W, Chen H and Huang B (2020) Fully-Automated Segmentation of Nasopharyngeal Carcinoma on Dual-Sequence MRI Using Convolutional Neural Networks. Front. Oncol. 10:166. doi: 10.3389/fonc.2020.00166

In this study, we proposed an automated method based on convolutional neural network (CNN) for nasopharyngeal carcinoma (NPC) segmentation on dual-sequence magnetic resonance imaging (MRI). T1-weighted (T1W) and T2-weighted (T2W) MRI images were collected from 44 NPC patients. We developed a dense connectivity embedding U-net (DEU) and trained the network based on the two-dimensional dual-sequence MRI images in the training dataset and applied post-processing to remove the false positive results. In order to justify the effectiveness of dual-sequence MRI images, we performed an experiment with different inputs in eight randomly selected patients. We evaluated DEU's performance by using a 10-fold cross-validation strategy and compared the results with the previous studies. The Dice similarity coefficient (DSC) of the method using only T1W, only T2W and dual-sequence of 10-fold cross-validation as different inputs were 0.620 ± 0.0642, 0.642 ± 0.118 and 0.721 ± 0.036, respectively. The median DSC in 10-fold cross-validation experiment with DEU was 0.735. The average DSC of seven external subjects was 0.87. To summarize, we successfully proposed and verified a fully automatic NPC segmentation method based on DEU and dual-sequence MRI images with accurate and stable performance. If further verified, our proposed method would be of use in clinical practice of NPC.

Keywords: nasopharyngeal carcinoma, magnetic resonance image, dual-sequence, convolutional neural networks, segmentation

INTRODUCTION

Nasopharyngeal carcinoma (NPC) is a cancer type arising from the nasopharynx epithelium with a unique pattern of geographical distribution, with high incidence in Southeast Asia and North Africa (1). NPC has an incidence rate of 0.2‰ in endemic regions. Radiation therapy (RT) has come as the only curative treatment because of the anatomic constraints and its sensitivity to irradiation (2).

The accurate delineation of NPC greatly influences radiotherapy planning. NPC cannot be clearly identified from the adjacent soft tissue on computed tomography (CT) image (3). Compared with CT, magnetic resonance imaging (MRI) has demonstrated superior soft tissue contrast,

thus has been used as a preferred modality to evaluate the regional, local and intracranial infiltration of NPC. Moreover, NPC has complex anatomical structure and often shares the similar intensities with the nearby tissues. The NPC often present high shape variability, making the NPC segmentation very challenging (4). In clinical practice, NPC are delineated manually by radiologists or oncologists, which is time-consuming and subjective. Compared with manual delineation, automatic segmentation methods can be faster and relatively objective.

The automatic or semi-automatic segmentation methods, such as the traditional machine learning (ML) methods (5–11), have already been applied to NPC segmentation. The traditional ML methods are subjective to extract hand-crafted features with specific methods. Alternatively, convolutional neural networks (CNNs) allow automatic features extraction and have shown great performance in the field of medical image analysis. For NPC segmentation, there are some studies based on CNNs. Wang et al. (4) and Ma et al. (12) extracted patches in 2-dimension (2D) MRI images and trained a CNN model to classify the patches for NPC segmentation. Wang et al. (4) showed that CNN performed better in segmentation tasks than the traditional ML methods. However, segmentation by patches would cost much time in training while just makes use of the information of small local regions. To overcome these limitations, other studies have applied fully convolutional network (FCN) (13) or U-net (14) structure in NPC segmentation. Men et al. (15) and Li et al. (16) applied an improved U-net to segment NPC in an end-to-end manner. The fully convolutional structure of U-net allows the network to realize pixel-wise segmentation and to input the whole image for NPC segmentation without extracting patches. Compared with extracting patches on images, fully convolutional structure can segment NPC with global image information and increase the segmentation efficiency. Based on FCN and U-net structure, there have been studies about NPC segmentation on multimodality images. Huang et al. (17) applied an improved U-net to segment NPC in PET and CT images. Ma et al. (18) applied a combined CNN to segment NPC in CT and MRI images. Similar to previous studies, the segmentation performance by using multimodality information was better than those by using single modality information. Recently, Huang et al. (19) proposed a dense convolutional network (DenseNet) showing great performance in the field of computer vision. DenseNet uses a densely connected path to concatenate the input features with the output features, enabling each micro-block to receive raw information from all previous micro-blocks. Inspired by the successful application of deep CNNs in NPC segmentation, in this study we proposed a dense connectivity embedding U-net (DEU) based on U-net, dense connectivity and dual-sequence MRI for accurate and automatic segmentation of NPC.

MATERIALS AND METHODS

Patient Data Acquisition and Pre-processing

Totally 44 NPC patients were retrospectively recruited from **** with 34 males and 10 females. The age of the patients ranged from 34 to 73 years old. The ethics committee of Panyu Central Hospital performed the ethical review and approved this study and waived the necessity to obtain informed written consent from the patients. The T1-weighted (T1W) and T2-weighted (T2W) images were both acquired with a 1.5T Siemens Avanto scanner (Siemens AG Medical Solutions, Erlangen, Germany). The spatial resolution of T1W images are $0.93 \times 0.93 \times 4$ mm^3 and T2W images are $0.48 \times 0.48 \times 4$ mm^3. The scanning range was from mandibular angle to suprasellar cistern (25 slices), or from suprasternal fossae to suprasellar cistern (45 slices). The gold standard of NPC boundary (including the primary tumor and the metastatic lymph node) was manually delineated by an experienced radiologist and double-checked by an experienced oncologist on the T2W images with reference to T1W images and saved as the gold standard images with a value of one in the lesions and 0 in the other regions. The diagnostic criteria for a detectable lymph node included the following: (1) lateral retropharyngeal nodes with a minimal axial dimension of $\geq$5 mm and 10 mm for all other cervical nodes, except for the retropharyngeal group, and if the minimum axial dimension of the lymph nodes $\geq$6 was considered high-risk metastatic; (2) lymph nodes with a contrast-enhancing rim or central necrosis; (3) nodal grouping (i.e., the presence of three or more contiguous and confluent lymph nodes as clusters); (4) extracapsular involvement of lymph nodes.

To make use of the information of both T1W and T2W images, we performed co-registration of T1W to T2W images by using Mattes mutual information (20) as correlation metric. To do this, a one plus one evolutionary method (21) (initial radius 0.004, maximum iterations 300) was used to find the best parameters. To resample the T2W images to the same spatial resolution as T1W images, the T2W images and the gold standard images of the same patients were down-sampled by using linear interpolation. The length and width of the T2W images and gold standard images were reduced by 50%. All the T2W and T1W images were normalized by performing min-max normalization. All the image slices were padded zero and cropped into 256×256 dimension. Totally 1950 pairs of T1W and T2W images were used for this study.

Automatic Segmentation of NPC by Deep Learning

To study the advantage of integrating dual-sequence information, we designed an experiment to compare different inputs, by using 10-fold cross-validation strategy. We trained three models for the comparisons of different inputs, namely, using only T1W, using only T2W and dual-sequence (both T1W and T2W) MRI images, respectively.

Comparison Between Different Inputs

Network architecture

We developed a DEU to inherit both advantages of dense connectivity and U-net-like connections. The network architecture is shown in **Figure 1**. The T1W and T2W

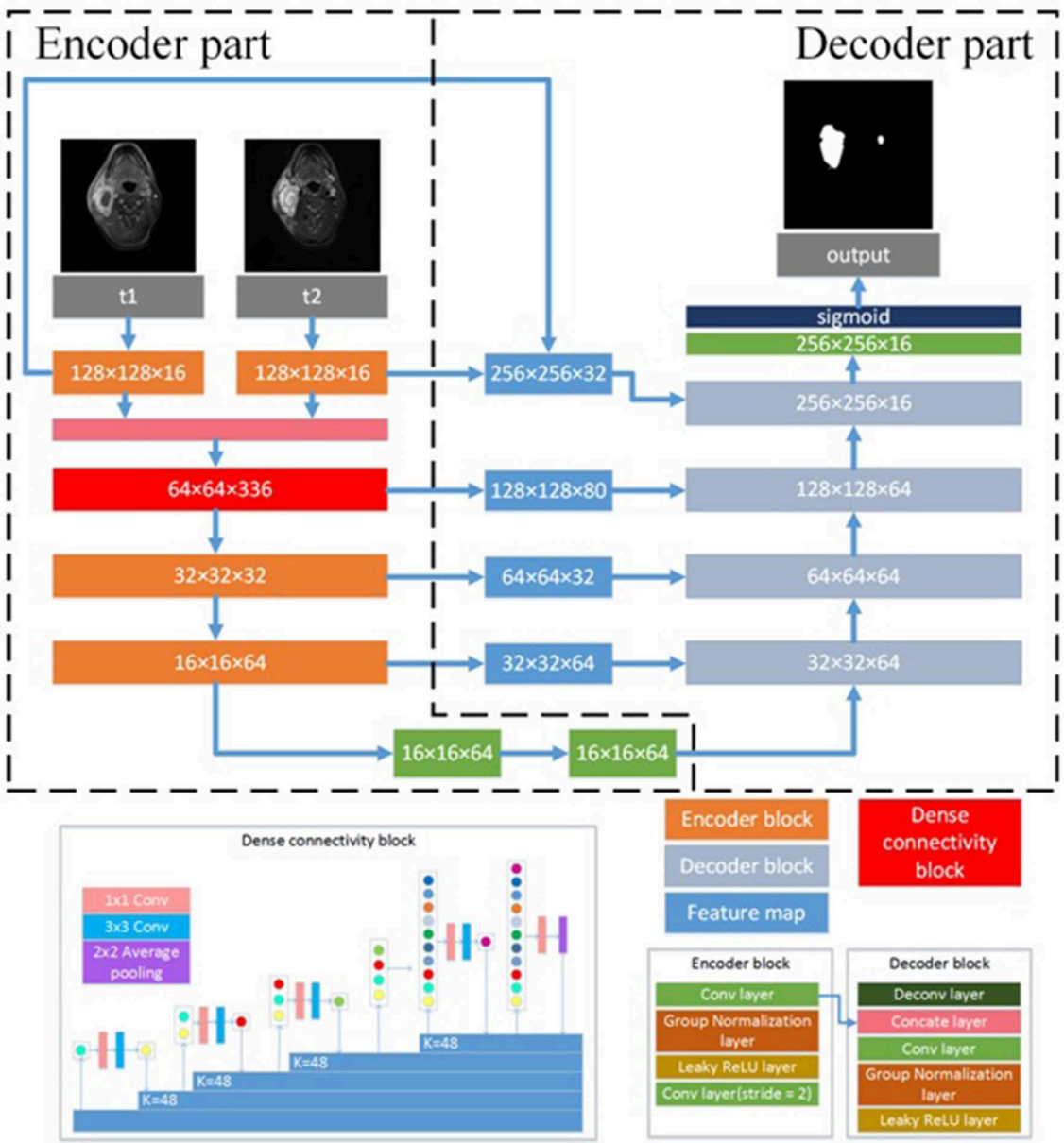

FIGURE 1 | Architecture of the proposed CNN model. N × N × C, N is the size of feature map and C is the number of feature maps. N × N Conv, the convolutional layer with N × N kernel size; K = N, N is the growth filters number; N × N Average pooling, the average pooling layer with N × N kernel size; Concate layer, the concatenation layer; ReLU, rectified linear unit.

images were inputted into the network by two independent paths, respectively. As an end-to-end segmentation framework, the structure consists of an encoder part and a symmetric decoder part.

The encoder part reduces the size of input data sets and extracts high representative features effectively. The decoder part recovers the extracted features to the same size of input images by deploying deconvolution, which is transposed convolution for upsampling. The encoder part consists of four encoder blocks and a dense connectivity block. An encoder block contains three 3 × 3 convolutional (conv) layers, two group normalization (GN) (22) layers and two leaky rectified linear unit (LReLU) (23) layers. The outputs of convolutional layer are inputted into a GN layer, and the groups of GN layer were set as 8. Because GN has shown better performance than batch normalization (BN) (24) with small batches (22), we employed GN in the proposed network. To optimize the effect of training and prevent gradient vanishing or exploding, each convolutional layer is followed by LReLU to the output of GN layer. The convolutional layer with two

strides is designed for downsampling the feature maps. LReLU is defined as:

$$y_i = \begin{cases} x_i & , x_i \geq 0 \\ \alpha x_i & , x_i < 0 \end{cases} \quad (1)$$

where α between 0 and 1 decides the slope of the negative part. It is set as 0.1 in the proposed network.

The dense connectivity block consists of a dense block and a transition block. The dense block is a direct connection from any layer to all subsequent layers, motivated by bottleneck structure (25). The dense block consists of GN-LReLU-conv (1 × 1 kernel size)-GN-LReLU-conv (3 × 3 kernel size). The transition block consists of a GN layer and an 1 × 1 convolutional layer followed by a 2 × 2 average pooling layer. Two encoder blocks are used to extract the low-level features of T1W images and T2W images, respectively, and then concatenate them in channel-wise as the input of the dense connectivity block. Another two encoder blocks are designed for the permutation and combination of the low-level features from the output of the dense connectivity block to acquire high-level features.

The decoder part consists of five decoder blocks. A decoder block contains a 3 × 3 deconvolutional layer (deconv), a concatenation layer, two 3 × 3 convolutional layers with stride 2, two LReLU and two GN layers. Deconvolution may cause information loss of the high-resolution images. To address this problem, the concatenation layer is used to fuse the feature maps in the convolution layers from the encoder part with the current feature maps in the deconvolutional layer. These skip-layers are able to capture more multi-scale contextual information and improve the accuracy of segmentation. At the final layer the feature maps are computed by a 1 × 1 convolutional layer with pixel-wise sigmoid.

With all the decoder blocks, the decoder part finally reconstructs the feature maps to an output image with the size of 256 × 256, the same as that of the input images. For the network optimization, the Dice loss (26) between the gold standard and the segmented results is calculated as objective function.

Model implementation details

We implemented the proposed DEU in Keras (27) using Tensorflow (28) backend, and trained it on Nvidia Geforce GTX 1080 TI with 11 GB GPU memory. The batch size was set as 1. We used Adam (29) optimizer with a learning rate of 0.0001 and the epochs number of 200. During each training epoch, data augmentation was applied to enlarge the training dataset and to reduce overfitting by flipping and re-scaling each image.

To further improve the segmentation accuracy, we performed post-processing to refine the segmentation results. Since the 2D network may ignore the context information of neighboring slices, the segmentation results with 2D network may include some isolated false positive (FP) areas. We extracted the segmentation results by using connected components algorithm on 3D images for each patient. We then removed the isolated regions which were segmented in only one slice to improve the segmentation accuracy.

The network architecture for the single sequence model is different from the dual-sequence model which is shown in **Figure 1**. The single sequence model has one single path for extracting features at the beginning of the network. The outputs of the first encoder block are fed to the dense connectivity block directly. The other structure of the single sequence model is the same as in DEU. We evaluated the single sequence model by using 10-fold cross-validation strategy and compared the performance of single sequence models with the dual-sequence model by using Mann-Whitney *U* test. We collected seven additional cases as an external validation dataset to evaluate the robustness and generalization ability of our dual-sequence model.

Performance evaluation

We used the testing dataset to evaluate the segmentation performance of all models by calculating Dice similarity coefficient (DSC) (30), sensitivity and precision as follows:

$$\mathbf{DSC} = \frac{2TP}{FP+2TP+FN} \quad (2)$$

$$\mathbf{Sensitivity} = \frac{TP}{TP+FN} \quad (3)$$

$$\mathbf{Precision} = \frac{TP}{TP+FP} \quad (4)$$

where true positive (TP) denotes the correctly identified tumor area, FP denotes the normal tissue that was incorrectly identified as a tumor, false negative (FN) denotes the tumor area that is incorrectly predicted as normal tissue. DSC describes the overlap between the segmentation results and the gold standard of NPC. Sensitivity describes the overlap between the correctly identified tumor area and the gold standard of NPC. Precision describes the ratio of the correctly identified tumor area in the segmentation result.

Comparison With Previous Studies

We evaluated the proposed method by using 10-fold cross-validation strategy. We also compared our results of DEU with the previous studies. However, performing a direct comparison across different studies is difficult due to differences in the datasets. Therefore, we directly compared our results with those in these publications, in terms of DSC. Although they may not be reasonably comparable, these comparisons to some extent provide insights about how our method outperforms the similar studies.

TABLE 1 | Comparisons of segmentation performance between different MRI sequences using 10-fold cross-validation strategy.

Input	DSC[a]	Sensitivity	Precision
T1W	0.620±0.064	0.642±0.070	0.654±0.072
T2W	0.642±0.118	0.654±0.115	0.688±0.146
T1W+T2W	0.721±0.036	0.712±0.045	0.768±0.045

[a] *DSC, Dice similarity coefficient.*

RESULTS

Comparison Between Different Network Inputs

As shown in **Table 1**, the mean DSC, sensitivity, precision of the models with different inputs (T1W only, T2W only, and dual-sequence) were 0.620 ± 0.064, 0.642 ± 0.118 and 0.721 ± 0.036, respectively in 10-fold cross-validation experiment. There were significant differences between the DSC values between the single sequence models and the dual-sequence model (T1W vs. dual-sequence, $p \leq 0.01$; and T2W vs. dual-sequence, $p = 0.047$), by Mann-Whitney U test. The mean DSC with dual-sequence MRI images input was higher than that with single-sequence MRI images input. An example of automatic segmentation result is shown in **Figure 2**, in which the DSC of our proposed method using only T1W, only T2W and dual-sequence MRI images were 0.721, 0.784, and 0.912, respectively. Two typical examples with poor results are shown in **Figure 3**, in which the DSC of our proposed method using dual-sequence MRI images were 0.610 and 0.467, respectively. The average DSC of these seven external cases was 0.87.

Comparison With Other Studies

With our trained DEU model in 10-fold cross-validation experiment, a tumor segmentation task for an example (a co-registered T1W image and a T2W image, two-dimensional) took about 0.02 s, and <1 s for a patient. The feature maps of DEU are shown in **Figure 1A**.

The median DSC in 44 patients was 0.735 (range, 0.383–0.946). The mean DSC, mean sensitivity, mean precision of all patients were 0.721 ± 0.036, 0.712 ± 0.045, 0.768 ± 0.045. The results of previous studies about NPC segmentation in MRI are shown in **Table 2**. The DSC in the study by Li et al. (16) was 0.736, however in their study they manually selected the images of tumor for segmentation, which means that their method was semi-automatic. Deng et al. (10) and Ma et al. (12) achieved a high DSC of 0.862 and 0.851, respectively, however, their method was applied on the MRI images containing the tumor and was also semi-automatic. Ma et al. (18) obtained mean DSC of 0.746, however, their method was applied on the slices containing the nasopharynx region. Song et al. (8), Yang et al. (9), and Huang et al. (17) obtained mean DSC of 0.761, 0.740 and 0.736, respectively, which was a little higher than our DSC, however in their study PET/CT images were used. The performance of Wang et al. (4) method (mean DSC of 0.725) was very close to our method, which was evaluated in only four patients. Men et al. (15) segmented NPC based on CT images and the mean DSC of 0.716 was slightly lower than ours.

DISCUSSION

We proposed an automated NPC segmentation method based on dual-sequence MRI images and CNN. We

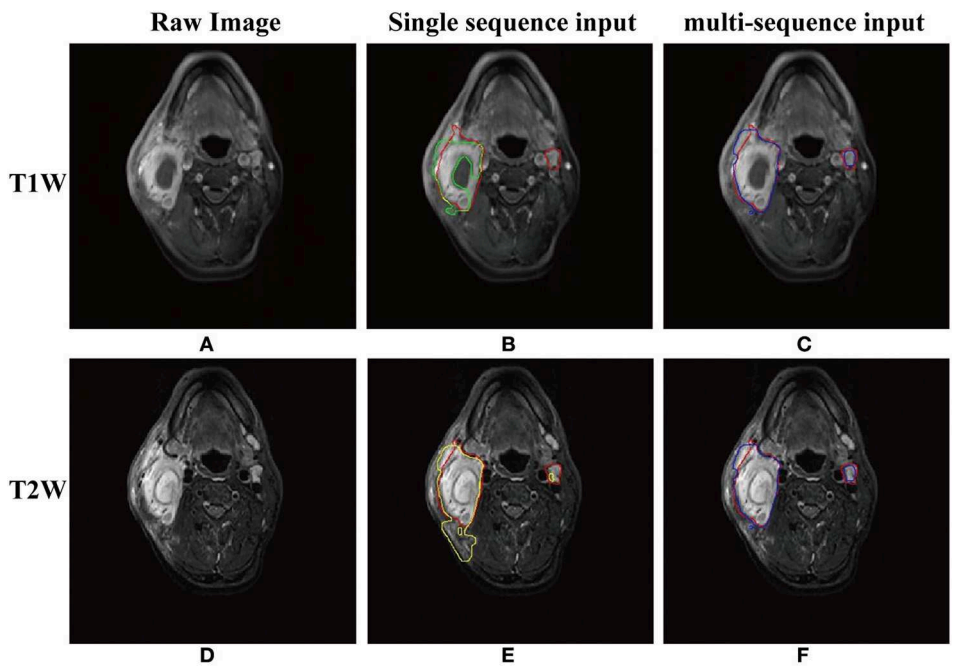

FIGURE 2 | An example of the segmentation results with T1W only, T2W only and dual-sequence images. **(A)** T1W image. **(B)** Automatic segmentation result with T1W image only (green line) and gold standard (red line) presented on the T1W image. Part of the lesion presented lower signal intensity in T1W image (arrow). **(C)**Automatic segmentation result with dual-sequence images (blue line) and gold standard (red line) presented on the T1W image. **(D)** T2W image. **(E)** Automatic segmentation result with T2W only image (yellow line) and gold standard (red line) presented on the T2W image. Some normal tissue beside the tumor presented high signal intensity as compared with the surrounding tissue (arrow). **(F)** Automatic segmentation result with dual-sequence images (blue line) and gold standard (red line) presented on the T2W image.

achieved better performance with dual-sequence MRI images than with single-sequence MRI images, as shown in **Table 1** and **Figure 2**. The good performance on the external validation dataset indicated that our model was robust.

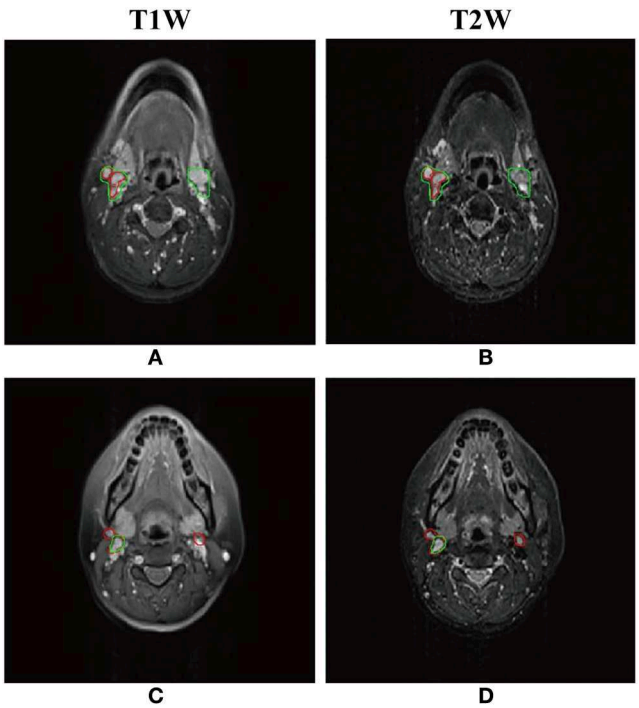

FIGURE 3 | Two typical examples of NPC segmentation with low accuracy. The Dice similarity coefficient (DSC) of first row and second row are 0.610 and 0.467, respectively. **(A,C)** Automatic segmentation result with dual-sequence images (green line) and gold standard (red line) presented on the T1W image. **(B,D)** Automatic segmentation result with dual-sequence images (green line) and gold standard (red line) presented on the T2W image.

As shown in **Figures 2A,D**, the image features of NPC in the T1W image and the T2W image were different. The T1W image depicted part of the lesion as a region with lower signal intensity (**Figure 2B**, arrow). Such low signal intensity region was incorrectly identified as normal tissue, because the network could not gain tumor features from the low signal intensity region. As shown in **Figure 2D**, the boundary of NPC was clearly shown in T2W image which was easy to segment by the network. Some normal tissue beside the tumor (**Figure 2E**, arrow) presented high signal intensity as compared with the surrounding tissue. This may cause that the normal tissue beside the tumor was incorrectly identified as tumor (**Figure 2E**). The proposed method extracted the different features from T1W and T2W images by two independent paths and fused them in the dense connectivity block. As show in **Figures 2C,F**, the high accuracy result with dual-sequence MRI showed that the different image information was fused as efficient features for more accurate segmentation.

The proposed CNN model has shown advantages in feature extraction and feature analysis. As shown in **Figure A1**, the feature maps of encoder part might have relatively high spatial resolution, but the features of tumor were not emphasized, since the encoder part was designed for extracting the features of tumor and normal tissue. The decoder part reconstructed the feature maps from encoder part to output the segmentation results, and in this procedure, the features of tumor were emphasized. As shown in **Figure A1**, the tumor in the feature map of the decoder part showed high signal intensity but had low spatial resolution. The skip-layer structure fused the high spatial resolution feature maps from encoder part and the feature maps of decoder part. The tumor in fused feature map showed high spatial resolution and high signal intensity. The feature maps showed that the skip-layer improved

TABLE 2 | Comparisons of segmentation performance between our proposed CNN model and the similar studies.

Studies	Algorithm	Images used	Average DSC[a]	Patient number	Journal
Deng et al. (10)	SVM[b]	DCE-MRI[c]	0.862	120	Contrast Media and Molecular Imaging, 2018
Song et al. (8)	Graph-based cosegmentation	PET	0.761	2	IEEE Transactions on Medical Imaging, 2013
Yang et al. (9)	MRFs[d]	PET, CT, MRI	0.740	22	Medical Physics, 2015
Stefano et al. (11)	AK-RW[e]	PET	0.848	18	Medical and Biological Engineering and Computing, 2017
Wang et al. (4)	CNN[f]	MRI	0.725	15	Neural Processing Letters, 2018
Ma et al. (12)	CNNs+3D graph cut	MRI	0.851	30	Experimental and Therapeutic Medicine, 2018
Men et al. (15)	DDNN[g]	CT	0.716	230	Frontiers in Oncology, 2017
Li et al. (16)	CNN	CE-MRI	0.890	29	Biomed Research International, 2018
Huang et al. (17)	CNN	PET-CT	0.736	22	Contrast Media and Molecular Imaging, 2018
Ma et al. (18)	C-CNN[h]	CT-MRI	0.746	90	Physics in Medicine and Biology, 2019
Proposed method	CNN	Dual-sequence MRI	0.721	44	–

[a]DSC, Dice similarity coefficient; [b]SVM, support vector machine; [c]DCE-MRI, dynamic contrast-enhanced magnetic resonance imaging; [d]MRFs, Markov random fields; [e]AK-RW, adaptive random walker with k-means; [f]CNN, convolutional neural network; [g]DDNN, deep deconvolutional neural network; [h]C-CNN, combined convolutional neural network.

the accuracy of segmentation. To summarize, our proposed network showed accurate NPC segmentation in dual-sequence MRI images.

As shown in **Table 2**, the mean DSC of the proposed method in 10-fold cross-validation experiment was 0.721 and some studies have reported higher DSC than ours. However, in the studies by Deng et al. (10), Stefano et al. (11), Song et al. (8), Ma et al. (12, 18), and Li et al. (16), their methods were not fully automatic with which the tumor were segmented in the manually drawn volume of interest. The proposed method allowed fully automatic tumor segmentation. Yang et al. (9) and Huang et al. (17) used tumor metabolic information in PET images which made the tumor was easily to be detected. Wang et al. (4) evaluated their method with only four patients. To summarize, we proposed a fully automatic segmentation method with accurate and stable performance in dual-sequence MRI images.

Our proposed method has some limitations. Firstly, the patients sample size was relatively small, and the patients were collected from single center. Future work with a lager sample, especially from multicenter, would be necessary to further verify our method. Secondly, the segmentation performance of the proposed method was unsatisfactory in some small lymph nodes. As shown in **Figure 3**, part of the normal lymph node and tumor were incorrectly identified. The reason may be that the image feature of normal lymph nodes was similar to that of abnormal lymph nodes in the axial MRI images. We may adapt the DEU to multi-view MRI images in future work. Thirdly, the co-registration of T1W and T2W images is still challenging. A method without co-registration may be proposed in future work.

In this study, we successfully proposed and verified an accurate and efficient automatic NPC segmentation method based on DEU and dual-sequence MRI images. Although both DenseNet and UNet has been applied widely in tumor segmentation tasks, no article has been published combining them for the automatic segmentation of the NPC on dual-sequence MRI. We the first time applied this method in the automatic segmentation of the NPC and showed more stable and better performance than other methods. With dual-sequence images, the combination of different features from T1W and T2W images increased the segmentation accuracy. The DEU extracted the features of T1W and T2W in different path automatically and fused the features with dense connectivity block, which also contributed to the increased accuracy. 10-fold cross-validation results showed that the proposed method gained good performance. Future studies may aim to improve the segmentation accuracy with improved network structure or domain knowledge, avoiding the co-registration between different modalities. If further verified with lager sample and multicenter data, our proposed method would be of use in clinical practice of NPC.

DATA AVAILABILITY STATEMENT

The datasets for this article are not publicly available because Panyu Central Hospital, the center from which the data were collected, does not agree to make the data publicly accessible. Requests to access the datasets should be directed to Prof. Bingsheng Huang, huangb@szu.edu.cn.

ETHICS STATEMENT

44 NPC patients were retrospectively recruited from Panyu Central Hospital. The ethics committee of Panyu Central Hospital performed the ethical review and approved this study, and waived the necessity to obtain informed written consent from the patients.

AUTHOR CONTRIBUTIONS

ZC, HC, BingH, and YY contributed conception and design of the study. YY, HC, YH, WD, and GZ organized the database. ZC and BinH performed the statistical analysis. ZC, BinH, and PZ wrote the first draft of the manuscript. All authors contributed to manuscript revision, read and approved the submitted version.

FUNDING

This study was jointly funded by Guangzhou Science and Technology Project (No. 201804010111); Science and Technology Plan Project of Panyu District, Guangzhou (No. 2017-Z04-08); and Shenzhen Science and Technology Project (No. JCYJ20160307114900292). Guangzhou Science and Technology Planning Project (No. 201903010073).

SUPPLEMENTARY MATERIAL

The Supplementary Material for this article can be found online at: https://www.frontiersin.org/articles/10.3389/fonc.2020.00166/full#supplementary-material

REFERENCES

1. Chang ET, Adami HO. The enigmatic epidemiology of nasopharyngeal carcinoma. *Cancer Epidemiol Biomarkers Prevent.* (2006) 15:1765–77. doi: 10.1158/1055-9965.EPI-06-0353
2. Peng H, Chen L, Chen YP, Li WF, Tang LL, Lin AH, et al. The current status of clinical trials focusing on nasopharyngeal carcinoma: A comprehensive analysis of ClinicalTrials. gov database. *PLoS ONE.* (2018) 13:e0196730. doi: 10.1371/journal.pone.0196730
3. Chua MLK, Wee JTS, Hui EP, Chan ATC. Nasopharyngeal carcinoma. *Lancet.* (2016) 387:1012–24. doi: 10.1016/S0140-6736(15)00055-0
4. Wang Y, Zu C, Hu G, Luo Y, Ma Z, He K, et al. Automatic tumor segmentation with deep convolutional neural networks for radiotherapy applications. *Neural Proc Lett.* (2018) 48:1323–34. doi: 10.1007/s11063-017-9759-3
5. Zhou J, Chan KL, Xu P, Chong VFH. Nasopharyngeal carcinoma lesion segmentation from MR images by support vector machine. In: *3rd IEEE International Symposium on Biomedical Imaging: Nano to Macro, 2006.* Arlington, VA: IEEE. (2006). p. 1364–1367.

6. Ritthipravat P, Tatanun C, Bhongmakapat T, Tuntiyatorn L. Automatic segmentation of nasopharyngeal carcinoma from CT images. In: *2008 International Conference on BioMedical Engineering and Informatics*. Sanya: IEEE (2008). p. 18–22.
7. Tatanun, C., Ritthipravat, P., Bhongmakapat T, Tuntiyatorn L. Automatic segmentation of nasopharyngeal carcinoma from CT images: Region growing based technique. In: *2010 2nd International Conference on Signal Processing Systems*. Dalian: IEEE (2010). p. V2-537-V532-541.
8. Song Q, Bai J, Han D, Bhatia S, Sun W, Rockey W, et al. Optimal co-segmentation of tumor in PET-CT images with context information. *IEEE Trans Med Imaging.* (2013) 32:1685–97. doi: 10.1109/TMI.2013.2263388
9. Yang J, Beadle BM, Garden AS, Schwartz DL, Aristophanous M. A multimodality segmentation framework for automatic target delineation in head and neck radiotherapy. *Med Phys.* (2015) 42:5310–20. doi: 10.1118/1.4928485
10. Deng W, Luo L, Lin X, Fang T, Liu D, Dan G, et al. Head and neck cancer tumor segmentation using support vector machine in dynamic contrast-enhanced MRI. *Contr Media Mol Imaging*. (2017) 2017:8612519. doi: 10.1155/2017/8612519
11. Stefano A, Vitabile S, Russo G, Ippolito M, Sabini MG, Sardina D, et al. An enhanced random walk algorithm for delineation of head and neck cancers in PET studies. *Med Biol Eng Comput*. (2017) 55:897–908. doi: 10.1007/s11517-016-1571-0
12. Ma Z, Wu X, Song Q, Luo Y, Wang Y, Zhou J. Automated nasopharyngeal carcinoma segmentation in magnetic resonance images by combination of convolutional neural networks and graph cut. *Exp Ther Med*. (2018) 16:2511–21. doi: 10.3892/etm.2018.6478
13. Long J, Shelhamer E, Darrell T. Fully convolutional networks for semantic segmentation. In: *Proceedings of the IEEE Conference on Computer Vision and Pattern Recognition*. Boston, MA: IEEE (2015). p. 3431–3440. doi: 10.1109/CVPR.2015.7298965
14. Ronneberger O, Fischer P, Brox T. (2015). *U-Net: Convolutional Networks for Biomedical Image Segmentation*. Munich: Springer International Publishing. p. 234–241.
15. Men K, Chen X, Zhang Y, Zhang T, Dai J, Yi J, et al. Deep deconvolutional neural network for target segmentation of nasopharyngeal cancer in planning computed tomography images. *Front Oncol*. (2017) 7:315. doi: 10.3389/fonc.2017.00315
16. Li Q, Xu Y, Chen Z, Liu D, Feng ST, Law M, et al. Tumor segmentation in contrast-enhanced magnetic resonance imaging for nasopharyngeal carcinoma: deep learning with convolutional neural network. *BioMed Res Int*. (2018) 2018:9128527. doi: 10.1155/2018/9128527
17. Huang B, Chen Z, Wu PM, Ye Y, Feng ST, Wong CO, et al. Fully automated delineation of gross tumor volume for head and neck cancer on PET-CT using deep learning: a dual-center study. *Contrast Media Mol Imaging.* (2018) 2018:8923028. doi: 10.1155/2018/8923028
18. Ma Z, Zhou S, Wu X, Zhang H, Yan W, Sun S, et al. Nasopharyngeal carcinoma segmentation based on enhanced convolutional neural networks using multi-modal metric learning. *Phys Med Biol.* (2019) 64:025005. doi: 10.1088/1361-6560/aaf5da
19. Huang G, Liu Z, van der Maaten L, Weinberger KQ. Densely connected convolutional networks. In: *Proceedings of the IEEE Conference on Computer Vision and Pattern Recognition*. Honolulu, HI, (2017). p. 4700–4708. doi: 10.1109/CVPR.2017.243
20. Mattes D, Haynor DR, Vesselle H, Lewellyn TK, Eubank W. Nonrigid multimodality image registration. In: *Medical Imaging 2001: Image Processing*. San Diego, CA: International Society for Optics and Photonics (2001). p. 1609–1621.
21. Styner M, Brechbühler C, Székely G, Gerig G. Parametric estimate of intensity inhomogeneities applied to MRI. *IEEE Trans Med Imaging.* (2000) 19:153–65. doi: 10.1109/42.845174
22. Wu Y, He K. Group normalization. In: *Proceedings of the European Conference on Computer Vision*. Munich: ECCV (2018). p. 3–19.
23. Liew SS, Khalil-Hani M, Bakhteri R. Bounded activation functions for enhanced training stability of deep neural networks on visual pattern recognition problems. *Neurocomputing.* (2016) 216:718–34. doi: 10.1016/j.neucom.2016.08.037
24. Ioffe S, Szegedy C. Batch normalization: accelerating deep network training by reducing internal covariate shift. *arXiv preprint* arXiv:1502.03167 (2015).
25. Szegedy C, Vanhoucke V, Ioffe S, Shlens J, Wojna Z. Rethinking the inception architecture for computer vision. In: *Proceedings of the IEEE Conference on Computer Vision and Pattern Recognition*. Las Vegas, NV, (2016). p. 2818–2826. doi: 10.1109/CVPR.2016.308
26. Milletari F, Navab N, Ahmadi A-S. V-net: fully convolutional neural networks for volumetric medical image segmentation. In: *2016 Fourth International Conference on 3D Vision (3DV)*. Stanford, CA: IEEE (2016). p. 565–571.
27. Chollet F. *Keras* (2015). Available online at: https://github.com/fchollet/keras
28. Abadi M, Barham P, Chen J, Chen Z, Davis A, Dean J. Tensorflow: a system for large-scale machine learning. In: *12th {USENIX} Symposium on Operating Systems Design and Implementation*. Savannah, GA: OSDI. (2016). p. 265–283.
29. Kingma DP, Ba J. Adam: a method for stochastic optimization. *arXiv preprint* arXiv:1412.6980 (2014).
30. Crum WR, Camara O, Hill DL. Generalized overlap measures for evaluation and validation in medical image analysis. *IEEE Trans Med Imaging.* (2006) 25:1451–61. doi: 10.1109/TMI.2006.880587

Conflict of Interest: The authors declare that the research was conducted in the absence of any commercial or financial relationships that could be construed as a potential conflict of interest.

frontiers in Oncology

ORIGINAL RESEARCH
published: 28 February 2020
doi: 10.3389/fonc.2020.00255

Stratification of Candidates for Induction Chemotherapy in Stage III-IV Nasopharyngeal Carcinoma: A Large Cohort Study Based on a Comprehensive Prognostic Model

Xue-Song Sun[1,2†], Bei-Bei Xiao[1,2†], Zi-Jian Lu[1,2†], Sai-Lan Liu[1,2], Qiu-Yan Chen[1,2], Li Yuan[1], Lin-Quan Tang[1,2] and Hai-Qiang Mai[1,2*]*

[1] Sun Yat-sen University Cancer Center, State Key Laboratory of Oncology in South China, Collaborative Innovation Center for Cancer Medicine, Guangdong Key Laboratory of Nasopharyngeal Carcinoma Diagnosis and Therapy, Guangzhou, China, [2] Department of Nasopharyngeal Carcinoma, Sun Yat-sen University Cancer Center, Guangzhou, China

Objective: To establish a prognostic index (PI) for patients with stage III-IV nasopharyngeal carcinoma (NPC) patients to personalize recommendations for induction chemotherapy (IC) before intensity-modulated radiotherapy (IMRT).

Patients and Methods: Patients received concurrent chemoradiotherapy (CCRT) with or without IC. Factors used to construct the PI were selected by a multivariate analysis of progression-free survival (PFS), which was the primary endpoint ($P < 0.05$). Five variables were selected based on a backward procedure in a Cox proportional hazards model: gender, T stage, N stage, lactate dehydrogenase (LDH), and Epstein–Barr virus (EBV) DNA. The cutoff value for the PI was determined by the receiver operating characteristic curve analysis.

Results: The present study involved 3,586 patients diagnosed with stage III-IV NPC. The cutoff value for PI was 0.8. The high-risk subgroup showed worse outcomes than did the low-risk subgroup on all endpoints: PFS, overall survival (OS), locoregional relapse-free survival (LRFS), and distant metastasis-free survival (DMFS). In the low-risk subgroup (PI < 0.8), patients showed comparable survival outcomes on all clinical endpoints regardless of IC application, whereas in the high-risk subgroup (PI > 0.8), the addition of IC significantly improved PFS, OS, and DMFS, but not LRFS. In multivariate analyses, IC was a protective factor for PFS, OS, and DMFS in the high-risk subgroup, while it had no significant benefit in the low-risk subgroup.

Conclusion: The proposed prognostic model effectively stratifies patients with stage III-IV NPC. High-risk patients are candidates for IC before CCRT, while low-risk patients are unlikely to benefit from it.

Keywords: nasopharyngeal carcinoma, Epstein–Barr virus DNA, induction chemotherapy, radiotherapy, survival

OPEN ACCESS

Edited by:
Jun Ma,
Sun Yat-sen University Cancer Center (SYSUCC), China

Reviewed by:
Lin Kong,
Fudan University Shanghai Cancer Center, China
Linglong Tang,
Sun Yat-sen University, China

****Correspondence:***
Lin-Quan Tang
tanglq@sysucc.org.cn
Hai-Qiang Mai
maihq@mail.sysu.edu.cn

† These authors have contributed equally to this work

Specialty section:
This article was submitted to Head and Neck Cancer, a section of the journal Frontiers in Oncology

Received: *26 July 2019*
Accepted: *14 February 2020*
Published: *28 February 2020*

Citation:
Sun X-S, Xiao B-B, Lu Z-J, Liu S-L, Chen Q-Y, Yuan L, Tang L-Q and Mai H-Q (2020) Stratification of Candidates for Induction Chemotherapy in Stage III-IV Nasopharyngeal Carcinoma: A Large Cohort Study Based on a Comprehensive Prognostic Model. Front. Oncol. 10:255. doi: 10.3389/fonc.2020.00255

INTRODUCTION

Nasopharyngeal carcinoma (NPC), a malignant disease of the nasopharyngeal epithelium, has an incidence rate of 20–50 cases per 100,000 people in epidemic areas, such as Southeast Asia (1, 2). As NPC has high sensitivity to irradiation and a distinct anatomical location, radiotherapy (RT) is currently the only curative treatment for NPC. For stage I NPC, radiotherapy has been reported to achieve an overall survival (OS) rate of over 90%. For locoregionally advanced disease, which represents 70–90% of newly diagnosed NPC cases, radiotherapy with concurrent chemoradiotherapy (CCRT) could improve OS; thus, it is regarded as standard treatment (3–5). However, over 20% of patients still develop distant metastasis after CCRT (6).

By lowering tumor volume and restricting occult micrometastasis, induction chemotherapy (IC) before RT has been proposed to further decrease distant metastasis risk. Previous studies have shown that IC might improve survival outcomes in patients with locoregionally advanced NPC (7, 8). Nevertheless, not all patients with locoregionally advanced NPC benefit from IC. Previous studies have reported that IC might not improve survival among patients with T3-4N0-1 NPC; in fact, IC has been associated with severe toxicity in this patient group (9, 10). Given the body of evidence, it is likely that patients at high risk might benefit from IC more than patients at low risk. As such, a prognostic score to differentiate high- and low-risk patients is required to assist in clinical decision-making.

The tumor, node, metastasis (TNM) staging system, which continues to be a globally recognized standard for assessing the prognosis of NPC, has been criticized as barely satisfactory, as it does not account for important prognostic factors, such as Epstein–Barr virus (EBV) DNA and serum lactate dehydrogenase (LDH) levels (11–13). Therefore, this study aimed to evaluate several potential prognostic factors and construct a prognostic score to classify risk status and identify suitable patients with stage III-IVa NPC that could benefit from IC, using data from a large cohort of patients.

MATERIALS AND METHODS

Patients

This study included 3,586 stage III-IVa NPC patients treated at Sun Yat-sen University Cancer Center (SYSUCC) from January 2008 to December 2013 who met the following inclusion criteria: (1) biopsy-confirmed NPC; (2) non-metastasis status at diagnosis; (3) stage III-IVa NPC, based on the 8th edition of the American Joint Committee on Cancer/International Union Against Cancer (AJCC/UICC) staging system; (4) no history of malignancy or synchronous cancer; (5) complete clinicopathological and treatment information; (6) treatment with IC + CCRT or CCRT alone. The study protocol was approved by the clinical research ethics committee of our cancer center, and written informed consent was obtained from each patient. The flowchart capturing patient inclusion process is shown in **Figure 1**.

Quantification of Plasma EBV DNA Levels

Plasma EBV DNA quantification method is described in the **Supplementary Material**.

Treatment

In our cohort, 2077 patients were treated with CCRT alone and 1509 patients were treated with IC before CCRT. The common IC regimens were cisplatin (80 mg/m^2) with 5-fluorouracil (800

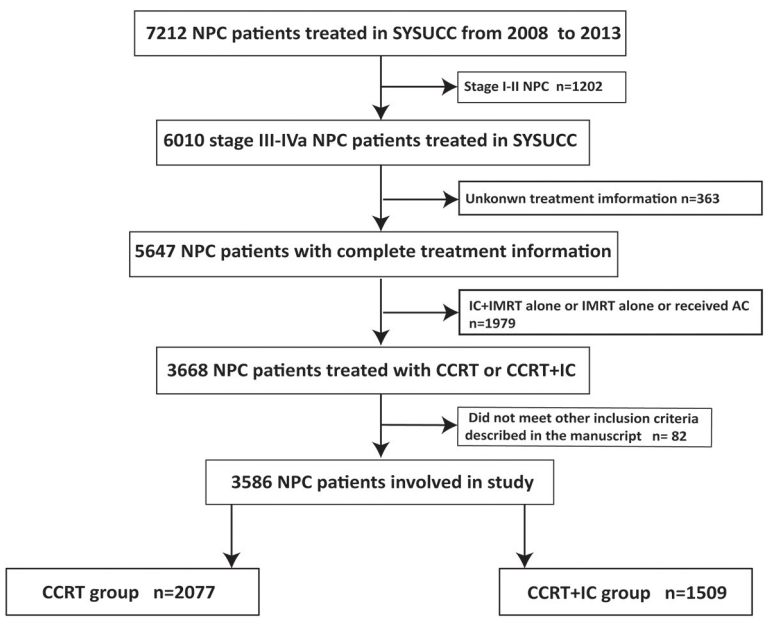

FIGURE 1 | Flowchart presenting patient inclusion process.

mg/m^2/day over 120 h), or cisplatin (80 mg/m^2) with docetaxel (80 mg/m^2), or cisplatin (60 mg/m^2) with 5-fluorouracil (600 mg/m^2 over 120 h), and docetaxel (60 mg/m^2) administered at 3-week intervals. Concurrent chemotherapy consisted of cisplatin/nedaplatin (80 or 100 mg/m^2) given in Week 1, 4, and 7 of radiotherapy, or cisplatin/nedaplatin (40 mg/m^2) given weekly during radiotherapy, beginning on the first day of radiotherapy. The radiotherapy technique used was intensity-modulated radiotherapy (IMRT), with 66–70 Gy to the primary lesion, 60–70 Gy to the involved neck fields, and 50–54 Gy of prophylactic irradiation to the neck. All patients received 5 fractions per week at a dose of 1.8–2.2 Gy per fraction. The IMRT plan was designed based on evidence from previous studies (14).

Follow-Up

All patients received comprehensive follow-up examinations every 3 months for the first 3 years and every 6 months thereafter. Follow-up examinations included semiannual quantitative EBV DNA determination, nasopharyngoscopy, head and neck magnetic resonance imaging, chest radiography, and abdominal sonography. If locoregional relapse and/or distant metastasis were suspected, a bone scan, or 18F-fluorodeoxyglucose positron emission tomography and computed tomography (PET/CT) were considered.

The primary endpoint of the present study was progression-free survival (PFS), which represented the time interval between first diagnosis and disease progression or death from any

TABLE 1 | Baseline characteristics of patients in the CCRT and CCRT + IC groups.

Characteristic	CCRT *n* (%)	CCRT + IC *n* (%)	*P*-value
Total	2,077	1,509	
Age, y			
≤46	1,009 (48.6)	769 (51.0)	0.166
>46	1,068 (51.4)	740 (49.0)	
Gender			
Female	552 (26.6)	354 (23.5)	0.036
Male	1,525 (73.4)	1,155 (76.5)	
Diabetes mellitus			
No	2,014 (97.0)	1,480 (98.1)	0.042
Yes	63 (3.0)	29 (1.9)	
Cardiovascular disease			
No	1,957 (94.2)	1,431 (94.8)	0.459
Yes	120 (5.8)	78 (5.2)	
T stage[a]			
T1	69 (3.3)	45 (3.0)	<0.001
T2	232 (11.2)	181 (12.0)	
T3	1,365 (65.7)	740 (49.0)	
T4	411 (19.8)	543 (36.0)	
N stage[a]			
N0	328 (15.8)	135 (8.9)	<0.001
N1	759 (36.5)	433 (28.7)	
N2	967 (41.7)	710 (47.1)	
N3	123 (5.9)	231 (15.3)	
LDH level			
≤245 U/L	1,981 (95.4)	1,399 (92.7)	0.001
>245 U/L	96 (4.6)	110 (7.3)	
EBV DNA level			
≤1,500 copies/ml	913 (44.0)	425 (28.2)	<0.001
>1,500 copies/ml	1,164 (56.0)	1,084 (71.8)	

CCRT, concurrent chemoradiotherapy; IC, induction chemotherapy; LDH, lactate dehydrogenase; EBV, Epstein–Barr virus.

[a]*According to the 8th edition of the UICC/AJCC staging system.*

P-values were calculated by a χ^2-test.

TABLE 2 | Multivariable analysis of prognostic factors for progression-free survival, overall survival, locoregional relapse–free survival, and distant metastasis–free survival.

Characteristic	HR	95%CI	*P* value
Progression-free survival			
Gender	1.369	1.113–1.684	0.003
T stage	1.441	1.200–1.729	<0.001
N stage			
N2 vs. N0-1	1.375	1.138–1.661	0.001
N3 vs. N0-1	1.925	1.468–2.525	<0.001
LDH level	1.414	1.055–1.897	0.021
EBV-DNA level	2.115	1.706–2.621	<0.001
Treatment method	0.761	0.640–0.905	0.002
Overall survival			
Age	1.447	1.146–1.827	0.002
Gender	1.993	1.442–2.755	<0.001
T stage	1.648	1.286–2.111	<0.001
N stage			
N2 vs. N0-1	1.679	1.290–2.187	<0.001
N3 vs. N0-1	2.468	1.692–3.599	<0.001
EBV-DNA level	2.330	1.703–3.189	<0.001
Treatment method	0.552	0.431–0.706	<0.001
Locoregional relapse–free survival			
T stage	1.544	1.151–2.072	0.004
EBV-DNA level	2.102	1.486–2.971	<0.001
Distant metastasis–free survival			
Gender	1.754	1.336–2.302	<0.001
Diabetes mellitus	1.622	0.982–2.680	0.059
T stage	1.360	1.088–1.701	0.007
N stage			
N2 vs. N0-1	1.434	1.134–1.813	0.003
N3 vs. N0-1	2.491	1.818–3.413	<0.001
EBV-DNA level	1.435	1.014–2.031	0.041
LDH level	2.378	1.813–3.119	<0.001
Treatment method	0.651	0.526–0.805	<0.001

HR, hazard ratio; CI, confidence interval; NPC, nasopharyngeal carcinoma; LDH, lactate dehydrogenase; EBV, Epstein–Barr virus. A Cox proportional hazards model was used to perform multivariate analyses. All variables were transformed into categorical variables. HRs were calculated for age (years) (>46 vs. ≤46), gender (male vs. female), diabetes mellitus (yes vs. no), cardiovascular disease (yes vs. no), T stage (T4 vs. T1-3), LDH level (>245 U/L vs. ≤245 U/L), EBV DNA level (>1,500 copies/ml vs. ≤1,500 copies/ml) and treatment method (CCRT + IC vs. CCRT). We selected variables using a backward stepwise approach. The P-value threshold was 0.1 (P > 0.1) for removing non-significant variables from the model.

cause. The following survival outcomes were secondary study endpoints: overall survival (OS) was defined as the time interval from the first diagnosis to death from any cause, while locoregional relapse–free survival (LRFS) and distant metastasis-free survival (DMFS) were defined as time from diagnosis to disease relapse in the nasopharynx or a neck lymph node, and to occurrence of distant metastasis, respectively. Patients lost to follow-up or alive without distant metastasis or locoregional recurrence at the last follow-up visit had their data censored.

Statistical Analysis

The patients' clinical characteristics and acute toxicity status were compared between treatment groups using the Pearson χ^2-test or Fisher's exact test. Kaplan-Meier curves were used to compare survival outcomes between study groups with a log-rank test. All variables were transformed into categorical variables. A Cox proportional hazards model with a backward method was used for multivariate analyses. Covariates that were statistically significant ($P < 0.05$) were selected to construct the PI. The cohort was divided into low- and high-risk subgroups by the cutoff value of the PI score, which was determined by a receiver operating characteristic (ROC) curve. All statistical analyses were conducted using SPSS v23 (IBM, Armonk, IL, USA).

RESULTS

Patients' Characteristics and Survival

From January 2008 to December 2013, 3586 patients were involved in this study. Then median age of our cohort at diagnosis was 46 years; 74.7% of patients were men. In total, 1509 patients (42.1%) received IC before CCRT. Patient characteristics by treatment group are shown in **Table 1**. Patients with stage T4 or N2-3 disease were more likely to receive IC than were patients with stage T1-3 ($P < 0.001$) or N0-1 ($P < 0.001$) disease. Male gender ($P = 0.036$), higher (>245 U/L) level of LDH ($P = 0.001$), and pretreatment EBV DNA >1,500 copies/ml ($P < 0.001$) were also significantly associated with IC treatment. During a median follow-up time of 44.9 months (interquartile range 32.8–61.9 months), 299 patients (8.3%) died. The OS rates at 3 and 5 years were 94.0 and 88.9%, respectively.

Prognostic Factors and Establishment of the Prognostic Index

In multivariate analysis, gender [hazard ratio (HR) = 1.369; 95% confidence interval (CI) = 1.113–1.684; $P = 0.003$], T stage (HR = 1.441; 95% CI = 1.200–1.729; $P < 0.001$), N stage (N2 vs. N0-1: HR = 1.375; 95% CI = 1.138–1.661; $P = 0.001$; N3 vs. N0-1: HR = 1.925; 95% CI = 1.468–2.525; $P < 0.001$), LDH level (HR = 1.414; 95% CI = 1.055–1.897; $P = 0.021$), and EBV DNA level (HR = 2.115; 95% CI = 1.706–2.621; $P < 0.001$) emerged as independent prognostic factors for PFS (**Table 2**). Subsequently, the PI was constructed based on weighting (derived by the log [adjusted HR]) of these five prognostic factors (**Table 3**). The results of multivariate analysis in terms of OS, LRFS, and DMFS are also shown in **Table 2**.

TABLE 3 | Prognostic score to predict progression-free survival.

Variable	Hazard ratio	Score [HR = exp (score)]
Gender		
Female	1	0
Male	1.369	0.314
T stage[a]		
T1-3	1	0
T4	1.441	0.365
N stage[a]		
N0-1	1	0
N2	1.375	0.318
N3	1.925	0.655
LDH level		
≤245 U/L	1	0
>245 U/L	1.414	0.346
EBV-DNA level		
≤1500 copies/ml	1	0
>1500 copies/ml	2.115	0.749

Hazard ratios were estimated by a Cox proportional hazards regression.
[a]*According to the 8th edition of the UICC/AJCC staging system.*

Risk Stratification

Using this PI model, we divided patients into low- and high-risk subgroups. The cutoff value was PI = 0.8, determined by the ROC analysis. Clinical characteristics of patients in two risk subgroups are shown in **Table 4**. Patients with lower PI (low-risk) achieved a significantly greater PFS compared with high-risk patients (3-year PFS rate: 92.1vs. 81.7%; $P < 0.001$). A similar association was found for OS, LRFS, and DMFS (3-year OS rate: 97.8 vs. 91.7%; $P < 0.001$; 3-year LRFS rate: 97.1 vs. 94.2%; $P < 0.001$; 3-year DMFS rate: 95.3 vs. 86.5%; $P < 0.001$; **Figures 2A–D**).

The Efficacy of IC in Risk-Based Subgroups

Given that patients in different risk subgroups were likely to suffer different tumor burden, we investigated the efficacy of IC in low- and high-risk patients and found that it differed between the subgroups. In the low-risk subgroup (PI < 0.8), non-significant differences were observed in PFS ($P = 0.422$), OS ($P = 0.100$), LRFS ($P = 0.455$), and DMFS ($P = 0.662$) between the IC + CCRT and CCRT groups (**Figures 3A–D**). However, in the high-risk subgroup, patients receiving IC + CCRT achieved greater PFS, OS, and DMFS than did patients receiving CCRT alone (3-year PFS rate: 83.5 vs. 77.9%, $P = 0.012$; 3-year OS rate: 94.0 vs. 89.4%, $P < 0.001$; 3-year DMFS rate: 88.6 vs. 84.2%, $P = 0.003$). There was no significant difference between two treatment groups in LRFS (**Figures 4A–D**).

In multivariate analysis, within the low-risk subgroup, there was no significant survival difference between two treatment

TABLE 4 | Clinical characteristics of patients in low- and high-risk subgroups.

Characteristic	Low-risk patients *n* (%)			High-risk patients *n* (%)		
	CCRT	CCRT + IC	*P-value*	CCRT	CCRT + IC	*P-value*
Total	972	414		1,105	1,095	
Age, y						
≤46	503 (51.7)	224 (54.1)	0.445	506 (45.8)	545 (49.8)	0.066
>46	469 (48.3)	190 (45.9)		599 (54.2)	550 (50.2)	
Gender						
Female	357 (36.7)	143 (34.5)	0.464	195 (17.6)	211 (19.3)	0.350
Male	615 (63.3)	271 (65.5)		910 (82.4)	884 (80.7)	
Diabetes mellitus						
No	943 (97.0)	408 (98.6)	0.097	1,071 (96.9)	1,072 (97.9)	0.179
Yes	29 (3.0)	6 (1.4)		34 (3.1)	23 (2.1)	
Cardiovascular disease						
No	911 (93.7)	400 (96.6)	0.028	1,046 (94.7)	1,031 (94.2)	0.643
Yes	61 (6.3)	14 (3.4)		59 (5.3)	64 (5.8)	
T stage[a]						
T1	26 (2.7)	6 (1.4)	<0.001	43 (3.9)	39 (3.6)	<0.001
T2	69 (7.1)	40 (9.7)		163 (14.8)	141 (12.9)	
T3	762 (78.4)	247 (59.7)		603 (54.6)	493 (45.0)	
T4	115 (11.8)	121 (29.2)		296 (26.8)	422 (38.5)	
N stage[a]						
N0	262 (27.0)	77 (18.6)	0.005	66 (6.0)	58 (5.3)	<0.001
N1	456 (46.9)	204 (49.3)		303 (27.4)	229 (20.9)	
N2	241 (24.8)	125 (30.2)		626 (56.7)	585 (53.4)	
N3	13 (1.3)	8 (1.9)		110 (10.0)	223 (20.4)	
LDH level						
≤245 U/L	957 (98.5)	410 (99.0)	0.462	1024 (92.7)	989 (90.3)	0.056
>245 U/L	15 (1.5)	4 (1.0)		81 (7.3)	106 (9.7)	
EBV DNA level						
≤1,500 copies/ml	880 (90.5)	371 (89.6)	0.621	33 (3.0)	54 (4.9)	0.021
>1,500 copies/ml	92 (9.5)	43 (10.4)		1,072 (97.0)	1,041 (95.1)	

CCRT, concurrent chemoradiotherapy; IC, induction chemotherapy; LDH, lactate dehydrogenase; EBV, Epstein–Barr virus.
[a]*According to the 8th edition of the UICC/AJCC staging system.*
P-values were calculated by a χ^2-test.

groups ($P > 0.05$ for all survival endpoints). In contrast, in the high-risk subgroup, the addition of IC was found to be protective for PFS (HR = 0.709; 95% CI, 0.585–0.858; $P = 0.002$), OS (HR = 0.466; 95% CI = 0.356–0.610; $P < 0.001$), and DMFS (HR = 0.633; 95% CI = 0.502–0.797; $P < 0.001$). There was no effect for LRFS (**Table 5**).

Acute Toxicity

Details of treatment-related acute toxicity experienced by patients receiving CCRT and CCRT + IC are presented in **Table 6**. The IC + CCRT group had a significantly higher proportion of grade 3–4 leukopenia (30.0 vs. 16.3%; $P < 0.001$) and neutropenia (37.8 vs. 15.2%; $P < 0.001$) than did the CCRT alone group. Between-group differences in other hematological toxicities, such as anemia or thrombocytopenia, were not significant. No significant differences in grade 3–4 hepatotoxicity or nephrotoxicity were observed between the treatment groups.

DISCUSSION

The present study identified independent prognostic factors for patients with stage III-IVa NPC in the IMRT era. Our study involved a large cohort and development of a PI to personalize treatment recommendations for IC. For patient stratification, the PI cutoff value was determined by the ROC analysis. We found that high-risk patients are likely to benefit from the addition of IC before CCRT, whereas low-risk patients are unlikely to benefit from it.

CCRT is standard treatment for locoregionally advanced NPC. As radiotherapy technology has developed, the local control rate of NPC has improved significantly (15). In

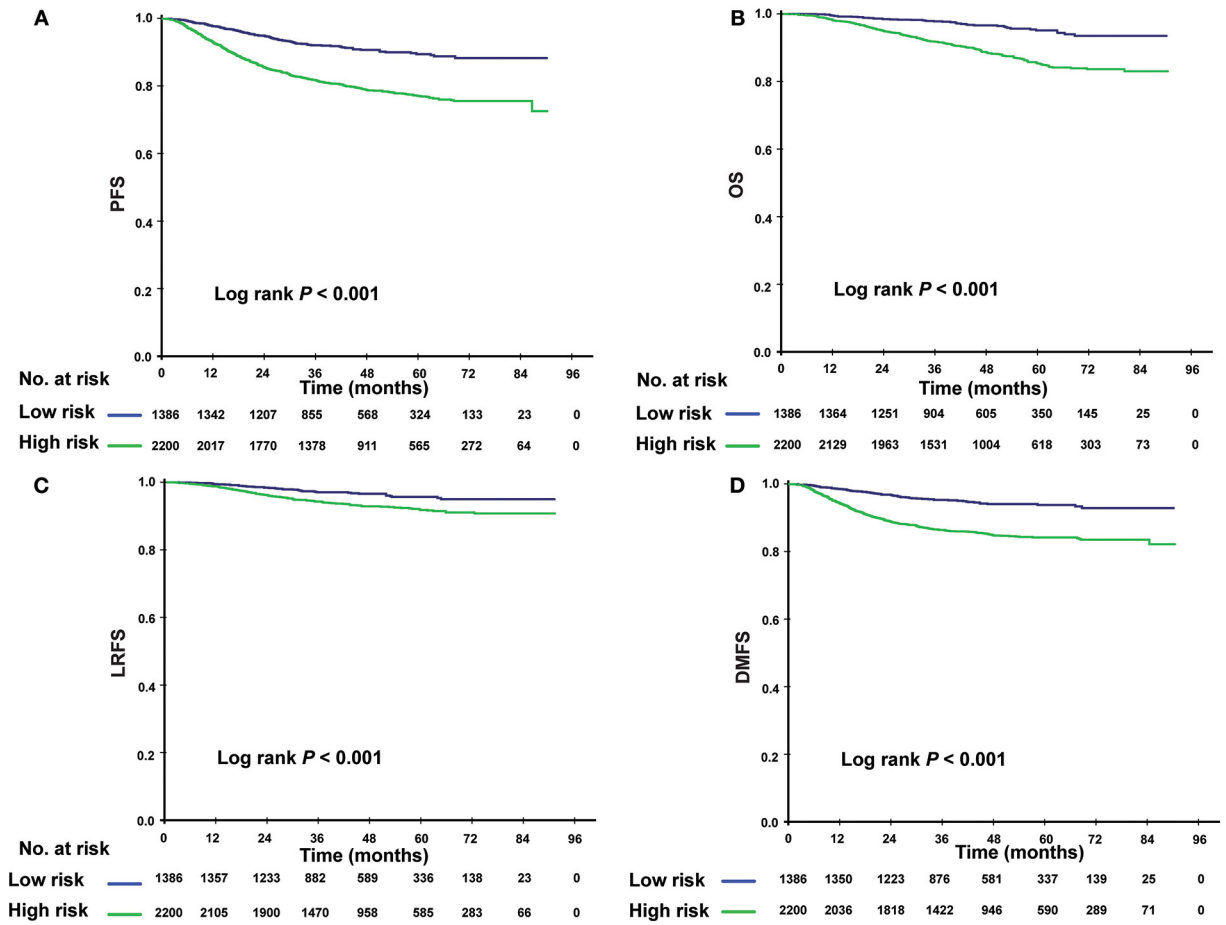

FIGURE 2 | Kaplan-Meier survival curves for the low- and high-risk subgroups. Results shown are for progression-free survival **(A)**, overall survival **(B)**, locoregional relapse–free survival **(C)**, and distant metastasis-free survival **(D)**. *P*-values are calculated using the log-rank test.

the IMRT era, occurrence of distant metastasis has become the predominant sign of failed treatment (16, 17). Recently, several clinical trials have provided evidence that IC before definitive CCRT is associated with lower incidence of distant metastases and further improved patient survival (7, 18, 19). However, according to studies among patients with stage T3-4 N0-1, clinical outcome was similar between the CCRT and IC + CCRT groups, indicating that IC might benefit only patients with a greater tumor burden (9, 10). Considering the toxicity and economic cost of chemotherapy, it is important to identify suitable patients who could benefit from additional IC.

The current AJCC/UICC stage classification is the main guideline for NPC risk stratification in clinical practice. However, this classification does not consider several variables that have been suggested as prognostic factors in NPC, such as age, gender, LDH, comorbidities, and, in particular, EBV DNA (11–13). Therefore, a more comprehensive prognostic model is urgently needed to accurately predict patients' clinical outcome.

In previous studies, several prognostic models were put forward to help select high-risk patients that might benefit from IC (20–22). Zhang et al. developed and validated a nomogram to predict individual benefit of IC based on a Phase III clinical trial (22). However, only 480 participants were involved in the establishment of the nomogram, and plasma EBV DNA was not included. Similarly, Du et al. created a prognostic model for distant metastasis in locally advanced NPC patients to identify high-risk patients who should receive IC, where the prognostic score was the sum of the number of prognostic factors (20). It was less rigorous in that different risk factors did not share the same weight in treatment failure. In our study, the PI scores were calculated based on the logarithm of HRs derived from multivariate analysis. To our knowledge, to-date, our study involved the largest cohort in establishing prognostic scores for selecting candidates for IC in stage III-IVa NPC.

We set PFS as the primary endpoint. In our results, five characteristics (gender, T stage, N stage, LDH level, and EBV DNA level) were selected and remained independent

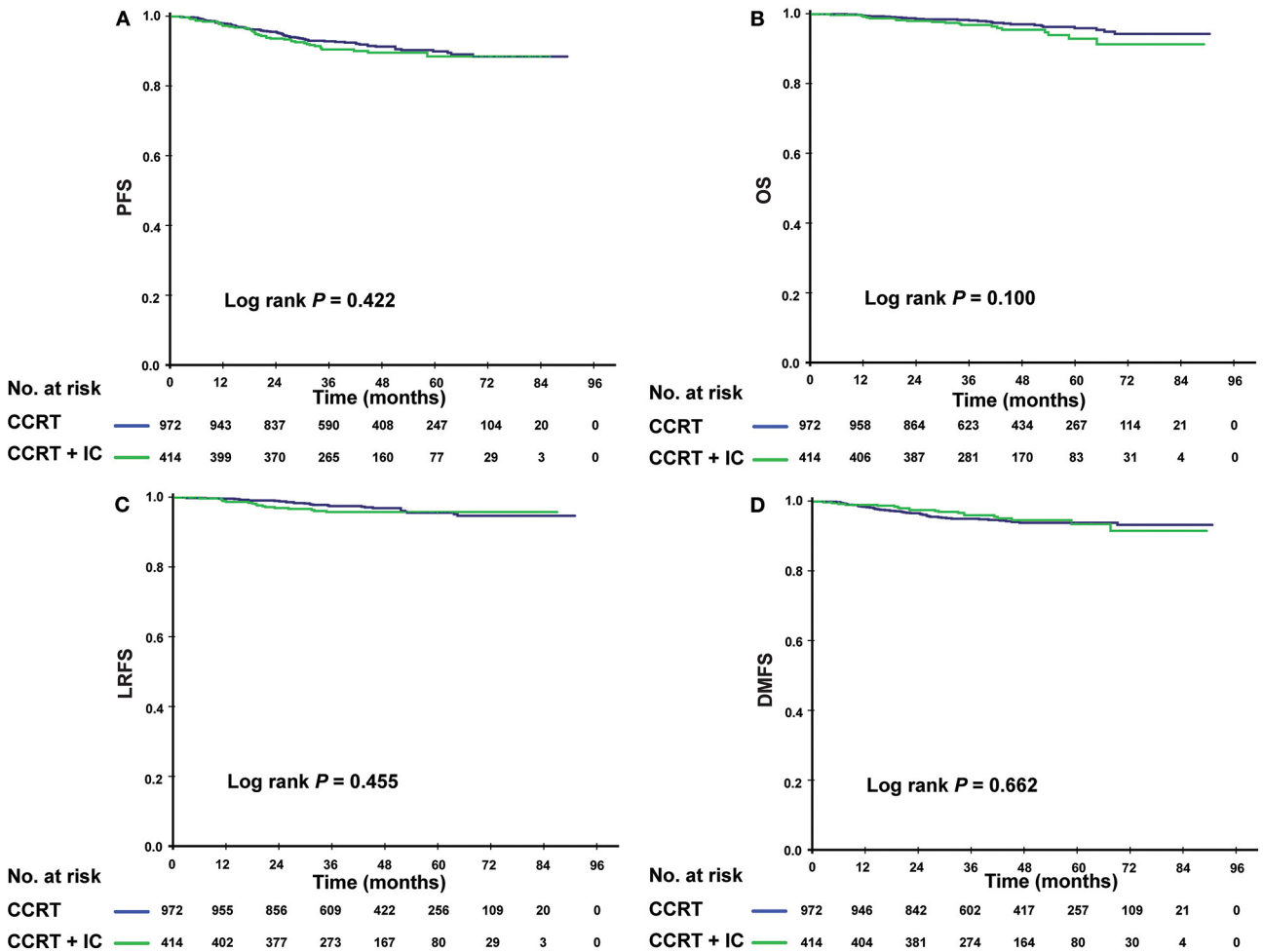

FIGURE 3 | Kaplan-Meier survival curves for the patients receiving concurrent chemoradiotherapy (CCRT), and induction chemotherapy combined with concurrent chemoradiotherapy (IC + CCRT) within the low-risk subgroup. Results shown are for progression-free survival **(A)**, overall survival **(B)**, locoregional relapse-free survival **(C)**, and distant metastasis–free survival **(D)**. *P*-values are calculated using the log-rank test.

factors in multivariate analysis. Previous studies have verified all five of these factors as important prognostic indicators (11). After the trade-off between sensitivity and specificity was resolved, the cutoff value of PI was determined as 0.8, with 1386 and 2200 patients identified as at low- and high-risk, respectively. Among patients with a higher PI, patients achieved a higher PFS rate, if they were in the IC + CCRT group. In contrast, no significant differences between the treatment groups were observed in the low-risk subgroup.

Collectively, our findings justify the recommendation of IC for patients identified as at high-risk, which could be explained by the following reasons. IC plays an important role in early eradication of tumor before radical radiotherapy. Patients in the high-risk subgroup suffer a greater tumor burden and higher risk of treatment failure. Some of them also might develop subclinical micrometastasis at diagnosis, which might indicate they should receive intensified therapy. Concurrently, induction chemotherapy can reduce tumor volume, which can support radiotherapy and shrink the target area. As a result, long-term toxicities, such as radiation encephalopathy, xerostomia, or trismus might improve to some extent. Therefore, the addition of IC could help these patients achieve longer disease-free survival. However, patients in the low-risk subgroup had a relatively satisfactory clinical outcome when treated with CCRT alone. Concurrently, additional toxic effects such as hepatoxicity or nephrotoxicity caused by IC may influence the survival benefit.

Our study shows great potential for application in clinical practice. Clinicians could evaluate the condition of stage III-IVa NPC patients before treatment using our PI system and select high-risk patients who may benefit from IC. However, it should be noted that more than 10% of high-risk patients still developed distant lesions in the IC + CCRT group, suggesting that a more intense therapy such as targeted therapy may be necessary for this subgroup (23, 24). Our

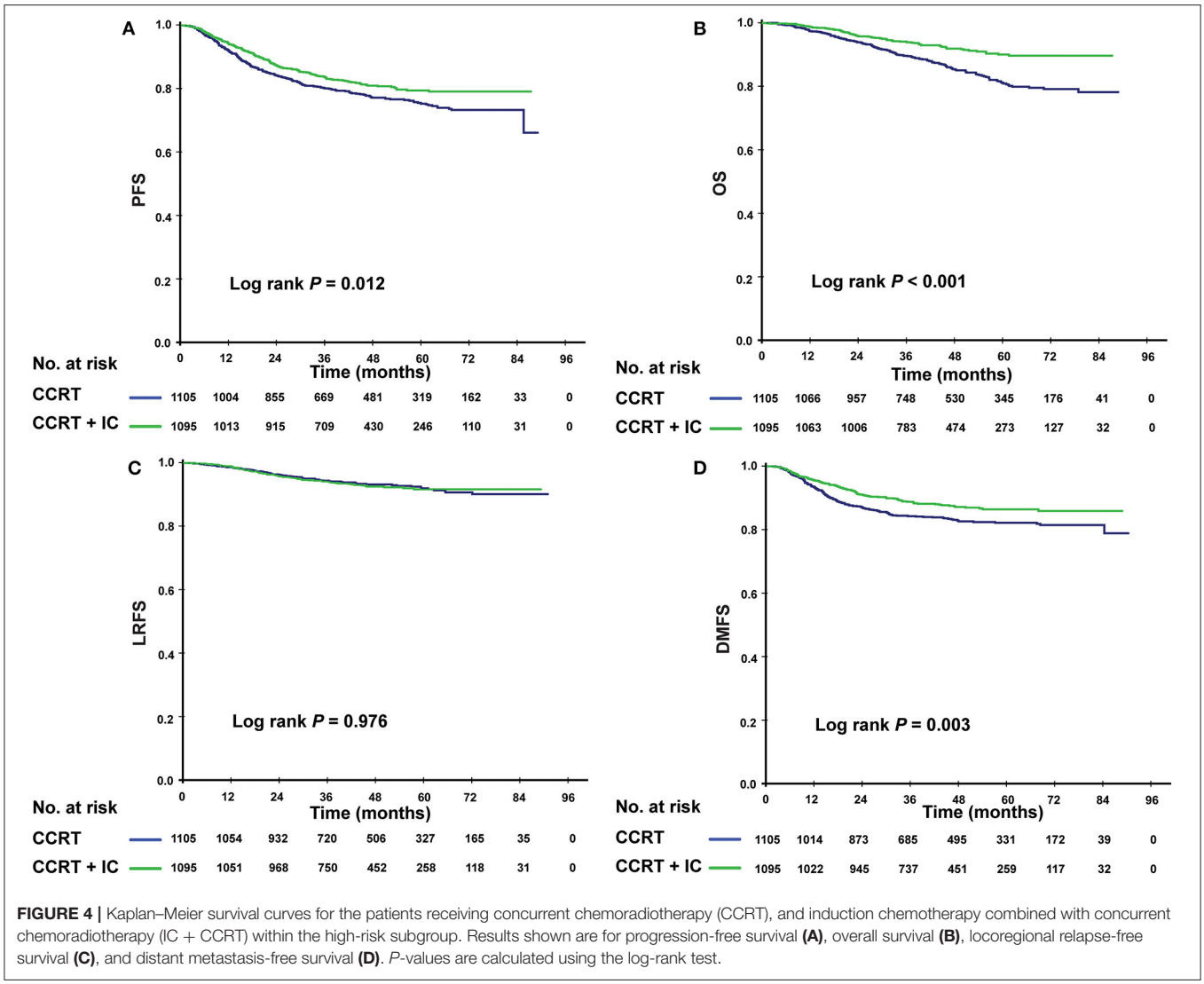

FIGURE 4 | Kaplan–Meier survival curves for the patients receiving concurrent chemoradiotherapy (CCRT), and induction chemotherapy combined with concurrent chemoradiotherapy (IC + CCRT) within the high-risk subgroup. Results shown are for progression-free survival **(A)**, overall survival **(B)**, locoregional relapse-free survival **(C)**, and distant metastasis-free survival **(D)**. *P*-values are calculated using the log-rank test.

group has launched a phase 1 study of tumor-infiltrating lymphocyte immunotherapy after CCRT in high-risk NPC; we were looking forward to the results of the phase 2 study (25).

Although this study is based on a large cohort, it has several limitations. First, it was a retrospective study, so survival outcomes might be affected by confounding factors, and accurate data on late toxicities could not be acquired. Secondly, the data were obtained from a single treatment center; therefore, our results should be validated by other datasets.

In conclusion, we proposed a PI model to predict whether patients could benefit from additional IC before CCRT and thereby to improve the decision-making process for patients with stage III-IVa NPC. Patients with higher PI (>0.8) are identified as at high-risk and would be likely to benefit from additional IC, whereas low-risk patients are unlikely to benefit from it.

DATA AVAILABILITY STATEMENT

The datasets analyzed in this article are not publicly available. Requests to access the datasets should be directed to maihq@mail.sysu.edu.cn.

ETHICS STATEMENT

This retrospective study was approved by the Clinical Research Committee of SYSUCC. Patients were required to provide written informed consent before enrolling in the study.

AUTHOR CONTRIBUTIONS

H-QM, L-QT, Q-YC, and LY: study concepts and manuscript review. X-SS, B-BX, Z-JL, and S-LL: study design, data acquisition, and data analysis and interpretation. X-SS, B-BX, and

TABLE 5 | Multivariate analysis of progression-free survival, overall survival, locoregional relapse–free survival, and distant metastasis–free survival in low- and high-risk subgroups.

Low-risk subgroup				High-risk subgroup			
Characteristic	**HR**	**95% CI**	***P*-value**	**Characteristic**	**HR**	**95% CI**	***P*-value**
Progression-free survival							
Gender	1.833	1.083–3.103	0.024	Gender	1.397	1.080–1.807	0.011
T stage	1.545	0.953–2.504	0.077	T stage	1.427	1.164–1.749	0.001
N stage				N stage			
N1 vs. N0	1.079	0.672–1.731	0.754	N1 vs. N0	1.486	1.182–1.867	0.001
N2 vs. N0	6.441	2.307–17.988	<0.001	N2 vs. N0	1.938	1.428–2.631	<0.001
EBV DNA level	3.603	1.806–7.189	<0.001	LDH level	1.437	1.066–1.936	0.017
				EBV DNA level	1.556	0.920–2.630	0.099
				Treatment method	0.709	0.585–0.858	<0.001
Overall survival							
Age	1.810	0.993–3.299	0.053	Age	1.351	1.048–1.741	0.020
Gender	5.075	1.557–16.537	0.007	Gender	1.774	1.222–2.577	0.003
Cardiovascular disease	2.787	1.22–6.365	0.015	T stage	1.511	1.156–1.975	0.003
T stage	2.382	1.135–5.001	0.022	N stage			
N stage				N1 vs. N0	1.657	1.222–2.246	0.001
N1 vs. N0	1.652	0.785–3.476	0.186	N2 vs. N0	2.310	1.537–3.472	<0.001
N2 vs. N0	11.017	1.082–112.183	0.043	Treatment method	0.466	0.356–0.610	<0.001
EBV DNA level	9.119	2.154–38.612	0.003				
Locoregional relapse–free survival							
T stage	1.961	0.990–3.887	0.054	T stage	1.431	1.028–1.991	0.034
EBV DNA level	2.331	1.055–5.149	0.036				
Distant metastasis–free survival							
Gender	2.382	1.126–5.039	0.023	Gender	1.840	1.309–2.586	<0.001
N stage				Diabetes mellitus	1.791	1.063–3.015	0.028
N2 vs. N0-1	1.072	0.606–1.897	0.812	T stage	1.295	1.015–1.651	0.037
N3 vs. N0-1	7.237	1.888–27.739	0.004	N stage			
EBV-DNA level	4.371	1.769–10.801	0.001	N2 vs. N0-1	1.506	1.141–1.988	0.004
				N3 vs. N0-1	2.366	1.667–3.358	<0.001
				LDH level	1.425	1.001–2.028	0.050
				Treatment method	0.633	0.502–0.797	<0.001

HR, hazard ratio; CI, confidence interval; LDH, lactate dehydrogenase; EBV, Epstein–Barr virus; CCRT, concurrent chemoradiotherapy; IC, induction chemotherapy.
A Cox proportional hazards model was used to perform multivariate analyses. All variables were transformed into categorical variables. HRs were calculated for age (years) (>46 vs. ≤46), gender (male vs. female), diabetes mellitus (yes vs. no), cardiovascular disease (yes vs. no), T stage (T4 vs. T1-3), LDH level (>245 U/L vs. ≤245 U/L), EBV DNA level (>1,500 copies/ml vs. ≤1,500 copies/ml) and treatment method (CCRT + IC vs. CCRT).
We selected variables with a backward stepwise approach. The P-value threshold was 0.1 ($P > 0.1$) for removing non-significant variables from the model.

TABLE 6 | Acute toxicities in patients between CCRT and CCRT + IC groups.

Adverse event (Toxicity grade)	**CCRT (*n* = 2,077)**		**CCRT + IC (*n* = 1,509)**		***P*-value**
	0–2 (%)	**3–4 (%)**	**0–2 (%)**	**3–4 (%)**	
Leukocytopenia	1,738 (83.7)	339 (16.3)	1,056 (70.0)	453 (30.0)	<0.001
Neutropenia	1,761 (84.8)	316 (15.2)	939 (62.2)	570 (37.8)	<0.001
Anemia	2,033 (97.9)	44 (2.1)	1,481 (98.2)	28 (1.8)	0.631
Thrombocytopenia	2,052 (98.8)	25 (1.2)	1,484 (98.3)	25 (1.7)	0.313
Hepatoxicity	2,054 (98.9)	23 (1.1)	1,482 (98.2)	27 (1.8)	0.112
Nephrotoxicity	2,077 (100.0)	0 (0.0)	1,507 (99.9)	2 (0.1)	0.177[a]

CCRT, concurrent chemoradiotherapy; IC, induction chemotherapy.
[a]P-value was calculated with the Pearson χ^2-test or Fisher's exact test.

Z-JL: quality control of data and algorithms, statistical analysis, and manuscript preparation and editing.

FUNDING

This work was supported by grants from the following organizations and institutions: National Key R&D Program of China (2017YFC1309003 and 2017YFC0908500), National Natural Science Foundation of China (Nos. 81425018, 81672868, and 81602371), Sun Yat-sen University Clinical Research 5010 Program (201707020039, 2014A020212103, and 16zxyc02), Sci-Tech Project Foundation of Guangzhou City (201707020039), National Key Basic Research Program of China (No. 2013CB910304), Special Support Plan of Guangdong Province (No. 2014TX01R145), Sci-Tech Project Foundation of Guangdong Province (No. 2014A020212103), Health & Medical Collaborative Innovation Project of Guangzhou City (No. 201400000001), National Science & Technology Pillar Program during the Twelfth 5-Year Plan Period (No. 2014BAI09B10), Ph.D. Start-up Fund of the Natural Science Foundation of Guangdong Province (2016A030310221), cultivation foundation for the junior teachers in Sun Yat-sen University (16ykpy28), foundation for major projects and new cross subjects in Sun Yat-sen University (16ykjc38), Central Universities Fundamental Research Funds the Natural Science Foundation of Guangdong Province for Distinguished Young Scholar (No. 2018B030306001), and Pearl River S&T Nova Program of Guangzhou (No. 201806010135).

SUPPLEMENTARY MATERIAL

The Supplementary Material for this article can be found online at: https://www.frontiersin.org/articles/10.3389/fonc.2020.00255/full#supplementary-material

REFERENCES

1. Torre L, Bray F, Siegel R, Ferlay J, Lortet-Tieulent J, Jemal A. Global cancer statistics, 2012. *CA Cancer J Clin.* (2015) 65:87–108. doi: 10.3322/caac.21262
2. Wei KR, Zheng RS, Zhang SW, Liang ZH, Li ZM, Chen WQ. Nasopharyngeal carcinoma incidence and mortality in China 2013. *Chin J Cancer.* (2017) 36:90. doi: 10.1186/s40880-017-0257-9
3. Lin JC, Jan JS, Hsu CY, Liang WM, Jiang RS, Wang WY. Phase III study of concurrent chemoradiotherapy versus radiotherapy alone for advanced nasopharyngeal carcinoma: positive effect on overall and progression-free survival. *J Clin Oncol.* (2003) 21:631–7. doi: 10.1200/JCO.2003.06.158
4. Chan A, Teo P, Ngan R, Leung T, Lau W, Zee B, et al. Concurrent chemotherapy-radiotherapy compared with radiotherapy alone in locoregionally advanced nasopharyngeal carcinoma: progression-free survival analysis of a phase III randomized trial. *J. Clin. Oncol.* (2002) 20:2038–44. doi: 10.1200/JCO.2002.08.149
5. Al-Sarraf M, LeBlanc M, Giri PG, Fu KK, Cooper J, Vuong T, et al. Chemoradiotherapy versus radiotherapy in patients with advanced nasopharyngeal cancer: phase III randomized Intergroup study 0099. *J Clin Oncol.* (1998) 16:1310–17. doi: 10.1200/JCO.1998.16.4.1310
6. Wu F, Wang R, Lu H, Wei B, Feng G, Li G, et al. Concurrent chemoradiotherapy in locoregionally advanced nasopharyngeal carcinoma: treatment outcomes of a prospective, multicentric clinical study. *Radiother Oncol.* (2014) 112:106–11. doi: 10.1016/j.radonc.2014.05.005
7. Sun Y, Li W, Chen N, Zhang N, Hu G, Xie F, et al. Induction chemotherapy plus concurrent chemoradiotherapy versus concurrent chemoradiotherapy alone in locoregionally advanced nasopharyngeal carcinoma: a phase 3, multicentre, randomised controlled trial. *Lancet Oncol.* (2016) 17:1509–20. doi: 10.1016/S1470-2045(16)30410-7
8. Chen YP, Tang LL, Yang Q, Poh SS, Hui EP, Chan ATC, et al. Induction chemotherapy plus concurrent chemoradiotherapy in endemic nasopharyngeal carcinoma: individual patient data pooled analysis of four randomized trials. *Clin Cancer Res.* (2018) 24:1824–33. doi: 10.1158/1078-0432.CCR-17-2656
9. Lan XW, Xiao Y, Zou XB, Zhang XM, OuYang PY, Xie FY. Outcomes of adding induction chemotherapy to concurrent chemoradiotherapy for stage T3N0-1 nasopharyngeal carcinoma: a propensity-matched study. *Onco Targets Ther.* (2017) 10:3853–60. doi: 10.2147/OTT.S133917
10. Wu LR, Yu HL, Jiang N, Jiang XS, Zong D, Wen J, et al. Prognostic value of chemotherapy in addition to concurrent chemoradiotherapy in T3-4N0-1 nasopharyngeal carcinoma: a propensity score matching study. *Oncotarget.* (2017) 8:76807–15. doi: 10.18632/oncotarget.20014
11. Tang LQ, Li CF, Li J, Chen WH, Chen QY, Yuan LX, et al. Establishment and validation of prognostic nomograms for endemic nasopharyngeal carcinoma. *J Natl Cancer Inst.* (2016) 108:djv291. doi: 10.1093/jnci/djv291
12. Peng XS, Xie GF, Qiu WZ, Tian YH, Zhang WJ, Cao KJ. Type 2 Diabetic mellitus is a risk factor for nasopharyngeal carcinoma: a 1:2 matched case-control study. *PLoS ONE.* (2016) 11:e0165131. doi: 10.1371/journal.pone.0165131
13. Lin JC, Wang WY, Chen KY, Wei YH, Liang WM, Jan JS, et al. Quantification of plasma Epstein-Barr virus DNA in patients with advanced nasopharyngeal carcinoma. *N Engl J Med.* (2004) 350:2461–70. doi: 10.1056/NEJMoa032260
14. Yu Z, Luo W, Zhou QC, Zhang QH, Kang DH, Liu MZ. Impact of changing gross tumor volume delineation of intensity-modulated radiotherapy on the dose distribution and clinical treatment outcome after induction chemotherapy for the primary locoregionally advanced nasopharyngeal carcinoma. *Ai zheng* (2009), 28:1132–37. doi: 10.5732/cjc.009.10435
15. Zhang M, Li J, Shen G, Zou X, Xu J, Jiang R, et al. Intensity-modulated radiotherapy prolongs the survival of patients with nasopharyngeal carcinoma compared with conventional two-dimensional radiotherapy: a 10-year experience with a large cohort and long follow-up. *Eur. J. Cancer.* (2015). 51:2587–95. doi: 10.1016/j.ejca.2015.08.006
16. Tang L, Chen Q, Fan W, Liu H, Zhang L, Guo L, et al. Prospective study of tailoring whole-body dual-modality [18F]fluorodeoxyglucose positron emission tomography/computed tomography with plasma Epstein-Barr virus DNA for detecting distant metastasis in endemic nasopharyngeal carcinoma at initial staging. *J. Clin. Oncol.* (2013) 31:2861–9. doi: 10.1200/JCO.2012.46.0816
17. Sun X, Su S, Chen C, Han F, Zhao C, Xiao W, et al. Long-term outcomes of intensity-modulated radiotherapy for 868 patients with nasopharyngeal carcinoma: an analysis of survival and treatment toxicities. *Radiother Oncol.* (2014) 110:398–403. doi: 10.1016/j.radonc.2013.10.020
18. Cao SM, Yang Q, Guo L, Mai HQ, Mo HY, Cao KJ, et al. Neoadjuvant chemotherapy followed by concurrent chemoradiotherapy versus concurrent chemoradiotherapy alone in locoregionally advanced nasopharyngeal carcinoma: a phase III multicentre randomised controlled trial. *Eur J Cancer.* (2017) 75:14–23. doi: 10.1016/j.ejca.2016.12.039
19. Zhang Y, Chen L, Hu GQ, Zhang N, Zhu XD, Yang KY, et al. Gemcitabine and cisplatin induction chemotherapy in nasopharyngeal carcinoma. *N Engl J Med.* (2019) 381:1124–35. doi: 10.1056/NEJMoa1905287
20. Du XJ, Tang LL, Chen L, Mao YP, Guo R, Liu X, et al. Neoadjuvant chemotherapy in locally advanced nasopharyngeal carcinoma: defining high-risk patients who may benefit before concurrent chemotherapy combined with intensity-modulated radiotherapy. *Sci Rep.* (2015) 5:16664. doi: 10.1038/srep16664

21. OuYang PY, Zhang LN, Xiao Y, Lan XW, Zhang XM, Ma J, et al. Validation of published nomograms and accordingly individualized induction chemotherapy in nasopharyngeal carcinoma. *Oral Oncol.* (2017) 67:37–45. doi: 10.1016/j.oraloncology.2017.01.009
22. Zhang Y, Li WF, Mao YP, Zhou GQ, Peng H, Sun Y, et al. Establishment of an integrated model incorporating standardised uptake value and N-classification for predicting metastasis in nasopharyngeal carcinoma. *Oncotarget.* (2016) 7:13612–20. doi: 10.18632/oncotarget.7253
23. Masmoudi A, Toumi N, Khanfir A, Kallel-Slimi L, Daoud J, Karray H, et al. Epstein-Barr virus-targeted immunotherapy for nasopharyngeal carcinoma. *Cancer Treat Rev.* (2007) 33:499–505. doi: 10.1016/j.ctrv.2007.04.007
24. Gottschalk S, Heslop HE, Rooney CM. Adoptive immunotherapy for EBV-associated malignancies. *Leuk Lymphoma.* (2005) 46:1–10. doi: 10.1080/10428190400002202
25. Li J, Chen Q, He J, Li Z, Tang X, Chen S, et al. Phase I trial of adoptively transferred tumor-infiltrating lymphocyte immunotherapy following concurrent chemoradiotherapy in patients with locoregionally advanced nasopharyngeal carcinoma. *Oncoimmunology.* (2015) 4:e976507. doi: 10.4161/23723556.2014.976507

Conflict of Interest: The authors declare that the research was conducted in the absence of any commercial or financial relationships that could be construed as a potential conflict of interest.

The handling Editor declared a shared affiliation, though no other collaboration, with the authors.

frontiers in Oncology

ORIGINAL RESEARCH
published: 31 March 2020
doi: 10.3389/fonc.2020.00356

Clinical Implications of Plasma Epstein–Barr Virus DNA in Children and Adolescent Nasopharyngeal Carcinoma Patients Receiving Intensity-Modulated Radiotherapy

Wenze Qiu[1,2], *Xing Lv*[2], *Xiang Guo*[2] *and Yawei Yuan*[1*]

[1] *Department of Radiation Oncology, Affiliated Cancer Hospital & Institute of Guangzhou Medical University, Guangzhou, China,* [2] *State Key Laboratory of Oncology in South China, Collaborative Innovation Center of Cancer Medicine, Sun Yat-sen University Cancer Center, Guangzhou, China*

Background: Plasma Epstein–Barr virus (EBV) DNA has been determined as a prognostic factor in adult nasopharyngeal carcinoma (NPC) patients. This study was designed to evaluate the prognostic value of plasma pretreatment EBV DNA in children and adolescent NPC patients receiving intensity-modulated radiotherapy (IMRT).

Methods: Pretreatment EBV DNA was retrospectively assessed in 147 children with newly diagnosed, non-metastatic NPC. All patients were treated using IMRT. Receiver operating characteristic (ROC) curve was used to identify the optimal EBV DNA cutoff point. Prognostic value was examined using a multivariate Cox proportional hazards model.

Results: The median follow-up for the entire cohort was 58 months (range, 10–119 months), and the 5-year survival rates for all patients were as follows: overall survival (OS), 88.7%; locoregional relapse-free survival, 95.2%; distant metastasis-free survival (DMFS), 84.8%; and disease-free survival (DFS), 81.5%. For ROC curve analysis, the optimal cutoff value of pretreatment EBV DNA load for DFS was 40,000 copies/mL. High plasma EBV DNA was significantly associated with poorer 5-year DMFS (70.6 vs. 89.1%, $P = 0.003$) and DFS (63.9 vs. 86.9%, $P < 0.001$). In multivariate analysis, high plasma EBV DNA was an independent predictor for DMFS and DFS.

Conclusions: Pretreatment EBV DNA level was a powerful prognostic discriminator for DMFS and DFS in children and adolescent NPC patients treated with IMRT.

Keywords: nasopharyngeal carcinoma, children and adolescent, Epstein–Barr virus, intensity-modulated radiotherapy, clinical implications

OPEN ACCESS

Edited by:
Jan Baptist Vermorken, University of Antwerp, Belgium

Reviewed by:
Thorsten Fuereder, Medical University of Vienna, Austria
Hong-Quan Duong, Hanoi University of Public Health, Vietnam

***Correspondence:**
Yawei Yuan
yuanyawei@gzhmu.edu.cn

Specialty section:
This article was submitted to Head and Neck Cancer, a section of the journal Frontiers in Oncology

Received: *15 November 2019*
Accepted: *28 February 2020*
Published: *31 March 2020*

Citation:
Qiu W, Lv X, Guo X and Yuan Y (2020) Clinical Implications of Plasma Epstein–Barr Virus DNA in Children and Adolescent Nasopharyngeal Carcinoma Patients Receiving Intensity-Modulated Radiotherapy. Front. Oncol. 10:356. doi: 10.3389/fonc.2020.00356

INTRODUCTION

Children and adolescent nasopharyngeal carcinoma (NPC) is rare, accounting for ∼1% of all cases of NPC in the endemic areas of southern China (1). Although the incidence varies extensively with racial and geographical factors, it constitutes 1–5% of all malignant tumors and 20–50% of all primary nasopharyngeal malignant tumors in this age group (2–4). Children and adolescent NPC is

distinguishable from the adult form of the disease because of its undifferentiated histology and the high incidence of advanced stage disease and its close association with Epstein–Barr virus (EBV) infection (1).

Because of the rarity of NPC in children, its epithelial cell origin, and occurrence in older children and adolescents, the treatment recommendations for childhood NPC typically follow guidelines established for adults. Radiotherapy (RT) is the primary treatment modality, and concurrent chemoradiotherapy with or without neoadjuvant/adjuvant chemotherapy is regarded as the standard of care for patients with locoregionally advanced NPC. In recent years, intensity-modulated radiation therapy (IMRT), which is associated with superior disease control and a lower treatment toxicity profile, has gradually replaced two-dimensional conventional radiotherapy as the mainstay RT technique for children and adolescent NPC patients (5).

Several clinical features, including age, gender, stage, RT technique, RT dose, and response to chemotherapy can predict the prognosis in children with NPC (5–10). However, the variable outcomes of patients within heterogeneous subgroups suggest that clinical features alone cannot precisely predict the treatment outcome. This prompted us to determine and evaluate prognostic factors tailored to children and adolescent patients.

Plasma EBV DNA is one of the most well-recognized biomarkers for NPC (11, 12). An expanding body of data has suggested that the EBV DNA load correlates with clinical stage and can be used for monitoring and prediction of the survival of NPC patients (13, 14). To the best of our knowledge, studies that explore whether treatment outcomes can be predicted by pretreatment levels of plasma EBV DNA in young NPC patients are rare. Although one retrospective study (15) has reported that plasma EBV DNA predicts worse outcomes in pediatric non-metastatic NPC patients, the findings were based on a relatively small sample size without using uniform IMRT technique.

Therefore, this retrospective study was conducted to confirm whether pretreatment plasma EBV DNA levels are able to accurately predict the prognosis of a large population of NPC patients in childhood and adolescence undergoing modern RT treatment.

MATERIALS AND METHODS

Patient and Staging Evaluation

A total of 147 children with NPC were treated by IMRT at the Sun Yat-sen University Cancer Center from June 2008 to December 2015. Patients were 7 to 20 years of age and histologically diagnosed with untreated non-metastatic NPC. All patients underwent a pretreatment evaluation including a complete physical examination, magnetic resonance imaging (MRI)/computed tomography (CT) of the nasopharynx and neck, chest radiography, abdominal ultrasonography, and single-photon emission computed tomography whole-body bone scan. Positron emission tomography was optional and was performed when clinically indicated. Patients were restaged by two radiation oncologists specializing in head and neck cancer according to the eighth edition of the American Joint Committee for Cancer Staging system (16), with disagreements resolved by consensus. This retrospective study was conducted in compliance with the institutional policy to protect the patients' private information and was approved by the institutional ethical committee. Informed consent was obtained from the subject and/or guardian.

TABLE 1 | Clinical characteristics of 147 patients with children and adolescent nasopharyngeal carcinoma.

Characteristics	No. of patients	%
Age, years		
≤17	79	53.7
>17	68	46.3
Gender		
Male	110	74.8
Female	37	25.2
Pathologic type		
WHO II	3	2.0
WHO III	144	98.0
Pretreatment BMI, kg/m^2		
<23	128	87.1
≥23	19	12.9
T Stage		
T1	4	2.7
T2	10	6.8
T3	61	41.5
T4	72	49.0
N Stage		
N0	4	2.7
N1	38	25.9
N2	77	52.4
N3	28	19.0
Overall stage		
I	1	0.7
II	5	3.4
III	55	37.4
IV	86	58.5
Combination with Chemotherapy		
No	3	2.0
NAC	20	13.6
CCT	34	23.1
NAC + CCT	90	61.2
Total dose of cisplatin, mg/m^2 [median (range)]	320 (0–480)	
Pretreatment plasma EBV Dna		
0	26	17.7
<10^3	14	9.5
<10^4	37	25.2
<10^5	50	34.0
<10^6	19	12.9
<10^7	1	0.7
Median level, copies/mL (interquartile range)	7,360 (660–39,200)	

BMI, body mass index; NAC, neoadjuvant chemotherapy; CCT, concurrent chemotherapy.

Quantification of Plasma EBV DNA

Before the start of treatment, peripheral venous blood (3 mL) was collected from each patient into EDTA-containing tubes and centrifuged at 3,000 g for 5 min. Total plasma DNA was extracted using a QIAamp DNA Blood Mini Kit (Qiagen, Hilden, Germany). Fluorescence polymerase chain reaction (PCR) was carried out using an EBV PCR quantitative diagnostic kit (Da-An Genetic Diagnostic Center, Guangzhou, China) targeting the BamHI-W region of the EBV genome. Data were analyzed using Applied Biosystems 7300 SDS software (Beijing, China).

Radiotherapy

All patients received IMRT as a primary treatment. The techniques of planning and delivery of IMRT were described previously (17, 18). Gross tumor volume (GTV) included the primary tumor and the enlarged lymph nodes. GTVnx included the sum of the primary tumor volume and the enlarged retropharyngeal nodes, whereas GTVnd was the volume of clinically involved gross cervical lymph nodes. High-risk clinical target volume (CTV1) was defined as the nasopharynx GTV plus a 5–10-mm margin (2–3 mm posteriorly if adjacent to the brainstem or spinal cord) to encompass the high-risk sites of the microscopic extension and the whole nasopharynx. Low-risk clinical target volume (CTV2) was defined as the high-risk clinical target volume plus a 5- to 10-mm margin (2–3 mm posteriorly if adjacent to the brainstem or spinal cord) to encompass the low-risk sites of the microscopic extension, including the skull base, clivus, sphenoid sinus, parapharyngeal space, pterygoid fossae, posterior parts of the nasal cavity, pterygopalatine fossae, retropharyngeal nodal regions, and the elective neck area from level IB to level V. A planning target volume (PTV) was created by adding a three-dimensional margin of 3–5 mm to the delineated target volume to compensate for the uncertainties in treatment setup and internal organ motion. The prescribed doses were 66–70, 64–70, 60–62, and 54–56 Gy, in 30–33 fractions, for the PTVs derived from GTVnx, GTVnd, CTV1, and CTV2, respectively. The dose constraints for organs at risk and planning organ at risk volumes were as described for the RTOG-0225 trial (19). All patients were treated following a routine schedule (one fraction daily, 5 days per week).

Chemotherapy

Chemotherapy regimens and administering schedules had some heterogeneity. Whereas, three patients (2.0%) were treated by RT alone, 20 patients (13.6%) received neoadjuvant chemotherapy before RT, 34 patients (23.1%) received concurrent chemotherapy, and 90 patients (61.2%) received neoadjuvant and concurrent chemotherapy.

Neoadjuvant chemotherapy included the following regimens: PF [consisting of cisplatin (1 day of 80–100 mg/m^2) and 5-fluorouracil (800–1,000 mg/m^2, by 120-h continuous intravenous infusion)], TP [consisting of docetaxel (1 day of 75 mg/m^2) or paclitaxel (1 day of 150–180 mg/m^2) and cisplatin (1 day of 75 mg/m^2)], and TPF [consisting of docetaxel (1 day of 60 mg/m^2) or paclitaxel (1 day of 135 mg/m^2), cisplatin (1 day of 60 mg/m^2), and 5-fluorouracil (500–800 mg/m^2, by 120-h continuous intravenous infusion)]. All regimens were administered at intervals of 3 weeks for two to four cycles. Concurrent chemotherapy consisted of cisplatin (80–100 mg/m^2) given in weeks 1, 4, and 7 of RT, or cisplatin (30–40 mg/m^2) given weekly during RT, beginning on the first day of RT.

Evaluation Criteria and Follow-Up

The treatment outcome was evaluated according to the Response Evaluation Criteria in Solid Tumors (version 1.1). All patients were evaluated weekly during radiation therapy, with a required follow-up after they completed RT: every 3 months in the first 2 years, every 6 months from the third to fifth years, and annually thereafter. The following examinations should be included in the follow-up: physical examination, routine blood test, biochemistry, plasma EBV DNA test, nasopharyngoscopy, chest X-ray or CT scan, abdominal ultrasonography, and nasopharynx + neck MRI scan with contrast.

Statistical Analysis

The following endpoints were assessed: locoregional relapse-free survival (LRRFS), distant metastasis-free survival (DMFS), disease-free survival (DFS), and overall survival (OS), and DFS was set as the primary endpoint. Locoregional relapse-free survival was measured from the end of RT to the date of the first observation of local or regional recurrence. Distant metastasis-free survival was measured from the end of RT to the date of the first observation of distant metastasis. Disease-free survival was measured from the end of RT to the date of

TABLE 2 | Associations between pretreatment EBV DNA and TNM staging.

Characteristics	No. of patients	%	Median (copies/mL)	Interquartile range (copies/mL)	*P*
T stage					0.743
T1–T3	75	51.0	5,790	110–41,800	
T4	72	49.0	9,890	900–35,350	
N stage					0.216
N0–1	42	28.6	4,325	60–40,825	
N2–3	105	71.4	10,500	1,915–39,500	
Overall stage					0.101
I–III	61	41.5	4,790	90–27,400	
IV	86	58.5	15,200	1,500–40,375	

the first observation of local or regional recurrence or distant metastasis. Overall survival was measured from the end of RT to the time of death or the time of last follow-up. We used χ^2 test for categorical variables and Mann-Whitney *U* tests for continuous variables to assess the differences between groups. Receiver operating characteristic (ROC) curve was obtained by plotting sensitivity against 1–specificity to evaluate performance of EBV DNA for predicting DFS. The optimal cutoff point of EBV DNA was identified based on Youden index, which was at the maximum sum of the sensitivity and specificity−1. The area under the curve (AUC) was used to assess the prognostic value of EBV DNA. An AUC of 0.5 represents a test with no discriminating ability (i.e., no better than chance), whereas an AUC of 1.0 represents a test with perfect discrimination (20–24). The Kaplan–Meier method was used to calculate actuarial survival rates and to draw survival curves, and the differences were compared using the log-rank test. Multivariate analysis was performed using the Cox proportional hazards model to define the independent risk factors for survival rates. The Statistical Package for the Social Sciences software package (SPSS 25.0, SPSS, Inc., Chicago, IL) was used, and a two-tailed $P < 0.05$ was considered to be statistically significant.

RESULTS

Patient Characteristics

Table 1 shows the demographic information of all the patients included in the study. The median age at diagnosis was 17 years (range, 7–20 years) with a male-to-female ratio of 2.97:1. Based on the World Health Organization (WHO) criteria, 98.0% of patients had type III disease, and 2.0% had type II disease. By TNM stage, 55 (37.4%) patients were at stage III, and 86 (58.5%) at stage IV. Chemotherapy was administered to 144 patients, whereas the other three were given RT alone. The median cumulative cisplatin dose during the entire treatment was 320 mg/m^2 (range, 0–480 mg/m^2).

The median concentration of plasma EBV DNA in our study was 7,360 copies/mL (interquartile range, 660–39,200 copies/mL). The median pretreatment plasma EBV DNA levels were described as stratified by different classifications. Advanced T stage, N stage, and clinical stage had higher median pretreatment plasma EBV DNA levels; however, the differences did not reach statistical significance (all $P > 0.05$; **Table 2**).

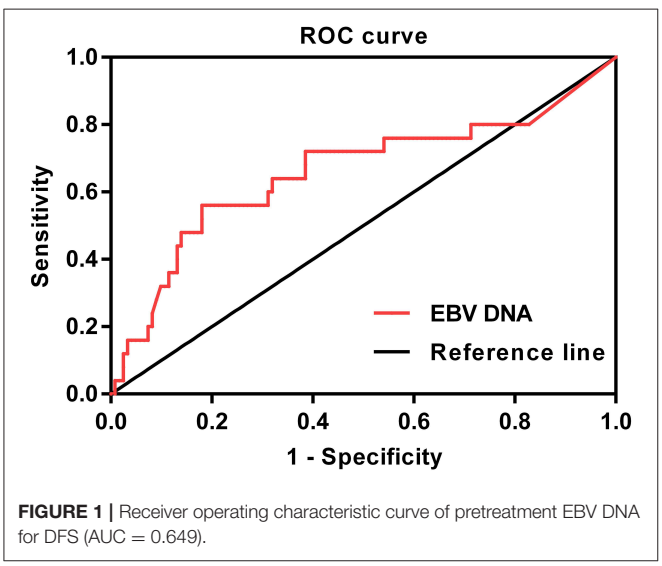

FIGURE 1 | Receiver operating characteristic curve of pretreatment EBV DNA for DFS (AUC = 0.649).

TABLE 3 | Baseline characteristics of the patients with children and adolescent NPC stratified by low vs. high pretreatment EBV DNA.

Characteristics	EBV DNA ≤40,000 (%, *n* = 113)	EBV DNA >40,000 (%, *n* = 34)	*P*
Age, years			0.915
≤17	61 (54.0)	18 (52.9)	
>17	52 (46.0)	16 (47.1)	
Gender			0.109
Male	81 (71.7)	29 (85.3)	
Female	32 (28.3)	5 (14.7)	
Pathologic type			1.000#
WHO II	3 (2.7)	0 (0)	
WHO III	110 (97.3)	34 (100.0)	
Pretreatment BMI, kg/m^2			1.000*
<23	98 (86.7)	30 (88.2)	
≥23	15 (13.3)	4 (11.8)	
T stage			0.603
T1	3 (2.7)	1 (2.9)	
T2	8 (7.1)	2 (5.9)	
T3	45 (39.8)	16 (47.1)	
T4	57 (50.4)	15 (44.1)	
N stage			0.564
N0	3 (2.7)	1 (2.9)	
N1	29 (25.7)	9 (26.5)	
N2	62 (54.9)	15 (44.1)	
N3	19 (16.8)	9 (26.5)	
Overall stage			0.748
I	1 (0.9)	0 (0)	
II	3 (2.7)	2 (5.9)	
III	44 (38.9)	11 (32.4)	
IV	65 (57.5)	21 (61.8)	
Combination with chemotherapy			0.092
No	2 (1.8)	1 (2.9)	
NAC	18 (15.9)	2 (5.9)	
CCT	28 (24.8)	6 (17.6)	
NAC + CCT	65 (57.5)	25 (73.5)	
Total dose of cisplatin, mg/m^2 (mean ± SD)	275.8 ± 95.3	291.8 ± 105.3	0.403

#*Fisher exact test.*
**Correction for continuity.*
BMI, body mass index; NAC, neoadjuvant chemotherapy; CCT, concurrent chemotherapy; SD, standard deviation.

Correlations Between Patient Characteristics and Pretreatment Plasma EBV DNA Levels

In this study, ROC curve was used to evaluate different cutoff points for pretreatment plasma EBV DNA levels (**Figure 1**). The AUC of pretreatment EBV DNA for DFS was 0.649, with a sensitivity of 54.2% and a specificity of 81.3% using the cutoff value of 39,500. At this point, the Youden index (sensitivity + specificity−1) was considered to be maximal. In order to facilitate and promote the clinical application of this biomarker, 40,000 copies/mL was taken as the optimum cutoff value to classify the patients into low and high pretreatment EBV DNA groups for further statistical analysis.

The correlations between pretreatment plasma EBV DNA levels and various clinicopathological features were examined. There was no significant difference in age, gender, histology, body mass index (BMI), stage, chemotherapy, or total dose of cisplatin between patients with low and high plasma EBV DNA levels (all $P > 0.05$; **Table 3**).

Survival Outcome

The median follow-up for the entire cohort was 58 months (range, 10–119 months), and the median failure times were 16 months (12–37 months) and 7 months (3–52 months) for local-regional recurrence and distant metastasis, respectively. The 5-year survival rates for all patients were as follows: OS, 88.7%; LRRFS, 95.2%; DMFS, 84.8%; and DFS, 81.5%. For patients receiving chemotherapy, the 5-year OS, LRRFS, DMFS, and DFS were 88.5, 95.1, 85.2, and 81.9%, respectively.

Univariate and Multivariate Analyses

Univariate analyses were performed using age, gender, BMI, T stage, N stage, chemotherapy, total dose of cisplatin and plasma EBV DNA levels as possible variables. As seen in **Table 4**, high plasma EBV DNA was significantly associated with poorer 5-year DMFS and DFS. The 5-year OS, LRRFS, DMFS, and DFS rates for high vs. low plasma EBV DNA group were 81.2 vs. 91.5% ($P = 0.193$), 89.4 vs. 96.8% ($P = 0.099$), 70.6 vs. 89.1% ($P = 0.003$), and 63.9 vs. 86.9% ($P < 0.001$), respectively (**Table 4** and **Figure 2**). In addition, patients with advanced T stage had poorer 5-year OS, DMFS, and DFS. The Cox regression method was used, and the above factors were taken as covariates for analysis. The results revealed that high plasma EBV DNA was an independent predictor for DMFS and DFS, and T stage was significantly associated with OS, DMFS, and DFS (**Table 5**). Variables, including age, gender, BMI, T stage, N stage, total dose of cisplatin, and plasma EBV DNA levels, were also taken

TABLE 4 | Univariate analysis of prognostic factors for 147 patients.

Variate	5-Year survival rate (%)							
	OS	*P*	LRRFS	*P*	DMFS	*P*	DFS	*P*
Age, years		0.927		0.809		0.878		0.823
≤17	88.5		96.8		84.6		81.9	
>17	88.7		94.3		84.9		80.9	
Gender		0.816		0.657		0.443		0.786
Male	89.2		95.8		83.4		81.2	
Female	87.6		93.4		89.0		82.7	
Pretreatment BMI, kg/m^2		0.634		0.347		0.846		0.895
<23	88.3		94.5		85.0		81.3	
≥23	92.9		100		83.6		83.6	
T stage		0.008		0.317		0.002		<0.001
T1–T3	97.2		97.3		94.6		93.2	
T4	80.2		92.6		74.7		69.4	
N stage		0.629		0.829		0.585		0.540
N0–1	90.4		93.9		88.0		84.6	
N2–3	88.1		95.7		83.5		80.3	
Pretreatment EBV DNA, copies/mL		0.193		0.099		0.003		<0.001
≤40,000	91.5		96.8		89.1		86.9	
>40,000	81.2		89.4		70.6		63.9	
Combination with chemotherapy		0.632		0.751		0.252		0.318
No	100.0		100.0		66.7		66.7	
Yes	88.5		95.1		85.2		81.9	
Total dose of cisplatin, mg/m^2		0.601		0.874		0.640		0.980
<320	87.8		94.6		85.2		80.3	
≥320	89.6		95.6		84.2		82.5	

BMI, body mass index; OS, overall survival; LRRFS, locoregional relapse-free survival; DMFS, distant metastasis-free survival; DFS, disease-free survival.

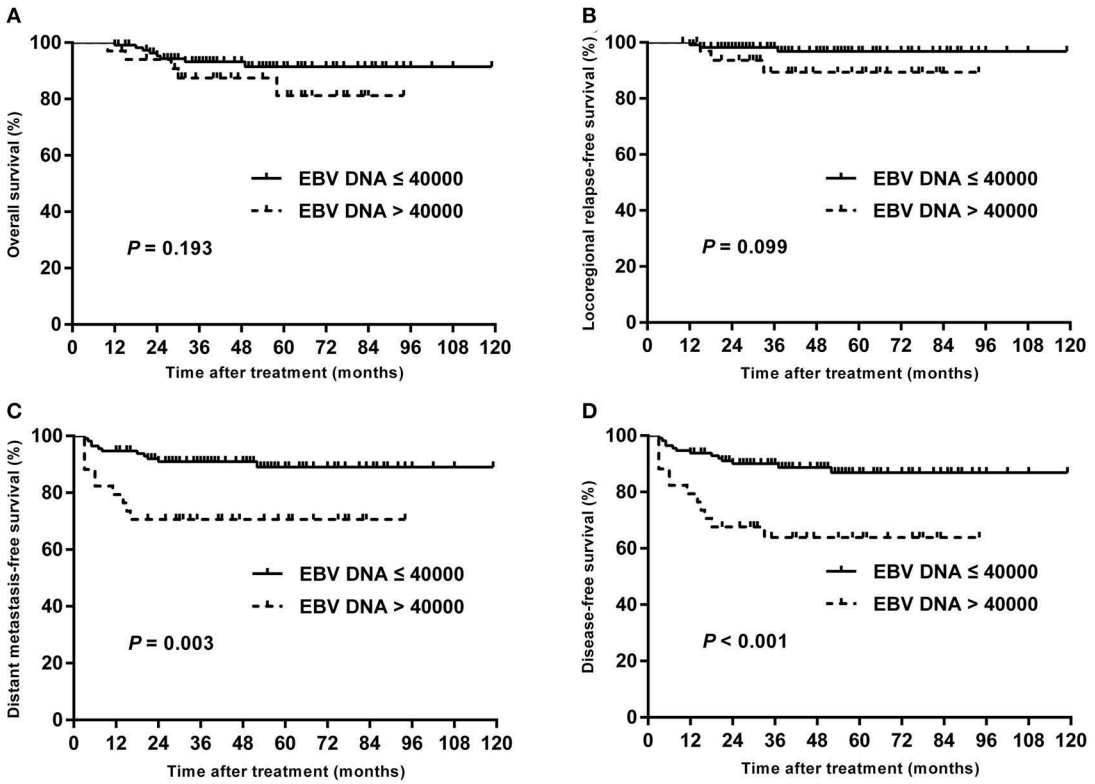

FIGURE 2 | Kaplan–Meier estimate of the OS **(A)**, LRRFS **(B)**, DMFS **(C)**, and DFS **(D)** of children and adolescent NPC patients according to pretreatment EBV DNA levels.

TABLE 5 | Multivariate analysis of prognostic factors for 147 patients.

Endpoint	Variate	HR	95% CI	*P*
OS	T stage: T4 vs. T1–T3	6.62	1.45–30.15	0.015
	Pretreatment EBV DNA: >40,000 vs. ≤40,000 copies/mL	2.56	0.82–7.98	0.106
LRRFS	T stage: T4 vs. T1–T3	2.67	0.47–15.21	0.301
	Pretreatment EBV DNA: >40,000 vs. ≤40,000 copies/mL	4.63	0.84–25.37	0.078
DMFS	T stage: T4 vs. T1–T3	5.46	1.82–16.37	0.002
	Pretreatment EBV DNA: >40,000 vs. ≤40,000 copies/mL	3.86	1.61–9.23	0.002
DFS	T stage: T4 vs. T1–T3	5.20	1.94–13.91	0.001
	Pretreatment EBV DNA: >40,000 vs. ≤40,000 copies/mL	4.25	1.91–9.46	<0.001

OS, overall survival; LRRFS, locoregional relapse-free survival; DMFS, distant metastasis-free survival; DFS, disease-free survival; HR, hazard ratio; CI, confidence interval.

for multivariate analysis in 144 patients receiving chemotherapy, and the results were similar to those in the entire cohort (**Supplemental Table 1**).

Subgroup Analysis Stratified by T Stage

In subgroup analysis of T1–T3 disease, the patients with high plasma EBV DNA levels presented with worse DMFS (84.2 vs. 98.1%; $P = 0.013$) and DFS (78.9 vs. 98.1%; $P = 0.003$), but with similar OS (94.7 vs. 98.0%; $P = 0.432$) and LRRFS (94.4 vs. 98.2%; $P = 0.423$; **Figure 3**). For patients with T4, statistical significance was also achieved for DMFS (53.3 vs. 80.4%; $P = 0.011$) and DFS (42.7 vs. 76.1%; $P = 0.007$), but not for OS (64.2 vs. 85.0%; $P = 0.178$) and LRRFS (80.8 vs. 95.2%; $P = 0.108$; **Figure 4**).

DISCUSSION

Plasma EBV DNA has been reported to have prognostic value in patients with non-metastatic NPC treated with conventional RT or IMRT (14, 25, 26). The present study, which involved a large cohort of NPC patients in childhood and adolescence treated with IMRT, is the first one to provide valuable data on treatment outcomes and the clinical value of EBV DNA levels. We have shown that IMRT resulted in a favorable prognosis

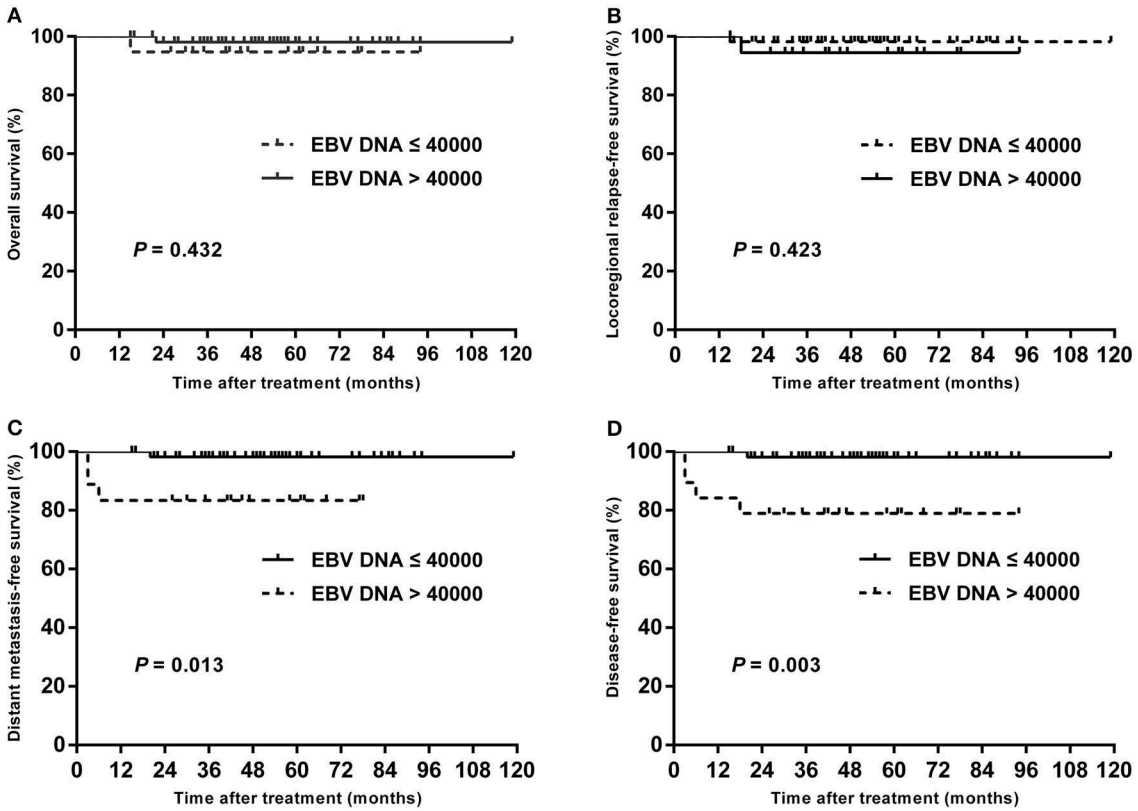

FIGURE 3 | Kaplan–Meier estimate of the OS **(A)**, LRRFS **(B)**, DMFS **(C)**, and DFS **(D)** of T1–T3 children and adolescent NPC patients according to pretreatment EBV DNA levels.

for children and adolescent NPC (5-year DFS, 81.5%), especially in patients with low pretreatment EBV DNA load (5-year DFS, 86.9%), which indicated that pretreatment EBV DNA level is an important prognostic factor in this age group.

In young patients, the predominant histology of NPC is an undifferentiated variant of disease (27–29), which was confirmed in our study where 98.0% of pediatric patients were histologically WHO type III. On the other hand, ∼96.0% of our patients presented in advanced clinical stage III or IV, similar to other reports with stage III–IV patients accounting for 92.0–97.3% (5, 7, 29).

A previous study by Chou et al. (30) showed that NPCs are correlated with EBV DNA infection as the virus infects the epithelial cells promoting the activation of proliferation signaling. Studies also have demonstrated that the circulating cell-free EBV DNA is mainly released from apoptotic and necrotic cancer cells. Consequently, circulating cell-free DNA could reflect the tumor load of NPC patients (31). According to previous studies, pretreatment EBV DNA levels have a strong relation with clinical stages of NPC (14, 25, 26). In our study, although the patient with advanced-stage NPC had higher levels of pretreatment EBV DNA, a positive correlation was not found between pretreatment EBV DNA concentrations and T stage, N stage, and TNM stage grouping (all $P > 0.05$). One reasonable explanation for this negative correlation is that children with NPC differ from their adult counterparts in having a closer association with EBV. Therefore, some children with early-stage NPC may also have high levels of pretreatment EBV DNA. Additionally, pretreatment plasma EBV DNA may not precisely predict the tumor burden for patients with children and adolescent NPC as the circulating cell-free plasma EBV DNA load only originates from apoptotic and necrotic tumor cells, rather than all circulating tumor cells (32). Furthermore, the small sample size of patients in each group could potentially affect the results.

Interestingly, the cutoff value for pretreatment EBV DNA in this study was 40,000 copies/mL, which was much higher than that in previous studies. For example, Chan et al. (33) chose the cutoff value for pretreatment EBV DNA on the basis of a measure of heterogeneity with the log-rank test statistic and reported that a cutoff value of 4,000 copies/mL was optimal for classifying patients into two groups and demonstrated a highly statistically significant difference in progression-free survival. In the study by Lin et al. (14), the median concentration of EBV DNA (1,500 copies/mL) was chosen as cutoff value, and they found that OS ($P < 0.001$) and relapse-free survival ($P = 0.02$) were significantly lower among patients with pretreatment plasma EBV DNA concentrations of at least 1,500 copies/mL than among those with concentrations of <1,500 copies/mL. However, study subjects in these reports were almost adult patients. Considering that

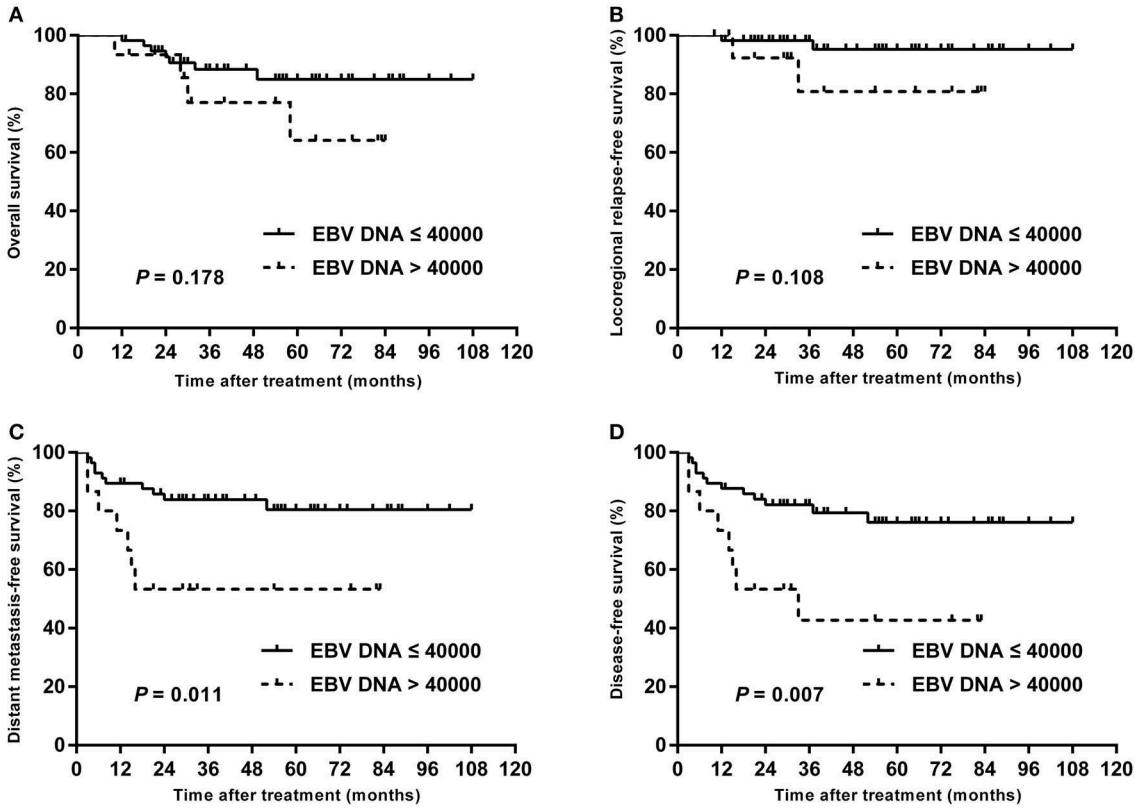

FIGURE 4 | Kaplan–Meier estimate of the OS **(A)**, LRRFS **(B)**, DMFS **(C)**, and DFS **(D)** of T4 children and adolescent NPC patients according to pretreatment EBV DNA levels.

the patients in the present study were specifically children and adolescents with locoregionally advanced disease and a higher pretreatment EBV DNA level, previous cutoff points might not be suitable for our study. Therefore, the metrics used to describe the prognostic quality of each potential cutoff point in our study were the AUC, the sensitivity, and the specificity, which were calculated using ROC analysis. The sensitivity and specificity were simultaneously maximized in order to determine the optimal pretreatment EBV DNA cutoff points. The cutoff value identified in ROC curve analysis was 40,000 copies/mL, and there was an extreme difference in the DFS of patients with low vs. high pretreatment EBV DNA. Furthermore, the optimal cutoff point of the pretreatment EBV DNA (40,000 copies/mL) was confirmed to be an independent prognostic factor for DMFS and DFS in both entire cohort and patients receiving chemotherapy by multivariate analysis. A previous study by Shen et al. (15) also used ROC curve to determine the optimal cutoff value for pretreatment EBV DNA load in childhood and adolescent patients; however, they found that a cutoff level of 7,500 copies/mL could predict outcomes with the best trade-off between sensitivity and specificity. This lower cutoff point may be due to the fact that the patients in their study were older (median age, 19 years; range, 6–21 years). In addition, owing to the relatively short follow-up time in their study, the calculation of ROC curve was based on 3-year survival outcome, which might have an influence on evaluating the cutoff value. Generally, we would like to suggest that the pretreatment EBV DNA cutoff point should be set to 40,000 copies/mL for children and adolescent NPC patients treated with IMRT.

A higher T stage has been reported as an unfavorable factor for survival (27, 34). In the present study, higher plasma EBV DNA and T4 category were independent predictors for DMFS and DFS. Furthermore, higher plasma EBV DNA remained an independent unfavorable prognostic factor in subgroup analysis stratified by T category.

In the current study, IMRT has provided excellent locoregional control in children and adolescent NPC patients with LRRFS of 95.2%. Nevertheless, the NPC failure pattern was not altered by IMRT, and distant metastasis remained the major pattern of failure, a result similar to the findings of other reports (5, 35, 36). We observed that a level of pretreatment EBV DNA >40,000 copies/mL was highly statistically significantly associated with the poorer DMFS and DFS. Such a subgroup of patients may benefit from systemic treatment before RT, which can eradicate micrometastases earlier. The Children's Oncology Group ARAR0331 study showed excellent event-free survival (EFS) and OS of induction chemotherapy plus concurrent chemoradiotherapy (CCRT) in childhood NPC patients (37). However, a large population, retrospective study by Liu et al. (38) showed that in adult NPC patients the addition of neoadjuvant

chemotherapy to CCRT could only reduce distant failure in patients with low risk of treatment failure (stage N0–1 disease and EBV DNA <4,000 copies/mL). In our study, 25 patients (73.5%) with high pretreatment EBV DNA received two to four cycles of induction cisplatin and 5-fluorouracil; or cisplatin and taxanes; or taxanes, cisplatin, and 5-fluorouracil, followed by cisplatin-based CCRT; however, the clinical outcome was far from satisfactory. On the other hand, previous studies by Ou et al. demonstrated that total dose of cisplatin more than 300 mg/m^2 in the whole course of treatment indicates a favorable prognosis of DFS, DMFS, and OS in locally advanced NPC treated with IMRT (39, 40). ARAR0331 study also observed a trend toward increased EFS for patients assigned to receive higher doses of cisplatin during CCRT (37). In the present study, however, patients with high EBV DNA levels received similar cumulative cisplatin dose to those with low EBV DNA levels ($P =$ 0.403). Therefore, future studies on the most effective regimens and ideal intensity of chemotherapy (e.g., cumulative cisplatin dose) in children and adolescent NPC patients with high EBV DNA levels are needed.

It should be noted that our study was subject to several limitations. First, the study is a retrospective series, which could have shortcomings such as selection bias. Second, because of the low incidence of childhood NPC, the number of patients who can be included is relatively limited, which might make the results of the study underpowered; thus, a larger sample size of patients is needed to confirm our findings. Third, the data were obtained exclusively at one center; therefore, these results must be validated by other datasets. The fourth concern was that we failed to include data regarding post-treatment EBV DNA; future studies need to continue to evaluate the prognostic value of post-treatment EBV DNA in children and adolescent NPC patients. Despite limitations above, this study still provides valuable reference for survival prediction of NPC patients in this age group.

CONCLUSIONS

In this study, we described the long-term outcomes for patients with children and adolescent NPC treated with definitive IMRT. Our results suggest that pretreatment EBV DNA >40,000 copies/mL is an independent adverse prognostic factor on DMFS and DFS for this group of patients.

DATA AVAILABILITY STATEMENT

The datasets generated for this study are available on request to the corresponding author.

ETHICS STATEMENT

The studies involving human participants were reviewed and approved by Human Ethics Approval Committee at Sun Yat-sen University Cancer Center. All subjects gave written informed consent in accordance with the Declaration of Helsinki.

AUTHOR CONTRIBUTIONS

WQ and YY conceived, designed and supervised the study. XL and XG collected and analyzed the data. WQ wrote the manuscript.

FUNDING

This study and work were supported by Guangzhou Key Medical Discipline Construction Project and Guangzhou High-level Clinical Key Training Specialty Construction Project.

ACKNOWLEDGMENTS

The chief acknowledgment is to the subjects who provided information for this study, and the research staff.

SUPPLEMENTARY MATERIAL

The Supplementary Material for this article can be found online at: https://www.frontiersin.org/articles/10.3389/fonc.2020.00356/full#supplementary-material

REFERENCES

1. Ayan I, Kaytan E, Ayan N. Childhood nasopharyngeal carcinoma: from biology to treatment. *Lancet Oncol.* (2003) 4:13–21. doi: 10.1016/S1470-2045(03)00956-2
2. Deutsch M, Mercado R Jr, Parsons JA. Cancer of the nasopharynx in children. *Cancer.* (1978) 41:1128–33. doi: 10.1002/1097-0142(197803)41:3<1128::AID-CNCR2820410348>3.0.CO;2-S
3. Ingersoll L, Woo SY, Donaldson S, Giesler J, Maor MH, Goffinet D, et al. Nasopharyngeal carcinoma in the young: a combined M.D. Anderson and stanford experience. *Int J Radiat Oncol Biol Phys.* (1990) 19:881–7. doi: 10.1016/0360-3016(90)90008-8
4. Pao WJ, Hustu HO, Douglass EC, Beckford NS, Kun LE. Pediatric nasopharyngeal carcinoma: long term follow-up of 29 patients. *Int J Radiat Oncol Biol Phys.* (1989) 17:299–305. doi: 10.1016/0360-3016(89)90443-4
5. Qiu WZ, Peng XS, Xia HQ, Huang PY, Guo X, Cao KJ. A retrospective study comparing the outcomes and toxicities of intensity-modulated radiotherapy versus two-dimensional conventional radiotherapy for the treatment of children and adolescent nasopharyngeal carcinoma. *J cancer Res Clin Oncol.* (2017) 143:1563–72. doi: 10.1007/s00432-017-2401-y
6. Gioacchini FM, Tulli M, Kaleci S, Magliulo G, Re M. Prognostic aspects in the treatment of juvenile nasopharyngeal carcinoma: a systematic review. *Eur Arch Otorhinolaryngol.* (2017) 274:1205–14. doi: 10.1007/s00405-016-4154-7
7. Ozyar E, Selek U, Laskar S, Uzel O, Anacak Y, Ben-Arush M, et al. Treatment results of 165 pediatric patients with non-metastatic nasopharyngeal carcinoma: a rare cancer network study. *Radiother Oncol.* (2006) 81:39–46. doi: 10.1016/j.radonc.2006.08.019
8. Hu S, Xu X, Xu J, Xu Q, Liu S. Prognostic factors and long-term outcomes of nasopharyngeal carcinoma in children and adolescents. *Pediatr Blood Cancer.* (2013) 60:1122–7. doi: 10.1002/pbc.24458

9. Afqir S, Ismaili N, Alaoui K, Ahid S, Lotz JP, Horn E, et al. Nasopharyngeal carcinoma in adolescents: a retrospective review of 42 patients. *Eur Arch Otorhinolaryngol*. (2009) 266:1767–73. doi: 10.1007/s00405-009-0911-1
10. Laskar S, Bahl G, Muckaden M, Pai SK, Gupta T, Banavali S, et al. Nasopharyngeal carcinoma in children: comparison of conventional and intensity-modulated radiotherapy. *Int J Radiat Oncol Biol Phys*. (2008) 72:728–36. doi: 10.1016/j.ijrobp.2008.01.032
11. Lo YM, Chan LY, Lo KW, Leung SF, Zhang J, Chan AT, et al. Quantitative analysis of cell-free Epstein-Barr virus DNA in plasma of patients with nasopharyngeal carcinoma. *Cancer Res*. (1999) 59:1188–91.
12. Leung SF, Zee B, Ma BB, Hui EP, Mo F, Lai M, et al. Plasma Epstein-Barr viral deoxyribonucleic acid quantitation complements tumor-node-metastasis staging prognostication in nasopharyngeal carcinoma. *J Clin Oncol*. (2006) 24:5414–8. doi: 10.1200/JCO.2006.07.7982
13. Chua MLK, Wee JTS, Hui EP, Chan ATC. Nasopharyngeal carcinoma. *Lancet*. (2016) 387:1012–24. doi: 10.1016/S0140-6736(15)00055-0
14. Lin JC, Wang WY, Chen KY, Wei YH, Liang WM, Jan JS, et al. Quantification of plasma Epstein-Barr virus DNA in patients with advanced nasopharyngeal carcinoma. *N Engl J Med*. (2004) 350:2461–70. doi: 10.1056/NEJMoa032260
15. Shen T, Tang LQ, Gu WG, Luo DH, Chen QY, Li PJ, et al. Plasma Epstein-Barr viral deoxyribonucleic acid predicts worse outcomes in pediatric nonmetastatic nasopharyngeal carcinoma patients: an observational study of 89 cases in an Endemic Area. *Medicine*. (2015) 94:e1945. doi: 10.1097/MD.0000000000001945
16. Amin MB, Greene FL, Edge SB, Compton CC, Gershenwald JE, Brookland RK, et al. *AJCC Cancer Staging Manual*. 8th ed. New York, NY: Springer International Publishing (2017).
17. Kam MK, Teo PM, Chau RM, Cheung KY, Choi PH, Kwan WH, et al. Treatment of nasopharyngeal carcinoma with intensity-modulated radiotherapy: the Hong Kong experience. *Int J Radiat Oncol Biol Phys*. (2004) 60:1440–50. doi: 10.1016/j.ijrobp.2004.05.022
18. Lai SZ, Li WF, Chen L, Luo W, Chen YY, Liu LZ, et al. How does intensity-modulated radiotherapy versus conventional two-dimensional radiotherapy influence the treatment results in nasopharyngeal carcinoma patients? *Int J Radiat Oncol Biol Phys*. (2011) 80:661–8. doi: 10.1016/j.ijrobp.2010.03.024
19. Lee N, Harris J, Garden AS, Straube W, Glisson B, Xia P, et al. Intensity-modulated radiation therapy with or without chemotherapy for nasopharyngeal carcinoma: radiation therapy oncology group phase II trial 0225. *J Clin Oncol*. (2009) 27:3684–90. doi: 10.1200/JCO.2008.19.9109
20. Hanley JA, McNeil BJ. The meaning and use of the area under a receiver operating characteristic (ROC) curve. *Radiology*. (1982) 143:29–36. doi: 10.1148/radiology.143.1.7063747
21. Zweig MH, Campbell G. Receiver-operating characteristic (ROC) plots: a fundamental evaluation tool in clinical medicine. *Clin Chem*. (1993) 39:561–77. doi: 10.1093/clinchem/39.4.561
22. Yin J, Samawi H, Linder D. Improved nonparametric estimation of the optimal diagnostic cut-off point associated with the Youden index under different sampling schemes. *Biom J*. (2016) 58:915–34. doi: 10.1002/bimj.201500036
23. Hoo ZH, Candlish J, Teare D. What is an ROC curve? *Emerg Med J*. (2017) 34:357–9. doi: 10.1136/emermed-2017-206735
24. Wu WM, Wang Y, Jiang HR, Yang C, Li XQ, Yan B, et al. Colorectal cancer screening modalities in Chinese population: practice and lessons in pudong new area of Shanghai, China. *Front Oncol*. (2019) 9:399. doi: 10.3389/fonc.2019.00399
25. Hou X, Zhao C, Guo Y, Han F, Lu LX, Wu SX, et al. Different clinical significance of pre- and post-treatment plasma Epstein-Barr virus DNA load in nasopharyngeal carcinoma treated with radiotherapy. *Clin Oncol*. (2011) 23:128–33. doi: 10.1016/j.clon.2010.09.001
26. Peng H, Guo R, Chen L, Zhang Y, Li WF, Mao YP, et al. Prognostic impact of plasma Epstein-Barr virus DNA in patients with nasopharyngeal carcinoma treated using intensity-modulated radiation therapy. *Sci Rep*. (2016) 6:22000. doi: 10.1038/srep22000
27. Sahai P, Mohanti BK, Sharma A, Thakar A, Bhasker S, Kakkar A, et al. Clinical outcome and morbidity in pediatric patients with nasopharyngeal cancer treated with chemoradiotherapy. *Pediatr Blood Cancer*. (2017) 64:259–66. doi: 10.1002/pbc.26240
28. Nikitovic M, Popovic-Vukovic M, Stanic D, Bokun J, Paripovic L, Ilic V, et al. Treatment outcome of childhood nasopharyngeal carcinoma: a single institution experience. *Int J Pediatr Otorhinolaryngol*. (2018) 113:168–72. doi: 10.1016/j.ijporl.2018.07.031
29. Liu W, Tang Y, Gao L, Huang X, Luo J, Zhang S, et al. Nasopharyngeal carcinoma in children and adolescents - a single institution experience of 158 patients. *Radiat Oncol*. (2014) 9:274. doi: 10.1186/s13014-014-0274-7
30. Chou J, Lin YC, Kim J, You L, Xu Z, He B, et al. Nasopharyngeal carcinoma–review of the molecular mechanisms of tumorigenesis. *Head Neck*. (2008) 30:946–63. doi: 10.1002/hed.20833
31. Fan H, Nicholls J, Chua D, Chan KH, Sham J, Lee S, et al. Laboratory markers of tumor burden in nasopharyngeal carcinoma: a comparison of viral load and serologic tests for Epstein-Barr virus. *Int J Cancer*. (2004) 112:1036–41. doi: 10.1002/ijc.20520
32. Lo YM, Leung SF, Chan LY, Lo KW, Zhang J, Chan AT, et al. Plasma cell-free Epstein-Barr virus DNA quantitation in patients with nasopharyngeal carcinoma. Correlation with clinical staging. *Ann N Y Acad Sci*. (2000) 906:99–101. doi: 10.1111/j.1749-6632.2000.tb06597.x
33. Chan AT, Lo YM, Zee B, Chan LY, Ma BB, Leung SF, et al. Plasma Epstein-Barr virus DNA and residual disease after radiotherapy for undifferentiated nasopharyngeal carcinoma. *J Natl Cancer Inst*. (2002) 94:1614–9. doi: 10.1093/jnci/94.21.1614
34. Zrafi WS, Tebra S, Tbessi S, Ouni S, Jebsi M, Bouaouina N. Undifferentiated carcinoma of nasopharyngeal type in children: clinical features and outcome. *Eur Ann Otorhinolaryngol Head Neck Dis*. (2017) 134:321–4. doi: 10.1016/j.anorl.2017.03.002
35. Tao CJ, Liu X, Tang LL, Mao YP, Chen L, Li WF, et al. Long-term outcome and late toxicities of simultaneous integrated boost-intensity modulated radiotherapy in pediatric and adolescent nasopharyngeal carcinoma. *Chin J Cancer*. (2013) 32:525–32. doi: 10.5732/cjc.013.10124
36. Guo Q, Cui X, Lin S, Lin J, Pan J. Locoregionally advanced nasopharyngeal carcinoma in childhood and adolescence: analysis of 95 patients treated with combined chemotherapy and intensity-modulated radiotherapy. *Head Neck*. (2016) 38(Suppl. 1):E665–72. doi: 10.1002/hed.24066
37. Rodriguez-Galindo C, Krailo MD, Krasin MJ, Huang L, McCarville MB, Hicks J, et al. Treatment of childhood nasopharyngeal carcinoma with induction chemotherapy and concurrent chemoradiotherapy: results of the children's oncology group ARAR0331 study. *J Clin Oncol*. (2019) 37:3369–76. doi: 10.1200/JCO.19.01276
38. Liu LT, Chen QY, Tang LQ, Guo SS, Guo L, Mo HY, et al. Neoadjuvant or adjuvant chemotherapy plus concurrent CRT versus concurrent CRT alone in the treatment of nasopharyngeal carcinoma: a study based on EBV DNA. *J Natl Compr Cancer Netw*. (2019) 17:703–10. doi: 10.6004/jnccn.2018.7270
39. Ou X, Zhou X, Shi Q, Xing X, Yang Y, Xu T, et al. Treatment outcomes and late toxicities of 869 patients with nasopharyngeal carcinoma treated with definitive intensity modulated radiation therapy: new insight into the value of total dose of cisplatin and radiation boost. *Oncotarget*. (2015) 6:38381–97. doi: 10.18632/oncotarget.5420
40. Ou X, Xu T, He X, Ying H, Hu C. Who benefited most from higher cumulative dose of cisplatin among patients with locally advanced nasopharyngeal carcinoma treated by intensity-modulated radiation therapy? A retrospective study of 527 cases. *J Cancer*. (2017) 8:2836–45. doi: 10.7150/jca.19725

Conflict of Interest: The authors declare that the research was conducted in the absence of any commercial or financial relationships that could be construed as a potential conflict of interest.

frontiers in Oncology

ORIGINAL RESEARCH
published: 17 April 2020
doi: 10.3389/fonc.2020.00437

Quality of Life Following Salvage Endoscopic Nasopharyngectomy in Patients With Recurrent Nasopharyngeal Carcinoma: A Prospective Study

*Wanpeng Li, Hanyu Lu, Juan Liu, Quan Liu, Huan Wang, Huankang Zhang, Xicai Sun, Li Hu, Weidong Zhao, Yurong Gu, Houyong Li and Dehui Wang**

Department of Otolaryngology-Head and Neck Surgery, Affiliated Eye Ear Nose and Throat Hospital, Fudan University, Shanghai, China

OPEN ACCESS

Edited by:
Yu-Pei Chen, Sun Yat-sen University Cancer Center (SYSUCC), China

Reviewed by:
Dong Dong, Zhengzhou University, China
Rongming Ge, Tongji Hospital, China
Jiang Yan, Affiliated Hospital of Qingdao University, China

***Correspondence:**
Dehui Wang
wangdehuient@sina.com

Specialty section:
This article was submitted to Head and Neck Cancer, a section of the journal Frontiers in Oncology

Received: *01 January 2020*
Accepted: *11 March 2020*
Published: *17 April 2020*

Citation:
Li W, Lu H, Liu J, Liu Q, Wang H, Zhang H, Sun X, Hu L, Zhao W, Gu Y, Li H and Wang D (2020) Quality of Life Following Salvage Endoscopic Nasopharyngectomy in Patients With Recurrent Nasopharyngeal Carcinoma: A Prospective Study. Front. Oncol. 10:437. doi: 10.3389/fonc.2020.00437

Background: This study aimed to assess the effect of endoscopic nasopharyngectomy in patients with recurrent nasopharyngeal carcinoma (NPC) on site-specific and sinonasal-related quality of life (QoL) before and after surgery using validated instruments.

Methods: Consecutive adult patients with recurrent NPC, who were treated via salvage endoscopic nasopharyngectomy, were prospectively enrolled at a single institution from January 2018 to December 2019. Each patient completed the Anterior Skull Base Questionnaire (ASBQ) and the 22-Item Sino-Nasal Outcome Test (SNOT-22) preoperatively, and then at regular intervals after surgery to assess their perceived QoL.

Results: Forty patients fulfilled the inclusion criteria. The median follow-up was 12 months (range, 2–24 months). Overall scores on the ASBQ and SNOT-22 at 3 or 12 weeks after surgery decreased significantly compared with before surgery ($p < 0.05$). At 6 months and 1 year postoperatively, there was no significant difference from the preoperative score. Subtotal resection was associated with worse overall ASBQ scores at 6 months and 1 year after endoscopic nasopharyngectomy ($p < 0.05$). Worse QoL was also associated with advanced T stage (rT3 and rT4) and pathological World Health Organization type III. Sex, age (<50 years), tumor necrosis, lymph node metastasis, and use of a nasoseptal flap approach did not impact postoperative QoL.

Conclusions: Site-specific and sinonasal-related QoL, measured using validated tools, demonstrated an overall maintenance of postoperative compared with preoperative QoL. Endoscopic endonasal resection is a valuable management choice in patients with recurrent NPC. In addition, subtotal resection was an important factor that negatively influenced postoperative QoL; as such, gross-total resection should be attempted in all patients to optimize QoL after surgery.

Keywords: nasopharyngeal carcinoma, recurrent, endoscopic, nasopharyngectomy, quality of life

INTRODUCTION

Nasopharyngeal carcinoma (NPC) has a high incidence in South China and Southeast Asia, with an obvious ethnic and geographical distribution (1). Radiotherapy is the first choice given the early susceptibility of NPC. However, ∼10% of patients experience local recurrence after radiotherapy. Re-irradiation for recurrent NPC may lead to poor curative effect, serious complications, and even death; therefore, surgical treatment of recurrent NPC has been advocated in many studies (2–4). Endoscopic nasopharyngectomy has been increasingly used due to advances in high-magnification technology, and the decreases in functional and cosmetic morbidities (5, 6). Evaluation of the curative effect of endoscopic nasopharyngectomy in the literature has mainly focused on resection, complications, survival rate, and other parameters. However, recent interest in outcome-based studies has led us to recognize the importance of patient perception of their health and the success of surgical interventions. Evaluation of these subjective parameters includes quality of life (QoL) measurements, questionnaires, and direct symptom scores (7).

QoL is a multidimensional metric, which describes an individual's overall perception of happiness. QoL instruments can be generalized, or site- or disease-specific. Data collected directly from patients are referred to as patient-reported outcome measures. Patient perception of QoL is an important indicator to measure the success of surgery, which can be used as an additional outcome measure. It is important to use effective instruments to assess the QoL of distinct sequelae associated with skull base disease and related approaches. In a prospective study involving 66 patients undergoing endoscopic skull base surgery, Edward et al. found that postoperative, site-specific QoL improved compared with the preoperative QoL (7). To our knowledge, no prospective studies have described changes in site-specific QoL in patients undergoing endoscopic nasopharyngectomy for recurrent NPC. Therefore, in this study, we measured postoperative QoL in a series of patients using acceptable site-specific QoL metrics and used their own preoperative QoL as an internal control. Two disease-specific instruments were used: the Anterior Skull Base Questionnaire (ASBQ) and the 22-Item Sinonasal Outcome Test (SNOT-22) (8, 9).

METHODS

Study Design and Data Sources

Consecutive adult patients with recurrent NPC who were treated via salvage endoscopic nasopharyngectomy were prospectively enrolled at the Department of Otorhinolaryngology of the Affiliated Eye Ear Nose and Throat Hospital (AEENTH) at Fudan University (Shanghai, China) from January 2018 to December 2019. All surgeries were performed by the senior author (DW). The Institutional Review Board of AEENTH at Fudan University approved this study. All patients who underwent endonasal endoscopic surgery for histologically confirmed NPC were identified. Patients selected for inclusion were adults >18 years of age who had completed preoperative assessment with the ASBQ and SNOT-22, and at ≥1 time point postoperatively. Those who required simultaneous neck dissection for metastatic lymph node disease, those who had undergone nasopharyngectomy for other types of malignancy, and those who were unable to complete the questionnaire because of illiteracy were excluded from this study.

The presence of recurrent NPC was detected by routine endoscopy or magnetic resonance imaging (MRI) of the nasopharynx, and confirmed by endoscopic biopsy. The choice of salvage treatment was determined according to tumor location, disease degree, the preferences of patients, and consultation with radiation oncologists and surgeons. All the patients with recurrent NPC were treated via salvage endoscopic nasopharyngectomy. If the tumor was confined to the posterior wall and midline of the nasopharynx, the resection range should reach the basisphenoid superiorly, prevertebral fascia posteriorly, and torus tubarius laterally. When the sphenoid sinus was involved by the tumor, bilateral sphenoidotomies should be performed to remove the floor of the sphenoid sinus, anterior wall, sphenoid rostrum, and intersphenoidal septum. The questionnaires were administered in person or by telephone interview. An independent doctor conducted all interviews to preclude any bias from doctor–patient interaction(s). Patient charts were reviewed for age, sex, tumor necrosis, T stage, lymph node metastasis, extent of resection, and pathological type.

In this study, two effective methods of QoL measurement were used, the ASBQ and SNOT-22. Both questionnaires were completed by each patient before the preoperative evaluation. Postoperative follow-up was performed at 3 weeks, 12 weeks, 6 months, and 1 year after endoscopic nasopharyngectomy, at which time each patient was again asked to complete the ASBQ and SNOT-22. Upon completion of the survey, endoscopic examination and intranasal debridement were performed during each visit. The main outcome measure of this study was postoperative changes in ASBQ scores, followed by postoperative changes in SNOT-22 scores.

Outcome Measures

The ASBQ consists of 35 items divided into six independent QoL areas: performance, physical function, vitality, pain, emotional impact, and specific symptoms. Responses are scored on a 5-item Likert scale, with each item scored from 1 to 5, and a total score ranging from 35 to 175. The total score is reported as an average item score of 1.0 to 5.0, with a lower score indicating worse QoL. The SNOT-22 questionnaire consists of 22 questions, with responses recorded on a 6-point Likert scale ranging from 0 to 5 points per item. Total scores range from 0 to 110, with a lower score indicating a better QoL.

Statistical Methods

Statistical analysis was performed using SPSS version 19.0 (IBM Corporation, Armonk, NY, USA). Each case served as its own historical control. The paired *t*-test was used to compare average preoperative and postoperative scores. The correlation between ASBQ and SNOT scores was analyzed by Pearson's correlation. Univariate analysis was performed using the unpaired *t* test. All *P* values were two-sided, and statistical significance was evaluated at the 0.05 alpha level.

TABLE 1 | Summary of tumor characteristics in 40 patients who underwent endoscopic nasopharyngectomy.

Characteristic	Total = 40	%
Sex		
Male	31	77.5
Female	9	22.5
Age		
<50	19	47.5
≥50	21	52.5
Tumor necrosis		
No	26	65.0
Yes	14	35.0
T stage		
T1	17	42.5
T2	5	12.5
T3	14	35
T4	4	10
Lymph node metastasis		
No	25	63.5
Yes	15	37.5
GTR		
No	10	25.0
Yes	30	75.0
Pathological type		
WHO type II	18	45.0
WHO type III	22	55.0
Nasoseptal flap		
NO	13	32.5
Yes	27	67.5

GTR, Gross-total resection; WHO, World Health Organization.

TABLE 2 | Overall postoperative ASBQ scores in patients who underwent endoscopic nasopharyngectomy.

Time since surgery	No. of patients	Mean ASBQ score (SD)		*P* value
		Preop	Postop	
3 weeks	32	3.38 (0.60)	2.49 (0.63)	<0.0001*
12 weeks	25	3.43 (0.64)	3.10 (0.68)	0.0444*
6 month	19	3.37 (0.64)	3.42 (0.72)	0.8062
1 year	20	3.22 (0.52)	3.49 (0.57)	0.1686

**p < 0.05, paired 2-tailed t-test. SD, standard deviation; ASBQ, Anterior Skull Base Questionnaire.*

RESULTS

Forty patients fulfilled inclusion criteria for inclusion in the study, 31 (77.5%) of whom were male and 9 (22.5%) were female, with a mean age of 50.7 years (range, 32–69 years). Tumor characteristics of the patients included in this study are summarized in **Table 1**. All the patients were previously treated with intensity modulated radiotherapy, and 26 patients received concurrently chemotherapy. The median time between initial radiotherapy and recurrence was 36 months (range 6–96 months). Tumor necrosis was observed in 14 (35.0%) patients. Tumors in this study were staged according to the rTNM staging system of the American Joint Committee on Cancer, as follows: rT1 ($n = 17$); rT2 ($n = 5$); rT3 ($n = 14$); and rT4 ($n = 4$). Fifteen (37.5%) patients experienced lymph node metastases. Gross-total resection (GTR) was performed in 30 of 40 operations (75.0%). The histological World Health Organization (WHO) lesion subtype in most patients was type III [$n = 22$ (55.0%)], followed by WHO type II [$n = 18$ (45.0%)]. Skull base defects repaired using a nasoseptal flap was presented in 27 cases (67.5%).

Overall ASBQ scores at 3 or 12 weeks after surgery decreased significantly compared with before surgery. At 6 months and 1 year postoperatively, there was no significant difference over the preoperative ASBQ score (**Table 2**). Independent examination of all subdomains of the ASBQ revealed significant decreases at 3 weeks after surgery, with further decreases in 3 of 6 subdomains (vitality, pain, emotional impact) at 12 weeks postoperatively. Finally, the subdomain of physical function demonstrated improvement at 1 year, while the other 5 subdomains at 6 months and 1 year did not differ significantly after endoscopic nasopharyngectomy (**Figure 1**).

SNOT-22 scores were higher (i.e., worse outcome) at 3 or 12 weeks after endoscopic nasopharyngectomy compared with preoperative scores. However, subsequent SNOT-22 scores at 6 months and 1 year postoperatively did not differ significantly from preoperative scores (**Table 3**). Overall, SNOT-22 and ASBQ scores demonstrated a significant inverse correlation preoperatively, and at 3 and 12 weeks postoperatively ($r = -0.613$, $r = -0.614$, $r = -0.744$, respectively) (**Table 4**). The direction of correlation reflected the inverse direction of scoring for the ASBQ and SNOT-22 questionnaires. Using ASBQ and SNOT-22, we identified four items from each instrument exhibiting the severe symptoms after 1-year follow-up of patients (**Table 5**). By ASBQ, sense of smell and nasal secretions were the most frequently reported item with high symptom burden (35% of patients reported scores of 1 or 2). Using the SNOT-22 instrument, sense of taste/smell demonstrated the highest symptom burden (40% of patients reported scores of 4 to 6).

Univariate analysis was performed for several variables at each postoperative time point (**Figure 2**). GTR was associated with better overall ASBQ scores and individual domain scores at 6 months and 1 year after endoscopic nasopharyngectomy ($p < 0.05$). rT3 and rT4 lesions adversely affected overall ASBQ scores at 1 year postoperatively. Pathological WHO type III lesions were associated with worse overall ASBQ scores at 6 months postoperatively. There were no significant differences in overall ASBQ scores in terms of sex, age (<50 years), tumor necrosis, lymph node metastasis, or nasoseptal flap approach. A limited number of patients were lost to follow-up, which included 8 patients after the 3-week postoperative visit, 8 patients after the 12-week visit, 7 patients after the 6-month visit, and 5 patients after the 12-month visit. In addition, reasons for loss to follow-up included inability to contact patient (e.g., phone number no longer valid), patient no-shows, and inability of patient to complete visit at each time point because of personal

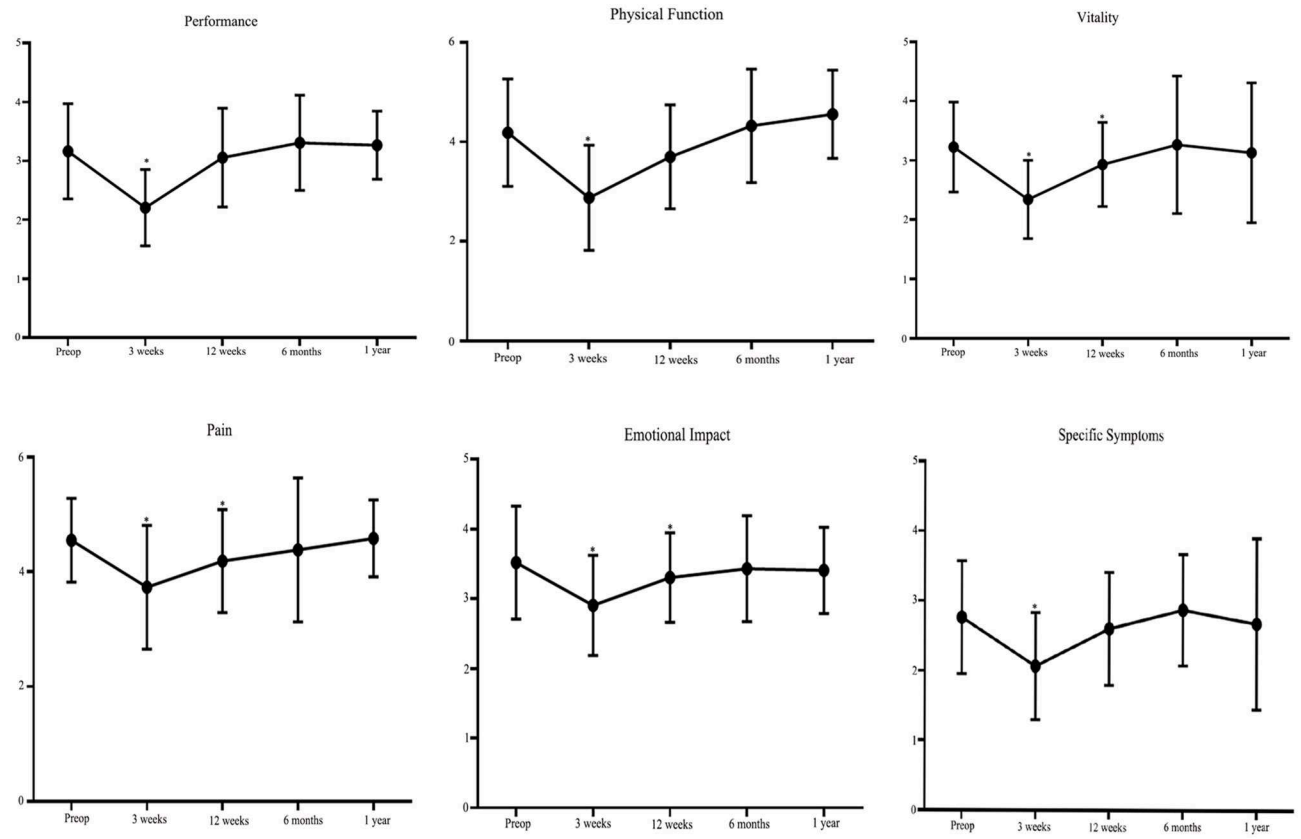

FIGURE 1 | Plots illustrating preoperative and postoperative scores for each of the six domains assessed using the Anterior Skull Base Questionnaire (ASBQ) after endoscopic nasopharyngectomy in patients with recurrent nasopharyngeal carcinoma. A higher score indicates better quality of life. *$p < 0.05$ (paired *t* test).

circumstances. Data are being collected for the remaining patients for future analysis.

DISCUSSION

The assessment of QoL is playing an increasingly important role in evaluating the efficacy of surgery and other substantive factors, such as the extent of resection, incidence of complications, time of progression, and survival rate. Gil et al. were the first to report a QoL study based on a site-specific questionnaire (ASBQ) for patients undergoing anterior skull base surgery. According to the results of their retrospective, cross-sectional study involving 40 patients undergoing open surgery, the authors found that the QoL was generally good, while malignant tumors, comorbidity, and radiotherapy were negative predictors of QoL. However, due to the lack of preoperative data, it was exceedingly difficult to conclude that QoL changes with time (10). The ASBQ was subsequently shown to be psychometrically effective in assessing site-specific QoL following anterior skull base surgery for both endoscopic and transcranial approaches (11, 12). Edward et al. prospectively assessed ASBQ before and after endoscopic skull base surgery in 85 patients and found that overall scores 6 months after surgery demonstrated significant improvement over preoperative scores (13). To avoid bias errors caused by other skull base diseases in the present study, we specifically evaluated changes in ASBQ scores in patients with recurrent NPC before and after endoscopic nasopharyngectomy and found that ASBQ scores at 6 months and 1 year postoperatively were not significantly different over preoperative ASBQ scores. Our results were different from those in some studies describing the assessment of ASBQ changes before and after skull base surgery. The main possible explanation for this difference is that most patients in those studies had benign lesions (7, 13–15).

TABLE 3 | Overall postoperative SNOT-22 scores in patients who underwent endoscopic nasopharyngectomy.

		Mean SNOT-22 Score (SD)		
Time since surgery	**No. of patients**	**Preop**	**Postop**	***P* value**
3 weeks	32	24.83 (19.71)	45.69 (25.08)	<0.0001*
12 weeks	25	23.64 (19.34)	34.44 (19.75)	0.0006*
6 month	19	22.95 (18.33)	30.26 (17.55)	0.098
1 year	20	24.15 (18.16)	23.95 (9.66)	0.9685

$p < 0.05$, paired 2-tailed t-test.SD, standard deviation; SNOT-22, 22-item Sinonasal Outcome Test.

Postoperative SNOT-22 scores in this study reflected the decrease in early postoperative sinonasal-related QoL, which is consistent with the expected effect of nasal edema, crusting, and nasal secretions after an endonasal surgical approach. These symptoms were usually relieved by postoperative debridement and nasal irrigation, and the SNOT-22 scores had improved to baseline values at 6 months and later time points after surgery. Similar findings were reported in a study in which SNOT-22 scores in 51 patients undergoing endonasal surgery for skull base tumors were significantly higher 6 to 12 months after surgery compared with the first 3 months (11). de Almeida reported that up to 98% of patients who underwent skull base surgery developed nasal crusting that lasted for 100 days (16). In addition, the overall SNOT-22 and ASBQ scores demonstrated a significant inverse correlation, which suggested that assessment using multiple instruments may provide complementary information. It also suggested that a shorter and more concise instrument may be developed to replace the two instruments that cover related domains.

In the literature, only a few studies have investigated the QoL of patients who experienced recurrent NPC after salvage surgery (17, 18). In a prospective, longitudinal study assessing the QoL of 185 patients who underwent nasopharyngectomy using the maxillary swing approach, Chan et al. reported that postoperative QoL of patients was good. However, the most

TABLE 4 | Correlation between SNOT-22 and ASBQ scores.

Time since surgery	ASBQ (n)	SNOT-22 (*n*)	Pearson correlation coefficient	*P* value
Preoperatively	40	40	−0.613	<0.0001*
3 weeks	32	32	−0.614	<0.0001*
12 weeks	25	25	−0.362	0.075
6 month	19	19	−0.744	<0.0001*
1 year	20	19	−0.398	0.082

*ASBQ, Anterior Skull Base Questionnaire; SNOT-22, 22-item Sinonasal Outcome Test; *p < 0.05, Pearson's correlation analysis.*

TABLE 5 | The items of ASBQ and SNOT-22 with severe symptoms after 1 year follow-up of patients.

	ASBQ		SNOT-22	
	Question/Item	Patients (%)	Question/Item	Patients (%)
Severe symptoms	"How would you define your sense of smell?	35	"Sense of taste/smell"	40
	"How would you define your amount of nasal secretions"	35	"Blockage/congestion of nose"	35
	"How would you define your sense of taste"	25	"Ear fullness"	30
	"How would you define your eye secretions and tears"	20	"Need to blow nose"	30

ASBQ, Anterior Skull Base Questionnaire; SNOT-22: 22-Item Sinonasal Outcome Test. Severe symptoms were indicated on ASBQ with scores of 1 or 2 and SNOT-22 with scores of 4 to 6.

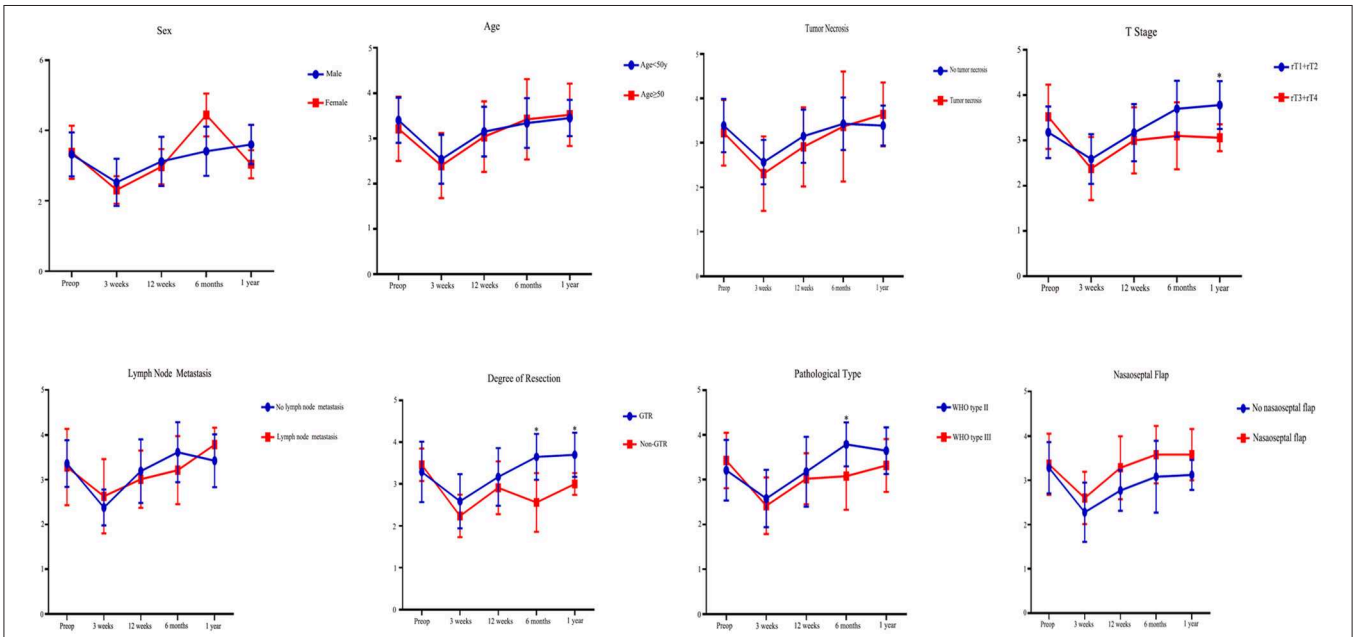

FIGURE 2 | Univariate analysis of Anterior Skull Base Questionnaire (ASBQ) scores for patients who underwent endoscopic nasopharyngectomy for recurrent nasopharyngeal carcinoma. A higher score indicates better quality of life. The *y*-axes represent the scores. *$p < 0.05$ (two-tailed *t* test).

common complications after surgery were trismus, palatal fistula, osteoradionecrosis, maxillary necrosis, and facial numbness and scar(s) (18). In addition, You et al. retrospectively assessed the QoL of patients with T1–T3 recurrent NPC who survived > 3 years after endoscopic nasopharyngectomy or intensity-modulated re-irradiation alone, they found that endoscopic nasopharyngectomy may be a more promising salvage treatment to maximize QoL benefits than re-irradiation (2). To our knowledge, there have been no prospective studies investigating the QoL of patients with recurrent NPC undergoing endoscopic salvage surgery. Results of the present prospective study revealed that short-term QoL after surgery was worse than before surgery; however, long-term QoL after surgery was essentially unchanged. Endoscopic surgery uses the natural passage of the nasal cavity to enter the pathological area of the nasopharynx, which shortens the operation path and reduces damage to the surrounding non-surgical area. In addition, it has the advantages of good illumination, clear vision, no facial incision, and rapid postoperative recovery. Endoscopic surgery can reach almost the same resection range as open surgery, and the QoL of patients after surgery is significantly improved (19, 20).

GTR was achieved using endoscopic surgery in most patients in this series, which resulted in better postoperative QoL than in patients who underwent subtotal resection, which may reflect a favorable sense of well-being by the patient who considers the surgery to be a success. The risk for local tumor recurrence is significantly lower in patients who undergo GTR compared with those who undergo subtotal resection (21). Achieving GTR in recurrent NPC is challenging due to the high incidence of submucosal extension beyond the boundary of the ulceration and the unique tumor configuration (22). Chan and Wei reported that 15-mm radial mucosal margins with the entire medial pterygoid muscle as the deep margin was adopted to ensure an acceptably high probability of achieving GTR during nasopharyngectomy (21). Meanwhile, some studies also reported that skull base tumor, such as pituitary adenomas and craniopharyngiomas, demonstrated a better QoL score after GTR (7, 14, 15).

Several limitations to this study merit consideration. First, a small sample size with long-term QoL data may have led to insufficient detection of some actual differences between QoL before and after surgery. Second, complications have a significant impact on QoL; however, we did not use this variable to stratify QoL due to the small number of complications. Third, surveys used to assess QoL are inherently limited because they may not capture disease-specific QoL changes caused by recurrent NPC and may reflect comorbidities. Finally, the outcomes in this study were based on observational data and, as such, the possibility of confounding factors cannot be excluded, such as socioeconomic status and educational level. However, the low variability in the observed preoperative and postoperative data points provides reassurance about the validity of QOL changes.

CONCLUSION

We report the first prospective study investigating site-specific and sinonasal-related QoL after endoscopic nasopharyngectomy in patients who experienced recurrent NPC. Validated QoL tools demonstrated an overall maintenance of postoperative compared with preoperative QoL. Therefore, endoscopic endonasal resection appeared to be a valuable management choice in patients with recurrent NPC. In addition, subtotal resection was an important factor that negatively influenced postoperative QoL; as such, GTR should be attempted in all patients to optimize QoL after surgery.

DATA AVAILABILITY STATEMENT

The raw data supporting the conclusions of this article will be made available by the authors, without undue reservation, to any qualified researcher.

ETHICS STATEMENT

The studies involving humans were reviewed and approved by the Institutional Review Board of AEENTH at Fudan University. The patients/participants provided their written informed consent to participate in this study.

AUTHOR CONTRIBUTIONS

DW and WL conceived and designed the study. WL, HLu, JL, QL, HW, and HZ acquired the data. WL, XS, LH, WZ, YG, and HLi drafted the manuscript. HLu performed the statistical analysis. DW supervised the study.

FUNDING

This work was financially supported by the National Natural Science Foundation of China (No. 81870703). The Joint Project of New Frontier Technology of Shanghai Shen-kang Hospital Development Center (SHDC 12018118).

ACKNOWLEDGMENTS

We thank all the participants for their contribution and participation.

REFERENCES

1. Yu MC, Yuan JM. Epidemiology of nasopharyngeal carcinoma. *Semin Cancer Biol.* (2002) 12:421–9. doi: 10.1016/S1044579X02000858
2. You R, Zou X, Hua YJ, Han F, Li L, Zhao C, et al. Salvage endoscopic nasopharyngectomy is superior to intensity-modulated radiation therapy for local recurrence of selected T1-T3 nasopharyngeal carcinoma - a case-matched comparison. *Radiother Oncol.* (2015) 115:399–406. doi: 10.1016/j.radonc.2015.04.024
3. Liu J, Yu H, Sun X, Wang D, Gu Y, Liu Q, et al. Salvage endoscopic nasopharyngectomy for local recurrent or residual nasopharyngeal carcinoma: a 10-year experience. *Int J*

Clin Oncol. (2017) 22:834–842. doi: 10.1007/s10147-017-1143-9
4. Vlantis AC, Lee DL, Wong EW, Chow SM, Ng SK, Chan JY. Endoscopic nasopharyngectomy in recurrent nasopharyngeal carcinoma: a case series, literature review, and pooled analysis. *Int Forum Allergy Rhinol.* (2017) 7:425–432. doi: 10.1002/alr.21881
5. Ho AS, Kaplan MJ, Fee WE, Jr., Yao M, Sunwoo JB, et al. Targeted endoscopic salvage nasopharyngectomy for recurrent nasopharyngeal carcinoma. *Int Forum Allergy Rhinol.* (2012) 2:166–73. doi: 10.1002/alr.20111
6. Hsu NI, Shen PH, Chao SS, Ong YK, Li CS. En bloc resection concept for endoscopic endonasal nasopharyngectomy: surgical anatomy and outcome. *Chin Med J (Engl).* (2014) 127:2934–9. doi: 10.3760/cma.j.issn.0366-6999.20133189
7. McCoul ED, Anand VK, Schwartz TH. Improvements in site-specific quality of life 6 months after endoscopic anterior skull base surgery: a prospective study. *J Neurosurg.* (2012) 117:498–506. doi: 10.3171/2012.6.JNS111066
8. Gil Z, Abergel A, Spektor S, Shabtai E, Khafif A, Fliss DM. Development of a cancer-specific anterior skull base quality-of-life questionnaire. *J Neurosurg.* (2004) 100:813–9. doi: 10.3171/jns.2004.100.5.0813
9. Piccirillo JF, Merritt MG, Jr., Richards ML. Psychometric and clinimetric validity of the 20-Item sino-nasal outcome test (SNOT-20). *Otolaryngol Head Neck Surg.* (2002) 126:41–7. doi: 10.1067/mhn.2002.121022
10. Gil Z, Abergel A, Spektor S, Cohen JT, Khafif A, Shabtai E, et al. Quality of life following surgery for anterior skull base tumors. *Arch Otolaryngol Head Neck Surg.* (2003) 129:1303–9. doi: 10.1001/archotol.129.12.1303
11. Cavel O, Abergel A, Margalit N, Fliss DM, Gil Z. Quality of life following endoscopic resection of skull base tumors. *J Neurol Surg B Skull Base.* (2012) 73:112–6. doi: 10.1055/s-0032-1301392
12. Gil Z, Fliss DM. Quality of life in patients with skull base tumors: current status and future challenges. *Skull Base.* (2010) 20:11–8. doi: 10.1055/s-0029-1242979
13. McCoul ED, Anand VK, Bedrosian JC, Schwartz TH. Endoscopic skull base surgery and its impact on sinonasal-related quality of life. *Int Forum Allergy Rhinol.* (2012) 2:174–81. doi: 10.1002/alr.21008
14. Patel KS, Raza SM, McCoul ED, Patrona A, Greenfield JP, Souweidane MM, et al. Long-term quality of life after endonasal endoscopic resection of adult craniopharyngiomas. *J Neurosurg.* (2015) 123:571–80. doi: 10.3171/2014.12.JNS141591
15. McCoul ED, Bedrosian JC, Akselrod O, Anand VK, Schwartz TH. Preservation of multidimensional quality of life after endoscopic pituitary adenoma resection. *J Neurosurg.* (2015) 123:813–20. doi: 10.3171/2014.11.JNS14559
16. de Almeida JR, Snyderman CH, Gardner PA, Carrau RL, Vescan AD. Nasal morbidity following endoscopic skull base surgery: a prospective cohort study. *Head Neck.* (2011) 33:547–51. doi: 10.1002/hed.21483
17. Ng RW, Wei WI. Quality of life of patients with recurrent nasopharyngeal carcinoma treated with nasopharyngectomy using the maxillary swing approach. *Arch Otolaryngol Head Neck Surg.* (2006) 132:309–16. doi: 10.1001/archotol.132.3.309
18. Chan YW, Chow VL, Wei WI. Quality of life of patients after salvage nasopharyngectomy for recurrent nasopharyngeal carcinoma. *Cancer.* (2012) 118:3710–8. doi: 10.1002/cncr.26719
19. Yu KH, Leung SF, Tung SY, Zee B, Chua DT, Sze WM, et al. Hong Kong nasopharyngeal carcinoma study, survival outcome of patients with nasopharyngeal carcinoma with first local failure: a study by the Hong Kong nasopharyngeal carcinoma study group. *Head Neck.* (2005) 27:397–405. doi: 10.1002/hed.20161
20. Wei WI. Salvage surgery for recurrent primary nasopharyngeal carcinoma. *Crit Rev Oncol Hematol.* (2000) 33:91–8. doi: 10.1016/S1040-8428(99)00069-4
21. Chan JY, Wei WI. Impact of resection margin status on outcome after salvage nasopharyngectomy for recurrent nasopharyngeal carcinoma. *Head Neck 38 Suppl.* (2016) 1:E594–9. doi: 10.1002/hed.24046
22. Chan JY, Wong ST, Wei WI. Whole-organ histopathological study of recurrent nasopharyngeal carcinoma. *Laryngoscope.* (2014) 124:446–50. doi: 10.1002/lary.24218

Conflict of Interest: The authors declare that the research was conducted in the absence of any commercial or financial relationships that could be construed as a potential conflict of interest.

frontiers in Oncology

ORIGINAL RESEARCH
published: 30 April 2020
doi: 10.3389/fonc.2020.00601

Circular RNA Expression Profiles in Nasopharyngeal Carcinoma by Sequence Analysis

Jing Yang[1†], Yongqian Gong[2†], Qingshan Jiang[2], Lijun Liu[2], Shuyan Li[2], Quanjun Zhou[2], Fang Huang[2] and Zhifeng Liu[2]*

[1] Department of Gastroenterology, The First Affiliated Hospital of University of South China, Hengyang, China,
[2] Department of Otorhinolaryngology, The First Affiliated Hospital of University of South China, Hengyang, China

Circular RNAs (circRNAs), as a burgeoning sort of non-coding RNAs (ncRNAs), can regulate the expression of parental genes as miRNA sponges. This study was designed to explore the circRNA expression profile of nasopharyngeal carcinoma (NPC). High-throughput sequencing was performed to identify the circRNA expression profile of NPC patients compared with healthy controls. A total of 93 upregulated circRNAs and 77 downregulated circRNAs were identified. The expression levels of the top three upregulated and three downregulated circRNAs annotated by circBase were validated by quantitative real-time PCR (qRT-PCR). GO and KEGG analyses showed that these differentially expressed circRNAs were potentially implicated in NPC pathogenesis. CircRNA-miRNA-target gene network analysis revealed a potential mechanism that hsa_circ_0002375 (circKITLG) may be involved in NPC through sponging up miR-3198 and interfering with its downstream targets. Silencing of circKITLG inhibited NPC cell proliferation, migration, and invasion *in vitro*. This study provides a leading and fundamental circRNA expression profile of NPC.

Keywords: circular RNA (circRNA), nasopharyngeal carcinoma (NPC), high-throughput sequencing, biomarkers, microRNA (miRNA)

OPEN ACCESS

Edited by:
Yu-Pei Chen,
Sun Yat-sen University Cancer Center (SYSUCC), China

Reviewed by:
Weibin Wang,
Zhejiang University, China
Haiping Pei,
Central South University, China

***Correspondence:**
Zhifeng Liu
liuzf@usc.edu.cn

† These authors have contributed equally to this work

Specialty section:
This article was submitted to Head and Neck Cancer, a section of the journal Frontiers in Oncology

Received: *29 October 2019*
Accepted: *01 April 2020*
Published: *30 April 2020*

Citation:
Yang J, Gong Y, Jiang Q, Liu L, Li S, Zhou Q, Huang F and Liu Z (2020) Circular RNA Expression Profiles in Nasopharyngeal Carcinoma by Sequence Analysis. Front. Oncol. 10:601. doi: 10.3389/fonc.2020.00601

INTRODUCTION

Nasopharyngeal carcinoma (NPC), the most common head and neck cancer, is associated with remarkable distinct geographical distribution and racial differences, and it is highly prevalent in east and southeast Asia (1, 2). The main causes of NPC include Epstein-Barr virus (EBV), genetic susceptibility, environmental factors, and so on (1). The radiotherapy and chemotherapy treatments used to treat NPC have been advanced. However, 30% of NPC patients will develop local relapsed and distant metastasis, and the outcomes of these patients remain frustrating (3, 4). Searching for the underlying NPC novel targets would help facilitate clinical treatment strategies.

CircRNAs are a novel class of ncRNA molecules, which are single-stranded, have covalently joined head 3′ and tail 5′, and are produced via backsplicing (5, 6). Due to the particular covalently closed circular molecular structure, circRNAs are highly resistant to degradation and more stable than conventional linear RNA (7). Though circRNAs were first identified in RNA viruses in the 1980's, they were initially considered to be splicing-associated noise (8). Currently, much research has demonstrated that circRNAs can function as microRNA (miRNA) sponges (9). Based on the function, more and more studies have revealed that circRNAs play an essential role in the regulation of gene expression and in physiology, pathology, and the initiation and progression of human diseases, especially tumorigenesis (10, 11).

Recently, circRNAs have been indicated to be potential biomarkers or therapeutic targets in various cancers, such as colorectal cancer (12), pancreatic cancer (13), hepatocellular carcinoma (14), bladder carcinoma (15), and lung adenocarcinoma (16). Exome capture transcriptome sequencing was used to compile a cancer circRNA landscape across 40 cancer types by Arul M. Chinnaiyan et al. (17). However, circRNA expression profiling and circRNAs as biomarkers in nasopharyngeal carcinoma have not been reported. Here, we profiled potential circRNA biomarkers in nasopharyngeal carcinoma presented by high-throughput sequencing.

MATERIALS AND METHODS

Patients and Tissue Specimen

Four fresh nasopharyngeal carcinoma tissue specimens and four matched healthy tissue specimens were acquired from nasopharyngeal carcinoma and nasopharyngitis patients via biopsy for circRNA high-throughput sequencing. Then, a total of 41 matched specimens, containing the specimens for sequencing, were used to validate the circRNA expression by qRT-PCR. The experimental tissue specimens were diagnosed based on strict pathologic examination. They had no other tumor history and did not undergo radiotherapy and chemotherapy before biopsy. Pathologic and clinical characteristics of nasopharyngeal carcinoma patients were based on the American Joint Committee on Cancer (AJCC) and the Union for International Cancer Control (UICC) TNM classification. Consent documents were obtained from all patients, and the Medical Ethics Committee of The First Affiliated Hospital of University of South China approved this study. Specimens were instantly stored in liquid nitrogen (−180°C) after biopsy.

Cell Culture

The human NPC cell lines HNE1, HNE2, HNE3, CNE1, CNE2, 5-8F, and HK1 were obtained from Hunan Province Key Laboratory of Tumor Cellular & Molecular Pathology (University of South China, Hengyang, China). The cancer cells were cultured with RPMI Medium (Hyclone) with 10% FBS (Sigma) and antibiotics (100 units/mL of penicillin and 100 μg/mL streptomycin) at 37°C and 5% CO_2.

Total RNA Extraction

Total RNA was isolated from the frozen tissues by TRIzol (Invitrogen, USA) based on the manufacturer's instructions. The quantity of the isolated RNA of each sample was tested using ND-1000 spectrophotometer (NanoDrop/Termo, Wilmington, DE). The OD260/OD280 ratio was used as the RNA purity index. If the OD260/OD280 ratio ranges between 1.8 and 2.1, the purity of RNA is qualified, and the QC results are determined as "Pass."

Library Construction and circRNA Sequencing

CircRNA sequencing was performed by Aksomics Inc (Shanghai, China). A total quantity of 1∼2 μg total RNA per sample was used to enrich circRNA using NEB Next® Poly(A) mRNA Magnetic Isolation Module (New England Biolabs, USA). Strand-specific CircRNA-seq libraries were constructed by KAPA Stranded RNA-Seq Library Prep Kit (KAPA, USA) with pretreated RNAs according to the manufacturer's protocol. The digested RNAs were fragmented into pieces and then used to synthesize first-strand and the second-strand cDNA. Next, the cDNA products were end-repaired, added a single "A" base, and Illumina sequencing adaptors were ligated onto the double-stranded cDNA. After libraries were purified and enriched by PCR, the quality of libraries was controlled by the Agilent 2100 Bioanalyzer (Agilent Technologies Inc, USA) using the Agilent DNA 1000 chip kit (Agilent Technologies Inc, USA). Finally, the double-stranded cDNA was denatured as single-stranded DNA and then sequenced for 150 cycles on an Illumina X-ten/NovaSeq system (Illumina, USA).

Data Analysis and Differentially Expressed circRNA Identification

Raw sequencing data were under Quality Control (QC) and filtered to remove the joint sequence and too short clips. Then, the trimmed data was aligned to the reference genome (GRCh37/hg19) using STAR software (version 2.5.2b). Differential expression for circRNA-seq data were calculated using the edgeR package (version 3.20.9) in the statistical R program (version 3.5.0). Genes with a fold change $\geq$ 2.0 or fold change $\leq$ 0.5 and $p < 0.05$ between cases and controls were selected as differentially expressed circRNAs. For annotation, these differentially expressed circRNAs were blasted by the circBase (18), and those that cannot be annotated were defined as novel circRNAs. The sequencing data that cannot be aligned to reference genome directly were subjected to the subsequent circRNA analysis by recognition of the reverse splicing event using CIRCexplorer2 software (version 2.3.2) (19). These differentially expressed circRNAs were visualized with a circular view by CIRCOS visualization software (20).

qRT-PCR Validation for the Expression of circRNA

Quantitative reverse-transcription polymerase chain reaction (qRT-PCR) was performed to validate the expression of circRNAs identified by sequencing. Six circRNAs annotated by circBase were selected, including the top three upregulated and three downregulated circRNAs. All the primers for candidate circRNAs are listed in **Table 2**, and these were purchased from Sangon Biotech (Shanghai, China). For qRT-PCR analysis, cDNA was synthesized from 1 μg of total RNA using the All-in-One First-Strand cDNA Synthesis kit (GeneCopoeia Inc, Santa Cruz, CA). The qRT-PCR analyses were performed by All-in-One qPCR Mix (GeneCopoeia Inc, USA) on ABI 7500HT qRT-PCR system (Applied Biosystems, Foster City, CA) as reactions: 95°C for 48 s, followed by 40 cycles of 95°C for 5 s and 62.5°C for 40 s. The reference gene was GAPDH, and the relative levels of gene expression were calculated using the $2^{-\Delta\Delta Ct}$ method.

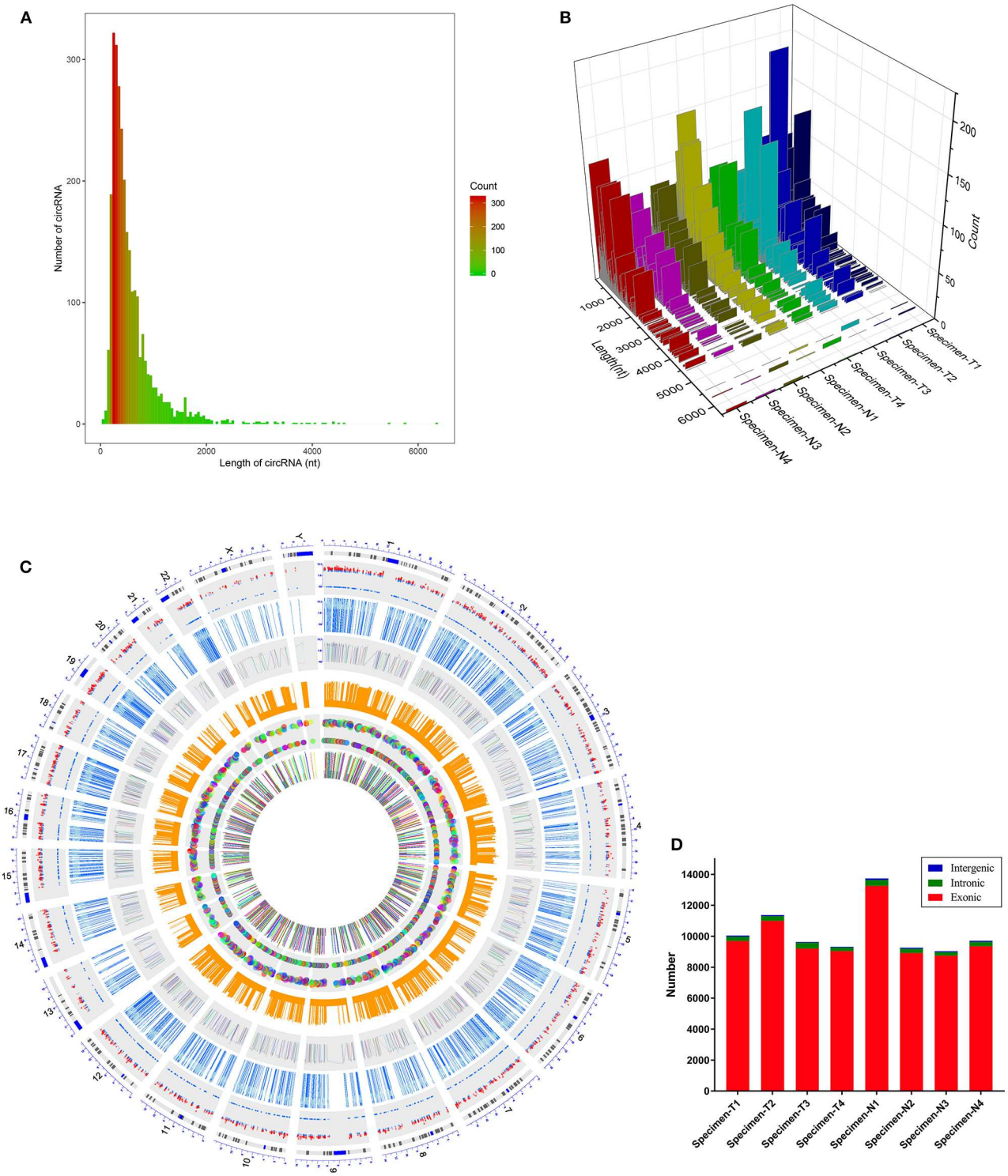

FIGURE 1 | Characteristics of the identified circRNAs in nasopharyngeal carcinoma and healthy controls. **(A,B)** Length distribution of the identified circRNAs. x-axis, the length of the detected circRNAs; y-axis, the abundance of circRNAs classified by different lengths. **(C)** Distribution of the candidate circRNAs on chromosomes. **(D)** Genomic origin of the identified circRNAs.

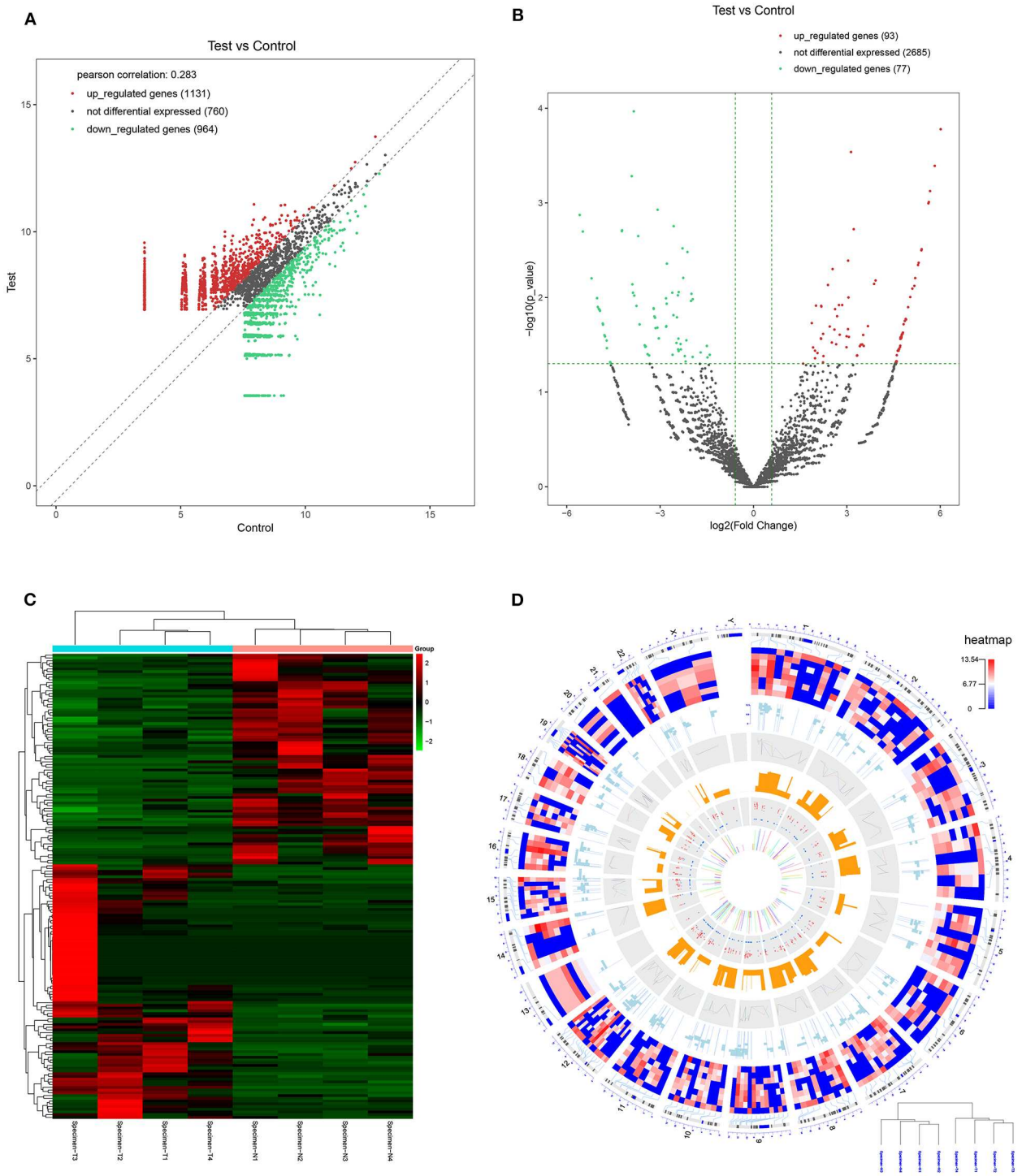

FIGURE 2 | CircRNA expression profile in nasopharyngeal carcinoma compared to healthy controls. **(A)** The expression of circRNAs in the four pairs of nasopharyngeal carcinoma tissues and healthy controls through the high-throughput sequencing. **(B)** Volcano plots of the differentially expressed circRNAs. Horizontal dotted line: $P = 0.05$ (–log10 scaled); red points: upregulated circRNAs with statistical significance; green points: downregulated circRNAs with statistical significance. **(C)** Heat map and hierarchical cluster analysis of all target circRNAs. Red strip: high relative expression; blue strip: low relative expression. **(D)** Heat map of differentially expressed circRNAs on human chromosomes.

GO and KEGG Pathway Analysis of circRNAs

The potential functions of differentially expressed circRNAs and their parental genes were analyzed by DAVID (https://david.ncifcrf.gov/). GO enrichment analysis was performed, in terms of biological process (BP), cellular component (CC), and molecular function (MF), with Gene Ontology (http://geneontology.org/). The KEGG enrichment analysis revealed the significantly enriched pathways of the parental genes of differentially expressed circRNAs analyzed using KEGG (http://www.genome.jp/kegg/).

CircRNA–miRNA–mRNA Interaction Prediction

CircRNAs as miRNAs sponges can indirectly interfere with the translation of the targeted mRNAs. We used miRanda software (version 3.3a) (21) (http://www.microrna.org/microrna/home.do) and RNAhybrid software (version 2.1.2) (22) (https://bibiserv.cebitec.uni-bielefeld.de/rnahybrid/) to predict the targeted miRNAs and mRNAs for hsa_circ_0002375 (circKITLG). The circRNA/miRNA/mRNA networks were visualized by Cytoscape software (version 3.7.0) (23) (https://cytoscape.org/).

Transfection

Small interfering RNAs (siRNAs) targeting circKITLG backsplice junction sites and negative control (NC) oligonucleotides were purchased from RIBOBIO (Ribobio Co.,Ltd., Guangzhou, China). The siRNA sequences were si-circKITLG#1, 5′-GTACATTGACTTGGATTCTCA-3′; si-circKITLG#2, 5′-ACATTGACTTGGATTCTCACT-3′; si-NC, and 5′-TTCTCCGAACGTGTCACGT-3′. Cells were transfected with final concentrations of 50 nM of siRNAs using the Lipofectamine 2000 (Invitrogen, Carlsbad, CA, USA) according to the manufacturer's instructions.

Cell Proliferation Assay

Cells were seeded into the 96-well plate (3×10^3 cells/well). A cell proliferation assay was performed at the indicated time points using CCK-8 kit (CCK8, Beyotime, Nanjing, China) according

TABLE 2 | A list of primers (F, forward and R, reverse) used in this study.

circRNA	Primer sequence
hsa_circ_0002375	F:5′- GTTGCAAGAGAAAGAGAGAGAGTT-3′
	R:5′- CGATTCCTGCAGATCCCTTC-3′
hsa_circ_0111974	F:5′- TCACAAAGCGCAGACGTAAA-3′
	R:5′- ATGAAGGACGAACAGCTGGAA-3′
hsa_circ_0081534	F:5′- GAACGGGGTATCCTCCTTAGC-3′
	R:5′- TTAGAGTGGCTATTGGCTGGG-3′
hsa_circ_0007439	F:5′- GGGAGAAAATGATCGTGGTGTT-3′
	R:5′- AGATTGCAGGTCTGGTGACAA-3′
hsa_circ_0000345	F:5′- GTGAAGAAGCCATCCTAGCAGA-3′
	R:5′- AGAACATTGGCTGTAGAACGGT-3′
hsa_circ_0138314	F:5′- GTCTGGTTGCCTTAGTGAGGG-3′
	R:5′- TCCCACCAAATGGATCTCTCTTC-3′
GAPDH	F:5′- CATGAGAAGTATGACAACAGCCT-3′
	R:5′-AGTCCTTCCACGATACCAAAGT-3′

F, forward; R, reverse.

TABLE 1 | Top 20 differentially expressed circRNAs in the nasopharyngeal carcinoma.

circRNA_ID	Chr	Locus	Strand	Gene_Name	Length	log2FC	*p*-value
hsa_circ_0002375	chr12	88898935–88939642	-	KITLG	844	6.0146682	0.00017
hsa_circ_0111974	chr1	216824314–216850833	-	ESRRG	533	5.8223723	0.00040
chr10:46121398-46135411:-	chr10	46121398–46135411	-	ZFAND4	1303	5.6740423	0.00075
hsa_circ_0081534	chr7	100417178–100417918	-	EPHB4	489	5.6344749	0.00098
hsa_circ_0025767	chr12	29904598–29911710	-	TMTC1	458	5.6178356	0.00101
hsa_circ_0088018	chr9	114190321–114195652	-	KIAA0368	342	5.4035426	0.00309
hsa_circ_0135761	chr8	132952745–132958880	+	EFR3A	356	5.3922431	0.00316
hsa_circ_0094943	chr11	110007387–110034104	+	ZC3H12C	1234	5.3060947	0.00430
hsa_circ_0079557	chr7	22306582–22357656	-	RAPGEF5	565	5.2869091	0.00453
hsa_circ_0066568	chr3	78763546–78767033	-	ROBO1	388	5.1949179	0.00622
hsa_circ_0007439	chr2	29006772–29011675	+	PPP1CB	224	−5.5835715	0.00134
chr19:6697354-6697805:-	chr19	6697354–6697805	-	C3	356	−5.4836046	0.00201
hsa_circ_0000345	chr11	77409531–77413540	-	RSF1	1982	−5.2024664	0.00624
chr19:42621401-42664544:-	chr19	42621401–42664544	-	POU2F2	336	−5.0259181	0.01015
hsa_circ_0138314	chr9	14672827–14680160	-	ZDHHC21	428	−5.0014845	0.01256
hsa_circ_0105201	chr16	22162015–22163955	+	VWA3A	276	−4.9682426	0.01319
chr9:100092435-100093049:+	chr9	100092435–100093049	+	AL512590.3	486	−4.9654478	0.01325
hsa_circ_0001913	chrX	19701940–19713859	-	SH3KBP1	336	−4.9523179	0.01341
hsa_circ_0004315	chr16	74491771–74493687	-	GLG1	229	−4.9392393	0.01356
hsa_circ_0025967	chr12	46319924–46322642	-	SCAF11	2718	−4.932998	0.01380

to the manufacturer's instructions. The optical density (OD) at 450 nm was determined with a microplate reader (Thermo Fisher Scientific, Waltham, MA, USA).

Colony Formation Assay

For colony formation assay, 24 h after transfection, cells were seeded into the 6-well plate (4×10^2 cells/well). The culture medium was replaced every 3 days for 2 weeks. Then the colonies were fixed using methanol for 20 min and stained by crystal violet (Beyotime, Nanjing, China) for 15 min.

Cell Migration and Invasion Assays

Cell migration ability was evaluated by wound healing assays. Cells were seeded into 6-well plates and scraped using 10 μl tips when cell confluence reached 90%. Cells were then cultured with serum-free medium for 48 h. The plates were photographed under a microscope at different time points. Cell invasion assays were conducted using Transwell chamber (Corning, NY, USA) coated with Matrigel (Corning, NY, USA). Cells suspended with serum-free medium were seeded into the upper chamber (2×10^4 cells/well), and the culture medium with 10% FBS was placed into the lower chamber. After 48 h, the cells on the upper surfaces of the Transwell chamber were removed with cotton swabs, and the cells on the lower surfaces were fixed with paraformaldehyde and stained by crystal violet. The stained cells were photographed and counted under a microscope.

Statistical Analysis

The statistical analyses were performed by SPSS18 software (SPSS Inc., IL, USA). The results were presented as the mean ± SD. For analysis, we used Student's *t*-test and One-way ANOVA between groups, and $P < 0.05$ was considered to be statistically significant. More specifically, $^{*}P < 0.05$; $^{**}P < 0.01$; and $^{***}P < 0.001$.

RESULTS

CircRNA Expression Profile in NPC

We first analyzed the circRNA expression profile of four matched tissues acquired from NPC and nasopharyngitis patients by high-throughput deep sequencing. More than 12 gigabytes (Gb) of sequenced data of each specimen were aligned to the reference genome (GRCh37/hg19) using STAR software (version 2.5.2b). A total of 2,855 circRNAs were identified in these samples. Of these, 192 circRNAs were previously unknown. The lengths of candidate circRNAs were mostly <2000 nucleotides (nt) (**Figures 1A,B**). These candidate circRNAs were annotated using the RefSeq database. The candidate circRNAs were distributed on all chromosomes, including sex chromosomes X and Y (**Figure 1C**). Among these candidate circRNAs' host genes, 96.5% originated from exonic regions, and the rest lay on intronic and unannotated regions (**Figure 1D**).

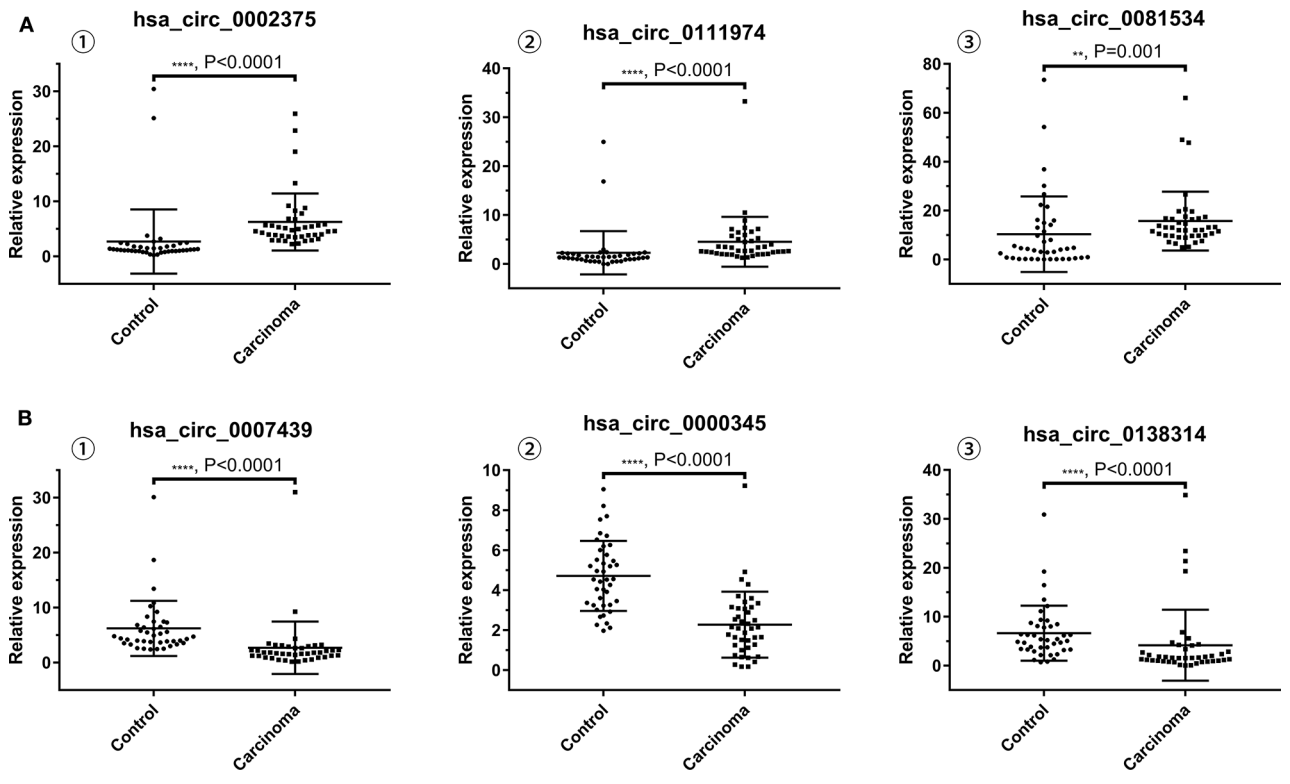

FIGURE 3 | Validation of the expression level of six selected circRNAs. **(A)** The levels of the top three upregulated circRNAs (hsa_circ_0002375, hsa_circ_0111974, and hsa_circ_0081534) in NPC tissues are significantly higher than normal tissues. **(B)** The levels of the top three downregulated circRNAs (hsa_circ_0007439, hsa_circ_0000345, and hsa_circ_0138314) in NPC tissues are significantly lower than normal tissues.

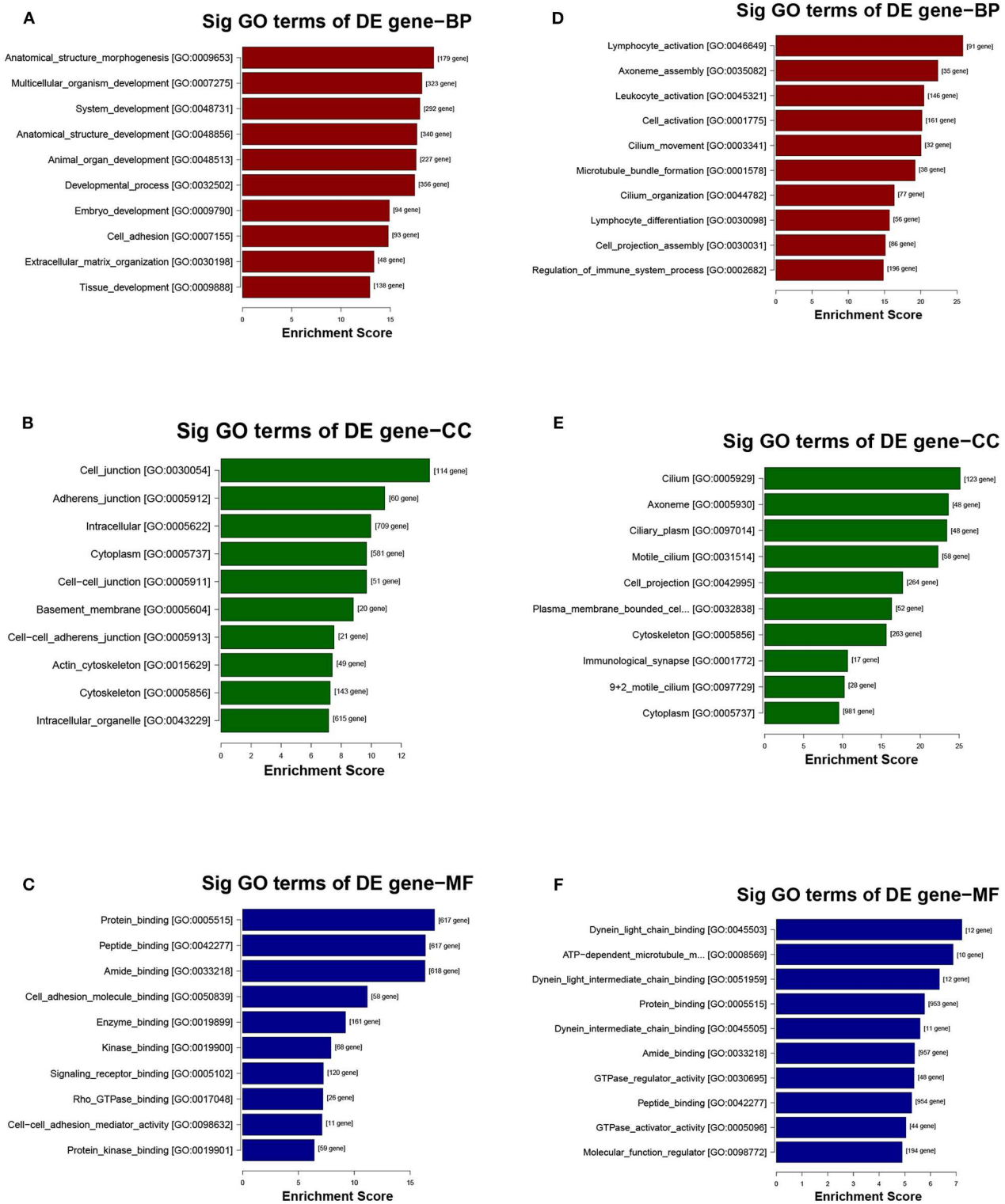

FIGURE 4 | GO analysis of the parental genes of the differentially expressed circRNAs, includes the following categories: biological process (BP), cellular component (CC) and molecular function (MF). **(A–C)** GO analysis corresponds with the upregulated circRNAs. **(D–F)** GO analysis corresponds with the downregulated circRNAs.

CircRNA expression profile was used to evaluate the variations between the NPC tissue specimens group and four matched normal tissue specimens group using the scatter plot (**Figure 2A**). Differentially expressed circRNAs with a statistical significance between the two groups were identified with fold change $\geq$ 2.0 or fold change $\leq$0.5 and $p < 0.05$. A total of 170 circRNAs were significantly differentially expressed, including 93 remarkably upregulated circRNAs and 77 significantly downregulated circRNAs visualized by volcano plots (**Figure 2B**) and a cluster heatmap (**Figure 2C**). The top 20 differentially expressed circRNAs are presented (**Table 1**). The differentially expressed circRNAs were distributed by heatmap on human chromosomes (**Figure 2D**).

Validation of Differentially Expressed circRNAs by qRT-PCR

To validate the RNA-seq results, the top three upregulated and three downregulated circRNAs annotated by circBase were selected for validation by qRT-PCR with outward-facing primers (**Table 2**) blasted to the circRNA transcripts.

The results of qRT-PCR revealed that the expression levels of hsa_circ_0002375 (circKITLG) ($P < 0.0001$), hsa_circ_0111974 (circESRRG) ($P < 0.001$), and hsa_circ_0081534 (circEPHB4) ($P = 0.001$) were significantly upregulated in the NPC specimens (**Figure 3A**), and the expression levels of hsa_circ_0007439 (circPPP1CB) ($P < 0.0001$), hsa_circ_0000345 (circRSF1) ($P < 0.001$), and hsa_circ_0138314 (circZDHHC21) ($P < 0.0001$) were significantly downregulated in the NPC specimens (**Figure 3B**).

GO and KEGG Pathway Analyses of Differentially Expressed circRNAs

The potential function and connection of the differentially expressed circRNAs and their parental genes were predicted using GO and KEGG analyses. The top 10 enrichment GO terms for differentially expressed circRNAs are shown. The most significant enriched GO terms in the biological process were related to the anatomical structure morphogenesis process (GO:0009653) and lymphocyte activation process (GO:0046649) (**Figures 4A,D**); the most significant enriched GO terms in cellular component were related to the cell junction (GO:0030054) and cilium process (GO:0005929) (**Figures 4B,E**); and the most significant enriched GO terms in molecular function were related to the protein binding (GO:0005515) and dynein light chain binding process (GO:0045503) (**Figures 4C,F**). The top 10 enriched pathways of KEGG pathway enrichment analysis are displayed in an enriched scatter diagram (**Figures 5A,B**). These results showed that the differentially expressed genes might be associated with tumor signaling pathways and immune signaling pathways.

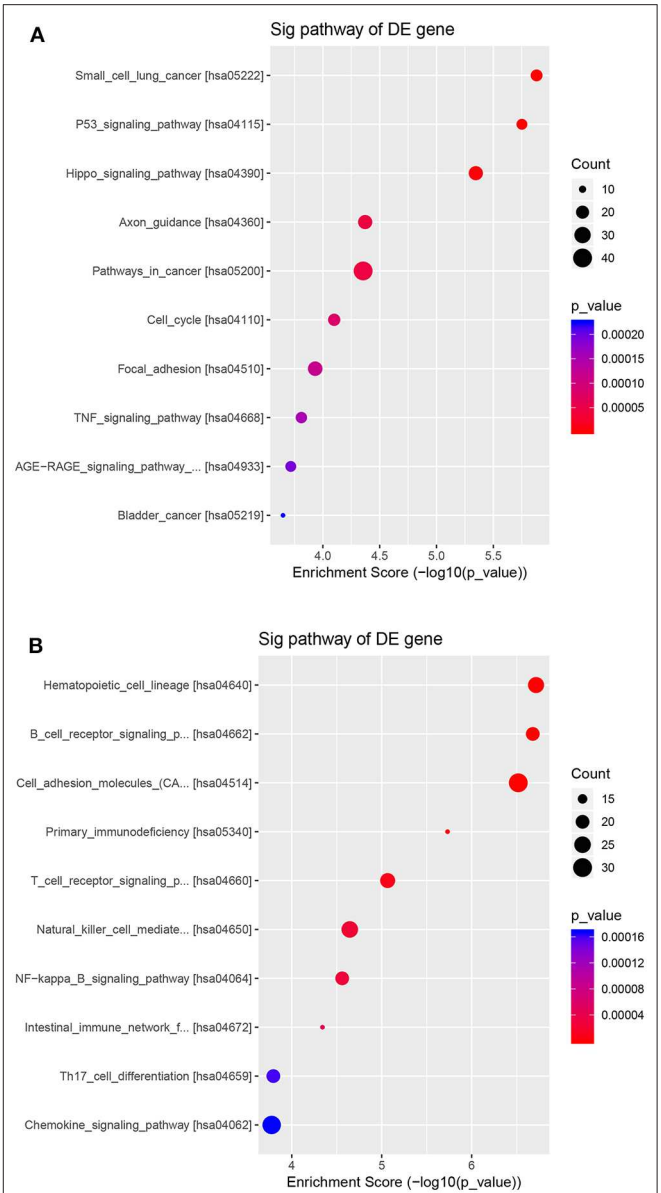

FIGURE 5 | KEGG pathway analyses of the parental genes of the differentially expressed circRNAs. The pathways correspond with **(A)** the upregulated circRNAs and **(B)** the downregulated circRNAs. The results are shown in a scatter plot. Enrichment factor refers to the ratio of the number of genes located in the pathway entry and the total number of genes in the pathway entry.

Prediction of the circRNA–miRNA–mRNA Interaction Network

The top upregulated circRNA hsa_circRNA_002375 (circKITLG), validated by qRT-PCR, was selected for analyzing the network between circRNAs and miRNAs by miRanda and RNAhybrid software. Only the circRNA and miRNA interactions predicted using both tools were considered. The potential functional network of circKITLG were presented (**Figure 6**).

Silencing of circKITLG Inhibited NPC Cell Proliferation, Migration, and Invasion *in vitro*

As shown in **Table 1** and **Figure 3A**, circKITLG was the top upregulated circRNA and validated by qRT-PCR. Hence, to further explore the biological functional roles of circRNAs in

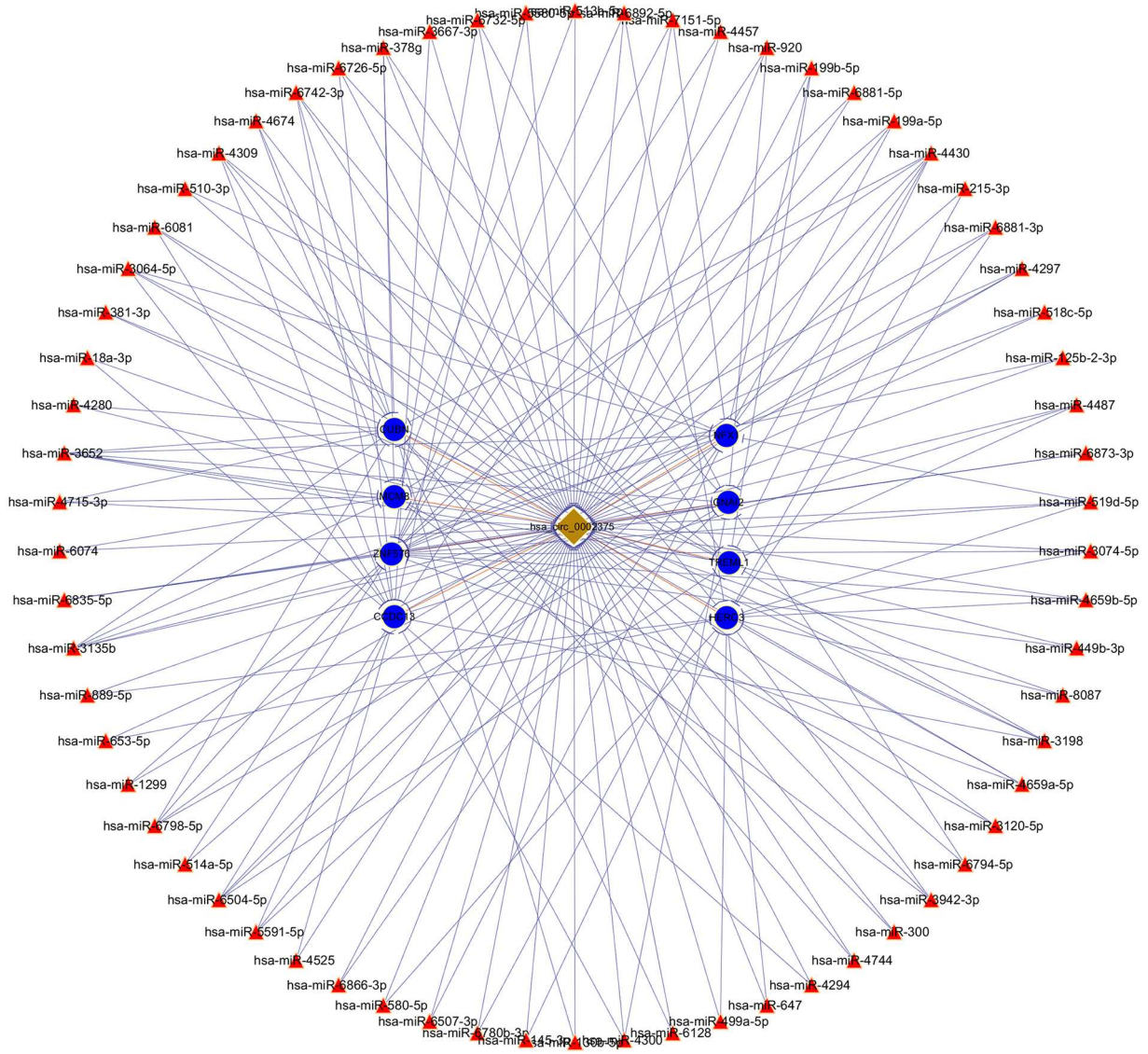

FIGURE 6 | CircRNA-miRNA-mRNA network analysis of the top upregulated circRNA hsa_circ_0002375 (circKITLG).

NPC *in vitro*, we selected circKITLG as a candidate circRNA for further investigation. The expression of circKITLG in seven NPC cell lines was measured by qRT-PCR, and the results demonstrated that circKITLG expression level was higher in HK1 and CNE2 cells than others (**Figure 7A**). Therefore, HK1 and CNE2 cell lines were chosen for silencing of circKITLG (**Figures 7B,C**). Cell proliferation was measured by the CCK-8 assay, and knockdown of circKITLG significantly attenuated cell proliferation in both HK1 and CNE2 cells (**Figure 7D**). The colony formation abilities of NPC cells were also markedly inhibited by silencing circKITLG (**Figure 7E**). Moreover, in the wound healing assays and transwell invasion assays, silencing of circKITLG significantly inhibited the migration and invasion abilities of HK1 and CNE2 cells (**Figures 7F,G**). Therefore, the above results demonstrated that silencing of circKITLG could inhibit the progression of NPC cells.

DISCUSSION

CircRNAs, as a burgeoning sort of non-coding RNA, could function as miRNA sponges, which can regulate the expression of parental genes (24, 25). A significant number of studies have revealed that circRNAs are implicated in various human diseases, including carcinomas (26). However, no NPC-associated circRNA has been identified by high-throughput sequencing. In this study, we presented a leading and primary circRNA expression profile in NPC using high-throughput sequencing.

In our research, a total of 93 upregulated circRNAs and 77 downregulated circRNAs were identified. Hsa_circ_0002375,

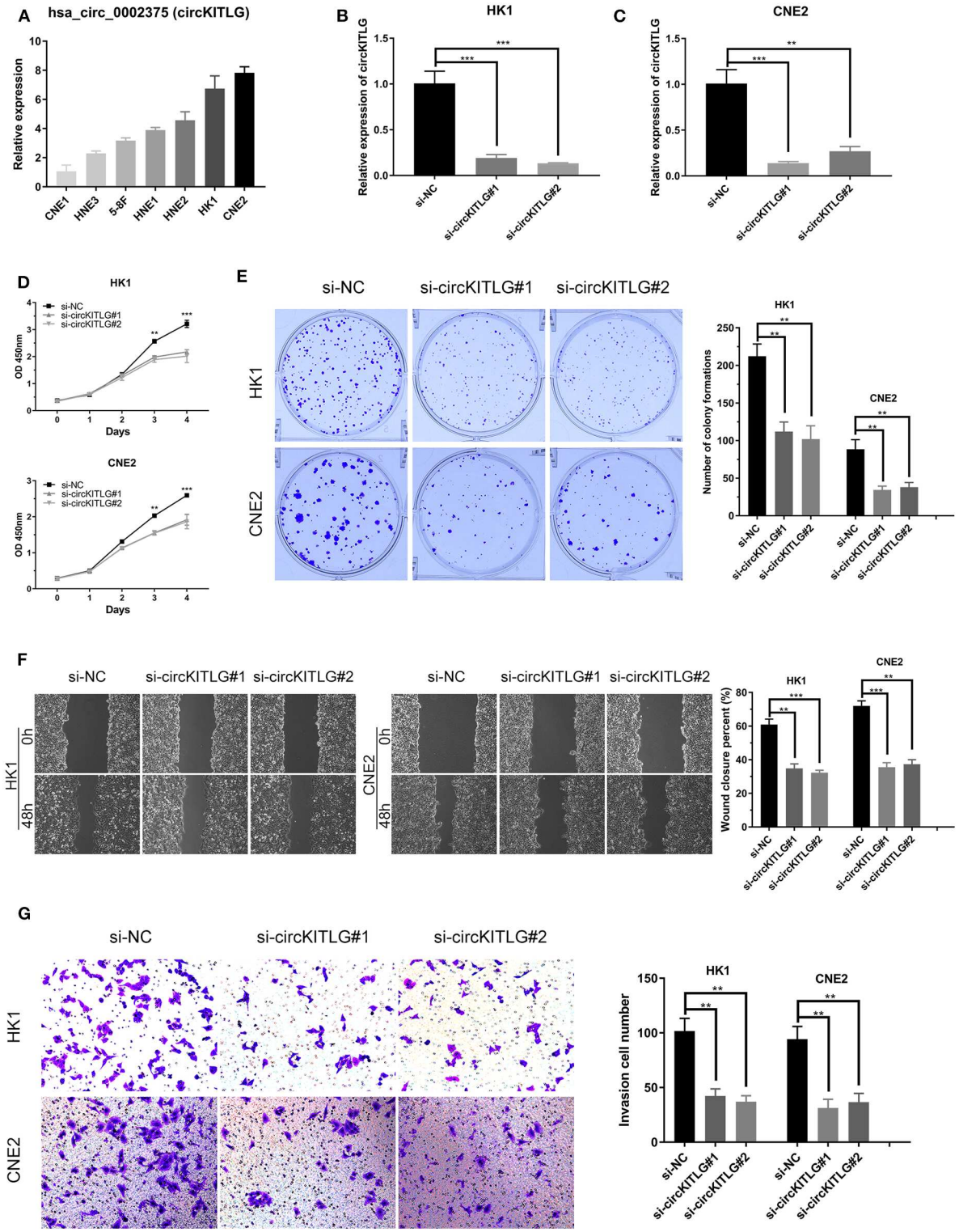

FIGURE 7 | Silencing of hsa_circ_0002375 (circKITLG) inhibited NPC cell proliferation, migration, and invasion. **(A,B)** Relative expression of circKITLG in 7 NPC cell lines was examined by qRT-PCR. **(C)** Results of qRT-PCR for circKITLG in HK1 and CNE2 cells treated with circKITLG siRNAs. **(D)** CCK-8 assay was performed to evaluate the growth of NPC cells after treatment with circKITLG siRNAs. **(E)** Colony formation assay was performed after transfected with NC or circKITLG siRNA. **(F,G)** Migration and invasion of NPC cells transfected with NC or circKITLG siRNA. $^{**}p < 0.01$ and $^{***}p < 0.001$.

hsa_circ_0111974, and hsa_circ_0081534 were the significantly upregulated circRNAs, and hsa_circ_0007439, hsa_circ_0000345, and hsa_circ_0138314 were the significantly downregulated circRNAs confirmed by qRT-PCR. After validation using qRT-PCR, six selected circRNAs were consistent with the RNA-seq data. These differentially expressed circRNAs may be used as biomarkers and therapeutic targets of NPC, while the exact roles of circRNAs requires further investigation.

CircRNAs were encoded from exons and/or introns of their parental genes (27). Our data showed that most of the circRNAs are from exons. Exonic circRNA is generated by the back-slicing process, an out-of-order arrangement of exons (28–30). Hsa_circ_0002375, hsa_circ_0111974, and hsa_circ_0081534 are spliced from KIT ligand (KITLG), estrogen related receptor gamma (ESRRG), and EPH receptor B4 (EPHB4), respectively, which play an essential role in cancer proliferation, metastasis and apoptosis. KITLG is the ligand of the tyrosine-kinase receptor, which is demonstrated as a novel target of miR-34c that inhibited the growth and invasion of colorectal cancer cells (31). ESRRG is a member of the estrogen receptor-related receptor (ESRR) family, which has been identified as a tumor suppressor gene in several cancers (32–36). EPHB4 is one of the EphB subfamily, the largest of receptor tyrosine kinases, which is known to facilitate vascularization in multiple carcinomas and is upregulated in various cancers, including upper aerodigestive cancers (37–40). Based on this, we think that circRNA may participate in development and prognosis of NPC.

According to the GO and KEGG pathway analyses, we explored the biological functions and potential mechanisms of circRNAs in NPC. We found that cell junction and cilium process affect the development of NPC. Moreover, the P53 and Hippo pathway has been shown to be related to the development and prognosis of NPC. CircRNAs, acting as miRNAs sponge, regulate the miRNA to impact cancer development and progress. Therefore, in this study, we predict a relationship between the circRNA and microRNA by *in silico* analyses. For example, the top upregulated circRNA hsa_circ_0002375 (circKITLG) potentially binds miR-3198. Kanzaki H et al. provided experimental evidence for the role of miR-3198 in in periodontal ligament cells through downregulates OPG expression in response to mechanical stress (41). *In vitro* experiments showed that knockdown of circKITLG could inhibit NPC cell proliferation, migration, and invasion. Each of these proves that circRNAs play an important role in NPC. To confirm whether these circRNAs are involved in the development of NPC, further functional and mechanistic studies and a larger cohort of patients are required.

In summary, we found that circRNAs were significantly differentially expressed in NPC compared with normal tissues in this study. CircRNAs play a key role in the development and progress of NPC and regulates cancer-related pathways. This study will help researchers to elucidate the mechanism of NPC tumorigenesis and progression and provide new clinical diagnostic markers and therapeutic targets.

DATA AVAILABILITY STATEMENT

The data in this article can be found in the GEO database with the link: https://www.ncbi.nlm.nih.gov/geo/query/acc.cgi?acc=GSE143797.

ETHICS STATEMENT

The studies involving human participants were reviewed and approved by The Medical Ethics Committee of The First Affiliated Hospital of University of South China. The patients/participants provided their written informed consent to participate in this study. Written informed consent was obtained from the individual(s) for the publication of any potentially identifiable images or data included in this article.

AUTHOR CONTRIBUTIONS

ZL designed this project. JY, YG, QJ, LL, SL, QZ, and FH performed the experiments.

FUNDING

This work was supported by the grants from the Hunan provincial Health and Family Planning Commission (20201947; B20180186), the Hunan Provincial Natural Science Foundation of China (2019JJ50547) and the Hunan Province Science and Technology Department (2017Sk50206).

REFERENCES

1. Chen YP, Chan ATC, Le QT, Blanchard P, Sun Y, Ma J. Nasopharyngeal carcinoma. *Lancet.* (2019) 394:64–80. doi: 10.1016/S0140-6736(19)30956-0
2. Wei F, Wu Y, Tang L, Xiong F, Guo C, Li X, et al. Trend analysis of cancer incidence and mortality in China. *Sci China Life Sci.* (2017) 60:1271–5. doi: 10.1007/s11427-017-9172-6
3. Zhang L, Huang Y, Hong S, Yang Y, Yu G, Jia J, et al. Gemcitabine plus cisplatin versus fluorouracil plus cisplatin in recurrent or metastatic nasopharyngeal carcinoma: a multicentre, randomised, open-label, phase 3 trial. *Lancet.* (2016) 388:1883–92. doi: 10.1016/S0140-6736(16)31388-5
4. Lee AW, Ma BB, Ng WT, Chan AT. Management of nasopharyngeal carcinoma: current practice and future perspective. *J Clin Oncol.* (2015) 33:3356–64. doi: 10.1200/JCO.2015.60.9347
5. Capel B, Swain A, Nicolis S, Hacker A, Walter M, Koopman P, et al. Circular transcripts of the testis-determining gene sry in adult mouse testis. *Cell.* (1993) 73:1019–30. doi: 10.1016/0092-8674(93)90279-Y
6. Wilusz JE, Sharp PA. Molecular biology. A circuitous route to noncoding RNA. *Science.* (2013) 340:440–1. doi: 10.1126/science.1238522
7. Chen Y, Li C, Tan C, Liu X. Circular RNAs: a new frontier in the study of human diseases. *J Med Genet.* (2016) 53:359–65. doi: 10.1136/jmedgenet-2016-103758
8. Sanger HL, Klotz G, Riesner D, Gross HJ, Kleinschmidt AK. Viroids are single-stranded covalently closed circular RNA molecules existing as highly base-paired rod-like structures. *Proc Natl Acad Sci USA.* (1976) 73:3852–6. doi: 10.1073/pnas.73.11.3852
9. Gao Y, Wang J, Zheng Y, Zhang J, Chen S, Zhao F. Comprehensive identification of internal structure and alternative splicing events in circular RNAs. *Nat Commun.* (2016) 7:12060. doi: 10.1038/ncomms12060

10. Guarnerio J, Bezzi M, Jeong JC, Paffenholz SV, Berry K, Naldini MM, et al. Oncogenic role of fusion-circRNAs derived from cancer-associated chromosomal translocations. *Cell.* (2016) 166:1055–6. doi: 10.1016/j.cell.2016.07.035
11. Zhong Y, Du Y, Yang X, Mo Y, Fan C, Xiong F, et al. Circular RNAs function as ceRNAs to regulate and control human cancer progression. *Mol Cancer.* (2018) 17:79. doi: 10.1186/s12943-018-0827-8
12. Zhu M, Xu Y, Chen Y, Yan F. Circular BANP, an upregulated circular RNA that modulates cell proliferation in colorectal cancer. *Biomed Pharmacother.* (2017) 88:138–144. doi: 10.1016/j.biopha.2016.12.097
13. Wang Y, Liu J, Liu C, Naji A, Stoffers DA. MicroRNA-7 regulates the mTOR pathway and proliferation in adult pancreatic beta-cells. *Diabetes.* (2013) 62:887–95. doi: 10.2337/db12-0451
14. Zhong L, Wang Y, Cheng Y, Wang W, Lu B, Zhu L, et al. Circular RNA circC3P1 suppresses hepatocellular carcinoma growth and metastasis through miR-4641/PCK1 pathway. *Biochem Biophys Res Commun.* (2018) 499:1044–9. doi: 10.1016/j.bbrc.2018.03.221
15. Zhong Z, Lv M, Chen J. Screening differential circular RNA expression profiles reveals the regulatory role of circTCF25-miR-103a-3p/miR-107-CDK6 pathway in bladder carcinoma. *Sci Rep.* (2016) 6:30919. doi: 10.1038/srep30919
16. Qiu M, Xia W, Chen R, Wang S, Xu Y, Ma Z, et al. The circular RNA circPRKCI promotes tumor growth in lung Adenocarcinoma. *Cancer Res.* (2018) 78:2839–2851. doi: 10.1158/0008-5472.CAN-17-2808
17. Vo JN, Cieslik M, Zhang Y, Shukla S, Xiao L, Zhang Y, et al. The landscape of circular RNA in cancer. *Cell.* (2019) 176:869–81.e13. doi: 10.1016/j.cell.2018.12.021
18. Chen J, Li Y, Zheng Q, Bao C, He J, Chen B, et al. Circular RNA profile identifies circPVT1 as a proliferative factor and prognostic marker in gastric cancer. *Cancer Lett.* (2017) 388:208–19. doi: 10.1016/j.canlet.2016.12.006
19. Zhang XO, Wang HB, Zhang Y, Lu X, Chen LL, Yang L. Complementary sequence-mediated exon circularization. *Cell.* (2014) 159:134–47. doi: 10.1016/j.cell.2014.09.001
20. Krzywinski M, Schein J, Birol I, Connors J, Gascoyne R, Horsman D, et al. Circos: an information aesthetic for comparative genomics. *Genome Res.* (2009) 19:1639–45. doi: 10.1101/gr.092759.109
21. Enright AJ, John B, Gaul U, Tuschl T, Sander C, Marks DS. MicroRNA targets in Drosophila. *Genome Biol.* (2003) 5:R1. doi: 10.1186/gb-2003-5-1-r1
22. Kruger J, Rehmsmeier M. RNAhybrid: microRNA target prediction easy, fast and flexible. *Nucleic Acids Res.* (2006) 34:W451–4. doi: 10.1093/nar/gkl243
23. Su G, Morris JH, Demchak B, Bader GD. Biological network exploration with Cytoscape 3. *Curr Protoc Bioinformatics.* (2014) 47:8.13.1–24. doi: 10.1002/0471250953.bi0813s47
24. Shang Q, Yang Z, Jia R, Ge S. The novel roles of circRNAs in human cancer. *Mol Cancer.* (2019) 18:6. doi: 10.1186/s12943-018-0934-6
25. Han B, Chao J, Yao H. Circular RNA and its mechanisms in disease: from the bench to the clinic. *Pharmacol Ther.* (2018) 187:31–44. doi: 10.1016/j.pharmthera.2018.01.010
26. Su M, Xiao Y, Ma J, Tang Y, Tian B, Zhang Y, et al. Circular RNAs in cancer: emerging functions in hallmarks, stemness, resistance and roles as potential biomarkers. *Mol Cancer.* (2019) 18:90. doi: 10.1186/s12943-019-1002-6
27. Chen LL, Yang L. Regulation of circRNA biogenesis. *RNA Biol.* (2015) 12:381–8. doi: 10.1080/15476286.2015.1020271
28. Li Z, Huang C, Bao C, Chen L, Lin M, Wang X, et al. Exon-intron circular RNAs regulate transcription in the nucleus. *Nat Struct Mol Biol.* (2015) 22:256–64. doi: 10.1038/nsmb.2959
29. Qu S, Yang X, Li X, Wang J, Gao Y, Shang R, et al. Circular RNA: a new star of noncoding RNAs. *Cancer Lett.* (2015) 365:141–8. doi: 10.1016/j.canlet.2015.06.003
30. He J, Xie Q, Xu H, Li J, Li Y. Circular RNAs and cancer. *Cancer Lett.* (2017) 396:138–44. doi: 10.1016/j.canlet.2017.03.027
31. Yang S, Li WS, Dong F, Sun HM, Wu B, Tan J, et al. KITLG is a novel target of miR-34c that is associated with the inhibition of growth and invasion in colorectal cancer cells. *J Cell Mol Med.* (2014) 18:2092–102. doi: 10.1111/jcmm.12368
32. Dong SS, Guo Y, Zhu DL, Chen XF, Wu XM, Shen H, et al. Epigenomic elements analyses for promoters identify ESRRG as a new susceptibility gene for obesity-related traits. *Int J Obes.* (2016) 40:1170–6. doi: 10.1038/ijo.2016.44
33. Su N, Qiu H, Chen Y, Yang T, Yan Q, Wan X. miR-205 promotes tumor proliferation and invasion through targeting ESRRG in endometrial carcinoma. *Oncol Rep.* (2013) 29:2297–302. doi: 10.3892/or.2013.2400
34. Kim JH, Choi YK, Byun JK, Kim MK, Kang YN, Kim SH, et al. Estrogen-related receptor gamma is upregulated in liver cancer and its inhibition suppresses liver cancer cell proliferation via induction of p21 and p27. *Exp Mol Med.* (2016) 48:e213. doi: 10.1038/emm.2015.115
35. Shen Z, Hu Y, Zhou C, Yuan J, Xu J, Hao W, et al. ESRRG promoter hypermethylation as a diagnostic and prognostic biomarker in laryngeal squamous cell carcinoma. *J Clin Lab Anal.* (2019) 33:e22899. doi: 10.1002/jcla.22899
36. Heckler MM, Thakor H, Schafer CC, Riggins RB. ERK/MAPK regulates ERRgamma expression, transcriptional activity and receptor-mediated tamoxifen resistance in ER+ breast cancer. *FEBS J.* (2014) 281:2431–42. doi: 10.1111/febs.12797
37. Kania A, Klein R. Mechanisms of ephrin-Eph signalling in development, physiology and disease. *Nat Rev Mol Cell Biol.* (2016) 17:240–56. doi: 10.1038/nrm.2015.16
38. Barquilla A, Pasquale EB. Eph receptors and ephrins: therapeutic opportunities. *Annu Rev Pharmacol Toxicol.* (2015) 55:465–87. doi: 10.1146/annurev-pharmtox-011112-140226
39. Pasquale EB. Eph receptors and ephrins in cancer: bidirectional signalling and beyond. *Nat Rev Cancer.* (2010) 10:165–80. doi: 10.1038/nrc2806
40. Chen Y, Zhang H, Zhang Y. Targeting receptor tyrosine kinase EphB4 in cancer therapy. *Semin Cancer Biol.* (2019) 56:37–46. doi: 10.1016/j.semcancer.2017.10.002
41. Kanzaki H, Wada S, Yamaguchi Y, Katsumata Y, Itohiya K, Fukaya S, et al. Compression and tension variably alter Osteoprotegerin expression via miR-3198 in periodontal ligament cells. *BMC Mol Cell Biol.* (2019) 20:6. doi: 10.1186/s12860-019-0187-2

Conflict of Interest: The authors declare that the research was conducted in the absence of any commercial or financial relationships that could be construed as a potential conflict of interest.

frontiers in Oncology

REVIEW
published: 14 May 2020
doi: 10.3389/fonc.2020.00600

Targeting Epstein-Barr Virus in Nasopharyngeal Carcinoma

Pok Man Hau[1], Hong Lok Lung[2], Man Wu[1], Chi Man Tsang[1], Ka-Leung Wong[3], Nai Ki Mak[2] and Kwok Wai Lo[1]**

[1] Department of Anatomical & Cellular Pathology and State Key Laboratory of Translational Oncology, The Chinese University of Hong Kong, Hong Kong, China, [2] Department of Biology, Hong Kong Baptist University, Hong Kong, China, [3] Department of Chemistry, Hong Kong Baptist University, Hong Kong, China

Nasopharyngeal carcinoma (NPC) is consistently associated with Epstein-Barr virus (EBV) infection in regions in which it is endemic, including Southern China and Southeast Asia. The high mortality rates of NPC patients with advanced and recurrent disease highlight the urgent need for effective treatments. While recent genomic studies have revealed few druggable targets, the unique interaction between the EBV infection and host cells in NPC strongly implies that targeting EBV may be an efficient approach to cure this virus-associated cancer. Key features of EBV-associated NPC are the persistence of an episomal EBV genome and the requirement for multiple viral latent gene products to enable malignant transformation. Many translational studies have been conducted to exploit these unique features to develop pharmaceutical agents and therapeutic strategies that target EBV latent proteins and induce lytic reactivation in NPC. In particular, inhibitors of the EBV latent protein EBNA1 have been intensively explored, because of this protein's essential roles in maintaining EBV latency and viral genome replication in NPC cells. In addition, recent advances in chemical bioengineering are driving the development of therapeutic agents targeting the critical functional regions of EBNA1. Promising therapeutic effects of the resulting EBNA1-specific inhibitors have been shown in EBV-positive NPC tumors. The efficacy of multiple classes of EBV lytic inducers for NPC cytolytic therapy has also been long investigated. However, the lytic-induction efficiency of these compounds varies among different EBV-positive NPC models in a cell-context-dependent manner. In each tumor, NPC cells can evolve and acquire somatic changes to maintain EBV latency during cancer progression. Unfortunately, the poor understanding of the cellular mechanisms regulating EBV latency-to-lytic switching in NPC cells limits the clinical application of EBV cytolytic treatment. In this review, we discuss the potential approaches for improvement of the above-mentioned EBV-targeting strategies.

Keywords: nasopharyngeal carcinoma, Epstein-Barr virus, EBNA1, cytolytic therapy, LMP1, BZLF1

OPEN ACCESS

Edited by:
Jun Ma,
Sun Yat-sen University Cancer Center (SYSUCC), China

Reviewed by:
Gaurisankar Sa,
Bose Institute, India
Lin Feng,
Sun Yat-sen University, China

***Correspondence:**
Hong Lok Lung
hllung2@hkbu.edu.hk
Kwok Wai Lo
kwlo@cuhk.edu.hk

Specialty section:
This article was submitted to Head and Neck Cancer, a section of the journal Frontiers in Oncology

Received: *03 January 2020*
Accepted: *01 April 2020*
Published: *14 May 2020*

Citation:
Hau PM, Lung HL, Wu M, Tsang CM, Wong K-L, Mak NK and Lo KW (2020) Targeting Epstein-Barr Virus in Nasopharyngeal Carcinoma. Front. Oncol. 10:600. doi: 10.3389/fonc.2020.00600

INTRODUCTION

Nasopharyngeal carcinoma (NPC) is a malignant epithelial tumor affecting the lining of lymphocyte-rich nasopharyngeal mucosa. It is a distinct type of head and neck cancer, and its unique pathogenesis is influenced by multiple etiological factors such as genetic predisposition, diet, and Epstein-Barr virus (EBV) infection (1–3). Although NPC is rarely found in most parts

of the world, it is prevalent in Southern China and Southeast Asia. There are up to 25 cases per 100,000 men in some parts of Southern China such as Zhong Shan City, Zhuhai, and Jiangmen. The high prevalence of NPC in these endemic regions implies that there are genetic and environmental factors that predispose individuals in these regions to develop this cancer (2, 3).

Notably, the strongest association with NPC risk has been consistently found in several variants of major histocompatibility complex (MHC) class I genes (4). Epidemiology studies have also documented dietary risk factors, such as consumption of salted fish or other preserved foods. The remarkable decrease of NPC incidence in some modern cities in endemic regions, such as Hong Kong, points to the effectiveness of changes in dietary habits for reducing exposure to these potential carcinogens (2, 5). Unlike other head and neck squamous carcinomas (HNSCCs), the major histological type of NPC is non-keratinizing carcinoma, either poorly or undifferentiated, showing characteristic features of rich lymphocytic infiltration and EBV infection. The link between EBV and NPC has been well-established by the fact that EBV DNA or transcripts are invariably detected in tumor cells, as well as the presence of a clonal EBV genome in NPC and precancerous lesions (6, 7). Next-generation sequencing-based studies have recently revealed that certain prevalent EBV strains are associated with an increased risk of NPC in Southern Chinese (8, 9). Strikingly, a link was found between EBV viral genomic variation and reportedly NPC-susceptible single nucleotide polymorphisms (SNPs) at the HLA locus (9). This new finding suggests that there is a complex interaction of genetic and viral factors involved in the pathogenesis of NPC.

The therapeutic management of NPC is based on the disease stage, according to the National Comprehensive Cancer Network guidelines (v. 2.2018). Radiotherapy (RT) alone is the major therapeutic strategy to manage early-stage disease (Stage I); RT in combination with concurrent chemotherapy (CRT) is used to manage intermediate (Stage II) to advanced stages of NPC (Stages III-IV) (2). According to a clinical study in Hong Kong, patients with early-stage NPC have favorable clinical outcomes and their survival rates with standalone RT are encouraging, with a 5-year overall survival rate of ∼90% (10). The adoption of intensity-modulated radiotherapy (IMRT) combined with conformal radiotherapy, which improves the diametric properties and reduces the toxicity of irradiative treatment, further significantly improves the locoregional control of NPC and the overall survival rate of patients (2, 11).

Nevertheless, >60% of newly diagnosed patients have a poor clinical outcome, as they usually present with advanced-stage disease. Most NPC patients will later develop loco-regional (5–15%) and distant treatment failures (15–30%) (2, 12). Furthermore, half of the patients with local recurrence also experience concurrent distant metastasis. In addition, ∼30% of patients with late-stage disease will experience distant recurrence following intensive concurrent CRT (2, 13).

Currently, the treatment of recurrent and metastatic NPC is challenging, and the clinical outcomes remain uncertain, possibly due to the profound heterogeneity of patients. Recent clinical studies of various new treatment strategies such as palliative systemic chemotherapy (e.g., gemcitabine plus cisplatin), targeted molecular therapies (e.g., VEGFR and EGFR inhibitors), and immunotherapies (e.g., adaptive T-cell therapy and immune checkpoint blockades) for controlling the progression of disease have shown a range of success rates (2, 12–14). Although the genomic landscape of NPC has recently been defined, disappointingly only a subset of NPC cases (>10%) was found to harbor immediately druggable somatic events, such as alterations of PIK3CA, FGFR3, and JAK1/2 (3, 15, 16). Moreover, the clinical benefits of the approved drugs targeting these potential oncogenic mutations still need to be confirmed in these patients. The discovery of frequent somatic alterations of MHC class I molecules also suggests that most NPC patients develop resistance to T-cell-based immunotherapy (3, 15). Thus, it is vital that effective therapeutic strategies are developed to address the unique features and specific molecular targets of NPC, to enable eradication of this deadly disease.

EBV INFECTION IN NPC

EBV, also known as human gammaherpesvirus 4, is a double-stranded DNA virus with a 170–180 kb genome that encodes nearly 100 genes for either latent or lytic infection of host cells. During the latent phase of infection, the viral genome remains episomal and expresses a group of latent genes (>10) for modulating various cellular mechanisms and exploiting host DNA polymerases for DNA replication. In contrast, lytic infection results in the expression of >80 lytic proteins and the extracellular release of viral particles during mandatory cell death.

Globally, over 90% of adults are healthy carriers of lifelong EBV infection, although the virus is now classified as a group I carcinogen. In healthy carriers, primary infection is followed by the persistence of EBV latency in only a few memory B-cells, and is under the control of the host's immune system. Nevertheless, the virus contributes to tumor initiation and clonal expansion of infected lymphoid and epithelial cells by inducing specific genetic/epigenetic changes (such as c-myc translocation and loss of *CDKN2A/p16*) or impairing host immune system (6, 17).

EBV is the first oncogenic virus identified in human cancer, and is etiologically linked to a remarkably wide range of human lymphoid malignancies (such as Burkitt lymphoma, classic Hodgkin lymphoma, B-cell lymphoma, and nasal NK/T-cell lymphoma), two distinct types of epithelial cancer, gastric cancer (GC), and NPC. Among the 200,000 new cases of EBV-associated cancers reported annually worldwide, 84,000 and 78,000 are GC and NPC, respectively. Nevertheless, EBV-associated GCs represent only ∼10% of all gastric cancers and are not endemic. In the endemic regions, such as Hong Kong and Southern China, almost all NPCs are of the non-keratinizing subtype, which is consistently associated with EBV infection (17, 18).

For the past three decades, studies have revealed that NPC tumorigenesis is driven by EBV infection and a combination of multiple genetic aberrations. It is believed that NPC is a clonal malignancy derived from a single progenitor cell that was latently infected with EBV (1, 3, 7). This is evidenced by the fact that

all episomal EBV genomes within NPC cells contain the same number of terminal repeats (TRs), which can only result from latent replication of EBV from one progenitor cell. However, in the EBV lytic cycle and its subsequent infection of epithelial cells, the linearized EBV genomes from the infectious virions undergo circularization by random joining of the TRs to form episomes, resulting in various numbers of TRs being present in each EBV episome within the latently infected cells (19, 20).

In an early study by Pathmanathan et al. (20), both EBV latent gene products (e.g., *EBERs* and LMP1) and homogeneous lengths of TR repeats were detected in NPC and precancerous lesions, suggesting that the clonal latent EBV infection is a crucial event in the initiation of this virus-associated cancer (20). Furthermore, our earlier genomic and functional studies have indicated that several specific genetic alterations (such as inactivation of *CDNK2A/p16* and tumor suppressors at chromosome 3p) in the premalignant nasopharyngeal epithelium support a cellular switch to state that maintains persistent latent EBV infection and predisposes individuals to NPC transformation (21–23). Indeed, persistent EBV latent infection and expression of latent viral genes are essential for NPC development. A type II latency program is observed in NPC, in which *EBER1/2*, EBNA1, LMP1, LMP2, BARF1, and multiple splicing non-coding RNAs and a number of miRNAs in *BART* regions are expressed. Several latent genes, such as *LMP1* and *LMP2*, are heterogeneously expressed in the tumor or during progression, while *EBERs* and *EBNA1* are consistently detected in all cancer cells (6, 18).

Notably, although loss of the EBV genome has been reported during long-term passage of some NPC cell lines *in vitro*, latent EBV infection is consistently detected in every tumor cell in patient-derived xenograft (PDX) models and clinical NPC specimens, in both primary or recurrent cases (6, 18, 24, 25). The continued presence of an episomal EBV genome and the requirement of multiple viral gene products for malignant transformation have been shown as key features of EBV-associated NPC.

Studies have also shown that multiple viral latent genes contribute to NPC tumorigenesis by generating various hallmarks of cancer. The oncogenic properties of these latent gene products and their contribution to NPC tumorigenesis have been extensively studied in epithelial cell lines over the past three decades (6, 18). Among these latent gene products, EBNA1 is the only protein that is expressed in all of the EBV-associated cancers: it is essential for governing the replication and mitotic segregation of the EBV episomes, thereby maintaining EBV genomes in latently infected cells. In addition, there is emerging evidence that EBNA1 plays roles in promoting cell survival upon DNA damage, inducing genetic instability and transcriptionally activating various cellular genes (26).

In addition to EBNA1, abundant non-polyadenylated RNAs, such as *EBER1* and *EBER2*, are also detected in all EBV-positive cancer cells. In latent infected epithelial cells, *EBERs* bind to auto-antigen La and ribosomal protein L22 to form ribonucleoprotein particles. This complex then binds to the PKR to prevent Fas-mediated apoptosis (27). Furthermore, these non-coding RNAs were also shown to promote tumor growth by stimulating secretion of autocrine insulin-like growth factor (IGF-1) and activating the NF-κB pathway via retinoic acid-inducible gene-1 (RIG-1) and toll-like receptor 3 (TLR3) signaling (28–30).

In NPC cells, multispliced long non-coding transcripts and viral miRNAs from the *BamH1 A* region of the EBV genome are abundantly expressed. As described in recent reviews, EBV-encoded miRNAs, *miR-BARTs*, target multiple viral and cellular genes to facilitate EBV latency, promote cell proliferation, enhance invasiveness, induce genome instability, inhibit apoptosis, and impair host immune response (6, 31, 32). Recent studies have also revealed that long non-coding RNAs (e.g., *RPMS1*) may epigenetically regulate cellular gene expression and maintain EBV latency by interfering with chromatin remodeling machinery, subsequently contributing to NPC tumorigenesis (33, 34). A BARF1 protein encoded by the *Bam H1-A* fragment is a homolog of human colony-stimulating factor 1 (CSF1) receptor, and this secreted viral protein is believed to enhance NPC tumorigenicity through activation of the CSF-1 signaling axis, suppression of apoptosis by activation of BCL-2, and upregulation of expression of NF-κB, RelA, and cyclin D1 (35).

LMP1 is a key EBV-encoded oncoprotein that functions as a potent activator of multiple signaling cascades, such as NF-κB, MAPK, JNK/AP1, and PI3K, to generate multiple cancer hallmarks (7, 36). Although LMP1 is only highly expressed in a subset of NPC specimens, the occurrence of LMP1 in preinvasive lesions implicates its contribution in transforming nasopharyngeal epithelial cells and tumor initiation (15, 20). LMP1 may enhance self-renewal properties and thus promote a cancer progenitor-like cell phenotype in a subpopulation of cancer cells, thereby driving the progression of NPC (36–38). LMP2A is another integral membrane protein that promotes stem-like properties and various oncogenic phenotypes by regulating multiple signaling pathways, such as PI3K/AKT, ERK, and RhoA (36, 38, 39). Unlike LMP2A, the function of LMP2B, which is encoded by an alternative first exon of the LMP2 gene, remains unclear.

Given the above oncogenic properties of EBV latent gene products and the unique virus-cell interactions, targeting these latent proteins and inducing lytic reactivation are thought to be possible approaches to cure this viral-associated epithelial cancer.

TARGETING EBV LATENT PROTEINS

The viral-encoded latent proteins EBNA1, LMP1, and LMP2 are expected to be potential therapeutic targets in NPC cells. The function of EBNA1 has been intensively studied because of its consistent expression in every tumor cell and its essential role in the maintenance of the EBV episomal genome. Indeed, the consistent expression and the biological importance of EBNA1 in viral DNA maintenance, replication, and segregation during viral latency and lytic reactivation make the EBNA1 protein a key therapeutic target. Research efforts over the past decade indicate that EBNA1 is a druggable protein, and selective agents targeting the DNA-binding site or dimerization interface have demonstrated efficacy in animals. The protein sequence of EBNA1 has little similarity to the cellular protein of the host,

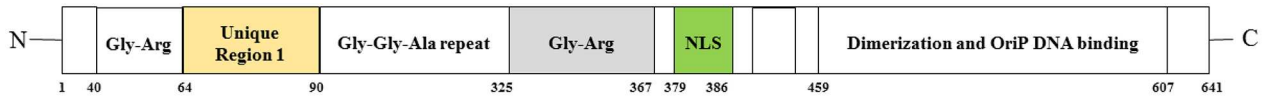

EBNA1 - RNA interaction	Zn coordination	Translational inhibition	EBNA1 - RNA interaction	DNA bind sites	Dimerization site
BRACO-19	ZRL_5P_4	PyDH2 and PhenDH2	BRACO-19	SC7, SC11, SC19, SC27	EiK1
				LB2, LB3, LB7	JLP2
				DSE3	L2P4
Netropsin			Netropsin	H31	ZRL_5P_4

FIGURE 1 | Functional regions in EBNA1. **(Upper)** Domains of EBNA1. NLS, nuclear localization sequence. **(Lower)** Agents reported to inhibit these domains. Refer to text for details.

except the reported similarities between the EBNA1 epitopes (PPPGMRPP and (GR)x) and the common human antigenic targets of the lupus autoantigens (Sm B'(PPPGMRPP) and Sm D1 (GR)x) (40). Nevertheless, it is expected that the off-target effect of a well-designed EBNA1-targeting agent would be minimal.

Therapeutic Targeting of EBNA1

It is now clear that EBNA1 interacts with certain host cell components to establish viral latency and mediate oncogenic transformation of the host cells (26, 41). EBNA1 is also considered to be a unique episome maintenance protein (42); several regions contributing to these processes have been identified (**Figure 1**). Early studies showed that EBNA1 siRNA could inhibit the growth of EBV-positive epithelial tumors and increase lytic DNA replication (43, 44). With the recent advances in the understanding of the structural biology of EBNA1, emerging evidence indicates that both EBNA1 dimers and oligomers participate in the control of viral latency. Here, we review the approaches that have been examined for the disruption of EBNA1 functions and the feasibility of targeting EBNA1 for treatment EBV-associated diseases (**Figure 2**, **Table 1**).

Interfere the RNA-Binding Function of LR1 and LR2 Regions in the EBNA1 Protein

The linking regions LR1 (amino acids 40–89, also known as GR1) and LR2 (amino acids 325–379, also known as GR2) are arginine- and glycine-rich regions that resemble the RGG motifs for RNA binding. It has previously been demonstrated that EBNA1 recruits the cellular origin recognition complex (ORC) to origin of replication (oriP) for episome maintenance or replication initiation (52). The recruitment of ORC to the dyad symmetry (DS) of oriP occurs through an RNA-dependent interaction with the RGG-like motifs in LR1 and LR2 (53). A subsequent study showed that LR1 and LR2 can bind to G-quadruplex-structured G-rich RNA (54). BRACO-19 is a G-quadruplex-interactive molecule. Norseen and coworkers further demonstrated that BRACO-19 could disrupt the tethering of EBNA1 to the metaphase chromosomes, indicating that G-quadruplex-interactive molecules may be developed as inhibitors of the LR1/LR2-dependent viral DNA attachment and replication in EBV-infected cells.

Interfere the Binding of LR1 and LR2 Regions Containing AT-Rich DNA

In addition to RNA binding, both the LR1 and LR2 regions have been shown to contain an AT-hook DNA-binding domain for the tethering of EBNA1 to chromosomal DNA. In LR1, the domain ATH1 (amino acids 40–54) resembles the AT-hook of high mobility group A (HMGA) protein (55). Sears and coworkers previously demonstrated that the ability of EBV to stably replicate and partition oriP plasmids correlates with the AT hook activity of EBNA1 (56). Chakravorty and Sugden further demonstrated that a small molecule, netropsin, not only inhibits the AT-hook DNA-binding activity of EBNA1 *in vitro* but also forces the loss of EBV genomes in an AT-hook dependent manner in epithelial and lymphoid cells (57). The results from these studies suggested that small molecule-based pharmacological blockade of AT-hook activity may effectively perturb the viral latency in EBV-infected cancer cells.

Target the Glycine-Alanine Repeats (GAr) Region of EBNA1 mRNA

The ability of EBV-latently infected cells to evade immune recognition is attributed to the presence of glycine-alanine repeats (GAr) in EBNA1. GAr (amino acids 90–325) is located near the N-terminal of EBNA1. Previous studies indicated that nascent GAr has the capacity to suppress the translation of its own mRNA *in cis* (58). The suppression of initiation of mRNA translation by GAr can also prevent the presentation of antigenic fragments generated from EBNA1 by class I MHC molecules (59). Hence, GAr-based reduction of translation of EBNA1 has been implicated as a relevant therapeutic target in EBV-latently infected cells.

Using a yeast-based genetic screening assay, Lista and coworkers found that nucleolin can directly interact with G-quadruplexes formed in GAr-encoding *EBNA1* mRNA. Furthermore, the process of GAr-mediated inhibition of EBNA1

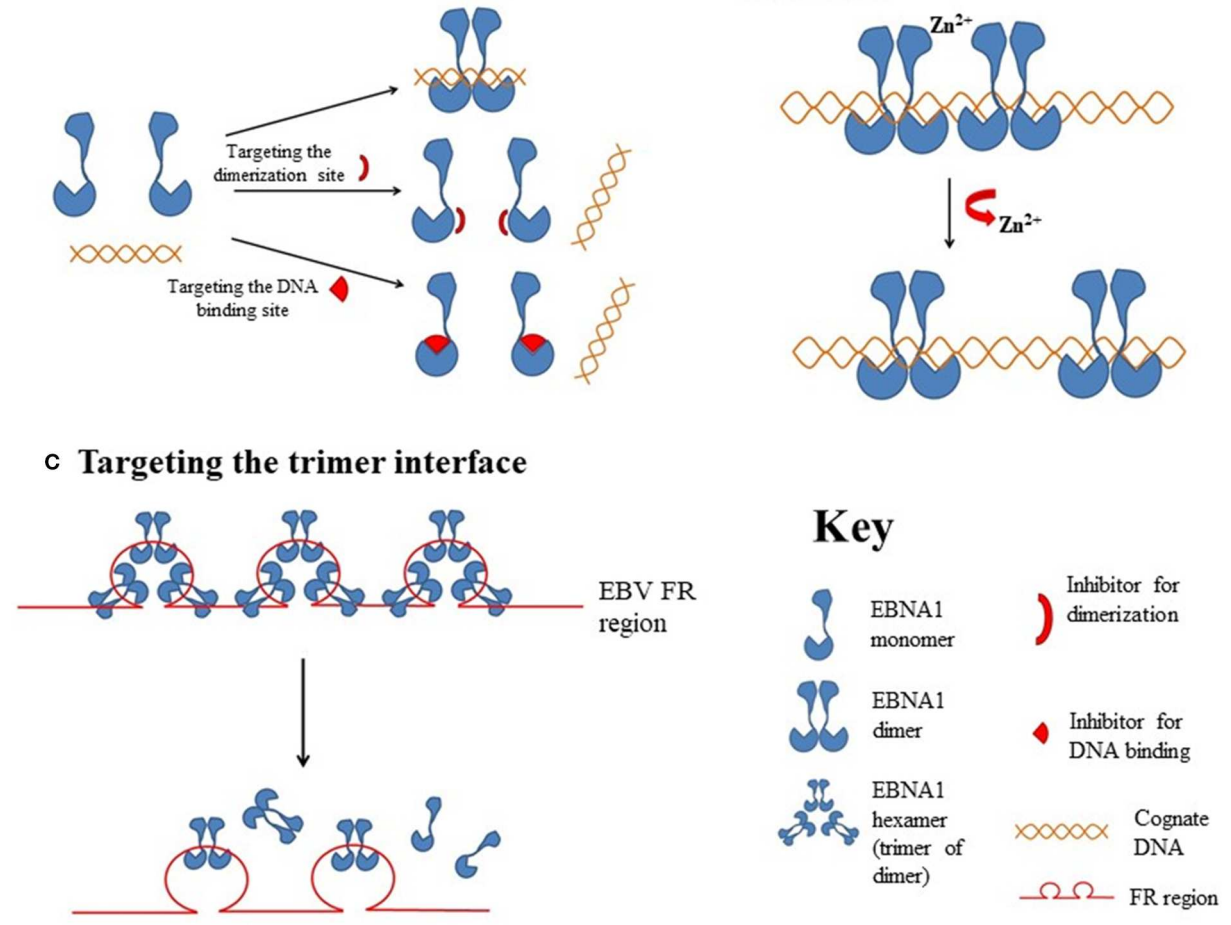

FIGURE 2 | Hypothetical diagrams of the EBNA1-targetable sites for therapeutic intervention. **(A)** Targeting the DNA binding or dimerization site of EBNA1. **(B)** Disruption of the EBNA1 dimer-dimer formation. **(C)** Targeting of the EBNA1 trimer interface.

expression and antigen presentation can be reversed by blocking the binding of nucleolin to *EBNA1* mRNA with G-quadruplex ligand PhenDC3 (60). Subsequently, a series of cationic bis(acylhydrazone) derivatives, representing shape analogs of PhenDC3, were synthesized and tested. Two compounds, PyDH2 and PhenDH2, were found to enhance the expression of EBNA1 in H1299 cells in a GAr-dependent manner (61). The results from these studies indicated that interruption of the interaction between nucleolin and GAr of EBNA1 mRNA for the restoration of immune recognition of infected cells may be a therapeutic strategy for the treatment of NPC.

Target the DNA Binding/Dimerization Site of EBNA1

The DNA-binding domain of EBNA1 is located between amino acids 459 and 598, near its C-terminal (62, 63). Under native conditions, EBNA1 exists as a dimer (64), and EBV replication and EBNA1 transactivation depend on the formation of an EBNA1 dimer and the binding of the dimer to EBV DNA. Crystallographic studies of the DNA-binding region of the EBNA1 protein revealed that this region has two structural domains: a core domain for EBNA1 dimerization and sequence-specific DNA interaction, and a flanking domain for DNA contact (45).

In early studies using a high-throughput virtual screen of 90,000 low molecular weight compounds, Li and coworkers demonstrated that a series of four compounds (SC7, SC11, SC19, and SC27) with an IC50 of ∼20 μM could physically inhibit EBNA1-DNA binding and reduce the number of EBV episomes in latently infected cells (65). Using a fluorescence polarization-based EBNA1/DNA binding high-throughput screening method, Thompson and coworkers, from the same group, identified several small-molecule inhibitors (LB2, LB3, and LB7 and LC7) from a library of 14,000 molecules that could selectively inhibit the binding of EBNA1 to DNA (46). In further studies using a fragment-based approach and X-ray crystallography, Messick and coworkers developed a series of 2,3-disubstituted benzoic

TABLE 1 | Therapeutic targeting of EBNA1 dimerization or multimerization.

Proposed targeting site	Remarks	References
DNA-binding site	• Molecular docking interaction analysis of compounds SC7 and SC19 identified several crucial residues such as Arg469 and Tyr518 of EBNA1	(45)
DNA-binding site	• Fragment-based approach and X-ray crystallography • A 2,3-disubstituted benzoic acid series that selectively inhibits the DNA-binding activity of EBNA1 • Suppresses tumor growth *in vivo*	(46)
Dimerization site	• Interruption by an engineered peptide $_{561}$YFMVF$_{565}$ with NLS RrRK. RrRK forms a salt with D_{602} • Suppresses tumor growth *in vivo*	(47)
Dimerization site	• A Zn^{2+} chelator conjugated with EBNA1-binding $_{561}$YFMVF$_{565}$ and NLS RrRK peptide • Inhibits EBNA1 oligomerization, suppresses tumor growth *in vivo*	(48)
Dimer-dimer interface	• At DS half-site • H-bond network involving residues R491 and D581	(49)
Dimer-dimer interface coordinated by Zn	• *In silico* protein structure modeling • Two conserved cysteine residues (Cys79 and Cys82) coordinate Zn^{2+} and facilitate the multimeric interactions	(50)
Interface between dimer and hexamer (trimer of dimers)	• EBNA1 forms hexamer at FR and hexamers stack to form an array of multiple hexagonal wheel. Essential for the maintenance of episome and latent infection • T585 is critical for the H-bonding network with adjacent residues as well as with residues from adjacent EBNA1 molecules	(51)

NLS, nuclear localization sequence; DS, dyad symmetry; FR, family of repeats.

acids that could selectively inhibit the DNA binding activity of EBNA1, and also suppress the growth of EBV-positive tumors in xenograft models (66). One of the inhibitors, VK-2019, is now in Phase I/IIa clinical trial (NCT03682055) in patients with EBV-positive NPC.

Most protein-protein interfaces are relatively flat, which means these sites are difficult to target with small-molecule drugs. Nonetheless, various protein-protein interfaces, such as dimerization interfaces, have emerged as a class of druggable targets (67–69). In EBNA1, interaction between dimerization interfaces is essential not only for the formation of EBNA1 dimer but also for the subsequent formation of the dimer-DNA complex, which makes the dimerization interface an attractive therapeutic target. A previous study showed that a short EBNA1 peptide (P85) covering amino acids 560–574 could effectively inhibit homodimerization of EBNA1 (47), and a peptide with a sequence of V_{560}CYFMVFL$_{566}$Q could substantially inhibit EBNA1- and oriP-dependent transcription of SEAP (secreted embryonic alkaline phosphatase) reporter in cells in a dose-dependent manner. Regarding the development of inhibitors for the dimerization interface, Jiang and coworkers demonstrated that a chemical probe consisting of nuclear localization sequence RrRK and the YFMVF motif could reduce the *in vitro* formation of EBNA1 dimer and inhibit *in vivo* growth of EBV-positive NPC (49).

EBNA1 Oligomers as Potential Targets

In addition to perturbing the functions of the EBNA1 dimer, interfering the formation of EBNA1 oligomers is another potential approach for disturbing EBV latency. The presence of two functionally distinct oligomeric states of EBNA1, namely a dimer-dimer and a trimer of dimers (hexamer), has recently been reviewed (42). According to the crystal structure of two "EBNA1 DNA-binding domain dimers" binding to a DS half-site, Lieberman and coworkers found that the dimer-dimer interface involves amino acids R491 and D581 and a hydrogen-bonding (H-bonding) network (70). Disruption of this interface could destabilize the formation of the dimer-dimer complex on the EBV DNA and subsequently impair the recruitment of MCM2 complex to oriP. The results from that study indicated that this dimer-dimer interface may be druggable by EBNA1-specific targeted therapeutic.

An early study showed that the unique region 1 (UR1) dimerizes upon coordinating with a zinc ion (Zn^{2+}) through a pair of essential cysteines within this region, and disruption of the zinc coordination prevented self-association and EBNA1-dependent transcriptional activity (50). In a computational study, full-length EBNA1 was used to develop monomeric and dimeric models (51). Hussain et al. found that adjacent dimers could link through Zn^{2+}, and that the bonding of Zn^{2+} with the N-terminal cysteines would facilitate the multimerization of the EBNA1 dimers. The results from these studies suggested that disruption of Zn^{2+} coordination might be an approach to prevent the oligomerization and the subsequent functions of EBNA1.

Apart from the formation of dimer-dimer complexes, the results from X-ray crystallographic studies show that EBNA1 may form a higher-order complex, namely a hexamer (trimer of dimers), as mentioned above (71). The formation of a hexameric structure at the family of repeats (FR) of oriP appears to be essential for the long-term maintenance of the EBV episomes. Among the trimer interface residues, namely R496, Q530, L582, M584, and T585, the last appears to be critical for the H-bonding network with both adjacent residues and adjacent EBNA1. As a T585 polymorphism is frequently found in Burkitt lymphoma and NPC, and the trimer interface is important for the maintenance of EBNA1 hexamer, this recently discovered interface may be another novel target for the disruption of the biological functions of EBNA1 multimers (72).

Development of EBNA1-Based Theranostic Agents

Theranostics is an innovative treatment modality that combines both diagnosis and targeted therapy, in the form of a single theranostic agent. Addition of an imaging moiety to the molecularly targeted agent would greatly facilitate the monitoring of the drug inside the cells or animal models. As mentioned above, EBNA1 is the only viral protein expressed in all EBV-infected cells, despite the existence of different latency types. The homodimerization of EBNA1 is known to be critical for EBNA1 to carry out all its major functions, such as viral DNA replication, segregation and maintenance of the EBV genome, and transcriptional activation/repression. In an early study, two types of inhibitors (peptide inhibitor P85, and small chemical inhibitor Eik1) were designed to target the DNA-binding/dimerization domain of EBNA1 (47). P85 contains a short EBNA1-derived β3 sheet (amino acids 560–566) that can target the region of the EBNA1 dimerization domain (amino acids 560–574). These EBNA1 inhibitors cannot be visualized inside the cells, and have low bioavailability due to their poor water solubility; to overcome this, we constructed a novel hybrid system containing a charged, water-soluble chromophore and an EBNA1-specific binding peptide $\mathbf{P_2}$, which was derived from the $Y_{561}FMVF_{565}$ amino acid residues of EBNA1 (73). This water-soluble chromophore-peptide bio-conjugate, $\mathbf{JLP_2}$, enables both simultaneous imaging and inhibition of EBNA1 *in vitro* in EBV-infected tumor cells. $\mathbf{JLP_2}$is the first generation of our EBNA1 dual-function bioprobes, and its cellular uptake can be evaluated directly by fluorescence detection; this is likely due to its slightly enhanced emission when bound to EBNA1, which disrupts EBNA1 formation, as indicated by cell-free assays. However, $\mathbf{JLP_2}$ lacks a specific subcellular location and is unable to penetrate the nucleus, and also does not show a significant responsive-binding fluorescent signal, which limits its further utility as an EBV-specific inhibitor.

A Nuclear Localizing EBNA1-Based Theranostic Agent: L_2P_4

Our subsequent study solved the problem of targeting the nuclear EBNA1 protein by incorporating a nuclear localization sequence (NLS) of the amino acid residues RrRK into the C-terminus of the penta-peptide $\mathbf{P_2}$(YFMVF). The resulting $\mathbf{P_4}$ (YFMVF-GG-RrRK) can occupy the first EBNA1 dimerization interface within the DNA-binding domain DBD (48, 49). The NLS sequence in $\mathbf{P_4}$ can form salt bridges with the adjacent dimerization interface, including several residues in the aspartate-rich tail of EBNA1 (D_{602}, D_{601}, D_{605}), which further enhances the interaction between $\mathbf{P_4}$and the EBNA1 monomer.

The fluorophore $\mathbf{L_2}$ was coupled with $\mathbf{P_4}$ to form the second-generation EBNA1 bioprobe $\mathbf{L_2P_4}$, which generates a responsive fluorescent signal when it binds with EBNA1 via induction of intermolecular charge transfer (ICT) in the **L2** fluorophore molecule. Confocal live-cell imaging clearly showed that the presence of NLS in $\mathbf{L_2P_4}$ enabled its penetration into the nuclei of EBV-positive cells, but not EBV-negative cells. $\mathbf{L_2P_4}$ can also significantly interfere with the EBNA1 dimerization, and it only inhibits the *in vitro* tumor-cell growth (leading to *in vivo* tumor suppression) of EBV-infected cells, and not of EBV-negative cells. The therapeutic potential of $\mathbf{L_2P_4}$ in EBV-associated malignancies is therefore evident.

L_2P_4-Based Lanthanide Upconversion Nanoparticles

To further enhance the stability of the EBNA1-binding peptide $\mathbf{P_4}$, to prolong its fluorescent lifetime and to minimize interference by biological autofluorescence, $\mathbf{P_4}$was conjugated with the lanthanide upconversion nanoparticles (UCNPs) $NaGdF_4$:Yb^{3+} and Er^{3+}@$NaGdF_4$ to form $\mathbf{UCNP\text{-}P_4}$ (74). Lanthanide-mediated upconversion is a well-known photophysical phenomenon characterized by the generation of high-energy photon/emission from low-energy photon/excitations. The $\mathbf{P_4}$peptide gained improved stability and biocompatibility from the solid support of UCNPs, which are quenched by the coating of $\mathbf{P_4}$ molecules, thus inducing aggregation of the UCNPs upon physical interaction with the EBNA1 protein molecules. This unique mechanism results in responsive UCNP emission and improves the signal-to-noise ratio for imaging purposes, while the original functions of $\mathbf{P_4}$, such as inhibition of EBNA1 dimerization and cytotoxicity to EBV-infected cells/tumors, are maintained.

L_2P_4-Based Zn^{2+} Binding Theranostic Agent ZRL_5P_4

A previous study indicated that Zn^{2+} is necessary for EBNA1 to dimerize and activate the *oriP*-enhanced transcription (50). Thus, we further modified the EBNA1-targeting peptide $\mathbf{P_4}$ by incorporating a zinc chelator (**ZRL5**) into the EBNA1-binding peptide $\mathbf{P_4}$, forming in $\mathbf{ZRL_5P_4}$ (75). $\mathbf{ZRL_5P_4}$ can respond independently to its interactions with Zn^{2+} and EBNA1 by emitting different fluorescence. $\mathbf{ZRL_5P_4}$ was shown to strongly bind EBNA1 and to have specific *in vitro* and *in vivo* growth-suppressive activities in EBV-positive NPC cells.

Interestingly, $\mathbf{ZRL_5P_4}$ could also selectively inhibit EBNA1 oligomerization, which occurs in the presence of Zn^{2+}, while this new probe had little effect on dimer formation. That is, although $\mathbf{L_2P_4}$ could completely suppress the dimerization in the absence of Zn^{2+}, its suppression of dimerization was only partial when Zn^{2+} was present, indicating that Zn^{2+} can assist the dimerization. Indeed, it was suggested that the N-terminal UR1 domain in EBNA1 is the second dimerization site, via the coordination of Zn^{2+}, beside the DBD (50). This is supported by our dot-blot binding assay showing that $\mathbf{ZRL_5P_4}$ could interact with UR1 to disrupt the oligomerization (unpublished observation), whereas $\mathbf{L_2P_4}$ showed no interaction and could not interfere with the multimerization, indicating that UR1 is responsible for a higher-order EBNA1 structure.

A fluorescent signal was emitted when $\mathbf{ZRL_5P_4}$ bound with EBNA1, and its interaction with both UR1 and DBD might explain why $\mathbf{ZRL_5P_4}$ could bind with EBNA1 and remain in the nuclei more than $\mathbf{L_2P_4}$. Furthermore, $\mathbf{ZRL_5P_4}$ can disrupt transactivation and induce EBV reactivation more potently than $\mathbf{L_2P_4}$, suggesting that EBNA1 oligomers are more important than the dimer in some of EBNA1's functions (75). Importantly, we found that treatment with $\mathbf{ZRL_5P_4}$ alone could reactivate EBV lytic induction by expressing the early and late EBV lytic genes and proteins. $\mathbf{ZRL_5P_4}$ can also specifically elevate Dicer1 and PML expression, molecular events that have been reported

to occur after the depletion of EBNA1 expression in EBV-infected cells (44, 76). Lytic induction is likely mediated by disruption of EBNA1 oligomerization and the subsequent change of Dicer1 expression.

To the best of our knowledge, **ZRL_5P_4** represents the first specific agent to disrupt the EBNA1 protein and to potently reactivate EBV from latency, leading to tumor cell lysis and/or induction of viral proteins that presumably can be targeted by immune cells and antiviral agents to eliminate EBV-infected tumor cells. Importantly, this study also suggests the EBNA1 oligomerization is associated with the maintenance of EBV latency.

EBNA1-Specific Gene Therapy

The consistent expression of EBNA1 in all latently infected cells is a unique feature of EBV-associated cancers, and has prompted researchers to investigate whether EBNA1-driven gene expression could be used as an EBV-specific targeted gene therapy for NPC. In 2002, Li et al. reported the first establishment of a recombinant adenovirus with wild-type p53 cloned downstream of the FR regions. Using this adenoviral vector, they successfully induced wild-type p53 expression in the EBV-positive NPC cell line C666-1 (77). The specific EBNA1-driven p53 expression retarded cell growth and induced apoptosis. Moreover, the combination of EBNA1-driven p53 expression and ionizing radiation decreased cancer-cell viability synergistically in both *in vitro* and *in vivo* NPC models, and the precise triggering of p53 expression on EBV-associated cells spared normal cells, leaving them unaffected.

The same research group has exploited such EBNA1-specific adenoviral vectors, confirming the utility of these constructs for inducing expression of BimS proapoptotic factor and FASL death ligand for effective treatment of NPC (78, 79). They have also generated a conditionally replicating adenovirus (CRA), adv.oriP.E1A, wherein E1A is expressed in an EBNA-1-dependent manner. Treatment of EBV-positive NPC cells with adv.oriP.E1A resulted in specific E1A expression and cytotoxicity, and combination of adv.oriP.E1A with ionizing radiation (i.e., RT) caused tumor regression in EBV-positive NPC xenografts and is associated with minimal systemic toxicity (80). Unfortunately, a study on the pharmacokinetics and biodistribution of EBV-specific transcriptionally targeted adenoviruses revealed that the vectors were mainly sequestered in the liver, limiting their potential clinical application. Nevertheless, strategies modifying the adenoviral vector have been shown to improve tumor uptake and reduce non-specific uptake, affording enhanced therapeutic efficacy (81).

In addition to adenovirus-based vectors, a novel minicircle non-viral vector, mc-oriP-IFNγ I, was developed to drive IFNγ expression by EBNA1 for effective targeting of EBV-positive tumor cells in NPC xenograft models via intratumoral injection (82). Similarly, an EBNA1-specific minicircle non-viral vector expressing *miR-31-5p* was constructed for EBV-specific targeted therapy. *miR-31* is a tumor suppressor microRNA commonly inactivated in NPC by homozygous deletion and promoter hypermethylation. Although mc-oriP-miR-31 inhibits cell proliferation and migration of C666-1 *in vitro* by EBV-specific induction of *miR-31*, *in vivo* studies on systemic delivery of this vector in NPC xenografts are needed to prove its therapeutic efficacy (83).

Meanwhile, the latent EBNA1 protein has also been exploited for oncolytic therapy via reactivation of the viral lytic cycle. Wang and co-workers (84) have reported EBV lytic reactivation in NPC cells by transfecting an EBNA1-driven CMV-BZLF1 expression plasmid (84). While the transfection of the CMV-driven BZLF1 plasmid induced moderate expression of BZLF1 in an EBV-infected epithelial cell line, the presence of an FR enhancer DNA element in the vector further promoted the induction of BZLF1, with BZLF1 triggering EBV reactivation, as shown by the expression of early and late viral genes, and causing in cell death. However, the vector could also induce mild expression of BZLF1 in EBV-negative cells, which may promote oncogenesis in patients' normal cells (6).

In addition to *BZLF1*, another immediate-early (IE) lytic gene, *BRLF1*, can also trigger EBV reactivation. Wang et al. have shown that EBNA1-driven BRLF1 expression induces EBV reactivation in C666-1 cells (85). A baculoviral vector with a *BRLF1* expression cassette cloned downstream of the EBV oriP enhancer element was designed to trigger lytic reactivation in various NPC cell lines. This EBNA1-driven BRLF1 viral vector was observed to cause lytic EBV DNA replication and cell death in infected tumor cells. Moreover, the baculovirus-infected NPC cells caused significant tumor-growth retardation in nude mice.

The above examples unambiguously suggest that EBNA1-FR interactions are a promising target for EBV-specific therapy. Nevertheless, the success of these EBNA1-specific gene therapeutic approaches is dependent on the efficiency of delivery of these vectors to the cancer cells. In this context, recent advances in non-viral delivery technologies mean that the antitumor effect of EBNA1-specific therapeutic constructs delivered by biocompatible nanoparticles in *in vivo* EBV-positive NPC models must also be investigated to confirm their utility in clinical applications.

Inhibition of Latent Membrane Proteins

LMP1 is believed to be a viral oncoprotein promoting transformation and progression of NPC via activation of multiple cellular signaling pathways, such as the NF-κB, PI3K/AKT, MAPK, and IRF pathways (36). Although high LMP1 expression has been reported in ∼25–30% of NPCs, a recent genomic study has revealed that this subgroup of tumors is characterized by a lack of somatic alterations for activating NF-κB signaling and other driver mutations (15). In low-LMP1-expressing tumor specimens, heterogeneous expression in a subpopulation of cancer cells was revealed by immunohistochemistry. As LMP1 has been shown to induce cancer stem/progenitor cells, the occurrence of such a subpopulation of LMP1-expressing cells may be important for maintaining the tumorigenic properties of NPC cells (37, 38). Thus, targeting LMP1 is hypothesized to be a potential therapeutic intervention for NPC, even in tumors exhibiting weak LMP1 expression. This hypothesis is supported by various LMP1-targeting studies in a native EBV-positive NPC cell line, C666-1, that weakly

expresses the LMP1 protein. While several studies on LMP1 targeting have been conducted in preclinical models, interesting clinical trial results have also been reported in a cohort of NPC patients (86, 87).

Among various RNA-interference technologies, inhibition of LMP1 expression by use of an RNA-cleaving DNAzyme has been extensively explored as a potential therapeutic strategy for NPC. DNAzymes are synthetic, single-stranded catalytic DNA molecules with excellent stability and activity in downregulating gene expression. They can be engineered to bind to the complementary sequence of RNA according to the Watson-Crick model. Upon binding to the target mRNA sequence, the DNAzyme can mediate the cleavage of RNA molecules at purine:pyrimidine junctions (86).

The general structure of a DNAzyme consists of a catalytic domain of 15 deoxyribonucleotides, flanked by two substrate-recognition domains, each containing seven to nine deoxyribonucleotides. In 2005, Lu et al. reported the first successful identification of the conserved regions of LMP1 targeted by DNAzymes (88). They further demonstrated the ability of a sequence-specific DNAzyme to knockdown LMP1 gene expression, impair downstream NF-κB signaling, and induce apoptosis in B95.8 cells. Due to the lack of EBV-positive LMP1-expressing NPC cell lines, their subsequent studies on NPC have only examined the inhibitory effects of these DNAzymes on LMP1-transfected epithelial cells (87, 89, 90). Interestingly, Ke et al. (89) have shown that a specific LMP1-targeted DNAzyme, DZ509, inhibited cell proliferation and induced apoptosis in an EBV-positive NPC cell line C666-1 with weak LMP1 expression (89). Intratumoral injections of this DNAzyme also significantly suppressed tumor growth in nude mice models. The vulnerability of C666-1 cells to the inhibition of LMP1 may imply the importance of weak LMP1 expression in tumorigenesis, supporting the therapeutic implications of this novel LMP1-targeting approach.

A clinical trial to evaluate the therapeutic efficiency of an LMP1-targeting DNAzyme, DZ1, as a radiosensitizer was conducted in a cohort of 40 patients with LMP1-positive NPC (87). The study found that there was a lower short-term tumor regression rate and altered tumor vasculature in the DZ1 treatment group. Furthermore, no adverse outcomes of the combined RT and DZ1 treatment were observed. In these clinical studies, DZ1 or control saline was directly injected into tumors with the guide of an endoscope, but not systematic administration. The utility of LMP1-targeted DNAzyme as a systemic treatment for NPC patients, especially with advanced disease, needs to be further elucidated using efficient *in vivo* delivery vehicles, such as nanoparticles (90).

Aside from EBNA1 and LMP1, only a few other latent EBV gene products have been targeted in NPC. Although LMP2 serves as a major viral antigen for developing therapeutic vaccines and T-cell-based immunotherapies in NPC patients, the effects of targeting LMP2 on tumor suppression in native EBV-positive NPC cells are not well-defined. The heterogeneous expression of LMP2 in tumor specimens also suggests that the clinical benefits of this approach may be limited. However, the role of LMP2A in promoting cancer stem-cell properties suggests that targeting LMP2 is a potential therapeutic strategy for this EBV-associated epithelial cancer.

CYTOLYTIC THERAPIES SWITCHING EBV LATENCY TO LYTIC CYCLE

Cytolytic therapy utilizes a naturally occurring virus or genetically engineered virus that can selectively lytic replicate and kill the host cells, without harming normal cells (91). Distinct from the HBV- and HPV-associated cancers, in which integration of the viral genome occurs as a critical event during transformation, clonal EBV episomes are consistently found in EBV-associated malignant diseases (3, 6). This episomal nature of the EBV genome implies that induction of the viral lytic cycle could serve as a cytolytic therapy to cure NPC. When latent EBV are induced into the lytic cycle, the IE proteins BZLF1 and BRLF1 must be expressed, as these further activate the transcription of early and late proteins to progress continue the lytic infection cycle (92). Lytic replication in EBV-positive NPC cells will result in cell disruption, for the release of infectious viral particles.

In addition to directly promoting cell death, lytic cycle induction can raise the potency of immune responses and induce susceptibility to antiviral agents in EBV-associated cancers. The early lytic proteins BGLF4 [EBV protein kinase (PK)] and BXLF1 [EBV thymidine kinase (TK)] are enzymes that can metabolize and activate prodrugs, such as ganciclovir (GCV), acyclovir (ACV), and fialuridine (FIAU). Although these antiviral agents have no effect on latently infected cells, phosphorylation of these prodrugs by EBV PK and TK during lytic reactivation induces premature termination of the nascent DNA and thus induces apoptosis, facilitating the cytotoxicity and bystander effect in the lytic and adjacent tumor cells (**Figure 3**) (92). By exploiting this unique feature, various approaches targeting the latent-lytic switch have been explored as potential therapeutic strategies for EBV-associated malignancies.

Latent-Lytic Switch in EBV-Infected Cells

In lymphocytes, EBV establishes a life-long latency stage upon infection, while it frequently undergoes lytic replication in the epithelial cells of healthy carriers. This is consistent with the fact that primary EBV infection takes place at the oral epithelium, after which the lytic infection of oral epithelial cells triggers the release of infectious virions that infect the surrounding B lymphocytes (6, 17). Despite the tendency of EBV to undergo lytic infection in epithelial cells, lytic reactivation is rarely detected in EBV-positive NPC tumor cells. This shows that the latent-lytic switch in NPC cells is tightly regulated by both viral latent genes and cellular factors.

Epigenetic modification of the viral genome, cellular transcription repressors, and a number of EBV-encoded microRNAs have been shown to contribute to inhibiting lytic gene expression (93–96). In latently infected cells, global methylation of the EBV genome interferes with BZLF1- and BRLF1-driven early and late lytic gene transcription and suppresses spontaneous EBV reactivation (93, 94). An EBV microRNA, *miR-BART20-5p*, directly inhibits the expression

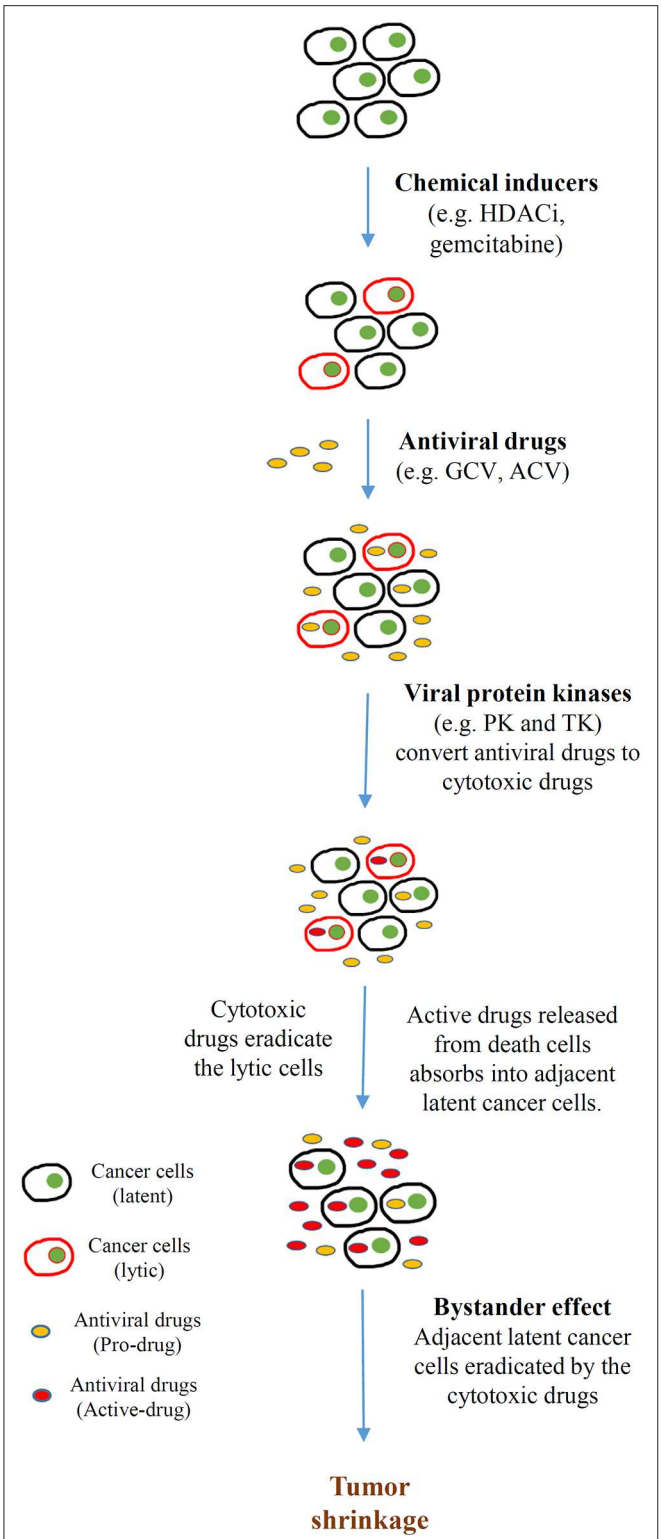

FIGURE 3 | Cytolytic therapy of Epstein-Barr virus (EBV)-associated cancers. Cancer cells harboring EBV in latent infection are induced to undergo reactivation by different chemical inducers [e.g., histone deacetylase inhibitors (HDACis), DNA-damaging agents (gemcitabine)]. Subsequently, the tumor is treated with antiviral drugs [e.g., ganciclovir (GCV), acyclovir (ACV)] that are *(Continued)*

FIGURE 3 | non-toxic unless converted from prodrugs to active drugs by a sequence of phosphorylation reactions. The monophosphorylated form of the antiviral drugs is first catalyzed by either BGLF4 (PK) or BXLF1 (TK), which are induced by the EBV immediate early (IE) genes BZLF1 and BRLF1. Subsequently, cellular kinases catalyze the formation of the cytotoxic diphosphate and triphosphate forms of the drugs. These cytotoxic drugs incorporate into the lytic cells, resulting in apoptosis. Apoptotic cells break down and release the toxic drugs to the tumor microenvironment. Adjacent latent cancer cells absorb the released drugs (the bystander effect) and are eradicated by them. This bystander effect then further promotes tumor shrinkage.

of BZLF1 and BRLF1 to maintain latency in EBV-associated gastric cancer (95). As shown in our recent study, several abundantly expressed miR-BARTs (*miR-BART5-5p, BART7-3p, BART9-3p,* and *BART14-3p*) inhibit lytic reactivation via suppression of ATM expression in NPC cells (96). Furthermore, the transcription of the two IE genes, *BZLF1* and *BRLF1*, is regulated by multiple transcription repressors including YY1, E2-2, MEF-2D, and ZEB1/2 in EBV-infected cells (92). Extensive studies have also revealed that multiple cellular events, such as aberrant protein kinase C (PKC), TGF-β and other signaling pathways, cell differentiation, hypoxia, DNA damage, and reactive oxygen species (ROS) induction play key roles in EBV lytic reactivation in B cells and epithelial cells, by activating the promoters of *BZLF1* and *BRLF1* (92). Nevertheless, the effects of these cellular factors on lytic-cycle induction remain to be defined in EBV-positive NPC cells.

Notably, induction of BZLF1 or BRLF1 alone is sufficient to activate the lytic cycle in EBV latently infected cells (97). BZLF1 and BRLF1 proteins are able to activate both their own and one another's promoters, resulting in efficient lytic-cycle induction. BZLF1 preferentially activates lytic promoters that are methylated, whereas BRLF1 preferentially activates unmethylated lytic promoters (92, 93). BZLF1 induces the transcription of BRLF1 by binding directly to Z-responsive element (ZRE) DNA elements on the BRLF1 promoter (Rp). In contrast, BRLF1 indirectly binds to the BZLF1 promoter (Zp) via interaction with other cellular factors, forming a positive loop to drive their transcription. Thus, the ability of EBV to switch from latent to lytic infection is largely determined by the presence of cellular transcriptional activators that stimulate Zp or Rp, and the inactivation of cellular transcriptional repressors that simultaneously suppress Zp or Rp (92). Then, these two IE proteins (*BZLF1* and *BRLF1*) cooperatively activate the promoters of early lytic genes involved in viral genome replication.

EBV lytic replication is initiated at two replication origins, known as oriLyts, in the EBV genome. This is accompanied by the related EBV-encoded replication proteins BALF5 (DNA polymerase), BMRF1 (DNA polymerase processivity factor, also called diffuse early antigen EA-D), BBLF2 (single-stranded DNA-binding protein), BBLF4 (helicase), BSLF1 (primase), and BBLF2/3 (a component of the helicase-primase complex). The late genes encoding structural proteins (viral capsid antigen and

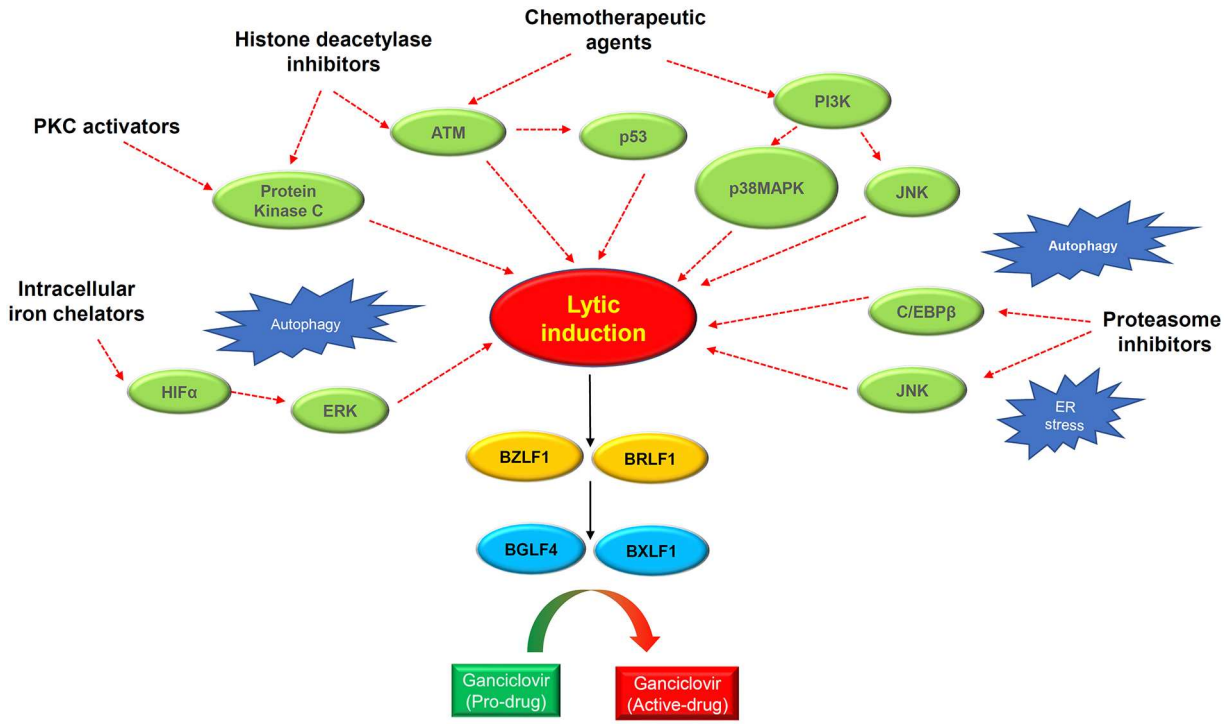

FIGURE 4 | Schematic diagram showing the rationales of lytic induction treatment of EBV-associated cancers. Multiple classes of chemical inducer trigger EBV lytic induction via activating different cellular signaling pathways with extensive cross-talks. Histone deacetylase inhibitors and protein kinase C (PKC) activators induce the PKCdelta and ATM signaling pathway. Chemotherapeutic agents activate the ATM-p53 signaling axis as well as the PI3K/p38MAPK/JNK signaling. Proteasome inhibitors trigger autophagy and ER stress which induce EBV reactivation via activating JNK and C/EBPβ. The intracellular iron chelators induce hypoxia via HIFα and ERK activation, causing EBV lytic induction. Through inducing the IE genes *BZLF1* and *BRLF1*, the chemical inducers switch on EBV lytic cycle. The expression of IE proteins further induces the early lytic proteins BGLF4 (protein kinase) and BXLF1 (thymidine kinase) which convert the ganciclovir into cytotoxic drugs to kill cancer cells during the cytolytic treatment.

gp350) are expressed after viral genome replication, to assist EBV virion production (97–99).

Lytic Cycle-Inducing Agents

Lytic reactivation of EBV can be observed in a small number of tumor cells in clinical specimens, as well as in the newly established EBV-positive NPC PDXs and cell lines (25). This observation strongly supports the potential clinical application of lytic induction therapy in NPC patients. To this end, multiple preclinical and clinical studies have been conducted over the past two decades to explore various lytic cycle-inducing agents for cytolytic reactivation therapy in EBV-associated NPC. These lytic inducers include chemotherapeutic agents, phorbol esters, histone deacetylase inhibitors (HDACis), and a number of novel chemical compounds identified by large-scale screening studies (**Figure 4**, **Table 2**).

Chemotherapeutic Agents

Several FDA-approved drugs for chemotherapy show cell-context-specific ability to switch latency to the lytic cycle in EBV-infected cells. The EBV lytic reactivation ability of these chemotherapeutic agents may contribute to the chemosensitivity of EBV-associated NPC. Two chemotherapeutic agents commonly used in NPC treatment, cisplatin and 5-fluorouracil (5-FU), were able to induce lytic reactivation and confer GCV susceptibility in the EBV-infected gastric cancer cell line AGS-EBV and an EBV-positive NPC PDX model, C18 (100). The activation of IE and early lytic genes by these drugs was found to be dependent on the MAPK/ERK, p38 MAPK, and PKCδ signaling pathways. Meanwhile, gemcitabine is also an effective chemotherapeutic agent in NPC patients, and reactivates BZLF1 expression in the EBV-positive NPC cell C666-1 (101). Gemcitabine induced functional EBV-lytic proteins BGLF4 (PK) and BXLF1(TK) were found in an EBV-associated gastric cancer (EBVaGC) mouse model by [125I]-FIAU-based single-photon emission computed tomography (SPECT) planar imaging. Notably, the induction of the EBV lytic cycle by gemcitabine is mediated by activation of the ATM/p53 genotoxic stress pathway (114).

Cytolytic viral activation (CLVA) therapy using a combination of gemcitabine, the HDACi valproic acid (VPA), and GCV has been developed as a novel NPC treatment. The combination of gemcitabine and VPA showed a synergistic effect on inducing expression of EBV lytic gene expression, while inclusion of GCV further enhanced the cytotoxicity in the tumor cells. In preclinical studies, the treatment induced the EBV lytic cycle and exerted

TABLE 2 | Chemical agents that reactivate the Epstein-Barr virus (EBV) lytic cycle in nasopharyngeal carcinoma (NPC).

Class of lytic inducers	Cell types	Mechanism of action	References
Conventional chemotherapeutics			
Cisplatin (CDDP)	C17 xenograft	DNA-damage agents cause inhibition of DNA replication by DNA intrastrand crosslinking (cisplatin), interference with base-excision DNA repair (gemcitabine), and interrupting thymidine synthesis by inhibiting thymidine synthase (5-FU)	(100)
5-Fluorouracil (5-FU)	C17 xenograft		(100)
Gemcitabine (GEM)	C666-1		(101)
Histone deacetylase inhibitors			
Suberoylanilide hydroxamic acid (SAHA)	C666-1	Inhibition of deacetylation of histones causes chromatin decondensation and interferes with gene transcription	(102, 103)
Valproic acid (VPA)	C666-1		(104)
Sodium butyrate (SB)	NA, HA		(104)
Trichostatin A (TSA)	NPC-TW01-NA; NPC-TW04-4A		(104, 105)
Romidepsin	HA and C6661		(106)
Protein kinase C (PKC) activators			
12-*O*-tetradecanoylphorbol-13-acetate (TPA)	NPC43	Activation of the PKC signaling pathway	(25)
DNA demethylating agents			
5-Azacytidine	Eight patients with NPC	Inhibition of DNA methyltransferase causing hypomethylation of DNA, restoration of gene expression	(107)
Intracellular ion chelators			
C7	C666-1, NPC43, HA, HONE1-EBV	Chemical compound contains a metal-binding moiety that chelates Fe^{2+} and results in activation of autophagy	(108–110)
Proteasome inhibitors			
Bortezomib	HA	Proteasome inhibitor binds to the catalytic site of the 26S proteasome, resulting in inhibition of protein degradation via the ubiquitin-mediated proteasome degradation pathway	(102)
ROS-related chemicals			
N-methyl-*N*′-nitro-*N*-nitrosoguanidine (MNNG)	NA, HA, and C6661	*N*-nitrosoguanidine results in ROS production, inducing EBV reactivation through a p53-dependent mechanism	(111, 112)
Other small synthetic organic compounds			
E11/E7/C8/A10	C6661 and HONE1-EBV	Nil	(108)
Antibacterial agents			
Clofoctol	C666-1	Activation of the unfolded protein response (UPR), which is a stress-signaling pathway that extends from the endoplasmic reticulum (ER) to the nucleus through the PERK-eIF2α-ATF4-CHOP axis (16)	(113)

ROS, reactive oxygen species.

cytotoxicity in both *in vitro* and *in vivo* EBV-positive NPC models (101, 115, 116). A pilot clinical study of CLVA therapy revealed that the treatment was well-tolerated and resulted in disease stabilization and improved quality of life in three patients with progressive end-stage NPC (101). Although the safety of the treatment was confirmed in a subsequent Phase I/II study on eight patients with recurrent or metastatic tumors, only partial clinical response and stable disease were observed, in two and three of the patients, respectively (117). These findings show that clinical benefit of CLVA treatment needs further evaluation in large-scale clinical studies that include a patient group receiving gemcitabine treatment only.

Histone Deacetylase Inhibitors

Histone acetylation is a reversible posttranslational modification that modifies chromatin structure, changing the accessibility of transcription activators and/or repressors to the gene promoters. The gross change of histone acetylation status in a particular gene locus is due to the respective activities of histone deacetylases (HDACs) and histone acetyltransferases (HATs) (118): HDACs deacetylate histones and other non-histone proteins, while HATs catalyze the transfer of acetyl groups from acetyl coenzyme A to the lysine residues of proteins. Both act as cofactors of different transcription regulators for modifying chromatin structure. To date, a variety of FDA-approved HDACis with high activity have been discovered (119). The HDACis are categorized into five groups according to their structure: that is, cyclic peptides, hydroxamic acids, benzamides, short-chain fatty acids, and sirtuin inhibitors (119).

In view of the chromatin-like structure of the EBV episome, the therapeutic potential of various classes of HDACi have been studied, aiming to reactivate the silenced EBV IE genes in the EBV-associated malignancies (4). Among the HDACis investigated in EBV-positive epithelial cancer cell lines, suberoylanilide hydroxamic acid (SAHA), alone or in combination with a proteasome inhibitor (bortezomib), was

found to be superior in terms of inducing EBV reactivation and causing cancer cell death (102, 120). As a class I HDACi, SAHA inhibits histone acetylase classes I and II via chelating the cofactor Zn^{2+} ion.

Notably, the combined treatment of bortezomib and SAHA enhanced ROS production, which caused cell apoptosis and at the same time suppressed virion production (121, 122). Concomitantly, ROS is proposed to be the intermediates of oxidative stress that mediate the EBV reactivation. A novel signaling mechanism in which ROS induces EBV reactivation was proposed by Huang and colleagues, based on the fact that ROS activates multiple signaling pathways, such as ATM, p38 MAPK, and JNKs, to induce p53-dependent EBV reactivation (111). Moreover, oxidative stress has been found to initiate BZLF1 transcription in the Raji cell line (123). These results indicate that the DNA damage response and ROS play a direct role in triggering EBV reactivation in response to various lytic induction treatments.

Although HDACi treatments are effective in triggering EBV reactivation in particular cell line models, their broad efficacy in cell line models remains in doubt, as varied ability of HDACis to trigger EBV reactivation in different cell lines has been highlighted recently (121). Moreover, the underlying mechanisms of the induction of IE genes by these treatments have generally not been investigated and therefore remain elusive. Although it is believed that the opened chromatin structures of IE promoters are critical for their induction, gene transcription does not occur efficiently unless transcription repressors are displaced from the IE promoters. Furthermore, SAHA is known to alter the acetylation of non-histone proteins as well (122). Thus, it is conceivable that understanding the acetylation status of other non-histone proteins will be critical to solve the discrepancy between different studies using HDACis.

Protein Kinase C (PKC) Activators

Early studies revealed that the phorbol ester 12-*O*-tetradecanoylphorbol-13-acetate (TPA) reactivates the EBV lytic cycle in various EBV-infected lymphoid cells through activation of the PKC signaling pathway (124, 125). Later, Gao and colleagues defined the mechanism of EBV lytic induction by TPA in epithelial cells. In EBV-infected gastric cell lines, they showed that TPA activates PKC and MAPK signaling to mediate the increased binding of NF-κB and AP-1 to the BZLF1 promoter for inducing EBV reactivation (126).

The involvement of PKC-delta activation in the EBV latent-lytic switch has also been shown in NPC cells treated with HDACi and the microtubule-depolymerizing agent nocodazole (127, 128). Although TPA alone can induce the lytic cycle in EBV-positive NPC cells in a cell-context-dependent manner, a combination of TPA and other HDACi may be needed to maximize the induction of EBV reactivation (25, 104). As TPA is a classical tumor-promoting agent and can cause skin carcinogenesis (129), it is intrinsically unsuitable as a clinical drug. Nevertheless, other clinically approved PKC activators are worth exploring for their potential ability to induce the lytic cycle in NPC cells.

Intracellular Iron Chelators

Using the recombinant EBV-infected epithelial cancer cell lines AGS-BX1 and NA, Choi and colleagues performed a high-throughput phenotypic screening of 50,240 novel small organic compounds for chemical inducers of the EBV lytic cycle (108). Five compounds showed dose-dependent induction of EBV lytic genes at micromolar concentrations and specific cytotoxicity in EBV-infected epithelial cells. While these compounds were structurally diverse and distinct from classical lytic inducers such as phorbol esters or HDACis, one of the novel compounds, C7, was demonstrated to induce the EBV lytic cycle in multiple native EBV-infected epithelial cancer cells, such as C666-1, SNU-719, and YCCEL1. In addition, a recent study has shown that combined treatment with C7 and an HDACi resulted in apoptosis-mediated synergistic killing of EBV-positive NPC cells (109).

As C7 contains a metal-binding moiety and functions as a chelator of intracellular iron, the group has further examined the ability of other iron chelators, such as Dp44mT, deferoxamine, deferiprone, and deferasirox, to reactivate the EBV lytic cycle in EBV-positive epithelial cancers. Their functional study revealed that C7 and the other iron chelators reactivate the EBV lytic cycle through the chelation of intracellular iron, resulting in HIF-1α induction, ERK1/2 activation, and initiation of autophagy. Thus, iron chelators appear to activate hypoxic signaling and autophagy to trigger lytic reactivation in EBV-positive epithelial cancer cells (110). The above studies have identified the clinically available iron chelators as a novel class of lytic inducer for potential cytolytic therapy.

Future Aspects

In the past decades, the development of EBV lytic-induction treatment for NPC has been hampered by the limited availability of patient-derived EBV-positive NPC models. Aside from the native EBV-positive NPC cell line C666-1, most of the preclinical studies on the efficacy of lytic inducers in reactivation of the EBV lytic cycle have been conducted on EBV-reinfected epithelial cells (e.g., EBV-CNE1, HA, HONE1-EBV) with undefined genome backgrounds. Due to the importance of cellular factors in the regulation of the latent-lytic switch in EBV, the response of NPC cells to different classes of lytic inducers is believed to be cell-context-specific. Specifically, NPC cells in each individual tumor might evolve and acquire different somatic changes to ensure EBV latency during cancer progression. This is evidenced by recent Phase I/II trials of CLVA treatment, in which the induction of the lytic cycle by gemcitabine and VPA appeared to vary among patients. This is itself consistent with preclinical findings that the combination of gemcitabine and VPA fails to induce the lytic cycle in some EBV-positive NPC cell lines, e.g., NPC43 and C17 (unpublished observation).

Furthermore, different efficiencies of HDACis or PKC activators in activating EBV lytic genes were observed in EBV-positive NPC cell lines (e.g., C666-1, NPC43, and C17) (25, 102–104). Recent genomic studies have also revealed that a number of somatic alterations (e.g., *TP53* and *TGFBR2* mutations) may contribute to the maintenance of EBV latency and regulation of the latent-lytic switch in NPC cells (15, 16, 130). Somatic

mutations of *TGFBR2* may prevent NPC cell differentiation, which is a key cellular factor for reactivation of the EBV lytic cycle. The important roles of the DNA damage response and ROS induction in EBV reactivation imply that the status of *TP53* mutations in NPC cells may determine their response to lytic-inducer treatment.

The use of more genomically characterized patient-derived NPC models and native EBV-infected cell lines in comprehensive studies on the association of somatic genetic changes in these tumors with their response to different classes of chemical inducer may allow us to develop effective cytolytic treatment strategies for NPC patients (24, 25). In addition, uncovering the cellular mechanisms of the resistance of tumor cells to lytic cycle induction is important for improving the efficacy of this treatment. As reported previously, the constitutive activation of the NF-κB, STAT3, and WNT signaling pathways modulates major cellular mechanisms and viral gene expression during NPC tumorigenesis (3, 6). However, the roles of these NPC-associated oncogenic-signaling pathways in the switching of persistent latent infection to the lytic cycle have not been defined. The combination treatment of EBV lytic inducers with selected targeted inhibitors of these specific pathways in EBV-positive NPC tumors may provide new insights on the cellular signals that regulate lytic reactivation.

Finally, the high expression of multiple immunogenic viral lytic antigens during EBV lytic reactivation is expected to raise potent immune responses during cytolytic therapy. However, the activation of multiple immunomodulatory lytic proteins such as BNLF2a, BILF1, BGLF5, BCLF1, and BARF1 may dampen the treatment efficiency (131). BNLF2a, BILF1, BGLF5, and BCLF1 deregulate the host antigen-processing pathway via targeting TAP1 (peptide transporter associated with antigen processing 1) and HLA (human leucocyte antigen) class 1 molecules, thereby evading elimination of EBV lytic infected cells by host cytotoxic T lymphocyte (CTL) responses. Furthermore, BCLF1 and BARF1 function as immunosuppressive cytokine and antagonist of M-CSF, respectively. In addition to reduce natural killer (NK) and CTL responses, these lytic proteins suppress T cell activity through inhibition of IFN-γ. Notably, somatic alterations of HLA class 1 molecules (HLA-A, HLA-B, HLA-C) and their transcription regulator (NLRC5) were reported in 30% of NPC in which the immune responses to the viral lytic antigens are impaired (15). It is interested to elucidate the effect of cytolytic therapy on the host immune surveillance by comprehensively characterizing the tumor microenvironment in NPC humanized mouse models. The findings will enhance our outstanding of the host immune response to EBV targeting treatment.

AUTHOR CONTRIBUTIONS

All authors listed have made a substantial, direct and intellectual contribution to the work, and approved it for publication.

FUNDING

KL was supported by the Research Grant Council, Hong Kong (Theme-based Research Scheme —T12-401/13-R; Collaborative Research Fund—C4001-18GF, C7027-16G; General Research Fund−14104415, 14138016, and 14117316), the Focused Innovations Scheme and Faculty Strategic Research (4620513) of the Faculty of Medicine, and the VC's One-off Discretionary Fund (VCF2014017, VCF2014015) of the Chinese University of Hong Kong. CT was supported by the General Research Fund (17110315 and 17111516) of the Research Grant Council, the Health and Medical Research Fund (05162386 and 13142201), and the NSFC/RGC Joint Research Scheme—N_HKU735/18. HL, K-LW, and NM were supported by the Hong Kong Baptist University (RC-IRMS/16-17/CHE, RC-ICRS/16-17/02A-BOL, RC-IRMS/16-17/01, and MPCF-002-2018/19) and Hong Kong Research Grants Council (HKBU 20301615 and 12300117, the NPC Area of Excellence, AoE/M 06/08 Center for Nasopharyngeal Carcinoma Research, and Research Grants Council Collaborative Research Fund Scheme C4001-18GF).

ACKNOWLEDGMENTS

We thank Core Utilities of Cancer Genome and Pathobiology of the Faculty of Medicine, The Chinese University of Hong Kong for providing support for our studies.

REFERENCES

1. Lo KW, To KF, Huang DP. Focus on nasopharyngeal carcinoma. *Cancer Cell*. (2004) 5:423–8. doi: 10.1016/S1535-6108(04)00119-9
2. Chen YP, Chan ATC, Le QT, Blanchard P, Sun Y, Ma J. Nasopharyngeal carcinoma. *Lancet*. (2019) 394:64–80. doi: 10.1016/S0140-6736(19)30956-0
3. Tsang CM, Lui VWY, Bruce JP, Pugh TJ, Lo KW. Translational genomics of nasopharyngeal cancer. *Semin Cancer Biol*. (2019) 61:84-100. doi: 10.1016/j.semcancer.2019.09.006
4. Su WH, Hildesheim A, Chang YS. Human leukocyte antigens and Epstein-Barr virus-associated nasopharyngeal carcinoma: old associations offer new clues into the role of immunity in infection-associated cancers. *Front Oncol*. (2013) 3:299. doi: 10.3389/fonc.2013.00299
5. Tsao SW, Yip YL, Tsang CM, Pang PS, Lau VM, Zhang G, et al. Etiological factors of nasopharyngeal carcinoma. *Oral Oncol*. (2014) 50:330–8. doi: 10.1016/j.oraloncology.2014.02.006
6. Tsao SW, Tsang CM, Lo KW. Epstein-Barr virus infection and nasopharyngeal carcinoma. *Philos Trans R Soc Lond B Biol Sci*. (2017) 372:20160270. doi: 10.1098/rstb.2016.0270
7. Raab-Traub N. Nasopharyngeal carcinoma: an evolving role for the Epstein-Barr virus. *Curr Top Microbiol Immunol*. (2015) 390:339–63. doi: 10.1007/978-3-319-22822-8_14
8. Hui KF, Chan TF, Yang W, Shen JJ, Lam KP, Kwok H, et al. High risk Epstein-Barr virus variants characterized by distinct polymorphisms in the EBER locus are strongly associated with nasopharyngeal carcinoma. *Int J Cancer*. (2019) 144:3031–42. doi: 10.1002/ijc.32049
9. Xu M, Yao Y, Chen H, Zhang S, Cao SM, Zhang Z, et al. Genome sequencing analysis identifies Epstein-Barr virus subtypes associated with

high risk of nasopharyngeal carcinoma. *Nat Genet*. (2019) 51:1131–36. doi: 10.1038/s41588-019-0436-5
10. Au KH, Ngan RKC, Ng AWY, Poon DMC, Ng WT, Yuen KT, et al. Treatment outcomes of nasopharyngeal carcinoma in modern era after intensity modulated radiotherapy (IMRT) in Hong Kong: a report of 3328 patients (HKNPCSG 1301 study). *Oral Oncol*. (2018) 77:16–21. doi: 10.1016/j.oraloncology.2017.12.004
11. Lee AW, Sze WM, Au JS, Leung SF, Leung TW, Chua DT, et al. Treatment results for nasopharyngeal carcinoma in the modern era: the Hon g Kong experience. *Int J Radiat Oncol Biol Phys*. (2005) 61:1107–16. doi: 10.1016/j.ijrobp.2004.07.702
12. Lee AW, Ma BB, Ng WT, Chan AT. Management of nasopharyngeal carcinoma: current practice and future perspective. *J Clin Oncol*. (2015) 33:3356–64. doi: 10.1200/JCO.2015.60.9347
13. Lee V, Kwong D, Leung TW, Lam KO, Tong CC, Lee A. Palliative systemic therapy for recurrent or metastatic nasopharyngeal carcinoma - how far have we achieved? *Crit Rev Oncol Hematol*. (2017) 114:13–23. doi: 10.1016/j.critrevonc.2017.03.030
14. Ma BBY, Hui EP, Chan ATC. Investigational drugs for nasopharyngeal carcinoma. *Expert Opin Investig Drugs*. (2017) 26:677–85. doi: 10.1080/13543784.2017.1324568
15. Li YY, Chung GT, Lui VW, To KF, Ma BB, Chow C, et al. Exome and genome sequencing of nasopharynx cancer identifies NF-κB pathway activating mutations. *Nat Commun*. (2017) 8:14121. doi: 10.1038/ncomms14121
16. Lin DC, Meng X, Hazawa M, Nagata Y, Varela AM, Xu L, et al. The genomic landscape of nasopharyngeal carcinoma. *Nat Genet*. (2014) 46:866–71. doi: 10.1038/ng.3006
17. Young LS, Yap LF, Murray PG. Epstein-Barr virus: more than 50 years old and still providing surprises. *Nat Rev Cancer*. (2016) 16:789–802. doi: 10.1038/nrc.2016.92
18. Tsao SW, Tsang CM, To KF, Lo KW. The role of Epstein-Barr virus in epithelial malignancies. *J Pathol*. (2015) 235:323–33. doi: 10.1002/path.4448
19. Raab-Traub N, Flynn K. The structure of the termini of the Epstein-Barr virus as a marker of clonal cellular proliferation. *Cell*. (1986) 47:883–9. doi: 10.1016/0092-8674(86)90803-2
20. Pathmanathan R, Prasad U, Sadler R, Flynn K, Raab-Traub N. Clonal proliferations of cells infected with Epstein-Barr virus in preinvasive lesions related to nasopharyngeal carcinoma. *N Engl J Med*. (1995) 333:693–8. doi: 10.1056/NEJM199509143331103
21. Chan AS, To KF, Lo KW, Mak KF, Pak W, Chiu B, et al. High frequency of chromosome 3p deletion in histologically normal nasopharyngeal epithelia from southern Chinese. *Cancer Res*. (2000) 60:5365–70.
22. Chan AS, To KF, Lo KW, Ding M, Li X, Johnson P, et al. Frequent chromosome 9p losses in histologically normal nasopharyngeal epithelia from southern Chinese. *Int J Cancer*. (2002) 102:300–3. doi: 10.1002/ijc.10689
23. Tsang CM, Yip YL, Lo KW, Deng W, To KF, Hau PM, et al. Cyclin D1 overexpression supports stable EBV infection in nasopharyngeal epithelial cells. *Proc Natl Acad Sci USA*. (2012) 109:E3473–82. doi: 10.1073/pnas.1202637109
24. Yip YL, Lin WT, Deng W, Tsang CM, Tsao SW. Establishment of nasopharyngeal carcinoma cell lines, patient-derived xenografts, and immortalized nasopharyngeal epithelial cell lines for nasopharyngeal carcinoma and Epstein–Barr Virus infection studies. In: Lee AWM, Lung ML, Ng WT, editors. *Nasopharyngeal Carcinoma - From Etiology to Clinical Practice*. London, UK: Academic Press (2019). p. 85–107. doi: 10.1016/B978-0-12-814936-2.00005-5
25. Lin W, Yip YL, Jia L, Deng W, Zheng H, Dai W, et al. Establishment and characterization of new tumor xenografts and cancer cell lines from EBV-positive nasopharyngeal carcinoma. *Nat Commun*. (2018) 9:4663. doi: 10.1158/1538-7445.AM2019-56
26. Frappier L. EBNA1. *Curr Top Microbiol Immunol*. (2015) 391:3–34. doi: 10.1007/978-3-319-22834-1_1
27. Nanbo A, Yoshiyama H, Takada K. Epstein-Barr virus-encoded poly(A)-RNA confers resistance to apoptosis mediated through Fas by blocking the PKR pathway in human epithelial intestine 407 cells. *J Virol*. (2005) 79:12280–5. doi: 10.1128/JVI.79.19.12280-12285.2005
28. Iwakiri D, Sheen TS, Chen JY, Huang DP, Takada K. Epstein-Barr virus-encoded small RNA induces insulin-like growth factor 1 and supports growth of nasopharyngeal carcinoma-derived cell lines. *Oncogene*. (2005) 24:1767–73. doi: 10.1038/sj.onc.1208357
29. Samanta M, Iwakiri D, Takada K. Epstein-Barr virus-encoded small RNA induces IL-10 through RIG-I-mediated IRF-3 signaling. *Oncogene*. (2008) 27:4150–60. doi: 10.1038/onc.2008.75
30. Li Z, Duan Y, Cheng S, Chen Y, Hu Y, Zhang L, et al. EBV-encoded RNA via TLR3 induces inflammation in nasopharyngeal carcinoma. *Oncotarget*. (2015) 6:24291–303. doi: 10.18632/oncotarget.4552
31. Lo AK, Dawson CW, Jin DY, Lo KW. The pathological roles of BART miRNAs in nasopharyngeal carcinoma. *J Pathol*. (2012) 227:392–403. doi: 10.1002/path.4025
32. Skalsky RL, Cullen BR. EBV noncoding RNAs. *Curr Top Microbiol Immunol*. (2015) 391:181–217. doi: 10.1007/978-3-319-22834-1_6
33. Verhoeven RJA, Tong S, Mok BW, Liu J, He S, Zong J, et al. Epstein-barr virus BART long non-coding RNAs function as epigenetic modulators in nasopharyngeal carcinoma. *Front Oncol*. (2019) 9:1120. doi: 10.3389/fonc.2019.01120
34. Marquitz AR, Mathur A, Edwards RH, Raab-Traub N. Host gene expression is regulated by two types of noncoding RNAs transcribed from the Epstein-barr virus BamHI a rightward transcript region. *J Virol*. (2015) 89:11256–68. doi: 10.1128/JVI.01492-15
35. Hoebe EK, Le Large TY, Greijer AE, Middeldorp JM. BamHI-A rightward frame 1, an Epstein-Barr virus-encoded oncogene and immune modulator. *Rev Med Virol*. (2013) 23:367–83. doi: 10.1002/rmv.1758
36. Dawson CW, Port RJ, Young LS. The role of the EBV-encoded latent membrane proteins LMP1 and LMP2 in the pathogenesis of nasopharyngeal carcinoma (NPC). *Semin Cancer Biol*. (2012) 22:144–53. doi: 10.1016/j.semcancer.2012.01.004
37. Kondo S, Wakisaka N, Muramatsu M, Zen Y, Endo K, Murono S, et al. Epstein-Barr virus latent membrane protein 1 induces cancer stem/progenitor-like cells in nasopharyngeal epithelial cell lines. *J Virol*. (2011) 85:11255–64. doi: 10.1128/JVI.00188-11
38. Port RJ, Pinheiro-Maia S, Hu C, Arrand JR, Wei W, Young LS, et al. Epstein-Barr virus induction of the Hedgehog signalling pathway imposes a stem cell phenotype on human epithelial cells. *J Pathol*. (2013) 231:367–77. doi: 10.1002/path.4245
39. Cen O, Longnecker R. Latent membrane protein 2 (LMP2). *Curr Top Microbiol Immunol*. (2015) 391:151–80. doi: 10.1007/978-3-319-22834-1_5
40. McClain MT, Heinlen LD, Dennis GJ, Roebuck J, Harley JB, James JA. Early events in lupus humoral autoimmunity suggest initiation through molecular mimicry. *Nat Med*. (2005) 11:85–9. doi: 10.1038/nm1167
41. Wilson JB, Manet E, Gruffat H, Busson P, Blondel M, Fahraeus R. EBNA1: oncogenic activity, immune evasion and biochemical functions provide targets for novel therapeutic strategies against Epstein-Barr virus-associated cancers. *Cancers*. (2018) 10:109. doi: 10.3390/cancers10040109
42. de Leo A, Calderon A, Lieberman PM. Control of viral latency by episome maintenance proteins. *Trends Microbiol*. (2019) 28:150–62. doi: 10.1016/j.tim.2019.09.002
43. Yin Q, Flemington EK. siRNAs against the Epstein barr virus latency replication factor, EBNA1, inhibit its function and growth of EBV-dependent tumor cells. *Virology*. (2006) 346:385–93. doi: 10.1016/j.virol.2005.11.021
44. Sivachandran N, Wang X, Frappier L. Functions of the Epstein-Barr virus EBNA1 protein in viral reactivation and lytic infection. *J Virol*. (2012) 86:6146–58. doi: 10.1128/JVI.00013-12
45. Cruickshank J, Shire K, Davidson AR, Edwards AM, Frappier L. Two domains of the Epstein-barr virus origin DNA-binding protein, EBNA1, orchestrate sequence-specific DNA binding. *J Biol Chem*. (2000) 275:22273–7. doi: 10.1074/jbc.M001414200
46. Thompson S, Messick T, Schultz DC, Reichman M, Lieberman PM. Development of a high-throughput screen for inhibitors of Epstein-barr virus EBNA1. *J Biomol Screen*. (2010) 15:1107–15. doi: 10.1177/1087057110379154

47. Kim SY, Song KA, Kieff E, Kang MS. Small molecule and peptide-mediated inhibition of Epstein-barr virus nuclear antigen 1 dimerization. *Biochem Biophys Res Commun*. (2012) 424:251–6. doi: 10.1016/j.bbrc.2012.06.095
48. Mahon KP, Potocky TB, Blair D, Roy MD, Stewart KM, Chiles TC, et al. Deconvolution of the cellular oxidative stress response with organelle-specific peptide conjugates. *Chem Biol*. (2007) 14:923–30. doi: 10.1016/j.chembiol.2007.07.011
49. Jiang L, Lan R, Huang T, Chan CF, Li H, Lear S, et al. EBNA1-targeted probe for the imaging and growth inhibition of tumours associated with the Epstein–barr virus. *Nat Biomed Eng*. (2017) 1:0042. doi: 10.1038/s41551-017-0042
50. Aras S, Singh G, Johnston K, Foster T, Aiyar A. Zinc coordination is required for and regulates transcription activation by Epstein-barr nuclear antigen 1. *PLoS Pathog*. (2009) 5:e1000469. doi: 10.1371/journal.ppat.1000469
51. Hussain M, Gatherer D, Wilson JB. Modelling the structure of full-length Epstein-barr virus nuclear antigen 1. *Virus Genes*. (2014) 49:358–72. doi: 10.1007/s11262-014-1101-9
52. Wu H, Kapoor P, Frappier L. Separation of the DNA replication, segregation, and transcriptional activation functions of Epstein-Barr nuclear antigen 1. *J Virol*. (2002) 76:2480–90. doi: 10.1128/jvi.76.5.2480-2490.2002
53. Norseen J, Thomae A, Sridharan V, Aiyar A, Schepers A, Lieberman PM. RNA-dependent recruitment of the origin recognition complex. *EMBO J*. (2008) 27:3024–35. doi: 10.1038/emboj.2008.221
54. Norseen J, Johnson FB, Lieberman PM. Role for G-quadruplex RNA binding by Epstein-Barr virus nuclear antigen 1 in DNA replication and metaphase chromosome attachment. *J Virol*. (2009) 83:10336–46. doi: 10.1128/JVI.00747-09
55. Singh G, Aras S, Zea AH, Koochekpour S, Aiyar A. Optimal transactivation by Epstein-Barr nuclear antigen 1 requires the UR1 and ATH1 domains. *J Virol*. (2009) 83:4227–35. doi: 10.1128/JVI.02578-08
56. Sears J, Ujihara M, Wong S, Ott C, Middeldorp J, Aiyar A. The amino terminus of Epstein-Barr virus (EBV) nuclear antigen 1 contains AT hooks that facilitate the replication and partitioning of latent EBV genomes by tethering them to cellular chromosomes. *J Virol*. (2004) 78:11487–505. doi: 10.1128/JVI.78.21.11487-11505.2004
57. Chakravorty A, Sugden B. The AT-hook DNA binding ability of the Epstein barr virus EBNA1 protein is necessary for the maintenance of viral genomes in latently infected cells. *Virology*. (2015) 484:251–8. doi: 10.1016/j.virol.2015.05.018
58. Apcher S, Komarova A, Daskalogianni C, Yin Y, Malbert-Colas L, Fåhraeus R. mRNA translation regulation by the gly-Ala repeat of Epstein-Barr virus nuclear antigen 1. *J Virol*. (2009) 83:1289–98. doi: 10.1128/JVI.01369-08
59. Apcher S, Daskalogianni C, Manoury B, Fåhraeus R. Epstein barr virus-encoded EBNA1 interference with MHC class I antigen presentation reveals a close correlation between mRNA translation initiation and antigen presentation. *PLoS Pathog*. (2010) 6:e1001151. doi: 10.1371/journal.ppat.1001151
60. Lista MJ, Martins RP, Billant O, Contesse MA, Findakly S, Pochard P, et al. Nucleolin directly mediates Epstein-Barr virus immune evasion through binding to G-quadruplexes of EBNA1 mRNA. *Nat Commun*. (2017) 8:16043. doi: 10.1038/ncomms16043
61. Reznichenko O, Quillévéré A, Martins RP, Loaëc N, Kang H, Lista MJ, et al. Novel cationic bis(acylhydrazones) as modulators of Epstein-Barr virus immune evasion acting through disruption of interaction between nucleolin and G-quadruplexes of EBNA1 mRNA. *Eur J Med Chem*. (2019) 178:13–29. doi: 10.1016/j.ejmech.2019.05.042
62. Ambinder RF, Mullen MA, Chang YN, Hayward GS, Hayward SD. Functional domains of Epstein-Barr virus nuclear antigen EBNA-1. *J Virol*. (1991) 65:1466–78. doi: 10.1128/JVI.65.3.1466-1478.1991
63. Ambinder RF, Shah WA, Rawlins DR, Hayward GS, Hayward SD. Definition of the sequence requirements for binding of the EBNA-1 protein to its palindromic target sites in Epstein-barr virus DNA. *J Virol*. (1990) 64:2369–79. doi: 10.1128/JVI.64.5.2369-2379.1990
64. Frappier L, O'Donnell M. Overproduction, purification, and characterization of EBNA1, the origin binding protein of Epstein-barr virus. *J Biol Chem*. (1991) 266:7819–26.
65. Li N, Thompson S, Schultz DC, Zhu W, Jiang H, Luo C, et al. Discovery of selective inhibitors against EBNA1 via high throughput *in silico* virtual screening. *PLoS ONE*. (2010) 5:e10126. doi: 10.1371/journal.pone.0010126
66. Messick TE, Smith GR, Soldan SS, McDonnell ME, Deakyne JS, Malecka KA, et al. Structure-based design of small-molecule inhibitors of EBNA1 DNA binding blocks Epstein-Barr virus latent infection and tumor growth. *Sci Transl Med*. (2019) 11:eaau5612. doi: 10.1126/scitranslmed.aau5612
67. Bai F, Morcos F, Cheng RR, Jiang H, Onuchic JN. Elucidating the druggable interface of protein-protein interactions using fragment docking and coevolutionary analysis. *Proc Natl Acad Sci USA*. (2016) 113:E8051–8. doi: 10.1073/pnas.1615932113
68. Gable JE, Lee GM, Acker TM, Hulce KR, Gonzalez ER, Schweigler P, et al. Fragment-based protein-protein interaction antagonists of a viral dimeric protease. *ChemMedChem*. (2016) 11:862–9. doi: 10.1002/cmdc.201500526
69. Gunderwala AY, Nimbvikar AA, Cope NJ, Li Z, Wang Z. Development of allosteric BRAF peptide inhibitors targeting the dimer interface of BRAF. *ACS Chem Biol*. (2019) 14:1471–80. doi: 10.1021/acschembio.9b00191
70. Malecka KA, Dheekollu J, Deakyne JS, Wiedmer A, Ramirez UD, Lieberman PM, et al. Structural basis for cooperative binding of EBNA1 to the Epstein-barr virus dyad symmetry minimal origin of replication. *J Virol*. (2019) 93:e00487-19. doi: 10.1128/JVI.00487-19
71. Deakyne JS, Malecka KA, Messick TE, Lieberman PM. Structural and functional basis for an EBNA1 hexameric ring in Epstein-Barr virus episome maintenance. *J Virol*. (2017) 91:e01046-17. doi: 10.1128/JVI.01046-17
72. Dheekollu J, Malecka K, Wiedmer A, Delecluse HJ, Chiang AK, Altieri DC, et al. Carcinoma-risk variant of EBNA1 deregulates Epstein-Barr virus episomal latency. *Oncotarget*. (2017) 8:7248–64. doi: 10.18632/oncotarget.14540
73. Jiang L, Lui YL, Li H, Chan CF, Lan R, Chan WL, et al. EBNA1-specific luminescent small molecules for the imaging and inhibition of latent EBV-infected tumor cells. *Chem Commun*. (2014) 50:6517–9. doi: 10.1039/C4CC01589D
74. Zha S, Fung YH, Chau HF, Ma P, Lin J, Wang J, et al. Responsive upconversion nanoprobe for monitoring and inhibition of EBV-associated cancers via targeting EBNA1. *Nanoscale*. (2018) 10:15632–40. doi: 10.1039/C8NR05015E
75. Jiang L, Lung HL, Huang T, Lan R, Zha S, Chan LS, et al. Reactivation of Epstein-Barr virus by a dual-responsive fluorescent EBNA1-targeting agent with Zn^{2+}-chelating function. *Proc Natl Acad Sci USA*. (2019) 116:26614–24. doi: 10.1073/pnas.1915372116
76. Mansouri S, Pan Q, Blencowe BJ, Claycomb JM, Frappier L. Epstein-Barr virus EBNA1 protein regulates viral latency through effects on let-7 microRNA and dicer. *J Virol*. (2014) 88:11166–77. doi: 10.1128/JVI.01785-14
77. Li JH, Chia M, Shi W, Ngo D, Strathdee CA, Huang D, et al. Tumor-targeted gene therapy for nasopharyngeal carcinoma. *Cancer Res*. (2002) 62:171–8.
78. Yip KW, Li A, Li JH, Shi W, Chia MC, Rashid SA, et al. Potential utility of BimS as a novel apoptotic therapeutic molecule. *Mol Ther*. (2004) 10:533–44. doi: 10.1016/j.ymthe.2004.05.026
79. Li JH, Shi W, Chia M, Sanchez-Sweatman O, Siatskas C, Huang D, et al. Efficacy of targeted FasL in nasopharyngeal carcinoma. *Mol Ther*. (2003) 8:964–73. doi: 10.1016/j.ymthe.2003.08.018
80. Chia MC, Shi W, Li JH, Sanchez O, Strathdee CA, Huang D, et al. A conditionally replicating adenovirus for nasopharyngeal carcinoma gene therapy. *Mol Ther*. (2004) 9:804–17. doi: 10.1016/j.ymthe.2004.03.016
81. Mocanu JD, Yip KW, Alajez NM, Shi W, Li JH, Lunt SJ, et al. Imaging the modulation of adenoviral kinetics and biodistribution for cancer gene therapy. *Mol Ther*. (2007) 15:921–9. doi: 10.1038/mt.sj.6300119
82. Zuo Y, Wu J, Xu Z, Yang S, Yan H, Tan L, et al. Minicircle-oriP-IFNγ: a novel targeted gene therapeutic system for EBV positive human nasopharyngeal carcinoma. *PLoS ONE*. (2011) 6:e19407. doi: 10.1371/journal.pone.0019407
83. Wu J, Tan X, Lin J, Yuan L, Chen J, Qiu L, et al. Minicircle-oriP-miR-31 as a novel EBNA1-specific miRNA therapy approach for nasopharyngeal carcinoma. *Hum Gene Ther*. (2017) 28:415–27. doi: 10.1089/hum.2016.136
84. Wang H, Zhao Y, Zeng L, Tang M, El-Deeb A, Li JJ, et al. BZLF1 controlled by family repeat domain induces lytic cytotoxicity in Epstein-Barr virus-positive tumor cells. *Anticancer Res*. (2004) 24:67–74.

85. Wang L, Shan L, Lo KW, Yin J, Zhang Y, Sun R, et al. Inhibition of nasopharyngeal carcinoma growth by RTA-expressing baculovirus vectors containing oriP. *J Gene Med*. (2008) 10:1124–33. doi: 10.1002/jgm.1237
86. Sun LQ, Cairns MJ, Saravolac EG, Baker A, Gerlach WL. Catalytic nucleic acids: from lab to applications. *Pharmacol Rev*. (2000) 52:325–47.
87. Cao Y, Yang L, Jiang W, Wang X, Liao W, Tan G, et al. Therapeutic evaluation of Epstein-Barr virus-encoded latent membrane protein-1 targeted DNAzyme for treating of nasopharyngeal carcinomas. *Mol Ther*. (2014) 22:371–7. doi: 10.1038/mt.2013.257
88. Lu ZX, Ye M, Yan GR, Li Q, Tang M, Lee LM, et al. Effect of EBV LMP1 targeted DNAzymes on cell proliferation and apoptosis. *Cancer Gene Ther*. (2005) 12:647–54. doi: 10.1038/sj.cgt.7700833
89. Ke X, Yang YC, Hong SL. EBV-LMP1-targeted DNAzyme restrains nasopharyngeal carcinoma growth in a mouse C666-1 xenograft model. *Med Oncol*. (2011) 28(Suppl. 1):S326–32. doi: 10.1007/s12032-010-9681-2
90. Zhou W, Ding J, Liu J. Theranostic DNAzymes. *Theranostics*. (2017) 7:1010–25. doi: 10.7150/thno.17736
91. Fukuhara H, Ino Y, Todo T. Oncolytic virus therapy: a new era of cancer treatment at dawn. *Cancer Sci*. (2016) 107:1373–9. doi: 10.1111/cas.13027
92. Kenney SC, Mertz JE. Regulation of the latent-lytic switch in Epstein-Barr virus. *Semin Cancer Biol*. (2014) 26:60–8. doi: 10.1016/j.semcancer.2014.01.002
93. Wille CK, Nawandar DM, Panfil AR, Ko MM, Hagemeier SR, Kenney SC. Viral genome methylation differentially affects the ability of BZLF1 versus BRLF1 to activate Epstein-Barr virus lytic gene expression and viral replication. *J Virol*. (2013) 87:935–50. doi: 10.1128/JVI.01790-12
94. Wille CK, Nawandar DM, Henning AN, Ma S, Oetting KM, Lee D, et al. 5-Hydroxymethylation of the EBV genome regulates the latent to lytic switch. *Proc Natl Acad Sci USA*. (2015) 112:E7257–65. doi: 10.1073/pnas.1513432112
95. Kim H, Choi H, Lee SK. Epstein-Barr virus microRNA miR-BART20-5p suppresses lytic induction by inhibiting BAD-mediated caspase-3-dependent apoptosis. *J Virol*. (2015) 90:1359–68. doi: 10.1128/JVI.02794-15
96. Lung RW, Hau PM, Yu KH, Yip KY, Tong JH, Chak WP, et al. EBV-encoded miRNAs target ATM-mediated response in nasopharyngeal carcinoma. *J Pathol*. (2018) 244:394–407. doi: 10.1002/path.5018
97. Hammerschmidt W, Sugden B. Identification and characterization of oriLyt, a lytic origin of DNA replication of Epstein-Barr virus. *Cell*. (1988) 55:427–33. doi: 10.1016/0092-8674(88)90028-1
98. Fixman ED, Hayward GS, Hayward SD. Trans-acting requirements for replication of Epstein-Barr virus ori-Lyt. *J Virol*. (1992) 66:5030–9. doi: 10.1128/JVI.66.8.5030-5039.1992
99. Tsurumi T, Fujita M, Kudoh A. Latent and lytic Epstein-Barr virus replication strategies. *Rev Med Virol*. (2005) 15:3–15. doi: 10.1002/rmv.441
100. Feng WH, Israel B, Raab-Traub N, Busson P, Kenney SC. Chemotherapy induces lytic EBV replication and confers ganciclovir susceptibility to EBV-positive epithelial cell tumors. *Cancer Res*. (2002) 62:1920–6.
101. Wildeman MA, Novalic Z, Verkuijlen SA, Juwana H, Huitema AD, Tan IB, et al. Cytolytic virus activation therapy for Epstein-Barr virus-driven tumors. *Clin Cancer Res*. (2012) 18:5061–70. doi: 10.1158/1078-0432.CCR-12-0574
102. Hui KF, Lam BH, Ho DB, Tsao SW, Chiang AK. Bortezomib and SAHA synergistically induce ROS-driven caspase-dependent apoptosis of nasopharyngeal carcinoma and block replication of Epstein-Barr virus. *Mol Cancer Ther*. (2013) 12:747–58. doi: 10.1158/1535-7163.MCT-12-0811
103. Hui KF, Ho DN, Tsang CM, Middeldorp JM, Tsao GS, Chiang AK. Activation of lytic cycle of Epstein-Barr virus by suberoylanilide hydroxamic acid leads to apoptosis and tumor growth suppression of nasopharyngeal carcinoma. *Int J Cancer*. (2012) 131:1930–40. doi: 10.1002/ijc.27439
104. Fang CY, Lee CH, Wu CC, Chang YT, Yu SL, Chou SP, et al. Recurrent chemical reactivations of EBV promotes genome instability and enhances tumor progression of nasopharyngeal carcinoma cells. *Int J Cancer*. (2009) 124:2016–25. doi: 10.1002/ijc.24179
105. Tsai PF, Lin SJ, Weng PL, Tsai SC, Lin JH, Chou YC, et al. Interplay between PKCdelta and Sp1 on histone deacetylase inhibitor-mediated Epstein-Barr virus reactivation. *J Virol*. (2011) 85:2373–85. doi: 10.1128/JVI.01602-10
106. Hui KF, Cheung AK, Choi CK, Yeung PL, Middeldorp JM, Lung ML, et al. Inhibition of class I histone deacetylases by romidepsin potently induces Epstein-Barr virus lytic cycle and mediates enhanced cell death with ganciclovir. *Int J Cancer*. (2016) 138:125–36. doi: 10.1002/ijc.29698
107. Chan AT, Tao Q, Robertson KD, Flinn IW, Mann RB, Klencke B, et al. Azacitidine induces demethylation of the Epstein-Barr virus genome in tumors. *J Clin Oncol*. (2004) 22:1373–81. doi: 10.1200/JCO.2004.04.185
108. Choi CK, Ho DN, Hui KF, Kao RY, Chiang AK. Identification of novel small organic compounds with diverse structures for the induction of Epstein-Barr virus (EBV) lytic cycle in EBV-positive epithelial malignancies. *PLoS ONE*. (2015) 10:e0145994. doi: 10.1371/journal.pone.0145994
109. Yiu SPT, Hui KF, Choi CK, Kao RYT, Ma CW, Yang D, et al. Intracellular iron chelation by a novel compound, C7, reactivates Epstein-Barr virus (EBV) lytic cycle via the ERK-autophagy axis in EBV-positive epithelial cancers. *Cancers*. (2018) 10:E505. doi: 10.3390/cancers10120505
110. Yiu SPT, Hui KF, Münz C, Lo KW, Tsao SW, Kao RYT, et al. Autophagy-dependent reactivation of Epstein-Barr virus lytic cycle and combinatorial effects of autophagy-dependent and independent lytic inducers in nasopharyngeal carcinoma. *Cancers*. (2019) 11:E1871. doi: 10.3390/cancers11121871
111. Huang SY, Fang CY, Wu CC, Tsai CH, Lin SF, Chen JY. Reactive oxygen species mediate Epstein-Barr virus reactivation by N-methyl-N′-nitro-N-nitrosoguanidine. *PLoS ONE*. (2013) 8:e84919. doi: 10.1371/journal.pone.0084919
112. Huang SY, Fang CY, Tsai CH, Chang Y, Takada K, Hsu TY, et al. N-methyl-N′-nitro-N-nitrosoguanidine induces and cooperates with 12-O-tetradecanoylphorbol-1,3-acetate/sodium butyrate to enhance Epstein-Barr virus reactivation and genome instability in nasopharyngeal carcinoma cells. *Chem Biol Interact*. (2010) 188:623–34. doi: 10.1016/j.cbi.2010.09.020
113. Lee J, Kosowicz JG, Hayward SD, Desai P, Stone J, Lee JM, et al. Pharmacologic activation of lytic Epstein-Barr virus gene expression without virion production. *J Virol*. (2019) 93:e00998-19. doi: 10.1128/JVI.00998-19
114. Lee HG, Kim H, Kim EJ, Park PG, Dong SM, Choi TH, et al. Targeted therapy for Epstein-Barr virus-associated gastric carcinoma using low-dose gemcitabine-induced lytic activation. *Oncotarget*. (2015) 6:31018–29. doi: 10.18632/oncotarget.5041
115. Stoker SD, Novalić Z, Wildeman MA, Huitema AD, Verkuijlen SA, Juwana H, et al. Epstein-Barr virus-targeted therapy in nasopharyngeal carcinoma. *J Cancer Res Clin Oncol*. (2015) 141:1845–57. doi: 10.1007/s00432-015-1969-3
116. Hsu CL, Kuo YC, Huang Y, Huang YC, Lui KW, Chang KP, et al. Application of a patient-derived xenograft model in cytolytic viral activation therapy for nasopharyngeal carcinoma. *Oncotarget*. (2015) 6:31323–34. doi: 10.18632/oncotarget.5544
117. Novalić Z, Verkuijlen SAWM, Verlaan M, Eersels JLH, de Greeuw I, Molthoff CFM, et al. Cytolytic virus activation therapy and treatment monitoring for Epstein-Barr virus associated nasopharyngeal carcinoma in a mouse tumor model. *J Med Virol*. (2017) 89:2207–16. doi: 10.1002/jmv.24870
118. Minucci S, Pelicci, PG. Histone deacetylase inhibitors and the promise of epigenetic (and more) treatments for cancer. *Nat Rev Cancer*. (2006) 6:38–51. doi: 10.1038/nrc1779
119. Hassell KN. Histone deacetylases and their inhibitors in cancer epigenetics. *Diseases*. (2019) 7:E57. doi: 10.3390/diseases7040057
120. Hui KF, Chiang AK. Suberoylanilide hydroxamic acid induces viral lytic cycle in Epstein-Barr virus-positive epithelial malignancies and mediates enhanced cell death. *Int J Cancer*. (2010) 126:2479–89. doi: 10.1002/ijc.24945
121. Daigle D, Gradoville L, Tuck D, Schulz V, Wang'ondu R, Ye J, et al. Valproic acid antagonizes the capacity of other histone deacetylase inhibitors to activate the Epstein-Barr virus lytic cycle. *J Virol*. (2011) 85:5628–43. doi: 10.1128/JVI.02659-10
122. Marks PK, Breslow R. Dimethyl sulfoxide to vorinostat: development of this histone deacetylase inhibitor as an anticancer drug. *Nat Biotechnol*. (2007) 25:84–90. doi: 10.1038/nbt1272
123. Lassoued S, Gargouri B, El Feki Ael F, Attia H, van Pelt J. Transcription of the Epstein-Barr virus lytic cycle activator BZLF-1 during oxidative stress induction. *Biol Trace Elem Res*. (2010) 137:13–22. doi: 10.1007/s12011-009-8555-y
124. Davies AH, Grand RJ, Evans FJ, Rickinson B. Induction of Epstein-Barr virus lytic cycle by tumor-promoting and non-tumor-promoting phorbol esters requires active protein kinase C. *J Virol*. (1991) 65:6838–44. doi: 10.1128/JVI.65.12.6838-6844.1991

125. Di Renzo L, Avila-Carino J, KleinE. Induction of the lytic viral cycle in Epstein Barr virus carrying Burkitt lymphoma lines is accompanied by increased expression of major histocompatibility complex molecules. *Immunol Lett*. (1993) 38:207–14. doi: 10.1016/0165-2478(93)90008-P
126. Gao X, Ikuta K, Tajima M, Sairenji T. 12-O-tetradecanoylphorbol-13-acetate induces Epstein-Barr virus reactivation via NF-kappaB and AP-1 as regulated by protein kinase C and mitogen-activated protein kinase. *Virology*. (2001) 286:91–9. doi: 10.1006/viro.2001.0965
127. Lee HH, Chang SS, Lin SJ, Chua HH, Tsai TJ, Tsai K, et al. Essential role of PKCdelta in histone deacetylase inhibitor-induced Epstein-Barr virus reactivation in nasopharyngeal carcinoma cells. *J Gen Virol*. (2008) 89:878–83. doi: 10.1099/vir.0.83533-0
128. Liu YR, Huang SY, Chen JY, Wang LH. Microtubule depolymerization activates the Epstein-Barr virus lytic cycle through protein kinase C pathways in nasopharyngeal carcinoma cells. *J Gen Virol*. (2013) 94:2750–8. doi: 10.1099/vir.0.058040-0
129. Rundhaug JE, Fischer SM. Molecular mechanisms of mouse skin tumor promotion. *Cancers*. (2010) 2:436–82. doi: 10.3390/cancers2020436
130. Chung AK, OuYang CN, Liu H, Chao M, Luo JD, Lee CY, et al. Targeted sequencing of cancer-related genes in nasopharyngeal carcinoma identifies mutations in the TGF-β pathway. *Cancer Med*. (2019) 8:5116–27. doi: 10.1002/cam4.2429
131. Morales-Sánchez A, Fuentes-Panana EM. The immunomodulatory capacity of an Epstein-Barr virus abortive lytic cycle: potential contribution to viral tumorigenesis. *Cancers*. (2018) 10:98. doi: 10.3390/cancers10040098

Conflict of Interest: The authors declare that the research was conducted in the absence of any commercial or financial relationships that could be construed as a potential conflict of interest.

frontiers in Oncology

REVIEW
published: 12 June 2020
doi: 10.3389/fonc.2020.00930

Quality of Life, Toxicity and Unmet Needs in Nasopharyngeal Cancer Survivors

Lachlan McDowell[1,2]*, *June Corry*[3,4], *Jolie Ringash*[5] and *Danny Rischin*[2,6]

[1] Department of Radiation Oncology, Peter MacCallum Cancer Centre, Melbourne, VIC, Australia, [2] Sir Peter MacCallum Department of Oncology, The University of Melbourne, Melbourne, VIC, Australia, [3] GenesisCare Radiation Oncology, Division Radiation Oncology, St. Vincent's Hospital, Melbourne, VIC, Australia, [4] Department of Medicine St Vincent's, The University of Melbourne, Melbourne, VIC, Australia, [5] Department of Radiation Oncology, Princess Margaret Cancer Centre/University of Toronto, Toronto, ON, Canada, [6] Department of Medical Oncology, Peter MacCallum Cancer Centre, Melbourne, VIC, Australia

OPEN ACCESS

Edited by:
Jun Ma,
Sun Yat-sen University Cancer Center (SYSUCC), China

Reviewed by:
Xu Liu,
Sun Yat-sen University Cancer Center (SYSUCC), China
Jo Patterson,
City Hospitals Sunderland NHS Foundation Trust, United Kingdom

***Correspondence:**
Lachlan McDowell
lachlan.mcdowell@petermac.org

Specialty section:
This article was submitted to Head and Neck Cancer, a section of the journal Frontiers in Oncology

Received: 03 January 2020
Accepted: 12 May 2020
Published: 12 June 2020

Citation:
McDowell L, Corry J, Ringash J and Rischin D (2020) Quality of Life, Toxicity and Unmet Needs in Nasopharyngeal Cancer Survivors. Front. Oncol. 10:930. doi: 10.3389/fonc.2020.00930

Concerted research efforts over the last three decades have resulted in improved survival and outcomes for patients diagnosed with nasopharyngeal carcinoma (NPC). The evolution of radiotherapy techniques has facilitated improved dose delivery to target volumes while reducing dose to the surrounding normal tissue, improving both disease control and quality of life (QoL). In parallel, clinical trials focusing on determining the optimal systemic therapy to use in conjunction with radiotherapy have been largely successful, resulting in improved locoregional, and distant control. As a consequence, neoadjuvant chemotherapy (NACT) prior to definitive chemoradiotherapy has recently emerged as the preferred standard for patients with locally advanced NPC. Two of the major challenges in interpreting toxicity and QoL data from the published literature have been the reliance on: (1) clinician rather than patient reported outcomes; and (2) reporting statistical rather than clinical meaningful differences in measures. Despite the lower rates of toxicity that have been achieved with highly conformal radiotherapy techniques, survivors remain at moderate risk of persistent and long-lasting treatment effects, and the development of late radiation toxicities such as hearing loss, cranial neuropathies and cognitive impairment many years after successful treatment can herald a significant decline in QoL. Future approaches to reduce long-term toxicity will rely on: (1) identifying individual patients most likely to benefit from NACT; (2) development of response-adapted radiation strategies following NACT; and (3) anticipated further dose reductions to organs at risk with proton and particle therapy. With increasing numbers of survivors, many in the prime of their adult life, research to identify, and strategies to address the unmet needs of NPC survivors are required. This contemporary review will summarize our current knowledge of long-term toxicity, QoL and unmet needs of this survivorship group.

Keywords: nasopharyngeal carcinoma, radiotherapy, chemotherapy, quality of life, survivorship, toxicity, unmet needs

INTRODUCTION

The last three decades have seen considerable progress in the management of patients diagnosed with nasopharyngeal cancer (NPC). While highly conformal radiotherapy (RT) remains the backbone of NPC treatment, the main research focus has been on optimal integration of systemic therapy for both radiosensitization to maximize locoregional control and eradication of micrometastatic disease to address the predominant mode of treatment failure (1, 2). The landmark intergroup 0099 study (3) established concomitant and adjuvant cisplatin-based chemotherapy as the standard of care, although much controversy followed, spawning a generation of clinical trials and meta-analyses targeted at identifying those patients most likely to derive benefit from additional systemic treatment (4–8). Flash forward to 2020 and neoadjuvant chemotherapy (NACT) in combination with platinum-based concurrent chemoradiation has become the preferred approach (9–12). In parallel, major technological advances in radiotherapy delivery have allowed for dose escalation to target volumes and reduced normal tissue dosing, resulting in improved disease control (13, 14), toxicity, and QoL (13–19).

While these successes should be celebrated, NPC survivors still harbor a substantial burden of long-term toxicity following successful treatment of their cancer. In endemic populations, the incidence of NPC shows a sharp increase from the third decade, peaking in the sixth decade; in low-risk populations, the incidence increases with age (20). As a consequence, the majority of patients afflicted with NPC are healthy middle-aged adults in the prime of their lives. While the most common and readily apparent radiation-induced toxicities of hearing loss, xerostomia, dysphagia, and hypothyroidism are well-quantified in the literature, survivors face numerous challenges. These include, amongst others, cognitive changes, fatigue, and emotional distress. Although targeted research is lacking, it is likely that NPC survivors will suffer from similar unmet needs to the general head and neck cancer (HNC) population, including workplace rehabilitation, sexual dysfunction and fear of cancer recurrence (21). The focus of this article will be to review our understanding of long-term toxicity, QoL and unmet needs and offer future avenues for targeted research in NPC populations.

TOXICITY AND QUALITY OF LIFE OUTCOMES

Much of our understanding of toxicities from prospective clinical trials has been reported through the eye of the clinician (**Table 1**). In contemporary oncology practice, the emphasis has shifted to patient-reported outcome measures (PROMs) as it is reasonably well-established that clinicians may unintentionally under report symptoms (46, 47) and their severity (48, 49) compared to patients. Only a few of the reported prospective series to date have included PROMs, including QoL assessments (**Table 1**). The most common PROM collected has been QoL, with the majority of studies using the validated European Organization for Research and Treatment of Cancer quality of life core questionnaire (EORTC QLQ-C30) and the accompanying head and neck module (EORTC QLQ- H&N35) (**Table 1**). The QLQ-C30 contains 30 items which map to a global health status/QoL score (composed of two items), five functional scales, three multi-item symptom scales, and six single symptom items (50); while the 35 items from the QLQ-H&N35 maps to seven symptom scales and 11 single items (51). Higher scores in the global QoL score and functional scales reflect better QoL or function, while on the symptom scales and items higher scores indicate an increased severity of symptomology. An additional challenge in interpreting QoL data in the current NPC literature has been the reliance on reporting statistically-determined differences rather than clinically meaningful differences, a limitation which has been identified across the oncology trials landscape (52). A commonly used "minimal clinically important difference" in the EORTC modules has been a difference of 10 (53), while Cocks and colleagues have ascribed numerical differences in the components of the EORTC QLQ-C30 as clinically trivial, small, medium or large (54). In the discussion that follows, the clinical difference proposed by Cocks et al. will be used in discussion on the QLQ-C30, and given there are no corresponding thresholds for the QLQ-H&N35, an estimate of 10 will be used to suggest a clinically meaningful differences in the components of that module.

Prospective Chemotherapy Studies

Chemoradiotherapy With or Without Neoadjuvant or Adjuvant Chemotherapy

The optimal integration of systemic treatment into the management of NPC has driven a large body of prospective clinical trials, both in endemic (2, 4, 6, 9–12, 22–24, 27–29, 31) and non-endemic regions (3, 25, 26, 30, 55, 56). NACT has emerged as the front runner, based on superior tolerability and compliance, but more importantly, has more consistently shown improvements in survival over concurrent cisplatin-based chemoradiotherapy (CRT) alone (9, 10, 22). Except where specifically mentioned, toxicity data has been reported from the perspective of the clinician.

The additional increase in toxicity from NACT appears to be manageable and limited to the treatment period, or shortly thereafter, with no differences in clinician-reported late toxicity. As anticipated, NACT results in higher rates of acute hematological toxicity, which in most cases is transient (9–11, 23, 24). While not a consistent finding, some studies report higher rates of nausea and/or vomiting (9–11, 23, 24) and severe mucositis (24) during the RT phase of treatment following NACT than without it. The data from these studies currently suggest that severe late toxicity (≥grade 3) is not enhanced with the addition NACT, however longer term reports are needed to confirm this finding (**Table 2**) (9, 12, 22–24). One of the concerns about combining cisplatin induction chemotherapy with concurrent cisplatin and radiation is the potential for increased toxicity related to the cumulative dose of cisplatin e.g., peripheral neuropathy. Indeed a higher rate of grade 1–4 peripheral neuropathy was reported in the gemcitabine-cisplatin induction study (9). In this trial there was also a higher incidence of acute nephrotoxic events. No difference in ototoxicity was

TABLE 1 | Selected NPC studies reporting long-term quality of life and toxicity and the instruments used.

Study	No.	Treatment	RT	QoL assessment	Toxicity measurement	
					Clinician-reported	Patient-reported
PROSPECTIVE CONCURRENT CRT ± NEO/ADJUVANT CHEMOTHERAPY						
Sun et al. (10) Li et al. (22)	241	HDC-CRT ± TPF induction	IMRT 100%	Not yet reported	Acute - CTCAE v3.0 Late - RTOG	No
Tan et al. (23)	172	LDC-CRT ± GCP induction	IMRT 98% 2D 4%	EORTC QLQ-C30 and H&N35	Acute - CTCAE RTOG Late - RTOG	EORTC QLQ-H&N35
Zhang (9)	480	HDC-CRT ± GC induction	IMRT 100%	No	Acute - CTCAE v4.0 Late - RTOG	No
Cao (11)	476	MDC-CRT ± PF induction	IMRT 43% 2D 57%	No	Acute - CTCAE v4.0 Late - RTOG	No
Hui (12)	65	LDC-CRT ± DP induction	3D	EORTC QLQ-C30 and H&N35	Acute - CTCAE v2.0 Late RTOG	EORTC QLQ-H&N35
Hong (24)	479	LDC-CRT ± MEPFL induction	IMRT 61% 3D 39%	No	Acute - CTCAE v3.0 Late RTOG	No
Fountzilas (25)	141	LDC-CRT ± CET induction	3D 100%	No	Acute - CTCAE v3.0 RTOG - Late RTOG	No
Frikha (26)	83	LDC-CRT ± TPF	IMRT 37%	No	CTCAE v3.0	No
Chen (6, 27)	508	LDC-CRT ± PF	IMRT 42% 3D 5% 2D 53%	No	Chemotherapy toxicity - CTCAE v3.0 RT toxicity - RTOG	No
PROSPECTIVE RT ALONE ± CONCURRENT WITH ADJUVANT OR ADJUVANT STUDIES						
Al-Sarraf et al. (3)	193	RT alone vs. HDC-CRT + PF	2D	No	SWOG	No
Wee et al. (4)	221	RT alone vs. HDC-CRT + PF	2D	No	Acute–RTOG	No
Lee et al. (28, 29)	348	RT alone vs. HDC-CRT + PF	2D 41% Mix 8% Conformal 61%	No	RTOG Chemo toxicities - WHO	No
Rossi et al. (30)	229	RT alone ± VAC	2D	No	Method/System NR	No
Chi et al. (31)	157	RT alone ± PF	2D	No	Method/System NR	No
OTHER PROSPECTIVE CHEMOTHERAPY STUDIES						
Chen, Li (5, 22)	230	RT alone vs LDC-CRT (stage II only)	2D	No	Acute–CTCAE Late–RTOG	No
Lee (2)	109	Weekly vs. triweekly CRT (+ Adjuvant)	IMRT 74% 2D-CRT 16%	EORTC QLQ-C30 and H&N35	Acute–RTOG	EORTC QLQ-H&N35
PROSPECTIVE INTENSITY-MODULATED vs. 2D/3D RADIOTHERAPY STUDIES						
Kam et al. (32)	60	IMRT vs. 2D	IMRT 50% 2D 50%	No	RTOG	No
Pow et al. (33)	46	IMRT vs. 2D	IMRT 52% 2D 48%	EORTC QLQ-C30 and H&N35	No	EORTC QLQ-H&N35
Peng et al. (14)	616	IMRT vs. 2D	IMRT 50% 2D 50%	No	CTCAE v3.0	No

(Continued)

TABLE 1 | Continued

Study	No.	Treatment	RT	QoL assessment	Toxicity measurement	
					Clinician-reported	Patient-reported
Fang et al. (34)	203	IMRT vs. 3D	IMRT 46% 3DCRT 54%	EORTC QLQ-C30 and H&N35	No	EORTC QLQ-H&N35
OTHER ENDEMIC STUDIES						
Fang et al. (17)	237	28% CRT	Conventional 64% (2D 26%, 2D + 3D boost 38%) Conformal 36% (3D 14%, IMRT 22%	EORTC QLQ-C30 and H&N35	No	EORTC QLQ-H&N35
Fang et al. (35)	68	CRT 100%	VMAT 100%	EORTC QLQ-C30 and H&N35	CTCAE v4.03	EORTC QLQ-H&N35
Hong et al. (36)	216	CRT 98%	IMRT 75%	EORTC QLQ-C30	Reported, but method/system not clear	Reported, but method/system not clear
Fang et al. (18)	356	CRT 35%	IMRT 24% 3D 16% 2D+3D boost 30% 2D 30%	EORTC QLQ-C30 and H&N35	No	EORTC QLQ-H&N35
Pan et al. (37)	106	CRT 48%	IMRT 56% 2D 44%	EORTC QLQ-C30 and H&N35	No	EORTC QLQ-H&N35
Tsai et al. (19)	242	CRT 66%	IMRT 41% Non-IMRT 59%	EORTC QLQ-C30	CTCAE v4.0	No
Wu et al. (38)	192	CRT 23%	2D 34% Co-60 66%	Chinese SF-36	No	No
Lee et al. (13)	1593	-	IMRT 28% 3D 45% 2D 27%	No	RTOG CTCAE v3.0	No
NON-ENDEMIC STUDIES						
Tonoli et al. (39)	136	CRT 91%	IMRT 95% 3D 5%	No	CTCAE v3.0	No
McDowell et al. (40)	107	CRT 93%	IMRT 100%	FACT-HN	CTCAE v4.03	MDASI-HN
Takiar et al. (41)	66	CRT 99%	IMRT 100%	No	CTCAE v4.0	No
Lastrucci et al. (42)	25	CRT 64%	IMRT 16% 3D 21% 2D 63%	FACT-NP XeQoLS	CTCAE v4.03	No
Talmi et al. (43)	28	CRT 64%	2D	(UW)-QoL	No	(UW)-QoL includes patient reported toxicity
Ghiggia et al. (44)	21	CRT 100%	NS	EORTC QLQ-C30 and H&N35	RTOG	EORTC QLQ-H&N35
Yee et al. (45)	82	CRT 77%	3D 43% 2D 57%	No	RTOG	No

RT, radiotherapy; QoL, Quality of Life; HDC, high dose/three weekly cisplatin; CRT, concurrent chemoradiotherapy; TPF, paclitaxel, cisplatin, 5-fluorouracil; IMRT, intensity-modulated radiotherapy; CTCAE, common terminology criteria of adverse events; RTOG, Radiation Therapy Oncology Group; LDC, low dose/weekly cisplatin; GCP, gemcitabine, carboplatin, paclitaxel; 2D, two dimensional radiotherapy; EORTC QLQ-C30, European organization for research and treatment of cancer core quality of life questionnaire; EORTC QLQ-H&N35, European organization for research and treatment of cancer head and neck quality of life questionnaire module; GC, gemcitabine, cisplatin; MDC, moderate dose/three weekly cisplatin; PF, cisplatin, fluorouracil; DP, docetaxel, cisplatin; 3D, three-dimensional radiotherapy; MEPFL, mitomycin, epirubicin, cisplatin, fluorouracil, leucovorin; CET, cisplatin, epirubicin, paclitaxel; SWOG, southwest oncology group; VAC, vincristine, Adriamycin, cyclophosphamide; VMAT, Volumetric Arc Therapy; FACT-HN, Functional Assessment of Cancer Therapy, Head & Neck cancer; MDASI-HN, MD Anderson symptom inventory, head and neck; FACT-NP, Functional Assessment of Cancer Therapy, Nasopharynx cancer; XeQoLS, University of Michigan Xerostomia-Related Quality of Life scale; (UW)-QoL, University of Washington Quality of Life Questionnaire.

reported, though it is possible that clinician reported late cisplatin side effects may underestimate the incidence.

Only two of these prospective NACT studies have reported QoL (**Table 3**) (12, 23). The larger, from Singapore, randomized 172 patients between concurrent weekly cisplatin (40 mg/m^2) with or without induction therapy using gemcitabine, carboplatin and paclitaxel (23). Almost all patients were treated with intensity-modulated radiotherapy (IMRT; 98%). The QLQ-C30

TABLE 2 | Selected studies reporting clinician-rated late toxicities (grade ≥3).

Study	No.	Treatment	RT	FU	Any ≥G3	Xerostomia	Dysphagia	Hearing	TLN	CN	Notes
PROSPECTIVE CONCURRENT CRT ± NEO/ADJUVANT CHEMOTHERAPY											
Li et al. (22)	480	HDC-CRT ± TPF induction	IMRT	5.9 y	9% (9 vs. 8%)	1% (0.8 vs. 2%)	NR	6% (6 vs. 6%)	0% (0 vs. 0%)	1% (2 vs. 1%)	No difference between arms
Tan et al. (23)	172	LDC-CRT ± GCP induction	IMRT 98% 2D 4%	3.4 y	NR	8% (11 vs. 5 NS)	NR	NR	NR	NR	No difference between arms
Zhang et al. (9)	480	HDC-CRT ± GC induction	IMRT	3.6 y	10% (11 vs. 9%)	3% (2 vs. 3%)	NR	6% (7 vs. 5%)	0.4% (1 vs. 0%)	0.8% (0.8 vs. 0.8%)	No difference between arms, except higher G1/2 peripheral neuropathy in induction arm
Hui et al. (12)	65	LDC-CRT ± DP induction	3D	3.0y FU	57% (65 vs. 50%)	NR	1.6% (4 vs. 0%)	10% (12 vs. 9%, NS)	NR	NR	No difference in late toxicity between arms
Hong et al. (24)	479	LDC-CRT ± MEPFL induction	IMRT 61% 3D 39%	6.0 y	15% (13 vs. 17%, NS)	2% (2 vs. 2%)	6% (4 vs. 7%)	NR	NR	NR	No difference between arms
Chen et al. (6, 27)	508	LDC-CRT alone vs. LDC-CRT + PF	IMRT 42% 3D 5% 2D 53%	5.7 y	24% (21 vs. 27%, p=0.14)	7% (6 vs. 7%)	NR	12% (11 vs. 13)	3% (3 vs. 3%)	2% (2 vs. 2%)	No difference in late toxicity between arms
PROSPECTIVE RT ALONE ± CONCURRENT WITH ADJUVANT STUDIES											
Lee et al. (28)	172	RT alone vs. HDC-CRT + PF	2D 41% Mix 8% Conf 61%	10.7 (min 10y FU)	52 vs. 47%, p=0.20)	NR	1.7% (2 vs. 1%)	24% (27 vs. 20%)	1% (2 vs. 0.6%)	6% (7 vs.5%	Chemotherapy did not increase late toxicity
OTHER PROSPECTIVE CHEMOTHERAPY STUDIES											
Chen, Li et al. (5, 22)	230	RT alone vs LDC-CRT	2D	10.4 y	26% vs. 35% (NS)	0 vs. 0%	NR	15 vs. 13%	10 vs. 6%	11 vs. 12	No difference in late toxicity between 3D and IMRT
PROSPECTIVE INTENSITY-MODULATED vs. 2D/3D RADIOTHERAPY STUDIES											
Kam et al. (32)	60	IMRT vs. 2D	IMRT 50% 2D 50%	1 y assessment	NR	39 vs. 82%*	NR	NR	NR	NR	
Peng et al. (14)	616	IMRT vs. 2D	IMRT 50% 3D 50%	3.5 y	NR	0 vs. 2 (≥G3) 10 vs. 29 (≥G2)	NR	26 vs. 84% (p<0.001)	21 vs. 13% (p=0.01)	4 vs. 9 (p=0.02)	Comparison of toxicity (grades) not clear in late analysis; significant differences across multiple late toxicities and additional for trismus and neck fibrosis
OTHER ENDEMIC STUDIES											
Fang et al. (35)	68	100% CRT	VMAT 100%	4 y cumulative incidence	3%	0%	NR	3%	0%	0%	Single arm VMAT report
Tsai et al. (19)	242	CRT 66%	IMRT 41% Non-IMRT 59%	EORTC QLQ-C30	CTCAE v4.0						
Lee et al. (13)	1593	-	IMRT 28% 3D 45% 2D 27%	6.8 y (0.2–18.4 y)	NR	NR	NR	IMRT 17% 3D 19% 2D 10%	IMRT 1% 3D 2% 2D 3%	IMRT 2% 3D 2% 2D 5%	

(Continued)

TABLE 2 | Continued

Study	No.	Treatment	RT	FU	Any ≥G3	Xerostomia	Dysphagia	Hearing	TLN	CN	Notes
NON-ENDEMIC STUDIES											
Tonoli et al. (39)	136	CRT 91%	IMRT 95% 3D 5%	At 3 y	NR	1%	6%	9%	NR	NR	
McDowell et al. (40)	107	93% CRT	IMRT	7.5 y	47%	1%	3%	43%	0%	10%	
Takiar et al. (41)	66	CRT 99%	IMRT 100%	3.2 y	49% (5 years)	2%	0%[#]	29%	14%	3%	
Yee et al. (45)	82	CRT 77%	3D 43% 2D 57%	9.2 y	6%	0%	0%	1%	1%	NR	
Lastrucci et al. (42)	25	CRT 64%	IMRT 16% 3D 21% 2D 63%	7.1 y	12%	0%	0%	0%	0%	0%	
Ghiggia et al. (44)	21	CRT 100%	NS	4.5 y	NS	19%	NS	NS	NS	NS	

RT, radiotherapy; FU, follow up; G3, grade 3 toxicity; TLN, temporal lobe necrosis; CN, cranial neuropathy; high dose/three weekly cisplatin; CRT, concurrent chemoradiotherapy; TPF, paclitaxel, cisplatin, 5-fluorouracil; IMRT, intensity-modulated radiotherapy; NR, not recorded; LDC, low dose/weekly cisplatin, GCP, gemcitabine, carboplatin, paclitaxel; 2D, two-dimensional radiotherapy; NS, not stated; GC, gemcitabine, cisplatin; DP, docetaxel, cisplatin; 3D, three-dimensional radiotherapy; MEPFL, mitomycin, epirubicin, cisplatin, fluorouracil, leucovorin; PF, cisplatin, 5-fluorouracil; Volumetric Arc Therapy.

[*]grade 2-4 xerostomia only reported; [#]2/66 (5%) required esophageal dilatation for esophageal strictures, but a feeding tube was not required.

and QLQ-H&N35 modules were collected at baseline, day 8 of cycle 2 in the NACT arm, during CRT (week 4), at the end of CRT, and at 3, 12, 24, and 60 months after treatment. Global QoL was similar between the two arms at all corresponding time points. Transient (and clinically small) differences favoring the CRT alone arm were observed in the EORTC QLQ-C30 dyspnoea (24.3 vs. 15.3; $p = 0.014$) and diarrhea (15.2 vs. 9.3; $p = 0.018$) scales. Somewhat counterintuitively patients in the CRT alone arm reported higher scores for pain, swallowing problems and pain killer use during treatment, and reported worse social contact at 3 months. It is unclear if these differences were purely statistical as the size of the difference was not included in the report. In all cases, these differences were isolated to the acute treatment and recovery period and differences resolved with follow up. In the smaller study of 65 patients reported by Hui et al., patients were randomized to CRT (with 3D-RT) with or without cisplatin-docetaxel induction (12). In both arms, declines were seen in the QLQ-C30 and QLQ-H&N35 scores compared to baseline in the acute treatment period, which gradually returned to baseline over time, and differences in global QoL scores did not differ between the arms at the measured times points. A deterioration in physical functioning scores was more marked in those receiving NACT during the treatment period (mean change in scores −42.9 vs. −27.7, $p = 0.0499$), although this resolved with further follow up. In the symptom scales, appetite (mean change 18.6 vs. −5.3; $p = 0.023$) and constipation (mean change 24.5 vs. −3.8; $p = 0.0075$) scores were worse in the NACT arm compared to the CRT alone arm at 4 weeks after CRT, but there were no differences at subsequent follow up. Differences by arm in the QLQ-H&N35 were seen only in the nutritional supplement score at the 24 month assessment only (mean change score, 10.0 vs. −23.5; $p = 0.025$), favoring the concurrent only arm.

In the single study to prospectively evaluate the addition of adjuvant chemotherapy (PF) following definitive chemoradiotherapy, Chen et al. found that severe late toxicity was similar between arms, with the exception of peripheral neuropathy, which was worse in the adjuvant arm, but the overall rate of severe toxicity (≥grade 3/4) was low (2 vs. 0.4%, $p = 0.05$) (6, 27).

Taken together, the published literature to date suggests that NACT or adjuvant chemotherapy is well-tolerated with manageable and time-limited toxicity compared to standard cisplatin-based CRT.

Prospective Studies of Chemotherapy Compared to Radiotherapy Alone

Radiotherapy as a single modality treatment is generally reserved for stage I disease (T1N0). While adding concurrent chemotherapy significantly improved survival in stage II patients (Chinese 1992 staging system) treated with 2D RT (5, 22), its necessity is under question in the IMRT era (57–59). In the prospective study by Chen et al., all patients were treated with 2D and the experimental arm consisted of weekly (30 mg/m2) cisplatin (5, 22). Patients in the CRT arm had a higher incidence of any severe acute toxicity (≥grade 3, 64 vs. 40%, $p < 0.001$), and a significant increase was observed for hematological toxicity, nausea and vomiting (9 vs. 0%, $p = 0.001$), and mucositis (46

TABLE 3 | Selected NPC studies reporting Quality of Life outcomes.

Study	No.	Treatment	RT	FU	QoL	QoL findings
PROSPECTIVE CONCURRENT CRT ± NEO/ADJUVANT CHEMOTHERAPY						
Tan et al. (23)	172	LDC-CRT ± GCP induction	IMRT 98% 2D 4%	3.4 y	EORTC QLQ-C30 and H&N35	No difference in global QoL, GCP arm worse dyspnea and diarrhea during CRT; H&N35, worse pain swallowing use of pain killers in GCP during CRT and for social contact at 3 m
Hui et al. (12)	65	LDC-CRT ± DP induction	3D	-	EORTC QLQ-C30 and H&N35	No difference in global QoL; Physical functioning more deterioration, appetite and constipation worse at 4 months in induction arm; all resolved with longer follow up; Only difference in H&N35 was nutritional supplement use in induction arm at 24m post treatment
OTHER PROSPECTIVE CHEMOTHERAPY STUDIES						
Lee et al. (2)	109	LDC vs. HDC CRT (+ adjuvant)	IMRT 74% 2D 16%	Last QoL at 12 m	EORTC QLQ-C30 and H&N35	Patients on weekly regimen showed better PF, EF and SF than the triweekly group and reported less appetite loss 3 weeks post treatment; Worse speech, social contact and sticky saliva in triweekly group; No differences at 3 and 12 m post treatment except dry mouth (3 m) and SF (12 m) post CRT
Pow et al. (33)	46	IMRT vs. 2D	IMRT 52% 2D 48%	Longitudinal assessment baseline, 2, 6 12 m post RT	EORTC QLQ-C30 and H&N35	No difference between IMRT and CRT global QoL at any point; at 12 m both global QoL scores = 64; No differences between baseline and 12 m post treatment, except global QoL, RF, EF were higher and insomnia lower than baseline in both groups; most of the domains showed improvement from 2 to 12 months. Role-physical, bodily pain, and physical function domains better in IMRT cohort
OTHER ENDEMIC STUDIES						
Fang et al. (17)	237	28% CRT	Conventional 64% (2D 26%, 2D + 3D boost 38%) Conformal 36% (3D 14%, IMRT 22%	-	EORTC QLQ-C30 and H&N35	Global QoL higher in conformal group (63 v51, $p<0.01$) Conformal outcomes better across multiple points including PF, EF CF, SF functioning domains; 6/12 QLQ-C30 symptom scales and 12/13 H&N35 symptom scales On UVA, QoL better in higher educated, higher income, employed, conformal technique and less medical comorbidities
Fang et al. (34)	203	CRT 55%	IMRT 46% 3D 54%	Longitduinal Baseline, during RT and 3, 12, and 24 m post RT	EORTC QLQ-C30 and H&N35	12 and 24 months global QoL 61 and 62; IMRT better global QoL, fatigue, taste, dry mouth and feeling ill at 3 m, improved with time; No other medical, sociodemographic factors predicted worse QoL; General trend of deterioration followed by recover in most QoL scales from baseline to during, and then after RT
Fang et al. (35)	68	CRT 100%	VMAT 100%	Longitudinal: baseline, during RT, 3 m, 12 m	EORTC QLQ-C30 and H&N35	12 months global QoL mean score 78; Generally maximal decline in most scales from baseline to mid treatment with improvement thereafter; Chemotherapy or medical or sociodemographics factors did not predict QoL score
Hong et al. (36)	216	CRT 98%	IMRT 75% Conformal 25%	4.4 y (mean)	EORTC QLQ-C30	Mean global QoL 74; no difference by time since treatment; factors associated with better QoL were older age, higher education, higher anxiety and depression scores, worse dry mouth and fatigue, and higher disease stage

(Continued)

TABLE 3 | Continued

Study	No.	Treatment	RT	FU	QoL	QoL findings
Fang et al. (18)	356	CRT 35%	IMRT 24% 3D 16% 2D+3D boost 30% 2D 30%	NR	EORTC QLQ-C30 and H&N35	Global QoL mean score 53; Age, gender, education, family income, CCI and RT technique associated with QoL; on multi-factor analysis education, family income and RT technique significant
Pan et al. (37)	106	CRT 48%	IMRT 56% 2D 44%	≥3 y (3.2–7.4 y)	EORTC QLQ-C30 and H&N35	Compared to CRT, RT alone patients reported better global QoL [77 vs. 68, $p < 0.001$)], PF, RF, EF; RT alone patients reported lower scores on selected symptom scales (fatigue, insomnia, financial problems, and weight gain); differences still apparent whether analyzed by RT technique
Tsai et al. (19)	242	CRT 66%	IMRT 41% Non-IMRT 59%	≥5 y	EORTC QLQ-C30	Mean global QoL 57; severe neuropathy, hearing loss and xerostomia associated with worse global QoL, all functional scales (PF, RF, EF, CF, SF, and some symptom scales.
Wu et al. (38)	192	CRT 23%	2D 34% Co-60 66%	3.6 y	Chinese SF-36	Most functional domains worse than general population. On multiple regression analysis medical comorbidities, monthly income, age, and T stage independently impacted global QoL
NON-ENDEMIC STUDIES						
McDowell et al. (40)	107	3% CRT	IMRT	7.5 y	FACT-HN	Mean total score FACT-HN 105.0 On UVA QoL associated with: marital status, employment status, time since treatment, chemotherapy, emotional distress, multiple clinician and patient-reported toxicities
Lastrucci et al. (42)	25	CRT 64%	IMRT 16% 3D 21% 2D 63%	7.1 y	FACT-NP XeQoLS	FACT-NP median 127; XeQoLS 31 younger patients better QoL; only xerostomia showed borderline association with global FACT-NP score (p=0.06)
Talmi et al. (43)	28	CRT 64%	2D	5.4 y (mean)	(UW)-QoL	Mean QoL score 4.2;
Ghiggia et al. (44)	21	CRT 100%	NS	4.5 y (mean)	EORTC QLQ-C30 and H&N35	Mean QoL score 74;

RT, radiotherapy; FU, follow up; QoL, Quality of Life; LDC, low dose/weekly cisplatin; CRT, concurrent chemoradiotherapy; IMRT, intensity-modulated radiotherapy; 2D, two-dimensional radiotherapy; GCP, gemcitabine, carboplatin, paclitaxel; EORTC QLQ-C30, European organization for research and treatment of cancer core quality of life questionnaire; EORTC QLQ-H&N35, European organization for research and treatment of cancer head and neck quality of life questionnaire module; GC, gemcitabine, cisplatin; DP, docetaxel, cisplatin; HDC, high dose/three weekly cisplatin; 3D, three-dimensional radiotherapy; PF, physical functioning; EF, emotional functioning; SF, social functioning; RF, role functioning; CF, cogntivie functioning; FACT-HN, Functional Assessment of Cancer Therapy, Head & Neck cancer; FACT-NP, Functional Assessment of Cancer Therapy, Nasopharynx cancer; XeQoLS, University of Michigan Xerostomia-Related Quality of Life scale; (UW)-QoL, University of Washington Quality of Life Questionnaire.
y, year.

vs. 33%, $p = 0.04$). At the 10 years follow up, there was no significant differences in late toxicity (RT 26 vs. CRT 35%). In a cross-sectional study which analyzed QoL outcomes in in stage II patients who had been treated with either RT alone or CRT, and a follow up time of at least 3 years, the authors reported that the addition of chemotherapy resulted in a detrimental impact on global QoL and a number of the functional and symptom scales from the QLQ-C30 and QLQ-H&N35 (37). When the analysis was restricted to patients treated only with IMRT, the authors reported a similar finding. In this study, the reported differences across the QLQ-C30 scores for the full and IMRT cohorts, which were in favor of the RT alone group would be considered small, with the exception of the financial problems item which would be considered of medium difference. In the IMRT alone cohort, there were some statistical differences favoring the RT alone group in the QLQ-H&N35 items, but only the less sexuality, nutritional supplements and weight gain items were in excess of ten points difference.

In the landmark studies which randomized patients to radiotherapy alone with or without concomitant and adjuvant chemotherapy, there was a predictable transient increase in severe hematological toxicity (3–5, 28, 29), mucositis (4, 5, 28), and nausea/vomiting (3–5, 28). Of these studies, the Hong Kong Nasopharyngeal Cancer Study Group NPC-9901 study published 10-year toxicity outcomes (28, 29). They reported no differences with respect to grade 3 or higher toxicities between the CRT and RT arms (52 vs. 47%, $p = 0.20$); and the majority of severe toxicity in both arms was attributable to ototoxicity, which was surprisingly similar between the arms (CRT 37 vs. RT alone 27%, $p = 0.19$). One interesting finding from this study was that severe

late toxicity was higher in the chemotherapy arm at 3 years, a difference which dissipated with longer follow up. Numerically there was a shorter average latency time to developing a severe toxicity in the chemotherapy group which did not reach statistical significance (4.2 years vs. 4.7 years, $p = 0.40$). However, this latency period is quite informative when interpreting late toxicity data from other clinical trials, where follow up may not extend beyond 5 years.

Prospective Concurrent Studies—Three Weekly or Weekly Chemotherapy?

The optimal schedule of concurrent cisplatin in the definitive setting remains an unanswered question across the breadth of HNC subsites, including NPC. This question has only been addressed prospectively in NPC in a phase II study from the Korean Cancer Study Group (2). The study found no differences between clinician reported toxicity in the acute phase of treatment. While global QoL was not significantly different at any point during the study, patients treated on the weekly arm showed improved physical ($p = 0.039$), emotional ($p = 0.019$), and social functioning ($p = 0.008$) compared to the triweekly group at 3 weeks after completion of CRT, but these differences diminished at subsequent follow up. On the symptom scales (QLQ-C30 and H&N35), the triweekly group reported more appetite loss ($p = 0.006$) and problems with speech ($p = 0.003$), social contact (p-0.043) and sticky saliva ($p = 0.019$) than the weekly group. These differences again largely resolved (dry mouth had a persistent difference at 3 months) with longer follow up. Although both chemotherapy and RT for HNC can cause significant hearing loss and dysfunction, this is not captured in either of the EORTC modules. While non-NPC HNC series have reported worse ototoxicity with high dose (three weekly) compared to low dose (weekly) (60, 61), in this study it was not captured in the PROMs and only acute treatment-related toxicity was recorded; with only two patients reported as developing hearing loss, one from each arm.

Meta-Analysis of Chemotherapy in NPC Trials—MAC-NPC

The Meta-Analysis of Chemotherapy in Nasopharynx Carcinoma (MAC-NPC) collaborative group included an analysis of acute and late toxicity differences with the addition of chemotherapy to RT alone (7). This analysis predates the most recent practice-changing NACT studies. Mirroring results from the included studies, the addition of chemotherapy resulted in a significant increase in acute hematological toxicity and nausea/vomiting and mucositis. In addition, acute ototoxicity and more profound weight loss were also significantly higher with chemotherapy. While most of the individual studies did not identify an increase in late toxicities, the pooled analysis reported significantly higher rates of long-term hearing deficits ($p = 0{\cdot}00068$) and a borderline increased risk of a cranial neuropathy ($p = 0.052$).

Prospective Radiotherapy Specific Studies

Impact of Radiotherapy Technique Changes

The introduction of IMRT revolutionized NPC treatment, allowing both improved target volume coverage and reduced dose to adjacent organs at risk (OARs). At least three randomized controlled trials have addressed the benefit of IMRT compared to historical RT techniques, including 2D and 3D RT (**Tables 1–3**) (14, 32, 33). Peng et al. reported on the largest RCT, with 616 patients randomized to either IMRT or 2D RT (14). Local control favored the IMRT arm, with a corresponding reduction in the incidence of both acute toxicities, including xerostomia (≥Grade 2; 57 vs. 28%, $p < 0.001$) and hearing loss (89 vs. 47%, $p < 0.001$) and late toxicities (median follow up 3.5 years), including temporal lobe necrosis (TLN; 21 vs. 13%, $p = 0.01$), cranial neuropathy (9 vs. 4%, $p = 0.02$), trismus (14 vs. 3% $p < 0.001$), neck fibrosis (11 vs. 2%, $p < 0.001$), xerostomia (≥G1 99 vs. 40%, $p < 0.001$), and hearing loss (85 vs. 26%, $p < 0.001$). There was no QoL assessment in this study.

Two smaller prospective randomized studies specifically focused on the benefit of IMRT over 2D treatment with respect to salivary gland function (32, 33). Kam et al. reported lower rates of severe (clinician-reported) xerostomia in the IMRT arm (39 vs. 82%, $p < 0.001$), with corresponding higher rates of measured salivary flow (32). A xerostomia PROM was included, with a trend to improvement in the IMRT group. Pow et al. also reported that functional salivary flow showed significantly better recovery in the IMRT cohort (33). It is important to note that the mean doses delivered to the parotid in this study was higher than is generally used (where possible) in contemporary practice, with a mean ipsilateral and contralateral parotid dose of 42 (range 31–51Gy) and 41Gy (range 33–42 Gy), respectively. Using the EORTC QoL modules and the SF-36 questionnaire, IMRT-treated patients reported improved role-physical, bodily pain, and physical function scores at 1 year (all $p < 0.05$). Both groups reported dry mouth and sticky saliva, but better recovery of these xerostomia-type symptoms were observed in the IMRT cohort.

In a series form Taiwan, Fang et al. reported a longitudinal, but non-randomized comparison of 203 NPC patients, with any stage (I-IV), treated with either IMRT ($N = 110$) or 3D-RT ($N = 93$) (34). In this study, allocation was on the basis of clinician preference or linac availability. The EORTC QLQ-C30 and QLQ-H&N35 modules were assessed at baseline, mid treatment (week 4) and 3, 12, and 24 months after completion of treatment. The majority of patients completed all assessments (71.4%). As expected, maximal deterioration was seen during treatment which improved with subsequent follow up, and the benefit of IMRT over 3D-RT appeared to be limited to the early recovery period. The IMRT arm showed clinically meaningful better outcomes at 3 months for global QoL (56 vs. 44), fatigue (29 vs. 39), taste (22 vs. 35), dry mouth (49 vs. 59) and feeling ill (25 vs. 36); these differences diminished with ongoing follow up. From the same institution, a longer follow up of more than 5 years (median follow up: non-IMRT group 8.5 years, IMRT group 6.4 years) reported better long term toxicity experience for the IMRT cohort relative to the 3D-RT group across multiple domains of the QLQ-C30 and QLQ-H&N35, including moderate differences in global QoL, cognitive and social functioning, and fatigue on the QLQ-C30; and large differences in speech and dry mouth and moderate differences in most of the QLQ-H&N35 scales (16).

The experience and use of volumetric arc therapy (VMAT), is also increasing, and although there have been no direct clinical comparisons between standard IMRT and VMAT, planning studies have shown enhanced sparing of the parotids, brain stem and spinal cord is possible (62).

Adaptive Radiotherapy

Adaptive strategies in HNC offer the promise of reducing the degree of normal tissue irradiation based on early tumor response. In a replanning series by Yang et al., the outcomes of 129 IMRT-treated patients were compared. All patients were advised to have a repeat simulation scan either before the 15th fraction (12%), the 25th fraction (61%) or both (27%). However, only 86 were replanned (67%), while 43 (33%) refused, and consequently received the same plan throughout the treatment course (63). Two-year locoregional control favored the replanned arm (97.2 vs. 92.4%, $p = 0.040$), with similar survival (89.8 vs. 82.2%, $p = 0.475$). A significant benefit favoring the replanning group was reported on components of both the QLQ-C30 (global QoL, role and social functional scales and the dyspnea, appetite, constipation and diarrhea symptom scales) and the QLQ-H&N35 (speech, social contact, and teeth, mouth opening, dry mouth and sticky saliva) modules. Most of the differences were appreciable during the treatment and the early recovery period, with a diminishing difference with further follow up; for example, the differences in global QoL at 1 month post treatment (61 vs. 48), were of a medium sized clinical difference, while the difference at 12 months (82 vs. 78) is considered a trivial to small clinical difference (54). There was an imbalance in global QoL at baseline, favoring the non-replanning group (77 vs. 68), and while the non-replanned group returned to baseline with time, the replanned group actually demonstrated a positive shift from baseline, so the difference may be more significant than the 12-months results suggest. The diminishing difference with longer follow up was noticeable across most scales, with the exception of sticky saliva (24 vs. 17) and dry mouth (33 vs. 25), which both showed an ongoing higher symptom burden in the non-replanned group. While this is a potentially appealing strategy to reduce toxicity, adaptive treatment and replanning is resource-intensive. Further research regarding efficacy and efficient implementation is needed before adaptive treatment is likely to become routine.

Post-induction Response-Adapted Strategies

Adapting radiation dose and target volumes based on NACT response offers yet another strategy for reducing long-term toxicity and potentially improving QoL (64, 65). While better rates of local control have been achieved with a dose to the primary GTV $\geq$ 66.5 Gy (1), this may not be required for controlling microscopic disease in the setting of a complete response to NACT, when assessed by metabolic, radiological and clinical means. Yang et al. reported the results of a prospective randomized study including 212 patients with target volumes based on either pre (Arm A) or post induction (Arm B) imaging following a cisplatin doublet (paclitaxel or 5-FU) (64). Target definitions and doses used in this protocol are outlined in **Table 4**. Both the primary GTV (45 vs. 26 cm^3, $p < 0.001$) and high dose CTV (367 vs. 305 cm^3, $p = 0.045$) were smaller in Arm B. There were no differences in disease outcomes between these arms, either in the initial report (median follow up 35 months) (64), or in the subsequent 4 years update presented at ASTRO in 2019 (surprisingly, the presented data numerically favored the post-IC group) (66). There were no differences observed in acute clinician-rated toxicity, but lower rates of dry mouth were reported at 2 years in Arm B (grade 0-1/2-3: 68%/32% Arm A vs. 76%/24%; Arm B; $p = 0.042$). With respect to QoL, measured by the EORTC QLQ-C30, statistically significant differences in cognitive function (76 vs. 65) and lower pain scores (76 vs. 67) were reported, with the estimated clinical impact of these differences considered medium and small, respectively (54). In both arms the entire nasopharynx with a margin and the entire pre induction disease was treated to 64Gy/33#, and the usual intermediate risk area was included to 54Gy/33#, irrespective of response. Other series have also reported outcomes with full dose (70 Gy) to the post induction volumes and reduced doses (60 Gy) to the pre induction tumor volume (67, 68). Future strategies aimed at reducing toxicity will need to implement a strategy of reducing wide field treatment of the critical structures of the base of skull and brain to almost curative doses of radiation, capitalizing on how best to assess treatment response.

Although large scale clinical trials are lacking, there is further suggestion in the literature that doses to gross disease below 70 Gy may provide adequate locoregional control in some patients. In a phase II study from the Peter MacCallum Center, 35 patients were treated with three cycles of induction epirubicin, cisplatin and 5-fluorouracil, followed by cisplatin-based chemoradiation (56). Radiation therapy was delivered with 2D planning to 60 Gy over 6 weeks at standard fractionation. After three cycles, 30/35 (86%) had a documented clinical and radiological (MRI/CT) response (2 complete, 28 partial). At a median follow up of 43 months only two patients had a locoregional relapse; one regional relapse in the elective nodal region (50 Gy) and one local (and concomitant distant) failure where the upper level of the field was limited to 54 Gy to remain under optic chiasm tolerance. In the previously mentioned retrospective study by Ng et al. a significant difference in local and regional control was reported when at least 66.5 Gy was delivered to the respective GTVs using IMRT (1). However, less than half (41.5%) received induction chemotherapy, and GTVs were contoured according to pre induction volumes. Other series have analyzed control rates in patients who failed to complete the prescribed course of treatment. Wang et al. performed a propensity match analysis comparing 234 patients completing the prescribed 70 Gy course of radiotherapy with 32 patients who did not complete treatment due to severe acute toxicities (69). In the entire cohort, 163/266 (61.5%) received NACT. The median dose in the non-completion group was 63.6 Gy (range 53–67.8 Gy) and the authors reported no difference in 5-years locoregional failure free survival (LRFS) between those receiving the reduced dose or the prescribed dose (92.5 vs. 91.7%; $p = 0.863$). Furthermore, radiation dose was not a significant variable in a univariate analysis of prognostic factors for LRFS. A smaller series (n=19) by Lu et al. concluded that patients who received a minimum of 54 Gy had a 5-years LRFS of 100% (70).

TABLE 4 | Target volumes used in the study by Yang et al. (64).

Target/Group	Group A (pre-induction)	Group B (post induction)
Imaging timing	Pre-induction CT and MR	CT and MR at day 14, cycle 2 of induction (cisplatin + paclitaxel or 5-FU)
Pre-IC GTVnx	Clinical + imaging findings pre-IC;	Clinical + imaging findings pre-IC;
Post-IC GTVnx	N/A	Clinical + imaging findings post-IC;
GTVnx (includes primary and retropharyngeal nodes)	Pre-IC GTVnx	Post-IC GTVnx
P-GTVnx dose (GTVnx +3–5 mm)	70Gy/33#	70Gy/33#
CTV1 (subclinical disease)	Pre-IC GTVnx + 0.5–1 cm margin Whole nasopharyngeal wall 0.5cm margin under normal pharyngeal mucosa	Post-IC GTVnx + 0.5–1 cm margin Pre-IC GTVnx Whole nasopharyngeal wall 0.5 cm margin under normal pharyngeal mucosa
P-CTV1 dose (CTV1 + 3–5 mm)	64Gy/33#	64Gy/33#
GTVnd	Clinical + imaging findings of gross nodal disease post-IC Pre-IC ECE was assessed and included based in pre-IC imaging	Clinical + imaging findings of gross nodal disease post-IC Pre-IC ECE was assessed and included based in pre-IC imaging
P-GTVnd dose (GTVnd +3–5 mm)	70Gy/33#	70Gy/33#
CTV2	Pre-IC CTV1 Posterior nasal cavity Posterior maxillary sinus Pterygopalatine fossa Part of posterior ethmoid sinus Parapharyngeal space Skull base Clivus (whole/partial depending on involvement)	Post-IC CTV1 Posterior nasal cavity Posterior maxillary sinus Pterygopalatine fossa Part of posterior ethmoid sinus Parapharyngeal space Skull base Clivus (whole/partial depending on involvement)
Pre-IC CTV2	Elective nodal irradiation	Elective nodal irradiation
P-CTV2 (CTV2 + 3-5mm)	54Gy/33#	54Gy/33#

CT, computed tomography; MR, magnetic resonance imaging; 5-FU, 5-Fluorouracil; IC- induction chemotherapy; GTVnx, nasopharynx gross tumor volume; P-GTV-nx, high dose primary planning target volume; CTV, clinical planning volume; P-CTV –planning target volume based on CTV; GTVnd, nodal gross tumor volume; P-GTVnd, high dose nodal planning target volume.

However, this was a subset of only nine patients, and further details reported that there were no local or regional relapses in the 5-years follow up period when a minimum dose of 60 Gy was given. While interesting and potentially hypothesis generating, retrospective series reporting on patients failing to complete treatment are limited by bias, small numbers and heterogeneity in chemotherapy regimens.

Dose reductions, particularly to the base of skull region will likely offer a more beneficial strategy to reduce the burden of toxicity in NPC survivors than other proposed approaches, such as a reduction of elective nodal volumes. Under the auspices of a clinical trial, dose and volume de-escalation based on NACT response, incorporating clinical, radiological (both structural and metabolic) and biological response (including EBV-titres) may provide a real opportunity to further improve outcomes for these patients.

Reducing Elective Nodal Volumes

Two regions that may be spared from routine elective irradiation include the submandibular (Ib) station and the low neck (Level IV/Vb). Level Ib involvement at diagnosis or as a site of subsequent failure is an infrequent occurrence, although the risk may be higher in the following situations: [1] where a level II node measures >20 mm or demonstrates radiological extracapsular extension; [2] where there are bilateral cervical LNs (N2); or [3] if the primary tumor extends into the oropharynx (71). While this is appealing strategy to reduce toxicity, the clinical impact is less clear. The main rationale for omitting level Ib is to reduce xerostomia, however Zhang et al. failed to demonstrate a statistically significant reduction in the frequency of grade 2 or higher xerostomia in 904 low risk patients whether they had bilateral Ib sparing, unilateral Ib sparing, or inclusion of bilateral Ib (10 vs. 14 vs. 18%, $p = 0.06$). In optimizing dose reduction to the submandibular gland, the tradeoff may be an increase in dose to other xerostomia-critical organs such as the parotid or oral cavity (72). While a dose constraint of <39 Gy has been proposed for the submandibular gland, based on improvements in stimulated and unstimulated salivary gland flow in non-NPC cohorts, it can be challenging to meet this when there is gross disease at level 2, and mean doses ≥50 Gy are generally expected (73). Although there have been studies looking at omitting the low neck in selected case of NPC, there is little comparative data at present to suggest improved clinical outcomes with this approach (58, 74).

Particle Therapy

Particle therapy offers the potential to reduce doses to OARs in HNC treatment (75, 76) and planning studies in NPC have shown improved metrics, with respect to both target coverage and OAR doses (77–80). However, clinical reports on efficacy and toxicity are limited (79, 81, 82). In a small retrospective series of 10 patients treated with intensity-modulated proton therapy (IMPT) from MD Anderson, Lewis et al. reported no late grade 3 toxicities (79); and grade 1 and 2 xerostomia were reported in 6 and 1 patient/s, respectively. The median follow up was only 24.5 months, shorter than the average latency time to development of severe toxicity (29). A case matched series from that institution (10 IMPT and 20 IMRT cases), reported lower rates of gastrostomy tube insertion during treatment in patients treated with IMPT, 65 vs. 20% ($p = 0.020$) (80). Results from a prospective phase II study from Massachusetts General Hospital are awaited, as to date this has only been presented in abstract form (81). In the abstract report, grade 3 or higher late hearing and weight loss was reported in 29 and 38% of patients, respectively, and 1/23 patients remained PEG dependent at 12 months.

Target Volume and Treatment Planning Heterogeneity

While the above studies have highlighted a number of different strategies focusing on reducing toxicity, two large sources of heterogeneity in the treatment planning process which may significantly impact toxicity are variations in target volume contouring and what constitutes an acceptable radiotherapy treatment plan (83–85). While the pioneering work of Peters et al. eloquently demonstrated the detrimental impact of poorly compliant radiotherapy treatment plans on long-term survival in HNC patients (86), a less obvious sin is that of over-contouring, which while resulting in locoregional control, may labor survivors with unnecessary morbidity. The findings from Peters et al. have spawned a generation of international consensus guidelines for HNC contouring and dose prioritization, including recommendations for NPC (87, 88), and while they may have reduced the variation to some degree, they have not completely mitigated it (85). In addition, an increasing recognition of the importance of HNC case volume and expertise (89, 90) and the value of peer-review in clinical practice (91, 92) will have hopefully further reduced this variation. However, with the recent number of immunotherapy trials opening, there has been a concerning trend in the number of trials failing to include a comprehensive radiotherapy quality assurance program (93). Clinician variability in both contouring and the variations accepted in radiotherapy treatment plans are arguably the most significant factors in determining long-term treatment toxicity, reducing the benefit of other toxicity-sparing measures mentioned above, and further ways to ensure the delivery of optimal treatment plans is required.

Toxicity and Quality of Life Reports From Non-endemic Areas

The majority of studies reporting toxicity and QoL arise from NPC endemic regions, with a few studies reporting from non-endemic regions (**Tables 1**–**3**).

A prospective study of 136 patients treated at 12 Italian centers from 2008 to 2010 included patients mostly treated with IMRT (95%) and focused on clinician-reported toxicity (39). At 3 years follow up, hearing loss was the most common grade 3 toxicity (8.6%), followed by dysphagia (5.5%), periodontal disease (4.3%) and xerostomia (1.3%). The frequency of the most common grade 2 toxicities were xerostomia (23.4%), hearing loss (12.9%), and dysphagia (12.3%).

One of the more comprehensive studies from a non-endemic region comes from a cross-sectional study conducted at the Princess Margaret Hospital in Toronto (40). This study included clinician and patient-reported toxicity, a QoL measure, audiometry testing, basal endocrine screening (thyroid and pituitary) and a cognitive and neurobehavioral assessment. There were 107 patients enrolled at a median follow up time of 7.5 years (4.1–11.1 years) following IMRT. The highest rated patient-reported toxicities/problems from the MDASI-HN were dry mouth, mucous, swallowing/chewing, memory and teeth and gums. The prevalence of ≥grade 3 toxicities was 47% (50/107); mostly hearing loss (43%), with a much smaller prevalence (11%) of non-hearing grade 3 toxicities, including 11 patients (10%) with ≥grade 3 cranial neuropathies. One-quarter of patients reported moderate to high levels of fatigue. On univariate analysis, a number of factors correlated with worse global QoL, including social factors (living, marital and employment status), treatment factors (time since treatment, use of chemotherapy), emotional distress (depression or anxiety) and multiple clinician graded toxicities (hearing, ear discharge, dysphagia, trismus, aspiration, and cranial neuropathy). When correlating patient-reported toxicity, every item of the MDASI-HN PRO correlated with QoL, indicating that the presence of any significant symptom has capacity to adversely impact QoL.

In a series of IMRT-treated patients with T4 disease, the MD Anderson Cancer Center reported long term toxicity in 66 patients treated with a mean follow up of 66 months (1–124 months) (41). The actuarial rate of Grade 3 toxicity was 36% at 3 years and 49% at 5 years. Hearing problems were the most frequent severe toxicity, but the rate of severe toxicity not attributable to hearing at 3 and 5 years was 23 and 33%, respectively. Cranial or peripheral neurotoxicity was reported in 15/66 patients (23%) including two patients with grade 3 radiation-induced optic neuropathy; the remaining cases (13/15) had grade 2 toxicity. Radiological TLN was demonstrated in nine patients (14%), two with reported cognitive impairment; cognitive impairment was reported in an additional two patients without TLN.

Factors Impacting on Long-Term Quality of Life

Factors which have been associated with QoL are summarized in **Table 5**. The studies show some conflicting findings, likely stemming from differences in patient populations, social constructs (particularly where sociodemographic factors are concerned) and variations in statistical methods to report predictive factors, including single or multi-factor models.

TABLE 5 | Selected studies reporting factors associated with patient-reported quality of life.

Factor/Study	Endemic					Non-endemic
	Fang et al. (17)	**Fang et al. (18)**	**Hong et al. (36)**	**Wu et al. (38)**	**Tsai et al. (19)**	**McDowell et al. (40)**
QoL measure	EORTC QLQ-C30 global health score	EORTC QLQ-C30 global health score	EORTC QLQ-C30 global health score	General health measure as a surrogate for global QoL	EORTC QLQ-C30 global health score	FACT-HN total score
Stats analysis	Univariable analysis: categorical chi-squared; multivariable logistic regression	GLM-MANOVA one factor and multifactor models	Multiple linear regression	UVA (ANOVA) and MVA (multiple stepwise regression)	GLM-MANOVA one factor and multifactor models	univariable linear regression
SOCIAL FACTORS						
Sex	No	Yes (1F only)	No	Yes (UVA only)	Yes (1F only)	No
Age	No	Yes (older better; 1F only)	Yes (younger worse)	Yes (older better on MVA and UVA)	No	No
Marital status	No	No	NR	No	No	Yes (divorce/separated worse than married/common law)
Living status	NR	NR	NR	NR	NR	Yes (living with others better than isolated)
Education level	Yes (higher education >12y better on UVA, not MVA (p=0.08)	Yes (higher educated better, both 1F and MF)	Yes (higher educated better)	No	Yes (both 1F and MF)	No
Employment status	Yes (employed better on UVA, not MVA)	NR	NR	No	NR	Yes (homemaker/caregiver and disability leave worse than full time employment)
Income	Yes (higher family income better on UVA and MVA)	Yes (higher family income better, both 1F and MF)	NR	Yes (higher income better QoL on MVA)	NR	NR
PATIENT FACTORS						
Medical comorbidities	Yes (presence comorbidity worse on both UVA and MVA)	Yes (1F only)	NR	Yes (lower better QoL; UVA and MVA)	NR	NR
Depression	NR	NR	Yes (higher worse QoL)	NR	NR	Yes (higher worse QoL)
Anxiety	NR	NR	Yes (higher worse QoL)	NR	NR	Yes (higher worse QoL)
Recurrence Worry	NR	NR	No	NR	NR	NR
TUMOR FACTORS						
T-category	NR	NR	NR	Yes (lower T better QoL on UVA and MVA)	NR	NR
N-category	NR	NR	NR	No	NR	NR
Stage	No	No	Yes (higher stage worse QoL)	No	No	No (stage IVB worse than stage I)
TREATMENT FACTORS						
Time since treatment	NR	No	No	No	Yes (both 1F and MF)	Yes (better with longer FU)
Chemotherapy	No	No	NR	No	Borderline on 1F (p = 0.058)	Yes (none better than any)
Radiation tech	Yes (3D/IMRT better than 2D on both UVA and MVA)	Yes (both 1F and MF; IMRT better)	NR	No	Yes (both 1F and MF)	N/A (all IMRT)

(Continued)

TABLE 5 | Continued

Factor/Study	Endemic					Non-endemic
	Fang et al. (17)	**Fang et al. (18)**	**Hong et al. (36)**	**Wu et al. (38)**	**Tsai et al. (19)**	**McDowell et al. (40)**
TOXICITY FACTORS						
Clinician-reported	NR	NR	* xerostomia and fatigue	NR	Neuropathy, hearing, xerostomia (both 1F and MF); Dysphagia and neck fibrosis (1F)	Hearing, ear discharge, dysphagia, trismus, dysarthria, aspiration, cranial neuropathy
Patient-reported toxicity	NR	NR	NR	NR		All items MDASI-HN correlated with QoL

*QoL, quality of life; EORTC QLQ-C30, European organization for research and treatment of cancer core quality of life questionnaire; FACT-HN, Functional Assessment of Cancer Therapy, Head & Neck cancer; GLM-MANOVA, general linear model multivariate analysis of variance; UVA, univariable analysis; ANOVA, analysis of variance; MVA, multivariable analysis; 1F, one factor analysis; NR, not recorded; MF, multifactor analysis; IMRT, intensity-modulated radiotherapy; MDASI-HN, MD Anderson symptom inventory, head and neck; * toxicity was graded as yes/no.*

Sociodemographic Factors

Age

In some studies worse QoL has been observed in younger patients (42) while others have shown the contrary (18, 36, 38), and some have shown no association (40).

Sex

In some series, male survivors have been reported to have improved long-term QoL (18, 19), while others have reported that sex does not influence QoL (17, 36, 40).

Marital status/living status

Marital status has not be shown to influence global QoL in studies from endemic regions (17–19, 38). In contrast, the aforementioned series from Toronto reported that divorced or separated patients, but not single or widowed patients scored lower global QoL scores compared to cohabitating (married/common law/other) patients (40).

Education, and employment status/income

Education status (17–19, 36), employment status (17, 40, 94) and income have all been associated with improved global QoL in NPC cohorts (17, 18, 38).

Patient Factors

Medical factors

Where included, the burden of medical comorbidities has been linked with worse QoL in NPC survivors (17, 18, 38).

Emotional distress

Similar to series reporting for other HNCs, higher rates of anxiety and depression correlate with worse global QoL (95–98), in both endemic and non-endemic NPC series (36, 40, 44, 99–101). A complex interplay and association exist between QoL, toxicity and emotional distress, and a higher burden of toxicity has been shown to correlate with worse emotional distress and QoL in NPC survivors (40, 100).

Other

QoL is a complex construct which may be affected by many different factors that may or may not be captured in PROMs currently used in clinical research, including consultation satisfaction, optimism and worry (102).

Treatment Factors

Chemotherapy

The actual impact of chemotherapy on long-term QoL is difficult to quantify, given most prospective NPC studies have not included QoL assessments. The two NACT trials which included QoL assessments suggest that the addition of NACT may have a transient, but not long-lasting impact on QoL (12, 23). Based on the cross-sectional series included in **Table 5**, impact was either absent (17, 18, 38) or identified only in single factor models (19, 40) without accounting for confounding variables such as stage. In a study limited to patients with stage II NPC, it was reported that the addition of concomitant chemotherapy resulted in worse long term global QoL (54). When isolating these results to IMRT-treated patients only, the reported difference in EORTC QLQ-C30 global QoL score was 86 vs. 79, a difference which could be considered small or clinically insignificant (54).

Radiotherapy technique

Although not all studies have shown a significant improvement in QoL with IMRT (33), most studies have reported a positive impact (15–19). Adaptive strategies, including treatment replanning (63) and response-adaptive target volume delineation following induction chemotherapy are discussed above and have also been reported to improve QoL (64–66).

Toxicity Factors

Table 5 presents studies reporting the impact of individual toxicities on long-term QoL. Most have used clinician-rated toxicity and found a significant correlation between some, but not all the measured toxicities (19, 36, 40). PRO measures, however may be more reliable. In a study using the MDASI-HN tool, the mean symptom burden showed strong correlation with global QoL (FACT-HN total, $r = 0.76$, $p < 0.001$), and every item of

the MDASI-HN inventory showed a very strong correlation with global QoL on univariate analysis, suggesting that the presence of any severe toxicity can adversely impact QoL (40).

Treatment Toxicity—Where Can We Further Our Understanding?

Following many years of clinical trials data there is still much to understand. This article has highlighted past reliance on clinician-reported toxicities and the presence of "severe" or grade 3 or higher toxicity. This approach does not discriminate the varying effects of individual toxicities on the patient (not all grade 3 toxicities will impact patients to the same degree), and may fail to direct enough attention to the significant impact that grade 1–2 toxicities can have on the long-term well-being of the patient. In terms of relying on clinician reports, it is well-appreciated that clinicians may under report both symptoms (46, 47) and their severity (48, 49) compared to patients. In the series reported above by McDowell et al. xerostomia was ranked "severe" (grade 3 CTCAE) by only 1% of clinicians, yet 49% of patients rated their problems with dry mouth in the severe range (≥7 on the MDASI-HN item) (40). This large discrepancy is only one example of where potentially we can further our understanding of toxicity, and future research should focus on what matters to patients. In addition to the well-established toxicities, such as xerostomia, dysphagia and hearing loss, it is worth highlighting additional toxicities requiring further research, such as neurotoxicity, endocrine dysfunction and fatigue.

Neurotoxicity

Cranial neuropathies

Cranial neuropathies can be catastrophic for the NPC survivor, heralding a significant decline in QoL (19, 40). The average latency period is between four and seven years after treatment, but shorter or longer intervals are reported (103–106), with few effective options to reverse or stabilize symptoms (107). In the IMRT era, radiation induced cranial neuropathies have been reported in up to 14% of patients (**Table 6**). Although any of the cranial nerves may be affected, the hypoglossal nerve is most frequently involved, owing to its tortuous course near the high dose region of the nasopharynx and upper neck (40, 106). A hypoglossal nerve palsy can remain stable or demonstrate insidious progression, rendering a patient dependent on a feeding tube. In the largest series, reported by Chow et al., T-stage and diabetes mellitus as well as the dose to the hypoglossal nerve (D1cc: <74 Gy 2.4% vs. ≥74 Gy 20.8%, $p < 0.001$) were all predictors for a hypoglossal nerve palsy (106). This highlights the importance of optimizing treatment plans, ensuring dose homogeneity around the base of skull and reducing hotspots, despite these being deemed as acceptable by current ICRU guidelines. Chemotherapy may be a factor: in the MAC-NPC analysis, there was a borderline increased risk of cranial neuropathies with the addition of chemotherapy to RT alone (11·4% vs. 8·7%, HR = 1·35 (1·00–1·82), $p = 0·052$) (7). The potential impact of NACT is unknown.

Cognitive and neurobehavioral toxicity

TLN is a well-recognized toxicity following NPC treatment (**Table 2**). IMRT-treated patients appear to have a significantly reduced risk of developing TLN (13). TLN has generally been reported as either symptomatic TLN, where the patient has a constellation of symptoms including reduced cognitive function with radiologic temporal lobe changes, or asymptomatic/radiologic TLN, where there is imaging evidence of necrosis in the temporal lobes, but the patient appears to be functioning normally from the perspective of the clinician. Prior to IMRT, TLN was shown to correlate with poorer cognitive function (99, 108), however this association has not been clearly demonstrated in IMRT-treated patients, although there are only few reports available (40, 109–112). In a cohort of 102 patients with a mean age and time since treatment of 56 and 7.5 years, respectively, McDowell et al. reported 32% of patents scoring in the neurocognitively impaired range (112). Asymptomatic TLN was reported in 22% of patients, which did not correlate with either objective (MoCA) or subjective (MDASI-HN memory problems item) cognitive assessment. In this series, frontal dysfunction was also high when self-rated by either the patient or their family member. Clinically significant rates of dysfunction in the domains of apathy, disinhibition and executive functioning were reported by 48, 35, and 39% of patients and 66, 53, and 56% of family members (who were reporting on the patients function), respectively. This study highlights the importance of measuring what matters; TLN has been used as a surrogate marker for radiation-induced damage to the brain and the designation of whether a patient is "symptomatic" has been based on a crude clinician assessment. However, directly measuring the functional impacts of our treatments, such as cognitive and frontal dysfunction provides more relevant and patient-focussed information, which can be used to counsel and consent patients. Cisplatin has also been implicated in cognitive dysfunction following cancer treatment (113), although the individual impacts of concurrent and neo/adjuvant chemotherapy and RT on cognition in NPC treatment have not been well-quantified in the literature.

Endocrine Dysfunction

Hypothyroidism

Compared to other HNC populations, NPC patients appear to be particularly vulnerable to developing primary hypothyroidism following neck irradiation (114). In IMRT series, up to 69% of survivors may develop hypothyroidism (40, 115–118). The median latency period has been reported in the range of 1.8–3.1 years (114–116), but the risk increases with further follow up and has been reported in excess of 10 years following treatment (114). Given this is a reversible toxicity which may significantly impact the QoL of survivors, all patients where the lower neck is irradiated should undergo indefinite biochemical screening following treatment. The National Comprehensive Cancer Network guidelines suggest testing thyroid-stimulating hormone every 6–12 months, but do not make a recommendation of duration (119).

TABLE 6 | Selected studies reporting cranial or hypoglossal neuropathies in NPC patients treated with IMRT.

Study	No.	Median follow up (range)	Incidence CN	Incidence hypoglossal neuropathy	Notes
Lee et al. (13)	444	NR *	1.6%	NR	IMRT lower rates than 2D (p=0.01)
Peng et al. (14)	306**	3.5y (0.1-6.9y)	3.9%	NR	IMRT lower rates than 2D (p=0.02)
Zhang et al. (9)	480	3.6y (2.9-5.4y)	3.8%	NR	G1/2 1.7% G3/4 2.1% combined arms of study; difference between NACT and CRT
Li et al. (22)	477	5.9y (0.1-7.5y)	3.7%	NR	G1/2–2.3% G3/4–1.4% Combined arms of study; difference between NACT and CRT
McDowell et al. (40)	107	7.5y (4.2-11.1)	14% (late)	13%	G1–6% G2–4% G3–4%
Chow et al. (106)	797	8.1y	NR	8.7%	74% unilateral; 26% bilateral;

*CN, cranial neuropathy; NR, not recorded; IMRT, intensity-modualted RT; G1/2, grade 1 or 2 toxicity; G3/4, grade 3 or 4 toxicity; NACT, neoadjuvant chemotherapy; CRT, concurrent chemoradiotherapy; * not reported for IMRT cohort separately, for entire study range was 0.2-18.2 years including 2D, 3D and IMRT. **306 in IMRT arm of this study.*

Pituitary dysfunction

In a meta-analysis of pituitary dysfunction in adult patients treated with cranial irradiation, the point prevalence in the pooled NPC studies was 0.74 (120). There are some limitations to this data and further research is needed to assess the true impact in the IMRT era, where the risk may be lower. One study which included basal screening reported a low rate of 1%, with a median follow up of 7.5y (4.1–11.1 y) (40). However, in other populations exposed to cranial irradiation hypopituitarism may develop many years after RT (120). There is a lack of data about the true prevalence of pituitary dysfunction in NPC survivors treated with IMRT and the absolute benefit of regular screening in this group is unknown.

Fatigue

Fatigue frequently ranks highly among NPC patient-reported toxicities (17–19, 40). Fatigue has many potential causes in the NPC survivor, including reversible causes such as poor nutritional intake, endocrine dysfunction and emotional distress, and irreversible causes such as a high treatment-related symptom burden or the presence of distant metastases. Efforts to exclude reversible causes should be undertaken where appropriate, as fatigue has been linked to worse QoL in NPC series (36, 40). In the two NACT series which included the QLQ-C30, long-term fatigue was not worse in the NACT arms (12, 23). Other factors, such as the volume of posterior fossa irradiated may also contribute, as this has been linked to higher rates of long-term fatigue (clinician reported) assessments in both NPC (121) and non-NPC HNC studies (122).

Unmet Needs

There has been little targeted research ascertaining unmet needs in NPC survivors, although studies in the general HNC population may be broadly translatable. Unmet needs cover a variety of domains that may not have been addressed at any point through the patients' cancer journey (123, 124), and include physical, psychological, informational, activities of daily living, social, spiritual/existential, nutritional, dental, communication, sexual and financial needs as well as access to care (125). A variety of validated tools exist to ascertain the unmet needs of cancer patients (125–127). In non-NPC HNC populations, patients frequently identify having an unmet need. For example, in a study of HNC survivors at the Princess Margaret Hospital, 61% (96/158) of survivors reported at least one unmet need, and patients with worse QoL reported an increased number of unmet needs (128).

Some of these domains are better understood than others. For instance, emotional distress has been reported in patients with NPC, and its presence often correlates with lower QoL (36, 40, 44). Fear of cancer recurrence is often cited an unmet need in HNC populations and in the study by Hong et al., frequent worry of recurrence was present in 18.5% of NPC patients (36). Workplace rehabilitation needs following treatment are also attracting increasing interest in the HNC literature. For instance in a Canadian study, which mostly included a migrant population from endemic areas, only 62% of patients who were employed prior to diagnosis and who were within working age at study enrolment (≤65) were working (median post-RT 7.5 years) (94). One-third of those who were working also reported working fewer hours than before their diagnosis (median 14 h, range 4–30). Patients who were working were younger, had a lower symptom burden, self-reported less changes in their frontal function and had private health benefits.

Conclusion and Future Directions

The outlook for patients with NPC has substantially improved over the last 30 years, as a consequence of concerted global research efforts and technological advancements in RT planning and delivery. Despite these improvements, many NPC patients will still develop significant long-term toxicities, negatively

impacting their QoL. Many opportunities offer early promise for reducing the burden of toxicity including adaptive RT, response-adapted treatment planning, and the potential offered by NACT, particle and proton therapy. Early research suggests these approaches may be beneficial in reducing toxicity and improving QoL. In designing future clinical trials, the focus needs to shift from clinician-reported to patient-reported outcomes, including both toxicity and QoL assessments, which have been lacking in most large-scale prospective studies to date. While there are a number of patient-reported tools appropriate for use in NPC patients, judicious selection of tools is required to ensure all significant treatment-related toxicity is being adequately captured. Currently, there is no "all encompassing" single tool for use during the treatment and survivorship phase of NPC treatment. As we continue to move into the era of immune and targeted therapies, additional toxicities and tools may need to be incorporated. In future studies, we would recommend including long-term follow up, in excess of 5 years is needed to fully quantify the development of late toxicities. Where reported, results from clinical trials should focus on reporting meaningful clinical differences in QoL measures rather than statistical differences which may be of little significance to patients. Targeted research to reduce the burden of toxicities such as cognitive and hearing impairment remain areas for future research, and clarifying the unmet needs of NPC survivors in endemic and non-endemic regions provides further opportunity to improve the survivorship experience.

AUTHOR CONTRIBUTIONS

LM designed the concept of the review and wrote the first draft of the manuscript. All others contributed to the manuscript revision, read, and approved the submitted version.

REFERENCES

1. Ng WT, Lee MC, Hung WM, Choi CW, Lee KC, Chan OS, et al. Clinical outcomes and patterns of failure after intensity-modulated radiotherapy for nasopharyngeal carcinoma. *Int J Radiat Oncol Biol Phys*. (2011) 79:420–8. doi: 10.1016/j.ijrobp.2009.11.024
2. Lee JY, Sun JM, Oh DR, Lim SH, Goo J, Lee SH, et al. Comparison of weekly versus triweekly cisplatin delivered concurrently with radiation therapy in patients with locally advanced nasopharyngeal cancer: a multicenter randomized phase II trial (KCSG-HN10-02). *Radiother Oncol.* (2016) 118:244–50. doi: 10.1016/j.radonc.2015.11.030
3. Al-Sarraf M, LeBlanc M, Giri PG, Fu KK, Cooper J, Vuong T, et al. Chemoradiotherapy versus radiotherapy in patients with advanced nasopharyngeal cancer: phase III randomized intergroup study 0099. *J Clin Oncol.* (1998) 16:1310–7. doi: 10.1200/JCO.1998.16.4.1310
4. Wee J, Tan EH, Tai BC, Wong HB, Leong SS, Tan T, et al. Randomized trial of radiotherapy versus concurrent chemoradiotherapy followed by adjuvant chemotherapy in patients with American joint committee on cancer/International union against cancer stage III and IV nasopharyngeal cancer of the endemic variety. *J Clin Oncol.* (2005) 23:6730–8. doi: 10.1200/JCO.2005.16.790
5. Chen QY, Wen YF, Guo L, Liu H, Huang PY, Mo HY, et al. Concurrent chemoradiotherapy vs radiotherapy alone in stage II nasopharyngeal carcinoma: phase III randomized trial. *J Natl Cancer Inst.* (2011) 103:1761–70. doi: 10.1093/jnci/djr432
6. Chen L, Hu CS, Chen XZ, Hu GQ, Cheng ZB, Sun Y, et al. Adjuvant chemotherapy in patients with locoregionally advanced nasopharyngeal carcinoma: long-term results of a phase 3 multicentre randomised controlled trial. *Eur J Cancer.* (2017) 75:150–8. doi: 10.1016/j.ejca.2017.01.002
7. Blanchard P, Lee A, Marguet S, Leclercq J, Ng WT, Ma J, et al. Chemotherapy and radiotherapy in nasopharyngeal carcinoma: an update of the MAC-NPC meta-analysis. *Lancet Oncol.* (2015) 16:645–55. doi: 10.1016/S1470-2045(15)70126-9
8. Baujat B, Audry H, Bourhis J, Chan AT, Onat H, Chua DT, et al. Chemotherapy in locally advanced nasopharyngeal carcinoma: an individual patient data meta-analysis of eight randomized trials and 1753 patients. *Int J Radiat Oncol Biol Phys.* (2006) 64:47–56. doi: 10.1016/j.ijrobp.2005.06.037
9. Zhang Y, Chen L, Hu GQ, Zhang N, Zhu XD, Yang KY, et al. Gemcitabine and cisplatin induction chemotherapy in nasopharyngeal carcinoma. *N Engl J Med.* (2019) 381:1124–35. doi: 10.1186/s40880-019-0385-5
10. Sun Y, Li WF, Chen NY, Zhang N, Hu GQ, Xie FY, et al. Induction chemotherapy plus concurrent chemoradiotherapy versus concurrent chemoradiotherapy alone in locoregionally advanced nasopharyngeal carcinoma: a phase 3, multicentre, randomised controlled trial. *Lancet Oncol.* (2016) 17:1509–20. doi: 10.1016/S1470-2045(16)30410-7
11. Cao SM, Yang Q, Guo L, Mai HQ, Mo HY, Cao KJ, et al. Neoadjuvant chemotherapy followed by concurrent chemoradiotherapy versus concurrent chemoradiotherapy alone in locoregionally advanced nasopharyngeal carcinoma: a phase III multicentre randomised controlled trial. *Eur J Cancer.* (2017) 75:14–23. doi: 10.1016/j.ejca.2016.12.039
12. Hui EP, Ma Bb Fau - Leung SF, Leung Sf Fau - King AD, King Ad Fau - Mo F, Mo F Fau - Kam MK, Kam Mk Fau - Yu BK, et al. Randomized phase II trial of concurrent cisplatin-radiotherapy with or without neoadjuvant docetaxel and cisplatin in advanced nasopharyngeal carcinoma. *J Clin Oncol.* (2009) 27:242–9. doi: 10.1200/JCO.2008.18.1545
13. Lee AW, Ng WT, Chan LL, Hung WM, Chan CC, Sze HC, et al. Evolution of treatment for nasopharyngeal cancer–success and setback in the intensity-modulated radiotherapy era. *Radiother Oncol.* (2014) 110:377–84. doi: 10.1016/j.radonc.2014.02.003
14. Peng G, Wang T, Yang KY, Zhang S, Zhang T, Li Q, et al. A prospective, randomized study comparing outcomes and toxicities of intensity-modulated radiotherapy vs. conventional two-dimensional radiotherapy for the treatment of nasopharyngeal carcinoma. *Radiother Oncol.* (2012) 104:286–93. doi: 10.1016/j.radonc.2012.08.013
15. Pan XB, Huang ST, Chen KH, Jiang YM, Ma JL, Qu S, et al. Intensity-modulated radiotherapy provides better quality of life than two-dimensional conventional radiotherapy for patients with stage II nasopharyngeal carcinoma. *Oncotarget.* (2017) 8:46211–8. doi: 10.18632/oncotarget.17582
16. Huang TL, Chien CY, Tsai WL, Liao KC, Chou SY, Lin HC, et al. Long-term late toxicities and quality of life for survivors of nasopharyngeal carcinoma treated with intensity-modulated radiotherapy versus non-intensity-modulated radiotherapy. *Head Neck.* (2016) 38(Suppl. 1):E1026–32. doi: 10.1002/hed.24150
17. Fang FM, Tsai WL, Chen HC, Hsu HC, Hsiung CY, Chien CY, et al. Intensity-modulated or conformal radiotherapy improves the quality of life of patients with nasopharyngeal carcinoma: comparisons of four radiotherapy techniques. *Cancer.* (2007) 109:313–21. doi: 10.1002/cncr.22396
18. Fang FM, Tsai WL, Lee TF, Liao KC, Chen HC, Hsu HC. Multivariate analysis of quality of life outcome for nasopharyngeal carcinoma patients after treatment. *Radiother Oncol.* (2010) 97:263–9. doi: 10.1016/j.radonc.2010.05.022
19. Tsai WL, Huang TL, Liao KC, Chuang HC, Lin YT, Lee TF, et al. Impact of late toxicities on quality of life for survivors of nasopharyngeal carcinoma. *BMC Cancer.* (2014) 14:856. doi: 10.1186/1471-2407-14-856
20. Chang ET, Adami HO. The enigmatic epidemiology of nasopharyngeal carcinoma. *Cancer Epidemiol Biomarkers Prev.* (2006) 15:1765–77. doi: 10.1158/1055-9965.EPI-06-0353

21. Nguyen NA, Ringash J. Head and neck cancer survivorship care: a review of the current guidelines and remaining unmet needs. *Curr Treat Options Oncol.* (2018) 19:44. doi: 10.1007/s11864-018-0554-9
22. Li WF, Chen NY, Zhang N, Hu GQ, Xie FY, Sun Y, et al. Concurrent chemoradiotherapy with/without induction chemotherapy in locoregionally advanced nasopharyngeal carcinoma: long-term results of phase 3 randomized controlled trial. *Int J Cancer.* (2019) 145:295–305. doi: 10.1002/ijc.32099
23. Tan T, Lim WT, Fong KW, Cheah SL, Soong YL, Ang MK, et al. Concurrent chemo-radiation with or without induction gemcitabine, carboplatin, and paclitaxel: a randomized, phase 2/3 trial in locally advanced nasopharyngeal carcinoma. *Int J Radiat Oncol Biol Phys.* (2015) 91:952–60. doi: 10.1016/j.ijrobp.2015.01.002
24. Hong RL, Hsiao CF, Ting LL, Ko JY, Wang CW, Chang JTC, et al. Final results of a randomized phase III trial of induction chemotherapy followed by concurrent chemoradiotherapy versus concurrent chemoradiotherapy alone in patients with stage IVA and IVB nasopharyngeal carcinoma-Taiwan cooperative oncology group (TCOG) 1303 Study. *Ann Oncol.* (2018) 29:1972–9. doi: 10.1093/annonc/mdy249
25. Fountzilas G, Ciuleanu, Bobos M, Kalogera-Fountzila A, Kalogera-Fountzila A, Eleftheraki AG, et al. Induction chemotherapy followed by concomitant radiotherapy and weekly cisplatin versus the same concomitant chemoradiotherapy in patients with nasopharyngeal carcinoma: a randomized phase II study conducted by the Hellenic Cooperative Oncology Group (HeCOG) with biomarker evaluation. *Ann Oncol.* (2012) 23:427–35. doi: 10.1093/annonc/mdr116
26. Frikha M, Auperin A, Tao Y, Elloumi F, Toumi N, Blanchard P, et al. A randomized trial of induction docetaxel-cisplatin-5FU followed by concomitant cisplatin-RT versus concomitant cisplatin-RT in nasopharyngeal carcinoma (GORTEC 2006-02). *Ann Oncol.* (2018) 29:731–6. doi: 10.1093/annonc/mdx770
27. Chen L, Hu CS, Chen XZ, Hu GQ, Cheng ZB, Sun Y, et al. Concurrent chemoradiotherapy plus adjuvant chemotherapy versus concurrent chemoradiotherapy alone in patients with locoregionally advanced nasopharyngeal carcinoma: a phase 3 multicentre randomised controlled trial. *Lancet Oncol.* (2012) 13:163–71. doi: 10.1016/S1470-2045(11)70320-5
28. Lee AW, Tung SY, Chua DT, Ngan RK, Chappell R, Tung R, et al. Randomized trial of radiotherapy plus concurrent-adjuvant chemotherapy vs radiotherapy alone for regionally advanced nasopharyngeal carcinoma. *J Natl Cancer Inst.* (2010) 102:1188–98. doi: 10.1093/jnci/djq287
29. Lee AWM, Tung SY, Ng WT, Lee V, Ngan RKC, Choi HCW, et al. A multicenter, phase 3, randomized trial of concurrent chemoradiotherapy plus adjuvant chemotherapy versus radiotherapy alone in patients with regionally advanced nasopharyngeal carcinoma: 10-year outcomes for efficacy and toxicity. *Cancer.* (2017) 123:4147–57. doi: 10.1002/cncr.30850
30. Rossi A, Molinari R, Boracchi P, Del Vecchio M, Marubini E, Nava M, et al. Adjuvant chemotherapy with vincristine, cyclophosphamide, and doxorubicin after radiotherapy in local-regional nasopharyngeal cancer: results of a 4-year multicenter randomized study. *J Clin Oncol.* (1988) 6:1401–10. doi: 10.1200/JCO.1988.6.9.1401
31. Chi KH, Chang Yc, Guo W-Y, Leung M-J, Shiau C-Y, Chen S-Y, et al. A phase III study of adjuvant chemotherapy in advanced nasopharyngeal carcinoma patients. *Int J Radiat Oncol Biol Phys.* (2002) 52:1238–44. doi: 10.1016/s0360-3016(01)02781-x
32. Kam MK, Leung SF, Zee B, Chau RM, Suen JJ, Mo F, et al. Prospective randomized study of intensity-modulated radiotherapy on salivary gland function in early-stage nasopharyngeal carcinoma patients. *J Clin Oncol.* (2007) 25:4873–9. doi: 10.1200/JCO.2007.11.5501
33. Pow EH, Kwong DL, McMillan AS, Wong MC, Sham JS, Leung LH, et al. Xerostomia and quality of life after intensity-modulated radiotherapy vs. conventional radiotherapy for early-stage nasopharyngeal carcinoma: initial report on a randomized controlled clinical trial. *Int J Radiat Oncol Biol Phys.* (2006) 66:981–91. doi: 10.1016/j.ijrobp.2006.06.013
34. Fang FM, Chien CY, Tsai WL, Chen HC, Hsu HC, Lui CC, et al. Quality of life and survival outcome for patients with nasopharyngeal carcinoma receiving three-dimensional conformal radiotherapy vs. intensity-modulated radiotherapy-a longitudinal study. *Int J Radiat Oncol Biol Phys.* (2008) 72:356–64. doi: 10.1016/j.ijrobp.2007.12.054
35. Fang FM, Huang TL, Lin YH, Chien CY, Chuang HC, Luo SD, et al. Concurrent chemoradiotherapy by simultaneously integrated boost volumetric-modulated arc therapy for nasopharyngeal carcinoma-toxicity/quality of life and survival. *Head Neck.* (2019) 41:1282–9. doi: 10.1002/hed.25551
36. Hong JS, Tian J, Han QF, Ni QY. Quality of life of nasopharyngeal cancer survivors in China. *Curr Oncol.* (2015) 22:e142–7. doi: 10.3747/co.22.2323
37. Pan XB, Huang ST, Chen KH, Jiang YM, Ma JL, Qu S, et al. Concurrent chemoradiotherapy degrades the quality of life of patients with stage II nasopharyngeal carcinoma as compared to radiotherapy. *Oncotarget.* (2017) 8:14029–38. doi: 10.18632/oncotarget.14932
38. Wu Y, Hu WH, Xia YF, Ma J, Liu MZ, Cui NJ. Quality of life of nasopharyngeal carcinoma survivors in Mainland China. *Qual Life Res.* (2007) 16:65–74. doi: 10.1007/s11136-006-9113-0
39. Tonoli S, Alterio D, Caspiani O, Bacigalupo A, Bunkheila F, Cianciulli M, et al. Nasopharyngeal carcinoma in a low incidence European area: a prospective observational analysis from the head and neck study group of the Italian society of radiation oncology (AIRO). *Strahlenther Onkol.* (2016) 192:931–43. doi: 10.1007/s00066-016-1052-2
40. McDowell LJ, Rock K, Xu W, Chan B, Waldron J, Lu L, et al. Long-Term late toxicity, quality of life, and emotional distress in patients with nasopharyngeal carcinoma treated with intensity modulated radiation therapy. *Int J Radiat Oncol Biol Phys.* (2018) 102:340–52. doi: 10.1016/j.ijrobp.2018.05.060
41. Takiar V, Ma D, Garden AS, Li J, Rosenthal DI, Beadle BM, et al. Disease control and toxicity outcomes for T4 carcinoma of the nasopharynx treated with intensity-modulated radiotherapy. *Head Neck.* (2016) 38(Suppl. 1):E925–33. doi: 10.1002/hed.24128
42. Lastrucci L, Bertocci S, Bini V, Borghesi S, De Majo R, Rampini A, et al. Late toxicity, evolving radiotherapy techniques, and quality of life in nasopharyngeal carcinoma. *Radiol Med.* (2017) 122:303–8. doi: 10.1007/s11547-016-0722-6
43. Talmi YP, Horowitz Z, Bedrin L, Wolf M, Chaushu G, Kronenberg J, et al. Quality of life of nasopharyngeal carcinoma patients. *Cancer.* (2002) 94:1012–7. doi: 10.1002/cncr.10342
44. Ghiggia A, Castelli L, Riva G, Tesio V, Provenzano E, Ravera M, et al. Psychological distress and coping in nasopharyngeal cancer: an explorative study in Western Europe. *Psychol Health Med.* (2017) 22:449–61. doi: 10.1080/13548506.2016.1220600
45. Yee D, Hanson J, Lau H, Siever J, Gluck S. Treatment of nasopharyngeal carcinoma in the modern era: analysis of outcomes and toxicity from a single center in a nonendemic area. *Cancer J.* (2006) 12:147–54. Available online at: https://journals.lww.com/journalppo/Abstract/2006/03000/Treatment_of_Nasopharyngeal_Carcinoma_in_the.11.aspx
46. Fromme EK, Eilers KM, Mori M, Hsieh YC, Beer TM. How accurate is clinician reporting of chemotherapy adverse effects? A comparison with patient-reported symptoms from the quality-of-life questionnaire C30. *J Clin Oncol.* (2004) 22:3485–90. doi: 10.1200/JCO.2004.03.025
47. Vogelzang NJ, Breitbart W, Cella D, Curt GA, Groopman JE, Horning SJ, et al. Patient, caregiver, and oncologist perceptions of cancer-related fatigue: results of a tripart assessment survey. The fatigue coalition. *Semin Hematol.* (1997) 34(3 Suppl. 2):4–12.
48. Ingham J, Portenoy R. The measurement of pain and other symptoms. In: Doyle DH, GWC, MacDonald N, editor. *Oxford Textboo of Palliative Medicine.* Oxford: Oxford University Press, (1998). p. 203–19.
49. Patrick DL, Ferketich SL, Frame PS, Harris JJ, Hendricks CB, Levin B, et al. National institutes of health state-of-the-science conference statement: symptom management in cancer: pain, depression, and fatigue, july 15-17, 2002. *J Natl Cancer Inst.* (2003) 95:1110–7. doi: 10.1093/jnci/djg014
50. Aaronson NK, Ahmedzai S, Bergman B, Bullinger M, Cull A, Duez NJ, et al. The European organization for research and treatment of cancer QLQ-C30: a quality-of-life instrument for use in international clinical trials in oncology. *J Natl Cancer Inst.* (1993) 85:365–76.
51. Bjordal K, Hammerlid E, Ahlner-Elmqvist M, de Graeff A, Boysen M, Evensen JF, et al. Quality of life in head and neck cancer patients: validation of the European organization for research and treatment of cancer quality of life questionnaire-H&N35. *J Clin Oncol.* (1999) 17:1008–19. doi: 10.1200/JCO.1999.17.3.1008

52. Cocks K, King MT, Velikova G, Fayers PM, Brown JM. Quality, interpretation and presentation of European organisation for research and treatment of cancer quality of life questionnaire core 30 data in randomised controlled trials. *Eur J Cancer.* (2008) 44:1793–8. doi: 10.1016/j.ejca.2008.05.008
53. Osoba D, Bezjak A, Brundage M, Zee B, Tu D, Pater J, et al. Analysis and interpretation of health-related quality-of-life data from clinical trials: basic approach of the National cancer institute of canada clinical trials group. *Eur J Cancer.* (2005) 41:280–7. doi: 10.1016/j.ejca.2004.10.017
54. Cocks K, King MT, Velikova G, Martyn St-James M, Fayers PM, Brown JM. Evidence-based guidelines for determination of sample size and interpretation of the European organisation for the research and treatment of cancer quality of life questionnaire core 30. *J Clin Oncol.* (2011) 29:89–96. doi: 10.1200/JCO.2010.28.0107
55. Lim AM, Corry J, Collins M, Peters L, Hicks RJ, D'Costa I, et al. A phase II study of induction carboplatin and gemcitabine followed by chemoradiotherapy for the treatment of locally advanced nasopharyngeal carcinoma. *Oral Oncol.* (2013) 49:468–74. doi: 10.1016/j.oraloncology.2012.12.012
56. Rischin D, Corry J, Smith J, Stewart J, Hughes P, Peters L. Excellent disease control and survival in patients with advanced nasopharyngeal cancer treated with chemoradiation. *J Clin Oncol.* (2002) 20:1845–52. doi: 10.1200/JCO.2002.07.011
57. Liu F, Jin T, Liu LA-O, Xiang Z, Yan R, Yang H. The role of concurrent chemotherapy for stage II nasopharyngeal carcinoma in the intensity-modulated radiotherapy era: a systematic review and meta-analysis. *PLoS ONE.* (2018) 13:e0194733. doi: 10.1371/journal.pone.0194733
58. Ou X, Shen C, Kong L, Wang X, Ding J, Gao Y, et al. Treatment outcome of nasopharyngeal carcinoma with retropharyngeal lymph nodes metastasis only and the feasibility of elective neck irradiation. *Oral Oncol.* (2012) 48:1045–50. doi: 10.1016/j.oraloncology.2012.04.011
59. Yi J, Zhao C, Chen X, Huang X, Gao L, Luo JW, et al. The value of adding chemotherapy to intensity modulated radiation therapy for stage II nasopharyngeal carcinoma: a multicenter phase 2 study. *Int J Radiat Oncol Biol Phys.* (2015) 93:S128. doi: 10.1016/j.ijrobp.2015.07.305
60. Noronha V, Joshi A, Patil VM, Agarwal J, Ghosh-Laskar S, Budrukkar A, et al. Once-a-week versus once-every-3-weeks cisplatin chemoradiation for locally advanced head and neck cancer: a phase III randomized noninferiority trial. *J Clin Oncol.* (2018) 36:1064–72. doi: 10.1200/JCO.2017.74.9457
61. Bauml JM, Vinnakota R, Anna Park YH, Bates SE, Fojo T, Aggarwal C, et al. Cisplatin every 3 weeks versus weekly with definitive concurrent radiotherapy for squamous cell carcinoma of the head and neck. *J Natl Cancer Inst.* (2019) 111:490–7. doi: 10.1093/jnci/djy133
62. Lu SH, Cheng JC, Kuo SH, Lee JJ, Chen LH, Wu JK, et al. Volumetric modulated arc therapy for nasopharyngeal carcinoma: a dosimetric comparison with tomotherapy and step-and-shoot IMRT. *Radiother Oncol.* (2012) 104:324–30. doi: 10.1016/j.radonc.2011.11.017
63. Yang H, Hu W, Wang W, Chen P, Ding W, Luo W. Replanning during intensity modulated radiation therapy improved quality of life in patients with nasopharyngeal carcinoma. *Int J Radiat Oncol Biol Phys.* (2013) 85:e47–54. doi: 10.1016/j.ijrobp.2012.09.033
64. Yang H, Chen X, Lin S, Rong J, Yang M, Wen Q, et al. Treatment outcomes after reduction of the target volume of intensity-modulated radiotherapy following induction chemotherapy in patients with locoregionally advanced nasopharyngeal carcinoma: a prospective, multi-center, randomized clinical trial. *Radiother Oncol.* (2018) 126:37–42. doi: 10.1016/j.radonc.2017.07.020
65. Xue F, Hu C, He X. Induction chemotherapy followed by intensity-modulated radiotherapy with reduced gross tumor volume delineation for stage T3-4 nasopharyngeal carcinoma. *Oncol Targets Ther.* (2017) 10:3329–36. doi: 10.2147/OTT.S140420
66. Xiang L, Wu J, Yang H, Lin S, Zhang J, Wen Q, et al. Four-year outcome after reduction of the target volume of intensity modulated radiotherapy following induction chemotherapy in locoregionally advanced nasopharyngeal carcinoma: a phase III, multicentre, randomised controlled trial. *Int J Radiat Oncol Biol Phys.* (2019) 105:S18. doi: 10.1016/j.ijrobp.2019.06.414
67. Wang L, Wu Z, Xie D, Zeng R, Cheng W, Hu J, et al. Reduction of target volume and the corresponding dose for the tumor regression field after induction chemotherapy in locoregionally advanced nasopharyngeal carcinoma. *Cancer Res Treat.* (2019) 51:685–95. doi: 10.4143/crt.2018.250
68. Zhao C, Miao JJ, Hua YJ, Wang L, Han F, Lu LX, et al. Locoregional control and mild late toxicity after reducing target volumes and radiation doses in patients with locoregionally advanced nasopharyngeal carcinoma treated with induction chemotherapy (IC) followed by concurrent chemoradiotherapy: 10-year results of a phase 2 study. *Int J Radiat Oncol Biol Phys.* (2019) 104:836–44. doi: 10.1016/j.ijrobp.2019.03.043
69. Wang X, Wang Y, Jiang S, Zhao J, Wang P, Zhang X, et al. Safety and effectiveness of de-escalated radiation dose in T1-3 nasopharyngeal carcinoma: a propensity matched analysis. *J Cancer.* (2019) 10:5057–64. doi: 10.7150/jca.33303
70. Lu T, Xie X, Guo Q, Zhan S, Lin C, Lin S, et al. Prognosis of nasopharyngeal carcinoma with insufficient radical dose to the primary site in the intensity-modulated radiotherapy era. *Head Neck.* (2019) 41:3516–24. doi: 10.1002/hed.25865
71. Zhang F, Cheng YK, Li WF, Guo R, Chen L, Sun Y, et al. Investigation of the feasibility of elective irradiation to neck level Ib using intensity-modulated radiotherapy for patients with nasopharyngeal carcinoma: a retrospective analysis. *BMC Cancer.* (2015) 15:709. doi: 10.1186/s12885-015-1669-z
72. Murdoch-Kinch CA, Kim HM, Vineberg KA, Ship JA, Eisbruch A. Dose-effect relationships for the submandibular salivary glands and implications for their sparing by intensity modulated radiotherapy. *Int J Radiat Oncol Biol Phys.* (2008) 72:373–82. doi: 10.1016/j.ijrobp.2007.12.033
73. Li M, Huang XG, Yang ZN, Lu JY, Zhan YZ, Xie WJ, et al. Effects of omitting elective neck irradiation to nodal level IB in nasopharyngeal carcinoma patients with negative level IB lymph nodes treated by intensity-modulated radiotherapy: a phase 2 study. *Br J Radiol.* (2016) 89:20150621. doi: 10.1259/bjr.20150621
74. Gao Y, Zhu G, Lu J, Ying H, Kong L, Wu Y, et al. Is elective irradiation to the lower neck necessary for N0 nasopharyngeal carcinoma? *Int J Radiat Oncol Biol Phys.* (2010) 77:1397–402. doi: 10.1016/j.ijrobp.2009.06.062
75. Steneker M, Lomax A, Schneider U. Intensity modulated photon and proton therapy for the treatment of head and neck tumors. *Radiother Oncol.* (2006) 80:263–7. doi: 10.1016/j.radonc.2006.07.025
76. Cozzi L, Fogliata A, Lomax A, Bolsi A. A treatment planning comparison of 3D conformal therapy, intensity modulated photon therapy and proton therapy for treatment of advanced head and neck tumours. *Radiother Oncol.* (2001) 61:287–97. doi: 10.1016/S0167-8140(01)00403-0
77. Taheri-Kadkhoda Z, Bjork-Eriksson T, Nill S, Wilkens JJ, Oelfke U, Johansson KA, et al. Intensity-modulated radiotherapy of nasopharyngeal carcinoma: a comparative treatment planning study of photons and protons. *Radiat Oncol.* (2008) 3:4. doi: 10.1186/1748-717X-3-4
78. Widesott L, Pierelli A, Fiorino C, Dell'oca I, Broggi S, Cattaneo GM, et al. Intensity-modulated proton therapy versus helical tomotherapy in nasopharynx cancer: planning comparison and NTCP evaluation. *Int J Radiat Oncol Biol Phys.* (2008) 72:589–96. doi: 10.1016/j.ijrobp.2008.05.065
79. Lewis GD, Holliday EB, Kocak-Uzel E, Hernandez M, Garden AS, Rosenthal DI, et al. Intensity-modulated proton therapy for nasopharyngeal carcinoma: decreased radiation dose to normal structures and encouraging clinical outcomes. *Head Neck.* (2016) 38(Suppl. 1):E1886–95. doi: 10.1002/hed.24341
80. Holliday EB, Garden AS, Rosenthal DI, Fuller CD, Morrison WH, Gunn GB, et al. Proton therapy reduces treatment-related toxicities for patients with nasopharyngeal cancer: a case-match control study of intensity-modulated proton therapy and intensity-modulated photon therapy. *Int J Part Ther.* (2015) 2:19–28. doi: 10.14338/IJPT-15-00011.1
81. Chan A, Adams JA, Weyman E, Parambi R, Goldsmith T, Holman A, et al. A phase II trial of proton radiation therapy with chemotherapy for nasopharyngeal carcinoma. *Int J Radiat Oncol Biol Phys.* (2012) 84:S151–2. doi: 10.1016/j.ijrobp.2012.07.391
82. Chan AW, Liebsch LJ, Deschler DG, Adams JA, Vrishali LV, McIntyre JF, et al. Proton radiotherapy for T4 nasopharyngeal carcinoma. *J Clin Oncol.* (2004) 22(Suppl. 14):5574. doi: 10.1200/jco.2004.22.14_suppl.5574
83. van der Veen J, Gulyban A, Nuyts S. Interobserver variability in delineation of target volumes in head and neck cancer. *Radiother Oncol.* (2019) 137:9–15. doi: 10.1016/j.radonc.2019.04.006
84. Weiss E, Hess CF. The impact of gross tumor volume (GTV) and clinical target volume (CTV) definition on the total accuracy in radiotherapy

theoretical aspects and practical experiences. *Strahlenther Onkol.* (2003) 179:21–30. doi: 10.1007/s00066-003-0976-5
85. Liu X, Le QT, Ma J. Focus on the number of radiation oncology trials or on clinical relevance—reply. *JAMA Oncol.* (2018) 4:1791–2. doi: 10.1001/jamaoncol.2018.5105
86. Peters LJ, O'Sullivan B, Giralt J, Fitzgerald TJ, Trotti A, Bernier J, et al. Critical impact of radiotherapy protocol compliance and quality in the treatment of advanced head and neck cancer: results from TROG 02.02. *J Clin Oncol.* (2010) 28:2996–3001. doi: 10.1200/JCO.2009.27.4498
87. Lee AW, Ng WT, Pan JJ, Poh SS, Ahn YC, AlHussain H, et al. International guideline for the delineation of the clinical target volumes (CTV) for nasopharyngeal carcinoma. *Radiother Oncol.* (2018) 126:25–36. doi: 10.1016/j.radonc.2017.10.032
88. Lee AW, Ng WT, Pan JJ, Chiang CL, Poh SS, Choi HC, et al. International guideline on dose prioritization and acceptance criteria in radiation therapy planning for nasopharyngeal carcinoma. *Int J Radiat Oncol Biol Phys.* (2019) 105:567–80. doi: 10.1016/j.ijrobp.2019.09.030
89. Wuthrick EJ, Zhang Q, Machtay M, Rosenthal DI, Nguyen-Tan PF, Fortin A, et al. Institutional clinical trial accrual volume and survival of patients with head and neck cancer. *J Clin Oncol.* (2015) 33:156–64. doi: 10.1200/JCO.2014.56.5218
90. Torabi SJ, Benchetrit L, Kuo Yu P, Cheraghlou S, Savoca EL, Tate JP, et al. Prognostic case volume thresholds in patients with head and neck squamous cell carcinoma. *JAMA Otolaryngol Head Neck Surg.* (2019) 145:708–15. doi: 10.1001/jamaoto.2019.1187
91. Amarasena I, Herschtal A, D'Costa I, Fua T, Tiong A, Geddes V, et al. Outcomes of routine intensity modulated radiation therapy quality assurance in a large head and neck cancer center. *Int J Radiat Oncol Biol Phys.* (2017) 98:541–6. doi: 10.1016/j.ijrobp.2017.02.215
92. McDowell L, Corry J. Radiation therapy quality assurance in head and neck radiotherapy - moving forward. *Oral Oncol.* (2019) 88:180–5. doi: 10.1016/j.oraloncology.2018.11.014
93. McDowell LJ, Corry J. A call to arms: radiation therapy quality assurance in the next generation of clinical trials. *Int J Radiat Oncol Biol Phys.* (2018) 102:1590–1. doi: 10.1016/j.ijrobp.2018.07.2001
94. So N, McDowell LJ, Lu L, Xu W, Rock K, Waldron J, et al. The prevalence and determinants of return to work in nasopharyngeal carcinoma survivors. *Int J Radiat Oncol Biol Phys.* (2019) 106:134–45. doi: 10.1016/j.ijrobp.2019.09.008
95. Ronis DL, Duffy SA, Fowler KE, Khan MJ, Terrell JE. Changes in quality of life over 1 year in patients with head and neck cancer. *Arch Otolaryngol Head Neck Surg.* (2008) 134:241–8. doi: 10.1001/archoto.2007.43
96. Howren MB, Christensen AJ, Karnell LH, Funk GF. Health-related quality of life in head and neck cancer survivors: impact of pretreatment depressive symptoms. *Health Psychol.* (2010) 29:65–71. doi: 10.1037/a0017788
97. Hammerlid E, Silander E, Hornestam L, Sullivan M. Health-related quality of life three years after diagnosis of head and neck cancer–a longitudinal study. *Head Neck.* (2001) 23:113–25. doi: 10.1002/1097-0347(200102)23:2<113::aid-hed1006>3.0.co;2-w
98. Barber B, Dergousoff J, Nesbitt M, Mitchell N, Harris J, O'Connell D, et al. Depression as a predictor of postoperative functional performance status (PFPS) and treatment adherence in head and neck cancer patients: a prospective study. *J Otolaryngol Head Neck Surg.* (2015) 44:38. doi: 10.1186/s40463-015-0092-4
99. Tang Y, Luo D, Rong X, Shi X, Peng Y. Psychological disorders, cognitive dysfunction and quality of life in nasopharyngeal carcinoma patients with radiation-induced brain injury. *PLoS ONE.* (2012) 7:e36529. doi: 10.1371/journal.pone.0036529
100. Lue BH, Huang TS, Chen HJ. Physical distress, emotional status, and quality of life in patients with nasopharyngeal cancer complicated by post-radiotherapy endocrinopathy. *Int J Radiat Oncol Biol Phys.* (2008) 70:28–34. doi: 10.1016/j.ijrobp.2007.06.053
101. Wang X, Lv Y, Li W, Gan C, Chen H, Liu Y, et al. Correlation between psychosocial distress and quality of life in patients with nasopharyngeal carcinoma following radiotherapy. *J Oncol.* (2018) 2018:3625302. doi: 10.1155/2018/3625302
102. Yu CL, Fielding R, Chan CL, Sham JS. Chinese nasopharyngeal carcinoma patients treated with radiotherapy: association between satisfaction with information provided and quality of life. *Cancer.* (2001) 92:2126–35. doi: 10.1002/cncr.1554
103. Kong L, Lu JJ, Liss AL, Hu C, Guo X, Wu Y, et al. Radiation-induced cranial nerve palsy: a cross-sectional study of nasopharyngeal cancer patients after definitive radiotherapy. *Int J Radiat Oncol Biol Phys.* (2011) 79:1421–7. doi: 10.1016/j.ijrobp.2010.01.002
104. Luk YS, Shum JS, Sze HC, Chan LL, Ng WT, Lee AW. Predictive factors and radiological features of radiation-induced cranial nerve palsy in patients with nasopharyngeal carcinoma following radical radiotherapy. *Oral Oncol.* (2013) 49:49–54. doi: 10.1016/j.oraloncology.2012.07.011
105. Rong X, Tang Y, Chen M, Lu K, Peng Y. Radiation-induced cranial neuropathy in patients with nasopharyngeal carcinoma. A follow-up study. *Strahlenther Onkol.* (2012) 188:282–6. doi: 10.1007/s00066-011-0047-2
106. Chow JCH, Cheung KM, Au KH, Zee BCY, Lee J, Ngan RKC, et al. Radiation-induced hypoglossal nerve palsy after definitive radiotherapy for nasopharyngeal carcinoma: clinical predictors and dose-toxicity relationship. *Radiother Oncol.* (2019) 138:93–8. doi: 10.1016/j.ijrobp.2019.06.290
107. McDowell LJ, Jacobson MC, Levin W. High-dose intravenous steroid regimen for radiation-induced hypoglossal nerve palsy. *Head Neck.* (2017) 39:E23–8. doi: 10.1002/hed.24600
108. Cheung MC, Chan AS, Law SC, Chan JH, Tse VK. Impact of radionecrosis on cognitive dysfunction in patients after radiotherapy for nasopharyngeal carcinoma. *Cancer.* (2003) 97:2019–26. doi: 10.1002/cncr.11295
109. Kiang A, Weinberg VK, Cheung KH, Shugard E, Chen J, Quivey JM, et al. Long-term disease-specific and cognitive quality of life after intensity-modulated radiation therapy: a cross-sectional survey of nasopharyngeal carcinoma survivors. *Radiat Oncol.* (2016) 11:127. doi: 10.1186/s13014-016-0704-9
110. Hsiao KY, Yeh SA, Chang CC, Tsai PC, Wu JM, Gau JS. Cognitive function before and after intensity-modulated radiation therapy in patients with nasopharyngeal carcinoma: a prospective study. *Int J Radiat Oncol Biol Phys.* (2010) 77:722–6. doi: 10.1016/j.ijrobp.2009.06.080
111. Mo YL, Li L, Qin L, Zhu XD, Qu S, Liang X, et al. Cognitive function, mood, and sleep quality in patients treated with intensity-modulated radiation therapy for nasopharyngeal cancer: a prospective study. *Psycho Oncol.* (2014) 23:1185–91. doi: 10.1002/pon.3542
112. McDowell LJ, Ringash J, Xu W, Chan B, Lu L, Waldron J, et al. A cross sectional study in cognitive and neurobehavioral impairment in long-term nasopharyngeal cancer survivors treated with intensity-modulated radiotherapy. *Radiother Oncol.* (2019) 131:179–85. doi: 10.1016/j.radonc.2018.09.012
113. Ongnok B, Chattipakorn N, Chattipakorn SC. Doxorubicin and cisplatin induced cognitive impairment: the possible mechanisms and interventions. *Exp Neurol.* (2020) 324:113118. doi: 10.1016/j.expneurol.2019.113118
114. Fan CY, Lin CS, Chao HL, Huang WY, Su YF, Lin KT, et al. Risk of hypothyroidism among patients with nasopharyngeal carcinoma treated with radiation therapy: a population-based cohort study. *Radiother Oncol.* (2017) 123:394–400. doi: 10.1016/j.radonc.2017.04.025
115. Lertbutsayanukul C, Kitpanit S, Prayongrat A, Kannarunimit D, Netsawang B, Chakkabat C. Validation of previously reported predictors for radiation-induced hypothyroidism in nasopharyngeal cancer patients treated with intensity-modulated radiation therapy, a post hoc analysis from a phase III randomized trial. *J Radiat Res.* (2018) 59:446–55. doi: 10.1093/jrr/rry036
116. Sommat K, Ong WS, Hussain A, Soong YL, Tan T, Wee J, et al. Thyroid V40 predicts primary hypothyroidism after intensity modulated radiation therapy for nasopharyngeal carcinoma. *Int J Radiat Oncol Biol Phys.* (2017) 98:574–80. doi: 10.1016/j.ijrobp.2017.03.007
117. Huang S, Wang X, Hu C, Ying H. Hypothalamic-pituitary-thyroid dysfunction induced by intensity-modulated radiotherapy (IMRT) for adult patients with nasopharyngeal carcinoma. *Med Oncol.* (2013) 30:710. doi: 10.1007/s12032-013-0710-9
118. Huang CL, Tan HW, Guo R, Zhang Y, Peng H, Peng L, et al. Thyroid dose-volume thresholds for the risk of radiation-related hypothyroidism in nasopharyngeal carcinoma treated with intensity-modulated radiotherapy-A single-institution study. *Cancer Med.* (2019) 8:6887–93. doi: 10.1002/cam4.2574

119. National Comprehensive Cancer Network. *Head and Neck Cancers*. (2019). Available online at: https://www.nccn.org/professionals/physician_gls/pdf/head-and-neck.pdf
120. Appelman-Dijkstra NM, Kokshoorn NE, Dekkers OM, Neelis KJ, Biermasz NR, Romijn JA, et al. Pituitary dysfunction in adult patients after cranial radiotherapy: systematic review and meta-analysis. *J Clin Endocrinol Metab.* (2011) 96:2330–40. doi: 10.1210/jc.2011-0306
121. Powell C, Schick U, Morden JP, Gulliford SL, Miah AB, Bhide S, et al. Fatigue during chemoradiotherapy for nasopharyngeal cancer and its relationship to radiation dose distribution in the brain. *Radiother Oncol.* (2014) 110:416–21. doi: 10.1016/j.radonc.2013.06.042
122. Gulliford SL, Miah AB, Brennan S, McQuaid D, Clark CH, Partridge M, et al. Dosimetric explanations of fatigue in head and neck radiotherapy: an analysis from the PARSPORT phase III trial. *Radiother Oncol.* (2012) 104:205–12. doi: 10.1016/j.radonc.2012.07.005
123. Harrison JD, Young JM, Price MA, Butow PN, Solomon MJ. What are the unmet supportive care needs of people with cancer? A systematic review. *Support Care Cancer.* (2009) 17:1117–28. doi: 10.1007/s00520-009-0615-5
124. Osse BH, Vernooij-Dassen Mj, de Vree BP, Schade E, Grol RP. Assessment of the need for palliative care as perceived by individual cancer patients and their families: a review of instruments for improving patient participation in palliative care. *Cancer.* (2000) 88:900–11. doi: 10.1002/(sici)1097-0142(20000215)88:4<900::aid-cncr22>3.0.co;2-2
125. Shunmugasundaram C, Rutherford C, Butow PN, Sundaresan P, Dhillon HM. Content comparison of unmet needs self-report measures used in patients with head and neck cancer: a systematic review. *Psychooncology.* (2019) 28:2295–306. doi: 10.1002/pon.5257
126. Ringash J, Bernstein LJ, Devins G, Dunphy C, Giuliani M, Martino R, et al. Head and neck cancer survivorship: learning the needs, meeting the needs. *Semin Radiat Oncol.* (2018) 28:64–74. doi: 10.1016/j.semradonc.2017.08.008
127. Rogers SN, El-Sheikha J, Lowe D. The development of a Patients Concerns Inventory (PCI) to help reveal patients concerns in the head and neck clinic. *Oral Oncol.* (2009) 45:555–61. doi: 10.1016/j.oraloncology.2008.09.004
128. Giuliani M, McQuestion M, Jones J, Papadakos J, Le LW, Alkazaz N, et al. Prevalence and nature of survivorship needs in patients with head and neck cancer. *Head Neck.* (2016) 38:1097–103. doi: 10.1002/hed.24411

Conflict of Interest: The authors declare that the research was conducted in the absence of any commercial or financial relationships that could be construed as a potential conflict of interest.

frontiers in Oncology

CLINICAL TRIAL
published: 07 August 2020
doi: 10.3389/fonc.2020.01314

Adding Concurrent Chemotherapy to Intensity-Modulated Radiotherapy Does Not Improve Treatment Outcomes for Stage II Nasopharyngeal Carcinoma: A Phase 2 Multicenter Clinical Trial

*Xiaodong Huang[1], Xiaozhong Chen[2], Chong Zhao[3], Jingbo Wang[1], Kai Wang[1], Lin Wang[3], Jingjing Miao[3], Caineng Cao[2], Ting Jin[2], Ye Zhang[1], Yuan Qu[1], Xuesong Chen[1], Qingfeng Liu[1], Shiping Zhang[1], Jianghu Zhang[1], Jingwei Luo[1], Jianping Xiao[1], Guozhen Xu[1], Li Gao[1] and Junlin Yi[1]**

[1] Department of Radiation Oncology, National Cancer Center/National Clinical Research Center for Cancer/Cancer Hospital, Chinese Academy of Medical Sciences and Peking Union Medical College, Beijing, China, [2] Department of Radiation Oncology, Zhejiang Province Cancer Hospital, Hangzhou, China, [3] State Key Laboratory of Oncology in South China, Department of Nasopharyngeal Carcinoma, Sun Yat-sen University Cancer Center, Collaborative Innovation Center for Cancer Medicine, Guangzhou, China

OPEN ACCESS

Edited by:
Jun Ma,
Sun Yat-sen University Cancer Center (SYSUCC), China

Reviewed by:
Nianyong Chen,
Sichuan University, China
Liangfang Shen,
Central South University, China

***Correspondence:**
Junlin Yi
yijunlin1969@163.com

Specialty section:
This article was submitted to Head and Neck Cancer, a section of the journal Frontiers in Oncology

Received: 14 November 2019
Accepted: 24 June 2020
Published: 07 August 2020

Citation:
Huang X, Chen X, Zhao C, Wang J, Wang K, Wang L, Miao J, Cao C, Jin T, Zhang Y, Qu Y, Chen X, Liu Q, Zhang S, Zhang J, Luo J, Xiao J, Xu G, Gao L and Yi J (2020) Adding Concurrent Chemotherapy to Intensity-Modulated Radiotherapy Does Not Improve Treatment Outcomes for Stage II Nasopharyngeal Carcinoma: A Phase 2 Multicenter Clinical Trial. Front. Oncol. 10:1314. doi: 10.3389/fonc.2020.01314

Purpose: To explore the efficacy of concomitant chemotherapy in intensity-modulated radiotherapy (IMRT) to treat stage II nasopharyngeal carcinoma (NPC).

Methods and Materials: In this randomized phase 2 study [registered with ClinicalTrials.gov (NCT01187238)], eligible patients with stage II (2010 UICC/AJCC) NPC were randomly assigned to either IMRT alone (RT group) or IMRT combined with concurrent cisplatin (40 mg/m^2, weekly) (CCRT group). The primary endpoint was overall survival (OS). The second endpoints included local failure-free survival (LFFS), regional failure-free survival (RFFS), disease-free survival (DFS), distant metastasis-free survival (DMFS), and acute toxicities.

Results: Between May 2010 to July 2012, 84 patients who met the criteria were randomized to the RT group ($n = 43$) or the CCRT group ($n = 41$). The median follow-up time was 75 months. The OS, LFFS, RFFS, DFS, and DMFS for the RT group and CCRT group were 100% vs. 94.0% ($p = 0.25$), 93.0% vs. 89.3% ($p = 0.79$), 97.7% vs. 95.1% ($p = 0.54$), 90.4% vs. 86.6% ($p = 0.72$), and 95.2% vs. 94.5% ($p = 0.77$), respectively. A total of 14 patients experienced disease failure, 7 patients in each group. The incidence of grade 2 to 4 leukopenia was higher in the CCRT group ($p = 0.022$). No significant differences in liver, renal, skin, or mucosal toxicity was observed between the two groups.

Conclusion: For patients with stage II NPC, concomitant chemotherapy with IMRT did not improve survival or disease control but had a detrimental effect on bone marrow function.

Keywords: nasopharyngeal carcinoma, intensity-modulated radiotherapy, concurrent chemoradiotherapy, stage II, treatment outcomes

INTRODUCTION

Nasopharyngeal carcinoma (NPC) has the highest incidence among head and neck cancers in Southeast Asia. Radiotherapy (RT) is the mainstay treatment modality for NPC. Concurrent chemoradiotherapy (CCRT), with or without adjuvant chemoradiotherapy, has been confirmed to have a significant survival benefit vs. RT alone for locally advanced NPC according to many prospective clinical trials and meta-analyses (1–6). Based on these studies, the NCCN guidelines have recommended CCRT with/without adjuvant chemotherapy as the standard treatment modality for patients with stage II–IVb (before the AJCC 8th edition) NPC since 2010 (7).

The benefit of concurrent chemoradiotherapy in locally advanced NPC is unquestionable. However, for stage II NPC, the role of concurrent chemotherapy remains unclear. The recommendation for concurrent chemoradiotherapy was based on only one phase 3 randomized trial published in 2011 by Chen et al. (8). In that trial, all patients were treated with two-dimensional radiation technique (2-DRT). Intensity-modulated radiotherapy (IMRT), which is characterized by advantageous dose distribution and reduced normal tissue exposure, has become to the mainstay radiation technique for NPC since the late 1990s. In the last two decades, the local control (LC) and overall survival (OS) of NPC have reached unprecedented levels with the use of IMRT, especially for patients with stage I/II disease, leading to almost 100% 3 year LC and OS, respectively (9). Therefore, it is rational to query whether any additional benefit can be introduced by the use of concurrent chemotherapy in stage II NPC treated with IMRT. To answer this, we conducted a multicenter phase 2 trial to assess whether concurrent chemotherapy could be omitted for patients with stage II NPC without compromising the overall treatment outcomes, yet avoiding the acute treatment-related toxicities associated with chemotherapy (1, 10–12).

PATIENTS AND METHODS

Study Design

This was a multicenter, randomized, phase 2 study. Eligible patients from three large cancer centers were registered and randomly assigned to receive either IMRT alone (IMRT group), or concurrent chemotherapy with IMRT (CCRT group). Patients were stratified according to the tumor (T) and node (N) classification using a central randomization method. The detailed study design is shown in a CONSORT flow diagram (**Figure 1**).

Patient Eligibility

Eligible patients were required to have newly pathologically proven stage II NPC according to the 2010 UICC/AJCC staging system (T2N0, T1N1, or T2N1), a Karnofsky performance status (KPS) $>$ 70, age ranging from 18 to 70 years, adequate hematological function (leukocyte count $> 4 \times 10^9$/L and platelet count $>100 \times 10^9$/L), normal renal function [serum creatinine level $\leq 1.25 \times$ the upper limit of normal (ULN)], and normal hepatic function [alanine aminotransferase (ALT), aspartate transaminase (AST), and bilirubin (BIL) $\leq 1.25 \times$ ULN].

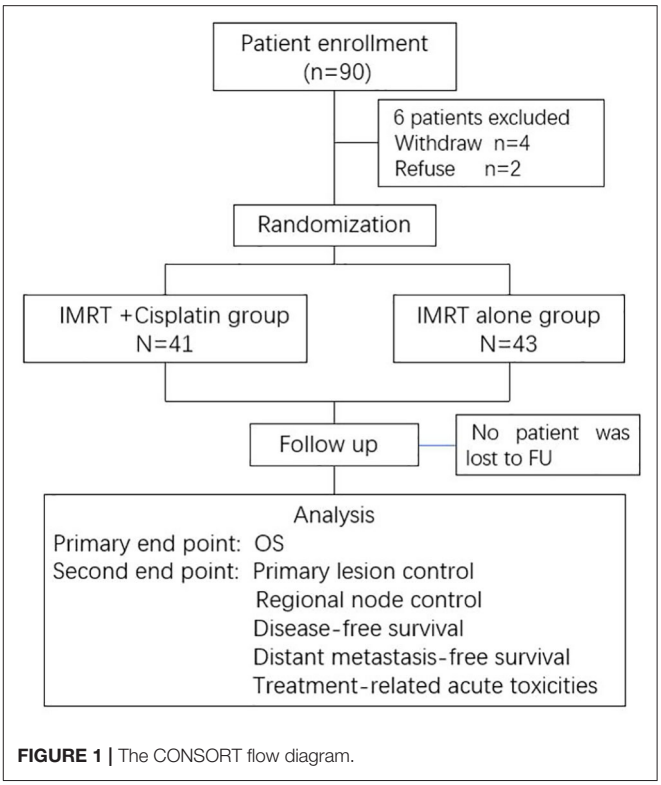

FIGURE 1 | The CONSORT flow diagram.

Exclusion criteria included previous receipt of chemotherapy or radiotherapy, any other cancer history within 5 years, and any severe comorbidities that contraindicated the treatment in the procedure.

Before registration, all patients should receive the following workups: physical examination; endoscopy examination of the nasopharynx; magnetic resonance imaging (MRI) and computed tomography (CT) of nasopharynx and neck; chest CT; and abdominal and pelvic CT or ultrasound.

This study was approved by the Ethics Committee of the Cancer Hospital, Chinese Academy of Medical Sciences, and was registered with ClinicalTrials.gov (NCT01187238). Written informed consent was obtained from all patients before enrollment in the study.

Treatment

All patients were treated using IMRT. Patients were immobilized using thermoplastic masks and simulated via a planning CT with 3 mm-thick slices. Intravenous contrast was strongly recommended. Target delineation was completed on the planning CT with the assistance of fused MRI images.

The gross tumor volume of the nasopharynx (GTVnx) was defined as the nasopharyngeal primary lesion displayed on simulation CT and diagnostic MRI. Cervical nodes with a short axis larger than 1 cm, with central necrosis, or a cluster of nodes large than 8 mm at level II, were considered positive and were named as GTVnd. The high-risk region of tumor invasion or nodal metastasis was defined as clinical tumor volume 1 (CTV1), including the entire nasopharynx,

retropharyngeal nodal region, skull base, clivus, pterygopalatine fossa, parapharyngeal space, sphenoid sinus, and the posterior third of the nasal cavity/maxillary sinuses. CTV1 also included the regions with a high risk of nodal involvement, such as the level II nodal region for N0 patients or the corresponding level plus the adjacent level of positive nodes for N1 patients. Other nodal regions, including the supraclavicular fossa, were defined as CTV2. GTVnx, GTVnd, CTV1, and CTV2 were uniformly expanded by a 3-mm margin to generate the planning target volumes PGTVnx, PTV1, and PTV2, respectively.

Radiotherapy was delivered using simultaneous-integrated boost (SIB) IMRT, and all doses were prescribed to the PTVs. Generally, an RT dose of 69.96 Gy/2.12 Gy/33 fractions and 60.06 Gy/1.82 Gy/33 fractions were prescribed to the PGTVnx/GTVnd and PTV1, respectively. If there was a prophylactic neck volume (CTV2, prescribed dose was 50.96 Gy/1.82 Gy/28 fractions), the patients were treated using a two-phase plan. First, 28 fractions were delivered to all PTVs, and then the remaining five fractions were only delivered to PGTVnx/GTVnd and PTV1. If there were retropharyngeal lymph nodes with a diameter > 2 cm, the prescribe doses were 2.24–2.36 Gy/fraction for 33 fractions. The dose constraints for organs at risk were as follows: Maximum dose (Dmax) to 3 mm of the brain stem planning organ at risk volume (PRV): < 54 Gy; Dmax of 5 mm of the spinal cord PRV: < 45 Gy; Dmax of the optic nerve, chiasm, and temporal lobe: < 54 Gy; and the percentage of the volume receiving 30–35 Gy (V30–35) of the parotid gland was $< 50\%$.

The patients randomized to the CCRT group also received concurrent chemotherapy of weekly cisplatin at 40 mg/m^2, which was started on the first day of IMRT. A maximum of seven cycles of chemotherapy could be administered during radiotherapy.

Follow-Up and Outcomes

All patients were followed up at 1 month after the completion of protocol treatment, every 3 months for the first 2 years and every 6 months for the 3rd to 5th years, and once a year thereafter. If there was suspicion of progression or toxicity, more frequent evaluations were allowed.

Statistical Consideration

The primary endpoint of this study was overall survival (OS), which was defined as the period of time from the start of treatment to death from any cause. Secondary endpoints included local failure-free survival (LFFS), regional failure-free survival (RFFS), progression-free survival (PFS), distant metastasis-free survival (DMFS), and treatment-related acute toxicities. The National Cancer Institute Common Toxicity Criteria of adverse event (version 4.0) was used to assess treatment-related acute toxicities (13).

The SPSS 20.0 software (IBM Corp., Armonk, NY, USA) was used to analyze the data. The survival data were estimated using the Kaplan–Meier method, and the survival intervals of two groups were compared using the log-rank test. The chi-squared test was used to compare differences in acute toxicities and patient characteristics between two groups.

TABLE 1 | The patients' characteristics between two groups.

Items	CCRT ($n = 41$)		IMRT alone ($n = 43$)		*P*
	n	%	*n*	%	
Gender					
Male	32	78.0	30	69.8	0.388
Female	9	22.0	13	30.2	
Age					
Median (Range)	48 (range 19–68)		46 (range 26–65)		
T stage					
T1	15	36.6	14	32.6	0.698
T2	26	63.4	29	67.4	
N stage					
N0	7	17.1	8	18.6	0.855
N1	34	82.9	35	81.4	
Radiation Dose					
Median (Range)	70 Gy (69.36–76.93 Gy)		70 Gy (69.7–74.25 Gy)		0.506

RESULTS

Patient's Characteristics

Between May 2010 and July 2012, a total of 90 patients from three large cancer centers were screened. Six patients withdrew from the study after providing signed informed consent. Finally, 84 patients entered this study and completed the required treatment as per protocol, with 43 in the IMRT group and 41 in the CCRT group. The patients' general characteristics are listed in **Table 1**. The baseline characteristics were well-balanced between the groups. The median age was 48 and 46 years old for the CCRT and IMRT groups, respectively. There was no difference in terms of T and N stage between the two groups. All patients received the RT dose as per protocol, with a median of 70 Gy for both groups. With regard to the CCRT group, a median of 6 cycles of concurrent chemotherapy were completed, including 13 patients (31.7%) receiving 7 cycles, 20 patients (48.8%) receiving 6 cycles, 5 patients (12.2%) receiving 5 cycles, and the other 3 patients receiving ≤ 3 cycles of chemotherapy.

Treatment Results

No patients were lost to follow-up. With a median follow-up time of 75 months, four patients died, including one from the IMRT group and three from the CCRT group. The 5 year OS, DFS, LFFS, RFFS, and DMFS for the whole cohort were 97.5, 88.7, 93.9, 96.4, and 94.9%, respectively. As shown in **Figure 2**, the OS, LFFS, RFFS, DFS, and DMFS of the IMRT and CCRT groups were 100% vs. 94.0% ($p = 0.25$), 93.0% vs. 89.3% ($p = 0.79$), 97.7% vs. 95.1% ($p = 0.54$), 90.4% vs. 86.6% ($p = 0.72$), and 95.2% vs. 94.5% ($p = 0.77$) respectively.

A total of 14 patients, 7 from each group, experienced treatment failure. There was no difference concerning the failure pattern between the two groups (**Table 2**). Five patients suffered distant metastasis with or without local–regional failure, including 4 patients with T2N1 and the other 1 with T2N0 diseases.

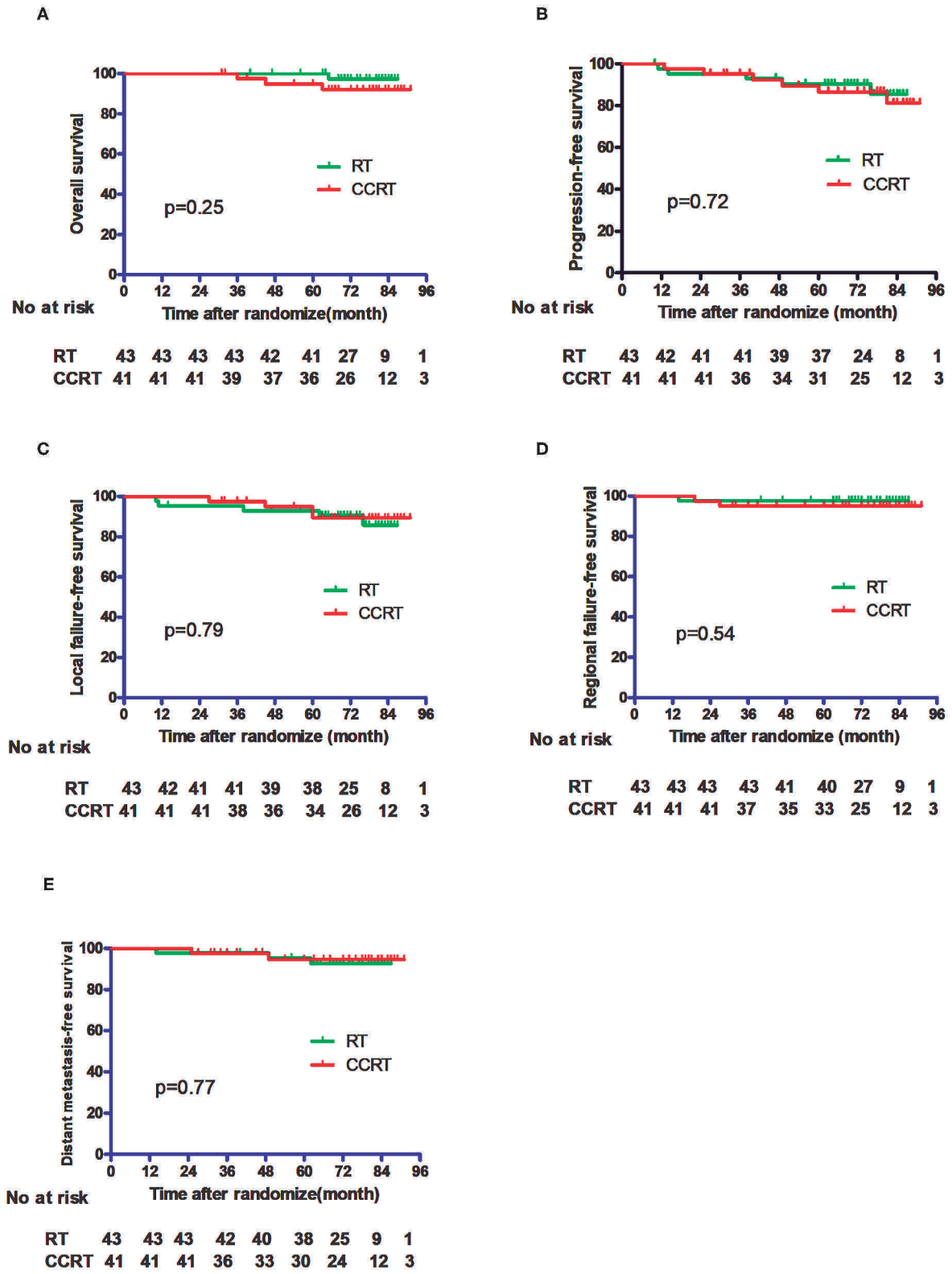

FIGURE 2 | Comparison of the treatment results between the IMRT alone group and the CCRT group. **(A)** Overall survival. **(B)** Progression-free survival. **(C)** Local failure-free survival. **(D)** Regional failure-free survival. **(E)** Distant metastasis-free survival.

TABLE 2 | Pattern of failure between IMRT and CCRT.

Failure pattern	CCRT ($n = 41$)		IMRT alone ($n = 43$)		*P*
	n	%	*n*	%	
Local	4	9.8	4	9.3	
Regional	1	2.4	0	0	
Distant Metastasis	2	4.8	1	2.3	
Local+Distant	0	0	1	2.3	
Regional+Distant	0	0	1	2.3	
Total	7	17.1	7	16.3	0.92

TABLE 3 | Treatment related acute toxicities.

	CCRT $n = 41$		IMRT alone $n = 43$		*P*
	n	%	*n*	%	
Hb	1	24	0	0	0.3
WBC	17	41.4	8	18.6	0.02
PLT	1	2.4	0	0	0.30
GI	15	36.6	6	14.0	0.02
Liver	1	2.4	0	0	0.30
Skin	10	24.4	9	20.9	0.70
Mucositis	27	65.9	27	62.8	0.70

Hb, hemoglobin; WBC, white blood cell; PLT, Platelet; GI, Gastrointestinal.

With regard to treatment-related adverse events, more grade 2–4 acute hematological ($p = 0.02$) and gastrointestinal ($p = 0.02$) toxicities were observed in the CCRT group than in the IMRT group. For hematological toxicity, a total of 5 patients presented $\geq$ G3 events in the entire study cohort. In the CCRT group, 3 grade 3 and 1 grade 4 events were observed whereas only 1 patient with grade 3 toxicity was reported in the IMRT alone group. A total of 5 patients experienced GI toxicities in the CCRT group, including 4 patients with grade 2 and 1 patient with grade 3 events. No $\geq$ G2 GI toxicity was observed in the IMRT group. There was no significant difference in terms of liver, renal, skin, and oral mucosa toxicities between the IMRT and CCRT groups (**Table 3**). No grade 3 xerostomia was observed in either group.

DISCUSSION

Our study demonstrated that adding concurrent cisplatin to IMRT did not improve treatment outcomes in patients with stage II NPC but increased treatment-related acute hematological and gastrointestinal toxicities.

There are limited data assessing the role of concurrent chemoradiotherapy for stage II NPC. The only published phase 3 trial (8) that compared CCRT with RT alone found that the use of concurrent chemotherapy significantly improved the 5 year OS (94.5% vs. 85.8%; $p = 0.007$), PFS (87.9% vs. 77.8%; $p = 0.017$), and DMFS (94.8% vs. 83.9%; $p = 0.007$). However, it should be noted that all patients in that study underwent two-dimensional conventional radiotherapy, which has been proven to be inferior to IMRT. In addition, in Chen's study (8), 31 out of 236 patients (13.1%) had N2 disease (stage III) according to the 7th AJCC staging system. Therefore, the advantage of CCRT for this subgroup might have confounded the overall evaluation, leading to an overestimation of the role of concurrent chemotherapy for patients with pure stage II disease. It should also be noted that in that study, CCRT did not improve local regional control, with 5 year loco-regional relapse-free survival rates of 93.0% vs. 91.1% ($p = 0.29$), but did improve the distant metastasis-free survival, with the rates of 94.8% vs. 83.9%; $p = 0.007$), indicating that the decreased distant metastasis-free survival contributed to the improved OS.

In the present study, all patients were staged according to the 7th AJCC staging system with the assistance of MRI and CT imaging; therefore, the patients' tumor burden was more homogeneous compared with that of the abovementioned study. Additionally, the patients were pre-stratified by N status, leading to a minimized influence of N stage on the treatment results. Correspondingly, the 5 year DMFS of the CCRT and RT alone groups were 95.2% vs. 94.5% ($p = 0.77$), which were numerically higher than those reported in the previous study. Hence, the need for CCRT to decrease distant metastasis in our study was relatively unnecessary.

Although it has been widely confirmed by many randomized studies and meta-analyses that concurrent chemoradiotherapy could offer better treatment results than radiotherapy alone in locally advanced NPC, all of these studies showed that concurrent chemotherapy increased treatment-related toxicities, especially hematological, gastrointestinal, oral mucosal, and skin toxicities (1, 4, 10, 11). Our study also verified that CCRT increased treatment-related toxicities, even in patients treated using IMRT.

In the last two decades, IMRT has been widely used because of its advantage of dose distribution (14–16). Studies have confirmed that the advantage of dose distribution could translate into clinical benefit, in terms of either OS or treatment-related toxicities, especially for patients whose tumor was located in the center of the skull base and is surrounded by many critical organs (17). For patients with T1/T2 or stage I/II disease, Kwong et al. (9) reported the survival results of 33 patients with T1, N0–N1, and M0 NPC treated by IMRT and revealed that the 3 year LC, DMFS, and OS were all 100%. Several large sample studies from NPC epidemic regions reported 5 year OS rates of 80–85% in the IMRT era (18–23).

Stage II NPC has a relatively low tumor burden and a low risk of distant metastasis and indeed excellent LC, OS, and DMFS could be achieved using IMRT; therefore, doubts were expressed as to whether concurrent chemoradiotherapy is really needed in the era of IMRT. Fangzheng et al. (24) analyzed 242 patients with stage II disease treated by IMRT retrospectively and observed no significant differences between patients who received IMRT alone ($n = 37$), induction chemotherapy plus IMRT ($n = 48$), induction chemotherapy plus CCRT ($n = 132$), and CCRT ($n = 25$), with 5 year OS rates of 94.7, 98.7, 92.9, and 93.4%, respectively.

There have been few randomized studies focusing on the role of CCRT for stage II NPC treated by IMRT. Chen et al. (25) reported a randomized study with the same design as the present study and obtained similar findings. In Chen's study, 168 patients were recruited, of whom 160 were eligible for

intent-to-treat analysis, with 81 in the CCRT group and 79 in the IMRT alone group. With a median follow-up of 61.5 months, the 5 year OS rates for the CCRT and IMRT alone groups were 91.4 and 88.6%, ($p = 0.562$). The 5 year DMFS rates were 93.82% in the CCRT arm and 93.67% in the IMRT alone arm ($p = 0.967$). There were significantly higher acute systemic side effects in the CCRT arm, especially the incidence of grade 3–4 hematological and gastrointestinal events ($p = 0.000$). Most of the locoregional recurrence (6/8, 75.0%) and distant metastases (6/7, 85.7%) occurred in the T2N1 group. Xu et al. (26) performed a systemic review and meta-analysis focusing on the value of chemoradiotherapy (CRT) in stage II NPC compared with that of RT alone. By including both 2D-RT and IMRT techniques, patients receiving CRT or RT alone achieved an equivalent OS, LRRFS, and DMFS ($p = 0.14$).

Considering that stage II consists of three subgroups (T1N1, T2N0, and T2N1), the prognosis and failure patterns might differ among these subgroups. In our study, a total of 5 patients experienced distant metastasis, including 4 harboring T2N1 tumor and the other 1 with T2N0 disease. Because of the relative small sample size and few events of distant metastasis in our study, it was not statistically meaningful for us to analyze the prognostic difference among the three subgroups. However, the T2N1 subgroup indeed accounted for the highest proportion of overall patients with distant failure. A series of publications provided retrospective evidence for this hypothesis. Leung et al. (27) found that patients with stage IIB disease had a higher distant failure rate when compared with patients in the stage I and stage IIA subgroups. Based on a database including 1,070 patients with NPC treated with RT alone from 1990 to 1998, Leung et al. (28) further reported a significantly higher isolated distant metastases rate (5.7% vs. 14.9%) for patients with T1–2N1 disease compared with that for the T2N0 subgroup. Similarly, Zong et al. (29) reported a 5 year accumulated distant metastasis rate of 10.8% in patients with T1–T2N1 disease vs. 0.1% in patients with T1–T2N0 NPC, accompanied by significantly different OS rates of 84.7% vs. 95.4% ($p = 0.005$). Xiao et al. (30) found that the accumulated distant metastasis-free survival rate was 81.2% for the T2N1 group, while the rates in the T1N1 and T2N0 groups were 95.6% and 97.5%, respectively, with corresponding 5 year OS rates of 73.1%, 95.6%, and 97.5%, respectively ($p = 0.000$). Even in Chen's (25) randomized study in which the design was similar to that of the present study, the T2N1 group demonstrated relatively worse outcomes compared with those of the other stage II subgroups, mainly because of increased failure in distant sites. The results of Chen's phase 3 study (8) confirmed that CCRT can decrease the distant metastasis rate for stage II NPC. Therefore, it would be important to distinguish patients with a higher risk of distant metastasis from general stage II patients to provide them with a more tailored treatment strategy. In recent decades, plasma-based Epstein–Barr virus DNA (EBV-DNA) evaluation has become an attractive prognostic biomarker. Leung et al. (27) observed that the probability of distant failure was significantly higher in patients with higher pretreatment plasma EBV-DNA levels (>4,000 copies/mL, $p = 0.0001$). Likewise, Du et al. (31) also verified that plasma EBV-DNA $\geq$ 4,000 copies/mL was independently associated with worse distant metastasis-free survival (DMFS) in 296 patients with stage II (AJCC 7th) NPC treated using IMRT.

In conclusion, this randomized phase 2 study demonstrated that adding concurrent chemotherapy to IMRT might not be necessary for stage II NPC. Considering the relatively small sample size and the implicit heterogeneity among patients with stage II disease, a further phase 3 study is warranted to confirm this finding in selected patients with stage II NPC with a lower risk of distant metastasis.

DATA AVAILABILITY STATEMENT

The datasets generated for this study are available on request to the corresponding author.

ETHICS STATEMENT

This study was approved by the Ethics Committee of the cancer hospital, Chinese Academy of Medical Sciences, and was registered with ClinicalTrials.gov (NCT01187238). Written informed consent was obtained for all patients before enrollment to the study.

AUTHOR CONTRIBUTIONS

JY designed the study, wrote the protocol, reviewed all the case record forms for eligibility and protocol violation, recruited the patients, and wrote the manuscript. XiC, CZ, and LG designed the study. XH and JW were responsible for the patient accrual, radiotherapy treatment, data collection, and wrote the manuscript. LW, JM, CC, TJ, YZ, KW, YQ, XuC, QL, SZ, JZ, JL, JX, and GX were responsible for radiotherapy treatment, the patients' data collection, and data management. All authors contributed to the article and approved the submitted version.

FUNDING

This present study was supported by the National Key Projects of Research and Development of China (2017YFC0107500) and the National Natural Sciences Foundation of China, 81172125/H1610.

REFERENCES

1. Al-Sarraf M, LeBlanc M, Giri PG, Fu KK, Cooper J, Vuong T, et al. Chemoradiotherapy versus radiotherapy in patients with advanced nasopharyngeal cancer: phase III randomized Intergroup study 0099. *J Clin Oncol.* (1998) 16:1310–7. doi: 10.1200/JCO.1998.16.4.1310
2. Lin JC, Jan JS, Hsu CY, Liang WM, Jiang RS, Wang WY. Phase III study of concurrent chemoradiotherapy versus radiotherapy alone for advanced

nasopharyngeal carcinoma: positive effect on overall and progression-free survival. *J Clin Oncol.* (2003) 21:631–7. doi: 10.1200/JCO.2003.06.158
3. Langendijk JA, Leemans CR, Buter J, Berkhof J, Slotman BJ. The additional value of chemotherapy to radiotherapy in locally advanced nasopharyngeal carcinoma: a meta-analysis of the published literature. *J Clin Oncol.* (2004) 22:4604–12. doi: 10.1200/JCO.2004.10.074
4. Lee AW, Lau WH, Tung SY, Chua DT, Chappell R, Xu L, et al. Preliminary results of a randomized study on therapeutic gain by concurrent chemotherapy for regionally-advanced nasopharyngeal carcinoma: NPC-9901 Trial by the Hong Kong Nasopharyngeal Cancer Study Group. *J Clin Oncol.* (2005) 23:6966–75. doi: 10.1200/JCO.2004.00.7542
5. Wee J, Tan EH, Tai BC, Wong HB, Leong SS, Tan T, et al. Randomized trial of radiotherapy versus concurrent chemoradiotherapy followed by adjuvant chemotherapy in patients with American Joint Committee on Cancer/International Union against cancer stage III and IV nasopharyngeal cancer of the endemic variety. *J Clin Oncol.* (2005) 23:6730–8. doi: 10.1200/JCO.2005.16.790
6. Baujat B, Audry H, Bourhis J, Chan AT, Onat H, Chua DT, et al. Chemotherapy in locally advanced nasopharyngeal carcinoma: an individual patient data meta-analysis of eight randomized trials and 1753 patients. *Int J Radiat Oncol Biol Phys.* (2006) 64:47–56. doi: 10.1016/j.ijrobp.2005.06.037
7. National Comprehensive Cancer Network (NCCN). *Clinical Practice Guidelines in Oncology*. Head and Neck Cancer, Version 1.2019 (2019). Available online at: https://wwwnccnorg/professionals/physician_gls/f_guidelinesasp
8. Chen QY, Wen YF, Guo L, Liu H, Huang PY, Mo HY, et al. Concurrent chemoradiotherapy vs. radiotherapy alone in stage II nasopharyngeal carcinoma: phase III randomized trial. *J Natl Cancer Inst.* (2011) 103:1761–70. doi: 10.1093/jnci/djr432
9. Kwong DL, Pow EH, Sham JS, McMillan AS, Leung LH, Leung WK, et al. Intensity-modulated radiotherapy for early-stage nasopharyngeal carcinoma: a prospective study on disease control and preservation of salivary function. *Cancer.* (2004) 101:1584–93. doi: 10.1002/cncr.20552
10. Chan AT, Teo PM, Ngan RK, Leung TW, Lau WH, Zee B, et al. Concurrent chemotherapy-radiotherapy compared with radiotherapy alone in locoregionally advanced nasopharyngeal carcinoma: progression-free survival analysis of a phase III randomized trial. *J Clin Oncol.* (2002) 20:2038–44. doi: 10.1200/JCO.2002.08.149
11. Kwong DL, Sham JS, Au GK, Chua DT, Kwong PW, Cheng AC, et al. Concurrent and adjuvant chemotherapy for nasopharyngeal carcinoma: a factorial study. *J Clin Oncol.* (2004) 22:2643–53. doi: 10.1200/JCO.2004.05.173
12. Lee AW, Yau TK, Wong DH, Chan EW, Yeung RM, Ng WT, et al. Treatment of stage IV(A-B) nasopharyngeal carcinoma by induction-concurrent chemoradiotherapy and accelerated fractionation. *Int J Radiat Oncol Biol Phys.* (2005) 63:1331–8. doi: 10.1016/j.ijrobp.2005.05.061
13. *The National Cancer Institute Common Toxicity Criteria of Adverse Event* (version 4.0). Available online at: https://evsncinihgov/ftp1/CTCAE/CTCAE_403/
14. Xia P, Fu KK, Wong GW, Akazawa C, Verhey LJ. Comparison of treatment plans involving intensity-modulated radiotherapy for nasopharyngeal carcinoma. *Int J Radiat Oncol Biol Phys.* (2000) 48:329–37. doi: 10.1016/S0360-3016(00)00585-X
15. Kam MK, Chau RM, Suen J, Choi PH, Teo PM. Intensity-modulated radiotherapy in nasopharyngeal carcinoma: dosimetric advantage over conventional plans and feasibility of dose escalation. *Int J Radiat Oncol Biol Phys.* (2003) 56:145–57. doi: 10.1016/S0360-3016(03)00075-0
16. Lee N, Xia P, Quivey JM, Sultanem K, Poon I, Akazawa C, et al. Intensity-modulated radiotherapy in the treatment of nasopharyngeal carcinoma: an update of the UCSF experience. *Int J Radiat Oncol Biol Phys.* (2002) 53:12–22. doi: 10.1016/S0360-3016(02)02724-4
17. Lee N, Harris J, Garden AS, Straube W, Glisson B, Xia P, et al. Intensity-modulated radiation therapy with or without chemotherapy for nasopharyngeal carcinoma: radiation therapy oncology group phase II trial 0225. *J Clin Oncol.* (2009) 27:3684–90. doi: 10.1200/JCO.2008.19.9109
18. Feng J, Hu FJ, Hu QY, Feng XL, Li B, Bao WA, et al. Evaluation of significance of the 7th edition of the International union against cancer/ American Joint Committee on cancer staging system for nasopharyngeal carcinoma with intensity-modulated radiotherapy. *Chin J Radiat Oncol.* (2015) 24:281–4. doi: 10.3760/cma.j.issn.1004-4221.2015.03.013
19. Yi J, Huang X, Gao L, Luo J, Zhang S, Wang K, et al. Intensity-modulated radiotherapy with simultaneous integrated boost for locoregionally advanced nasopharyngeal carcinoma. *Radiat Oncol.* (2014) 9:56. doi: 10.1186/1748-717X-9-56
20. Sun X, Su S, Chen C, Han F, Zhao C, Xiao W, et al. Long-term outcomes of intensity-modulated radiotherapy for 868 patients with nasopharyngeal carcinoma: an analysis of survival and treatment toxicities. *Radiother Oncol.* (2014) 110:398–403. doi: 10.1016/j.radonc.2013.10.020
21. Ng WT, Lee MC, Chang AT, Chan OS, Chan LL, Cheung FY, et al. The impact of dosimetric inadequacy on treatment outcome of nasopharyngeal carcinoma with IMRT. *Oral Oncol.* (2014) 50:506–12. doi: 10.1016/j.oraloncology.2014.01.017
22. Hung TM, Chen CC, Lin CY, Ng SH, Kang CJ, Huang SF, et al. Prognostic value of prepontine cistern invasion in nasopharyngeal carcinoma treated by intensity-modulated radiotherapy. *Oral Oncol.* (2014) 50:228–33. doi: 10.1016/j.oraloncology.2013.12.005
23. Zong J, Lin S, Lin J, Tang L, Chen B, Zhang M, et al. Impact of intensity-modulated radiotherapy on nasopharyngeal carcinoma: validation of the 7th edition AJCC staging system. *Oral Oncol.* (2015) 51:254–9. doi: 10.1016/j.oraloncology.2014.10.012
24. Fangzheng W, Chuner J, Quanquan S, Zhimin Y, Tongxin L, Jiping L, et al. Addition of chemotherapy to intensity-modulated radiotherapy does not improve survival in stage II nasopharyngeal carcinoma patients. *J Cancer.* (2018) 9:2030–7. doi: 10.7150/jca.25042
25. Chen S, Meng Y, Shen Y, Ning X, Xiong C, Lin Z, et al. Chemotherapy may not be necessary in stage II nasopharyngeal carcinoma treated with intensity-modulated radiation therapy. *Int J Radiat Oncol Biol Phys.* (2018) 102:S125–6. doi: 10.1016/j.ijrobp.2018.06.313
26. Xu C, Zhang LH, Chen YP, Liu X, Zhou GQ, Lin AH, et al. Chemoradiotherapy versus radiotherapy alone in stage II nasopharyngeal carcinoma: a systemic review and meta-analysis of 2138 patients. *J Cancer.* (2017) 8:287–97. doi: 10.7150/jca.17317
27. Leung SF, Chan AT, Zee B, Ma B, Chan LY, Johnson PJ, et al. Pretherapy quantitative measurement of circulating Epstein-Barr virus DNA is predictive of posttherapy distant failure in patients with early-stage nasopharyngeal carcinoma of undifferentiated type. *Cancer.* (2003) 98:288–91. doi: 10.1002/cncr.11496
28. Leung TW, Tung SY, Sze WK, Wong FC, Yuen KK, Lui CM, et al. Treatment results of 1070 patients with nasopharyngeal carcinoma: an analysis of survival and failure patterns. *Head Neck.* (2005) 27:555–65. doi: 10.1002/hed.20189
29. Zong J, Ma J, Tang L, Huang Y, Liu LZ, Lin AH, et al. A study of the combined treatment strategy for patients with nasopharyngeal carcinoma based on the analysis of the treatment results from 749 cases. *Bull Chin Cancer.* (2005) 14:538–42. doi: 10.3969/j.issn.1004-0242.2005.08.017
30. Xiao WW, Han F, Lu TX, Chen CY, Huang Y, Zhao C. Treatment outcomes after radiotherapy alone for patients with early-stage nasopharyngeal carcinoma. *Int J Radiat Oncol Biol Phys.* (2009) 74:1070–6. doi: 10.1016/j.ijrobp.2008.09.008
31. Du XJ, Tang LL, Mao YP, Guo R, Sun Y, Lin AH, et al. Circulating EBV DNA, globulin and nodal size predict distant metastasis after intensity-modulated radiotherapy in stage II nasopharyngeal carcinoma. *J Cancer.* (2016) 7:664–70. doi: 10.7150/jca.14183

Conflict of Interest: The authors declare that the research was conducted in the absence of any commercial or financial relationships that could be construed as a potential conflict of interest.

The handling editor declared a shared affiliation, though no other collaboration, with several of the authors CZ, LW, and JM.

frontiers in Oncology

ORIGINAL RESEARCH
published: 12 August 2020
doi: 10.3389/fonc.2020.01076

A Field Test of Major Value Frameworks in Chemotherapy of Nasopharyngeal Carcinoma—To Know, Then to Measure

Yuan Zhang[1†], *Xu Liu*[1†], *Ying-Qin Li*[1†], *Ling-Long Tang*[1], *Lei Chen*[1,2] *and Jun Ma*[1*]

[1] State Key Laboratory of Oncology in South China, Guangdong Key Laboratory of Nasopharyngeal Carcinoma Diagnosis and Therapy, Department of Radiation Oncology, Collaborative Innovation Center of Cancer Medicine, Sun Yat-sen University Cancer Center, Guangzhou, China, [2] Department of Radiation Oncology, University of Texas M.D. Anderson Cancer Center, Houston, TX, United States

OPEN ACCESS

Edited by:
Dirk Van Gestel,
Free University of Brussels, Belgium

Reviewed by:
Wai Tong Ng,
Pamela Youde Nethersole Eastern Hospital, Hong Kong
Ester Orlandi,
Istituto Nazionale dei Tumori (IRCCS), Italy

***Correspondence:**
Jun Ma
majun2@mail.sysu.edu.cn

[†] These authors have contributed equally to this work

Specialty section:
This article was submitted to Head and Neck Cancer, a section of the journal Frontiers in Oncology

Received: 03 September 2019
Accepted: 29 May 2020
Published: 12 August 2020

Citation:
Zhang Y, Liu X, Li Y-Q, Tang L-L, Chen L and Ma J (2020) A Field Test of Major Value Frameworks in Chemotherapy of Nasopharyngeal Carcinoma—To Know, Then to Measure. Front. Oncol. 10:1076. doi: 10.3389/fonc.2020.01076

Background: The European Society for Medical Oncology (ESMO) and the American Society of Clinical Oncology (ASCO) have independently developed their own frameworks to assess the benefits of different cancer treatment options, which have significant implications in health science and policy. We aimed to compare these frameworks in nasopharyngeal carcinoma.

Methods: We identified all randomized controlled trials of systemic chemotherapies for nasopharyngeal carcinoma until April 5th, 2020. Trials were eligible if significant differences favoring the experimental group in a prespecified primary or secondary outcome were reported. Two assessors independently scored the trials and the final scores were determined by consensus.

Results: Fifteen trials were included in the analysis. Five different toxicity grading criteria were applied to the 15 trials. Ten (66.7%) trials did not report grade 1–2 toxicities and eight (53.3%) did not report late toxicities. The number of acute toxicities reported was strikingly different (17 vs. 8) in two trials using the same regimen. All trials met the ESMO criteria for a high level of benefit. However, significant variations in ASCO scores between trials were observed (mean [standard deviation]: 38.9 [20.0]).

Conclusions: The underreporting and inconsistent reporting of toxicities would significantly impair the assessment of value using any framework. Moreover, there is a concern that the ASCO framework generated highly inconsistent scoring for treatments that met the ESMO criteria for a high level of benefit. The anomalies identified in the frameworks function would be helpful in their future improvement.

Keywords: value framework, European Society for Medical Oncology, Magnitude of Clinical Benefit Scale, American Society of Clinical Oncology, drug therapy, nasopharyngeal neoplasms

INTRODUCTION

The goal of any cancer therapy is to help patients live longer, or live better, or both. In the clinic, oncologists, and patients need to discuss the balance of benefit and toxicity associated with different treatment options, to make the best decision for each patient. The European Society for Medical Oncology (ESMO) and the American Society of Clinical Oncology (ASCO) have proposed and updated frameworks to assess the value of cancer treatment options (1, 2).

Nasopharyngeal carcinoma (NPC) is prevalent in Southern China, Southeast Asia, North Africa, the Middle East, and Alaska (3). Radiotherapy (RT) is the primary treatment for non-metastatic NPC. Multiple randomized controlled trials (RCTs) have shown that combining chemotherapy with RT improves outcome in loco-regionally advanced NPC. However, different sequences (induction, concurrent, adjuvant, and their combinations) and regimens of chemotherapy were used in these RCTs and controversy remains over which treatment option is optimal (4). In recurrent or metastatic NPC, chemotherapy is the mainstay of treatment and various regimens have been used in the clinic.

Recently, researchers have used the ESMO and ASCO frameworks to assess systemic therapies for cancers (5–8). However, to the best of our knowledge, no study has tested these frameworks in NPC. We applied the updated ESMO and ASCO value frameworks to RCTs investigating systemic chemotherapies in NPC.

MATERIALS AND METHODS

Literature Search

This systematic analysis aimed to include all relevant published trials on systemic chemotherapies in NPC. The following electronic databases were searched to identify potentially eligible trials: PubMed, Web of Science, and the Central Registry of Controlled Trials of the Cochrane Library (CENTRAL). The search was supplemented by a manual search of the reference lists of primary studies, review articles, meta-analyses, and relevant books. To search PubMed and Web of Science, we adopted a search algorithm used in the latest individual patient data meta-analysis of chemotherapy in NPC (4). For CENTRAL, we used the Medical Subject Heading "nasopharyngeal neoplasms" to search for studies. The language and time were not limited in the search, which was performed on April 5th, 2020.

The search algorithms were as follows:

PubMed:
((nasopharyngeal neoplasms/drug therapy [MAJR] OR nasopharyngeal neoplasms/radiotherapy [MAJR]) AND (clinical trial [Publication Type] AND (random* OR (Phase III)Fields: Title Word))) OR ((nasopharyngeal neoplasms/drug therapy [MAJR] OR nasopharyngeal neoplasms/radiotherapy [MAJR]) AND (clinical trial, phase III [Publication Type] OR randomized controlled trial [Publication Type]))

Web of Science:
TS = (nasopharyn* OR cavum) AND TS = (chemotherapy OR chemoradiation OR chemoradiotherapy OR radiochemotherapy OR radio-chemotherapy OR pharmacotherapy) AND TS = (cancer* OR carcinoma* OR adenocarcinoma* OR malignan* OR tumor* OR tumor* OR neoplasm) AND TS = (random*) AND TS = (trial*) NOT TS = (retrospective*)
Refined by: DOCUMENT TYPES: (CLINICAL TRIAL)
Timespan: All years. Databases: WOS.

CENTRAL:
#1 = MeSH descriptor: [Nasopharyngeal Neoplasms] explode all trees
#2 = random*
#3 = #1 and #2

Study Selection

The following criteria were applied to the selection of RCTs:

1) RCTs reporting significant differences favoring the experimental group in a prespecified primary or secondary outcome. Trials with "negative" results were excluded, as they were not assessable according to the frameworks. This is in accordance to the ESMO-Magnitude of Clinical Benefit Scale (MCBS) version 1.1 stating that only "adequately powered studies showing statistically significant improvement in the primary outcomes or secondary outcomes" should be scored (2).
2) At least 50% of trial participants had NPC;
3) At least 30 patients had been included in each arm;
4) Trials using split-course RT were excluded.

Two authors (YZ and XL) independently performed the literature search and study selection. Any inconsistencies were discussed until consensus was reached.

Frameworks

The updated ASCO–Value Framework (ASCO-VF) and ESMO-MCBS both quantify gains in overall survival (OS) or its surrogates (e.g., disease-free survival [DFS]) (1, 2). In ASCO-VF, the hazard ratio (HR) is subtracted from one and the result is multiplied by 100 to derive a Clinical Benefit Score; in ESMO-MCBS, HRs, and/or survival gains are linked to a particular grade in a pre-specified manner. For example, in the curative setting, a $>5\%$ improvement of OS at ≥ 3 years follow-up translates to a grade of A. Both scales use different forms for treatment in curative and palliative setting.

Toxicity and quality-of-life (QoL) data are used to adjust the scores or grades in both frameworks. For ASCO-VF, different points are assigned to every "clinically meaningful toxicity" based on its frequency and severity (e.g., 2.0 points for every grade 3 or 4 toxicity with a frequency $\geq 5\%$). The percentage difference in the sum of toxicity points between the two regimens is then multiplied by -20 to obtain a Toxicity Score. If the test regimen is more toxic than the comparator, the toxicity score is negative and vice versa. In the ESMO-MCBS, some prespecified severe toxicities are explicitly outlined and grades reduced by 1 level if

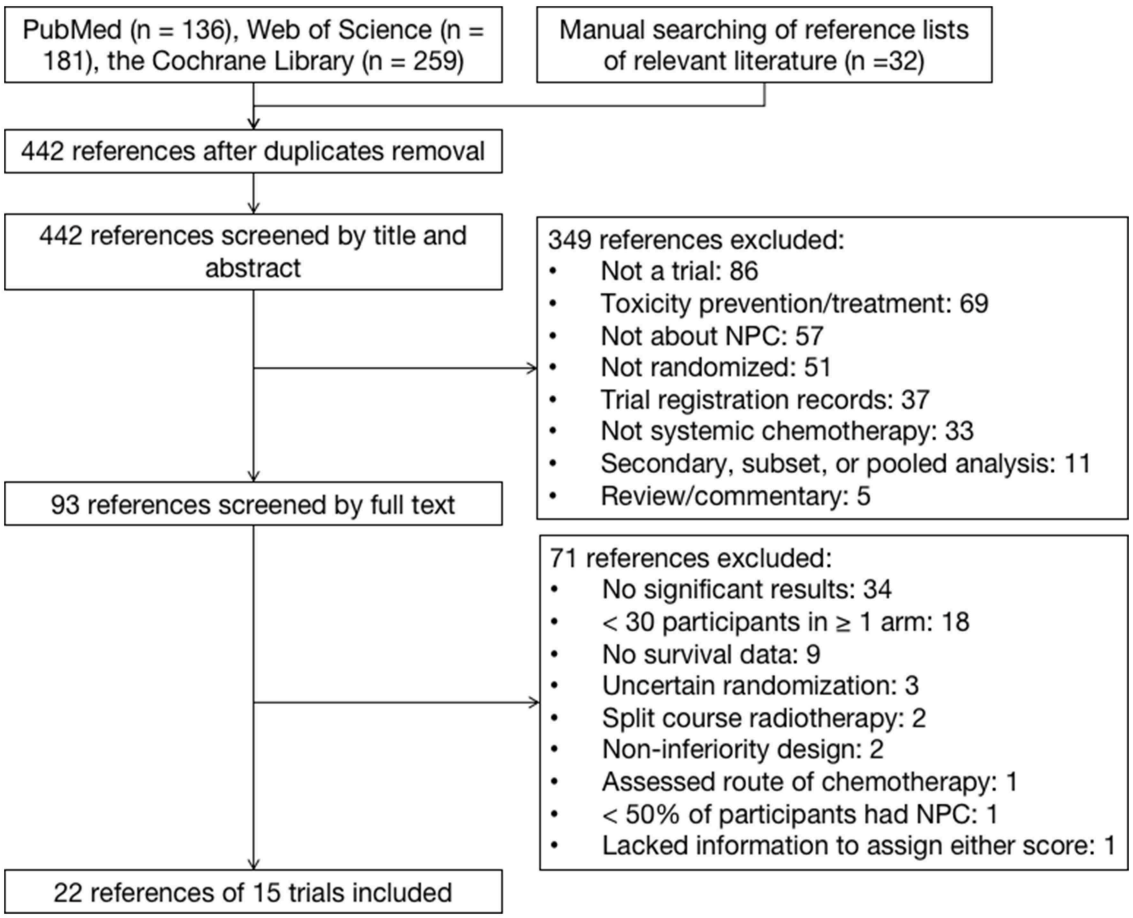

FIGURE 1 | Identification of trials on systemic chemotherapies in patients with nasopharyngeal carcinoma.

toxic effects meet any of these prespecifications (e.g., a statistically significant increase of toxic death rate >2%).

Both frameworks award bonus for a "tail of the survival curve effect." The ASCO-VF award 16–20 bonus points if there is a 50% or greater improvement in the proportion of patients alive with the test regimen at the time point on the survival curve that is 2 × the median survival of the comparator regimen. The ESMO-MCBS requires an upgrade of 1 level if there is a long-term plateau in the survival curve. Final ASCO-VF scores, termed Net Health Benefit, are the sum of Clinical Benefit Score, Toxicity Score and any bonus points (possible range −20 to more than 120 with bonus point allocation); ESMO-MCBS grades are ranked C, B, or A (for the curative setting), and 1, 2, 3, 4, or 5 (for the palliative setting). ESMO-MCBS defines "substantial clinical benefit" as a grade of 4, 5, B, or A whereas ASCO-VF includes no explicit definition.

Data Abstraction, Scoring, and Statistical Analysis

Firstly, two assessors (YZ, XL) independently scored the trials according to both frameworks. Secondly, the two assessors discussed the results and determined the final scores by consensus. Bias in trials was evaluated by one assessor (XL) using the Cochrane risk of bias assessment tool (9). Data were collected in an Excel file designed for this study. Descriptive statistics were used to summarize the scoring.

RESULTS

The electronic and manual search identified 195 references after the removal of duplicates. After screening, 22 references for 15 trials were eligible (**Figure 1**). Only one study was excluded because of insufficient information to assign a score for either framework. The median sample size of the 13 included trials was 284. Eleven trials investigated chemotherapy in the curative treatment of non-metastatic NPC, including four trials comparing concurrent chemoradiation (CCRT) plus adjuvant chemotherapy (AC) vs. RT alone, four trials comparing CCRT vs. RT alone, and five trials comparing induction chemotherapy (IC) plus CCRT vs. CCRT (**Table 1**). Two trials investigated palliative treatment of recurrent or metastatic NPC: one compared cisplatin and gemcitabine vs. cisplatin and fluorouracil and the other compared cisplatin and fluorouracil every 2 weeks vs. every 4 weeks (**Table 2**).

We found significant variation in the reporting of toxicities. Among the 13 trials, five different toxicity grading criteria were

TABLE 1 | Summary of trials in the curative treatment of non-metastatic, newly diagnosed nasopharyngeal carcinoma.

Study	No. of Pts	Stage	RT Technique	RT Dose (Gy)	Chemotherapy Regimen		
					Induction	Concurrent	Adjuvant
CCRT+AC vs. RT							
INT-0099 (10)	193	III–IV	2D	70	None	Cisplatin 100 D1 Q3W*3	Cisplatin 80 D1; 5FU 1,000 D1–4 Q4w*3
SQNP01 (11)	221	III–IV	2D	70	None	Cisplatin 25 D1–4 Q3W*3	Cisplatin 20 D1–4; 5FU 1,000 D1–4 Q4w*3
NPC-9901 (12–14)	348	Any T, N2–3	Mixed 2D and conformal	≥66	None	Cisplatin 100 D1 Q3W*3	Cisplatin 80 D1; 5FU 1,000 D1–4 Q4W*3
SYSUCC-02 (15, 16)	316	III–IV	2D	>66	None	Cisplatin 40 D1 QW during RT	Cisplatin 80 D1; 5FU 800 D1–5 Q4W*3
CCRT vs. RT							
TVGH-93 (17)	284	III–IV	2D	70–74	None	Cisplatin 20 D1–4; 5FU 400 D1–4 Q4W*2	None
PWHQEH-94 (18, 19)	350	II–IV	2D	66	None	Cisplatin 40 QW*8	None
SYSUCC-01 (20, 21)	115	III–IV	2D	70–74	None	Oxaliplatin 70 D1 QW*6	None
SYSUCC-03 (22)	230	II–III	2D	68–70	None	Cisplatin 30 QW during RT	None
IC+CCRT vs. CCRT							
NPC-008 (23)	65	III–IVB	Mixed 2D and IMRT	66	Docetaxel 75 D1; Cisplatin 75 D1 Q3w*2	Cisplatin 40 QW during RT	None
GORTEC 2006-02 (24)	83	T2b-4 and/or N1–N3	Mixed IMRT and non-IMRT (not specified)	70	Docetaxel 75 D1; Cisplatin 75 D1; 5FU 750 D1–5 Q3w*3	Cisplatin 40 QW during RT	None
SYSUCC-PF (25, 26)	476	III-IVB (excluding T3N0–1)	Mixed 2D and IMRT		Cisplatin 80 D1; 5FU 800 D1–5 Q3W*2	Cisplatin 80 D1 Q3W*3	None
SYSUCC-TPF (27, 28)	480	III-IVB (excluding T3–4N0)	IMRT	70	Docetaxel 60 D1; Cisplatin 60 D1; 5FU 600 D1–5 Q3w*3	Cisplatin 100 D1 Q3W*3	None
SYSUCC-GP IC (29)	480	III-IVB (excluding T3–4N0)	IMRT	70	Gemcitabine 1g D1,8; Cisplatin 80mg D1 Q3w*3	Cisplatin 100 D1 Q3W*3	None

AC, adjuvant chemotherapy; CCRT, concurrent chemoradiotherapy; IC, induction chemotherapy; IMRT, intensity-modulated radiation therapy; INT-0099, Southwest Oncology Group-coordinated Intergroup trial; No., number; NPC, nasopharyngeal carcinoma; Pts, patients; PWHQEH, Prince of Wales Hospital, Queen Elizabeth Hospital; RT, radiotherapy; SQNP, Singapore Naso-Pharynx; SYSUCC, Sun Yat-sen University Cancer Center; 2D, 2-dimension conventional radiotherapy; TVGH, Taichung Veterans General Hospital, Taiwan.

used, including criteria developed by the Southwest Oncology Group, the World Health Organization, and the Radiation Therapy Oncology Group, and the National Cancer Institute Common Terminology Criteria for Adverse Events. Ten (66.7%) studies did not report grade 1–2 toxicities and eight (53.3%) did not report late toxicities. The number of acute toxicities reported was strikingly different (17 vs. 8) in two trials using the same regimen (10, 11). Moreover, no trial reported QoL data.

Scoring With the ESMO-MCBS and ASCO-VF

All 15 trials were assessable with the ESMO-MCBS. Among 13 trials in the curative setting, 12 (92.3%) trials were graded at the highest ESMO grade of A and one trial was grade B. Both trials in the palliative setting were graded at ESMO grade 4. Thus, all trials met the ESMO threshold for substantial benefit.

Fourteen of 15 trials were assessable using the ASCO-VF. One trial comparing CCRT vs. RT did not provide HR for

TABLE 2 | Summary of trials in the treatment of recurrent or metastatic nasopharyngeal carcinoma.

Study	No. of patients	Eligible patients	Experimental arm	Control arm
SYSUCC-GP (30)	362	Recurrent or metastatic	Cisplatin + gemcitabine	Cisplatin + fluorouracil
Guangxi-10 (31)	103	Metastatic	Cisplatin + fluorouracil, every 2 weeks[a]	Cisplatin + fluorouracil, every 4 weeks[a]

GP, cisplatin and gemcitabine; SYSUCC, Sun Yat-sen University Cancer Center.
[a]After chemotherapy, residual lesions were treated with additional radiotherapy.

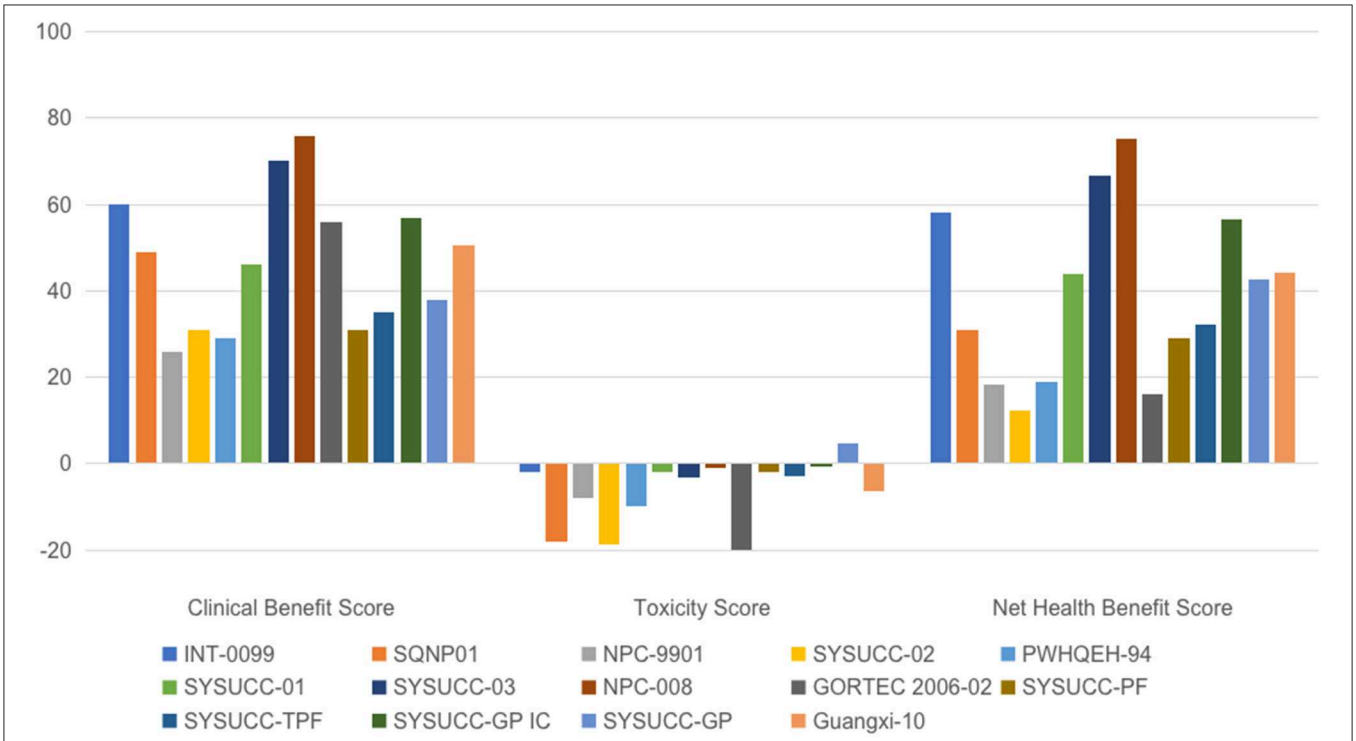

FIGURE 2 | Scoring of trials evaluating chemotherapy in nasopharyngeal carcinoma using the ASCO value framework. ASCO, American Society of Clinical Oncology; GP, cisplatin, and gemcitabine; INT-0099, Southwest Oncology Group-coordinated Intergroup trial; NPC, nasopharyngeal carcinoma; PF, cisplatin, and fluorouracil; PWHQEH, Prince of Wales Hospital, Queen Elizabeth Hospital; SQNP, Singapore Naso-Pharynx; SYSUCC, Sun Yat-sen University Cancer Center, China; TPF, docetaxel, cisplatin, and fluorouracil.

survival, meaning it could not be evaluated using the ASCO-VF (17). Another trial comparing IC plus CCRT vs. CCRT reported a statistically significant improvement in the primary endpoint of DFS (HR = 0.44; 95% CI: 0.20–0.97, $p = 0.042$). However, there was no significant difference in OS (HR = 0.40; 95% CI: 0.15–1.04, $p = 0.059$) with a median follow-up of 43.1 months. Because the OS data was not mature, the trial was evaluated on the basis of DFS results after discussion between the two assessors. As shown in **Figure 2**, significant variations in ASCO Clinical Benefit Score (mean: 46.8; standard deviation [SD]: 15.8), Toxicity Score (mean: 7.8; SD: 11.3), and Net Health Benefit Score (mean: 38.9; SD: 20.0) between trials were noticed.

DISCUSSION

To the best of our knowledge, this study is the first to test the ESMO and ASCO frameworks in trials evaluating chemotherapy in NPC. We found significant variation in the reporting of toxicities, including different grading criteria and deficiencies in the reporting of grade 1–2 and long-term toxicities. These results are consistent with previous evidence suggesting that the reporting of toxicity data from RCTs needs improvement (32). The underreporting and inconsistent reporting of toxicities would significantly impair the assessment of value using any framework in any possible settings, not only in NPC. Compliance with established guidance on toxicity reporting and

TABLE 3 | Comparison of toxicity assessment using the current ASCO value framework and a proposed continuous system[a].

	Radiotherapy alone arm ($n = 176$)		Concurrent chemoradiotherapy arm ($n = 174$)	
Stomatitis	**Grade 3**	**Grade 4**	**Grade 3**	**Grade 4**
Incidence (%)	34.7	1.1	44.3	4.6
Current ASCO framework				
Toxicity points	2		2	
Percentage difference	0			
Toxicity score[b]	0			
A proposed continuous system				
Toxicity points	$3 \times 0.347 = 1.041$	$4 \times 0.011 = 0.044$	$3 \times 0.443 = 1.329$	$3 \times 0.046 = 0.138$
Sum	1.085		1.467	
Percentage difference	1.467/1.085 – 1 = 0.352			
Toxicity score[b]	$0.352 \times 20 = 7.04$			

ASCO, American Society of Clinical Oncology.

[a] *Based on data in the PWHQEH-94 trial comparing concurrent chemoradiotherapy vs. radiotherapy alone (18).*

[b] *toxicity score = 20×the percentage difference in toxicity points between the two regimens, according to the ASCO value framework.*

sharing of clinical trial data may help mitigate this problem (33, 34). Moreover, subjective toxicities are at high risk of underreporting by physicians, even when prospectively collected within randomized trials (35). This strongly supports the need for incorporation of patient-reported outcomes and QoL data into toxicity reporting in clinical trials (36).

Our two assessors had a perfect agreement in the ESMO-MCBS analysis except in the assessment of one trial in the palliative setting (30). The ESMO-MCBS requires upgrading one level if the new treatment is associated with "statistically significantly less grade 3–4 toxicities impacting on daily well-being" compared with the standard therapy in the non-curative setting. In the trial comparing cisplatin and gemcitabine vs. cisplatin and fluorouracil in recurrent or metastatic NPC (SYSUCC-GP), the overall incidences of grade 3–4 toxicities were not significantly different between the two arms (43.3 vs. 35.8%, $p = 0.18$), while the experimental arm had significantly fewer grade 3–4 mucosal inflammation (0 vs. 14.5%, $p < 0.001$) (30). Our two assessors differed on whether this met the criteria for upgrade. After discussion, they decided that no upgrade should be done. More detailed guidance on this criterion might help avoid discrepancy in the future.

For the ASCO framework, however, wide variation in the initial independent analysis occurred between the two assessors, mainly due to the different interpretation of "clinically meaningful toxicity." The ASCO-VF defined "clinically meaningful toxicities" as toxicities other than laboratory abnormality only, which might be ambiguous and prone to different interpretations. For example, grade 1–2 hyponatremia may be symptomless while grade 3–4 hyponatremia might cause symptoms like fatigue. A clearer definition would facilitate more consistent scoring, which was also suggested by de Hosson et al. (6).

Our results demonstrated good applicability of both frameworks. Trials included in this study achieved highly consistent grades using the ESMO-MCBS. The ASCO-VF, however, gave very inconsistent and disparate scoring. For example, in the curative setting, all except one trial met the ESMO criteria for the highest level of benefit (grade A), while significant variations were found in the ASCO-VF scoring of Clinical Benefit, Toxicity as well as the final Net Health Benefit.

An important difference between these two frameworks is that the ESMO-MCBS places increasing weights on the toxicity profile as the treatment effects moves from curative to increasing palliative settings, while the calculation of toxicity score in the ASCO-VF is the same regardless of curative or palliative setting. For example, in the curative setting, for a new treatment regimen that improved the OS by >5%, the ESMO-MCBS would score a grade of A regardless of toxicity, while the ASCO-VF would take toxicity into consideration. In theory, the ASCO approach might be more reasonable. However, this is also part of the reason why the ASCO-VF score has significant variations. Conversely, unlike the ESMO-MCBS, the ASCO-VF didn't mention grade 5 toxicity (treatment-related death), which we believe is of vital importance in assessing toxicities.

For ASCO-VF, each toxicity is assigned a score between 0.5 and 2.0, based on grade and frequency. However, these points are arbitrary, not intuitive, and this may have obscured the actual differences in toxicity. For example, in the PWHQEH-94 trial comparing CCRT vs. RT alone, grade 3–4 stomatitis was observed in 48.9 and 35.8% of patients in the CCRT and RT-only groups, respectively, with a significant difference of 13.1% ($p = 0.002$) (18). However, when grading using the ASCO criteria, both groups scored two points, despite the apparent clinically relevant difference. In the original ASCO framework, the HR for survival was also assigned a score of 1–5 on the basis of the magnitude of difference (e.g., 5 for an HR < 0.2). While in the revised framework, a continuous scoring system is used to avoid arbitrary cut-offs (1). In the same vein, a continuous scoring system for toxicity might more accurately reflect the absolute difference in toxicity, as shown in **Table 3**. Such calculations could be easily performed once the framework is converted to a software application, as planned by ASCO (1).

The study had some limitations. Firstly, only trials reporting significant results favoring the experimental arm were assessable using the frameworks. However, our study was a field test

of ESMO and ASCO frameworks in systemic chemotherapy of NPC and not aimed at determining the value of different treatment options. A balanced value assessment requires the consideration of all relevant studies, whether they report significant findings or not, which was beyond the scope of this study. Secondly, our research was limited to RCTs investigating systemic chemotherapy in NPC; the applicability of value frameworks in other treatments or other diseases might be different. Nevertheless, there is a strong probability that similar situations apply to other settings. Thirdly, no trials included in the current study reported QoL data. It was not clear how such data will impact value assessments. Finally, only 6 of 13 trials in the curative setting used intensity-modulated radiotherapy, which has become the standard of care in NPC (37).

In conclusion, significant variations regarding toxicity reporting were found in trials evaluating chemotherapy in NPC. Both frameworks could be applied to the systemic chemotherapy of NPC. However, there is concern that the ASCO-VF generated highly inconsistent scoring for treatments that met the ESMO criteria for high level of benefit. The successful future application of value frameworks requires consistent reporting of toxicities as well as iterative refining and intergroup alignment of different frameworks.

DATA AVAILABILITY STATEMENT

The raw data supporting the conclusions of this article will be made available by the authors, without undue reservation.

AUTHOR CONTRIBUTIONS

Study design: YZ and JM. Data collection: YZ, XL, and Y-QL. Revision of the manuscript, data analysis, and interpretation: All authors. Writing of the manuscript: YZ. Statistical analysis: YZ, XL, and Y-QL.

FUNDING

This work was supported by the Guangdong Medical Science and Technology Research Fund [grant number A2017005]; the Natural Science Foundation of Guang Dong Province [grant number 2017A030312003]; and the Health and Medical Collaborative Innovation Project of Guangzhou City, China [grant number 201803040003]. The funders of the study had no role in study design, data collection, data analysis, data interpretation, or writing of this report.

ACKNOWLEDGMENTS

We thank Prof. Nathan I Cherny (the ESMO-MCBS Task Force, and Cancer Pain and Palliative Medicine Service, Department of Medical Oncology, Shaare Zedek Medical Center, Jerusalem, Israel) for reading earlier drafts of the manuscript and offered valuable editorial suggestions. We thank editors and the reviewers for their insightful comments and great help to improve this work.

REFERENCES

1. Schnipper LE, Davidson NE, Wollins DS, Blayney DW, Dicker AP, Ganz PA, et al. Updating the American Society of Clinical Oncology value framework: revisions and reflections in response to comments received. *J Clin Oncol.* (2016) 34:2925–34. doi: 10.1200/JCO.2016.68.2518
2. Cherny NI, Dafni U, Bogaerts J, Latino NJ, Pentheroudakis G, Douillard JY, et al. ESMO-Magnitude of Clinical Benefit Scale version 1.1. *Ann Oncol.* (2017) 28:2340–66. doi: 10.1093/annonc/mdx310
3. Torre LA, Bray F, Siegel RL, Ferlay J, Lortet-Tieulent J, Jemal A. Global cancer statistics, 2012. *CA Cancer J Clin.* (2015) 65:87–108. doi: 10.3322/caac.21262
4. Ribassin-Majed L, Marguet S, Lee AWM, Ng WT, Ma J, Chan ATC, et al. What is the best treatment of locally advanced nasopharyngeal carcinoma? An individual patient data network meta-analysis. *J Clin Oncol.* (2017) 35:498–505. doi: 10.1200/JCO.2016.67.4119
5. Del Paggio JC, Sullivan R, Schrag D, Hopman WM, Azariah B, Pramesh CS, et al. Delivery of meaningful cancer care: a retrospective cohort study assessing cost and benefit with the ASCO and ESMO frameworks. *Lancet Oncol.* (2017) 18:887–94. doi: 10.1016/S1470-2045(17)30415-1
6. de Hosson LD, Veenendaal LMV, Schuller Y, Zandee WT, de Herder WW, Tesselaar MET, et al. Clinical benefit of systemic treatment in patients with advanced pancreatic and gastrointestinal neuroendocrine tumours according to ESMO-MCBS and ASCO framework. *Ann Oncol.* (2017) 28:3022–7. doi: 10.1093/annonc/mdx547
7. Tibau A, Molto C, Ocana A, Templeton AJ, Del Carpio LP, Del Paggio JC, et al. Magnitude of clinical benefit of cancer drugs approved by the US Food and Drug Administration. *J Natl Cancer Inst.* (2018) 110:486–92. doi: 10.1093/jnci/djx232
8. Vivot A, Jacot J, Zeitoun JD, Ravaud P, Crequit P, Porcher R. Clinical benefit, price and approval characteristics of FDA-approved new drugs for treating advanced solid cancer, 2000-2015. *Ann Oncol.* (2017) 28:1111–6. doi: 10.1093/annonc/mdx053
9. Higgins JP, Altman DG, Gotzsche PC, Juni P, Moher D, Oxman AD, et al. The Cochrane Collaboration's tool for assessing risk of bias in randomised trials. *BMJ.* (2011) 343:d5928. doi: 10.1136/bmj.d5928
10. Al-Sarraf M, LeBlanc M, Giri PG, Fu KK, Cooper J, Vuong T, et al. Chemoradiotherapy versus radiotherapy in patients with advanced nasopharyngeal cancer: phase III randomized Intergroup study 0099. *J Clin Oncol.* (1998) 16:1310–7. doi: 10.1200/JCO.1998.16.4.1310
11. Wee J, Tan EH, Tai BC, Wong HB, Leong SS, Tan T, et al. Randomized trial of radiotherapy versus concurrent chemoradiotherapy followed by adjuvant chemotherapy in patients with American Joint Committee on Cancer/International Union against cancer stage III and IV nasopharyngeal cancer of the endemic variety. *J Clin Oncol.* (2005) 23:6730–8. doi: 10.1200/JCO.2005.16.790
12. Lee AW, Lau WH, Tung SY, Chua DT, Chappell R, Xu L, et al. Preliminary results of a randomized study on therapeutic gain by concurrent chemotherapy for regionally-advanced nasopharyngeal carcinoma: NPC-9901 Trial by the Hong Kong Nasopharyngeal Cancer Study Group. *J Clin Oncol.* (2005) 23:6966–75. doi: 10.1200/JCO.2004.00.7542
13. Lee AW, Tung SY, Chua DT, Ngan RK, Chappell R, Tung R, et al. Randomized trial of radiotherapy plus concurrent-adjuvant chemotherapy vs radiotherapy alone for regionally advanced nasopharyngeal carcinoma. *J Natl Cancer Inst.* (2010) 102:1188–98. doi: 10.1093/jnci/djq287
14. Lee AWM, Tung SY, Ng WT, Lee V, Ngan RKC, Choi HCW, et al. A multicenter, phase 3, randomized trial of concurrent chemoradiotherapy plus adjuvant chemotherapy versus radiotherapy alone in patients with regionally advanced nasopharyngeal carcinoma: 10-year outcomes for efficacy and toxicity. *Cancer.* (2017) 123:4147–57. doi: 10.1002/cncr.30850

15. Chen Y, Liu MZ, Liang SB, Zong JF, Mao YP, Tang LL, et al. Preliminary results of a prospective randomized trial comparing concurrent chemoradiotherapy plus adjuvant chemotherapy with radiotherapy alone in patients with locoregionally advanced nasopharyngeal carcinoma in endemic regions of china. *Int J Radiat Oncol Biol Phys.* (2008) 71:1356–64. doi: 10.1016/j.ijrobp.2007.12.028
16. Chen Y, Sun Y, Liang SB, Zong JF, Li WF, Chen M, et al. Progress report of a randomized trial comparing long-term survival and late toxicity of concurrent chemoradiotherapy with adjuvant chemotherapy versus radiotherapy alone in patients with stage III to IVB nasopharyngeal carcinoma from endemic regions of China. *Cancer.* (2013) 119:2230–8. doi: 10.1002/cncr.28049
17. Lin JC, Jan JS, Hsu CY, Liang WM, Jiang RS, Wang WY. Phase III study of concurrent chemoradiotherapy versus radiotherapy alone for advanced nasopharyngeal carcinoma: positive effect on overall and progression-free survival. *J Clin Oncol.* (2003) 21:631–7. doi: 10.1200/JCO.2003.06.158
18. Chan AT, Teo PM, Ngan RK, Leung TW, Lau WH, Zee B, et al. Concurrent chemotherapy-radiotherapy compared with radiotherapy alone in locoregionally advanced nasopharyngeal carcinoma: progression-free survival analysis of a phase III randomized trial. *J Clin Oncol.* (2002) 20:2038–44. doi: 10.1200/JCO.2002.08.149
19. Chan AT, Leung SF, Ngan RK, Teo PM, Lau WH, Kwan WH, et al. Overall survival after concurrent cisplatin-radiotherapy compared with radiotherapy alone in locoregionally advanced nasopharyngeal carcinoma. *J Natl Cancer Inst.* (2005) 97:536–9. doi: 10.1093/jnci/dji084
20. Wu X, Huang PY, Peng PJ, Lu LX, Han F, Wu SX, et al. Long-term follow-up of a phase III study comparing radiotherapy with or without weekly oxaliplatin for locoregionally advanced nasopharyngeal carcinoma. *Ann Oncol.* (2013) 24:2131–6. doi: 10.1093/annonc/mdt163
21. Zhang L, Zhao C, Peng PJ, Lu LX, Huang PY, Han F, et al. Phase III study comparing standard radiotherapy with or without weekly oxaliplatin in treatment of locoregionally advanced nasopharyngeal carcinoma: preliminary results. *J Clin Oncol.* (2005) 23:8461–8. doi: 10.1200/JCO.2004.00.3863
22. Chen QY, Wen YF, Guo L, Liu H, Huang PY, Mo HY, et al. Concurrent chemoradiotherapy vs radiotherapy alone in stage II nasopharyngeal carcinoma: phase III randomized trial. *J Natl Cancer Inst.* (2011) 103:1761–70. doi: 10.1093/jnci/djr432
23. Hui EP, Ma BB, Leung SF, King AD, Mo F, Kam MK, et al. Randomized phase II trial of concurrent cisplatin-radiotherapy with or without neoadjuvant docetaxel and cisplatin in advanced nasopharyngeal carcinoma. *J Clin Oncol.* (2009) 27:242–9. doi: 10.1200/JCO.2008.18.1545
24. Frikha M, Auperin A, Tao Y, Elloumi F, Toumi N, Blanchard P, et al. A randomized trial of induction docetaxel-cisplatin-5FU followed by concomitant cisplatin-RT versus concomitant cisplatin-RT in nasopharyngeal carcinoma (GORTEC 2006-02). *Ann Oncol.* (2018) 29:731–6. doi: 10.1093/annonc/mdx770
25. Cao SM, Yang Q, Guo L, Mai HQ, Mo HY, Cao KJ, et al. Neoadjuvant chemotherapy followed by concurrent chemoradiotherapy versus concurrent chemoradiotherapy alone in locoregionally advanced nasopharyngeal carcinoma: a phase III multicentre randomised controlled trial. *Eur J Cancer.* (2017) 75:14–23. doi: 10.1016/j.ejca.2016.12.039
26. Yang Q, Cao SM, Guo L, Hua YJ, Huang PY, Zhang XL, et al. Induction chemotherapy followed by concurrent chemoradiotherapy versus concurrent chemoradiotherapy alone in locoregionally advanced nasopharyngeal carcinoma: long-term results of a phase III multicentre randomised controlled trial. *Eur J Cancer.* (2019) 119:87–96. doi: 10.1016/j.ejca.2019.07.007
27. Sun Y, Li WF, Chen NY, Zhang N, Hu GQ, Xie FY, et al. Induction chemotherapy plus concurrent chemoradiotherapy versus concurrent chemoradiotherapy alone in locoregionally advanced nasopharyngeal carcinoma: a phase 3, multicentre, randomised controlled trial. *Lancet Oncol.* (2016) 17:1509–20. doi: 10.1016/S1470-2045(16)30410-7
28. Li WF, Chen NY, Zhang N, Hu GQ, Xie FY, Sun Y, et al. Concurrent chemoradiotherapy with/without induction chemotherapy in locoregionally advanced nasopharyngeal carcinoma: long-term results of phase 3 randomized controlled trial. *Int J Cancer.* (2019) 145:295–305. doi: 10.1002/ijc.32099
29. Zhang Y, Chen L, Hu GQ, Zhang N, Zhu XD, Yang KY, et al. Gemcitabine and cisplatin induction chemotherapy in nasopharyngeal carcinoma. *N Engl J Med.* (2019) 381:1124–35. doi: 10.1056/NEJMoa1905287
30. Zhang L, Huang Y, Hong S, Yang Y, Yu G, Jia J, et al. Gemcitabine plus cisplatin versus fluorouracil plus cisplatin in recurrent or metastatic nasopharyngeal carcinoma: a multicentre, randomised, open-label, phase 3 trial. *Lancet.* (2016) 388:1883–92. doi: 10.1016/S0140-6736(16)31388-5
31. Liang Y, Bu JG, Cheng JL, Gao WW, Xu YC, Feng J, et al. Selective radiotherapy after distant metastasis of nasopharyngeal carcinoma treated with dose-dense cisplatin plus fluorouracil. *Asian Pac J Cancer Prev.* (2015) 16:6011–7. doi: 10.7314/APJCP.2015.16.14.6011
32. Ioannidis JP, Lau J. Completeness of safety reporting in randomized trials: an evaluation of 7 medical areas. *JAMA.* (2001) 285:437–43. doi: 10.1001/jama.285.4.437
33. Ioannidis JP, Evans SJ, Gotzsche PC, O'Neill RT, Altman DG, Schulz K, et al. Better reporting of harms in randomized trials: an extension of the CONSORT statement. *Ann Intern Med.* (2004) 141:781–8. doi: 10.7326/0003-4819-141-10-200411160-00009
34. Taichman DB, Backus J, Baethge C, Bauchner H, de Leeuw PW, Drazen JM, et al. Sharing clinical trial data–a proposal from the international committee of medical journal editors. *N Engl J Med.* (2016) 374:384–6. doi: 10.1056/NEJMe1515172
35. Di Maio M, Gallo C, Leighl NB, Piccirillo MC, Daniele G, Nuzzo F, et al. Symptomatic toxicities experienced during anticancer treatment: agreement between patient and physician reporting in three randomized trials. *J Clin Oncol.* (2015) 33:910–5. doi: 10.1200/JCO.2014.57.9334
36. Jim HS, McLeod HL. American Society of Clinical Oncology value framework: importance of accurate toxicity data. *J Clin Oncol.* (2017) 35:1133–4. doi: 10.1200/JCO.2016.69.2079
37. Peng G, Wang T, Yang KY, Zhang S, Zhang T, Li Q, et al. A prospective, randomized study comparing outcomes and toxicities of intensity-modulated radiotherapy vs. conventional two-dimensional radiotherapy for the treatment of nasopharyngeal carcinoma. *Radiother Oncol.* (2012) 104:286–93. doi: 10.1016/j.radonc.2012.08.013

Conflict of Interest: The authors declare that the research was conducted in the absence of any commercial or financial relationships that could be construed as a potential conflict of interest.

frontiers in Oncology

ORIGINAL RESEARCH
published: 25 August 2020
doi: 10.3389/fonc.2020.01469

Clinical Characteristics and Prognostic Factors of Early and Late Recurrence After Definitive Radiotherapy for Nasopharyngeal Carcinoma

Feng Li[1,2,3,4], *Fo-Ping Chen*[1,2,3,4], *Yu-Pei Chen*[1,2,3,4], *Yue Chen*[1,2,3,4], *Xiao-Jun He*[1,2,3,4], *Xiao-Dan Huang*[1,2,3,4], *Zi-Qi Zheng*[1,2,3,4], *Wei-Hong Zheng*[1,2,3,4], *Xu Liu*[1,2,3,4], *Ying Sun*[1,2,3,4] *and Guan-Qun Zhou*[1,2,3,4]*

[1] Department of Radiation Oncology, Sun Yat-sen University Cancer Center, Guangzhou, China, [2] State Key Laboratory of Oncology in South China, Sun Yat-sen University Cancer Center, Guangzhou, China, [3] Collaborative Innovation Center of Cancer Medicine, Sun Yat-sen University Cancer Center, Guangzhou, China, [4] Guangdong Key Laboratory of Nasopharyngeal Carcinoma Diagnosis and Therapy, Sun Yat-sen University Cancer Center, Guangzhou, China

OPEN ACCESS

Edited by:
Raffaele Solla,
Institute of Biostructure and Bioimaging (IBB), Italian National Research Council, Italy

Reviewed by:
Cesare Piazza,
Istituto Nazionale dei Tumori (IRCCS), Italy
Xing Lv,
Sun Yat-sen University, China
Emma D'Ippolito,
Istituto Nazionale Tumori Fondazione G. Pascale (IRCCS), Italy

***Correspondence:**
Guan-Qun Zhou
zhougq@sysucc.org.cn

Specialty section:
This article was submitted to Head and Neck Cancer, a section of the journal Frontiers in Oncology

Received: 04 November 2019
Accepted: 10 July 2020
Published: 25 August 2020

Citation:
Li F, Chen F-P, Chen Y-P, Chen Y, He X-J, Huang X-D, Zheng Z-Q, Zheng W-H, Liu X, Sun Y and Zhou G-Q (2020) Clinical Characteristics and Prognostic Factors of Early and Late Recurrence After Definitive Radiotherapy for Nasopharyngeal Carcinoma. Front. Oncol. 10:1469. doi: 10.3389/fonc.2020.01469

We investigated the clinical characteristics, prognostic factors, and post-recurrence prognostic factors of early- and late-recurrence patients for nasopharyngeal carcinoma (NPC) after definitive intensity-modulated radiation therapy (IMRT). This was a single-center retrospective analysis of patients in China from January 2010 to December 2015. The prognostic factors for overall survival (OS) and post-recurrence OS of early- and late-recurrence patients were identified using univariate and multivariate Cox regression analyses. Of the 9,468 patients included, 409 (4.3%), 325 (3.4%), and 182(1.9%) developed purely local recurrence, purely regional recurrence, and locoregional recurrence during follow-up, respectively. In the purely local recurrence group, 192 patients (46.9%) developed early local recurrence (ETR), and 217 patients (53.1%) developed late local recurrence (LTR). Of the 192 ETR patients, multivariate Cox regression analysis revealed that age and gender were independent risk factors of OS, and post-recurrence best supportive treatment (PRBST) was associated with poorer post-recurrence OS. Of the 217 LTR patients, the results revealed that baseline value of EBV-DNA was an independent risk factor for OS, while PRBST was associated with poorer post-recurrence OS. In the purely regional recurrence group, 183 patients (56.3%) developed early regional recurrence (ENR), and 142 patients (43.7%) developed late regional recurrence (LNR). Of the 183 ENR patients, multivariate Cox regression analysis revealed that alcohol abuse and TNM stage were independent risk factors of OS, while alcohol drinkers and PRBST were associated with poorer post-recurrence OS. Of the 142 LNR patients, PRBST was associated with poorer post-recurrence OS. In the locoregional recurrence group, 87 patients (47.8%) developed early locoregional recurrence (ELR), and 95 patients (52.2%) developed late locoregional recurrence (LLR). Of the 87 ELR patients, multivariate Cox regression analysis revealed that N stage and

TNM stage were independent risk factors of OS, and N2/3 stage and PRBST were associated with poorer post-recurrence OS. Of the 95 LLR patients, the results revealed that T stage was an independent risk factor for OS, while T3/4 stage and PRBST were associated with poorer post-recurrence OS. Patients with LTR/LNR/LLR demonstrate significantly better OS compared with patients with ETR/ENR/ELR, Nevertheless, post-recurrence OS between patients with ETR/ENR/ELR and LTR/LNR/LLR was not significantly different.

Keywords: nasopharyngeal carcinoma, radiotherapy, prognosis, early locoregional recurrence, late locoregional recurrence

INTRODUCTION

Nasopharyngeal carcinoma (NPC), a malignant tumor that originates in the nasopharyngeal epithelium, is endemic in Southern China, Southeast Asia, North Africa, the Middle East, and Alaska (1, 2). As a result of its complex anatomical location and high radiosensitivity, radiotherapy with or without chemotherapy is the primary treatment modality for NPC (3, 4), and the application of IMRT has greatly improved locoregional control in NPC (5). However, the long-term prognosis remains unsatisfactory, given the high rate of locoregional recurrence of up to 5–10% in patients after definitive IMRT (6). This study focuses on the failure patterns of NPC except distant metastasis, which was separated clearly in three subgroups: (1) purely local recurrence (on the T site only), (2) purely regional recurrence (on the N site only), (3) locoregional recurrence (on the T and N sites simultaneously). Meanwhile, time to cancer recurrence differs in such patients, and the three subgroups were divided into ETR and LTR, ENR and LNR, and ELR and LLR, respectively, based on the time to recurrence after radiotherapy (7–9). To the best of our knowledge, research focusing on early and late recurrence in NPC patients remains rare and limited. Accordingly, we aimed to identify the clinical characteristics and prognostic factors of ETR and LTR, ENR and LNR, and ELR and LLR in a large cohort of patients with NPC who underwent long-term follow-up, providing data to clinicians for planning surveillance strategies.

PATIENTS AND METHODS

Patient Selection

This study was performed according to the ethical principles of the Declaration of Helsinki, and the Sun Yat-sen University Cancer Center review board approved the study protocol. Written informed consent was obtained from all patients for their data to be used in clinical research without affecting their treatment options or violating their privacy. We retrospectively reviewed the records of all 9,468 patients with biopsy-proven NPC who had been treated with IMRT at our center between January 2010 and December 2015. All patients had completed a pretreatment evaluation including complete patient history, physical examination, hematology and biochemistry profiles, nasopharynx and neck magnetic resonance imaging (MRI), chest radiography, abdominal ultrasonography, and whole-body bone scan or positron emission tomography/computed tomography (PET/CT). All patients were restaged according to the 8th Union for International Cancer Control/American Joint Committee on Cancer staging system (10, 11). RT+Chemo was defined as treatment with both radiotherapy and chemotherapy, including induction chemotherapy and/or concurrent chemotherapy and/or adjuvant chemotherapy. Treatment options after recurrence were divided into four parts: salvage surgery, re-irradiation, chemotherapy, and best supportive treatment. During the study period, our institutional guidelines recommended no chemotherapy for stage I–IIA NPC, concurrent chemoradiation therapy for stage IIB NPC, and concurrent chemoradiation therapy with or without neoadjuvant/adjuvant chemotherapy for stage III to IVA–B NPC.

Follow-Up Schedule and Definition of ETR and LTR, ENR and LNR, and ELR and LLR

Patients attended follow-up visits every 3 months during the first 2 years, every 6 months during years 3–5, and annually thereafter or until death. Scheduled surveillance including fiberoptic endoscopy and head and neck CT/MRI scans was performed every 3 months during the first year and annually during years 2–5. Local recurrence was diagnosed by fiberoptic endoscopy and biopsy or nasopharynx and skull base CT/MRI scans. Regional recurrence was diagnosed by pathological examination with fine-needle aspiration or surgery or by radiology with neck CT/MRI scans. Additional tests were ordered whenever necessary. In this study, purely local recurrence was defined as recurrence on the T site only, which was divided into ETR and LTR according to time to NPC recurrence of $\leq$2 years and $>$2 years. Purely regional recurrence was defined as recurrence on the N site only, which was divided into ENR and LNR according to time to NPC recurrence of $\leq$2 years and $>$2 years, and locoregional recurrence was defined as recurrence on the T and N sites simultaneously, which was divided into ELR and LLR according to the time to NPC recurrence of $\leq$2 years and $>$2 years.

Abbreviations: NPC, nasopharyngeal carcinoma; IMRT, intensity-modulated radiation therapy; ETR, early purely local recurrence; LTR, late purely local recurrence; ENR, early purely regional recurrence; LNR, late purely regional recurrence; ELR, early locoregional recurrence; LLR, late locoregional recurrence; OS, overall survival; WHO, World Health Organization; TNM, tumor-node-metastasis; MRI, magnetic resonance imaging; PET/CT, positron-emission tomography/computed tomography; UICC/AJCC, Union for International Cancer Control/American Joint Committee on Cancer; EBV, Epstein-Barr virus; HR, hazard ratio; CI, Confidence interval; RT, radiotherapy; Chemo, chemotherapy; PRBST, Post-recurrence best supportive treatment.

TABLE 1 | Comparison of clinical characteristics of ETR and LTR patients in the purely local recurrence group.

Characteristic	Total (n = 409)%	ETR group (n = 192)%	LTR group (n = 217)%	*P*-value
Age (years)				0.203
≤46 years	199 (48.7)	87 (45.3)	112 (51.6)	
>46 years	210 (51.3)	105 (54.7)	105 (48.4)	
Gender				0.282
Male	303 (74.1)	147 (76.6)	156 (71.9)	
Female	106 (25.9)	45 (23.4)	61 (28.1)	
Smoking status				0.535
Non-smoker	243 (59.4)	111 (57.8)	132 (60.8)	
Smoker	166 (40.6)	81 (42.2)	85 (39.2)	
Alcohol abuse				0.804
Non-drinker	368 (90.0)	172 (89.6)	196 (90.3)	
Drinker	41 (10.0)	20 (10.4)	21 (9.7)	
Tumor family history				0.410
No	308 (75.3)	141 (73.4)	167 (77.0)	
Yes	101 (24.7)	51 (26.6)	50 (23.0)	
Cranial nerve symptom				0.741
N0	356 (87.0)	166 (86.5)	190 (87.6)	
Yes	53 (13.0)	26 (13.5)	27 (12.4)	
Baseline value of EBV-DNA				0.212
≤2,000	189 (46.2)	95 (49.5)	94 (43.3)	
>2,000	220 (53.8)	97 (50.5)	123 (56.7)	
Histological type				0.218
WHO I/II	18 (4.4)	11 (5.7)	7 (3.2)	
WHO III	391 (95.6)	181 (94.3)	210 (96.8)	
T stage				0.084
1/2	60 (14.7)	22 (11.5)	38 (17.5)	
3/4	349 (85.3)	170 (88.5)	179 (82.5)	
N stage				0.258
0/1	274 (67.0)	134 (69.8)	140 (64.5)	
2/3	135 (33.0)	58 (30.2)	77 (35.5)	
TNM stage				0.416
I/II	46 (11.2)	19 (9.9)	27 (12.4)	
III/IV	363 (88.8)	173 (90.1)	190 (87.6)	
Induction chemotherapy				0.927
No	195 (47.7)	92 (47.9)	103 (47.5)	
Yes	214 (52.3)	100 (52.1)	252 (52.5)	
Concurrent chemotherapy				0.171
No	86 (21.0)	46 (24.0)	40 (18.4)	
Yes	323 (79.0)	146 (76.0)	17781.6)	
Adjuvant chemotherapy				0.404
No	388 (94.9)	184 (95.8)	204 (94.0)	
Yes	21 (5.1)	8 (4.2)	13 (6.0)	
Post-recurrence treatment options				0.073
BST	47 (11.5)	26 (13.5)	21 (9.7)	
Salvage surgery	19 (4.7)	8 (4.2)	11 (5.1)	
Re-irradiation	203 (49.6)	83 (43.2)	120 (55.3)	
Chemotherapy	140 (34.2)	75 (39.1)	65 (29.9)	

TABLE 2 | Comparison of clinical characteristics of ENR and LNR patients in the purely regional recurrence group.

Characteristic	Total (n = 325)%	ENR group (n = 183)%	LNR group (n = 142)%	*P*-value
Age (years)				0.094
≤46 years	175 (53.8)	106 (57.9)	69 (48.6)	
>46 years	150 (46.2)	77 (42.1)	73 (51.4)	
Gender				0.567
Male	261 (80.3)	149 (81.4)	112 (78.9)	
Female	64 (19.7)	34 (18.6)	30 (21.1)	
Smoking status				0.165
Non-smoker	192 (59.1)	102 (55.7)	90 (63.4)	
Smoker	133 (40.9)	81 (44.3)	52 (36.6)	
Alcohol abuse				0.420
Non-drinker	266 (81.8)	147 (80.3)	119 (83.8)	
Drinker	59 (18.2)	36 (19.7)	23 (16.2)	
Tumor family history				0.796
No	229 (70.5)	130 (71.0)	99 (69.7)	
Yes	96 (29.5)	53 (29.0)	43 (30.3)	
Cranial nerve symptom				0.936
N0	304 (93.5)	171 (93.4)	133 (93.7)	
Yes	21 (6.5)	12 (6.6)	9 (6.3)	
Baseline value of EBV-DNA				0.009
≤2,000	84 (25.8)	37 (20.2)	47 (33.1)	
>2,000	241 (74.2)	146 (79.8)	95 (66.9)	
Histological type				0.183
WHO I/II	12 (3.7)	9 (4.9)	3 (2.1)	
WHO III	313 (96.3)	174 (95.1)	139 (97.9)	
T stage				0.337
1/2	117 (36.0)	70 (38.3)	47 (33.1)	
3/4	208 (64.0)	113 (61.7)	95 (66.9)	
N stage				0.157
0/1	139 (42.8)	72 (39.3)	67 (47.2)	
2/3	186 (57.2)	111 (60.7)	75 (52.8)	
TNM stage				0.606
I/II	59 (18.2)	35 (19.1)	24 (16.9)	
III/IV	266 (81.8)	148 (80.9)	118 (83.1)	
Induction chemotherapy				0.077
No	111 (34.2)	55 (30.1)	56 (39.4)	
Yes	214 (65.8)	128 (69.9)	86 (60.6)	
Concurrent chemotherapy				0.625
No	47 (14.5)	28 (15.3)	19 (13.4)	
Yes	278 (85.5)	155 (84.7)	123 (86.6)	
Adjuvant chemotherapy				0.113
No	295 (90.8)	162 (88.5)	133 (93.7)	
Yes	30 (9.2)	21 (11.5)	9 (6.3)	
Post-recurrence treatment options				0.689
BST	17 (5.2)	9 (4.9)	8 (5.6)	
Salvage surgery	162 (49.9)	94 (51.4)	68 (47.9)	
Re-irradiation	64 (19.7)	32 (17.5)	32 (22.5)	
Chemotherapy	82 (25.2)	48 (26.2)	34 (24.0)	

TABLE 3 | Comparison of clinical characteristics of ELR and LLR patients in the locoregional recurrence group.

Characteristic	Total ($n = 182$)%	ELR group ($n = 87$)%	LLR group ($n = 95$)%	*P*-value
Age (years)				0.088
≤46 years	101 (55.5)	54 (62.1)	47 (49.5)	
>46 years	81 (44.5)	33 (37.9)	48 (50.5)	
Gender				0.162
Male	138 (75.8)	70 (80.5)	68 (71.6)	
Female	44 (24.2)	17 (19.5)	27 (28.4)	
Smoking status				0.870
Non-smoker	112 (61.5)	53 (60.9)	59 (62.1)	
Smoker	70 (38.5)	34 (39.1)	36 (37.9)	
Alcohol abuse				0.569
Non-drinker	154 (84.6)	75 (86.2)	79 (83.2)	
Drinker	28 (15.4)	12 (13.8)	16 (16.8)	
Tumor family history				0.603
No	137 (75.3)	67 (77.0)	70 (73.7)	
Yes	45 (24.7)	20 (23.0)	25 (26.3)	
Cranial nerve symptom				0.427
N0	172 (94.5)	81 (93.1)	91 (95.8)	
Yes	10 (5.5)	6 (6.9)	4 (4.2)	
Baseline value of EBV-DNA				0.728
≤2,000	63 (34.6)	29 (33.3)	34 (35.8)	
>2,000	119 (65.4)	58 (66.7)	61 (64.2)	
Histological type				0.246
WHO I/II	10 (5.5)	3 (3.4)	7 (7.4)	
WHO III	172 (94.5)	84 (96.6)	88 (92.6)	
T stage				0.552
1/2	39 (21.4)	17 (19.5)	22 (23.2)	
3/4	143 (78.6)	70 (80.5)	73 (76.8)	
N stage				0.316
0/1	97 (53.3)	43 (49.4)	54 (56.8)	
2/3	85 (46.7)	44 (50.6)	41 (43.2)	
TNM stage				0.826
I/II	22 (12.1)	11 (12.6)	11 (11.6)	
III/IV	160 (87.9)	76 (87.4)	84 (88.4)	
Induction chemotherapy				0.399
No	77 (42.3)	34 (39.1)	43 (45.3)	
Yes	105 (57.7)	53 (60.9)	52 (54.7)	
Concurrent chemotherapy				0.203
No	29 (15.9)	17 (19.5)	12 (12.6)	
Yes	153 (84.1)	70 (80.5)	83 (87.4)	
Adjuvant chemotherapy				0.065
No	173 (95.1)	80 (92.0)	93 (97.9)	
Yes	9 (4.9)	7 (8.0)	2 (2.1)	
Post-recurrence treatment options				0.415
BST	9 (4.9)	5 (5.7)	4 (4.2)	
Salvage surgery	43 (23.6)	22 (25.3)	21 (22.1)	
Re-irradiation	70 (38.5)	28 (32.2)	42 (44.2)	
Chemotherapy	60 (33.0)	32 (36.8)	28 (29.5)	

Statistical Analysis

The patients' clinical and pathological characteristics were summarized using frequencies and percentages for categorical covariates and medians and ranges for continuous covariates. The clinicopathological characteristics and treatment modalities among the patients with ETR and LTR, ENR and LNR, and ELR and LLR were compared using the chi-square test. The OS and post-recurrence OS were calculated with the Kaplan–Meier method, and differences between survival curves were assessed with the log-rank test. The prognostic factors of OS and post-recurrence OS of the patients with ETR and LTR, ENR and LNR, and ELR and LLR were evaluated using multivariate Cox regression analysis. $P < 0.05$ was considered significant. Statistical analyses were performed using SPSS version 23.0 (IBM).

RESULTS

Comparison of Clinical Characteristics Between Patients With ETR and LTR, ENR and LNR, and ELR and LLR

Of the 9,468 patients included, 409 (4.3%) developed purely local recurrence, 325 (3.4%) developed purely regional recurrence, and 182 (1.9%) developed locoregional recurrence. Among the 409 patients with purely local recurrence, in whom the median time to recurrence was 25.4 months (range, 3.7–86.3 months), 207 patients (50.6%) died, 303 patients (74.1%) were male, 106 patients (25.9%) were female, and the median age was 47.0 years. At a median follow-up of 44.5 months (range, 9.9–104.9 months), 192 patients (46.9%) developed ETR, with a median time to recurrence of 15.4 months (range, 3.7–24.0 months); 217 patients (53.1%) developed LTR, with a median time to recurrence of 36.7 months (range, 24.1–86.3 months). After recurrence, 47 patients (11.5%) received BST, 19 patents (4.7%) were undergoing salvage surgery, 203 patients (49.6%) received re-irradiation, and 140 patients (34.2%) received chemotherapy. Among the 325 patients with purely regional recurrence, 114 patients (35.1%) died, 261 patients (80.3%) were male, 64 patients (19.7%) were female, and the median age was 45.0 years. At a median follow-up of 49.3 months (range, 7.9–111.0 months), 183 patients (56.3%) developed ENR, with a median time to recurrence of 14.5 months (range, 1.8–23.9 months), and 142 patients (43.7%) developed LNR, with a median time to recurrence of 37.5 months (range, 24.4–80.1 months). Among the 182 patients with locoregional recurrence, 88 patients (48.4%) died, 138 patients (75.8%) were male, 44 patients (24.2%) were female, and the median age was 44.0 years. At a median follow-up of 49.9 months (range, 6.9–101.8 months), 87 patients (47.8%) developed ELR, with a median time to recurrence of 14.70 months (range, 4.90–23.63 months), and 95 patients (52.2%) developed LLR, with a median time to recurrence of 34.63 months (range, 24.07–94.13 months). **Tables 1**–**3** illustrate the comparisons of the baseline clinical characteristics between the patients with ETR and LTR, ENR and LNR, and ELR and LLR. The difference was significant in the baseline value of EBV-DNA between ENR and LNR groups ($P = 0.009$). No significant differences were found in the

TABLE 4 | Univariate and multivariate analysis of prognostic factors of ETR and LTR in the purely local recurrence group.

Characteristic	ETR group		LTR group	
	Univariate *P*-value HR (95% CI)	Multivariate *P*-value	Univariate *P*-value HR (95% CI)	Multivariate *P*-value
Age (years)	0.005	0.006	0.888	NS
≤46 years	Reference			
>46 years	1.645 (1.153–2.346)		/	
Gender	0.008	0.020	0.179	NS
Male	Reference			
Female	0.589 (0.377–0.920)		/	
Smoking status	0.293	NS	0.264	NS
Non-smoker				
Smoker	/		/	
Alcohol abuse	0.211	NS	0.043	NS
Non-drinker				
Drinker	/		/	
Tumor family history	0.883	NS	0.079	NS
No				
Yes	/		/	
Cranial nerve symptom	0.025	NS	0.836	NS
No				
Yes	/		/	
Baseline value of EBV-DNA	0.381	NS	0.015	0.017
≤2000			Reference	
>2000	/		1.817 (1.115–2.962)	
Histological type	0.257	NS	0.399	NS
WHO I/II				
WHO III	/		/	
T stage	0.110	NS	0.184	NS
1/2				
3/4	/		/	
N stage	0.074	NS	0.150	NS
0/1				
2/3	/		/	
TNM stage	0.069	NS	0.479	NS
I/II				
III/IV			/	
RT+/Chemo	0.316	NS	0.182	NS
RT alone				
RT+Chemo	/		/	

clinicopathological characteristics between ETR and LTR, ENR and LNR, and ELR and LLR.

Prognostic Factors Associated With OS

The prognostic factors contributing to long-term OS in ETR and LTR, ENR and LNR, and ELR and LLR were investigated using univariate and multivariate analyses (**Tables 4–6**). The effects of clinical factors on the OS with ETR group were evaluated. Age > 46 years and male gender were significantly associated with poorer OS. Cox regression modeling predicted that age [hazard ratio [HR], 1.645; 95% confidence interval [CI], 1.153–2.346; $P = 0.006$], gender (HR, 0.589; 95% CI, 0.377–0.920; $P = 0.020$) were independent risk factors of OS. Of the 217 patients with LTR, a baseline value of EBV-DNA > 2,000 was significantly associated with poorer OS. Cox regression modeling identified the baseline value of EBV-DNA (HR, 1.817; 95% CI, 1.115–2.962; $P = 0.017$) as an independent risk factor of OS. The effects of clinical factors on the OS with ENR group were evaluated. Alcohol drinking and TNM stage III/IV were significantly associated with poorer OS. Cox regression modeling predicted that alcohol abuse [hazard ratio [HR], 3.070; 95% confidence interval [CI], 1.551–6.076; $P = 0.001$], TNM stage (HR, 2.394; 95% CI, 1.178–4.864; $P = 0.016$) were independent risk factors of OS. Of the 142 patients with LNR, no clinical characteristics were significantly associated with OS. The effects of clinical factors on the OS with ELR group were also evaluated.

TABLE 5 | Univariate and multivariate analysis of prognostic factors of ENR and LNR in the purely regional recurrence group.

Characteristic	ETR group		LTR group	
	Univariate *P*-value HR (95% CI)	Multivariate *P*-value	Univariate *P*-value HR (95% CI)	Multivariate *P*-value
Age (years)	0.437	NS	0.997	NS
≤46 years				
>46 years	/		/	
Gender	0.749	NS	0.885	NS
Male				
Female	/		/	
Smoking status	0.264	NS	0.705	NS
Non-smoker				
Smoker	/		/	
Alcohol abuse	0.032	0.001	0.970	NS
Non-drinker	Reference			
Drinker	3.070 (1.551–6.076)		/	
Tumor family history	0.599	NS	0.796	NS
No				
Yes	/		/	
Cranial nerve symptom	0.035	NS	0.315	NS
No				
Yes	/		/	
Baseline value of EBV-DNA	0.090	NS	0.323	/ NS
≤2,000				
>2,000	/		/	
Histological type	0.979	NS	0.234	NS
WHO I/II				
WHO III	/		/	
T stage	0.353	NS	0.580	NS
1/2				
3/4	/		/	
N stage	0.048	NS	0.192	NS
0/1				
2/3	/		/	
TNM stage	0.037	0.016	0.494	NS
I/II	Reference			
III/IV	2.394 (1.178–4.864)		/	
RT+/Chemo	0.823	NS	0.740	NS
RT alone				
RT+Chemo	/		/	

Cox regression modeling predicted that N stage [hazard ratio [HR], 2.391; 95% confidence interval [CI], 1.328–4.271; $P = 0.004$], TNM stage (HR, 1.874; 95% CI, 1.248–2.812; $P = 0.002$) were independent risk factors of OS. Of the 95 patients with LLR, Cox regression modeling identified T stage (HR, 3.675; 95% CI, 1.241–10.882; $P = 0.019$) as an independent risk factor of OS. The patients with LTR/LNR/LLR demonstrated significantly better OS than the patients with ETR/ENR/ELR (**Figures 1A**, **2A**, **3A**), with a median OS of 33.1 months (range, 9.9–104.9 months)/53.0 months (range, 25.2–103.7 months), 44.1 months (range, 7.9–103.3 months)/53.6 months (range, 29.6–111.0 months), and 39.10 months (range, 6.90–85.27 months)/58.9 months (range, 33.6–101.8 months), respectively.

Prognostic Factors Associated With Post-recurrence OS

The clinical factors and treatment modalities of post-recurrence OS in ETR and LTR, ENR and LNR, and ELR and LLR were elevated by univariate and multivariate analyses (**Tables 7**–**9**). Of the 192 patients with ETR, PRBST was significantly associated with poorer OS. Of the 217 patients with LTR patients, Cox regression modeling identified post-recurrence treatment options ($P = 0.000$) was an independent risk factor of post-recurrence OS. Of the 183 patients with ENR, Cox regression modeling predicted that alcohol abuse (HR, 3.750; 95% CI, 1.909–7.367; $P = 0.000$) and post-recurrence treatment options ($P = 0.000$) were independent risk factors of post-recurrence OS. Of

TABLE 6 | Univariate and multivariate analysis of prognostic factors of ELR and LLR in the locoregional recurrence group.

Characteristic	ETR group		LTR group	
	Univariate *P*-value HR (95% CI)	Multivariate *P*-value	Univariate *P*-value HR (95% CI)	Multivariate *P*-value
Age(years)	0.069	NS	0.063	NS
≤46 years				
>46 years	/		/	
Gender	0.837	NS	0.101	NS
Male				
Female	/		/	
Smoking status	0.245	NS	0.483	NS
Non-smoker				
Smoker	/		/	
Alcohol abuse	0.194	NS	0.817	NS
Non-drinker				
Drinker	/		/	
Tumor family history	0.106	NS	0.095	NS
No				
Yes	/		/	
Cranial nerve symptom	0.139	NS	0.771	NS
No				
Yes	/		/	
Baseline value of EBV-DNA	0.110	NS	0.600	NS
≤2,000				
>2,000	/		/	
Histological type	0.646	NS	0.392	NS
WHO I/II				
WHO III	/		/	
T stage	0.557	NS	0.020	0.019
1/2			Reference	
3/4	/		3.675 (1.241–10.882)	
N stage	0.026	0.004	0.966	NS
0/1	Reference			
2/3	2.391 (1.328–4.271)		/	
TNM stage	0.363	0.002	0.047	NS
I/II	Reference			
III/IV	1.874 (1.248–2.812)		/	
RT+/Chemo	0.765	NS	0.403	NS
RT alone				
RT+Chemo	/		/	

the 142 patients with LNR patients, Cox regression modeling predicted post-recurrence treatment options ($P = 0.000$) was an independent risk factor of post-recurrence OS. Of the 87 patients with ELR, Cox regression modeling predicted that N stage (HR, 2.216; 95% CI, 1.225−4.009; $P = 0.008$) and post-recurrence treatment options ($P = 0.000$) were independent risk factors of post-recurrence OS. Of the 95 patients with LLR patients, Cox regression modeling predicted that T stage (HR, 4.111; 95% CI, 1.337–12.635; $P = 0.014$) and post-recurrence treatment options ($P = 0.000$) were independent risk factors of post-recurrence OS. Post-recurrence OS was not significantly different between ETR and LTR, ENR and LNR, and ELR and LLR groups (**Figures 1B**, **2B**, **3B**), with a median post-recurrence OS of 16.2 months (range, 0–93.0 months) and 12.2 months (range, 0.2–69.1 months), 28.1 months (range, 0.5–92.6 months) and 15.9 months (range 0–62.6 months), and 22.6 months (range, 0–63.7 months) and 15.3 months (range, 0.6–71.4 months), respectively.

DISCUSSION

Here, we investigated the clinical characteristics and prognostic factors predicting OS and post-recurrence OS in NPC patients with ETR and LTR, ENR and LNR, and ELR and LLR. In this retrospective study, 409 (4.3%) developed purely local recurrence, 325 (3.4%) developed purely regional recurrence,

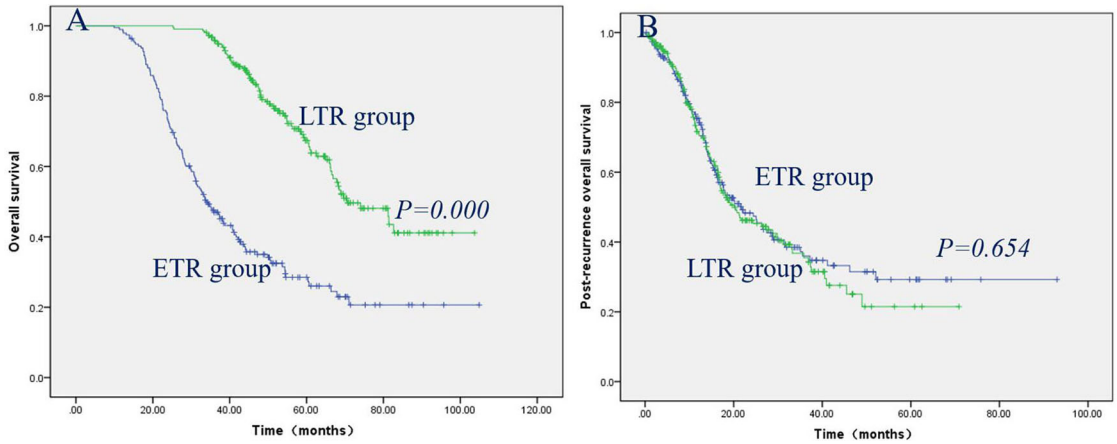

FIGURE 1 | Patients with LTR had significantly better OS than patients with ETR **(A)**, while post-recurrence OS did not reach significance between the patients with LTR and ETR **(B)**.

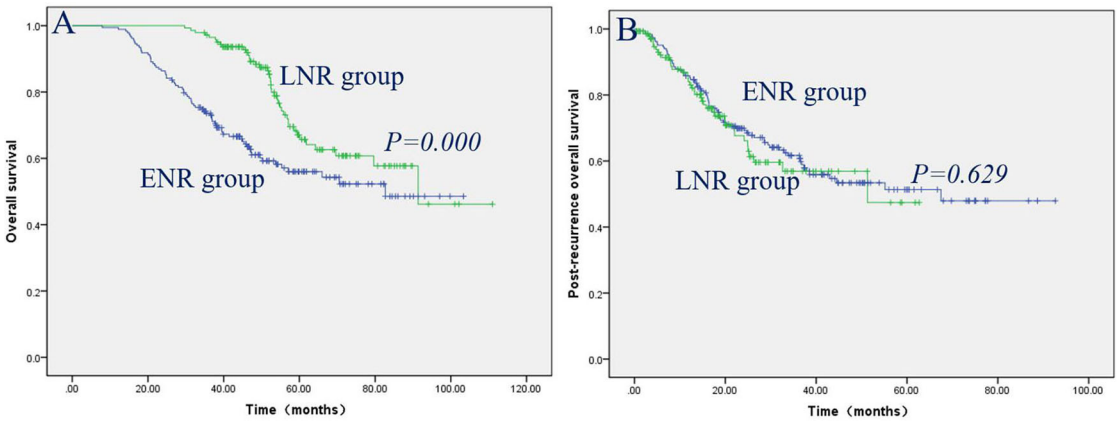

FIGURE 2 | Patients with LNR had significantly better OS than patients with ENR **(A)**, while post-recurrence OS did not reach significance between the patients with LNR and ENR **(B)**.

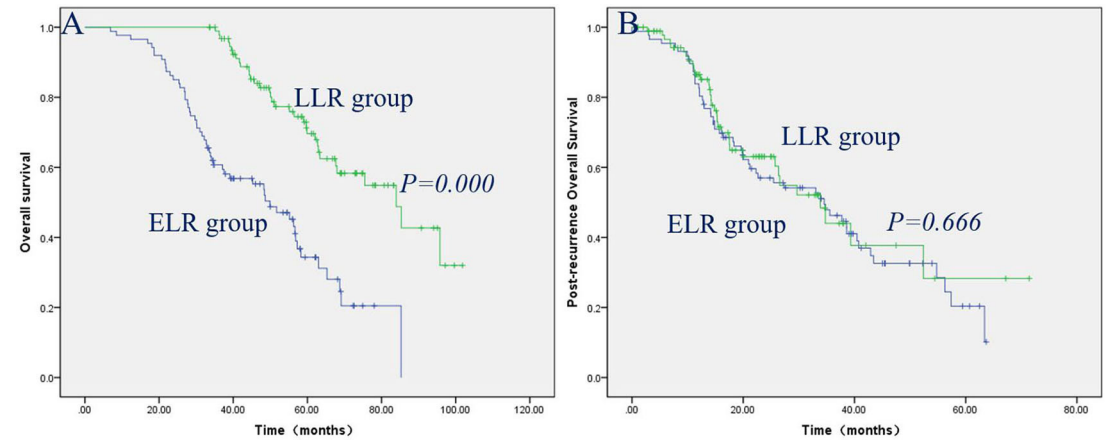

FIGURE 3 | Patients with LLR had significantly better OS than patients with ELR **(A)**, while post-recurrence OS did not reach significance between the patients with LLR and ELR **(B)**.

TABLE 7 | Univariate and multivariate analysis of post-recurrence prognostic factors of ETR and LTR in the purely local recurrence group.

Characteristic	ETR group		LTR group	
	Univariate *P*-value HR (95% CI)	Multivariate *P*-value	Univariate *P*-value HR (95% CI)	Multivariate *P*-value
Age (years)	0.013	NS	0.144	NS
≤46 years				
>46 years	/		/	
Gender	0.014	NS	0.299	NS
Male				
Female	/		/	
Smoking status	0.386	NS	0.262	NS
Non-smoker				
Smoker	/		/	
Alcohol abuse	0.296	NS	0.038	NS
Non-drinker				
Drinker	/		/	
Tumor family history	0.786	NS	0.077	NS
No				
Yes	/		/	
Cranial nerve symptom	0.061	NS	0.994	NS
No	/			
Yes	/		/	
Baseline value of EBV-DNA	0.299	NS	0.055	NS
≤2,000				
>2,000	/		/	
Histological type	0.296	NS	0.794	NS
WHO I/II				
WHO III	/		/	
T stage	0.124	NS	0.297	NS
1/2				
3/4	/		/	
N stage	0.095	NS	0.486	NS
0/1				
2/3	/		/	
TNM stage	0.095	NS	0.669	NS
I/II				
III/IV	/			
Post-recurrence treatment options	0.000	0.000	0.007	/ 0.019
BST	Reference		Reference	
Salvage surgery	0.162 (0.065–0.407)		0.983 (0.359–2.691)	
Re-irradiation	0.226 (0.135–0.378)		0.369 (0.184–0.739)	
Chemotherapy	0.302 (0.184–0.497)		0.554 (0.270–1.138)	

and 182 (1.9%) developed locoregional recurrence, which is similar to the results of previous studies from other centers in China (12, 13); 192 patients (46.9%) developed early ETR, and 217 patients (53.1%) developed LTR, 183 patients (56.3%) developed ENR, and 142 patients (43.7%) developed LNR, while 87 patients (47.8%) developed ELR, and 95 patients (52.2%) developed LLR, which suggests that the incidence of early and late recurrence is nearly the same. The patients with LTR/LNR/LLR demonstrated significantly better OS than the patients with ETR/ENR/ELR, which is consistent with previous studies on renal cell carcinoma and intrahepatic cholangiocarcinoma (14, 15), while post-recurrence OS did not reach significance between the ETR and LTR, ENR and LNR, and ELR and LLR groups, which suggests that post-recurrence OS does not depend on the time of recurrence.

Multivariate Cox regression analysis revealed that age and gender were independent risk factors for OS with ETR, and the baseline value of EBV-DNA was an independent risk factor for OS with LTR; alcohol abuse and TNM stage were independent risk factors for OS with ENR, and no clinical characteristics were associated with OS with LTR, and N stage and TNM stage were independent risk factors for OS with ELR; and T

TABLE 8 | Univariate and multivariate analysis of post-recurrence prognostic factors of ENR and LNR in the purely regional recurrence group.

Characteristic	ETR group		LTR group	
	Univariate *P*-value HR (95% CI)	Multivariate *P*-value	Univariate *P*-value HR (95% CI)	Multivariate *P*-value
Age (years)	0.462	NS	0.847	NS
≤46 years				
>46 years	/			/
Gender	0.804	NS	0.670	NS
Male				
Female	/		/	
Smoking status	0.208	NS	0.715	NS
Non-smoker				
Smoker	/		/	
Alcohol abuse	0.045	0.000	0.717	NS
Non-drinker	Reference			
Drinker	3.750 (1.909–7.367)		/	
Tumor family history	0.539	NS	0.858	NS
No				
Yes	/		/	
Cranial nerve symptom	0.029	NS	0.373	NS
No				
Yes	/		/	
Baseline value of EBV-DNA	0.138	NS	0.377	NS
≤2,000				
>2,000	/		/	
Histological type	0.910	NS	0.209	NS
WHO I/II				
WHO III	/		/	
T stage	0.327	NS	0.910	NS
1/2				
3/4	/		/	
N stage	0.070	NS	0.362	NS
0/1				
2/3	/		/	
TNM stage	0.041	NS	0.790	NS
I/II				
III/IV	/		/	
Post-recurrence treatment options	0.000	0.000	0.025	0.031
BST	Reference		Reference	
Salvage surgery	0.100 (0.042–0.238)		0.200 (0.065–0.619)	
Re-irradiation	0.159 (0.058–0.433)		0.266 (0.080–0.886)	
Chemotherapy	0.687 (0.309–1.528)		0.328 (0.100–1.071)	

stage was an independent risk factor for OS with LLR. In addition, multivariate Cox regression analysis revealed that post-recurrence treatment option was an independent risk factor of post-recurrence OS with ETR and LTR, while alcohol abuse and post-recurrence treatment option were independent risk factors of post-recurrence OS with ENR, and PRBST was associated with poorer post-recurrence OS with LNR. Meanwhile, N stage and post-recurrence treatment options were independent risk factors for post-recurrence OS with ELR, and T stage and post-recurrence treatment options were independent risk factors for post-recurrence OS with LLR. It has been suggested that patients with early initial T stage have a more favorable prognosis (16), which is consistent with the LLR patients in the present study. Post-recurrence treatment options including salvage surgery, re-irradiation, and chemotherapy are very important for NPC recurrence patients, which was shown that post-recurrence treatment options mentioned above have a better prognosis compared with PRBST.

There are various hypotheses for the occurrence of early and late recurrence. A probable hypothesis is the discrepancy of NPC tumor cell radiosensitivity. Recent studies have shown that apoptosis, DNA damage repair, a hypoxic microenvironment,

TABLE 9 | Univariate and multivariate analysis of post–recurrence prognostic factors of ELR and LLR in the locoregional recurrence group.

Characteristic	ETR group		LTR group	
	Univariate *P*-value HR (95% CI)	Multivariate *P*-value	Univariate *P*-value HR (95% CI)	Multivariate *P*-value
Age (years)	0.069	NS	0.296	NS
≤46 years				
>46 years	/		/	
Gender	0.982	NS	0.076	NS
Male				
Female	/		/	
Smoking status	0.284	NS	0.055	NS
Non-smoker				
Smoker	/		/	
Alcohol abuse	0.255	NS	0.489	NS
Non-drinker				
Drinker	/		/	
Tumor family history	0.144	NS	0.075	NS
No				
Yes	/		/	
Cranial nerve symptom	0.050	NS	0.563	NS
No				
Yes	/		/	
Baseline value of EBV-DNA	0.140	NS	0.963	NS
≤2,000				
>2,000	/		/	
Histological type	0.741	NS	0.056	NS
WHO I/II				
WHO III	/		/	
T stage	0.387	/	0.006	0.014
1/2			Reference	
3/4			4.111 (1.337–12.635)	
N stage	0.020	0.008	0.472	/
0/1	Reference			
2/3	2.216 (1.225–4.009)			
TNM stage	0.252	NS	0.028	NS
I/II				
III/IV	/		/	
Post-recurrence treatment options	0.002	0.007	0.000	0.000
BST	Reference		Reference	
Salvage surgery	0.238 (0.073–0.770)		0.277 (0.028–1.749)	
Re-irradiation	0.282 (0.090–0.885)		0.565 (0.071–1.476)	
Chemotherapy	0.666 (0.227–1.952)		0.736 (0.343–1.284)	

and autophagy can be involved in regulating radiotherapy resistance (17–19), which results in the difference in early and late recurrence. A study from Japan shed light on the biological impact of DNA methylation status as a predictive biomarker of early recurrence in ovarian cancers (20). It has been suggested that the tumor dormancy-reactivation hypothesis might be applicable to NPC (21, 22). Furthermore, surgery for removing breast tumors may lead to the appearance of growth factors in the circulation in response to surgical wounding, which may terminate the dormancy of the tumor foci and result in accelerated recurrence (7, 23). Although the main treatment of NPC is radiotherapy instead of surgery, it may also give rise to the appearance and an increase of growth factors to result in the occurrence of recurrence. Therefore, it is reasonable to speculate that there might be intrinsic biological differences between patients with early and late recurrence, and this warrants further studies.

The definitions of ETR and LTR, ENR and LNR, and ELR and LLR were applied with 2 years as the cut-off point, which have also been proposed and proven in recent studies (8, 9, 24). Hence, the frequency and intensity of follow-up should be strengthened at the initial 2 years. However, the application of

2 years for differentiating early recurrence from late recurrence remains controversial, and several studies have used 5 years as another major demarcation point (14, 25, 26). We applied 5 years for differentiating early recurrence from late recurrence and we found that there are very few cases of early recurrence; the number imbalance between the two groups is likely to lead to statistical problems.

There are two new features in the present study that differ from previous reports. First, this study figured out the prognostic factors of OS and post-recurrence OS in NPC patients with ETR and LTR, ENR and LNR, and ELR and LLR in detail. Second, this study has a large sample size with long median-time follow-up, which might help oncologists predict patients' prognosis and design individualized follow-up strategies. Although our study yielded some unique results, certain limitations should be noted. First, this is a retrospective single-center study, which has inherent biases. Second, the study merely explores the impact of baseline clinical characteristics on post-recurrence OS rather than post-recurrence clinical characteristics, which are principal elements of post-recurrence OS. Third, some information was lacking because of the long follow-up duration. However, we believe that the present results are noteworthy and reliable because this is the only such large-cohort study to date.

CONCLUSIONS

The present study shows that age and gender were independent risk factors of OS with ETR, and the baseline value of EBV-DNA was an independent risk factor of OS with LTR. Alcohol abuse and TNM stage were independent risk factors for OS with ENR, while N stage and TNM stage were independent risk factors of OS with ELR; and T stage was an independent risk factor for OS with LLR patients. In addition, post-recurrence treatment option was an independent risk factor of post-recurrence OS with ETR and LTR. Alcohol abuse and post-recurrence treatment option were independent risk factors of post-recurrence OS with ENR, and PRBST was associated with poorer post-recurrence OS with LNR. Meanwhile, N stage and post-recurrence treatment options were independent risk factors for post-recurrence OS with ELR, and T stage and post-recurrence treatment options were independent risk factors for post-recurrence OS with LLR. Patients with LTR/LNR/LLR demonstrate significantly better OS compared with patients with ETR/ENR/ELR, whereas post-recurrence OS is not significantly different between patients with ETR/ENR/ELR and LTR/LNR/LLR. Further studies are warranted to confirm our results.

DATA AVAILABILITY STATEMENT

The datasets generated for this study are available on request to the corresponding author.

ETHICS STATEMENT

This study was performed according to the ethical principles of the Declaration of Helsinki, and the Sun Yat-sen University Cancer Center review board approved the study protocol. Written informed consent was obtained from all patients for their data to be used in clinical research without affecting their treatment options or violating their privacy.

AUTHOR CONTRIBUTIONS

FL, F-PC, Y-PC, and G-QZ conceived and designed the study. YC, X-JH, X-DH, and Z-QZ contributed cases data collection. W-HZ, XL, and YS analyzed the data. FL, F-PC, and G-QZ wrote the paper. All authors read and approved the final manuscript.

FUNDING

This study was supported by grants from the Chinese postdoctoral fund (No. 2019M653214).

ACKNOWLEDGMENTS

The chief acknowledgment is to the subjects who provided information for this study and the research staff.

REFERENCES

1. Chua MLK, Wee JTS, Hui EP, Chan ATC. Nasopharyngeal carcinoma. *Lancet.* (2016) 387:1012–24. doi: 10.1016/S0140-6736(15)00055-0
2. Wei KR, Zheng RS, Zhang SW, Liang ZH, Ou ZX, Chen WQ. Nasopharyngeal carcinoma incidence and mortality in China in 2010. *Chin. J. Cancer.* (2014) 33:381–7. doi: 10.5732/cjc.014.10086
3. Chan AT. Nasopharyngeal carcinoma. *Ann Oncol.* (2010) 21 (Suppl. 7): vii308–12. doi: 10.1093/annonc/mdq277
4. Lee AW, Lin JC, Ng WT. Current management of nasopharyngeal cancer. *Semin. Radiat. Oncol.* (2012) 22:233–44. doi: 10.1016/j.semradonc.2012.03.008
5. Lai SZ, Li WF, Chen L, Luo W, Chen YY, Liu LZ, et al. How does intensity-modulated radiotherapy versus conventional two-dimensional radiotherapy influence the treatment results in nasopharyngeal carcinoma patients? *Int. J. Radiat. Oncol. Biol. Phys.* (2011) 80:661–8. doi: 10.1016/j.ijrobp.2010.03.024
6. Lee AW, Ma BB, Ng WT, Chan AT. Management of nasopharyngeal carcinoma: current practice and future perspective. *J Clin Oncol.* (2015) 33:3356–64. doi: 10.1200/JCO.2015.60.9347
7. Retsky M, Demicheli R, Hrushesky WJ. Does surgery induce angiogenesis in breast cancer? Indirect evidence from relapse pattern and mammography paradox. *Int J Surg.* (2005) 3:179–87. doi: 10.1016/j.ijsu.2005.08.002
8. Yamada S, Hatta W, Shimosegawa T, Takizawa K, Oyama T, Kawata N, et al. Different risk factors between early and late cancer recurrences in patients without additional surgery after noncurative endoscopic submucosal dissection for early gastric cancer. *Gastrointest Endosc.* (2019) 89:950–60. doi: 10.1016/j.gie.2018.11.015
9. Mortensen MS, Lauritsen J, Kier MG, Bandak M, Appelt AL, Agerbæk M, et al. Late relapses in stage I testicular cancer patients on surveillance. *Eur Urol.* (2016) 70:365–71. doi: 10.1016/j.eururo.2016.03.016
10. Tang LL, Chen YP, Mao YP, Wang ZX, Guo R, Chen L, et al. Validation of the 8th edition of the UICC/AJCC staging system for nasopharyngeal carcinoma

from endemic areas in the intensity-modulated radiotherapy era. *J Natl Compr Canc Netw.* (2017) 15:913–9. doi: 10.6004/jnccn.2017.0121
11. OuYang PY, Xiao Y, You KY, Zhang LN, Lan XW, Zhang XM, et al. Validation and comparison of the 7th and 8th edition of AJCC staging systems for non-metastatic nasopharyngeal carcinoma, and proposed staging systems from Hong Kong, Guangzhou, and Guangxi. *Oral Oncol.* (2017) 72:65–72. doi: 10.1016/j.oraloncology.2017.07.011
12. Wu LR, Liu YT, Jiang N, Fan YX, Wen J, Huang SF, et al. Ten-year survival outcomes for patients with nasopharyngeal carcinoma receiving intensity-modulated radiotherapy: an analysis of 614 patients from a single center. *Oral Oncol.* (2017) 69:26–32. doi: 10.1016/j.oraloncology.2017.03.015
13. Yi JL, Gao L, Huang XD, Li SY, Luo JW, Cai WM, et al. Nasopharyngeal carcinoma treated by radical radiotherapy alone: ten-year experience of a single institution. *Int J Radiat Oncol Biol Phys.* (2006) 65: 161–8. doi: 10.1016/j.ijrobp.2005.12.003
14. Kroeger N, Choueiri TK, Lee JL, Bjarnason GA, Knox JJ, MacKenzie MJ, et al. Survival outcome and treatment response of patients with late relapse from renal cell carcinoma in the era of targeted therapy. *Eur Urol.* (2014) 65:1086–92. doi: 10.1016/j.eururo.2013.07.031
15. Wang C, Pang S, Si-Ma H, Yang N, Zhang H, Fu Y, et al. Specific risk factors contributing to early and late recurrences of intrahepatic cholangiocarcinoma after curative resection. *World J Surg Oncol.* (2019) 17:2. doi: 10.1186/s12957-018-1540-1
16. Yu KH, Leung SF, Tung SY, Zee B, Chua DT, Sze WM, et al. Survival outcome of patients with nasopharyngeal carcinoma with first local failure: a study by the Hong Kong Nasopharyngeal Carcinoma Study Group. *Head Neck.* (2005) 27:397–405. doi: 10.1002/hed.20161
17. Lu ZX, Ma XQ, Yang LF, Wang ZL, Zeng L, Li ZJ, et al. DNAzymes targeted to EBV-encoded latent membrane protein-1 induce apoptosis and enhance radiosensitivity in nasopharyngeal carcinoma. *Cancer Lett.* (2008) 265:226–38. doi: 10.1016/j.canlet.2008.02.019
18. Zhai X, Yang Y, Wan J, Zhu R, Wu Y. Inhibition of LDH-A by oxamate induces G2/M arrest, apoptosis and increases radiosensitivity in nasopharyngeal carcinoma cells. *Oncol Rep.* (2013) 30:2983–91. doi: 10.3892/or.2013.2735
19. Yang S, Chen J, Guo Y, Lin H, Zhang Z, Feng G, et al. Identification of prognostic biomarkers for response to radiotherapy by DNA microarray in nasopharyngeal carcinoma patients. *Int J Oncol.* (2012) 40:1590–600. doi: 10.3892/ijo.2012.1341
20. Mase S, Shinjo K, Totani H, Katsushima K, Arakawa A, Takahashi S, et al. ZNF671 DNA methylation as a molecular predictor for the early recurrence of serous ovarian cancer. *Cancer Sci.* (2019) 110:1105–16. doi: 10.1111/cas.13936
21. Naumov GN, Townson JL, MacDonald IC, Wilson SM, Bramwell VH, Groom AC, et al. Ineffectiveness of doxorubicin treatment on solitary dormant mammary carcinoma cells or late-developing metastases. *Breast Cancer Res Treat.* (2003) 82:199–206. doi: 10.1023/B:BREA.0000004377.12288.3c
22. Braun S, Kentenich C, Janni W, Hepp F, de Waal J, Willgeroth F, et al. Lack of effect of adjuvant chemotherapy on the elimination of single dormant tumor cells in bone marrow of high-risk breast cancer patients. *J Clin Oncol.* (2000) 18:80–6. doi: 10.1200/JCO.2000.18.1.80
23. Tagliabue E, Agresti R, Carcangiu ML, Ghirelli C, Morelli D, Campiglio M, et al. Role of HER2 in wound-induced breast carcinoma proliferation. *Lancet.* (2003) 362:527–33. doi: 10.1016/S0140-6736(03)14112-8
24. Calderaro J, Petitprez F, Becht E, Laurent A, Hirsch TZ, Rousseau B, et al. Intra-tumoral tertiary lymphoid structures are associated with a low risk of early recurrence of hepatocellular carcinoma. *J Hepatol.* (2019) 70:58–65. doi: 10.1016/j.jhep.2018.09.003
25. Lee JH, Kim HI, Kim MG, Ha TK, Jung MS, Kwon SJ. Recurrence of gastric cancer in patients who are disease-free for more than 5 years after primary resection. *Surgery.* (2016) 159:1090–8. doi: 10.1016/j.surg.2015.11.002
26. Ichiyanagi O, Naito S, Ito H, Kabasawa T, Narisawa T, Kanno H, et al. Levels of 4EBP1/eIF4E activation in renal cell carcinoma could differentially predict its early and late recurrence. *Clin Genitourin Cancer.* (2018) 16:e1029–58. doi: 10.1016/j.clgc.2018.06.002

Conflict of Interest: The authors declare that the research was conducted in the absence of any commercial or financial relationships that could be construed as a potential conflict of interest.

frontiers in Oncology

ORIGINAL RESEARCH
published: 08 September 2020
doi: 10.3389/fonc.2020.01678

Internal Ribosome Entry Sites Mediate Cap-Independent Translation of Bmi1 in Nasopharyngeal Carcinoma

Hongbo Wang[1,2†], Yunjia Zhu[1†], Lijuan Hu[2,3†], Yangyang Li[4], Guihong Liu[5], Tianliang Xia[2], Dan Xiong[2,6], Yiling Luo[2], Binliu Liu[2], Yu An[2], Manzhi Li[2], Yuehua Huang[1], Qian Zhong[2] and Musheng Zeng[2]**

[1] Guangdong Provincial Key Laboratory of Liver Disease Research, The Third Affiliated Hospital of Sun Yat-sen University, Guangzhou, China, [2] State Key Laboratory of Oncology in South China, Collaborative Innovation Center for Cancer Medicine, Sun Yat-sen University Cancer Center, Guangzhou, China, [3] Beijing Key Laboratory of Hematopoietic Stem Cell Transplantation, Peking University People's Hospital, Peking University Institute of Hematology, Beijing, China, [4] Department of Pathology, Sun Yat-sen Memorial Hospital, Guangzhou, China, [5] Tungwah Hospital of Sun Yat-sen University, Dongguan, China, [6] Department of Laboratory Medicine, Luohu District People's Hospital, Shenzhen, China

OPEN ACCESS

Edited by:
Jan Baptist Vermorken,
University of Antwerp, Belgium

Reviewed by:
Katrin Schröder,
University Hospital Frankfurt, Germany
Hong-Quan Duong,
Hanoi University of Public Health, Vietnam

***Correspondence:**
Qian Zhong
zhongqian@sysucc.org.cn
Musheng Zeng
zengmsh@mail.sysu.edu.cn

[†] These authors have contributed equally to this work

Specialty section:
This article was submitted to Head and Neck Cancer, a section of the journal Frontiers in Oncology

Received: 30 October 2019
Accepted: 29 July 2020
Published: 08 September 2020

Citation:
Wang H, Zhu Y, Hu L, Li Y, Liu G, Xia T, Xiong D, Luo Y, Liu B, An Y, Li M, Huang Y, Zhong Q and Zeng M (2020) Internal Ribosome Entry Sites Mediate Cap-Independent Translation of Bmi1 in Nasopharyngeal Carcinoma. Front. Oncol. 10:1678. doi: 10.3389/fonc.2020.01678

Bmi1 is overexpressed in multiple human cancers. We previously reported the oncogenic function and the transcription regulation mechanisms of Bmi1 in nasopharyngeal carcinoma (NPC). In this study, we observed that the mRNA and the protein levels of Bmi1 were strictly inconsistent in NPC cell lines and cancer tissues. The inhibitors of proteasome and lysosome could not enhance the protein level of Bmi1, indicating that Bmi1 may be post-transcriptionally regulated. The IRESite analysis showed that there were two potential internal ribosome entry sites (IRESs) in the 5′-untranslated region (5′-UTR) of Bmi1. The luciferase assay demonstrated that the 5′-UTR of Bmi1 has IRES activity, which may mediate cap-independent translation. The IRES activity of the Bmi1 5′-UTR was significantly reduced after the mutation of the two IRES elements. Taken together, these results suggested that the IRES elements mediating translation is a novel post-transcriptional regulation mechanism of Bmi1.

Keywords: internal ribosome entry sites, Bmi1, nasopharyngeal carcinoma, 5′-untranslated region, translational activity

HIGHLIGHTS

- We observed that the mRNA and the protein levels of Bmi1 were strictly inconsistent.
- The inhibitors of proteasome and lysosome could not enhance the protein level of Bmi1.
- The 5′-UTR of Bmi1 mRNA contains potential internal ribosome entry sites.
- The 5′-UTR of Bmi1 mediated cap-independent translation.
- The mutation of the two IRES elements reduced the IRES activity of the Bmi1 5′-UTR.

Abbreviations: 5′-UTR, 5′-untranslated region; CSCs, cancer stem cells; IRES, internal ribosome entry sites; NPC, nasopharyngeal carcinoma; NPECs, nasopharyngeal epithelial cells; PCBP, poly (rC)-binding protein; PRC1, polycomb-repressive complex 1; PTB, polypyrimidine tract-binding protein; unr, upstream of N-ras.

INTRODUCTION

Nasopharyngeal carcinoma (NPC) is a common malignant tumor in Southern China and Southeast Asia. Chemotherapy and radiation therapy are the preferred options for the treatment of NPC. However, the 5-year survival rate is only 50 to 75% (1). Therefore, it is very important to elucidate the molecular mechanism underlying the progression of NPC.

Bmi1, a member of the polycomb-repressive complex 1 (PRC1), participates in the self-renewal of hematopoietic and neural stem cells, embryogenesis, cell cycle regulation, senescence, chemoresistance, recurrence of cancer stem cells, and tumor progression (2, 3). Bmi1 is upregulated in tumor cells and tissue and associated with poor prognosis in various human cancers including breast cancer (4), lymphomas (5), melanoma (6), colon cancer (7), ovarian cancer (8), hepatocellular carcinoma (9), NPC (10, 11), lung cancer (12), and neuroblastoma (13). We previously reported that the overexpression of Bmi1 promoted immortalization and epithelial–mesenchymal transition (EMT) in nasopharyngeal epithelial cells (11, 14). The knockdown of Bmi1 reverses EMT and suppresses the metastasis of NPC cells. Xu et al. reported that the knockdown of Bmi1 sensitizes $CD44^+$ nasopharyngeal cancer stem-like cells to radiotherapy (15). These findings indicate that Bmi1 may serve as a potential therapeutic target for NPC (16).

The overexpression of Bmi1 in cancers could be caused by different mechanisms. We previously reported that Sp1 and c-Myc regulate the transcription of Bmi1 mRNA in NPC (17). Nowak reported that E2F1 and MYCN promote the transcription of Bmi1 in neuroblastomas (18). Hypoxia-induced Twist1 directly enhances Bmi1 transcription and cooperates with Bmi1 to induce EMT and stemness properties in head and neck squamous cell carcinoma (19). SALL4 and c-Myb regulates the transcription of Bmi1 in hematopoietic and leukemic cells, while nuclear factor kB (NF-kB) and the sonic hedgehog-activated Gli1 are its potent transcription factors in Hodgkin lymphoma and medulloblastoma cells, respectively (20–23). In addition to transcriptional regulation, miR-200C (24), miR-141 (25), miR-203 (26), miR-15a (27), miR-183 (26), miR-218 (28), miR-320a (10), and miR-16 (27) target Bmi1 and suppress its expression. Moreover, Bmi1 expression may also be regulated post-translationally. BetaTrCP promotes the ubiquitination and the degradation of Bmi1 protein in breast cancer cells (29). C18Y polymorphism in the RING finger domain of Bmi1 promotes its degradation through the ubiquitin–proteasome system (30). The PS domain of Bmi1 is involved in its proteolysis, and it negatively regulates the function of Bmi1 oncoprotein (31). Although there are mountains of studies addressing the regulation of Bmi1 in the transcriptional, post-transcriptional, and post-translational levels, there are few studies about the role of internal ribosome entry site (IRES) elements in the regulation of Bmi1 expression.

Protein biosynthesis includes cap-dependent and cap-independent initiations, which are directed by IRES. Since the discovery of the IRES elements in the 5′-untranslated regions (5′-UTRs) of the encephalomyocarditis virus (32) and the poliovirus (33), IRESs have been found to be contained in the 5′-UTR of a number of viral and eukaryotic cellular mRNAs, including proto-oncogenes, growth factors, receptors, and transcription factors (34). Cellular mRNA with IRES elements could regulate angiogenesis, mitosis, various stress situations, and nutritional and osmotic control (35). IRES *trans*-acting factors (ITAFs) are RNA binding proteins which are required for IRES-mediated translation and thus specifically enhance the protein level of mRNA with IRES elements. PTBP1 (36), PCBP1 (37), HnRNP A1 (38, 39), HnRNP C (40), and DAP5 (41) are the reported ITAFs which regulate the translation of numerous oncogenes, such as MYC, FGF2, IGF1R, CDK1, cyclin D1, etc.

In the present study, we reported that there are two IRES motifs in the 5′-UTR of the human Bmi1. The mutation of the two IRES elements partially inhibited the translational activity of the Bmi1 5′-UTR. These results demonstrated that IRES elements might mediate the translation of Bmi1 in NPC.

MATERIALS AND METHODS

Materials

Proteasome inhibitor MG132 (Calbiochem, San Diego, CA, United States) was used at a final concentration of 10 and 20 μM for 8 h. The cell was treated with lysosomal inhibitor NH_4Cl (Guangzhou Chemical Reagent Factory, China) at a final concentration of 10 and 20 mM for 8 h. The β-gal was purchased from Sigma.

Cell Culture

HNE1, CNE2, and C666-1 cells (the human nasopharyngeal carcinoma cells) were grown in RPMI1640 medium, supplemented with 10% fetal bovine serum (Gibco, Grand Island, NY, United States). MCF10A cells (the immortalized primary human mammary epithelial cells) were maintained in keratinocyte/serum-free medium (Gibco). MCF7 cells (the human breast cancer cells) were grown in Dulbecco's modified Eagle's medium (Gibco) supplemented with 10% fetal bovine serum (Gibco). The cells were grown in a humidified 5%-CO_2 incubator at 37°C and passaged with standard cell culture techniques.

Patients and Specimens

Four paraffin-embedded slides and the paired mRNA from NPC specimens were obtained from Sun Yat-sen University Cancer Center (17). Informed consent was obtained from each patient prior to surgery, and the study was approved by the Institute Research Ethics Committee of Sun Yat-sen University Cancer Center.

Immunohistochemistry

An immunohistochemical analysis of Bmi1 expression in NPC specimens was performed as previously described (11). Each slide was incubated overnight with rabbit antibody against human Bmi1 (Proteintech Group, Wuhan, China).

Plasmid Constructs

The plasmid (pRBMIF) was constructed by the insertion of the 5′-UTR of Bmi1 (GenBank accession number: NM_005180.6)

PCR-amplified from the cDNA of C666-1 into the *Eco*RI/*Nco*I sites between the Renilla and the Firefly luciferase in the dual luciferase vector pRF (42) (a generous gift from Dr. Anne Willis, University of Leicester, United Kingdom). The 5′-UTR of Bmi1 containing mutant IRES1, IRES2, or both was obtained through the overlap extension PCR method, with pRBMIF as the template, and inserted in the plasmid (pRF), named as mIRES1, mIRES2, and mIRES1 + 2, respectively. The primers used in the overlap extension PCR were as follows: mutant IRES1, 5′-CCA CCATCGCATCGCACGCTTCGCATCGCCCCGCTCGCACGC ACACACACGGC-3′ and mutant IRES2, 5′-CGTCATGCACC GGGGGCTGCTTCGCATCGTGCTCGGCCGCCGCCGCCTC CTCCCGCTCC-3′.

Western Blotting Analysis

Western blotting analysis was performed as previously described (43). The cells were harvested and lysed with a cell lysis buffer [50 mM Tris–HCl (pH 7.4), 150 mM NaCl, 1.0% NP-40, 5 mM EDTA, and protein inhibitor cocktail]. The cell lysates were subjected to SDS-PAGE and immunoblotted with Bmi1 (Proteintech Group, Wuhan, China), α-tubulin (Sigma), glyceraldehyde-3-phosphate dehydrogenase (GAPDH; Santa Cruz Biotechnology, Santa Cruz, CA, United States), and p53 (Santa Cruz Biotechnology) as indicated.

Transient Transfections and IRES Activity Assays

CNE2 (1×10^5) cells were seeded into 24-well plates 16 h prior to transfection, at about 70–80% confluency. The cells were co-transfected with 200 ng of the indicated dicistronic reporter plasmids and 100 ng of β-galactosidase reporter plasmid using Lipofectamine 2000 (Invitrogen) according to the manufacturer's protocol. β-Galactosidase reporter plasmid serves as an internal control to correct the differences in both the transfection and the harvesting efficiencies. At 24 h following transfection, cell extracts were harvested using a passive lysis buffer (Promega, Madison, WI, United States) and then subjected to the translational activity assays. The Firefly and the Renilla luciferase activities were determined using the dual-luciferase reporter assay system (Promega). The β-galactosidase activity was analyzed with the galactosidase enzyme assay system (44). The translational activity was determined as the ratios of Firefly to Renilla luciferase activities relative to the value of the β-galactosidase activity.

RT-PCR and Quantitative RT-PCR Analysis

Total RNA was extracted with TRIzol reagent (Invitrogen) as described previously (17). According to the manufacturer's instructions, the first-strand cDNA was synthesized using 2 μg of the total RNA with a reverse transcriptase kit (Promega). The total RNA was treated with DNAseI for the Firefly and the Renilla luciferase gene-transfected cell and qRT-PCR analysis. The mRNA level was evaluated by qRT-PCR with Power SYBR Green qPCR SuperMix-UDG (Invitrogen) on an LC480 detection system (Roche). GAPDH was used as an internal control to normalize the relative expression. The relative gene expression was calculated by $2^{\Delta Ct}$, where ΔCt = Ct (internal control) – Ct (unknown). The following primers were used in the qRT-PCR analysis: qBmi1pF, 5′-TGGCTCGCATTC ATTTTCTG-3′; qBmi1pR, 5′-TGTGGCATCAATGAAGT ACCCT-3′; qGAPDHpF, 5′-CTCCTCCTGTTCGACAGT CAGC-3′; qGAPDHpR, 5′-CCCAATACGACCAAATCC GTT-3′; qFireflypF, 5′-CGGATTACCAGGGATTTCA GTC-3′; qFireflypR, 5′-ATCTCACGCAGGCAGTTC TATG-3′; qRenillapF, 5′-GCCTCGTGAAATCCCGTTAGT-3′; and qRenillapR, 5′-TCTTGGCACCTTCAACAATAGC-3′.

The full-length 5′-UTR of Bmi1 was 623 bp and was amplified using specific primers (BMI-UTRpF: 5′-GGAA TTCGAGCCATTTTGGAGCCGGTG-3′ and BMI-UTRpR: 5′-CATGCCATGG TTCTGCTTGATAAAAAATCCCGG-3′). The internal reference gene was ACTIN (ACTINpF: 5′-CGCGAGAA GATGACCCAGAT-3′ and ACTINpR: 5′-GGGCATACCC CTCGTAGATG-3′), and the final product was about 500 bp long. These products were analyzed by electrophoresis on 1.0% agarose gel.

IRES and RNAfold Analyses

The IRESite[1] presents curated experimental evidence of many eukaryotic viral and cellular IRES regions (45). RNAfold[2] is the web-based algorithm which was used for the predictions of the RNA secondary structure.

Statistical Analysis

All data analyses were conducted with GraphPad Prism version 5.0 (GraphPad Software, San Diego, CA, United States). The results were representative of at least three independent experiments.

Data were presented as mean ± standard error of the mean obtained with triplicate samples. The analysis of the differences between groups was determined with a *t*-test, and differences with $p < 0.05$ were considered as statistically significant.

RESULTS

The mRNA and the Protein Levels of Bmi1 Were Inconsistent in Nasopharyngeal Carcinoma Cancer Cells and Cancer Tissues

To explore the mechanism underlying the high expression of Bmi1, the mRNA and the protein levels of Bmi1 in NPC and breast cancer cells were determined. As shown in **Figure 1**, the expression of Bmi1 mRNA in C666-1 cells was only 1.5-fold higher than in CNE2 cells (**Figure 1A**). However, the Bmi1 protein level in C666-1 cells was 6.6-folds higher than in CNE2 cells (**Figures 1B,C**). In addition to NPC cells, the protein level in MCF7 cell was 2.8-folds higher than in MCF10A cells, while Bmi1 mRNA was almost equal in MCF10A and MCF7 cells (**Figures 1A–C**).

[1]http://www.iresite.org

[2]http://nhjy.hzau.edu.cn/kech/swxxx/jakj/dianzi/Bioinf4/miRNA/miRNA1.htm

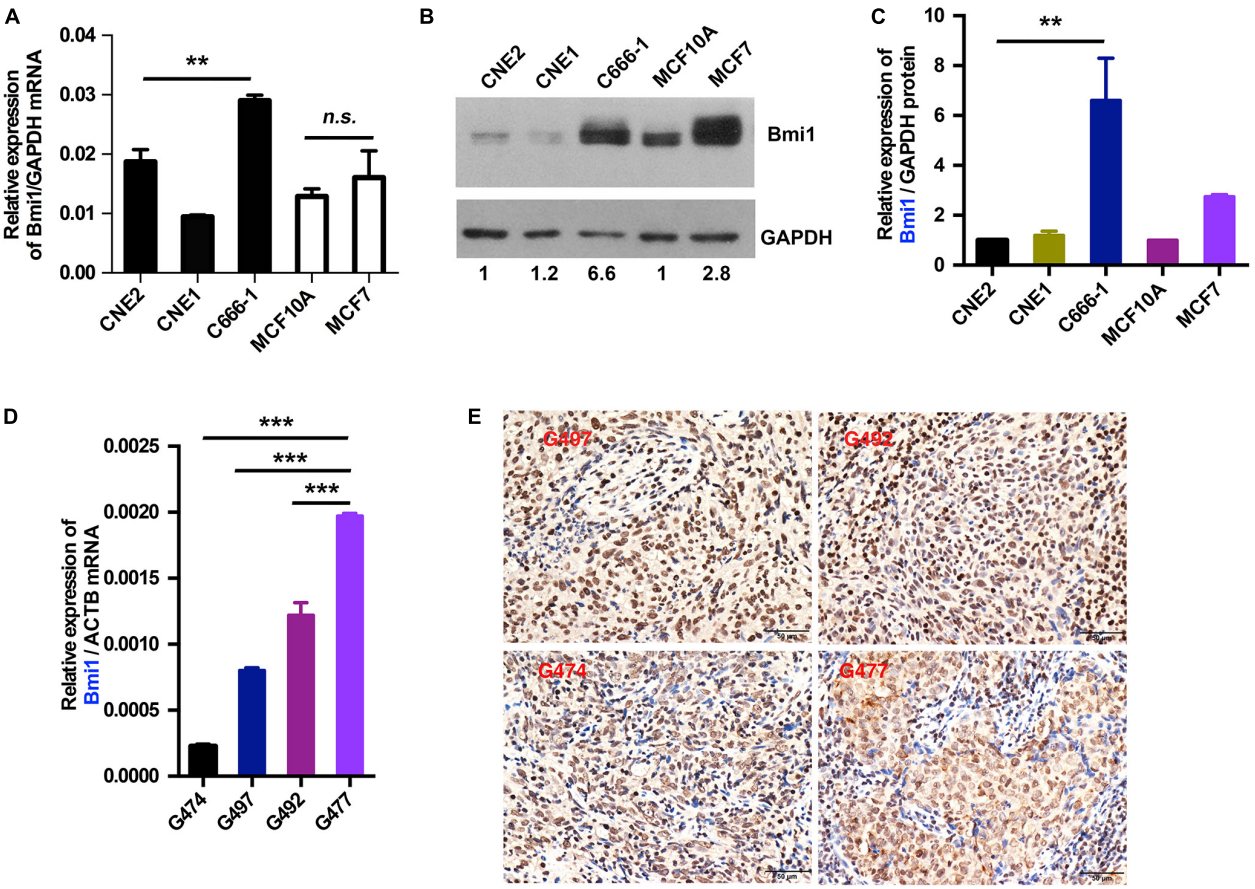

FIGURE 1 | The mRNA and protein levels of Bmi1 are inconsistent in nasopharyngeal carcinoma, breast cancer cell lines, and nasopharyngeal carcinoma tissues. **(A,B)** The protein and mRNA levels of Bmi1 were analyzed by qRT-PCR **(A)** and Western blot **(B)** in CNE2, C666-1, MCF10A, and MCF7 cell lines. GAPDH was used as internal control. **(C)** The intensity of the bands was determined with ImageJ software. **(D,E)** The mRNA and protein levels of Bmi1 were analyzed by qRT-PCR **(D)** and immunohistochemistry staining **(E)** in nasopharyngeal carcinoma tissues. *ACTB* was used as qPCR internal control. A representative result of three independent experiments is shown ($n = 3$). The graphs show the mean ± SEM. $^{**}P < 0.01$, $^{***}P < 0.001$; Student's *t*-test.

To clinically show the inconsistency between the mRNA and the protein levels of Bmi1, we analyzed the expression of Bmi1 mRNA and protein in NPC tissue. As shown in **Figures 1D,E**, the expression of Bmi1 mRNA in G477 NPC tissue was higher than in G474, G497, and G492. However, immunohistochemical staining showed that the Bmi1 protein level in G474, G497, and G492 was higher than in G477 NPC tissue.

Taken together, the mRNA and the protein levels of Bmi1 were not strictly correlated in NPC cancer cells and tissues, indicating that Bmi1 expression was not only regulated in the transcriptional level but may also be regulated in the post-transcriptional level in NPC cells and cancer specimens.

Inhibitors of Proteasome and Lysosome Could Not Enhance the Protein Level of Bmi1

To determine whether Bmi1 was regulated at the posttranslational level in NPC cell lines, the effects of proteasomal inhibitors (MG132), and lysosomal inhibitors (NH_4Cl) on the protein level of Bmi1 were analyzed. CNE2 cells were cultured in the presence of the indicated concentration of MG132 and NH_4Cl for 8 h. As shown in **Figure 2A**, compared to the DMSO-treated cells, MG132 and NH_4Cl obviously enhanced the protein level of p53 (the positive control for proteasomal degradation) and LC3-II (the positive control for lysosomal degradation), respectively. However, both MG132 and NH_4Cl could not enhance the protein level of Bmi1 in CNE2 cells. In addition, the NPC cell lines HNE1 and C666-1 were also treated with MG132 for 8 h. The protein level of Bmi1 was not enriched, while the protein level of p53 was obviously increased in MG132-treated cells (**Figure 2B**). These data indicated that the expression of Bmi1 might be post-transcriptionally regulated in the proteasome-independent and lysosome-independent degradation pathway.

Two Internal Ribosome Entry Sites Are Identified in Bmi1 5′-UTR

To further explore the potential mechanisms underlying the inconsistency between the mRNA and the protein level of Bmi1, we analyzed the region from −639 to +1 (the translation initiation site ATG was assigned as +1) of the Bmi1 5′-UTR

using the IRESite online software. As shown in **Figure 3A**, there were four potential IRES motifs, which were named as IRES1 (−579/−549), IRES2 (−324/−291), IRES3 (−275/−255), and IRES4 (−222/−213). The RNAfold online software was used to analyze the secondary structure of the Bmi1 5′-UTR. As shown in **Figure 3B**, the IRES1 and IRES2 motif in the 5′-UTR region of Bmi1 could form the putative KMI1 stem loop structure which may bind PTBP1. These results suggested that the two

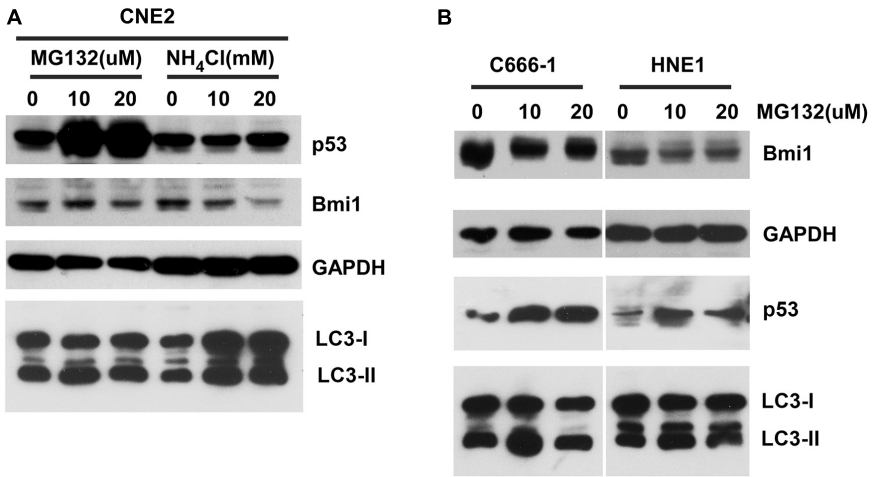

FIGURE 2 | The inhibitors proteasome and lysosome do not have effects on Bmi1 protein expression in nasopharyngeal carcinoma (NPC) cells. NPC cells CNE2 **(A)**, C666-1, and HNE1 **(B)** were seeded into six-well plates, then treated with the indicated concentrations of MG132 and NH_4Cl for 8 h, then subjected to western blot. p53 served as the positive control for the role of MG132 in proteasomal degradation. LC3-II served as the positive control for the role of NH_4Cl in lysosomal degradation. GAPDH was used as a loading control. The data represent three sets of independent experiments.

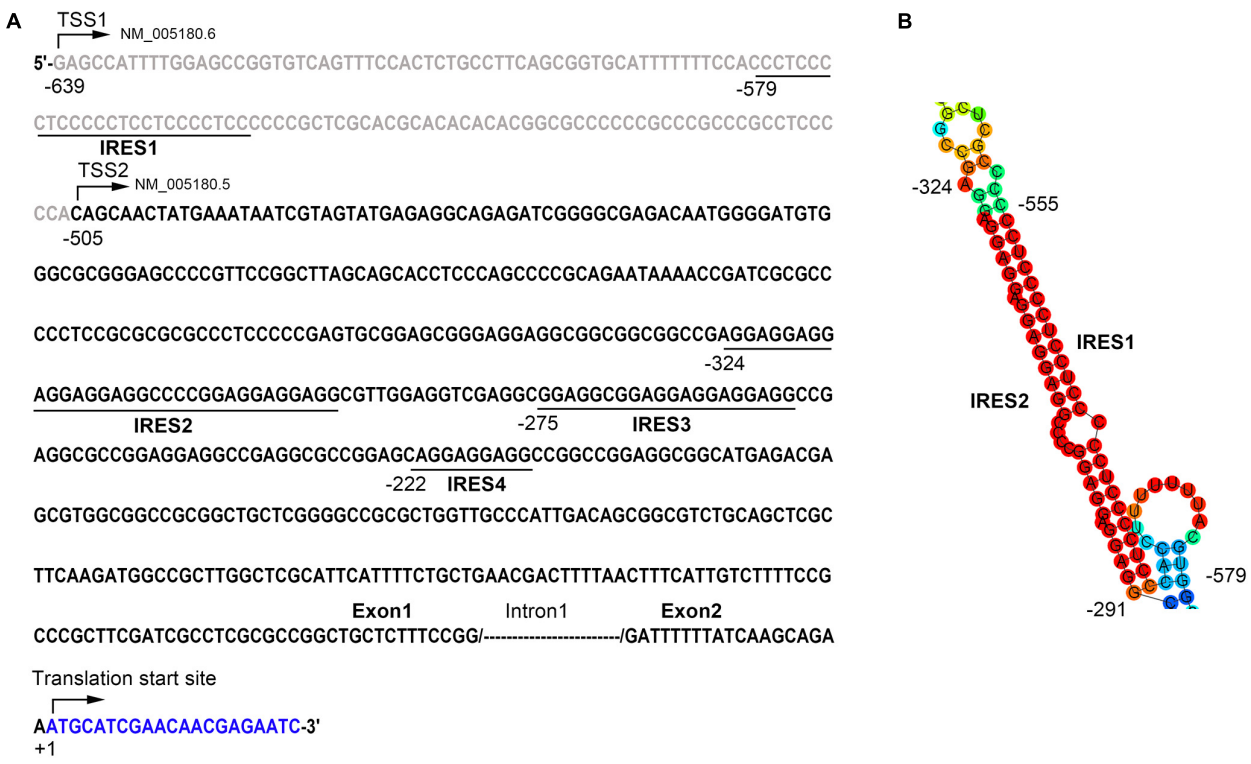

FIGURE 3 | The 5′-UTR region of Bmi1 contains the potential internal ribosome entry sites (IRES) motifs. **(A)** IRESite database analyses of the region from −639 to +1 of Bmi1 5′-UTR sequence; the translation initiation site ATG was assigned as +1. There are four potential IRES elements. **(B)** The secondary structure of the Bmi1 5′-UTR predicated by RNAfold database showing that the IRES1 and IRES2 motifs form a KMI1 stem loop structure.

potential IRES motifs in the Bmi1 5′-UTR may activate the translation of Bmi1.

The Bmi1 5′-UTR Promoted Translation

There are two transcriptional versions of Bmi1 mRNA (NM 005180.6 and NM 005180.5) with different transcription start sites (TSS). The long 5′-UTR (−623/+30) was named as TSS1 and the short 5′-UTR (−414/+30) was named as TSS2 (**Figure 4A**). RT-PCR demonstrated that both the long and the short 5′-UTRs were expressed in the four cell lines tested, including CNE2, C666-1, MCF10A, and MCF7 cells (**Figure 4B**).

To test whether the Bmi1 5′-UTR could enhance Bmi1 protein translation, the dicistronic reporter plasmid (named as pRBMIF) was constructed. As shown in **Figure 4C**, the Bmi1 5′-UTR (−623/+1) was inserted between the Renilla and the Firefly luciferase in the plasmid (pRF), with the 5′-UTR of c-myc as the positive control (pRMF). The plasmids

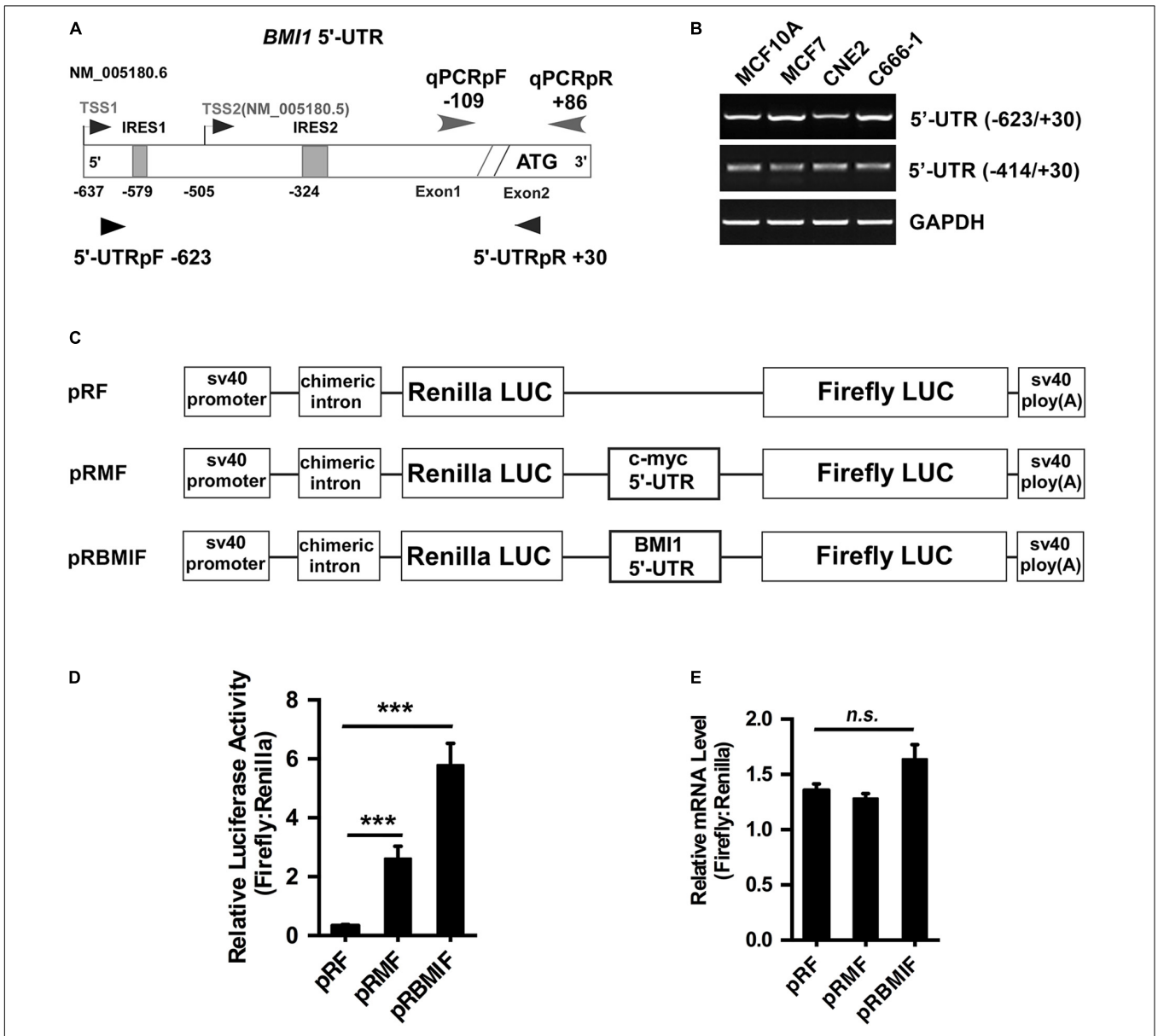

FIGURE 4 | The 5′-UTR promotes the translation of Bmi1 in CNE2 cells. **(A)** Diagram of the full-length Bmi1 5′-UTR. **(B)** The Bmi1 5′-UTR in CNE2, C666-1, MCF7, and MCF10A cells was analyzed by PCR. **(C)** Construction of the dicistronic reporter plasmid. The 5′-UTRs of c-myc and Bmi1 were subcloned between the Renilla and the Firefly luciferase in the dual luciferase vector pRF, named as pRMF and pRBMIF, respectively. The plasmid pRMF served as the positive control. **(D)** The translational activity analysis of the 5′-UTR in CNE2 cells. The plasmids pRF, pRMF, and pRBMIF were transfected into CNE2 cells. Luciferase activity was detected 24 h post-transfection and presented as relative internal ribosome entry sites activity (Firefly luciferase/Renilla luciferase). **(E)** The mRNA expression ratio of Firefly to Renilla luciferase in CNE2 cells. A representative result of three independent experiments is shown ($n = 3$). The graphs show the mean ± SEM. ***$P < 0.001$; Student's *t*-test.

pRF, pRBMI1F, and pRMF were transfected into CNE2 cell lines. As shown in **Figure 4D**, the luciferase activity of Firefly compared to that of Renilla is 20-folds higher in pRBMIF-transfected cells than in pRF-transfected cells. However, there is no significant difference in the ratio of the mRNA level of Firefly to that of Renilla luciferase in CNE2 cells (**Figure 4E**). These results suggested that the Bmi1 5′-UTR can effectively activate Bmi1 translation.

IRES1 and IRES2 Mediate the Translational Activity of the Bmi1 5′-UTR

To investigate whether IRES1 and IRES2 regulate the 5′-UTR mediating Bmi1 translation, IRES1 and IRES2 were point-mutated (**F**igures 5A,B). The mutants of IRES1 and IRES2 were cloned into the pRF plasmid and named as mut-IRES1 and mut-IRES2, respectively. The double mutants of both IRES1 and IRES2 were also constructed and named as mut-IRES1 + 2. These plasmids were transfected into CNE2 cells for 24 h, followed by luciferase assays. As shown in **Figure 5C**, compared to the wild-type control (pRBMIF), the translational activity of mIRES1 and mIRES2 significantly decreased. In addition, double mutations of IRES1 and IRES2 led to an additional decrease in the translational activity, suggesting that both IRES1 and IRES2 were required for the translational activity of the Bmi1 5′-UTR.

DISCUSSION

Bmi1, a component of PRC1, has been implicated in the tumorigenesis of multiple tumors. It is over-expressed and correlated with a poor prognosis in NPC. However, the mechanism underlying its higher expression remains to be investigated. In this study, we found that the mRNA and the protein level of Bmi1 were not strictly consistent in NPC cancer cells and tissues. We then identified two IRES elements which played an important role in the translational activity of the Bmi1 5′ UTR using the dicistronic reporter plasmid assay. These results elucidated a novel post-transcriptional mechanism of Bmi1 (**Figure 1**).

We previously identified the region from +167 to +232 and the region from −536 to −134 as the core promoter

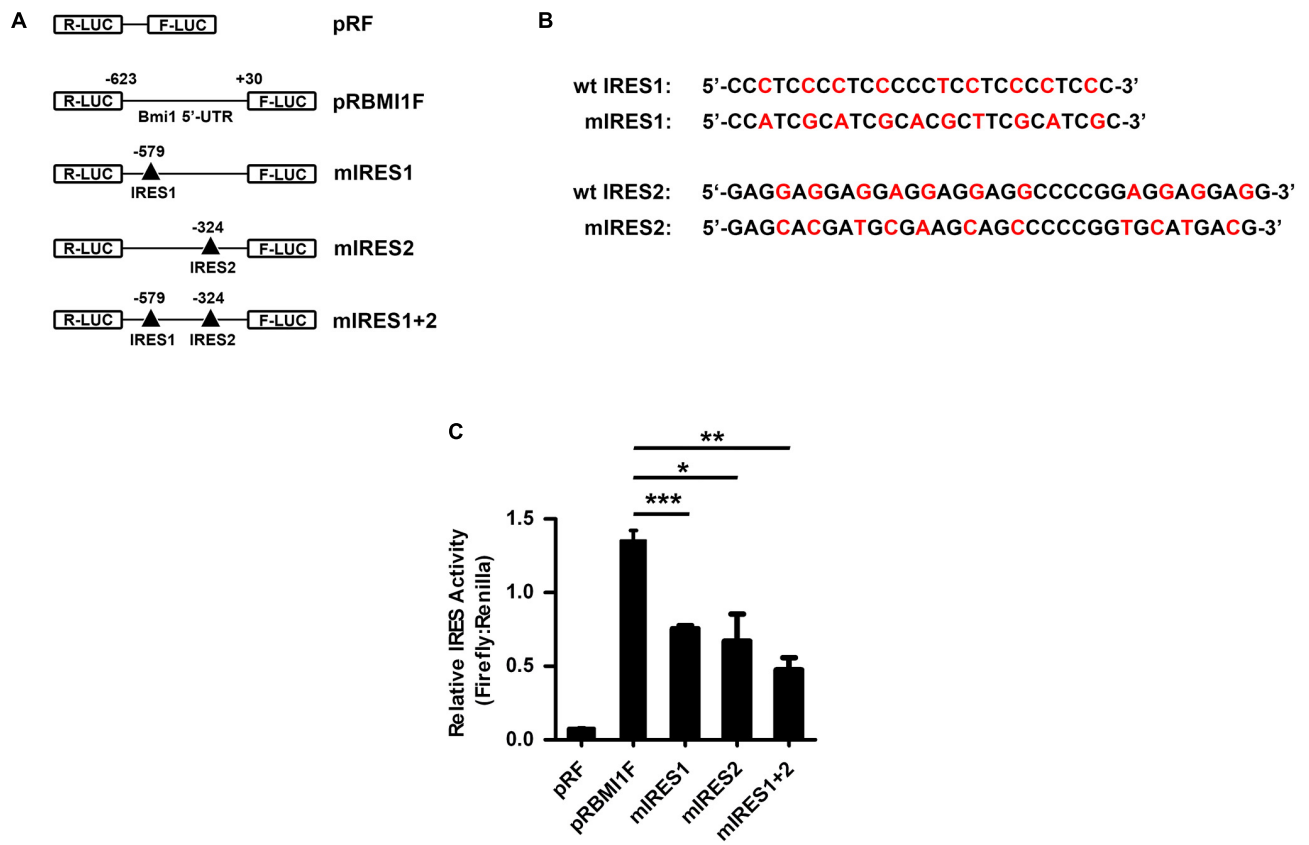

FIGURE 5 | IRES1 and IRES2 mediate the translational activity of 5′-UTR in CNE2 cells. **(A)** Schematic of the potential IRES1 and IRES2 elements in the Bmi1 5′-UTR. The mutation is labeled as "Δ." The IRES1 and IRES2 or double mutations of Bmi1 5′-UTR were subcloned in pRF vector and were designated as mut-IRES1, mut-IRES2, and mut-IRES1 + 2. **(B)** The IRES1 and IRES2 mutant base was labeled as red. **(C)** The translational activity analysis of the IRES 1 and IRES2 mutant 5′-UTR of Bmi1 in CNE2 cells. The plasmids containing the IRES1 and IRES2 mutant 5′-UTR were transfected into CNE2 cells. Luciferase activity was detected at 24 h post-transfection. A representative result of three independent experiments is shown ($n = 3$). The graphs show the mean ± SEM. $^{*}P < 0.05$, $^{**}P < 0.01$, and $^{***}P < 0.001$; Student's *t*-test.

regions of the Bmi1 gene. The transcriptional activity of the Bmi1 promoter is mainly mediated by the Sp1 binding site cluster (+181/+214) and the E-box elements (−181). It is interesting that the Sp1 binding site cluster (+181/+214, the NM 005180.5 transcription start site was assigned as +1) and IRES2 (−324/−291, the translation initiation site ATG was assigned as +1) are the same sites, suggesting that this region may regulate both the transcription and the translation of Bmi1 in NPC cells (17). With the relative transcriptional activity of IRES2, its cryptic promoter activity does not make a significant contribution to Firefly luciferase expression in Bmi1 5′-UTR (**Figure 4E**). To understand the significance of the IRES elements in the regulation of Bmi1 translational activity, the IRES1 and IRES2 motifs were truncated. The translational activity of the IRES mutants was significantly reduced but did not abrogate (**Figure 5**), suggesting that there are additional potential IRESs in the Bmi1 5′-UTR.

To investigate whether there are mutations of IRES1 and IRES2 in the Bmi1 5′UTR, the RNA-seq data from 113 patients with NPC (GSE102349, https://www.ncbi.nlm.nih.gov/geo/query/acc.cgi?acc=GSE102349) were analyzed for the mutation of IRES2 in the Bmi1 5′-UTR. The G/A mutation (GGAG GAGGAGGAGGAGGCCCCGGAGGAGGAGG → AGAGG AGGAGGAGGAGGCCCCGGAGGAGGAGG) was found in the IRES2 motif of the sample (SRR5908825). No mutation was found in the IRES2 motif of the rest of the 112 samples (**Supplementary Figure 1**). It is hard to analyze the mutation in the IRES1 element, which locates nearby the transcription start sites of Bmi1. The data suggested that the mutation of BMI1 IRES is a rare event.

In addition to the IRES element, the ITAFs are required for IRES-mediated cap-independent translation. The expression level of the ITAFs may also affect the translation of Bmi1. Therefore, it is very important to further identify ITAFs and analyze their expression levels in cancer patients. IRES1 and IRES2 form the stem loop structure of KMI1, which could bind to PTBP1 (46). To identify whether PTBP1 regulated the translational activity of the Bmi1 5′ UTR, we assessed the effect of PTBP1 knockdown on Bmi1 expression. Both the mRNA level and the protein level of Bmi1 did not change in the PTBP1-knockdown CNE2 cells. Therefore, it is important to further identify the ITAFs which may regulate the translational activity of Bmi1.

In conclusion, the IRES motifs in the 5′-UTR regulated the translation of Bmi1. The ITAFs–Bmi1 pathway may play an important role in the development of NPC and other tumors. It is urgent to explore the ITAFs that bind to Bmi1 IRES elements and thus regulate the translation of Bmi1. The identification of ITAFs would provide a potential therapeutic target for NPC treatment.

DATA AVAILABILITY STATEMENT

All datasets generated for this study are included in the article/**Supplementary Material**. The authenticity of this article has been validated by uploading the key raw data onto the Research Data Deposit public platform (www.researchdata.org.cn), with the approval number RDDB2020000951.

ETHICS STATEMENT

The studies involving human participants were reviewed and approved by The Institute Research Ethics Committee of Sun Yat-sen University Cancer Center. The patients/participants provided their written informed consent to participate in this study.

AUTHOR CONTRIBUTIONS

MZ, HW, and QZ designed and oversaw the project. HW, YZ, LH, and GL performed the key experiments, analyzed the data, and wrote the manuscript. YiL and DX performed the cell culture and western blotting. BL and YaL performed the immunohistochemistry assays. TX performed the bioinformatic analysis. YH, ML, and YA provided technical support and important materials. All the authors read and approved the final manuscript.

FUNDING

This work was supported by grants from the National Natural Science Foundation of China (grant nos. 81672703, 81402252, 81772883, and 81302037), National Key Research and Development Program (2017YFC0908501), and the Sun Yat-sen University Young Talent Teachers Plan (15ykpy28).

ACKNOWLEDGMENTS

We thank Dr. Anne Willis (University of Leicester, United Kingdom) for gifting us with the dual luciferase vector pRF and pRMF.

SUPPLEMENTARY MATERIAL

The Supplementary Material for this article can be found online at: https://www.frontiersin.org/articles/10.3389/fonc.2020.01678/full#supplementary-material

REFERENCES

1. Wei WI, Sham JS. Nasopharyngeal carcinoma. *Lancet*. (2005) 365:2041–54. doi: 10.1016/S0140-6736(05)66698-6
2. Park IK, Morrison SJ, Clarke MF. Bmi1, stem cells, and senescence regulation. *J Clin Invest*. (2004) 113:175–9. doi: 10.1172/JCI200420800
3. Siddique HR, Saleem M. Role of BMI1, a stem cell factor, in cancer recurrence and chemoresistance: preclinical and clinical evidences. *Stem Cells*. (2012) 30:372–8. doi: 10.1002/stem.1035
4. Hoenerhoff MJ, Chu I, Barkan D, Liu ZY, Datta S, Dimri GP, et al. BMI1 cooperates with H-RAS to induce an aggressive breast cancer phenotype with brain metastases. *Oncogene*. (2009) 28:3022–32. doi: 10.1038/onc.2009.165

5. van Galen JC, Muris JJ, Oudejans JJ, Vos W, Giroth CP, Ossenkoppele GJ, et al. Expression of the polycomb-group gene BMI1 is related to an unfavourable prognosis in primary nodal DLBCL. *J Clin Pathol*. (2007) 60:167–72. doi: 10.1136/jcp.2006.038752
6. Wei Y, Du Y, Chen X, Li P, Wang Y, Zang W, et al. Expression patterns of microRNA-218 and its potential functions by targeting CIP2A and BMI1 genes in melanoma. *Tumour Biol*. (2014) 35:8007–15. doi: 10.1007/s13277-014-2079-6
7. Du J, Li Y, Li J, Zheng J. Polycomb group protein Bmi1 expression in colon cancers predicts the survival. *Med Oncol*. (2010) 27:1273–6. doi: 10.1007/s12032-009-9373-y
8. Hu X, Feng Y, Zhang D, Zhao SD, Hu Z, Greshock J, et al. A functional genomic approach identifies FAL1 as an oncogenic long noncoding RNA that associates with BMI1 and represses p21 expression in cancer. *Cancer Cell*. (2014) 26:344–57. doi: 10.1016/j.ccr.2014.07.009
9. Chiba T, Miyagi S, Saraya A, Aoki R, Seki A, Morita Y, et al. The polycomb gene product BMI1 contributes to the maintenance of tumor-initiating side population cells in hepatocellular carcinoma. *Cancer Res*. (2008) 68:7742–9. doi: 10.1158/0008-5472.CAN-07-5882
10. Qi X, Li J, Zhou C, Lv C, Tian M. MicroRNA-320a inhibits cell proliferation, migration and invasion by targeting BMI-1 in nasopharyngeal carcinoma. *FEBS Lett*. (2014) 588:3732–8. doi: 10.1016/j.febslet.2014.08.021
11. Song LB, Zeng MS, Liao WT, Zhang L, Mo HY, Liu WL, et al. Bmi-1 is a novel molecular marker of nasopharyngeal carcinoma progression and immortalizes primary human nasopharyngeal epithelial cells. *Cancer Res*. (2006) 66:6225–32. doi: 10.1158/0008-5472.CAN-06-0094
12. Meng X, Wang Y, Zheng X, Liu C, Su B, Nie H, et al. shRNA-mediated knockdown of Bmi-1 inhibit lung adenocarcinoma cell migration and metastasis. *Lung Cancer*. (2012) 77:24–30. doi: 10.1016/j.lungcan.2012.02.015
13. Ochiai H, Takenobu H, Nakagawa A, Yamaguchi Y, Kimura M, Ohira M, et al. Bmi1 is a MYCN target gene that regulates tumorigenesis through repression of KIF1Bbeta and TSLC1 in neuroblastoma. *Oncogene*. (2010) 29:2681–90. doi: 10.1038/onc.2010.22
14. Song LB, Li J, Liao WT, Feng Y, Yu CP, Hu LJ, et al. The polycomb group protein Bmi-1 represses the tumor suppressor PTEN and induces epithelial-mesenchymal transition in human nasopharyngeal epithelial cells. *J Clin Invest*. (2009) 119:3626–36.
15. Xu XH, Liu XY, Su J, Li DJ, Huang Q, Lu MQ, et al. ShRNA targeting Bmi-1 sensitizes CD44(+) nasopharyngeal cancer stem-like cells to radiotherapy. *Oncol Rep*. (2014) 32:764–70. doi: 10.3892/or.2014.3267
16. Alajez NM, Shi W, Hui AB, Yue S, Ng R, Lo KW, et al. Targeted depletion of BMI1 sensitizes tumor cells to P53-mediated apoptosis in response to radiation therapy. *Cell Death Differ*. (2009) 16:1469–79. doi: 10.1038/cdd.2009.85
17. Wang HB, Liu GH, Zhang H, Xing S, Hu LJ, Zhao WF, et al. Sp1 and c-Myc regulate transcription of BMI1 in nasopharyngeal carcinoma. *FEBS J*. (2013) 280:2929–44. doi: 10.1111/febs.12299
18. Nowak K, Kerl K, Fehr D, Kramps C, Gessner C, Killmer K, et al. BMI1 is a target gene of E2F-1 and is strongly expressed in primary neuroblastomas. *Nucleic Acids Res*. (2006) 34:1745–54. doi: 10.1093/nar/gkl119
19. Yang MH, Hsu DS, Wang HW, Wang HJ, Lan HY, Yang WH, et al. Bmi1 is essential in Twist1-induced epithelial-mesenchymal transition. *Nat Cell Biol*. (2010) 12:982–92. doi: 10.1038/ncb2099
20. Yang J, Chai L, Liu F, Fink LM, Lin P, Silberstein LE, et al. Bmi-1 is a target gene for SALL4 in hematopoietic and leukemic cells. *Proc Natl Acad Sci USA*. (2007) 104:10494–9. doi: 10.1073/pnas.0704001104
21. Waldron T, De Dominici M, Soliera AR, Audia A, Iacobucci I, Lonetti A, et al. c-Myb and its target Bmi1 are required for p190BCR/ABL leukemogenesis in mouse and human cells. *Leukemia*. (2012) 26:644–53. doi: 10.1038/leu.2011.264
22. Dutton A, Woodman CB, Chukwuma MB, Last JI, Wei W, Vockerodt M, et al. Bmi-1 is induced by the Epstein-Barr virus oncogene LMP1 and regulates the expression of viral target genes in Hodgkin lymphoma cells. *Blood*. (2007) 109:2597–603. doi: 10.1182/blood-2006-05-020545
23. Rao JS, Gopinath S, Malla RR, Alapati K, Gorantla B, Gujrati M, et al. Cathepsin B and uPAR regulate self-renewal of glioma-initiating cells through GLI-regulated Sox2 and Bmi1 expression. *Carcinogenesis*. (2012) 34:550–9. doi: 10.1093/carcin/bgs375
24. Liu S, Tetzlaff MT, Cui R, Xu X. miR-200c inhibits melanoma progression and drug resistance through down-regulation of BMI-1. *Am J Pathol*. (2012) 181:1823–35. doi: 10.1016/j.ajpath.2012.07.009
25. Dimri M, Carroll JD, Cho JH, Dimri GP. microRNA-141 regulates BMI1 expression and induces senescence in human diploid fibroblasts. *Cell Cycle*. (2013) 12:3537–46. doi: 10.4161/cc.26592
26. Wellner U, Schubert J, Burk UC, Schmalhofer O, Zhu F, Sonntag A, et al. The EMT-activator ZEB1 promotes tumorigenicity by repressing stemness-inhibiting microRNAs. *Nat Cell Biol*. (2009) 11:1487–95. doi: 10.1038/ncb1998
27. Bhattacharya R, Nicoloso M, Arvizo R, Wang E, Cortez A, Rossi S, et al. MiR-15a and MiR-16 control Bmi-1 expression in ovarian cancer. *Cancer Res*. (2009) 69:9090–5. doi: 10.1158/0008-5472.CAN-09-2552
28. Zhu Y, Yu F, Jiao Y, Feng J, Tang W, Yao H, et al. Reduced miR-128 in breast tumor-initiating cells induces chemotherapeutic resistance via Bmi-1 and ABCC5. *Clin Cancer Res*. (2011) 17:7105–15. doi: 10.1158/1078-0432.CCR-11-0071
29. Sahasrabuddhe AA, Dimri M, Bommi PV, Dimri GP. betaTrCP regulates BMI1 protein turnover via ubiquitination and degradation. *Cell Cycle*. (2011) 10:1322–30. doi: 10.4161/cc.10.8.15372
30. Zhang J, Sarge KD. Identification of a polymorphism in the RING finger of human Bmi-1 that causes its degradation by the ubiquitin-proteasome system. *FEBS Lett*. (2009) 583:960–4. doi: 10.1016/j.febslet.2009.02.023
31. Yadav AK, Sahasrabuddhe AA, Dimri M, Bommi PV, Sainger R, Dimri GP. Deletion analysis of BMI1 oncoprotein identifies its negative regulatory domain. *Mol Cancer*. (2010) 9:158. doi: 10.1186/1476-4598-9-158
32. Hoffman MA, Palmenberg AC. Mutational analysis of the J-K stem-loop region of the encephalomyocarditis virus IRES. *J Virol*. (1995) 69:4399–406. doi: 10.1128/JVI.69.7.4399-4406.1995
33. Schmid M, Wimmer E. IRES-controlled protein synthesis and genome replication of poliovirus. *Arch Virol Suppl*. (1994) 9:279–89. doi: 10.1007/978-3-7091-9326-6_28
34. Jackson RJ. The current status of vertebrate cellular mRNA IRESs. *Cold Spring Harb Perspect Biol*. (2013) 5:a011569. doi: 10.1101/cshperspect.a011569
35. Komar AA, Hatzoglou M. Cellular IRES-mediated translation: the war of ITAFs in pathophysiological states. *Cell Cycle*. (2011) 10:229–40. doi: 10.4161/cc.10.2.14472
36. Cobbold LC, Wilson LA, Sawicka K, King HA, Kondrashov AV, Spriggs KA, et al. Upregulated c-myc expression in multiple myeloma by internal ribosome entry results from increased interactions with and expression of PTB-1 and YB-1. *Oncogene*. (2010) 29:2884–91. doi: 10.1038/onc.2010.31
37. Pickering BM, Mitchell SA, Evans JR, Willis AE. Polypyrimidine tract binding protein and poly r(C) binding protein 1 interact with the BAG-1 IRES and stimulate its activity in vitro and in vivo. *Nucleic Acids Res*. (2003) 31:639–46. doi: 10.1093/nar/gkg146
38. Bonnal S, Pileur F, Orsini C, Parker F, Pujol F, Prats AC, et al. Heterogeneous nuclear ribonucleoprotein A1 is a novel internal ribosome entry site trans-acting factor that modulates alternative initiation of translation of the fibroblast growth factor 2 mRNA. *J Biol Chem*. (2005) 280:4144–53. doi: 10.1074/jbc.M411492200
39. Jo OD, Martin J, Bernath A, Masri J, Lichtenstein A, Gera J. Heterogeneous nuclear ribonucleoprotein A1 regulates cyclin D1 and c-myc internal ribosome entry site function through Akt signaling. *J Biol Chem*. (2008) 283:23274–87. doi: 10.1074/jbc.M801185200
40. Kim JH, Paek KY, Choi K, Kim TD, Hahm B, Kim KT, et al. Heterogeneous nuclear ribonucleoprotein C modulates translation of c-myc mRNA in a cell cycle phase-dependent manner. *Mol Cell Biol*. (2003) 23:708–20. doi: 10.1128/MCB.23.2.708-720.2003
41. Marash L, Liberman N, Henis-Korenblit S, Sivan G, Reem E, Elroy-Stein O, et al. DAP5 promotes cap-independent translation of Bcl-2 and CDK1 to facilitate cell survival during mitosis. *Mol Cell*. (2008) 30:447–59. doi: 10.1016/j.molcel.2008.03.018
42. Evans JR, Mitchell SA, Spriggs KA, Ostrowski J, Bomsztyk K, Ostarek D, et al. Members of the poly (rC) binding protein family stimulate the activity of the c-myc internal ribosome entry segment in vitro and in vivo. *Oncogene*. (2003) 22:8012–20. doi: 10.1038/sj.onc.1206645
43. Wang HB, Zhang H, Zhang JP, Li Y, Zhao B, Feng GK, et al. Neuropilin 1 is an entry factor that promotes EBV infection of nasopharyngeal epithelial cells. *Nat Commun*. (2015) 6:6240. doi: 10.1038/ncomms7240

44. Russell D, Sambrook J. *Molecular Cloning: A Laboratory Manual (Third Edition)*. Cold Spring Harbor, NY: Cold Spring Harbor Laboratory Press. (2000).
45. Mokrejs M, Masek T, Vopalensky V, Hlubucek P, Delbos P, Pospisek M. IRESite–a tool for the examination of viral and cellular internal ribosome entry sites. *Nucleic Acids Res*. (2010) 38:D131–6. doi: 10.1093/nar/gkp981
46. Mitchell SA, Spriggs KA, Bushell M, Evans JR, Stoneley M, Le Quesne JP, et al. Identification of a motif that mediates polypyrimidine tract-binding protein-dependent internal ribosome entry. *Genes Dev*. (2005) 19:1556–71. doi: 10.1101/gad.339105

Conflict of Interest: The authors declare that the research was conducted in the absence of any commercial or financial relationships that could be construed as a potential conflict of interest.

frontiers in Oncology

ORIGINAL RESEARCH
published: 24 September 2020
doi: 10.3389/fonc.2020.518110

Role of IMRT/VMAT-Based Dose and Volume Parameters in Predicting 5-Year Local Control and Survival in Nasopharyngeal Cancer Patients

Nicola Alessandro Iacovelli[1†], Alessandro Cicchetti[2†], Anna Cavallo[3], Salvatore Alfieri[4], Laura Locati[4], Eliana Ivaldi[1], Rossana Ingargiola[1], Domenico A. Romanello[1], Paolo Bossi[4], Stefano Cavalieri[4], Chiara Tenconi[3], Silvia Meroni[3], Giuseppina Calareso[5], Marco Guzzo[6], Cesare Piazza[6], Lisa Licitra[4,7], Emanuele Pignoli[3], Fallai Carlo[1] and Ester Orlandi[1,8]*

[1] Radiotherapy Unit 2, Fondazione IRCCS Istituto Nazionale dei Tumori di Milano, Milan, Italy, [2] Prostate Cancer Program, Fondazione IRCCS Istituto Nazionale dei Tumori di Milano, Milan, Italy, [3] Medical Physics Unit, Fondazione IRCCS Istituto Nazionale dei Tumori di Milano, Milan, Italy, [4] Head and Neck Medical Oncology Unit, Fondazione IRCCS Istituto Nazionale dei Tumori di Milano, Milan, Italy, [5] Department of Radiology, Fondazione IRCCS Istituto Nazionale dei Tumori di Milano, Milan, Italy, [6] Department of Otolaryngology, Head and Neck Surgery, Fondazione IRCCS, Istituto Nazionale dei Tumori di Milano, Milan, Italy, [7] Department of Oncology and Hemato-Oncology, University of Milan, Milan, Italy, [8] Radiotherapy Unit 1, Fondazione IRCCS Istituto Nazionale dei Tumori, Milan, Italy

Objective: This study aimed to look into the relationship between intensity-modulated-radiotherapy (IMRT)- or volumetric-modulated-arc-therapy (VMAT)-based dose–volume parameters and 5-year outcome for a consecutive series of non-metastatic nasopharyngeal cancer (NPC) patients (pts) treated in a single institution in a non-endemic area in order to identify potential prognostic factors.

Materials and methods: A retrospective analysis of consecutive non-metastatic NPC pts treated curatively with IMRT or VMAT and chemotherapy (CHT) between 2004 and 2014 was conducted. One patient was in stage I (0.7%), and 24 pts (17.5%) were in stage II, 38 pts (27.7%) in stage III, 29 pts (21.2%) in stage IVA, and 45 pts (32.8%) in stage IVB. Five pts (3.6%) received radiotherapy (RT) alone. Of the remaining 132 pts (96.4%), 30 pts (21.9%) received CHT concomitant to RT, and 102 pts (74.4%) were treated with induction CHT followed by RT-CHT. IMRT was given with standard fractionation at a total dose of 70 Gy. Clinical outcomes investigated in the study were local control (LC), disease-free survival (DFS), and overall survival (OS). Kaplan–Meier (KM) analysis was performed for the outcomes considering dose and coverage parameters, staging, and RT technique.

Results: Overall, 137 pts were eligible for this retrospective analysis. With a median follow-up of 70 months (range 12–143), actuarial rates at 5 years were LC 90.4, DFS 77.2, and OS 82.8%. For this preliminary study, T stage was dichotomized as T1, T2, T3 vs. T4. At 5 years, the group T1–T2–T3 reported an LC of 93%, a DFS of 79%, and an OS of 88%, whereas T4 pts reported LC, DFS, and OS, respectively, of 56, 50, and 78%. Pts with V95% > 95.5% had better LC ($p = 0.006$). Pts with D99% > 63.8 Gy had better LC ($p = 0.034$) and OS ($p = 0.005$). The threshold value of 43.2 cm^3 of GTVT

OPEN ACCESS

Edited by:
Jun Ma,
Sun Yat-sen University Cancer Center (SYSUCC), China

Reviewed by:
Ying Sun,
Sun Yat-sen University Cancer Center (SYSUCC), China
Chaosu Hu,
Fudan University, China

***Correspondence:**
Anna Cavallo
anna.cavallo@istitutotumori.mi.it

[†] These authors have contributed equally to this work

Specialty section:
This article was submitted to Head and Neck Cancer, a section of the journal Frontiers in Oncology

Received: 06 December 2019
Accepted: 17 August 2020
Published: 24 September 2020

Citation:
Iacovelli NA, Cicchetti A, Cavallo A, Alfieri S, Locati L, Ivaldi E, Ingargiola R, Romanello DA, Bossi P, Cavalieri S, Tenconi C, Meroni S, Calareso G, Guzzo M, Piazza C, Licitra L, Pignoli E, Carlo F and Orlandi E (2020) Role of IMRT/VMAT-Based Dose and Volume Parameters in Predicting 5-Year Local Control and Survival in Nasopharyngeal Cancer Patients. Front. Oncol. 10:518110. doi: 10.3389/fonc.2020.518110

was prognostic for LC ($p = 0.016$). To predict the risk of local recurrence at 5 years, we constructed a nomogram which combined GTVT with D99% relative to HRPTV.

Conclusions: We demonstrated the prognostic value of some dose–volume parameters, although in a retrospective series, this is potentially useful to improve planning procedure. In addition, for the first time in a non-endemic area, a threshold value of GTVT, prognostic for LC, has been confirmed.

Keywords: nasopharyngeal carcinoma (NPC), intensity-modulated radiation therapy (IMRT), gross tumor volume (GTV), dose-volume parameters, outcomes, nomogram, volumetric-modulated arc therapy (VMAT)

INTRODUCTION

Intensity modulated radiation therapy (IMRT) is an important milestone in the management of nasopharyngeal carcinoma (NPC), providing lowered frequency of serious radiation-induced late toxicities without compromising local control (LC) and survival compared to previous radiotherapy (RT) techniques (1). A radiation–dose response for NPC has been demonstrated with dose escalation of IMRT-based therapy by using both additional sequential boost over 66 Gy (2) and increasing biologically equivalent doses up to over 70 Gy by simultaneous integrated boost (SIB) IMRT (3–5). Still, the outcomes after IMRT remain unsatisfactory in T4 tumors, most of all because their proximity to critical neurological structures compromises planning target coverage and therefore undermines LC. In the most recently published NPC series, concerning endemic regions and providing the longest follow-ups to date, T1–T3 diseases had excellent LC unlike T4 lesions (6–8). Also, T4 patients are well-known to be at high risk of developing distant metastases or even dying, so they require an aggressive systemic approach by adding induction and/or adjuvant chemotherapy (CHT) (9–12). Assuming that CHT may make up for coverage defects of the target volume, it is still hard to set a benchmark for dosimetric adequacy. As a matter of fact, data correlating IMRT-based dose parameters and outcome are scanty, making it difficult to identify their potential prognostic role.

Even in the IMRT era, the therapeutic choice in NPC cases is primarily driven by the tumor–node–metastasis (TNM) staging system. Several previous studies from endemic regions have described some indicators resulting from imaging, i.e., gross tumor volume (GTV) of primary tumor as defined by magnetic resonance imaging (MRI), as prognosticators with a potential to increase the precision of TNM criteria (13–15). However, in low-incidence areas, the impact of primary tumor GTV has never been investigated.

The first aim of this study was to look into the relationship between IMRT- or volumetric-modulated-arc-therapy (VMAT)-based dose and volume parameters and outcome at 5 years for a consecutive series of NPC patients treated in a single institution in a non-endemic area, in order to identify potential prognostic factors. Secondly, we aimed to establish novel target volume constraints for planning optimization.

MATERIALS AND METHODS

Study Population

From May 2004 to April 2014, 160 consecutive patients with non-metastatic NPC received curative IMRT or VMAT with or without CHT at our institution. Eligibility criteria for this retrospective analysis were as follows: a minimum follow-up of 5 years, MRI before any treatment, and availability of full clinical and dosimetric data. Thus, 137 patients out of 160 met the inclusion criteria and were considered for this analysis. Over the course of the analysis, all patients were restaged according to the AJCC 2010 staging classification seventh edition (16). This study was approved by the ethics committee of the "Fondazione IRCCS Istituto Nazionale dei Tumori di Milano," and all patients signed an informed consent to use their data for research purposes in line with the policy of our institution. The study was performed in accordance with the ethical standards laid down in the 1975 Declaration of Helsinki and all subsequent revisions.

Treatment

Radiotherapy

Details of target volume delineation and IMRT planning and delivery procedures have been previously reported (17). There were no changes in delineation strategies during the entire study period. In synthesis, GTV included nasopharyngeal primary tumor and involved lymph nodes as demonstrated by clinical, endoscopic, and imaging data (MRI and ^{18}F-FDG PET/CT), i.e., global GTV (gGTV). For this study purpose, we retrospectively contoured the following GTVs separately: nasopharyngeal primary tumor (GTVT) and involved nodes (GTVN), deriving from the sum of involved lymph nodes including retropharyngeal involved nodes (GTVNRP) and involved nodes other than retropharyngeal (GTVNNRP). For patients receiving induction CHT (iCHT), all GTVs were contoured on pre-CHT magnetic resonance images.

A high-risk (HR) clinical target volume (CTV), including both GTVT and GTVN with an anisotropic margin ranging from 0 to 25 mm taking into account subclinical disease, and a low-risk (LR) CTV have been defined for all patients, whereas an intermediate-risk (IR) CTV was contoured in selected cases. Planning target volumes (PTVs) were generated by adding a 3-mm margin to corresponding CTVs, i.e., high-dose (HD) PTV (HDPTV), intermediate-dose (ID) PTV (IDPTV), and low-dose (LD) PTV (LDPTV). The goal for HDPTV was usually to deliver

at least 95% of the prescribed dose (PD) to at least 95% of HDPTV without exceeding tolerance doses to neurological organs at risk (n-OARs).

During the study period, RT was given with conventional fractionation (2–2.12 Gy per fraction) according to some technical approaches. From 2004 to 2009, IMRT was routinely delivered with the step-and-shoot technique with a 7-coplanar 6-MV photon beam arrangement. Two approaches were used: (i) a purely sequential (SEQ) approach, with conventional fractionation (2 Gy per fraction) up to 50–54 Gy to LDPTV and 70 Gy to HDPTV; and (ii) a mixed approach SEQ-SIB, which comprised a first phase of 30 fractions of 1.8 Gy to LDPTV (PD = 54 Gy) and 2–2.12 Gy to HDPTV (PD = 60–63.6 Gy) followed by a boost of five 2-Gy or three 2.12-Gy fractions to HDPTV (PD = 70 Gy). When defined, IDPTV received 60–66 Gy with 2-Gy fractions in either SEQ or SEQ-SIB mode. Since 2009, VMAT, with two to four coplanar arcs, has been gradually implemented in our practice, eventually becoming the standard technique for this disease in our center. A SIB regimen was given in 33 fractions with a PD of 69.96 and 56.1 Gy to HDPTV and LDPTV, respectively. When defined, IDPTV was planned to receive 59.4 Gy in 33 fractions.

For PTV coverage, the following parameters were recorded unrelated to the RT technique: minimum dose (D99%), maximum dose (D1%), mean dose (DMean), and the percentage of target volume receiving 95% (V95%) and 100% (V100%) of its PD.

Chemotherapy

Patients at stages I and IIA received exclusive RT, whereas patients at stages IIB–III–IV received concomitant platinum-based CHT. iCHT with docetaxel, cisplatin, and 5-fluorouracil was added to patients with a potential higher risk of distant metastasis, according to our previously reported institutional policies (18).

Follow-up

After RT completion, patients were clinically evaluated at predefined intervals, typically every 3–6 months for the first 3 years and annually thereafter. MRI and ^{18}F-FDG-PET were prescribed on a regular basis and when deemed necessary according to patients' disease status.

Statistical Analysis

Survival and recurrence time observations were plotted according to the Kaplan–Meier method starting from the first day of treatment (CHT or RT, whichever came first). Overall survival (OS) was defined as the time from treatment start until death from any cause. Disease-free survival (DFS) was defined as the time from treatment start to disease recurrence or death. LC was defined as the time from treatment start until local recurrence. Actuarial 5-year rates of LC, DFS and OS were calculated.

The following dose and volume parameters for HDPTV were studied as potential prognostic factors of OS, DFS, and LC: D99, D1%, DMean, V95, and V100% of the PD. This is because recurrences occurred mostly "in field" or were classified as "marginal" to HDPTV (17). Moreover, GTVT, GTVN, GTVNNRP, GTVNRP, and RT technique—conventional IMRT vs. VMAT—were investigated.

TABLE 1 | Clinical and treatment-related characteristics of the 137 patients included in the study.

		Total	Percentage (%) or range
All patients		137	100
Sex	Male	96	70.1
	Female	41	29.9
Age (median)		49	18–92
ECOG	0–1	131	95.6
	2	6	4.4
Histology	Keratinizing squamous cell carcinoma (WHO type 1)	1	0.7
	Non-keratinizing (WHO type 2)	2	1.5
	Undifferentiated (WHO type 2)	134	97
Neck surgery*		22	16.1
Stage T	1	48	35.0
	2	31	22.6
	3	19	13.9
	4	39	28.5
Stage N	0	4	2.9
	1	29	21.2
	2	59	43.1
	3a	14	10.2
	3b	31	22.6
Stage	I	1	0.7
	II	24	17.5
	III	38	27.7
	IVA	29	21.2
	IVB	45	32.9
Treatment	RT alone	5	3.6
	RT-CHT	30	21.9
	iCHT + RT-CHT	102	74.5
RT technique	IMRT	73	53.3
	VMAT	64	46.7
b-EBV-DNA**	Median	510	0–150,075
	Negative (pts)	36	29.3
	UQ + Q + Q^+ (pts)	87	70.7

ECOG, Eastern Cooperative Oncology Group.

**Excisional biopsy or functional or radical laterocervical dissection.*

***Only 123 patients out of 137; b-EBV-DNA was stratified into four groups: negative (b-EBV-DNA = 0); UQ, positive but unquantifiable (0 < b-EBV-DNA < 102 copies per milliliter); Q, positive and quantifiable (102 ≤ b-EBV-DNA ≤ 15 × 102 copies per milliliter); Q^+, strongly positive and quantifiable (b-EBV-DNA > 15 × 102 copies per milliliter). For details, see Alfieri et al. (18).*

We looked into correlations between HDPTV parameters and LC and not LRC because difficulties in target volume coverage are linked in particular with primary tumor extension (in particular T4) rather than nodal disease.

The maximal chi-square method was used to determine the optimal cutoff values for the association between continuous parameters and clinical outcomes. Thus, each feature has been dichotomized according to the quartile of their distribution closest to the derived best cutoff. Kaplan–Meier actuarial curves were generated for the significant parameters (with a $p < 0.05$ resulting from the *t*-test), and a log-rank test was used to verify if curve separation was statistically significant ($p < 0.05$) even considering the time dependence of the corresponding survival curve. Univariable Cox regression analysis was performed to estimate the hazard ratio (HR) associated with the variables.

Univariate and multivariate Cox regression analyses were finally performed for 5-year rates of OS, DFS, and LC including all the dosimetric variables and the following clinical factors: T stage, N stage, and overall stage. The latter were dichotomized as T1–T2–T3 vs. T4, N0–N1–N2 vs. N3a–N3b, and stages I–II–III vs. IVA–IVB. For that analysis, patients with an event within 5 years were selected together with those who are event free and had a minimum follow-up of 5 years. Finally, a nomogram was computed starting from the Cox proportional hazard regression model.

All statistical analyses were performed in the KNIME environment (KNIME GmbH, Germany) coupled to R software (www.r-project.org).

RESULTS

Clinical and treatment-related characteristics of the 137 patients included in this study are shown in **Table 1**. One patient was in stage I (0.7%), and 24 patients (17.5%) were in stage II, 38 patients (27.7%) in stage III, 29 patients (21.2%) in stage IVA, and 45 patients (32.8%) in stage IVB. In particular, 39 patients (28.5%) were stage T4.

As for CHT, five patients out of 137 did not receive CHT according to disease stage. Thirty patients out of 137 received concomitant platinum-based CHT with a median cumulative platinum dose of 225 mg/sm (range 150–300 mg/sm; mean 244 mg/sm). iCHT was administered in 102 out of 137 patients followed by concomitant CHT; 100 patients received TP schedule with or without 5FU, and two patients received PF schedule. All patients continued with platinum-based CHT concomitant to RT, with a median cumulative platinum dose of 250 mg/sm (range 50–300 mg/sm; mean 235 mg/sm).

The median follow-up period was 75.2 months (range: 12–141.1 months). Actuarial rates at 5 and 8 years were, respectively, 90.4 and 88.1% for LC, 77.2 and 74.3% for DFS, and 82.8 and 82.8% for OS. OS, DFS, and LC curves for the entire population are shown in **Figure 1**.

Sixteen out of 137 patients developed distant metastases (11.7 %) during the follow-up period, with three of them showing also a local recurrence of the disease.

Dose and volume statistics for the entire population are shown in **Table 2**. *t*-test results for parameter selection are reported in the (**Supplementary Table 1**) together with the distribution of the dosimetric variables selected for survival analysis in terms of mean value and standard deviation, stratified according to OS, DFS, and LC (**Supplementary Table 2**).

The results of univariate Cox regression analysis for LC, DFS, and OS on the whole set of parameters are reported in **Supplementary Tables 3–5**.

As for RT parameters, we found that V95, V100, D99, DMean relative to HDPTV and GTVT, and RT technique were significant for LC, and V95% relative to HDPTV and RT technique were significant for DFS. Finally, V95, V100, D99% relative to HDPTV, and RT technique were significant for OS.

Figure 2 shows the survival curves for the independent prognostic parameters common to all the analyzed outcomes: HDPTV V95, V100, and D99%. Due to the natural correlation between V95 and V100%, we decided to select HDPTV V95%

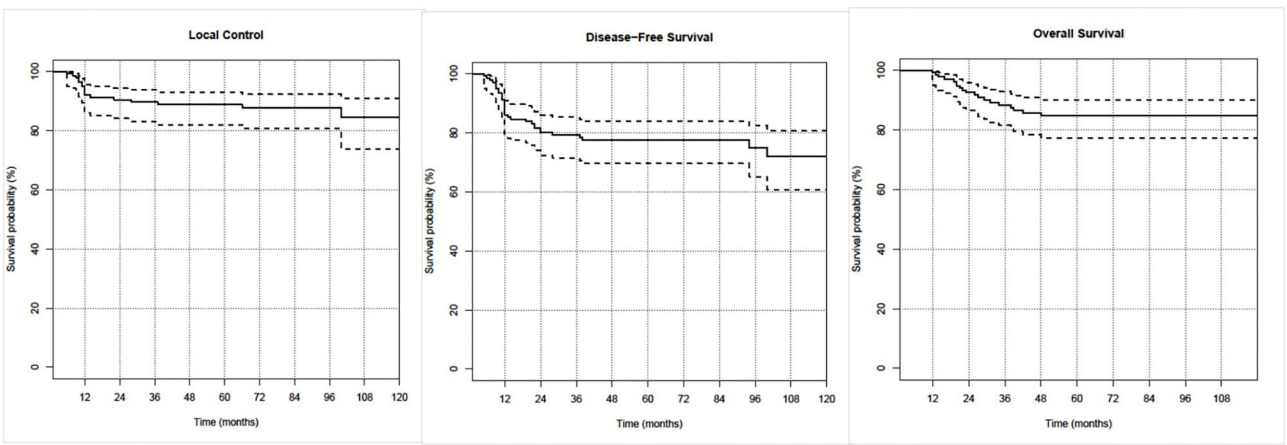

FIGURE 1 | Kaplan–Meier curves of the three investigated clinical outcomes.

TABLE 2 | Dose and volume statistics.

Variable	Mean ± SD	Range (min–max)	I quartile	Median	III quartile
GTVT (cm^3)	33.3 ± 34.8	2.2–173.3	7.6	21.1	43.2
GTVN (cm^3)	39.9 ± 47.9	0.2–332.7	9.0	25.1	55.2
GTVNRP (cm^3)	5.1 ± 8.1	0.2–43.3	2.2	4.0	9.7
GTVNNRP (cm^3)	34.6 ± 45.7	0.5–326.1	7.5	21.0	47.7
V95% (HDPTV) (%)	93.5 ± 15.0	16.1–100.0	95.5	98.4	99.7
V100% (HDPTV) (%)	60.3 ± 24.7	0–99.5	47.8	62.5	79.6
D1% (HDPTV) (Gy)	74.3 ± 2.5	67.8–84.3	72.9	74.3	75.4
D99% (HDPTV) (Gy)	65.2 ± 3.0	53.6–70.4	63.8	65.9	67.5
DMean (HDPTV) (Gy)	70.3 ± 1.7	65.1–75.7	69.8	70.4	71.1
HDPTV Volume (cm^3)	295.1 ± 140.2	58.1–833.0	188.0	289.0	378.0

for its major clinical–dosimetric value, which also had the lowest *p*-value. Variables were then dichotomized as described before (quartile closest to the best cutoff). In particular, HDPTV V95 and D99% were dichotomized according to the second and first quartiles of their distribution, respectively, for OS, the third quartile for DFS, and the first quartile for LC. HR and log-rank *p*-value for the new dichotomized variables were also reported in the figure.

In particular, different cutoffs of dose–volume parameters were found to be prognostic for the three outcomes considered: V95% higher than 98.4, 95.5, and 99.75% led to statistically better OS, LC, and DFS, respectively; D99% higher than 63.8, 63.8, and 67.5 Gy guaranteed statistically better OS, LC, and DFS, respectively.

Another significant RT parameter for LC was GTVT (HR = 3.07 and $p = 0.015$), which was dichotomized to its third quartile. Patients with GTVT bigger than 43.2 cm^3 had worse LC (**Supplementary Figure 1**). As mentioned before, all outcomes were significantly better with VMAT compared to step-and-shoot IMRT (**Supplementary Figure 1**).

Among clinical parameters, we found overall stage and T stage as significant prognosticators for LC and DFS, respectively (**Supplementary Figure 1**).

In addition, we found significant differences for patients treated with different RT modalities and for patients with different T stages. **Table 3** shows the corresponding actuarial rates at 5 years for LC, DFS, and OS.

As a consequence, we decided to perform a subanalysis of the survival curves as a function of T stage (T1–T2–T3 vs. T4) and RT technique (VMAT vs. IMRT). A new combined variable, obtained from the two parameters, was studied in terms of survival: the results for the four groups are shown in **Figure 3**. Forty-one T1–T2–T3 and 23 T4 stage patients were treated with VMAT, while 57 T1–T2–T3 and 16 T4 stage patients were treated with IMRT. In particular, T4 stage patients treated with VMAT had similar survival rates compared to patients with T1–T2–T3 stages treated with step-and-shoot IMRT.

The group of T1–T2–T3 stage patients treated with VMAT (the group with best outcomes) was considered as reference for HR computing in the other patients' groups. This was not possible for LC (**Figure 3B**), where the reference group did not have any event (making it impossible to compute HR). However, it is easily understandable that HRs should be similar (but higher) to the OS ones. For this specific case, T4 stage patients treated with VMAT were considered as reference in HR computing.

Moreover, we can see how the curves of intermediate groups (T1–T2–T3 stages treated with IMRT and T4 stage treated with VMAT) are similar in LC and DFS but not in OS.

The distribution of the significant dose–volume parameters for the four groups is shown in **Figure 4**.

Finally, we decided to work with a multivariable model which took into account continuous (dosimetric or volumetric variables) or ordinal variables (stage and T stage). Due to the limited number of events, we tested all the possible models with two covariates that were found significant in univariate analysis (see **Supplementary Materials**). A bivariate model including GTVT and HDPTV D99% was found for LC. Hazard ratios for GTVT and HDPTV D99% as continuous variables in the bivariate model were 1.01 (*p*-value 0.04) and 0.88 (*p*-value 0.04), respectively. Area under the ROC curve for this model was 0.74, while it was 0.68 for the two univariate models with GTVT or HDPTV D99% (HRs were 1.01 with a *p*-value of 0.01 and 0.86 with a *p*-value of 0.01).

A nomogram for the risk of LC at 5 and 8 years (**Figure 5**) was derived from the two-variable Cox regression model.

DISCUSSION

To our knowledge, this series had the longest follow-up for an NPC patient cohort in a low-incidence area.

Clinical outcomes were consistent with NPC series treated with IMRT and CHT reported in literature in endemic areas (6–8). Au and colleagues reported 5- and 8-year LC of 88.7% and 85.8%, progression-free survival (PFS) of 70.2 and 62.6%, OS of 78.2 and 68.5%, respectively. Sun et al. analyzing the prognostic factors in a series of 868 NPC patients showed 5-year disease-specific survival (DSS), local recurrence-free survival (LRFS), and PFS rates up to 84.7, 91.8, and 77.0%, respectively. As in these series, we confirmed the adverse prognostic role of advanced overall stage and T4 stage. However, treatment-related

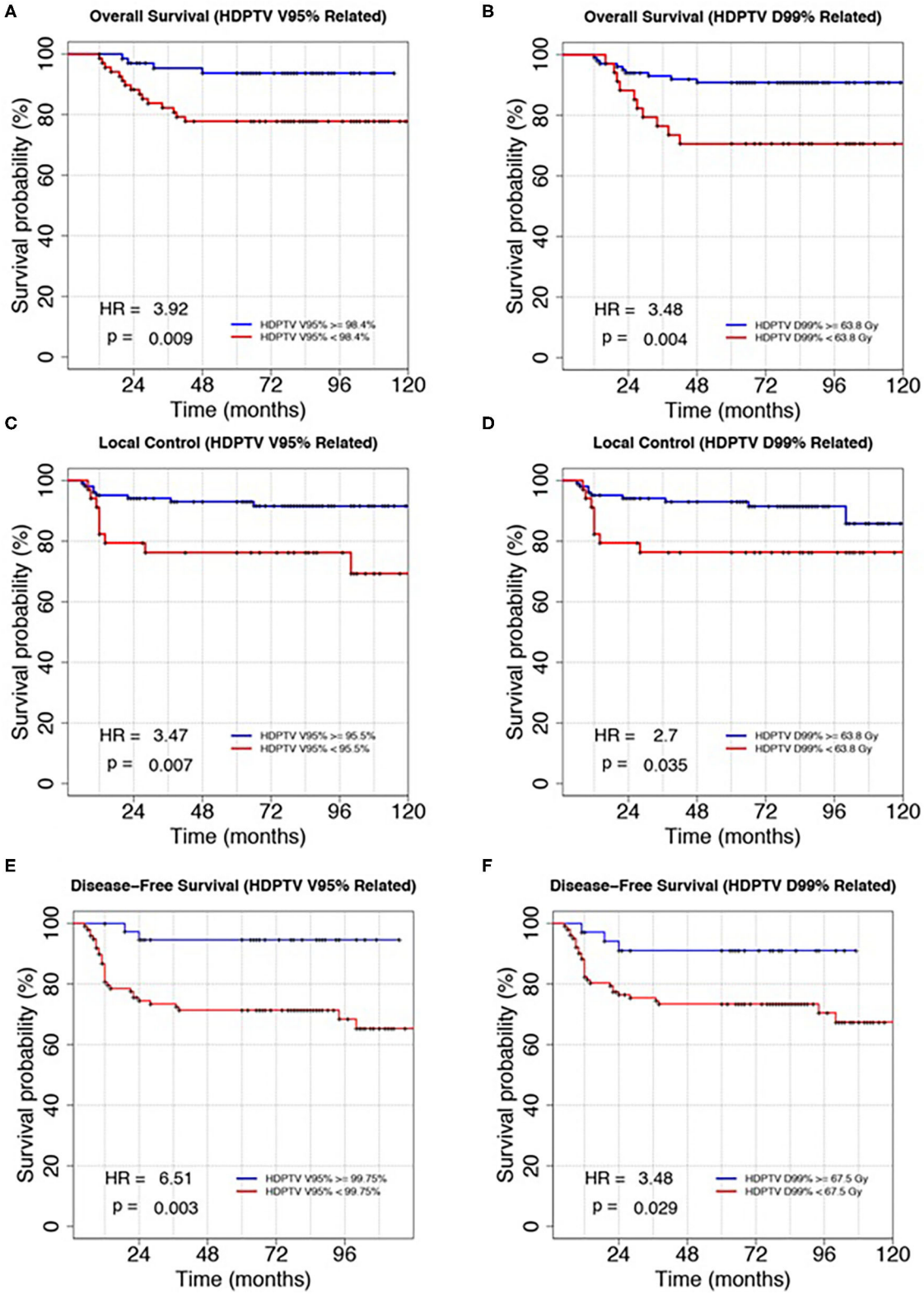

FIGURE 2 | Kaplan–Meier plots of overall survival, local control, and disease-free survival discriminating patients according to the HDPTV V95% **(A,C,E)** and HDPTC D99% **(B,D,F)**. Variables were dichotomized according to the method described in the main text. Hazard ratio (HR) and log-rank *p*-value were reported in the bottom left corner of each plot.

TABLE 3 | Statistical values of KM analysis for the three outcomes: survival rates, hazard ratios, and *p*-values.

Parameter		LC (%)	LC stat.	DFS (%)	DFS stat.	OS (%)	OS stat.
T1–T2–T3	98/137	93.9	HR = 5.64, $p < 0.001$	81.6	HR = 2.36, $p = 0.017$	88.9	HR = 2.04, $p = 0.12$
T4	39/137	71.8		64.4		79.5	
VMAT	64/137	95.3	HR = 3.76, $p = 0.027$	89.1	HR = 3.02, $p = 0.007$	96.9	HR = 7.35, $p = 0.03$
IMRT	73/137	80.8		65.8		76.7	

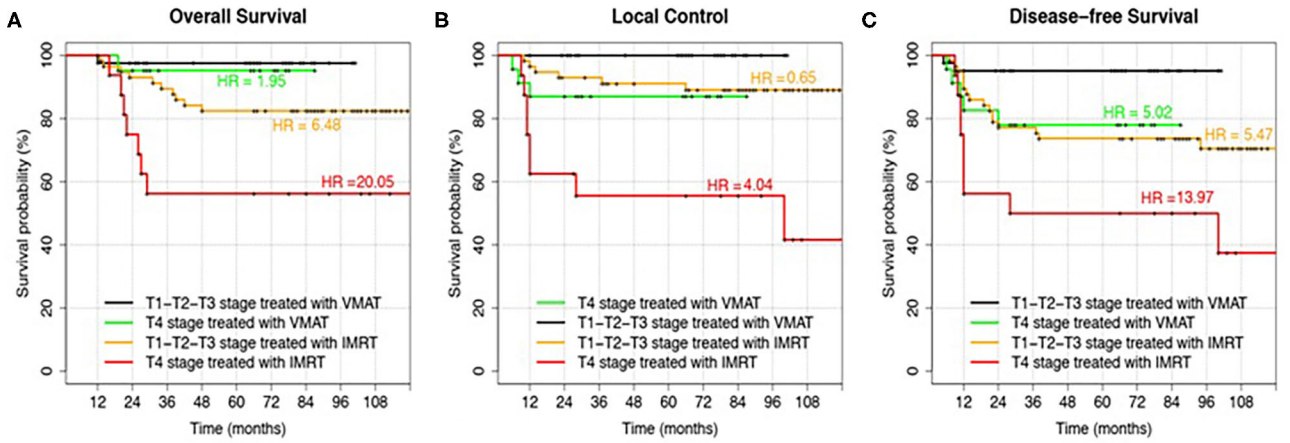

(%OS - %LC - %DFS)	VMAT	IMRT	*T-stage alone*
T1-T2-T3	41 (98-100-95)	57(82-89-72)	*98(89-94-82)*
T4	23(96-87-78)	16(56-50-44)	*39(79-72-64)*
RTT alone	*64(97-95-89)*	*73(77-71-66)*	137(86-88-77)

FIGURE 3 | Kaplan–Meier curves for the analyzed outcomes: Overall Survival **(A)**, Local Control **(B)** and Disease-free Survival **(C)**. Patients were stratified according to the T-stage (T1–T2–T3 vs T4) and RT modality (IMRT vs VMAT). Hazard Ratio (HR) for the comparison of each group with the low-risk class (T1–T2–T3 treated with VMAT) were reported. In Local Control, HR were computed using T4 treated with VMAT as reference since no events were recorded in the low-risk class. HR = 1.95 and HR = 0.65 had a *p*-value > 0.05. HR = 5.02 had a *p*-value < 0.05. All the other HRs had a *p*-value > 0.01.

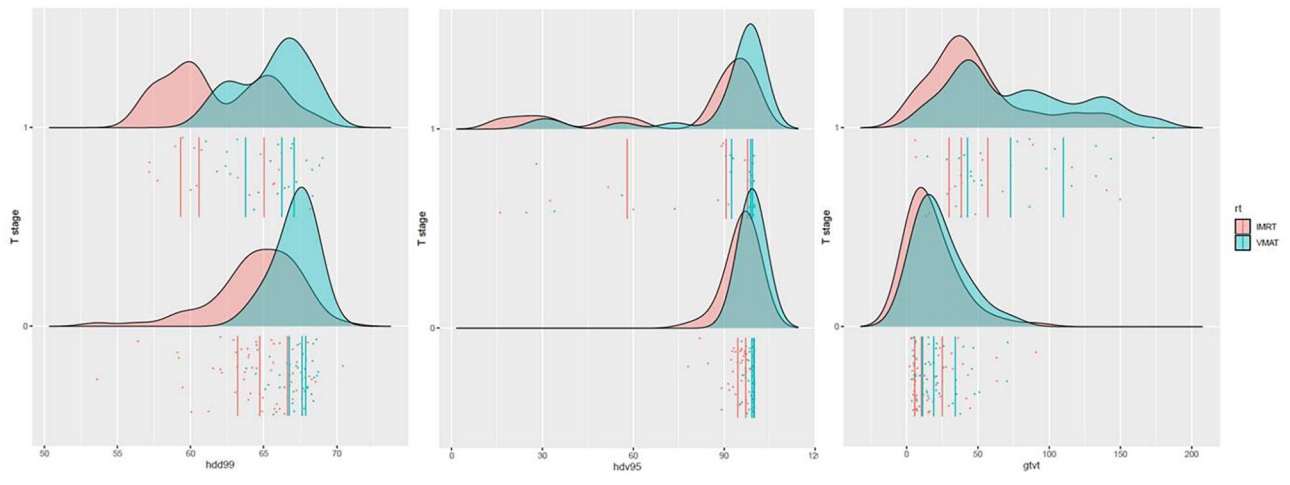

FIGURE 4 | Distribution of D99, V95%, and GTVT. Patients were stratified according to the T stage (T1–T2–T3 = 0 vs. T4 = 1) and RT modality (IMRT vs. VMAT).

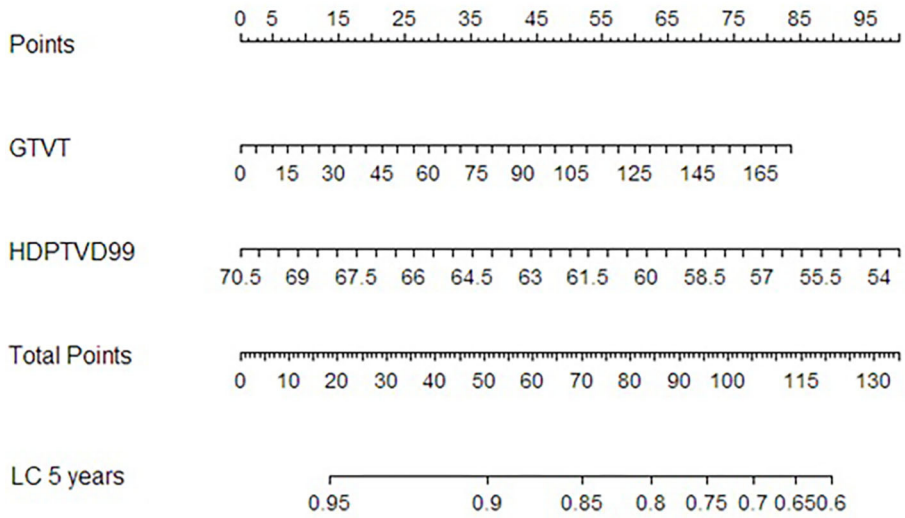

FIGURE 5 | Nomogram for local control at 5 years after RT derived from the Cox proportional hazard regression model with GTVT and HDPTV D99% as variables.

factors as a potential prognosticator on predicting outcome are less investigated.

Indeed, it is well-known that NPC is highly sensitive to ionizing radiation and total RT doses normally regarded as tumoricidal, allowing adequate LC and survival are ≥66 Gy (19); nonetheless, the correlation between precise dose–volume factors and clinical results has not been sufficiently investigated yet.

In the present analysis, we were able to demonstrate a prognostic impact of specific dose–volume parameters generated by IMRT techniques on long-term outcome for a homogeneous NPC patient cohort, although retrospectively. A better target coverage with higher values of V95 and D99% relative to HDPTV proved to significantly improve 5-year LC, DFS, and OS. Ng et al. in their study of 444 NPC patients, showed that underdosing a small portion, 3.4 cm^3, of the primary GTV (GTVT), because of its proximity to critical structures, correlated with a worse outcome in terms of LC and DFS (19). Analogously, when analyzing the prognostic factors in a series of 868 NPC patients, Sun et al. concluded that the minimum dose to the GTV (which could be interpreted as D99%) of at least 65.6 Gy was a prognostic factor of LRFS, PFS, and DSS (8).

Interestingly and contrarily to the previous series, we found different D99% cutoffs for DFS compared to OS and LC. This could probably be explained by the impact of advanced lymph nodal disease on distant metastases and/or by the difference in delineation procedure, because they considered only primary tumor and retropharyngeal lymph nodes while we considered HDPTV encompassing also neck nodal disease.

Recently, a panel of experts in head and neck RT published a guideline on dose prioritization and acceptance criteria for NPC (20). They recommended a minimum dose to the GTV of at least 68.6 Gy, with an acceptable minimum dose set at 66.5 Gy, in line with Ng et al. and PTV coverage with ≥95% of the PD to the entire volume, or ≥93% of the PD to at least 99% of the volume.

IMRT is a major breakthrough in the treatment of NPC. It has been refined over time, till the evolution in VMAT, allowing the radiation dose to be efficiently delivered using a dynamic modulated arc. It is capable of producing highly conformal dose distributions with steep dose gradients and complex isodose surfaces, so as to improve target coverage and OAR sparing in cancers of the oropharynx, hypopharynx, and larynx (21). Indeed, in our previous works, we found a better target coverage with VMAT compared to conventional IMRT, in particular linked to a higher value of V100% (17, 22). This can explain why in our analysis the patients receiving VMAT had better 5-year LC, DFS, and OS compared to conventional IMRT. This result however has to be taken with caution, considering that in our institution, step-and-shoot IMRT has been employed up to 2009 and VMAT technique thereafter and that a learning curve exists in the use of IMRT for head and neck cancer. The evolution in imaging techniques to better define disease extension and a higher use of CHT should also be taken into account.

Another significant finding of our work was the prognostic value of GTVT on the LC trend and the identification of a volume point of GTVT for the prediction of LC at 5 years (43.2 cm^3). This represents the first data in a low-incidence region. The GTVT meaning on the prognosis of NPC patients treated with IMRT has been extensively debated in several studies from endemic areas, with impact on different outcome endpoints probably due to the heterogeneity of samples and different imaging systems to define GTVT. Our finding is in line with data from endemic regions. In NPC, Feng et al. found that a large GTVT is a negative prognostic factor for LRC at 5 years (RR = 2.454, $p = 0.002$), with a 40-ml cutoff (23). Analyzing 321 patients with NPC, Wu et al. found a statistically significant correlation between GTVT and LC, DM, DFS, and OS (all $p < 0.05$) at univariate and multivariate analyses. According to the ROC curve analysis, the two cutoffs of 49 and 19 ml of GTV T were determined for LC and distant

control, respectively (24). He et al. came to similar conclusions (25) when they found GTVT >46.4 ml to be an independent unfavorable prognostic indicator for OS, LRFS, DMFS, and DFS after IMRT in locally advanced NPC patients, with a prognostic value superior to the T category. We were not able to find a significant correlation between nodal GTVs and outcomes: no data have been published in literature on this topic, suggesting that major outcome prognosticators are overall stage and N stage (6, 8).

To come up with a useful approach to predict the risk of local recurrence at 5 years, so as to facilitate personalized management of NPC patients, we constructed a nomogram which combined the GTVT with D99% relative to HRPTV. This nomogram could help clinicians with decision making, enabling them to perform inexpensive, earlier identification of NPC patients at high risk of local recurrence after IMRT. Several previous studies have developed nomograms for individual local recurrence risk assessment in NPC patients based on clinical and radiomic variables. For example, Zhang et al. built a nomogram including age, body mass index (BMI), GTVT, and ethmoidal sinus invasion (26), whereas Chen et al. (27) included age, the neutrophil/leukocyte ratio, pathological type, GTVT, maxillary sinus invasion, ethmoidal sinus invasion, and lacerated foramen invasion. Another nomogram including gender, age, hemoglobin, N stage, and radiomic features has been proposed by Zhang et al. (28). A novelty of our nomogram is the integration of a specific dose–volume parameter (D99%) with a clinical variable (GTVT): this could turn out to be useful in critical T4 cases in which the proximity to surrounding structures could compromise target coverage. When evaluating an RT plan, in particular in those with a larger GTV abutting critical structures, a greater effort in plan optimization (taking care that D99% is at least equal to 63.8 Gy) could play an important role in terms of outcome. When that is not possible, maybe a different approach considering mixed beam therapy could be evaluated (e.g., proton boost). However, this research is retrospective, and our sample size limited. Thus, our nomogram still requires further validation; we will validate its efficiency in other NPC patient cohorts in the following studies.

For T4 patients, to overcome difficulties in dose optimization during planning when the target volume abuts critical structures and reduce late toxicities, a change in the standard practice of contouring the GTVT on pre-iCHT MRI is under investigation. Recent papers have reported the outcomes of NPC patients treated with IMRT, defining the gGTV on post-iCHT MRI, so as to reduce the volume. Yang et al. observed no significant differences in 1-, 2-, and 3-year OS, PFS, LRFFS, and DMFS with volume reduction after iCHT (29). Analogously, the experiences of Zhao et al. (30) and Xue et al. (31) reported good results in terms of disease control with mild toxicities. The dose–volume parameters to take into account in these situations are still to be defined and constitute an interesting field for future research.

We acknowledge the limitations of our study, primarily the retrospective nature of the analysis and the small sample size, although in a low-incidence region. Another limitation was that we did not discriminate the dosimetry only for lymph nodal disease and primary tumor alone. Finally, in our nomogram, we focused only on dose–volume parameters without considering clinical and biochemical data, as other authors did (29–31).

CONCLUSIONS

In our analysis, we demonstrated the prognostic value of some dose–volume parameters, although in a retrospective series. The identification of a precise relationship between IMRT/VMAT plan results and clinical outcome is of paramount importance to finally establish dose–volume parameters serving as planning goal templates not only for routine clinical practice, within an institutional RT quality assurance program, but also for designing prospective NPC trials. In addition, for the first time, in a non-endemic area, a threshold value of GTVT, prognostic for LC, has been confirmed. Finally, to predict the risk of local recurrence at 5 years, we constructed a nomogram which combined the GTVT with D99% relative to HRPTV.

DATA AVAILABILITY STATEMENT

The datasets generated for this study are available on request to the corresponding author.

AUTHOR CONTRIBUTIONS

NI and EO conceived and designed the research. NI and ACa collected the data. NI, EO, ACi, and ACa analyzed and interpreted the data. NI, EO, ACi, and ACa prepared and wrote the manuscript. All authors commented on the manuscript and have given their final approval for submission. All authors contributed to the article and approved the submitted version.

SUPPLEMENTARY MATERIAL

The Supplementary Material for this article can be found online at: https://www.frontiersin.org/articles/10.3389/fonc.2020.518110/full#supplementary-material

REFERENCES

1. Zhang B, Mo Z, Du W, Wang Y, Liu L, Wei Y. Intensity-modulated radiation therapy versus 2D-RT or 3D-CRT for the treatment of nasopharyngeal carcinoma: a systematic review and meta-analysis. *Oral Oncol.* (2015) 51:1041–6. doi: 10.1016/j.oraloncology.2015.08.005
2. Wang TJC, Riaz N, Cheng SK, Lu JJ, Lee NY. Intensity-modulated radiation therapy for nasopharyngeal carcinoma: a review. *J Radiat Oncol.* (2012) 1:129–46. doi: 10.1007/s13566-012-0020-4
3. Lee N, Xia P, Quivey JM, Sultanem K, Poon I, Akazawa C, et al. Intensity-modulated radiotherapy in the treatment of NPC: an update of the UCSF experience. *Int J Radiat Oncol Biol Phys.* (2002) 53:12–22. doi: 10.1016/S0360-3016(02)02724-4
4. Wolden SL, Chen WC, Pfi ster DG, Kraus DH, Berry SL, Zelefsky MJ. IMRT for NPC: update of the memorial sloan-kettering experience. *Int J Radiat Oncol Biol Phys.* (2006) 64:57–62. doi: 10.1016/j.ijrobp.2005.03.057
5. Tham IW, Hee SW, Yeo RM, Salleh PB, Lee J, Tan TWK, et al. Treatment of NPC using IMRT–the NCC Singapore experience. *Int*

J Radiat Oncol Biol Phys. (2009) 75:1481–6. doi: 10.1016/j.ijrobp.2009.01.018
6. Au KH, Ngan RKC, Ng AWY, Poon DMC, Ng WT, Yuen KT, et al. Treatment outcomes of nasopharyngeal carcinoma in modern era after intensity modulated radiotherapy (IMRT) in Hong Kong: a report of 3328 patients (HKNPCSG 1301 study). *Oral Oncol.* (2018) 77:16–21. doi: 10.1016/j.oraloncology.2017.12.004
7. Wu L, Zhang X, Xie X, Lu Y, Wu F, He X. Validation of the 8th edition of AJCC/UICC staging system for nasopharyngeal carcinoma: results from a non-endemic cohort with 10-year follow-up. *Oral Oncol.* (2019) 98:141–6. doi: 10.1016/j.oraloncology.2019.09.029
8. Sun X, Su S, Chen C, Han F, Zhao C, Xiao W, et al. Long-term outcomes of intensity-modulated radiotherapy for 868 patients with nasopharyngeal carcinoma: an analysis of survival and treatment toxicities. *Radiother Oncol.* (2014) 110:398–403. doi: 10.1016/j.radonc.2013.10.020
9. Baujat B, Audry H, Bourhis J, Chan ATC, Onat H, Chua DTT, et al. Chemotherapy as an adjunct to radiotherapy in locally advanced nasopharyngeal carcinoma. *Cochrane Database Syst Rev.* (2006) 28:CD004329. doi: 10.1002/14651858.CD004329.pub2
10. Langendijk JA, Leemans CR, Buter J, Berkhof J, Slotman BJ. The additional value of chemotherapy to radiotherapy in locally advanced nasopharyngeal carcinoma: a meta-analysis of the published literature. *J Clin Oncol.* (2004) 22:4604–12. doi: 10.1200/JCO.2004.10.074
11. OuYang PY, Xie C, Mao YP, Zhang Y, Liang XX, Su Z, et al. Significant efficacies of neoadjuvant and adjuvant chemotherapy for nasopharyngeal carcinoma by meta-analysis of published literature-based randomized, controlled trials. *Ann Oncol.* (2013) 24:2136–46. doi: 10.1093/annonc/mdt146
12. Blanchard P, Lee AW, Leclercq J, Marguet S, Ng WT, Ma J, et al. Chemotherapy and radiotherapy in nasopharyngeal carcinoma: an update of the MAC-NPC meta-analysis. *Lancet Oncol.* (2015) 16:645–55. doi: 10.1016/S1470-2045(15)70126-9
13. Liu D, Long G, Mei Q, Hu G. Primary tumor volume should be included in the TNM staging system of nasopharyngeal carcinoma. *Med Hypotheses.* (2014) 82:486–7. doi: 10.1016/j.mehy.2014.01.032
14. Liu L, Liang S, Li L, Mao Y, Tang L, Tian L, et al. Prognostic impact of magnetic resonance imaging-detected cranial nerve involvement in nasopharyngeal carcinoma. *Cancer.* (2009) 115:1995–2003. doi: 10.1002/cncr.24201
15. Liu X, Liu LZ, Mao YP, Chen L, Tang LL, Zhou GQ, et al. Prognostic value of magnetic resonance imaging-detected cranial nerve invasion in nasopharyngeal carcinoma. *Br J Cancer.* (2014) 110:1465–71. doi: 10.1038/bjc.2014.27
16. Edge SB, Byrd DR, Compton CC, Fritz AG, Greene FL, Trotti A. *AJCC Cancer Staging Manual.* 7th ed. New York, NY: Springer (2010).
17. Orlandi E, Tomatis S, Potepan P, Bossi P, Mongioj V, Carrara M, et al. Critical analysis of locoregional failures following intensity-modulated radiotherapy for nasopharyngeal carcinoma. *Future Oncol.* (2013) 9:103–14. doi: 10.2217/fon.12.166
18. Alfieri S, Iacovelli NA, Marceglia S, Lasorsa I, Resteghini C, Taverna F, et al. Circulating pre-treatment Epstein-Barr virus DNA as prognostic factor in locally-advanced nasopharyngeal cancer in a nonendemic area. *Oncotarget.* (2017) 8:47780–9. doi: 10.18632/oncotarget.17822
19. Ng WT, Lee MC, Chang AT, Chan OS, Chan LL, Cheung FY, et al. The impact of dosimetric inadequacy on treatment outcome of nasopharyngeal carcinoma with IMRT. *Oral Oncol.* (2014) 50:506–12. doi: 10.1016/j.oraloncology.2014.01.017
20. Lee AW, Ng WT, Pan JJ, Chiang CL, Poh SS, Choi HC, et al. International guideline on dose prioritization and acceptance criteria in radiation therapy planning for nasopharyngeal carcinoma. *Int J Radiat Oncol Biol Phys.* (2019) 105:567–80. doi: 10.1016/j.ijrobp.2019.09.030
21. Vanetti E, Clivio A, Nicolini G, Fogliata A, Ghosh-Laskar S, Agarwal JP, et al. Volumetric modulated arc radiotherapy for carcinomas of the oro-pharynx, hypo-pharynx and larynx: a treatment planning comparison with fixed field IMRT. *Radiother Oncol.* (2009) 92:111–7. doi: 10.1016/j.radonc.2008.12.008
22. Orlandi E, Giandini T, Iannacone E, De Ponti E, Carrara M, Mongioj V, et al. Radiotherapy for unresectable sinonasal cancers: dosimetric comparison of intensity modulated radiation therapy with coplanar and non-coplanar volumetric modulated arc therapy. *Radiother Oncol.* (2014) 113:260–6. doi: 10.1016/j.radonc.2014.11.024
23. Feng M, Wang W, Fan Z, Fu B, Li J, Zhang S Lang J. Tumor volume is an independent prognostic indicator of local control in nasopharyngeal carcinoma patients treated with intensity-modulated radiotherapy. *Radiat Oncol.* (2013) 8:208. doi: 10.1186/1748-717X-8-208
24. Wu Z, Su Y, Zeng RF, Gu MF, Huang SM. Prognostic value of tumor volume for patients with nasopharyngeal carcinoma treated with concurrent chemotherapy and intensity-modulated radiotherapy. *J Cancer Res Clin Oncol.* (2014) 140:69–76. doi: 10.1007/s00432-013-1542-x
25. He YX, Wang Y, Cao PF, Shen L, Zhao YJ, Zhang ZJ, et al. Prognostic value and predictive threshold of tumor volume for patients with locally advanced nasopharyngeal carcinoma receiving intensity-modulated radiotherapy. *Chin J Cancer.* (2016) 35:96. doi: 10.1186/s40880-016-0159-2
26. Zhang LL, Li Y,Hu J, Zhou G, Chen L, Li W, Lin A, et al. Proposal of a pretreatment nomogram for predicting local recurrence after intensity-modulated radiation therapy in T4 nasopharyngeal carcinoma: a retrospective review of 415 chinese patients. *Cancer Res Treat.* (2018) 50:1084–1095. doi: 10.4143/crt.2017.359
27. Chen FP, Lin L, Qi ZY, Zhou GQ, Guo R, Hu J, et al. Pretreatment nomograms for local and regional recurrence after radical radiation therapy for primary nasopharyngeal carcinoma. *J Cancer.* (2017) 8:2595–603. doi: 10.7150/jca.20255
28. Zhang L, Zhou H, Gu D, Tian J, Zhang B, Dong D, et al. Radiomic nomogram: pretreatment evaluation of local recurrence in nasopharyngeal carcinoma based on MR imaging. *J Cancer.* (2019) 10:4217–25. doi: 10.7150/jca.33345
29. Yang H, Chen X, Lin S, Rong J, Yang M, Wen Q, et al. Treatment outcomes after reduction of the target volume of intensity-modulated radiotherapy following induction chemotherapy in patients with locoregionally advanced nasopharyngeal carcinoma: a prospective, multi-center, randomized clinical trial. *Radiother Oncol.* (2018) 126:37–42. doi: 10.1016/j.radonc.2017.07.020
30. Zhao C, Miao JJ, Hua YJ, Wang L, Han F, Lu LX, et al. Locoregional control and mild late toxicity after reducing target volumes and radiation doses in patients with locoregionally advanced nasopharyngeal carcinoma treated with induction chemotherapy (IC) followed by concurrent chemoradiotherapy: 10-Year results of a phase 2 study. *Int J Radiation Oncol Biol Phys.* (2019) 104:836–44. doi: 10.1016/j.ijrobp.2019.03.043
31. Xue F, Hu C, He X. Induction chemotherapy followed by intensity-modulated radiotherapy with reduced gross tumor volume delineation for stage T3-4 nasopharyngeal carcinoma. *Onco Targets Ther.* (2017) 10:3329–36. doi: 10.2147/OTT.S140420

Conflict of Interest: The authors declare that the research was conducted in the absence of any commercial or financial relationships that could be construed as a potential conflict of interest.

Advantages of publishing in Frontiers

OPEN ACCESS
Articles are free to read for greatest visibility and readership

FAST PUBLICATION
Around 90 days from submission to decision

HIGH QUALITY PEER-REVIEW
Rigorous, collaborative, and constructive peer-review

TRANSPARENT PEER-REVIEW
Editors and reviewers acknowledged by name on published articles

Frontiers
Avenue du Tribunal-Fédéral 34
1005 Lausanne | Switzerland

Visit us: www.frontiersin.org
Contact us: frontiersin.org/about/contact

REPRODUCIBILITY OF RESEARCH
Support open data and methods to enhance research reproducibility

DIGITAL PUBLISHING
Articles designed for optimal readership across devices

FOLLOW US
@frontiersin

IMPACT METRICS
Advanced article metrics track visibility across digital media

EXTENSIVE PROMOTION
Marketing and promotion of impactful research

LOOP RESEARCH NETWORK
Our network increases your article's readership